INSIGHTS IN EXPERIMENTAL PHARMACOLOGY AND DRUG DISCOVERY: 2021

EDITED BY: Salvatore Salomone and Andres Trostchansky
PUBLISHED IN: Frontiers in Pharmacology

frontiers Research Topics

Frontiers eBook Copyright Statement

The copyright in the text of individual articles in this eBook is the property of their respective authors or their respective institutions or funders. The copyright in graphics and images within each article may be subject to copyright of other parties. In both cases this is subject to a license granted to Frontiers.

The compilation of articles constituting this eBook is the property of Frontiers.

Each article within this eBook, and the eBook itself, are published under the most recent version of the Creative Commons CC-BY licence. The version current at the date of publication of this eBook is CC-BY 4.0. If the CC-BY licence is updated, the licence granted by Frontiers is automatically updated to the new version.

When exercising any right under the CC-BY licence, Frontiers must be attributed as the original publisher of the article or eBook, as applicable.

Authors have the responsibility of ensuring that any graphics or other materials which are the property of others may be included in the CC-BY licence, but this should be checked before relying on the CC-BY licence to reproduce those materials. Any copyright notices relating to those materials must be complied with.

Copyright and source acknowledgement notices may not be removed and must be displayed in any copy, derivative work or partial copy which includes the elements in question.

All copyright, and all rights therein, are protected by national and international copyright laws. The above represents a summary only. For further information please read Frontiers' Conditions for Website Use and Copyright Statement, and the applicable CC-BY licence.

ISSN 1664-8714
ISBN 978-2-88974-726-9
DOI 10.3389/978-2-88974-726-9

About Frontiers

Frontiers is more than just an open-access publisher of scholarly articles: it is a pioneering approach to the world of academia, radically improving the way scholarly research is managed. The grand vision of Frontiers is a world where all people have an equal opportunity to seek, share and generate knowledge. Frontiers provides immediate and permanent online open access to all its publications, but this alone is not enough to realize our grand goals.

Frontiers Journal Series

The Frontiers Journal Series is a multi-tier and interdisciplinary set of open-access, online journals, promising a paradigm shift from the current review, selection and dissemination processes in academic publishing. All Frontiers journals are driven by researchers for researchers; therefore, they constitute a service to the scholarly community. At the same time, the Frontiers Journal Series operates on a revolutionary invention, the tiered publishing system, initially addressing specific communities of scholars, and gradually climbing up to broader public understanding, thus serving the interests of the lay society, too.

Dedication to Quality

Each Frontiers article is a landmark of the highest quality, thanks to genuinely collaborative interactions between authors and review editors, who include some of the world's best academicians. Research must be certified by peers before entering a stream of knowledge that may eventually reach the public - and shape society; therefore, Frontiers only applies the most rigorous and unbiased reviews.
Frontiers revolutionizes research publishing by freely delivering the most outstanding research, evaluated with no bias from both the academic and social point of view. By applying the most advanced information technologies, Frontiers is catapulting scholarly publishing into a new generation.

What are Frontiers Research Topics?

Frontiers Research Topics are very popular trademarks of the Frontiers Journals Series: they are collections of at least ten articles, all centered on a particular subject. With their unique mix of varied contributions from Original Research to Review Articles, Frontiers Research Topics unify the most influential researchers, the latest key findings and historical advances in a hot research area! Find out more on how to host your own Frontiers Research Topic or contribute to one as an author by contacting the Frontiers Editorial Office: frontiersin.org/about/contact

INSIGHTS IN EXPERIMENTAL PHARMACOLOGY AND DRUG DISCOVERY: 2021

Topic Editors:
Salvatore Salomone, University of Catania, Italy
Andres Trostchansky, Universidad de la República, Uruguay

Citation: Salomone, S., Trostchansky, A., eds. (2022). Insights in Experimental Pharmacology and Drug Discovery: 2021. Lausanne: Frontiers Media SA.
doi: 10.3389/978-2-88974-726-9

Table of Contents

frontiers in Pharmacology

EDITORIAL
published: 28 February 2022
doi: 10.3389/fphar.2022.870830

Editorial: Insights in Experimental Pharmacology and Drug Discovery: 2021

Andres Trostchansky[1] *and Salvatore Salomone*[2]*

[1]Facultad de Medicina, Universidad de la República, Montevideo, Uruguay, [2]Department of Biomedical and Biotechnological Sciences, University of Catania, Catania, Italy

Keywords: experimental pharmacology, drug discovery, natural compounds, pain—drug therapy, Alzhaimer's disease (AD)

Editorial on the Research Topic

Insights in Experimental Pharmacology and Drug Discovery: 2021

This Research Topic was intended to focus on new insights, novel developments, current challenges, latest discoveries, recent advances, and future perspectives in Experimental Pharmacology and Drug Discovery. When launching this section, 12 years ago, we stated that it would deal with the analysis of those biological mechanisms targetable by drugs and/or affecting their action (Salomone, 2010). This analysis may be carried out at molecular, cellular, organ/organism level, with a further fourth level of analysis, individualized pharmacology, which takes into account the impact of genetics and epigenetics on drug efficacy and toxicity, to optimize drug therapy for each individual. Drug discovery may move from new chemical entities, conceived to target specific molecular and cellular processes relevant for a disease mechanism, but often takes the reverse way, which is moving from approved drugs to the study of their mechanisms, potentially exploitable to cure other, often unrelated, diseases (drug repurposing). Unexpectedly, our section has also seen a continuously growing number of submissions focusing on natural compounds, which are part of the traditional pharmacopeia in some cultures, particularly the Chinese one, but whose specific mechanisms are not known. These studies, when carried out according to the standards of modern pharmacology (pure substances, precisely known concentrations/doses, concentration-response relationship), may provide useful information not only to understand and implement the correct use of traditional medicine but, more importantly, to provide new lead compounds, specifically directed toward relevant pathophysiological targets.

Five original papers of this RT focus on natural compounds. Wei et al. report on apigenin, a hydroxy flavone active component of some herbal extracts, proposed to treat xerostomia. Based on the prevalence of xerostomia in menopausal women, they hypothesized that sex steroids may be involved in this condition, a mechanism also related to aquaporin 5 expression. Data obtained *in vitro* (human salivary gland cells challenged with estradiol) and *in vivo* (ovariectomized mice) indicated that apigenin upregulates aquaporin 5. This finding was paralleled by functional improvement *in vivo*, e.g., restoration of saliva flow rates by apigenin or estradiol, presumably through ERα signaling. Thus, apigenin appears as a potential therapeutic approach to treat xerostomia, particularly when associated with estrogen reduction. Further studies may indicate additional therapeutic uses of apigenin in conditions where ovary endocrine function is reduced. Qian et al. report on the effects of β-sitosterol, a plant-derived sterol, on synovial angiogenesis, as a potential treatment for rheumatoid arthritis. By using *in vitro* (human umbilical vein endothelial cells) and *in vivo* (collagen-induced arthritis mice) models, the authors tested the hypothesis that

OPEN ACCESS

Edited and reviewed by:
Maria Grazia Morgese, University of Foggia, Italy

***Correspondence:**
Salvatore Salomone
salomone@unict.it

Specialty section:
This article was submitted to Experimental Pharmacology and Drug Discovery, a section of the journal Frontiers in Pharmacology

Received: *07 February 2022*
Accepted: *11 February 2022*
Published: *28 February 2022*

Citation:
Trostchansky A and Salomone S (2022) Editorial: Insights in Experimental Pharmacology and Drug Discovery: 2021. Front. Pharmacol. 13:870830. doi: 10.3389/fphar.2022.870830

sitosterol inhibits VEGF signaling. *In vitro* data showed that β-sitosterol decreased cell proliferation and migration, while *in vivo* data showed a decrease of the swelling degree and the damage of bone and cartilage, inhibition of the synovial angiogenesis, and reduced expression of VEGFR2. These data, while providing a mechanistic rationale for β-sitosterol use in chronic articular inflammation, by showing anti-VEGF effects may suggest further investigations for its effects in experimental disease models involving VEGF signaling, and/or lead optimization to increase potency, specificity, and selectivity. He et al. investigated a phthalide derivative, levistilide A, to expand functional human umbilical cord blood stem cells *ex vivo*. Following a preliminary screening of natural compounds, levistilide A was selected for further testing. The experimental results showed levistilide A increased the numbers of stem cells and enhanced their colony formation ability. Furthermore, treatment with levistilide A improved rapid engraftment of stem cells with multilineage differentiation. These effects might be related to the reduction of reactive oxygen species (ROS) levels. In this respect other antioxidants should be compared to discriminate between general, ROS-related, protection and potential specific effects of levistilide A. Zhu et al. reported on potential anticancer effects of α-mangostin, a molecule extracted from the hull of the mangosteen. In several *in vitro* assays in different cancer cell lines, α-mangostin increased apoptotic mechanisms, including PARP cleavage, BAX induction, and blockade of AKT signaling, this latter effect was attributed to an α-mangostin-induced degradation of retinoid X receptor. Finally, α-mangostin seemed also active in some *in vitro* assays of migration and invasion. Because most of these effects occur at relatively high (supra micromolar) α-mangostin concentrations, these data deserve further refinement, e. g. lead optimization, to generate a molecular species further testable in *in vivo* settings. Wang et al. attempted to elucidate the mechanisms underlying the antiplatelet effect of berberine and its metabolite berberrubine. Docking and *in vitro* experiments suggested that these compounds inhibit the Rasa3-Rap1 pathway, which is critical for ADP-induced integrin activation (Stefanini et al., 2015). Furthermore, the berberine effect depended on PI3K activation. The antiplatelet effect was confirmed in an *in vivo* thrombosis model (carrageenan-induced thrombosis in mouse tail). The antithrombotic effects of such natural compounds are intriguing, because they point to novel, potentially exploitable, molecular and cellular mechanisms. However, again, additional studies are warranted to achieve, potency, specificity, and selectivity, sufficient for further pharmaceutical development.

Besides the pharmacological characterization of natural compounds, a leading domain in our specialty is Neuropharmacology/Neuroscience, both in terms of discovering novel targetable processes, as well as in terms of studying drug mechanisms, through repurposing and/or pharmacological profiling of new chemical entities. In the Neuropharmacology context, two submissions deal with amyloid-β (Aβ)-related neuroinflammation, two others with potential therapeutic approaches for neuropathic pain. Caruso et al. attempted to elucidate the neuroprotective mechanism of second-generation antidepressants against Aβ-induced neurotoxicity. They report that chronic treatment with vortioxetine or fluoxetine prevented oxidative stress in the hippocampus of Aβ-injected mice and decreased a number of inflammatory markers, including inducible nitric oxide synthase and NADPH oxidase 2, while increased glutathione peroxidase 1, an antioxidant enzyme. Neuroprotection by vortioxetine and fluoxetine was also confirmed *in vitro*, in neuronal cultures challenged with Aβ oligomers. These drugs are commonly used to treat depression associated with Alzheimer's disease; the present data suggest that they may also exert neuroprotection, which remains to be assessed in clinical settings. The other report by Morgese et al. is also somehow related to Alzheimer's disease and depression because it attempts to determine whether depression and the associated increase in pain perception occur in an animal model of Aβ-induced neurotoxicity. Intracerebroventricularly Aβ-injected rats displayed memory impairment associated with increased pain susceptibility to mechanical (but not to thermal) stimuli. Many biomarkers were found correlated with the above functional alterations, including increased glutamate, kynurenine, and dopamine and reduced serotonin in the hypothalamus, Cystatin-C, increased, serotonin and melatonin decreased in plasma, with urinary levels paralleling plasma levels. This animal study opens to the possibility of using these biomarkers as an approach for precision medicine.

Kappa opioid agonist have therapeutic potential to treat pain and itch but induce central side effects, such as sedation and dysphoria. Peripherally-restricted kappa-opioid agonists are developed to minimize these adverse effects, because of their scarce penetration in CNS. Wang et al. analyzed the effects of HSK21542, a peripherally-restricted kappa-opioid receptor agonist, in mouse models. HSK21542 showed a brain/plasma concentration ratio of 0.001 and significantly inhibited pain-and hitch-related behaviors, without significant central effects (locomotor activity, respiratory depression). Therefore, this compound seems a promising candidate for treating pain and pruritus and confirms the value of peripherally-restricted kappa-opioid agonists. The other study, by Fidilio et al. tests the hypothesis that reduced levels of transforming growth factor-β1 (TGF-β1) might be involved in aberrant pain processing. By using LP2, a dual-target mu and delta-opioid receptor agonist in the rat chronic constriction injury model, they found a decreased TGF-β1 and TGF-β type II receptor in the spinal cord and rescue of TGF-β1 and TGF-β type II receptor levels in LP2-treated animals. These data suggest that the rescue of TGF-β1 signalling in spinal microglia might be therapeutically relevant and that this might be achieved with the dual opioid receptor targeting approach.

Other reports in this RT deal with mechanisms and targets in cancer, diabetes, chronic inflammation. Lee et al. examined the role of B lymphocyte-induced maturation protein-1 (Blimp-1) in squamous cell carcinoma, in cell lines. They found that a number of stimuli increasing EGF signaling upregulate Blimp-1, while the EGFR inhibitor gefitinib blocks Blimp-1. Moreover, Blimp-1 silencing enhanced cell migration. They conclude that the function of Blimp-1 as a

negative regulator of cell migration provides a new therapeutic target in squamous cell carcinoma. Zhang et al. report on the protective effects of polyethylene glycol loxenatide, a long-acting glucagon-like peptide-1 analog, in db/db diabetic mice. They found that, in addition to the known, insulin-related, effect, loxenatide inhibited oxidative stress and decreased pro-inflammatory markers (TNF-α, IL-6, and MCP-1), while increasing anti-inflammatory IL-10. Rong et al. report that photodynamic therapy with a photosensitizer is beneficial for 2,4,6-trinitrobenzene sulfonic acid-induced ulcerative colitis in rats. This treatment seems to act via inhibition of Amine oxidase copper-containing 1 and is accompanied by a decrease of several inflammatory markers.

Finally, two reviews examine the pharmacological potential of some chemical classes of compounds as antimicrobial treatments. Brishty et al. summarize the literature on benzimidazole derivatives, Long et al. the literature on fusidic acid derivatives. Besides the structure-activity information, these reviews also point to potential uses of these derivatives, even in contexts distinct from infectious diseases, such as chronic inflammatory diseases and cancer.

AUTHOR CONTRIBUTIONS

All authors listed have made a substantial, direct, and intellectual contribution to the work and approved it for publication.

REFERENCES

Salomone, S. (2010). Analytical and Experimental Pharmacology, Challenges Ahead. *Front. Pharmacol.* 1, 119. doi:10.3389/fphar.2010.00119

Stefanini, L., Paul, D. S., Robledo, R. F., Chan, E. R., Getz, T. M., Campbell, R. A., et al. (2015). RASA3 Is a Critical Inhibitor of RAP1-Dependent Platelet Activation. *J. Clin. Invest.* 125, 1419–1432. doi:10.1172/JCI77993

Conflict of Interest: The authors declare that the research was conducted in the absence of any commercial or financial relationships that could be construed as a potential conflict of interest.

Publisher's Note: All claims expressed in this article are solely those of the authors and do not necessarily represent those of their affiliated organizations, or those of the publisher, the editors and the reviewers. Any product that may be evaluated in this article, or claim that may be made by its manufacturer, is not guaranteed or endorsed by the publisher.

Copyright © 2022 Trostchansky and Salomone. This is an open-access article distributed under the terms of the Creative Commons Attribution License (CC BY). The use, distribution or reproduction in other forums is permitted, provided the original author(s) and the copyright owner(s) are credited and that the original publication in this journal is cited, in accordance with accepted academic practice. No use, distribution or reproduction is permitted which does not comply with these terms.

frontiers in Pharmacology

ORIGINAL RESEARCH
published: 30 August 2021
doi: 10.3389/fphar.2021.739658

α-Mangostin Induces Apoptosis and Inhibits Metastasis of Breast Cancer Cells via Regulating RXRα-AKT Signaling Pathway

*Xiuzhi Zhu[1,2], Jialin Li[3], Huiting Ning[2], Zhidong Yuan[2], Yue Zhong[2], Suzhen Wu[2] and Jin-Zhang Zeng[1]**

[1]School of Pharmaceutical Sciences, Xiamen University, Xiamen, China, [2]School of Basic Medicine, Gannan Medical University, Ganzhou, China, [3]School of Pharmacy, Gannan Medical University, Ganzhou, China

Mangostin, which has the function of anti-inflammatory, antioxidant, and anticancer, etc, is one of the main active ingredients of the hull of the mangosteen. The main objective of the study was to elucidate its anti-cancer function and possible mechanism. α-Mangostin was separated and structurally confirmed. MTT method was used to check the effect of mangostin on breast cancer cell proliferation. Then the effect of α-Mangostin on the transcriptional activity of RXRα was tested by dual-luciferase reporter gene assay. And Western blot (WB) was used to detect the expression of apoptosis-related proteins or cell cycle-associated proteins after treatment. Also, this study was to observe the effects of α-Mangostin on the invasion of breast cancer cell line MDA-MB-231. α-Mangostin regulates the downstream effectors of the PI3K/AKT signaling pathway by degrading RXRα/tRXRα. α-Mangostin can trigger PARP cleavage and induce apoptosis, which may be related to the induction of upregulated BAX expression and downregulation of BAD and cleaved caspase-3 expression in MDA-MB-231 cells through blockade of AKT signaling. The experiments verify that α-Mangostin have evident inhibition effects of invasion and metastasis of MDA-MB-231 cells. Cyclin D1 was involved in the anticancer effects of α-Mangostin on the cell cycle in MDA-MB-231 cells. α-Mangostin induces apoptosis, suppresses the migration and invasion of breast cancer cells through the PI3K/AKT signaling pathway by targeting RXRα, and cyclin D1 has involved in this process.

Keywords: α-mangostin, apoptosis, RXRα/tRXRα, cyclin D1, breast cancer

OPEN ACCESS

Edited by:
Andres Trostchansky, Universidad de la República, Uruguay

Reviewed by:
Benoit Paquette, University of Sherbrooke, Canada
Noor Ayad Hussein, University of Toledo, United States

****Correspondence:***
Jin-Zhang Zeng
jzzeng@xmu.edu.cn

Specialty section:
This article was submitted to Experimental Pharmacology and Drug Discovery, a section of the journal Frontiers in Pharmacology

Received: *11 July 2021*
Accepted: *18 August 2021*
Published: *30 August 2021*

Citation:
Zhu X, Li J, Ning H, Yuan Z, Zhong Y, Wu S and Zeng J-Z (2021) α-Mangostin Induces Apoptosis and Inhibits Metastasis of Breast Cancer Cells via Regulating RXRα-AKT Signaling Pathway. Front. Pharmacol. 12:739658. doi: 10.3389/fphar.2021.739658

INTRODUCTION

Mangostin is a series of natural compounds isolated from the epicarp of the fruits of *Garcinia Mangostana Linn* which is one of the most popular herbal medicines (Nguyen et al., 2020). In traditional Chinese medicine, the fruit hull of mangosteen has been widely used in the treatment of diarrhea, diabetes, and cancer for centuries (Ittiudomrak et al., 2019; Zou et al., 2019). Also, the mangosteen fruit rind extracts have free radical scavenging and anti-acne activities (Phan et al., 2018). Since Mangostin was first isolated and identified in mangosteen fruit rind extracts (Zhang et al., 2017; Yeong et al., 2020), many biological activities and pharmacological studies of α-Mangostin have been performed in subsequent studies (Zhang et al., 2018). A suppression effect of α-Mangostin has been shown in breast cancer cells. α-Mangostin can indirectly induce the

apoptosis of leukemia HL60 cells and human DLD-1 colon cancer cells through a reduction of mitochondrial transmembrane potential (Fu et al., 2018; Lee et al., 2018), and also inhibits the proliferation of DLD-1 cells in the G1 phase (Nakagawa et al., 2007). The cytotoxicity of more than 10 types of compounds extracted from the epicarp of the mangosteen fruit has been tested, of which α-Mangostin was the most toxic to human leukemia cell lines (Jasek et al., 2014; Austin et al., 2015). The toxicity of methanol extracts from mangosteen shells on human breast cancer SKBR3 cells was also confirmed (Scolamiero et al., 2018; Bissoli and Muscari, 2020), and the authors speculated that the active ingredient causes apoptosis by inhibiting low-density lipoprotein (LDL) oxidation and acid sheath phospholipase activity.

We have confirmed that α-Mangostin is highly toxic to human breast cancer SKBR3, MCF-7, and MDA-MB-231 cells. The experiments revealed that α-Mangostin can bind with RXRα in cells and is a good antagonist of this receptor. RXRα is a non-steroidal nuclear receptor, and the conformation of its ligand-binding domain (LBD) helix 12 (Chen et al., 2014) changes to regulate biological function when the corresponding ligand is present (Ishizawa et al., 2012). RXRα has a non-genetic function in the cytoplasm in addition to its transcriptional function in the nucleus (Chen et al., 2014). Recent studies have shown that RXRα can be truncated by restrictive hydrolysis in many tumor cells (Zheng et al., 2019), to produce RXRα with missing N-terminus, called tRXRα (truncated RXRα) (Zhou et al., 2010). Truncated RXRα is mainly localized to the cytoplasm, regulating downstream PI3K through interactions with p85, which activates the PI3K/AKT survival pathway and promotes the disorderly proliferation of tumor cells (Jiang et al., 2013).

The invasive metastasis of breast cancer is a complex evolutionary process with multiple factors and steps, regulated by the expression of multiple genes (Hamurcu et al., 2018). The breast cancer cells invasion is the main reason of recurrence after tumor resection (Fuste et al., 2016). So, chemotherapy is generally the main treatment for invasive breast cancer. Paclitaxel is commonly used for the treatment of invasive breast cancer since the 90s (Zhong et al., 2010). But this clinical drug has shortcomings as well, such as side effects, drug resistance, etc. So far, the treatment of triple negative breast cancer (TNBC) is still difficulty. There is an urgent need for suitable targeted drugs and more effective drugs for TNBC(Fuste et al., 2016).

In this study, we examined whether tRXRα serves as an intracellular target mediating the biological activities of α-Mangostin. Also, we investigated the mechanism by which α-Mangostin acts to promote tumor cell apoptosis and inhibit invasion and metastasis. Furthermore, we explored the possibility of dissociating the anticancer effects of α-Mangostin from its cell cycle inhibition activity.

MATERIALS AND METHODS

Extraction and Separation

The fruits of Mangosteen were bought directly from the fruit market in Xiamen, China. The fruits were authenticated as *Garcinia Mangostana. Linn* by Professor Jin-zhang Zeng (School of pharmaceutical sciences and State Key Laboratory of Cellular Stress Biology, Xiamen University). The epicarp of the fruits (3 kg) was air-dried at room temperature and pulverized, then extracted with 95% ethanol (20 L) three times (36 h per time) at room temperature to yield an extract. The latter was concentrated in vacuo to yield a residue (504 g), which was suspended in H_2O and partitioned with Ethyl acetate. The solvent was evaporated under reduced pressure to afford an Ethyl acetate extract (209 g). The Ethyl acetate extract was subjected to silica gel column chromatography (200–300 mesh) with a gradient eluant system of CH_2CL_2-CH_3OH (80: 1-40:1, v/v) to yield 8 fractions. TLC (thin-layer chromatography) was employed to monitor the process. Fraction 6 was subjected to silica gel column chromatography eluted with petroleum ether–Ethyl acetate (4:1–1:1, v/v) to afford 2 subfractions 6.1–6.2. Fraction 6.2 followed by semi-preparative HPLC with 94% ethanol to give compounds 1 (67 mg), 2 (72 mg), and 3 (36 mg). The chromatographic column used in this method is the capillary column of C-18ODS (20*250 mm).

Structure Identification

The compounds were characterized by proton nuclear magnetic resonance, mass spectrometry, and elemental analysis. The compound 3 was identified as α-Mangostin according to the chromatographic behavior and mass spectral data by comparison with those of control. Spectral data: 1H-NMR (400 MHz,CDCl3):δ 1.62(6H,S, 19-CH_3,20-CH_3),1.73(3H,s, 14-CH3), 1.77(3H,s, 15-CH_3), 3.20(2H,d,J = 6.8 Hz,H-11), 3.79(3H,S, 7-OCH_3),4.09(2H,d,J = 6.8 Hz,H-16),5.16(2H,m,H-12, H-17),6.36(1H,S,H-4),6.80(1H,S,H-5),10.80(1H,brs,C-3-OH),13.78(1H,S,C-1-OH).13C-NMR (100MHz, $CDCl_3$):δ 17.9(C-19), 18.2(C-14), 21.4(C-11), 25.8(C-15,20), 26.6(C-16), 62.0(7-OCH_3), 93.3((C-4), 102.8(C-5),101.6(C-9a), 108.5(C-2), 112.2(C-8a), 121.5(C-12), 123.1(C-17), 133.1(C-13), 135.6(C-18), 137.0(C-8), 142.5(C-7), 154.5(C-4a), 155.3(C-10a), 155.8(C-6), 160.6(C-1), 161.6(C-3), 182.0(C-9).

Cell Lines and Plasmids

The MCF-7, SKBR-3, MDA-MB-231, and HEK-293 T cells were obtained from the Type Culture Collection of the Chinese Academy of Sciences (Shanghai, China), and grown in DMEM (dulbecco's modified eagle medium) supplemented with 10% fetal bovine serum (PAN Biotech, SA) at 37°C in an incubator containing 5% CO2. The pGAL4-RXRα-LBD plasmid was obtained by inserting the RXRα ligand-binding domain (LBD) cDNA sequence (amino acids 198–462) in-frame with the GAL4 DBD coding sequence in the pBind vector.

CCND1 and RXRα siRNA

CCND1 and RXRα siRNA was purchased from DHARMACON and was transfected into cells using RNAi- MAX reagent.

MTT Assay of Cell Viability and Proliferation

Three breast cancer cell lines were seeded at a density of 5–10 × 10^4 cells/well in 96-well plates containing 100 μL medium (DMEM containing 10% FBS) for 18 h. Thereafter, the culture

medium was removed and replaced with 100 μL medium (serum-free DMEM) containing various concentrations (40, 20, 10, 5, 2.5, and 1.2 μM) of α-Mangostin or 0.1% (v/v) dimethyl sulfoxide (DMSO) solvent only (control). The cells were grown for another 48 h. Subsequently, 10 μL MTT solution (5 g/L) was added to each well and the culture plates were incubated for 4 h to allow formazan formation. The culture medium was then removed, the formazan was solubilized by the addition of 150 μL DMSO, and the absorbance at 560 nm (A560) was measured with a microplate reader to calculate cell viability (%). The IC50(50% inhibitive concentration) value of the compound was calculated by Graphpad Prism 6.0.

Apoptosis and Cell Cycle Analysis

The MDA-MB-231 cells were cultured at a density of 4×10^5 cells/well in 6-well plates containing 1,600 μL medium for overnight culture. Then, the cells were treated with various concentrations of α-Mangostin, meanwhile, 5 μM concentration of paclitaxel acted as a control. The cells were harvested at the indicated times by trypsinization with 0.05% (w/v) trypsin in 0.5 mM ethylenediaminetetraacetic acid solution. The cells were then washed twice with cold phosphate-buffered saline (PBS), using centrifugation at 1,000 × g for 5 min at 4°C to harvest the cells each time. For apoptosis detection, the cell pellets were resuspended in 50 μL binding buffer (10 mM HEPES, pH 7.4, 140 mM NaCl, and 2.5 mM $CaCl_2$) and stained with 5 μL annexin V-Alexa Fluor 488 and 5 μL PI for 30 min at room temperature in the dark. For the cell cycle study, the cell pellets were fixed in 200 μL cold 70% (v/v) ethanol at −20°C overnight, harvested, and washed as described above. The washed cell pellet was then suspended in 250 μL PBS containing 0.1 g/L RNase A and incubated at 37°C for 30 min. Thereafter, it was washed as described above, resuspended in staining buffer (12.5 μL PI (1 g/L in PBS)), and incubated at room temperature for 30 min in the dark. The samples were then analyzed by flow cytometry on an FC 500 MPL cytometer that recorded 10,000 events per sample. The experiment was performed in triplicate.

Transient Transfection and Reporter Assays

293 T cells were grown in DMEM supplemented with 10% FBS. For dual-luciferase reporter assays, cells were seeded at a concentration of 5×10^4 cells per well in 24-well plates and transfected with pGL5 luciferase reporter vector (40 ng/well) and pGAL4-RXRα-LBD expression vector (40 ng/well). Cells were then incubated with various concentrations of compounds for 12 h. Luciferase activities were measured using the Dual-Luciferase Assay System Kit.

SPR (Surface Plasmon Resonance) Measurements

Binding experiments were carried out using Biacore S200 SPR sensors with control software version 3.0 and Sensor Chip CM5 (carboxymethylated dextran surface). All assays were carried out at 25°C. For the pre-binding experiment, pure RXRα-LBD protein was dissolved with acetate buffers with different pH values (pH4.0, pH4.5, pH5.0, and pH5.5) and flowed through the surface of the chip at a rate of 5 μL/min. Then, the chip surface was activated following a standard EDC/NHS protocol with Biacore PBS-EP buffer used as the running buffer. RXRα-LBD protein at a concentration of 0.4 g/L in 10 mM phosphate buffer pH 5.0 was then injected for 12 min followed by a 7- min injection of 1 M ethanolamine to inactivate residual active groups. Typically, approximately 2000 RU receptor protein was immobilized per flow cell. By reference to the coupling steps of RXRα-LBD protein, the protein was coupled to the chip. For the preparation of the α-Mangostin solution, the insoluble residue was pelleted by centrifugation and discarded. α-Mangostin was injected into the protein channel and blank channel at seven concentrations (0.625 nM, 1.25 nM, 2.5 nM, 5 nM, 10 nM, 20 nM, and 40 nM). The supernatant (200 μL) was injected at a flow rate of 20 μL/min. The protein binding period was set to 3 min, and the dissociation period was set to 300 s. The chip was regenerated with glycine-HCl (pH 2.5, 10 mM).

Western Blotting

Cell lysates were prepared by lysing cells with lysis buffer (RIPA) containing 50 mM Tris-HCl, 150 mM NaCl, 1 mM EDTA, 0.1% SDS, 1% Na-deoxycholate, 1% Triton X-100, pH 7.4 with a cocktail of proteinase inhibitors on ice for 30 min. The cells were fixed with 80 μL/well cell lysates in 12-well plates. Equal amounts of the lysates were electrophoresed on 8% SDS-PAGE gels and transferred onto polyvinylidene difluoride membranes. The membranes were blocked with 5% nonfat milk in Tris-Buffered Saline and Tween 20 [50 mmol/L Tris–HCl (pH 7.4), 150 mmol/L NaCl, and 0.1% Tween 20] for 1 h, incubated with various primary antibodies for 48 h and detected with either anti-rabbit (1:5,000) or anti-mouse (1: 5,000) secondary antibodies for 1 h. The final immunoreactive products were detected using enhanced chemiluminescence (ECL).

Molecular Docking

The three-dimensional structure of human RXRα (PDB code: 3A9E) was downloaded from the Protein Data Bank. Protein preparation was performed by Chimera and autodock software and was saved as a locked PDB file for docking. Schrodinger software glide module was used to calculate the molecular docking of α-Mangostin and RXRα, list the possible binding sites, and determine the docking energy.

Statistical Analyses

The quantitative data were obtained by three or more repeated experiments. Data were analyzed using an analysis of variance or Student's t-test and were presented as the mean and standard error of the mean (±SEM).

RESULTS

α-Mangostin Inhibits Proliferation and Induces Apoptosis of Breast Cancer Cells

We first assessed the anti-proliferative effects of α-Mangostin in breast cancer cells. MCF-7, MDA-MB-231, and SKBR-3 cells were treated with increasing concentrations of α-Mangostin (0,

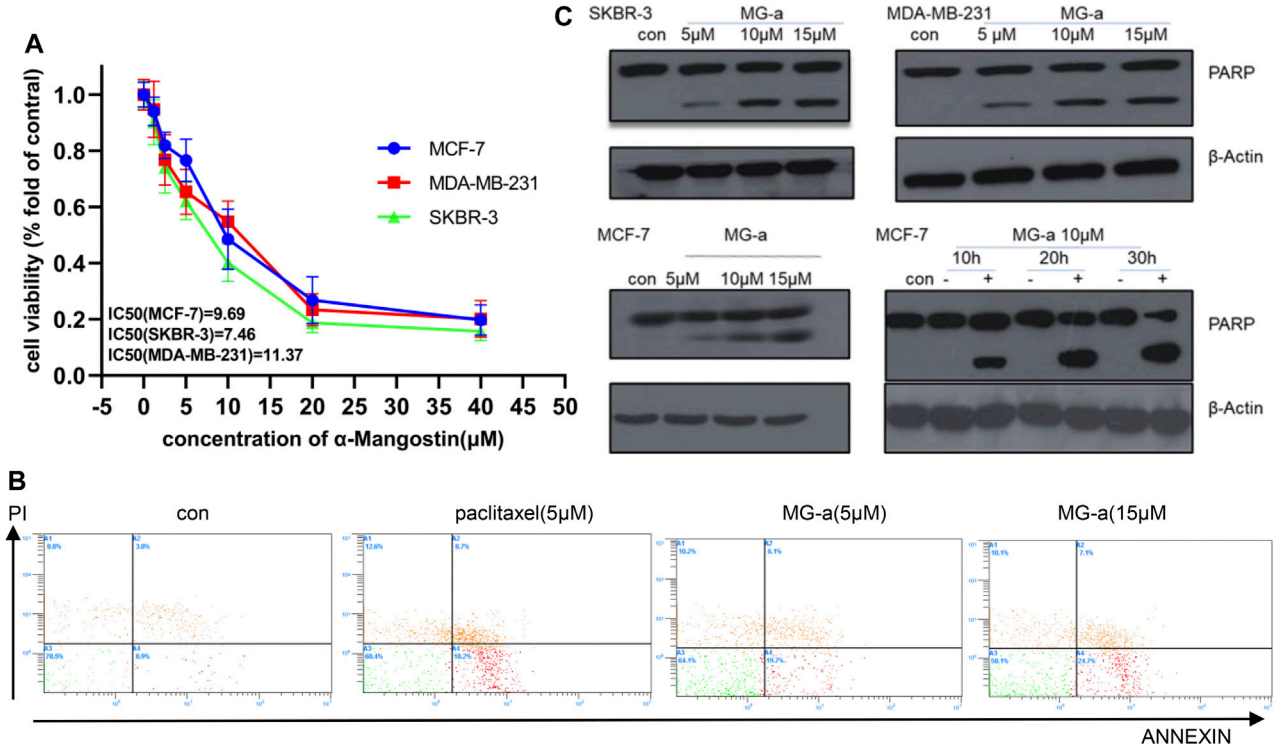

FIGURE 1 | α-Mangostin (MG-a) inhibits proliferation and induces apoptosis of breast cancer cells. **(A)** α-Mangostin reduces breast cancer proliferation. **(B)** Apoptosis of MDA-MB-231cells treated with MG-a was assessed by flow cytometry. **(C)** PARP expression levels were determined by western blotting analysis in breast cancer cells after α-Mangostin treatment.

1.2, 2.5, 5, 10, 20, and 40 μM) for 48 h α-Mangostin significantly inhibited breast cancer cell proliferation in a dose-dependent manner. (**Figure 1A**). The IC50 values of α-Mangostin against MCF-7, MDA-MB-231, and SKBR-3 cells were 9.69, 11.37, and 7.46 μM, respectively. We used Annexin-V and PI double staining to detect the cytotoxicity of α-Mangostin by flow cytometry. MDA-MB-231 cells were treated with α-Mangostin using paclitaxel as a positive control. α-Mangostin could induce apoptosis of MDA-MB-231 cells in a concentration-dependent manner (**Figure 1B**).

To further verify the apoptotic effects of α-Mangostin in breast cancer cells at the molecular level, we detected the cleavage of PARP in MCF-7, SKBR-3, MDA-MB-231 cells by western blotting. The PARP protein in these cell lines had been significantly cleaved, and the cleavage increased with the increase in α-Mangostin concentration over 20 h treatment (**Figure 1C**). Meanwhile, the cleavage of PARP proteins in the MCF-7 cells increased in a time-dependent manner through treatment with 10 μM α-Mangostin.

The Apoptotic Effects of α-Mangostin Depend on the PI3K/Akt Signaling Pathway

Because of potential influence on suppressing the migration and invasion of TNBC Cells *in Vitro* by α-Mangostin, we chose MDA-MB-231 to perform further experiments. Western blotting was used to detect cleaved caspase-3 and BCL-2 protein family expression in MDA-MB-231 cells (**Figure 2**). Endogenous cleaved caspase-3 mostly related to BCL-2 protein family. The expression of BAD and BAX was affected by α-Mangostin. A graded decrease in BAD expression was detected following treatment of cells with the concentration gradient of α-Mangostin for 24 h, while BAX expression increased (**Figure 2B**).

The PI3K/Akt signaling pathway is one of the most important survival pathways in cells and has a very close relationship with tumor development (Zhang et al., 2018). We further explored whether α-Mangostin induces apoptosis through the PI3K/Akt signaling pathway. The expression of Akt was almost unchanged with the increase in α-Mangostin concentration, while the expression of P-Akt decreased in turn (**Figure 2C**). After treatment with 10 μM α-Mangostin, the expression of P-Akt (activated Akt) protein in cells was significantly reduced. P-Akt was significantly suppressed compared with that of the control group. To further verify whether the induction of apoptosis of breast cancer cells by α-Mangostin depends on the PI3K/Akt signaling pathway, we added PI3K/Akt inhibitor LY294002 (20 μM) to the medium of MDA-MB-231 cells for 6 h. Then the cells were treated with α-Mangostin for 20 h. The expression of P-Akt protein in cells was then detected.

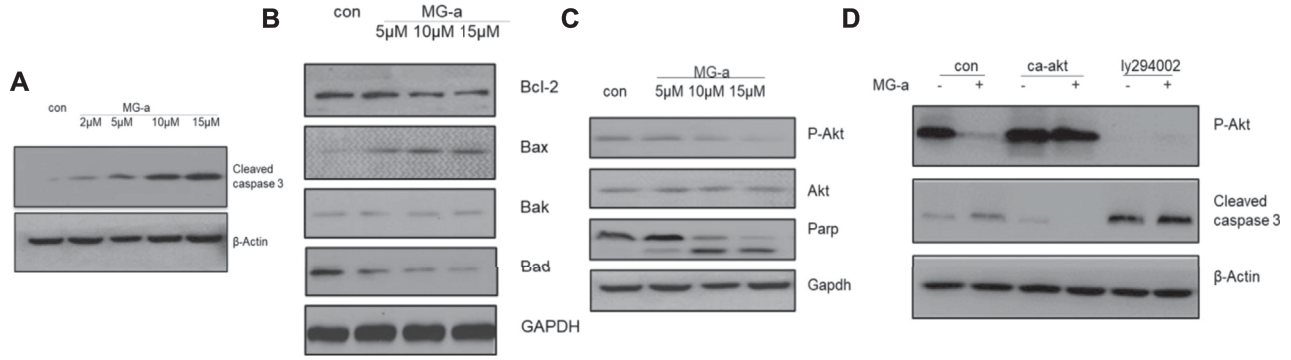

FIGURE 2 | The apoptotic effects of α-mangostin depend on the PI3K/Akt signaling pathway. Cell apoptosis in MDA-MB-231 cells treated with α-Mangostin depends on the PI3K/Akt signaling pathway. **(A)** The expression levels of cleaved caspase-3 were determined by western blotting analysis in MDA-MB-231 cells after α-Mangostin treatment. **(B)** The expression levels of BCL-2 family proteins were determined by western blotting analysis in MDA-MB-231 cells after α-Mangostin treatment. **(C)** and **(D)**, The western blotting analysis demonstrated that PI3K/Akt signaling is required for the apoptosis of MDB-MD-231 cells induced by α-Mangostin.

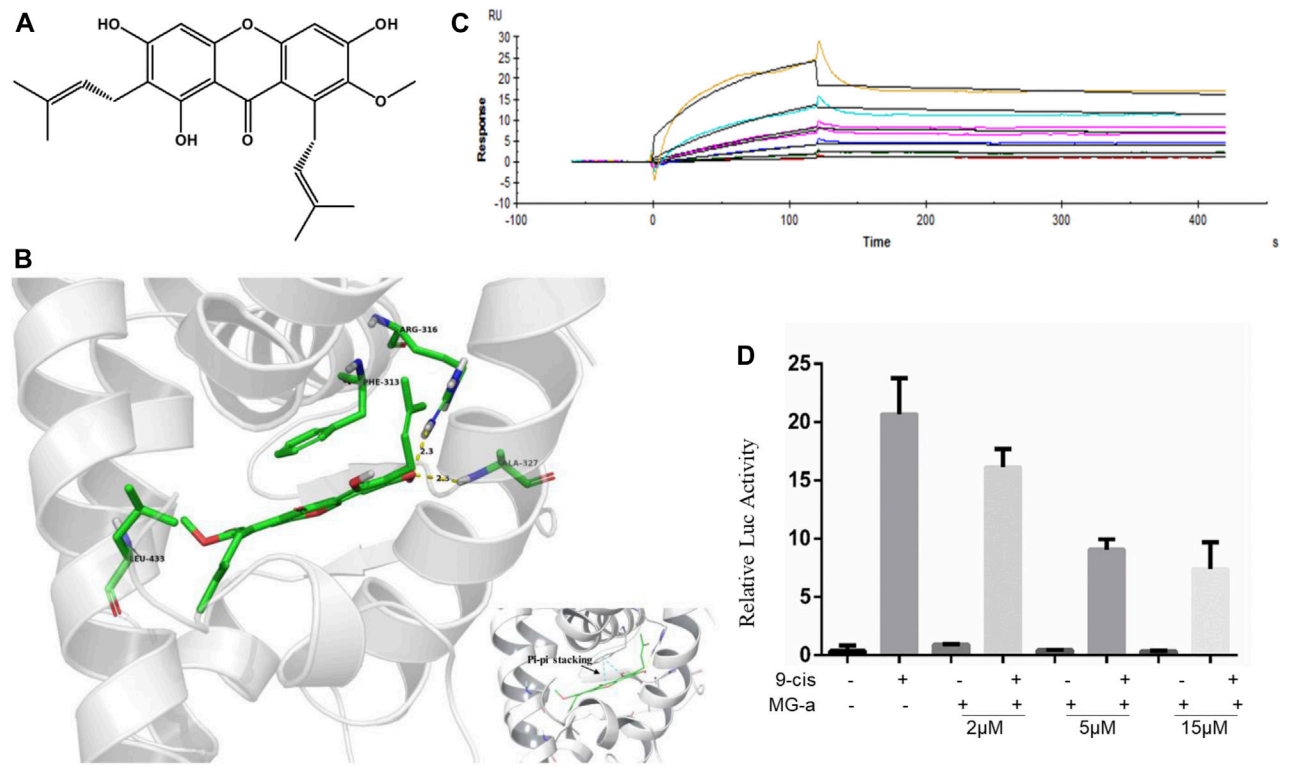

FIGURE 3 | α-Mangostin induces apoptosis by targeting RXRα. **(A)** The structural formula of α-Mangostin. **(B)** The results of molecular docking: α-Mangostin interacts with amino acid residues Arg-316, Ala327, and Leu-433 of RXRα LBD. A pi-pi stacking is formed with amino acid residue Phe-313. **(C)** Antagonistic effect of α-Mangostin (2, 5, 15 μM). 293 T cells transfected with PBind-RXR/LBD and PG5 expression vector were treated with or without 10–7 mol/L 9-cisRA in the absence or presence of different concentrations of α-Mangostin. Reporter activities were measured and normalized. One of three independent experiments is shown. **(D)** SPR analysis of the interaction of MG-a with RXRα (α-Mangostin solution was injected into the RXR-LBD protein channel and blank channel at seven concentrations (0.625, 1.25, 2.5, 5, 10, 20, and 40 nM).

LY294002 inhibited the activation of Akt (**Figure 2D**) and enhanced the inhibitory effect of α-Mangostin on P-Akt. Our laboratory constructed a plasmid expressing continuously activated Akt (CA-Akt) by generating a point mutation in a critical region. We transfected the plasmid into MDA-MB-231 cells. After 24 h, the cells were treated with 10 μM α-Mangostin.

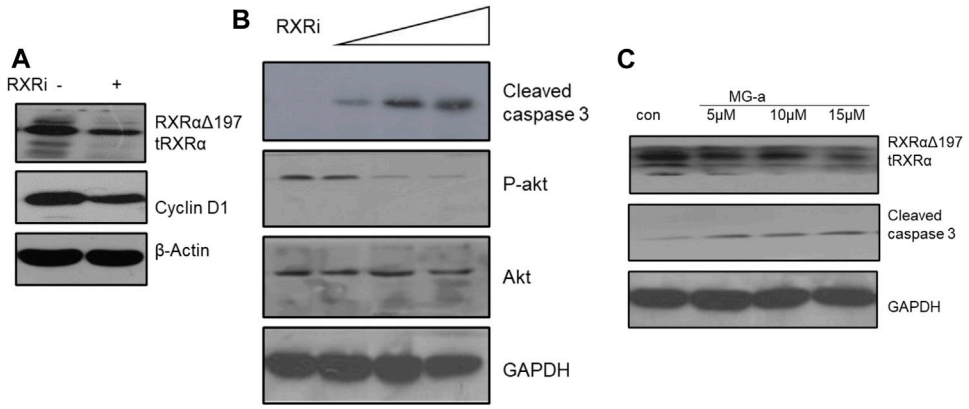

FIGURE 4 | α-Mangostin induces the degradation of RXRα/tRXR and inhibits Akt activity in MDA-MB-231 cells. **(A,B)** The expression levels of cyclin D1 and P-Akt were determined by western blotting analysis in MDA-MB-231 cells after knockdown of RXRα. **(C)** The expression levels of RXRα/tRXR and cleaved caspase-3 were determined by western blotting analysis in MDA-MB-231 cells after α-Mangostin treatment.

We observed many apoptotic cells in the control group, while the apoptosis of MDA-MB-231 cells expressing CA-Akt was much less. Western blotting demonstrated the cleavage of caspase-3 was reduced by continuous activation of Akt (**Figure 2D**).

α-Mangostin Induces Apoptosis by Targeting RXRα

α-Mangostin belongs to the xanthone group of compounds (Chen et al., 2018). Its structural formula is shown in **Figure 3A**. In the current study, molecular docking was further examined to explore the binding of RXRα with α-Mangostin. The aligned structures of the original X-ray and docking are shown in **Figure 3B**. α-Mangostin mainly depends on the hydrogen bond and π-π interaction with RXRα amino acid residues. The value of the docking energy between RXRα and α-Mangostin is −10.235 kcal/mol. The results showed that the docking effect was good and indicated that α-Mangostin may have a strong binding effect on RXRα. The binding energy values are related to the interaction between the compounds and amino acid residues of target proteins.

RXRα is usually in an inactivated state as a transcription factor bound with a repressor. If ligands combine with RXRα and block the repressor, RXRα can be bound with the specific sequence in the target promoter and promote the expression of the target gene. The Dual-luciferase assays shows the results (**Figure 3C**) of the competitive binding of α-Mangostin to the RXRα ligand-binding domain. The natural ligand 9-cis-RA could significantly activate the reporting gene system, but this activity was inhibited by different concentrations of α-Mangostin (2, 5, and 15 μM).

The SPR measurements show that the gradient concentrations of α-Mangostin (0.625, 1.25, 2.5, 5, 10, 20, and 40 μM) flowed through the chip channel. As can be seen from the curve of α-Mangostin binding with RXRα (**Figure 3D**), the signal was obvious. The results showed that the KD value was $3.897*10^{-5}$ M and thus the binding affinity of RXRα for α-Mangostin was expecting. Moreover, the dissociation process between α-Mangostin and RXRα was slow and occurred via another process other than a common non-covalent combination, indicating that the binding of α-Mangostin and RXRα may be mainly covalent.

α-Mangostin Induces the Degradation of RXRα/tRXR and Inhibits Akt Activity in MDA-MB-231 Cells

Based on the above experiments, we demonstrated that α-Mangostin can target binding to RXRα/tRXRα and can also induce the apoptosis of breast cancer cells through the Akt pathway. However, it is unclear as to what role RXRα/tRXRα has in the regulation of PI3K/Akt signaling. To explore this, we used siRNA technology to knockdown RXRα/truncated RXRα (**Figure 4A**), and then detected the effect of α-Mangostin on Akt by western blotting (**Figure 4B**). The results show treatment with α-Mangostin suppressed the phosphorylation of Akt and activated caspase-3 after knockdown of RXRα/truncated RXRα (**Figure 4C**).

The Effect of α-Mangostin on MDA-MB-231 Cell Cycle Depends on Cyclin D1

Our studies have shown that α-Mangostin can significantly inhibit the proliferation of human breast cancer cells. We know that inhibition of cell proliferation is usually closely related to blockade of the cell cycle. Therefore, to comprehensively explore the molecular mechanism of the inhibitory effect of α-Mangostin, we analyzed its effect on the cell cycle of MDA-MB-231. In the flow cytometry analysis, it was found that the proportion of S phase cells increased significantly after treatment for 6 h with α-Mangostin (5 μM). and the proportion of cells in G2/M also increased after treatment for

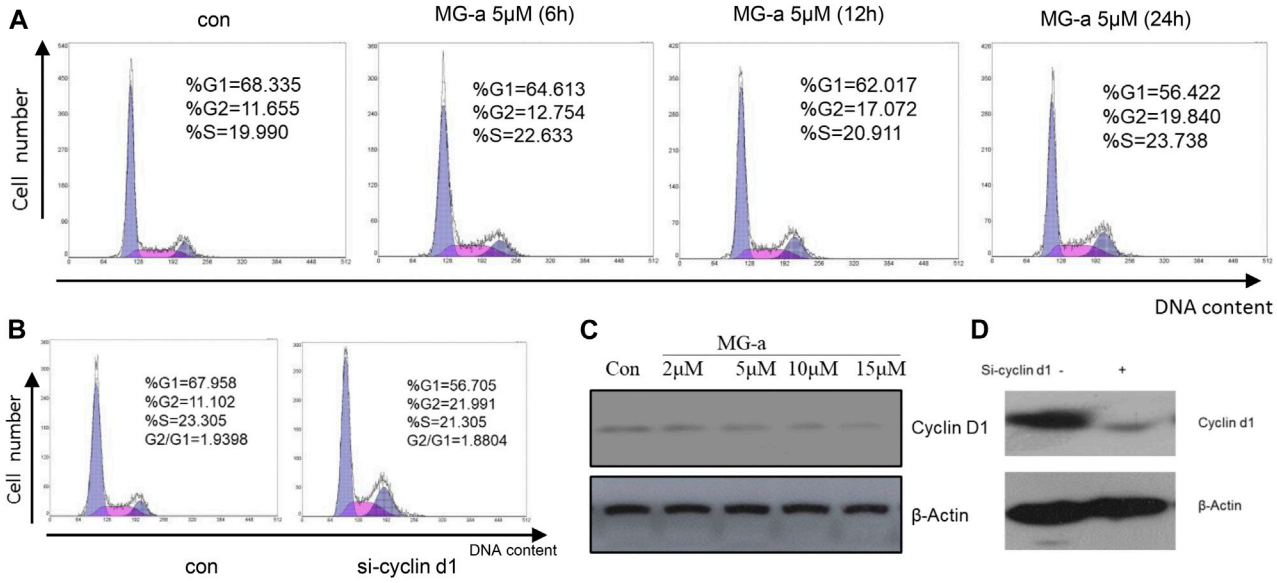

FIGURE 5 | The effect of α-Mangostin on the MDA-MB-231 cell cycle depends on cyclin D1. **(A)** The sub-G1 ratio in MDA-MB-231 cells treated with MG-a was examined by flow cytometry. Cells were exposed to 5 μM MG-a at the indicated times, after which cells were harvested and stained with PI. FACS was used to measure the sub-G1 percentage. **(B)** The sub-G1 ratio in MDA-MB-231 cells treated with siCCND1 was examined using flow cytometry. **(C,D)** The expression levels of cyclin D1 were determined by western blotting analysis in MDA-MB-231 cells after α-Mangostin treatment **(C)** and knockdown of RXRα **(D)**.

12 h with α-Mangostin (5 μM). Meanwhile, the proportion of MDA-MB-231 cells in G0/G1 showed a decreasing trend after treatment with 5 μM α-Mangostin. This suggests that α-Mangostin can arrest MDA-MB-231 cells in S and G0/G1 phase (**Figure 5A**).

Cyclin D1 is a regulator of cell cycle protein-dependent kinase CDKs, which have an important effect on the blockade of the cell cycle (Body et al., 2017). The effects of siCCND1 on inhibiting MDA-MB-231 cell proliferation and blockade of the cell cycle (**Figure 5B**). We treated the MDA-MB-231 cells with a concentration gradient of α-Mangostin for 24 h, and then the expression of cyclin D1 was detected by western blotting. Cyclin D1 expression decreased with increased α-Mangostin concentration (**Figure 5C**). siRNA knockdown of RXRα resulted in obviously reduced expression of cyclin D1 (**Figure 5D**), indicating that RXRα was able to regulate cyclin D1. Therefore, we speculate that the blockade of the cell cycle by α-Mangostin depends on the RXRα/cyclin D1 signaling pathway.

α-Mangostin Suppressed the Migration and Invasion of TNBC Cells *in Vitro*

To examine the anticancer effect of α-Mangostin on TNBC cells, we treated the highly aggressive MDA-MB-231 cells with α-Mangostin in different concentrations (2, 5, and 15 mM, respectively). Then we used wound-healing and transwell assay to determine whether α-Mangostin had the potential to inhibit breast cancer cell migration and invasion. α-Mangostin could concentration dependently slow down the wound healing process comparing to the control group (**Figures 6A** similar effect was observed in transwell assay, the invaded cells were decreased in α-Mangostin -treated groups when compared with the control group (**Figure 6B**). All these results suggested that α-Mangostin had the anticancer capability through influencing the proliferation, migration, and invasion of TNBC cells.

The Inhibitory Effect of α-Mangostin on Breast Cancer Cell Migration and Invasion Is Also Dependent on the tRXR/Akt/Cyclin D1 Pathway

Clinical studies show high expression of Cyclin D1 are often found in aggressive breast cancer, especially TNBC (**Figure 7A**). The clinical samples were collected from The First Affiliated Hospital of Gannan Medical University.) We speculate that cyclin D1 play a major role to promote tumor cell invasion and metastasis. Therefore, the MDA-MB-231 cells were used to verify the effect of knocking down Cyclin D1 on cell migration and invasion. The results of the Wound Healing Assay, the Transwell Assay and Western Blot Analysis all showed the migrated ability and invasive ability of MDA-MB-231 cells decline after being treated with si- Cyclin D1(**Figure 7C,D**).

DISCUSSION

The antitumor activity of α-Mangostin has been demonstrated in numerous studies (Asasutjarit et al., 2019; Ittiudomrak et al.,

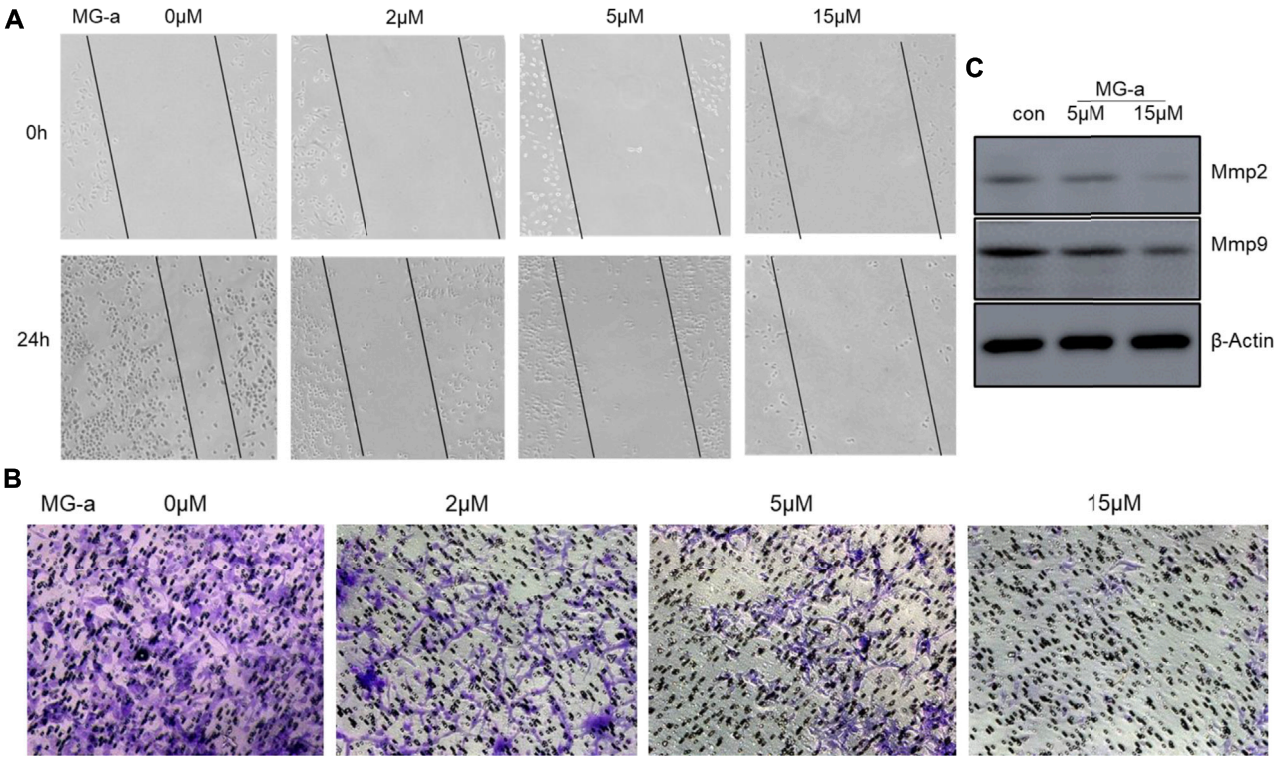

FIGURE 6 | α-mangostin suppressed the migration and invasion of TNBC Cells *in Vitro*. **(A)** The cell migration ability was determined by wound healing assay. **(B)** The cell migration and invasion were determined by Transwell assay. **(C)** The expression levels of Mmp2 and Mmp9 were determined by western blotting analysis in MDA-MB-231 cells after α-Mangostin treatment.

2019). Apoptosis of breast cancer cells induced by α-Mangostin has also been reported (Lee et al., 2010; Mardianingrum et al., 2020), but its specific molecular mechanism remains unclear. In this study, we first validated the findings of previous studies and verified that α-Mangostin could induce apoptosis of breast cancer cells *in vitro*. Flow cytometry experiments demonstrated that α-Mangostin promoted apoptosis with an efficiency that was similar to paclitaxel. Cell apoptosis is under the control of many signal transduction pathways and changes in homeostasis (Bissoli and Muscari, 2020). The cleavage of PARP proteins is a necessary factor for programmed cell death. α-Mangostin could induce PARP cleavage in breast cancer cells in a concentration and time-dependent manner. It also had a strong effect on inhibiting proliferation and inducing apoptosis in three breast cancer cell lines.

In many tumor cells including breast cancer cells, the nuclear receptor RXRα is hydrolyzed by a restricted protease. This results in RXRα with N-terminal deletion (Chen et al., 2014), known as tRXRα (truncated RXRα). Subcellular localization studies indicated that tRXRα is distributed in the cytoplasm. tRXRα can interact with p85 (a regulatory subunit of PI3K), and then activate Akt and the downstream PI3K/Akt pathway, promoting tumor processes (Xia et al., 2016). tRXRα is expressed specifically in tumor cells as an essential growth and survival factor. Thus, it is considered as a potential anti-tumor target. The ligand-binding domain of RXRα with N-terminal deletion remained the same as RXRα in our experiments. α-Mangostin can specifically target both RXRα and tRXRα, and we confirmed that α-Mangostin can degrade RXRα/tRXR in a concentration-dependent manner. Because tRXRα was the main factor activating PI3K/Akt in tumor cells, α-Mangostin could also inhibit the activity of Akt in a concentration-dependent manner.

The PI3K/Akt signaling pathway is closely related to tumor development. Inhibition of Akt activation may affect several downstream proteins, and can also induce apoptosis and suppress proliferation of tumor cells. α-Mangostin can regulate BCL-2 protein family members, and it can also activate caspase-3 and then trigger apoptosis in breast cancer cells. BCL-2 family proteins and caspase-3 protein are closely related to apoptosis. Further experiments revealed that the caspase-3 was no longer activated by α-Mangostin in MDA-MB-231 cells transfected with continuously activated Akt (CA-Akt). Apoptosis was reversed, and the proliferation of cells was almost unaffected. Furthermore, α-Mangostin had little effect on apoptosis following the treatment of MDA-MB-231 cells with LY294002 Akt inhibitor. So α-Mangostin-induced apoptosis of breast cancer cells depends on the PI3K/Akt signaling pathway.

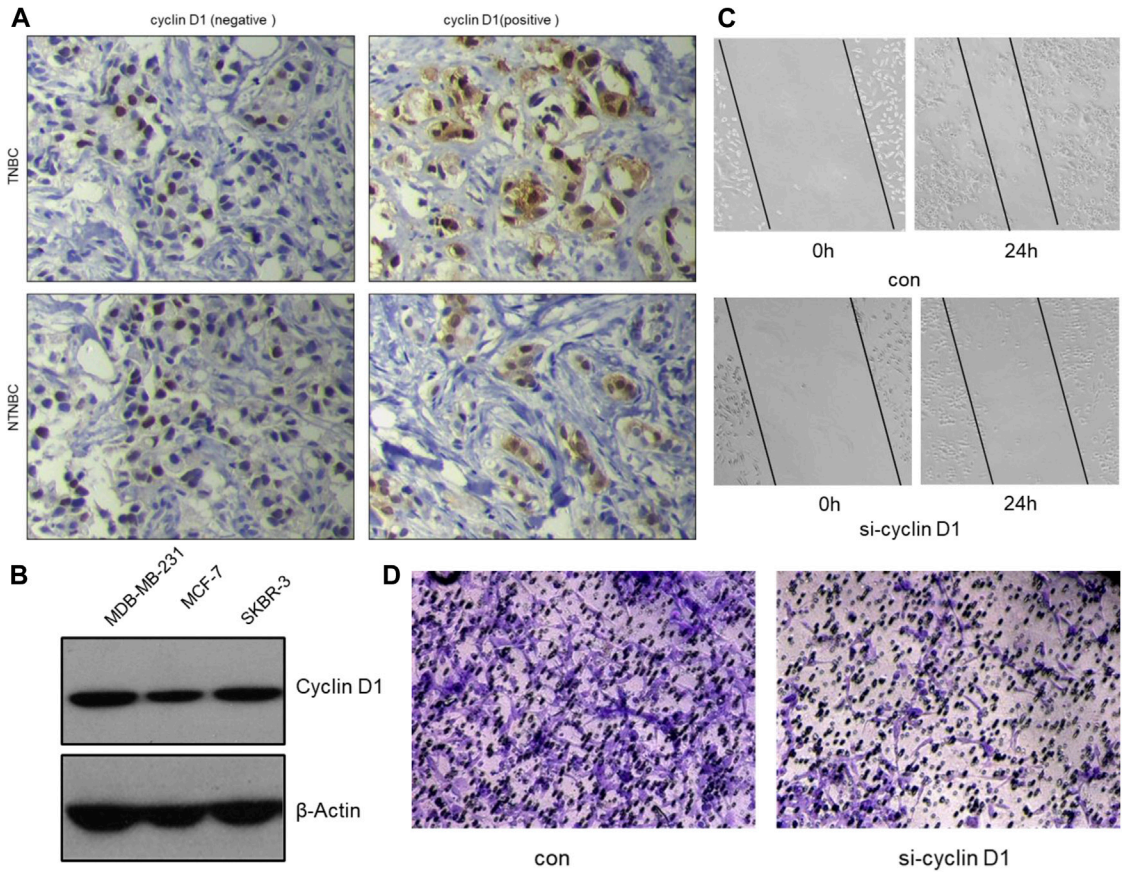

FIGURE 7 | The inhibitory effect of α-mangostin on breast cancer cell migration and invasion is also dependent on the tRXR/Akt/cyclin D1 pathway. **(A)** Representative images for the different expression of cyclin D1 by immunohistochemistry in tissues samples from TNBC and NTNBC patients. **(B)** The different expression of cyclin D1 by western blotting in different breast cancer cell lines. **(C,D)** The inhibitory effect of MG-a on MDA-MB-231 cells migration/invasion.

The loss of control of cell cycle regulation, resulting in unlimited tumor cell proliferation, is an essential attribute of tumors. The mechanism of cell cycle regulation disorder is an important cause of cell proliferation dropout, which leads to cancer. Cyclin D1 is a critical cell cycle regulator and a candidate proto-oncogene, whose deregulation has been implicated in the pathogenesis of several cancer types (Montalto and De Amicis, 2020), including breast cancer. It regulates cell cycle progression by binding to CDK4 or CDK6, forming tight complexes. Thus, cyclin D1 has been an area of focus in cancer research. In this study, the effect of α-Mangostin on the cell cycle of MDA-MB-231 was analyzed by flow cytometry. The results showed that α-Mangostin could arrest MDA-MB-231 cells in S and G2/M phases. The alterations in MDA-MB-231 cell cycle progression by treatment with α-Mangostin are dependent on cyclin D1.

The experiments verify that α-Mangostin has evident inhibition effects of invasion and metastasis of MDA-MB-231 cells. Many previous studies have demonstrated that Mmp-2 and Mmp-9 are closely related to tumor invasion and metastasis (Lee et al., 2010). The two matrix metalloproteinases have been used as indicators of invasive and migratory capacity in many studies. α-Mangostin was shown to significantly down-regulate Mmp-2 and Mmp-9 in Western blot experiments, thereby providing for the ability to inhibit invasion and metastasis of MDA-MB-231 cells. Do the inhibitory effects of α-Mangostin also depend mainly on the tRXR/Akt/cyclin D1 pathway? α-Mangostin can down-regulate the expression of cyclin D1, and the lower expression of cyclin D1 have inhibition effects on migration and invasion of MDA-MB-231 cells *in vitro*. It suggests that the inhibitory effect of α-Mangostin on breast cancer cell migration and invasion is also dependent on the tRXR/Akt/cyclin D1 pathway.

CONCLUSION

α-Mangostin occupies the binding pocket of RXRα and that the ligand antagonizes the effects of RXRα. α-Mangostin induces apoptosis of breast cancer cells through the PI3K/Akt signaling pathway by targeting RXRα, and cyclin D1 has involved in this process.

DATA AVAILABILITY STATEMENT

The original contributions presented in the study are included in the article/supplementary material, further inquiries can be directed to the corresponding author.

ETHICS STATEMENT

Ethical review and approval was not required for the study on human participants in accordance with the local legislation and institutional requirements. The patients/participants provided their written informed consent to participate in this study.

AUTHOR CONTRIBUTIONS

ZZ conceived and designed the experiments; XZ, HN performed the experiments; SW, YZ and JL analyzed the data; ZY contributed analysis tools; XZ wrote the paper.

FUNDING

This work was supported by grants from Natural Science. Foundation of China (Grant Numbers 82073866, 81673467, 31471273, 31461163002/RGC N_HKU 740/14), Natural Science. Foundation of Fujian Province (2019I0002) and Leading Talents in Scientific and Technological Innovation, Double Hundred Talents Program of Fujian Province.

REFERENCES

Asasutjarit, R., Meesomboon, T., Adulheem, P., Kittiwisut, S., Sookdee, P., Samosornsuk, W., et al. (2019). Physicochemical Properties of Alpha-Mangostin Loaded Nanomeulsions Prepared by Ultrasonication Technique. *Heliyon* 5 (9), e02465. doi:10.1016/j.heliyon.2019.e02465

Austin, G., Holcroft, A., Rinne, N., Wang, L., and Clark, R. E. (2015). Evidence that the Pregnane X and Retinoid Receptors PXR, RAR and RXR May Regulate Transcription of the Transporter hOCT1 in Chronic Myeloid Leukaemia Cells. *Eur. J. Haematol.* 94 (1), 74–78. doi:10.1111/ejh.12409

Bissoli, I., and Muscari, C. (2020). Doxorubicin and α-Mangostin Oppositely Affect Luminal Breast Cancer Cell Stemness Evaluated by a New Retinaldehyde-dependent ALDH Assay in MCF-7 Tumor Spheroids. *Biomed. Pharmacother.* 124, 109927. doi:10.1016/j.biopha.2020.109927

Body, S., Esteve-Arenys, A., Miloudi, H., Recasens-Zorzo, C., Tchakarska, G., Moros, A., et al. (2017). Cytoplasmic Cyclin D1 Controls the Migration and Invasiveness of Mantle Lymphoma Cells. *Sci. Rep.* 7 (1), 13946. doi:10.1038/s41598-017-14222-1

Chen, G., Li, Y., Wang, W., and Deng, L. (2018). Bioactivity and Pharmacological Properties of α-mangostin from the Mangosteen Fruit: a Review. *Expert Opin. Ther. Pat.* 28 (5), 415–427. doi:10.1080/13543776.2018.1455829

Chen, L., Wang, Z. G., Aleshin, A. E., Chen, F., Chen, J., Jiang, F., et al. (2014). Sulindac-derived RXRα Modulators Inhibit Cancer Cell Growth by Binding to a Novel Site. *Chem. Biol.* 21 (5), 596–607. doi:10.1016/j.chembiol.2014.02.017

Fu, T., Wang, S., Liu, J., Cai, E., Li, H., Li, P., et al. (2018). Protective Effects of α-mangostin against Acetaminophen-Induced Acute Liver Injury in Mice. *Eur. J. Pharmacol.* 827, 173–180. doi:10.1016/j.ejphar.2018.03.002

Fusté, N. P., Ferrezuelo, F., and Garí, E. (2016). Cyclin D1 Promotes Tumor Cell Invasion and Metastasis by Cytoplasmic Mechanisms. *Mol. Cel Oncol* 3 (5), e1203471. doi:10.1080/23723556.2016.1203471

Hamurcu, Z., Delibaşı, N., Geçene, S., Şener, E. F., Dönmez-Altuntaş, H., Özkul, Y., et al. (2018). Targeting LC3 and Beclin-1 Autophagy Genes Suppresses Proliferation, Survival, Migration and Invasion by Inhibition of Cyclin-D1 and uPAR/Integrin β1/Src Signaling in Triple Negative Breast Cancer Cells. *J. Cancer Res. Clin. Oncol.* 144 (3), 415–430. doi:10.1007/s00432-017-2557-5

Ishizawa, M., Kagechika, H., and Makishima, M. (2012). NR4A Nuclear Receptors Mediate Carnitine Palmitoyltransferase 1A Gene Expression by the Rexinoid HX600. *Biochem. Biophys. Res. Commun.* 418 (4), 780–785. doi:10.1016/j.bbrc.2012.01.102

Ittiudomrak, T., Puthong, S., Roytrakul, S., and Chanchao, C. (2019). α-Mangostin and Apigenin Induced Cell Cycle Arrest and Programmed Cell Death in SKOV-3 Ovarian Cancer Cells. *Toxicol. Res.* 35 (2), 167–179. doi:10.5487/TR.2019.35.2.167

Jasek, E., Gajda, M., Lis, G. J., Jasińska, M., and Litwin, J. A. (2014). Combinatorial Effects of PARP Inhibitor PJ34 and Histone Deacetylase Inhibitor Vorinostat on Leukemia Cell Lines. *Anticancer Res.* 34 (4), 1849–1856.

Jiang, P., Zhang, W. Y., Li, H. D., Cai, H. L., and Xue, Y. (2013). Repeated Haloperidol Administration Has No Effect on Vitamin D Signaling but Increase Retinoid X Receptors and Nur77 Expression in Rat Prefrontal Cortex. *Cell. Mol. Neurobiol.* 33 (3), 309–312. doi:10.1007/s10571-012-9902-7

Lee, D., Kim, Y. M., Jung, K., Chin, Y. W., and Kang, K. S. (2018). Alpha-Mangostin Improves Insulin Secretion and Protects INS-1 Cells from Streptozotocin-Induced Damage. *Int. J. Mol. Sci.* 19 (5). doi:10.3390/ijms19051484

Lee, Y. B., Ko, K. C., Shi, M. D., Liao, Y. C., Chiang, T. A., Wu, P. F., et al. (2010). Alpha-Mangostin, a Novel Dietary Xanthone, Suppresses TPA-Mediated MMP-2 and MMP-9 Expressions through the ERK Signaling Pathway in MCF-7 Human Breast Adenocarcinoma Cells. *J. Food Sci.* 75 (1), H13–H23. doi:10.1111/j.1750-3841.2009.01407.x

Mardianingrum, R., Yusuf, M., Hariono, M., Mohd Gazzali, A., and Muchtaridi, M. (2020). α-Mangostin and its Derivatives against Estrogen Receptor Alpha. *J. Biomol. Struct. Dyn.*, 1–14. doi:10.1080/07391102.2020.1841031

Montalto, F. I., and De Amicis, F. (2020). Cyclin D1 in Cancer: A Molecular Connection for Cell Cycle Control, Adhesion and Invasion in Tumor and Stroma. *Cells* 9 (12). doi:10.3390/cells9122648

Nakagawa, Y., Iinuma, M., Naoe, T., Nozawa, Y., and Akao, Y. (2007). Characterized Mechanism of Alpha-Mangostin-Induced Cell Death: Caspase-independent Apoptosis with Release of Endonuclease-G from Mitochondria and Increased miR-143 Expression in Human Colorectal Cancer DLD-1 Cells. *Bioorg. Med. Chem.* 15 (16), 5620–5628. doi:10.1016/j.bmc.2007.04.071

Nguyen, M. H., Nguyen, D. T., and Nguyen, P. T. M. (2020). Apoptosis Induction by α-mangostin-loaded Nanoparticles in Human Cervical Carcinoma Cells. *Z. Naturforsch C J. Biosci.* 75 (5-6), 145–151. doi:10.1515/znc-2020-0001

Phan, T. K. T., Shahbazzadeh, F., Pham, T. T. H., and Kihara, T. (2018). Alpha-mangostin Inhibits the Migration and Invasion of A549 Lung Cancer Cells. *PeerJ* 6, e5027. doi:10.7717/peerj.5027

Scolamiero, G., Pazzini, C., Bonafè, F., Guarnieri, C., and Muscari, C. (2018). Effects of α-Mangostin on Viability, Growth and Cohesion of Multicellular Spheroids Derived from Human Breast Cancer Cell Lines. *Int. J. Med. Sci.* 15 (1), 23–30. doi:10.7150/ijms.22002

Xia, Y., Chen, J., Gong, C., Chen, H., and Sun, J. (2016). α-Mangostin, a Natural Agent, Enhances the Response of NRAS Mutant Melanoma to Retinoic Acid. *Med. Sci. Monit.* 22, 1360–1367. doi:10.12659/msm.898204

Yeong, K. Y., Khaw, K. Y., Takahashi, Y., Itoh, Y., Murugaiyah, V., and Suzuki, T. (2020). Discovery of Gamma-Mangostin from Garcinia Mangostana as a Potent and Selective Natural SIRT2 Inhibitor. *Bioorg. Chem.* 94, 103403. doi:10.1016/j.bioorg.2019.103403

Zhang, K. J., Gu, Q. L., Yang, K., Ming, X. J., and Wang, J. X. (2017). Anticarcinogenic Effects of α-Mangostin: A Review. *Planta Med.* 83 (3-04), 188–202. doi:10.1055/s-0042-119651

Zhang, Y., Sun, Z., Pei, J., Luo, Q., Zeng, X., Li, Q., et al. (2018). Identification of α-Mangostin as an Agonist of Human STING. *ChemMedChem* 13 (19), 2057–2064. doi:10.1002/cmdc.201800481

Zhang, Y., Wang, S., Qian, W., Ji, D., Wang, Q., Zhang, Z., et al. (2018). uc.338 Targets P21 and Cyclin D1 via PI3K/AKT Pathway Activation to Promote Cell

Proliferation in Colorectal Cancer. *Oncol. Rep.* 40 (2), 1119–1128. doi:10.3892/or.2018.6480

Zheng, Y., Comaills, V., Burr, R., Boulay, G., Miyamoto, D. T., Wittner, B. S., et al. (2019). COX-2 Mediates Tumor-Stromal Prolactin Signaling to Initiate Tumorigenesis. *Proc. Natl. Acad. Sci. U S A.* 116 (12), 5223–5232. doi:10.1073/pnas.1819303116

Zhong, Z., Yeow, W. S., Zou, C., Wassell, R., Wang, C., Pestell, R. G., et al. (2010). Cyclin D1/cyclin-dependent Kinase 4 Interacts with Filamin A and Affects the Migration and Invasion Potential of Breast Cancer Cells. *Cancer Res.* 70 (5), 2105–2114. doi:10.1158/0008-5472.CAN-08-1108

Zhou, H., Liu, W., Su, Y., Wei, Z., Liu, J., Kolluri, S. K., et al. (2010). NSAID Sulindac and its Analog Bind RXRalpha and Inhibit RXRalpha-dependent AKT Signaling. *Cancer Cell* 17 (6), 560–573. doi:10.1016/j.ccr.2010.04.023

Zou, W., Yin, P., Shi, Y., Jin, N., Gao, Q., Li, J., et al. (2019). A Novel Biological Role of α-Mangostin via TAK1-NF-Kb Pathway against Inflammatory. *Inflammation* 42 (1), 103–112. doi:10.1007/s10753-018-0876-6

Conflict of Interest: The authors declare that the research was conducted in the absence of any commercial or financial relationships that could be construed as a potential conflict of interest.

Publisher's Note: All claims expressed in this article are solely those of the authors and do not necessarily represent those of their affiliated organizations, or those of the publisher, the editors and the reviewers. Any product that may be evaluated in this article, or claim that may be made by its manufacturer, is not guaranteed or endorsed by the publisher.

Copyright © 2021 Zhu, Li, Ning, Yuan, Zhong, Wu, Zeng. This is an open-access article distributed under the terms of the Creative Commons Attribution License (CC BY). The use, distribution or reproduction in other forums is permitted, provided the original author(s) and the copyright owner(s) are credited and that the original publication in this journal is cited, in accordance with accepted academic practice. No use, distribution or reproduction is permitted which does not comply with these terms.

frontiers in Pharmacology

ORIGINAL RESEARCH
published: 06 October 2021
doi: 10.3389/fphar.2021.749365

The Multimodal MOPr/DOPr Agonist LP2 Reduces Allodynia in Chronic Constriction Injured Rats by Rescue of TGF-β1 Signalling

Annamaria Fidilio[1,2†], Margherita Grasso[2,3†], Rita Turnaturi[4], Giuseppe Caruso[2], Federica Maria Spitale[5], Nunzio Vicario[5], Rosalba Parenti[5], Salvatore Spoto[2], Nicolò Musso[6], Agostino Marrazzo[4], Santina Chiechio[2,3], Filippo Caraci[2,3], Lorella Pasquinucci[4‡] and Carmela Parenti[2‡]*

[1]Department of Biomedical and Biotechnological Sciences, Section of Pharmacology, University of Catania, Catania, Italy, [2]Department of Drug and Health Sciences, Section of Pharmacology and Toxicology, University of Catania, Catania, Italy, [3]Oasi Research Institute - IRCCS, Troina, Italy, [4]Department of Drug and Health Sciences, Section of Medicinal Chemistry, University of Catania, Catania, Italy, [5]Department of Biomedical and Biotechnological Sciences, Section of Physiology, University of Catania, Catania, Italy, [6]Department of Biomedical and Biotechnological Sciences, Section of Biochemistry, University of Catania, Catania, Italy

Neuropathic pain is one of the most disabling forms of chronic pain and it is characterized by hyperalgesia and allodynia linked to an aberrant processing of pain transmission and to neuroinflammation. Transforming growth factor-β1 (TGF-β1) is an anti-inflammatory cytokine, which protects against neuroinflammation. It has been demonstrated that TGF-β1 and opioid receptors signalling crosstalk results in an improvement of endogenous opioid analgesia, but it is not known whether mu opioid peptide receptor (MOPr) or delta opioid peptide receptor (DOPr) agonists can positively modulate TGF-β1 pathway. In the present study, we examined the correlation between anti-allodynic effect of LP2, a dual-target MOPr/DOPr agonist, and TGF-β1 signalling in the chronic constriction injury (CCI) model. We detected a significant decrease of active TGF-β1 and of its type II receptor TGFβ-R2 levels in the spinal cord from CCI rats and a selective deficit of TGF-β1 in microglia cells both at days 11 and 21 post-ligature, as assessed by immunofluorescence analysis. LP2, when administered from the 11 days post-ligature to 21 days, was able to reduce CCI-induced mechanical allodynia by rescue of TGF-β1 and TGFβ-R2 levels. Our data suggest that the rescue of TGF-β1 signalling by dual-target MOPr/DOPr agonist LP2 could be mediated by DOPr activation in spinal microglia, thus the dual-target approach could represent a novel pharmacological approach to increase the analgesic efficacy of MOPr agonists.

Keywords: neuropathic pain, transforming growth factor-β1 (TGF-β1), dual target MOPr/DOPr agonist, analgesia, microglia

OPEN ACCESS

Edited by:
Andres Trostchansky, Universidad de la República, Uruguay

Reviewed by:
Carmen De Caro, University of Catanzaro, Italy
Marta Valenza, Sapienza University of Rome, Italy

***Correspondence:**
Filippo Caraci
carafil@hotmail.com

[†]These authors have contributed equally to this work

[‡]These authors share last authorship

Specialty section:
This article was submitted to Experimental Pharmacology and Drug Discovery, a section of the journal Frontiers in Pharmacology

Received: *29 July 2021*
Accepted: *17 September 2021*
Published: *06 October 2021*

Citation:
Fidilio A, Grasso M, Turnaturi R, Caruso G, Spitale FM, Vicario N, Parenti R, Spoto S, Musso N, Marrazzo A, Chiechio S, Caraci F, Pasquinucci L and Parenti C (2021) The Multimodal MOPr/DOPr Agonist LP2 Reduces Allodynia in Chronic Constriction Injured Rats by Rescue of TGF-β1 Signalling. Front. Pharmacol. 12:749365. doi: 10.3389/fphar.2021.749365

INTRODUCTION

Neuropathic pain, one of the most complex and disabling forms of chronic pain, is currently defined as "pain arising as a direct consequence of a lesion or disease affecting the somatosensory system" (Treed et al., 2008). It is often associated with different pathological conditions such as diabetes mellitus, cancer, vascular and infectious diseases. It is characterized by typical symptoms such as an exaggerated pain perception of noxious stimuli (more commonly known as hyperalgesia) as well as non-noxious stimuli (allodynia), linked to an aberrant processing of pain transmission (Costigan, et al., 2009). The underlying mechanisms include complex interactions between neurons, glia, and cells of the immune system through neurotransmitters, cytokines, and inflammatory mediators (Mika et al., 2013), so that neuropathic pain may now be considered as a "neuroimmune disorder" (Malcangio, 2019). Glia cells, which represent about 70% of the cells in the central nervous system (CNS), and microglia activation, with a shift in the balance between pro-inflammatory and anti-inflammatory cytokines, play a key role in sensitization processes (Gwak et al., 2017; Caraci et al., 2019). Pro-inflammatory cytokines such as Interleukin (IL)-1, IL-6, IL-15, IL-17, IL-18, tumor necrosis factor-alfa (TNF-α), and interferon-gamma (IFN-γ) play a key role in the processes of central sensitization, while the induction of anti-inflammatory cytokines [IL-10, IL-4, or transforming growth factor-β1 (TGF-β1)] can exert a protective role against neuroinflammatory events underlying neuropathic pain (Uçeyler et al., 2007; Chen et al., 2013; Caraci et al., 2019). Thus, anti-nociceptive strategies include inhibition of pro-inflammatory cytokines and use of anti-inflammatory cytokines (Shubayev et al., 2010). It has been hypothesized that a deficit of TGF-β1 signalling might contribute to the pathophysiology of chronic pain (Lantero et al., 2012). TGF-β1 can counteract the development of chronic neuropathic pain (Lantero et al., 2014) and exert anti-allodynic and analgesic effects in animal models of neuropathic pain (Echeverry et al., 2009; Lantero et al., 2014). Moreover, TGF-β1 is involved in the pathogenesis of depressive disorders, which often occur in comorbidity with chronic pain (Caraci et al., 2018). Echeverry et al. also observed that recombinant TGF-β1, delivered into the spinal cord of rats, was effective not only in preventing, but also in reversing the hypersensitivity evoked by damage to peripheral nerve through different mechanisms, i.e. blocking microglial cells proliferation, inhibiting spinal microglial activation, and reducing the expression of pro-inflammatory cytokines (Echeverry et al., 2009). Furthermore, Lantero et al. demonstrated that pre- and post-synaptic modulation of the endogenous opioid system by TGF-β1 signalling can prevent the development of allodynia and improve the analgesic efficacy of both endogenous and exogenous opioid agonists both in inflammatory and neuropathic pain conditions (Lantero et al., 2014).

Available therapies with mu opioid peptide receptor (MOPr) agonists often provide incomplete pain relief and treatment-related side effects are common such as respiratory depression, constipation, and tolerance (Chou et al., 2015). A novel drug discovery strategy in chronic pain is the development of MOPr/delta opioid peptide receptor (DOPr) dual-target compounds able to activate MOPr as well as DOPr (Martínez-Navarro et al., 2019). The MOPr/DOPr simultaneous targeting is supported by the co-expression of both receptors in areas involved in pain modulation and by the crucial role of MOPr activation in the regulation of DOPr trafficking (Scherrer et al., 2009). Moreover, activation of DOPr leads to fewer typical opioid side effects.

We previously reported that the dual-target benzomorphan-based compound LP2 was able to simultaneously bind and activate MOPr (K_i = 1.08 nM, IC_{50} = 21.5 nM) and DOPr (K_i = 6.6 nM, IC_{50} = 4.4 nM) (Pasquinucci et al., 2017). In tail-flick and formalin test LP2 was found to produce significant anti-nociceptive (ED_{50} = 0.9 mg/kg i.p.) and anti-inflammatory (ED_{50} = 0.88 and 0.79 mg/kg i.p., phases I and II of formalin test) effects (Pasquinucci et al., 2019). In rats subjected to unilateral sciatic nerve chronic constriction injury (CCI), we already showed that LP2 significantly inhibits the development of mechanical allodynia and prevents CCI-induced Cx43 alterations and pro-apoptotic signalling in the CNS (Vicario et al., 2019a). These findings prompted us to further examine the molecular mechanisms underlying the analgesic effects of the MOPr/DOPr agonist LP2 in the CCI model. Presently, it is not known whether MOPr and/or DOPr agonists can positively modulate TGF-β1 pathway and whether the rescue of TGF-β1 signalling can contribute to increase the analgesic effects of MOPr/DOPr compounds. Thus, in the present study we examined the hypothesis that CCI can induced an impairment of the TGF-β1 pathway and that the anti-allodynic effects of LP2 in the CCI rat model can be mediated by an increased expression of TGF-β1 and its type 2 receptor (TGFβ-R2) at spinal cord level along the time course of neuropathic pain.

MATERIALS AND METHODS

Animal Model of Neuropathic Pain

Experiments were carried out on male Sprague-Dawley rats (Envigo Laboratories), weighing 180–200 gr. Animals were set at a constant temperature (23–25°C) between 9:00 am and 15:00 pm. This study was performed according to the European Communities Council directive and Italian regulations (EEC Council 2010/63/EU and Italian D. Lgs. no. 26/2014) and approved by Italian Ministry of Health (OPBA Project 946/2018-PR) in order to replace, reduce, and refine the use of laboratory animals. The model used to induce neuropathic pain was the CCI model, according to Bennett and Xie. (1988), with secondary (minor) modifications (Parenti, et al., 2013). Animals were put in a chamber, anesthetized with isoflurane inhalation (4% induction, 2% for maintenance), and an incision was made underneath the hipbone, parallel to the common sciatic nerve, which was exposed. Later, four ligatures (4/0 chromic silk, Ethicon) were tied firmly around the nerve, proximal to the trifurcation of the nerve at about 1 mm spacing, observing a twitch in the respective hind limb. In the SHAM rats, the sciatic nerve was exposed, but there were not made any ligatures. Then, rats were randomly assigned to three different groups: SHAM-vehicle, CCI-vehicle, and CCI + LP2. Starting

from 11 days post-ligatures (dpl), after the measurements of allodynic thresholds, CCI groups received a daily intraperitoneal (i.p.) injection of either vehicle or LP2 (0.9 mg/kg) up to 21 dpl.

Evaluation of Mechanical Allodynia

Allodynia, already measured in the present CCI model in Vicario et al. (2019a), has been reproduced in a new cohort of rats. Rats were allocated and allowed to acclimate for 20 min in a wire mesh bottom test chamber. The ventral surface of the hind paw was mechanically stimulated from below with an ascending series of calibrated Von Frey's filaments, which bending forces ranging from 0.02 to 30 g. The "up-down" method was used to evaluate the withdrawal threshold, increasing and decreasing sequentially the stimulus strength (Dixon, 1980). Behavioural assessment of mechanical allodynia has been performed at 0 (before surgery), 11, 16 and 21 dpl.

Ex vivo Tissue Processing

At 11, 16, and 21 dpl, rats were anesthetized with an i.p. injection of ketamine (10 mg/ml) and xylazine (1.17 mg/ml), and transcardially perfused with 0.5 M ethylenediaminetetraacetic acid (EDTA) in normal saline, followed by ice cold 4% paraformaldehyde (PFA) in phosphate-buffered saline (PBS) (pH = 7.4) (Sigma-Aldrich, St Louis, MO).

Spinal cords were isolated and post-fixed in 4% PFA in PBS at 4°C overnight. Tissue samples were then washed in PBS and cryo-preserved in 30% sucrose in PBS at 4°C for 3 days. Samples were embedded in optimum cutting temperature (OCT) medium and snap frozen in liquid nitrogen for cryosectioning using a cryostat (Reichert-Jung 2800). Twenty μm-thick axial section of spinal cords from the lumbar enlargement (L4-L5) were collected and stored at −80°C until use.

RNA Isolation and Quantification

Total RNA was extracted from spinal cord slices (thickness of 20 μm) using the commercial RNeasy FFPE kit (Qiagen, Hilden, Germany) according to the manufacturer's recommendations, with different modifications carried out in order to improve the yield and purity of the extracted RNA. Briefly, the slides containing spinal cord slices were taken out from the −80°C and left to dry at room temperature (RT). Next, each slide was washed at least three times by using DEPC water and the spinal cord slides were harvested by employing a sterile scalpel and moved to microcentrifuge tubes. After the addition of Buffer PKD, each sample was vortexed, centrifuged, and mixed with proteinase K. Following three different incubation steps (56, 80, and 4°C) and one centrifugation, the supernatant of each sample was transferred to a new microcentrifuge tube. Each tube was therefore added with a mixture of DNase Booster Buffer and DNase I stock and incubated at RT. At the end of the incubation, Buffer RBC and ethanol (100%) were added and the total solution content was moved to the RNeasy MinElute spin column. After two washing steps (Buffer RPE), the RNA was eluted by the addition to the columns of RNase-free water. The concentration of total RNA recovered from spinal cord slices was determined by measuring the fluorescence with Qubit fluorometer (Thermo Fisher Scientific, Waltham, MA, United States) and the absorbance at 260 nm with NanoDrop® ND-1000 (Thermo Fisher Scientific). The first allows more accurate measurements in terms of quantity compared with commonly used methods absorbance-based because the dyes part of the Qubit kit fluoresce only when bound to RNA. The additional measurement with NanoDrop® ND-1000 was carried out to verify the purity of the samples by analyzing the absorbance curves.

Gene Expression Analysis by Quantitative Real-Time PCR (qRT-PCR)

Gene expression analysis by qRT-PCR was performed as previously described (Caruso et al., 2019) with slight modifications. The reverse transcription of 20 ng of total RNA (for each sample) was accomplished by using the SuperScript III First-Strand Synthesis SuperMix kit (Thermo Fisher Scientific), while the quantification of each cDNA sample loaded in a 384-well plate was achieved by using a LightCycler® 480 System (Roche Molecular Systems, Inc., Pleasanton, CA, United States). The list containing the information of each primer used for this study is reported in **Table 1**. The protocol employed for sample amplification, fluorescence data collection, and sample quantification is the same previously described elsewhere (Caruso et al., 2019).

Western Blot Analysis

To evaluate TGF-β1 and TGFβ-R2 expression levels, the slides containing eight spinal cord slices for each rat, obtained by the procedure described in the *Ex vivo Tissue Processing* paragraph, were washed three times by using deionized water. Next the samples were pooled by employing a sterile scalpel and harvested into microcentrifuge tubes. The samples were resuspended in 3% sodium dodecyl sulfate (SDS) RIPA buffer supplemented by phosphatases and proteases inhibitors (1:100 dilution), incubated for 20 min at 100°C, and for 20 min at 4°C, then were sonicated and subsequently centrifuged for 15 min at 15.000× g in refrigerate centrifuge to remove cellular debris.

Protein quantification was performed using a Pierce™ BCA protein assay kit (Thermo Fisher Scientific), according to the manufacturer's specifications; subsequently, 30 μg of total proteins were denatured at 95°C for 10 min, subjected to NuPage™ 10% bis–tris gel electrophoresis (Thermo Fisher Scientific) and transferred to nitrocellulose membranes.

The membranes were blotted with anti-TGF-β1 (1:500, Abcam ab92486, Cambridge, United Kingdom), anti-TGFβ-R2 (1:500, Cell signaling Technology Inc., Danvers, MA, United States; 79424), anti-GAPDH (1:2000, Millipore MAB 374, Burlington, MA, United States), and anti-β-actin (1:1000, Sigma Aldrich, St Louis, MO; A4700) primary antibodies in blocking buffer at 4°C overnight. After washing in tris-buffered saline (TBS)/Tween 20 × 0.1%, the membranes were incubated for 1 h with IRDye® 800CW or 680LT secondary antibodies (1: 15000) at RT in the dark. Bands were visualized using an Odyssey® infrared imaging system (LI-COR Biosciences, Lincoln, NE, United States), while the densitometric analysis was carried out by using ImageJ software.

TABLE 1 | The list of primers used for quantitative real-time PCR (qRT-PCR).

Official name[a]	Official symbol	Alternative titles/symbols	Detected transcript	Amplicon length	Cat. No[b]
interleukin 1 beta	Il1b	Il-1b; IL-1beta; IL-1β	NM_008361 XM_006498795	150 bp 682 bp	QT01048355
interleukin 6	Il6	Il-6	NM_031168	128 bp	QT00098875
transforming growth factor, beta 1	Tgfb1	Tgfb; Tgfb-1; TGFbeta1; TGF-beta1	NM_011577	145 bp	QT00145250
transforming growth factor, beta receptor 2	Tgfbr2	Tgfbr2T; TGF-beta 2	NM_031132 XM_008766690	99 bp	QT00182315

[a]*https://www.ncbi.nlm.nih.gov/gene/*
[b]*https://www.qiagen.com/it/shop/pcr/real-time-pcr-enzymes-and-kits/two-step-qrt-pcr/quantitect-primer-assays/*

Immunofluorescence

Immunofluorescence was performed as previously described (Gulino et al., 2019; Vicario et al., 2021). Briefly, sections were washed in PBS and incubated with blocking buffer (10% normal goat serum (NGS) and 0.1% Triton X-100 in PBS) for 1 h at RT. Sections were then incubated overnight at 4°C with the following primary antibodies: mouse monoclonal (A60) anti-NeuN (Millipore Cat. No. MAB377, RRID: AB_2298772, 1:100), mouse monoclonal anti-GFAP (BD Biosciences Cat. No. 610566, RRID: AB_397916, 1: 100), goat polyclonal anti-IBA1 (Novus Biologicals, Cat. No. NB100-1028, RRID: AB_521594, 1:500), and rabbit polyclonal anti-TGF-β1 (Abcam Cat. No. ab92486, RRID: AB_10562492, 1:100). The following day, sections were washed in 0.1% Triton X-100 in PBS 3 times at RT and then incubated 1 h at RT with appropriate combination of secondary antibodies: goat polyclonal anti-mouse (Alexa Fluor 488, Thermo Fisher Scientific, Cat. No. A-11001, RRID: AB_2534069, 1:1.000), goat polyclonal anti-rabbit (Alexa Fluor 564, Molecular Probes, Cat. No. A-11010, RRID: AB_143156, 1:1.000) and donkey anti-goat (Alexa Fluor 647, Thermo Fisher Scientific, Cat. No. A-21447, RRID: AB_2535864, 1:1.000). Nuclei were counterstained with DAPI (1:10.000, Invitrogen, Waltham, MA, United States) for 5 min at RT and then mounted with BrightMount mounting medium (Abcam). Digital images were acquired using a Leica DM IRB fluorescence microscope and with Leica TCS SP8 confocal microscope and profile plots for immunofluorescence images were obtained as previously described (Vicario et al., 2019a; Spitale et al., 2020). Briefly, confocal images of ipsilateral dorsal horns were analyzed using ImageJ software. For each population marker (i.e. NeuN, Gfap, or Iba1) a profile plot was calculated and superimposed to the corresponding TGF-β1 profile plot in order to highlight proximity and/or colocalization.

Statistical Analysis

Statistical analysis was performed by using GraphPad Prism 9 (GraphPad Software, La Jolla, CA). Two-tailed unpaired Student's t-test was used for comparison of $n = 2$ groups. Comparisons of $n > 2$ groups were performed using a one-way analysis of variance (ANOVA). Statistical analyses of behavioral assessment of mechanical allodynia were performed using a two-way ANOVA repeated measure. One-way ANOVA, followed by Bonferroni's post hoc test, was used for multiple comparisons on molecular markers. Only two-tailed *p*-values of less than 0.05 were considered statistically significant. All data are represented as means ± SEM.

RESULTS

The MOPr/DOPr Agonist LP2 Reduces the Mechanical Allodynia in CCI Rats

We first evaluated the antinociceptive effect of LP2 through the behavioral assessment of mechanical allodynia following the experimental paradigm shown in **Figure 1A**. Neuropathic pain condition, produced by CCI model, decreased the withdrawal threshold, with a significant reduction at 11 dpl in CCI animals as compared to SHAM rats (**Figure 1B**). LP2 administration, started from 11 dpl (after withdrawal threshold measurements) recovered the withdrawal threshold at 16 and 21 dpl of CCI + LP2 treated rats as compared to CCI-vehicle rats.

Molecular Mechanisms Underlying the Anti-allodynic Effects of LP2: The Key Role of TGF-β1

In order to assess the impact of CCI on neuroinflammation in the spinal cord, the gene expression of TGF-β1 and its receptor (TGFβ-R2) along with two well-known pro-inflammatory cytokines, IL-6 and IL-1β, was firstly investigated in the spinal cord at 11 dpl in SHAM and CCI animal groups (**Figure 2**).

CCI represents a validated animal model of neuropathic pain where neuroinflammation in the spinal cord is known to play a key role in central sensitization (Nong and Lan, 2018). Interestingly we found that CCI significantly decreased the expression levels of TGF-β1 (**Figure 2A**) and of its receptor TGFβ-R2 (**Figure 2B**), while raised both IL-6 (**Figure 2C**) and IL-1β (**Figure 2D**) mRNA expression levels compared to the rats belonging to the SHAM group ($p < 0.05$ for all cytokines).

To understand the molecular mechanisms underlying the anti-allodynic effects of LP2 in CCI rats, we then assessed whether LP2 exerted its analgesic effects in our animal model of neuropathic pain by counteracting neuroinflammatory phenomena induced by CCI (SHAM *vs.* CCI *vs.* CCI + LP2) after 5 and 10 days of LP2 treatment, respectively (i.e. at 16 and 21 dpl) (**Figures 3**, **4**). **Figures 3A,B** clearly shows that the significant decrease in mRNA expression levels of TGF-β1 induced by CCI, still persisting after 16 and 21 days ($p < 0.05$ *vs* SHAM). The same effect was observed for the TGFβ-R2 gene expression at 16 and 21 dpl (**Figures 4A,B**) ($p < 0.05$ *vs.* SHAM).

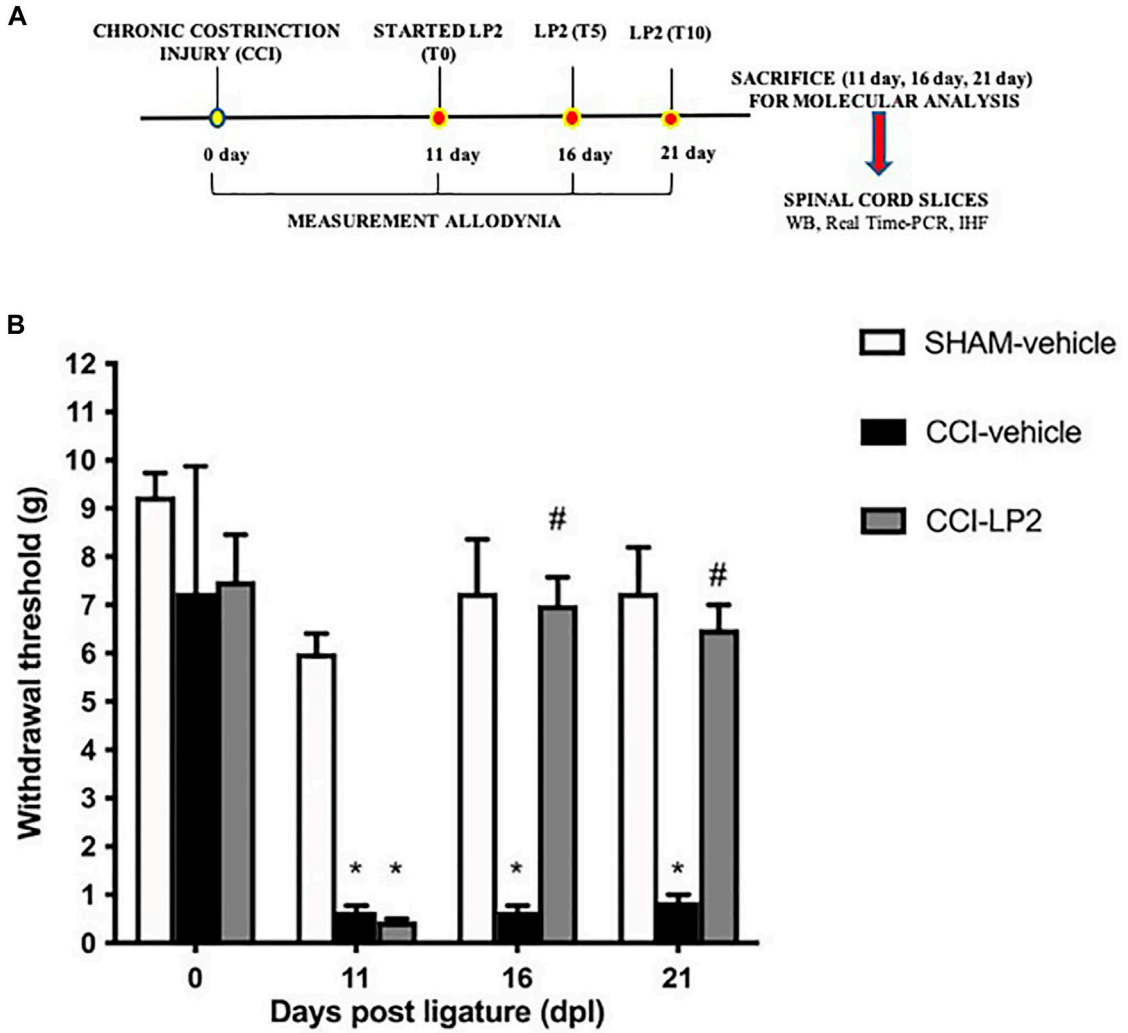

FIGURE 1 | The MOPr/DOPr agonist LP2 shows an anti-allodynic effect in CCI animal model. **(A)** Schematic representation of the experimental design. WB = Western Blot; Real Time-PCR = Real Time Polymerase Chain Reaction; IHF = Immunohistofluorescence analysis. **(B)** Withdrawal thresholds measured with von Frey's filaments on SHAM-vehicle, on SHAM-vehicle, CCI-vehicle, and CCI + LP2-treated rats at 0, 11 (before the start of LP2 administration), 16, and 21 dpl. Data are shown as mean ± SEM of n = 8 rats per group. $^{*}p < 0.001$ vs SHAM-vehicle. $^{\#}p < 0.001$ vs. CCI-vehicle.

Interestingly we found that the treatment with LP2 completely rescued both TGF-β1 (**Figures 3A,B**) and TGFβ-R2 (**Figures 4A,B**) mRNA levels in CCI rats ($p < 0.05$ *vs.* CCI) after 5 and 10 days of treatment. Unlike TGF-β1 and TGFβ-R2, the treatment with LP2 was not able to counteract the increased production of IL-6 and IL-1β CCI-induced (data not shown).

TGF-β1 activity in the CNS is regulated not only at a transcriptional level, but it shows a complex post-translational regulation through the conversion of latent TGF-β1 to active TGF-β1 by a variety of proteases, among which matrix metalloproteinase 2 (MMP-2) and matrix metalloproteinase 9 (MMP-9) play a central role in this conversion (Caraci et al., 2018).

To validate the role of TGF-β1 as a new pharmacological target in neuropathic pain, we therefore quantified the protein levels of active TGF-β1 and its receptor (TGFβ-R2) in the spinal cord of CCI rats both in the absence and in the presence of LP2 treatment. Interestingly, we found that CCI procedure was able to induce a significant decrease of active TGF-β1 (**Figures 3C,D**) and TGFβ-R2 levels (**Figures 4C,D**) only 21 dpl ($p <$ 0.05 *vs.* SHAM), but not at 16 dpl. Most importantly, LP2 treatment was able to rescue both TGF-β1 and TGFβ-R2 levels when compared with those in CCI rats ($p < 0.05$ *vs.* CCI; **Figures 3C,D**; **Figures 4C,D**), suggesting that only a long treatment with LP2 is able to rescue the TGF-β1 pathway in CCI rats.

The Multimodal MOPr/DOPr Agonist LP2 Induces an Increase of TGF-β1 Which Colocalizes With Iba1 in CCI Rats

To evaluate the expression and localization of TGF-β1 in CCI model, we analyzed ipsilateral dorsal horns cell population

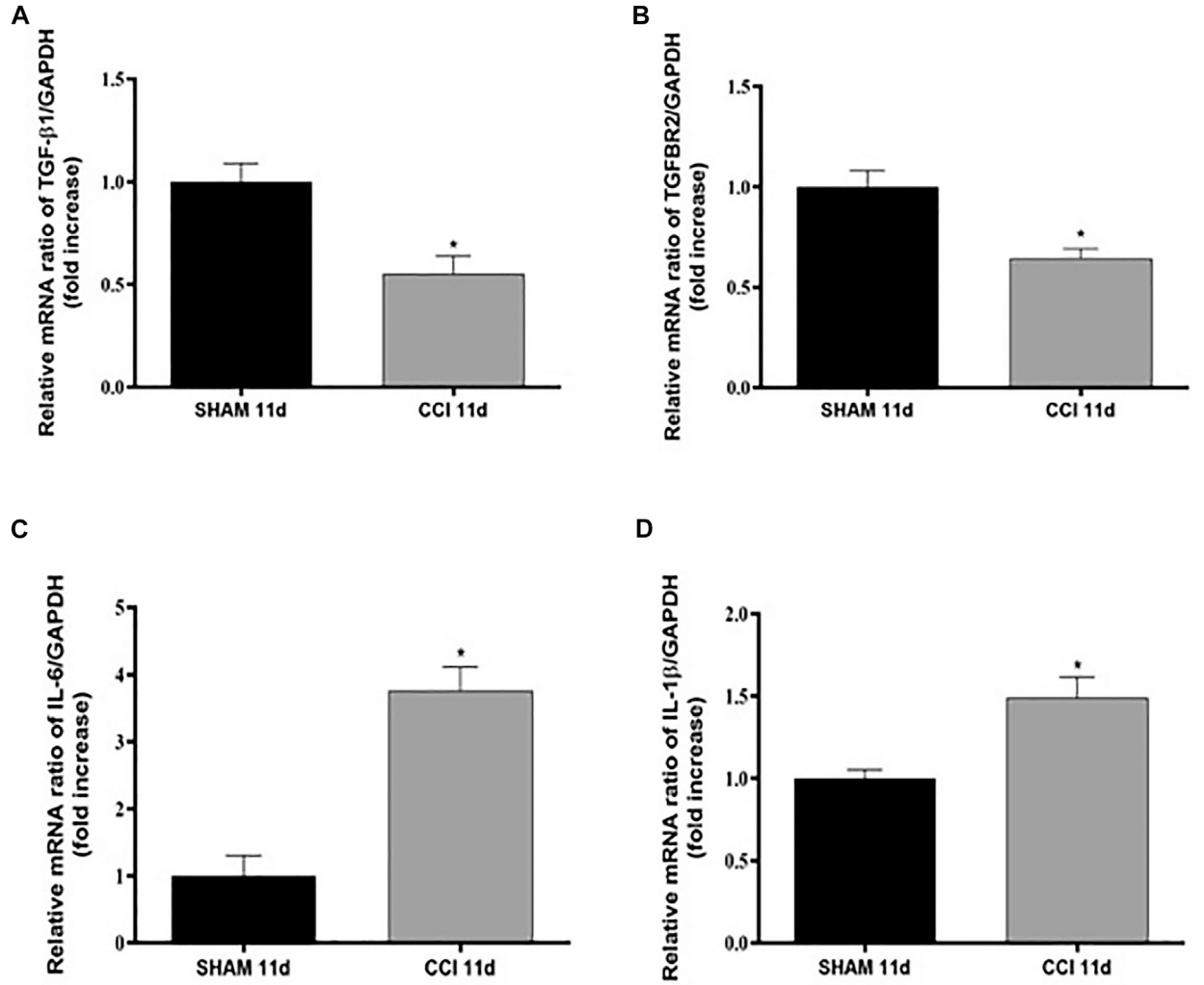

FIGURE 2 | CCI increases pro-inflammatory cytokines levels and reduces TGF-β1 levels 11 dpl. Measurement of **(A)** TGF-β1 (t = 3,593, df = 4; F, DFn, Dfd = 1,031, 2, 2), **(B)** TGFβ-R2 (t = 3,761, df = 4; F, DFn, Dfd = 3,027, 2, 2), **(C)** IL-6 (t = 5,955, df = 6; F, DFn, Dfd = 1,332, 3, 3), and **(D)** IL-1β (t = 3,206, df = 5; F, DFn, Dfd = 6,952, 3, 2) mRNA expression levels (RT-qPCR) in spinal cord of SHAM or CCI rats after 11 days. The abundance of each mRNA of interest was expressed relative to the abundance of GAPDH mRNA, as an internal control. Data are shown as mean ± SEM of n = 3–4 rats per group. Statistical analysis was performed using Student's t-test. *$p < 0.05$ *vs.* SHAM.

(i.e., NeuN positive neurons, GFAP positive astrocytes, and Iba1 positive microglial cells) and their potential colocalization or proximity to TGF-β1 in the early phase of the neuropathy (**Figures 5A–C**). We observed that CCI induced an overall reduction of TGF-β1, which was found to be in close proximity to NeuN positive cells (**Figure 5A**) and to colocalize with Iba1 positive cells (**Figure 5C**). These data demonstrate a selective deficit of TGF-β1 in the spinal microglia in the CCI model. Such a deficit was also observed in the chronic stage of CCI (i.e., 21 dpl, **Figures 5D–F**). Indeed, profile plot analysis revealed that LP2 treatment was able to increase peri-neuronal TGF-β1 signals (**Figure 5D**), which weakly colocalize with NeuN (**Figure 5D**) and GFAP (**Figure 5E**) positive cells. Interestingly we found a strong colocalization between TGF-β1 and Iba1 positive cells (**Figure 5F**), thus indicating a critical role of microglial cells in the rescue of TGF-β1 mediated by LP2.

DISCUSSION

Neuropathic pain represents a chronic pathological condition with a significant negative impact on a patient's quality of life with a prevalence among the general population ranging from 3 to 17% (Cavalli et al., 2019). Since the typical symptoms of this disease are often unresponsive to conventional therapy, new pharmacological targets have to be identified to improve current therapeutic approaches. In this scenario, the CCI model represents a validated animal model of neuropathic pain useful to identify the molecular mechanisms underlying chronic pain development as well as novel pharmacological targets for its management (Boccella et al., 2018; Coraggio et al., 2018; Caraci et al., 2019).

DOR represents a novel pharmacological target in the treatment of chronic neuropathic pain (Kabli and Cahill, 2007;

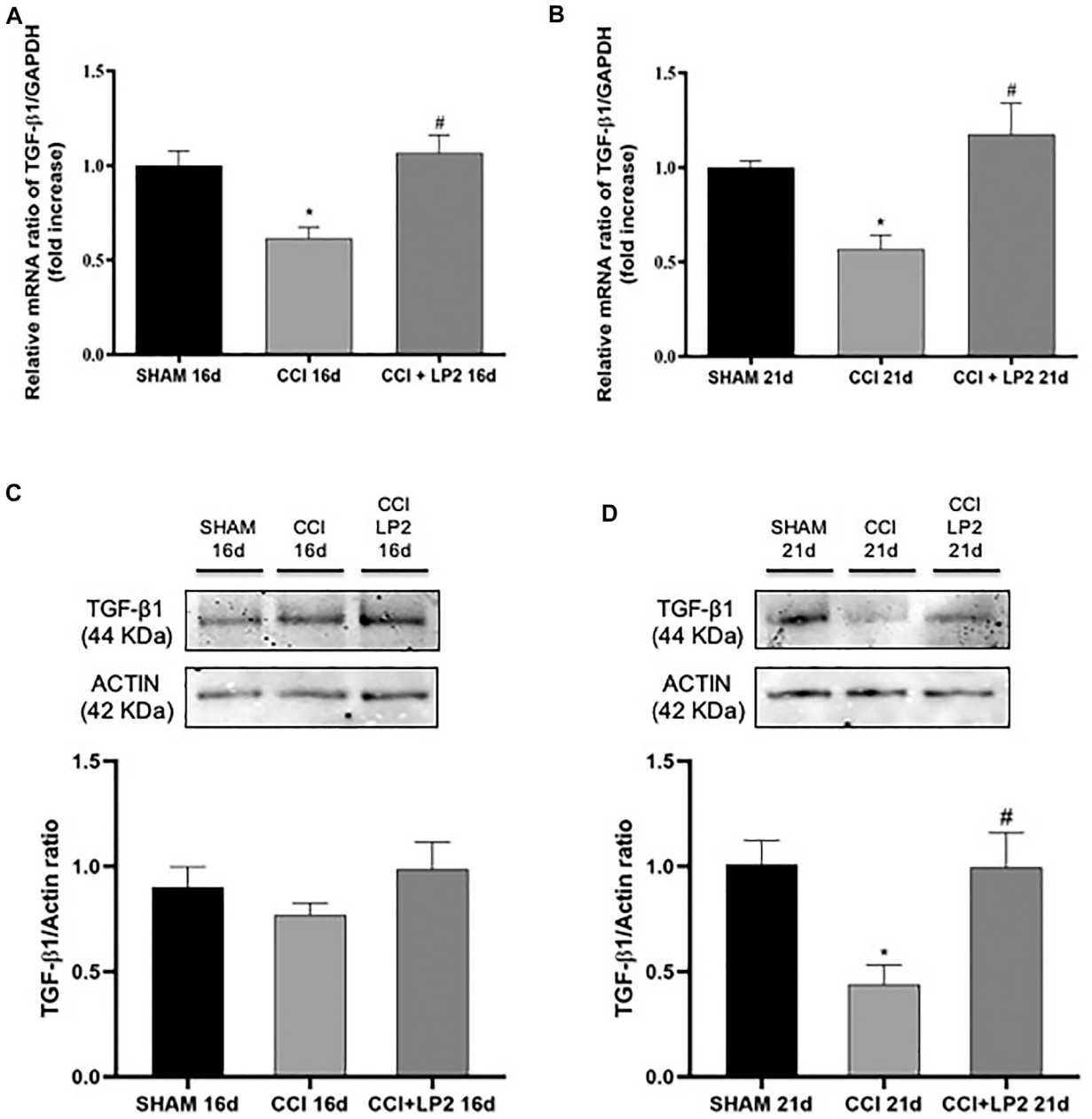

FIGURE 3 | LP2 treatment rescues TGF-β1 levels at 16 and 21 days after chronic constriction injury. Measurement of **(A–C)** TGF-β1 at 16 days and **(B–D)** TGF-β1 at 21 days mRNA and protein expression levels in spinal cord of SHAM, CCI, and CCI + LP2 rats. **(A–B)** The abundance of each mRNA of interest was expressed relative to the abundance of GAPDH mRNA, as an internal control. Data are shown as mean ± SEM of $n = 3$ rats per group. TGF-β1 16 days [$F(2, 6) = 10{,}02$]; TGF-β1 21 days [$F(2, 7) = 9{,}961$]. **(C–D)** Representative immunoblots of TGF-β1 (44 kDa) in total protein extracts from spinal cord tissues at 16 ($F(2, 15) = 1{,}222$) and 21 [$F(2, 9) = 6{,}638$] dpl. Histograms refer to independent experiments means ± SEM of the TGF-β1 densitometric values normalized against actin used as internal control. Data are shown as mean ± SEM of $n = 4–6$ rats per group. Statistical analysis was performed using one-way ANOVA with Bonferroni's *post-hoc* analysis. *$p < 0.05$ *vs.* SHAM; #$p < 0.05$ *vs.* CCI.

Cahill et al., 2020). Recent studies have demonstrated that DOPr agonists counteract and prevent nociceptive behaviors in various chronic pain models, including neuropathic pain, while having minimal effect on sensory thresholds in the absence of injury (Turnaturi et al., 2019). We have previously demonstrated that the multimodal MOPr/DOPr agonist LP2 produced a significant anti-nociceptive and anti-inflammatory effect in tail-flick and formalin test, respectively (Pasquinucci et al., 2017; Pasquinucci et al., 2019). Moreover, the repeated administration of LP2 significantly inhibited the development of mechanical allodynia in neuropathic rats subjected to CCI and prevented CCI-induced Cx43 alterations and pro-apoptotic signalling in the

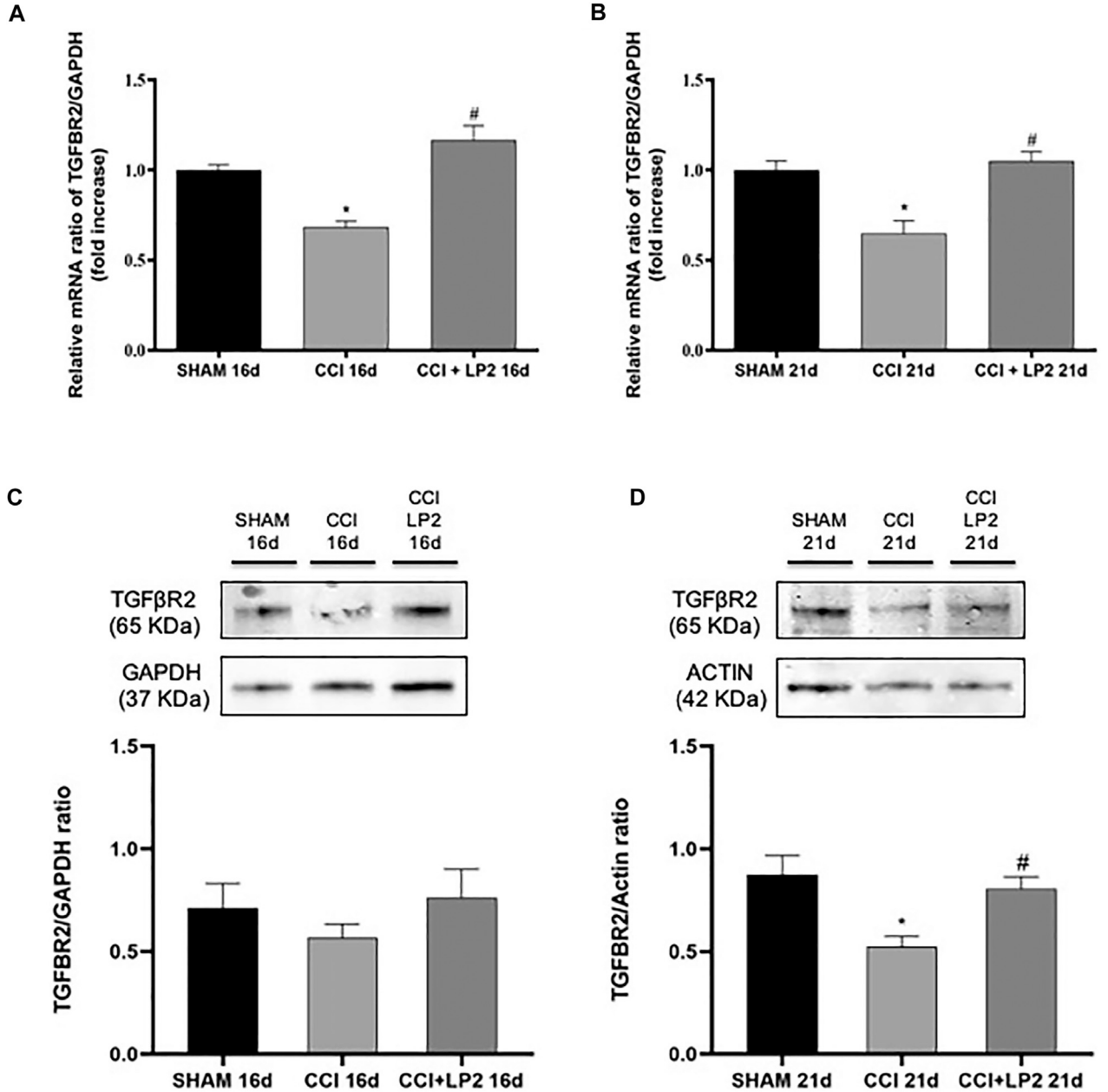

FIGURE 4 | CCI induces a reduction of TGFβ-R2 mRNA and protein expression levels reversed by a chronic treatment with LP2. Effects induced by CCI procedure in the absence or presence of LP2 treatment at 16 and 21 dpl on TGFβ-R2 levels evaluated by RT-qPCR and western blot analysis. **(A–B)** The abundance of each mRNA of interest was expressed relative to the abundance of GAPDH mRNA, as an internal control. Data are shown as mean ± SEM of $n = 3$ rats per group. TGFβ-R2 16 days [$F(2, 7) = 22,66$]; TGFβ-R2 21 days [$F(2, 5) = 13,51$]. **(C–D)** Representative immunoblots of TGFβ-R2 (65 kDa) in total protein extracts from spinal cord tissues at 16 [$F(2, 12) = 0,8078$] and 21 [$F(2, 12) = 7,197$] dpl. Histograms refer to independent experiments means ± SEM of the TGFβ-R2 densitometric values normalized against GAPDH and actin used as internal controls by one-way ANOVA with Bonferroni's *post-hoc* for statistical analysis. Data are shown as mean ± SEM of $n = 4–6$ rats per group. $^*p < 0.05$ *vs.* SHAM, $\#p < 0.05$ *vs.* CCI.

CNS (Vicario, et al., 2019a; Vicario, et al., 2019b). Despite selective MOPr agonists are the cornerstones of moderate-to-severe acute pain treatment, their effectiveness and safety in chronic pain conditions is controversial. In contrast to MOPr, DOPr density and activity are up-regulated in chronic pain models and analgesic effects of DOPr selective agonists are enhanced during persistent inflammation (Turnaturi et al., 2019). Moreover, the activation of MOPr plays a crucial role in the regulation of the trafficking and membrane targeting of DOPr in conditions of persistent inflammation (Gendron et al., 2007). Direct coupling of MOPr-DOPrs in the form of hetero-oligomers has been demonstrated in the spinal cord tissue and it

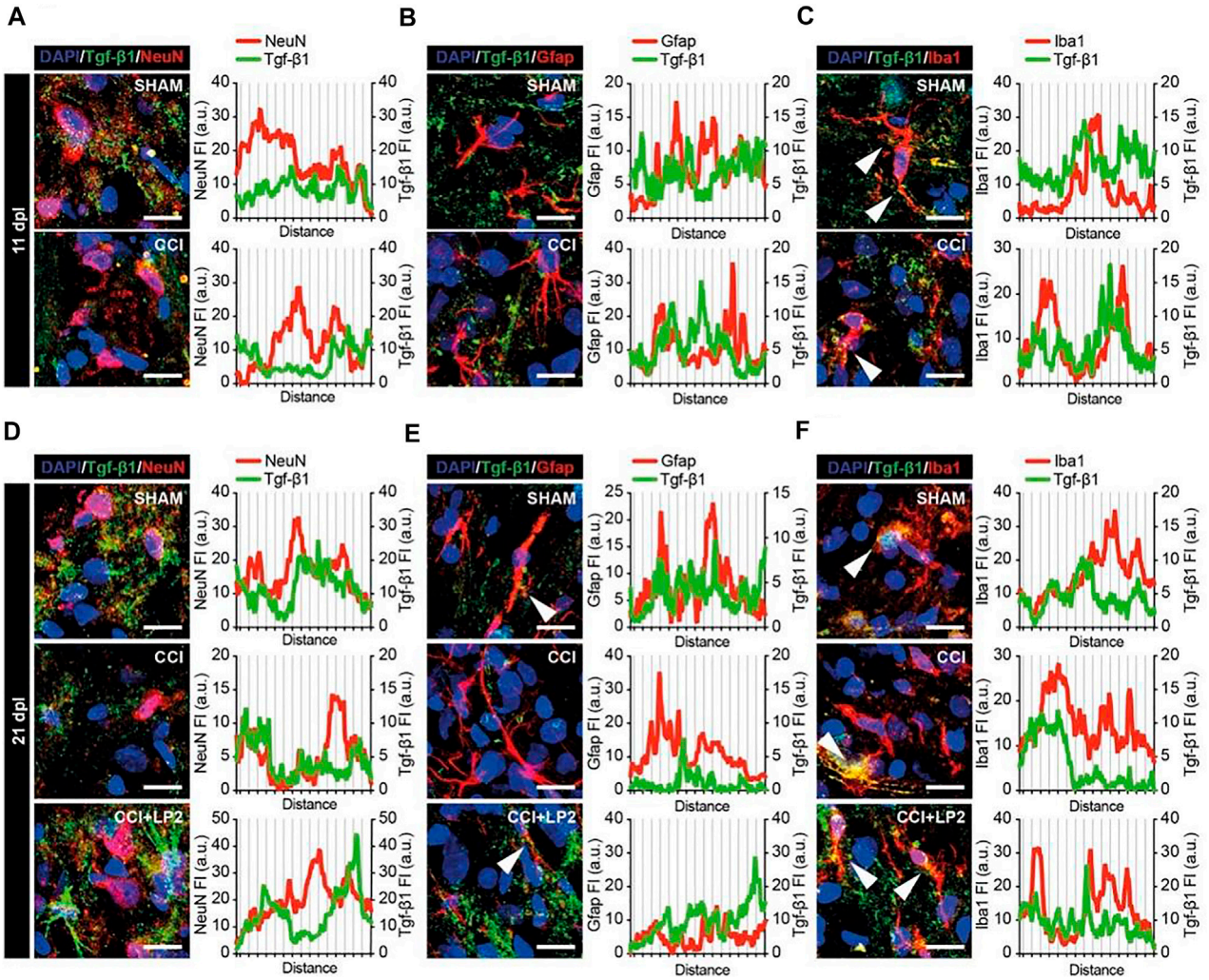

FIGURE 5 | TGF-β1 profile in neurons, astrocytes and microglial cells in ipsilateral dorsal horns of CCI spinal cord. Representative confocal images of TGF-β1 (green) and NeuN **(**red in **A**–**D)**, GFAP **(**red in **B**–**E**) and Iba1 **(**red in **C**–**F)** immunohistofluorescence analysis in ipsilateral dorsal horns of SHAM and CCI rats at 11 dpl **(A**–**C)** and of SHAM, CCI and CCI + LP2 treated rats at 21 dpl **(D**–**F).** Scale bars 10 μm. Profile plots of mean fluorescence intensity, expressed as arbitrary units (a.u.), are also shown.

was proposed to underlie the anti-nociceptive synergy between MOPr and DOPr agonists (Gomes et al., 2004). Thus, simultaneous activation of MOPr and DOPr with a dual target compound delivers potent analgesia in experimental models of chronic pain with strongly reduced dependence and tolerance development on the course of repeated administration (Starnowska-Sokół and Przewłocka, 2020). Nevertheless, the molecular mechanisms underlying the analgesic effects of DOPr agonists are still unclear as well as the different contribute of glial cells and neurons in the allodynic effects of these compounds. It is known that prolonged morphine treatment *in vivo* induces the translocation of DOPrs from intracellular compartments to neuronal plasma membranes (Hack et al., 2005). DORs are also strongly expressed both in astrocytes and microglial cells (Turchan-Cholewo et al., 2008), but it is presently unknown the contribute of glial DORs in the analgesic effects of DOPr agonists.

Recent studies have demonstrated that the activation of glial cells, in particular microglia, toward a pro-inflammatory state plays a central role in the transition from acute to chronic pain (Coraggio et al., 2018; Caraci et al., 2019; Myers et al., 2006), also contributing to a state of opioid analgesic tolerance (Holdridge et al., 2007). In particular, peripheral damage and hyperactivity of primary sensory neurons promote neuroinflammation, in the spinal cord, through the release of several pro-inflammatory cytokines (e.g., TNF-α and IL-1β) by both activated astrocytes and microglial cells (Ji et al., 2014; Lees et al., 2015), finally leading to central sensitization and pain chronicization (Ji et al., 2014). Interestingly, the repeated activation of DOPr reduces the release of pro-inflammatory cytokines, such as TNF-α (Vicario et al.,

2016), suggesting an impact of DOPr agonists on neuroinflammation in animal models of neuropathic pain. Along this line, an alternative approach that has been recently adopted in drug discovery in neuropathic pain is to develop new compounds able to promote the release of anti-inflammatory cytokines endowed with a neuroprotective and analgesic efficacy (Guo et al., 2021; Piotrowska, et al., 2016). Among microglial anti-inflammatory cytokines, TGF-β1 has a protective role against the development of chronic neuropathic pain by inhibiting neuroinflammation and promoting the expression of endogenous opioids within the spinal cord (Lantero et al., 2012). TGF-β1 pathway has been proposed as a novel pharmacological target to increase the analgesic effects of opioids (Onichtchouk et al., 1999; Lantero et al., 2014; de la Puerta et al., 2019). In addition, a TGF-β1-opioid receptor signalling crosstalk results in improvement of endogenous and exogenous opioid analgesia in experimental models of neuropathic pain (Lantero et al., 2012; Lantero et al., 2014).

Starting from this evidence, we therefore examined the impact of CCI on mRNA levels of pro-inflammatory (IL-1β and IL-6) and anti-inflammatory (TGF-β1) cytokines in the spinal cord observing that CCI procedure increased IL-1β and IL-6 levels at 11 days. These results are in accordance with previous findings showing a TNF-α induction in the same model in the sciatic nerve (Vicario et al., 2016). Previous works have also demonstrated an induction of IL-1β and IL-6 in affected nerves from CCI models (Khan et al., 2018; Liu et al., 2020). To the best of our knowledge our data demonstrate for the first time an induction of these cytokines in the spinal cord of CCI rats which co-occurs with a reduction of the expression levels of TGF-β1 and TGFβ-R2 mRNAs 11 dpl compared with SHAM control animals. Interestingly, in our model a significant decrease of both active TGF-β1 levels and TGFβ-R2 levels was detected only 21 dpl, suggesting a long-term and post-transcriptional regulation of TGF-β1 and its receptor in the CCI model or alternatively a selective deficit of them in sub-population of cells from spinal cord (microglial cells vs astrocytes/neurons; see below). TGF-β1 plays a protective role against the development of chronic neuropathic pain and the first demonstration of the anti-nociceptive effects of TGF-β1 has been obtained by Chen et al. (2013), with intrathecal administration of this peptide able to reduce both spinal neuroinflammation and excitoxicity (Chen et al., 2013). In the same animal model, it has been demonstrated that the down-regulation of p38 and extracellular signal-regulated kinase (ERK) activity influences TGF-β1-induced analgesia during neuropathy (Chen et al., 2016). Different groups have analyzed the neurobiological links between TGF-β1 and opioid system in animal models of neuropathic pain (Tramullas et al., 2010; Lantero et al., 2014). Increased levels of a transmembrane pseudo-receptor structurally similar to TGF-β type I receptors, BAMBI (bone morphogenetic protein and activin membrane-bound inhibitor), and TGF-β receptors have been detected in areas with a high density of opioid receptors such as the cingulate cortex, periaqueductal grey matter, and the dorsal horns of the spinal cord, key areas of the inhibitory modulation of pain transmission (Tramullas et al., 2010). An enhancement of TGF-β1 signalling has been observed in mice lacking the TGF-β pseudo-receptor BAMBI, which leads to an increased synaptic release of opioid peptides and to a naloxone-reversible hypoalgesic/antiallodynic phenotype. In in vivo neuropathic pain models, the pleiotropic protective effects of TGF-β1 are achieved by the inhibition of neuroinflammatory phenomena (Echeverry et al., 2009; Chen et al., 2015), suppression of the neuronal hyperexcitability (Chen et al., 2013) and endogenous opioid system activation (Onichtchouk et al., 1999; Lantero et al., 2014; de la Puerta et al., 2019). Nevertheless, all these studied have not deeply investigated the possible presence of a TGF-β1 signalling deficit in the CCI model.

In the present work we demonstrated a selective deficit of TGF-β1 and its receptor in microglia cells from spinal cord of CCI rats detectable both at days 11 and 21 dpl as assessed by immunofluorescence analysis. Previous studies have found conflicting data on TGF-β1 levels in the CCI model, with reduced expression of this factor in dorsal root ganglion from CCI mice, followed by an increase at day 10 post-ligature (Xie et al., 2019) or reduced levels of TGF- β1 and its type I receptor in the red nucleus of rats 2 weeks after spared nerve injury (SNI) (Wang et al., 2015). Further studies are needed in the rat model of CCI to understand whether the selective deficit of TGF-β1 and/or its receptor in microglia can be detected in an early phase of pain chronicization.

It is well-known that a 2 weeks subcutaneous infusion with recombinant TGF-β1 showed an anti-allodynic effect when compared with saline in mice subjected to sciatic nerve injury (Lantero et al., 2012), but alternative and more feasible approaches should be developed to rescue TGF-β1 levels in animal models of neuropathic pain. In the present work we demonstrated, for the first time, that a chronic treatment (10 days) with the multimodal MOPr/DOPr agonist LP2 was able to rescue the levels of active TGF-β1 and of TGFβ-R2 in the spinal cord from CCI rats and, most importantly, in microglial cells. Interestingly Reddy et al. found that activation of DOR in transplanted mesenchymal stem cells with the synthetic peptide (D-Ala^2, D-Leu^5)-enkephalin (DADLE) promotes the secretion of anti-inflammatory cytokines (IL-10/IL-4/TGF-β) (Reddy and Sen, 2017). Further studies are therefore needed, in primary cultures of microglial cells, to analyze the effects of LP2 as well as other DOPr agonists on TGF-β1 synthesis. A recent study, conducted in a neuropathic pain rat model generated through spinal nerve ligation (SNL), demonstrated that valproate mitigates SNL-induced allodynia by modulating microglial function, inhibiting neuroinflammatory response, finally promoting the expression of anti-inflammatory cytokines (TGF-β, IL-10 and IL-4) (Guo et al., 2021).

Our study, conducted in a validated animal model of neuropathic pain, is the first to demonstrate that the dual target MOPr/DOPr agonist LP2, when administered from the 11 dpl to 21 days, is able to reduce CCI-induced mechanical allodynia by rescue of TGF-β1 and TGFβ-R2 levels. Moreover, our results show the possible role played by microglial cells in modulating the rescue of TGF-β1 levels promoted by LP2 treatment. We believe that the rescue of TGF-β1 signalling by dual-target MOPr/DOPr agonist LP2 could be mediated by DOR

activation in spinal microglia and might represent a novel pharmacological approach to increase opioid analgesic efficacy of selective MOPr agonists.

DATA AVAILABILITY STATEMENT

The raw data supporting the conclusions of this article will be made available by the authors, without undue reservation.

ETHICS STATEMENT

The animal study was reviewed and approved by the Institutional Animal Care and Use Committee (IACUC) of the University of Catania and by the Italian Ministry of Health (DDL 26/2014 and previous legislation; OPBA Project 946/2018-PR). Animal care followed Italian (D.M. 116192) and EEC (O.J. of E.C.L 358/1 12/18/1986) regulations on protection of animals used for experimental and scientific purposes.

AUTHOR CONTRIBUTIONS

CP, LP, and FC gave substantial contributions to the conception and design of the work. AF, MG, RT, FS, NV, SS, NM, and GC performed the experiments. FC, AF, MG, NV, and GC analyzed the data. RP, SC, AM, LP participated in the design of the study. FC and CP drafted the work. All authors approved the version to be published.

FUNDING

This research was conducted with the support of the University of Catania, PIA.CE.RI. 2020-2022-Linea di intervento 2-Project DETTAGLI (UPB 57722172125). Is was also partially funded by grant from the Italian Ministero dell'Istruzione, dell'Università e della Ricerca, PRIN 2017, Grant no. 2017XKWWK9_004 to RP. This research was also funded by University of Catania, Programma Ricerca di Ateneo unict 2020-2022- Linea 3; Project Asclepio (UPB 57722172132). NV was supported by the PON AIM R&I 2014-2020-E66C18001240007. FMS was supported by the International Ph.D. program in Neuroscience (Department of Biomedical and Biotechnological Sciences, University of Catania, Italy). This study has been funded by the Italian Ministry of Health - Ricerca Corrente 2021 - Linea 4.

ACKNOWLEDGMENTS

The authors acknowledge the Center for Advanced Preclinical *in vivo* Research (CAPiR) and the confocal microscopy facility at the Bio-Nanotech Research and Innovation Tower (BRIT) of the University of Catania, for the technical contribution of the staff.

REFERENCES

Bennett, G. J., and Xie, Y. K. (1988). A Peripheral Mononeuropathy in Rat that Produces Disorders of Pain Sensation Like Those Seen in Man. *Pain.* 33 (1), 87–107. doi:10.1016/0304-3959(88)90209-6

Boccella, S., Guida, F., Palazzo, E., Marabese, I., de Novellis, V., Maione, S., et al. (2018). Spared Nerve Injury as a Long-Lasting Model of Neuropathic Pain. *Methods Mol. Biol.* 1727, 373–378. doi:10.1007/978-1-4939-7571-6_28

Cahill, C. M., Holdridge, S. V., Liu, S., Xue, L., Magnussen, C., Ong, E., et al. (2020). Delta Opioid Receptor Activation Modulates Affective Pain and Modality-Specific Pain Hypersensitivity Associated With Chronic Neuropathic Pain. *J. Neurosci. Res.*, 1–20. doi:10.1002/jnr.24680

Caraci, F., Merlo, S., Drago, F., Caruso, G., Parenti, C., and Sortino, M. A. (2019). Rescue of Noradrenergic System as a Novel Pharmacological Strategy in the Treatment of Chronic Pain: Focus on Microglia Activation. *Front. Pharmacol.* 10, 1024. doi:10.3389/fphar.2019.01024

Caraci, F., Spampinato, S. F., Morgese, M. G., Tascedda, F., Salluzzo, M. G., Giambirtone, M. C., et al. (2018). Neurobiological Links Between Depression and AD: The Role of TGF-B1 Signaling as a New Pharmacological Target. *Pharmacol. Res.* 130, 374–384. doi:10.1016/j.phrs.2018.02.007

Caruso, G., Fresta, C. G., Musso, N., Giambirtone, M., Grasso, M., Spampinato, S. F., et al. (2019). Carnosine Prevents Aβ-Induced Oxidative Stress and Inflammation in Microglial Cells: A Key Role of TGF-B1. *Cells.* 8 (1), 64. doi:10.3390/cells8010064

Cavalli, E., Mammana, S., Nicoletti, F., Bramanti, P., and Mazzon, E. (2019). The Neuropathic Pain: An Overview of the Current Treatment and Future Therapeutic Approaches. *Int. J. Immunopathol. Pharmacol.* 33, 2058738419838383. doi:10.1177/2058738419838383

Chen, G., Park, C. K., Xie, R. G., and Ji, R. R. (2015). Intrathecal Bone Marrow Stromal Cells Inhibit Neuropathic Pain via TGF-β Secretion. *J. Clin. Invest.* 125 (8), 3226–3240. doi:10.1172/JCI80883

Chen, N. F., Chen, W. F., Sung, C. S., Lu, C. H., Chen, C. L., Hung, H. C., et al. (2016). Contributions of P38 and ERK to the Antinociceptive Effects of TGF-B1 in Chronic Constriction Injury-Induced Neuropathic Rats. *J. Headache Pain.* 17 (1), 72. doi:10.1186/s10194-016-0665-2

Chen, N. F., Huang, S. Y., Chen, W. F., Chen, C. H., Lu, C. H., Chen, C. L., et al. (2013). TGF-β1 Attenuates Spinal Neuroinflammation and the Excitatory Amino Acid System in Rats With Neuropathic Pain. *J. Pain.* 14 (12), 1671–1685. doi:10.1016/j.jpain.2013.08.010

Chou, R., Turner, J. A., Devine, E. B., Hansen, R. N., Sullivan, S. D., Blazina, I., et al. (2015). The Effectiveness and Risks of Long-Term Opioid Therapy for Chronic Pain: a Systematic Review for a National Institutes of Health Pathways to Prevention Workshop. *Ann. Intern. Med.* 162 (4), 276–286. doi:10.7326/M14-2559

Coraggio, V., Guida, F., Boccella, S., Scafuro, M., Paino, S., Romano, D., et al. (2018). Neuroimmune-Driven Neuropathic Pain Establishment: A Focus on Gender Differences. *Int. J. Mol. Sci.* 19 (1), 281. doi:10.3390/ijms19010281

Costigan, M., Scholz, J., and Woolf, C. J. (2009). Neuropathic Pain: a Maladaptive Response of the Nervous System to Damage. *Annu. Rev. Neurosci.* 32, 1–32. doi:10.1146/annurev.neuro.051508.135531

de la Puerta, R., Carcelén, M., Francés, R., de la Fuente, R., Hurlé, M. A., and Tramullas, M. (2019). BMP-7 Protects Male and Female Rodents against Neuropathic Pain Induced by Nerve Injury through a Mechanism Mediated by Endogenous Opioids. *Pharmacol. Res.* 150, 104470. doi:10.1016/j.phrs.2019.104470

Dixon, W. J. (1980). Efficient Analysis of Experimental Observations. *Annu. Rev. Pharmacol. Toxicol.* 20, 441–462. doi:10.1146/annurev.pa.20.040180.002301

Echeverry, S., Shi, X. Q., Haw, A., Liu, H., Zhang, Z. W., and Zhang, J. (2009). Transforming Growth Factor-Beta1 Impairs Neuropathic Pain Through Pleiotropic Effects. *Mol. Pain.* 5, 16. doi:10.1186/1744-8069-5-16

Gendron, L., Pintar, J. E., and Chavkin, C. (2007). Essential Role of Mu Opioid Receptor in the Regulation of Delta Opioid Receptor-Mediated

Antihyperalgesia. *Neuroscience.* 150 (4), 807–817. doi:10.1016/j.neuroscience.2007.09.060

Gomes, I., Gupta, A., Filipovska, J., Szeto, H. H., Pintar, J. E., and Devi, L. A. (2004). A Role for Heterodimerization of Mu and delta Opiate Receptors in Enhancing Morphine Analgesia. *Proc. Natl. Acad. Sci. U S A.* 101 (14), 5135–5139. doi:10.1073/pnas.0307601101

Gulino, R., Vicario, N., Giunta, M. A. S., Spoto, G., Calabrese, G., Vecchio, M., et al. (2019). Neuromuscular Plasticity in a Mouse Neurotoxic Model of Spinal Motoneuronal Loss. *Int. J. Mol. Sci.* 20 (6), 1500. doi:10.3390/ijms20061500

Guo, A., Li, J., Luo, L., Chen, C., Lu, Q., Ke, J., et al. (2021). Valproic Acid Mitigates Spinal Nerve Ligation-Induced Neuropathic Pain in Rats by Modulating Microglial Function and Inhibiting Neuroinflammatory Response. *Int. Immunopharmacol.* 92, 107332. doi:10.1016/j.intimp.2020.107332

Gwak, Y. S., Hulsebosch, C. E., and Leem, J. W. (2017). Neuronal-Glial Interactions Maintain Chronic Neuropathic Pain After Spinal Cord Injury. *Neural Plast.* 2017, 2480689. doi:10.1155/2017/2480689

Hack, S. P., Bagley, E. E., Chieng, B. C., and Christie, M. J. (2005). Induction of Delta-Opioid Receptor Function in the Midbrain After Chronic Morphine Treatment. *J. Neurosci.* 25 (12), 3192–3198. doi:10.1523/JNEUROSCI.4585-04.2005

Holdridge, S. V., Armstrong, S. A., Taylor, A. M., and Cahill, C. M. (2007). Behavioural and Morphological Evidence for the Involvement of Glial Cell Activation in delta Opioid Receptor Function: Implications for the Development of Opioid Tolerance. *Mol. Pain.* 3, 7. doi:10.1186/1744-8069-3-7

Ji, R. R., Xu, Z. Z., and Gao, Y. J. (2014). Emerging Targets in Neuroinflammation-Driven Chronic Pain. *Nat. Rev. Drug Discov.* 13, 533–548. doi:10.1038/nrd4334

Kabli, N., and Cahill, C. M. (2007). Anti-Allodynic Effects of Peripheral Delta Opioid Receptors in Neuropathic Pain. *Pain.* 127 (1-2), 84–93. doi:10.1016/j.pain.2006.08.003

Khan, J., Noboru, N., Imamura, Y., and Eliav, E. (2018). Effect of Pregabalin and Diclofenac on Tactile Allodynia, Mechanical Hyperalgesia and Pro Inflammatory Cytokine Levels (IL-6, IL-1β) Induced by Chronic Constriction Injury of the Infraorbital Nerve in Rats. *Cytokine.* 104, 124–129. doi:10.1016/j.cyto.2017.10.003

Lantero, A., Tramullas, M., Díaz, A., and Hurlé, M. A. (2012). Transforming Growth Factor-β in Normal Nociceptive Processing and Pathological Pain Models. *Mol. Neurobiol.* 45 (1), 76–86. doi:10.1007/s12035-011-8221-1

Lantero, A., Tramullas, M., Pílar-Cuellar, F., Valdizán, E., Santillán, R., Roques, B. P., et al. (2014). TGF-β and Opioid Receptor Signaling Crosstalk Results in Improvement of Endogenous and Exogenous Opioid Analgesia Under Pathological Pain Conditions. *J. Neurosci.* 34 (15), 5385–5395. doi:10.1523/JNEUROSCI.4405-13.2014

Lees, J. G., Fivelman, B., Duffy, S. S., Makker, P. G., Perera, C. J., and Moalem-Taylor, G. (2015). Cytokines in Neuropathic Pain and Associated Depression. *Mod. Trends Pharmacopsychiatry.* 30, 51–66. doi:10.1159/000435932

Liu, M. X., Zhong, J., Xia, L., Dou, N. N., and Li, S. T. (2020). IL-6 Contributes to Nav1.3 Up-Regulation in Trigeminal Nerve Following Chronic Constriction Injury. *Neurol. Res.* 42 (6), 504–514. doi:10.1080/01616412.2020.1747719

Malcangio, M. (2019). Role of the Immune System in Neuropathic Pain. *Scand. J. Pain.* 20 (1), 33–37. doi:10.1515/sjpain-2019-0138

Martínez-Navarro, M., Maldonado, R., and Baños, J. E. (2019). Why Mu-Opioid Agonists Have Less Analgesic Efficacy in Neuropathic Pain?. *Eur. J. Pain.* 23 (3), 435–454. doi:10.1002/ejp.1328

Mika, J., Zychowska, M., Popiolek-Barczyk, K., Rojewska, E., and Przewlocka, B. (2013). Importance of Glial Activation in Neuropathic Pain. *Eur. J. Pharmacol.* 716 (1-3), 106–119. doi:10.1016/j.ejphar.2013.01.072

Myers, R. R., Campana, W. M., and Shubayev, V. I. (2006). The Role of Neuroinflammation in Neuropathic Pain: Mechanisms and Therapeutic Targets. *Drug Discov. Todaytoday.* 11 (1-2), 8–20. doi:10.1016/S1359-6446(05)03637-8

Nong, X., and Lan, Y. (2018). Picroside II Attenuates CCI-Induced Neuropathic Pain in Rats by Inhibiting Spinal Reactive Astrocyte-Mediated Neuroinflammation Through the NF-Kb Pathway. *Neurochem. Res.* 43 (5), 1058–1066. doi:10.1007/s11064-018-2518-7

Onichtchouk, D., Chen, Y. G., Dosch, R., Gawantka, V., Delius, H., Massagué, J., et al. (1999). Silencing of TGF-Beta Signalling by the Pseudoreceptor BAMBI. *Nature.* 401 (6752), 480–485. doi:10.1038/46794

Parenti, C., Turnaturi, R., Aricò, G., Gramowski-Voss, A., Schroeder, O. H., Marrazzo, A., et al. (2013). The Multitarget Opioid Ligand LP1's Effects in Persistent Pain and in Primary Cell Neuronal Cultures. *Neuropharmacology.* 71, 70–82. doi:10.1016/j.neuropharm.2013.03.008

Pasquinucci, L., Turnaturi, R., Montenegro, L., Caraci, F., Chiechio, S., and Parenti, C. (2019). Simultaneous Targeting of MOR/DOR: A Useful Strategy for Inflammatory Pain Modulation. *Eur. J. Pharmacol.* 847, 97–102. doi:10.1016/j.ejphar.2019.01.031

Pasquinucci, L., Turnaturi, R., Prezzavento, O., Arena, E., Aricò, G., Georgoussi, Z., et al. (2017). Development of Novel LP1-Based Analogues With Enhanced delta Opioid Receptor Profile. *Bioorg. Med. Chem.* 25 (17), 4745–4752. doi:10.1016/j.bmc.2017.07.021

Piotrowska, A., Kwiatkowski, K., Rojewska, E., Makuch, W., and Mika, J. (2016). Maraviroc Reduces Neuropathic Pain Through Polarization of Microglia and Astroglia - Evidence From *In Vivo* and *In Vitro* Studies. *Neuropharmacology.* 108, 207–219. doi:10.1016/j.neuropharm.2016.04.024

Reddy, L. V. K., and Sen, D. (2017). DADLE Enhances Viability and Anti-Inflammatory Effect of Human MSCs Subjected to 'Serum Free' Apoptotic Condition in Part via the DOR/PI3K/AKT Pathway. *Life Sci.* 191, 195–204. doi:10.1016/j.lfs.2017.10.024

Scherrer, G., Imamachi, N., Cao, Y. Q., Contet, C., Mennicken, F., O'Donnell, D., et al. (2009). Dissociation of the Opioid Receptor Mechanisms that Control Mechanical and Heat Pain. *Cell.* 137 (6), 1148–1159. doi:10.1016/j.cell.2009.04.019

Shubayev, V., Kato, K., and Meyers, R. (2010). "Cytokines in Pain," in *Translational Pain Research From Mouse to Man*. Editors L. Kruger and A. R. Light (CRC Press/Taylor & Francis). Chapter 8.

Spitale, F. M., Vicario, N., Rosa, M. D., Tibullo, D., Vecchio, M., Gulino, R., et al. (2020). Increased Expression of Connexin 43 in a Mouse Model of Spinal Motoneuronal Loss. *Aging (Albany NY).* 12 (13), 12598–12608. doi:10.18632/aging.103561

Starnowska-Sokół, J., and Przewłocka, B. (2020). Multifunctional Opioid-Derived Hybrids in Neuropathic Pain: Preclinical Evidence, Ideas and Challenges. *Molecules.* 25 (23), 5520. doi:10.3390/molecules25235520

Tramullas, M., Lantero, A., Díaz, A., Morchón, N., Merino, D., Villar, A., et al. (2010). BAMBI (Bone Morphogenetic Protein and Activin Membrane-Bound Inhibitor) Reveals the Involvement of the Transforming Growth Factor-Beta Family in Pain Modulation. *J. Neurosci.* 30 (4), 1502–1511. doi:10.1523/JNEUROSCI.2584-09.2010

Treed, R. D., Jensen, T. S., Campbell, J. N., Cruccu, G., Dostrovsky, J. O., Griffin, J. W., et al. (2008). Neuropathic Pain: Redefinition and a Grading System for Clinical and Research Purposes. *Neurology.* 70 (18), 1630–1635. doi:10.1212/01.wnl.0000282763.29778.59

Turchan-Cholewo, J., Dimayuga, F. O., Ding, Q., Keller, J. N., Hauser, K. F., Knapp, P. E., et al. (2008). Cell-specific Actions of HIV-Tat and Morphine on Opioid Receptor Expression in Glia. *J. Neurosci. Res.* 86 (9), 2100–2110. doi:10.1002/jnr.21653

Turnaturi, R., Chiechio, S., Salerno, L., Rescifina, A., Pittalà, V., Cantarella, G., et al. (2019). Progress in the Development of More Effective and Safer Analgesics for Pain Management. *Eur. J. Med. Chem.* 183, 111701. doi:10.1016/j.ejmech.2019.111701

Uçeyler, N., Tscharke, A., and Sommer, C. (2007). Early Cytokine Expression in Mouse Sciatic Nerve after Chronic Constriction Nerve Injury Depends on Calpain. *Brain Behav. Immun.* 21 (5), 553–560. doi:10.1016/j.bbi.2006.10.003

Vicario, N., Pasquinucci, L., Spitale, F. M., Chiechio, S., Turnaturi, R., Caraci, F., et al. (2019a). Simultaneous Activation of Mu and Delta Opioid Receptors Reduces Allodynia and Astrocytic Connexin 43 in an Animal Model of Neuropathic Pain. *Mol. Neurobiol.* 56 (11), 7338–7354. doi:10.1007/s12035-019-1607-1

Vicario, N., Bernstock, J. D., Spitale, F. M., Giallongo, C., Giunta, M. A. S., Li Volti, G., et al. (2019b). Clobetasol Modulates Adult Neural Stem Cell Growth via Canonical Hedgehog Pathway Activation. *Int. J. Mol. Sci.* 20 (8), 1991. doi:10.3390/ijms20081991

Vicario, N., Parenti, R., Arico', G., Turnaturi, R., Scoto, G. M., Chiechio, S., et al. (2016). Repeated Activation of Delta Opiod Receptors Counteracts Nerve Injury-Induced TNF-α Up-Regulation in the Sciatic Nerve of Rats With Neuropathic Pain: A Possible Correlation With Delta Opiod Receptors-Mediated Antiallodinic Effect. *Mol. Pain.* 12, 1744806916667949. doi:10.1177/1744806916667949

Vicario, N., Spitale, F. M., Tibullo, D., Giallongo, C., Amorini, A. M., Scandura, G., et al. (2021). Clobetasol Promotes Neuromuscular Plasticity in Mice After Motoneuronal Loss via Sonic Hedgehog Signaling, Immunomodulation and Metabolic Rebalancing. *Cell Death Dis.* 12 (7), 625. doi:10.1038/s41419-021-03907-1

Wang, J., Yu, J., Ding, C. P., Han, S. P., Zeng, X. Y., and Wang, J. Y. (2015). Transforming Growth Factor-Beta in the Red Nucleus Plays Antinociceptive Effect Under Physiological and Pathological Pain Conditions. *Neuroscience.* 291, 37–45. doi:10.1016/j.neuroscience.2015.01.059

Xie, J., Ren, J., Liu, N., Wu, C., Xiao, D., Luo, H., et al. (2019). Pretreatment With AM1241 Enhances the Analgesic Effect of Intrathecally Administrated Mesenchymal Stem Cells. *Stem Cell Int.* 2019, 7025473. doi:10.1155/2019/7025473

Conflict of Interest: The authors declare that the research was conducted in the absence of any commercial or financial relationships that could be construed as a potential conflict of interest.

Publisher's Note: All claims expressed in this article are solely those of the authors and do not necessarily represent those of their affiliated organizations, or those of the publisher, the editors and the reviewers. Any product that may be evaluated in this article, or claim that may be made by its manufacturer, is not guaranteed or endorsed by the publisher.

Copyright © 2021 Fidilio, Grasso, Turnaturi, Caruso, Spitale, Vicario, Parenti, Spoto, Musso, Marrazzo, Chiechio, Caraci, Pasquinucci and Parenti. This is an open-access article distributed under the terms of the Creative Commons Attribution License (CC BY). The use, distribution or reproduction in other forums is permitted, provided the original author(s) and the copyright owner(s) are credited and that the original publication in this journal is cited, in accordance with accepted academic practice. No use, distribution or reproduction is permitted which does not comply with these terms.

frontiers in Pharmacology

ORIGINAL RESEARCH
published: 08 October 2021
doi: 10.3389/fphar.2021.734603

Berberine and Its Main Metabolite Berberrubine Inhibit Platelet Activation Through Suppressing the Class I PI3Kβ/Rasa3/Rap1 Pathway

Can Wang[1,2], Yangyang Cheng[3], Yuanhui Zhang[3], Hongtao Jin[4], Zengyan Zuo[3], Aiping Wang[4], Jianmei Huang[1], Jiandong Jiang[2,3]* and Weijia Kong[3]**

[1]School of Chinese Materia Medica, Beijing University of Chinese Medicine, Beijing, China, [2]State Key Laboratory of Bioactive Substance and Function of Natural Medicines, Institute of Materia Medica, Chinese Academy of Medical Sciences and Peking Union Medical College, Beijing, China, [3]Department of Virology and NHC Key Laboratory of Biotechnology of Antibiotics, Institute of Medicinal Biotechnology, Chinese Academy of Medical Sciences and Peking Union Medical College, Beijing, China, [4]New Drug Safety Evaluation Center, Institute of Materia Medica, Chinese Academy of Medical Sciences and Peking Union Medical College, Beijing, China

OPEN ACCESS

Edited by:
Andres Trostchansky,
Universidad de la República, Uruguay

Reviewed by:
Libin Zhou,
Shanghai Jiao Tong University School of Medicine, China
Emilio Hirsch,
University of Turin, Italy

***Correspondence:**
Jianmei Huang
hjm70@139.com
Jiandong Jiang
jiang.jdong@163.com
Weijia Kong
kongweijia@imb.pumc.edu.cn

Specialty section:
This article was submitted to Experimental Pharmacology and Drug Discovery, a section of the journal Frontiers in Pharmacology

Received: 01 July 2021
Accepted: 06 September 2021
Published: 08 October 2021

Citation:
Wang C, Cheng Y, Zhang Y, Jin H, Zuo Z, Wang A, Huang J, Jiang J and Kong W (2021) Berberine and Its Main Metabolite Berberrubine Inhibit Platelet Activation Through Suppressing the Class I PI3Kβ/Rasa3/Rap1 Pathway. Front. Pharmacol. 12:734603. doi: 10.3389/fphar.2021.734603

Background: Berberine (BBR), a natural product, was reported to inhibit platelet aggregation; however, the molecular mechanisms remain unclear. This study aims to investigate the effects and mechanisms of BBR in inhibiting platelet activation and thrombus formation.

Methods: Flow cytometry, immunofluorescence, and Western blot were used to determine the inhibitory effects and mechanisms of BBR and its main metabolite berberrubine (M2) on platelet activation *in vitro* and *ex vivo*. Purified integrin αIIbβ3, class I PI3K kit, and molecular docking were used to identify the possible targets of BBR and M2. A carrageenan-induced mouse thrombosis model was used to evaluate the effects of BBR on thrombus formation *in vivo*.

Results: *In vitro*, BBR and M2 significantly inhibited ADP-induced integrin αIIbβ3 activation, reduced the level of P-selectin on the platelet membrane, and suppressed the binding of fibrinogen to the platelets. In this process, BBR and M2 greatly suppressed the PI3K/Akt pathway and inhibited Rasa3 membrane translocation and Rap1 activation. Furthermore, BBR and M2 selectively inhibited class I PI3Kβ, perhaps through binding to its active site. The activities of BBR were stronger than those of M2. After oral administration, BBR significantly inhibited the PI3K/Akt pathway and Rap1 activation and suppressed ADP-induced platelet activation and carrageenan-induced thrombosis in mice without prolonging bleeding time.

Conclusions: We reveal for the first time the possible targets and mechanisms of BBR and M2 in inhibiting platelet activation. Our research may support the future clinical application of BBR as an antiplatelet drug in the prevention or treatment of thrombotic diseases.

Keywords: berberine, berberrubine, platelet activation, class I PI3Kβ, thrombus formation

INTRODUCTION

Thrombotic diseases and the related cardiovascular or cerebrovascular events, such as myocardial infarction or stroke, are the leading causes of mortality and morbidity worldwide (Caron and Anand, 2017; Thomas et al., 2018; Wang et al., 2018). Inhibiting thrombus formation is a directly effective way for the prevention or treatment of cardiovascular or cerebrovascular diseases (Asada et al., 2018). Currently, there are two main types of drugs used in clinics for the treatment of thrombus formation: anticoagulant drugs (Mega and Simon, 2015; Honda et al., 2016) and antiplatelet drugs (Jing et al., 2011; Patrono et al., 2017; Binsaleh et al., 2018). However, bleeding risk is a common challenge for these drugs in clinical use (Patrono et al., 2017). Moreover, a recent study showed that warfarin, a kind of vitamin K antagonist that has been used for prophylaxis or the treatment of thromboembolic events for 64 years, may increase the risk of myelodysplastic syndrome (Verma et al., 2019). Therefore, the development of more safe and effective antithrombotic drugs is of scientific and clinical significance.

A variety of natural products isolated from traditional Chinese medicine have shown good safety and pharmacological activity in anti-thrombosis (Huang et al., 2010; Song et al., 2019). Berberine (BBR), a natural product isolated from *Coptis chinensis*, has been used for the treatment of bacterial diarrhea in clinics for many years in China (National Pharmacopoeia Committee, 2015), and no side effects of hemorrhagic tendencies have been reported (Wang et al., 2018). BBR has beneficial effects against a variety of chronic diseases (Kong et al., 2004; Zhang et al., 2010; Pirillo and Catapano, 2015; Zou et al., 2017). As early as the 1980s, researchers had reported that BBR was able to inhibit platelet aggregation, both in preclinical and clinical studies (Chen and Xie, 1986; Chu et al., 1989; Huang et al., 1989). BBR also inhibited thrombus formation effectively in animal models. For example, we previously reported that BBR significantly inhibited thrombus formation in the inferior vena cava in rats fed a normal or high-fat diet (Wang et al., 2018).

Currently, the mechanisms of BBR in inhibiting platelet activation and aggregation remain unclear. In addition, whether or not the metabolites of BBR have antiplatelet activities is unknown. Among the BBR metabolites, berberrubine (M2) (**Figure 1**) is the main metabolite and accounts for 65.1% of all BBR metabolites in the liver (Tan et al., 2013). Therefore, in this research, we aim to investigate the antiplatelet effects and possible mechanisms of BBR and M2, and our results prove that BBR and M2 suppress platelet activation through inhibiting the class I PI3Kβ/Rasa3/Rap1 pathway, which is related to the antithrombotic effect of BBR.

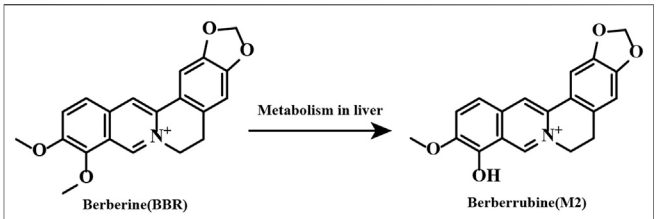

FIGURE 1 | Chemical structures of BBR and its main metabolite M2.

MATERIALS AND METHODS

Mice

All C57BL/6N mice (males, 6–7 weeks old, 18–20 g) and BALB/c mice (males, 6–7 weeks old, 18–20 g) were purchased from Beijing Vital River Laboratory Animal Technology Co., Ltd. The mice were kept in a room at a temperature of 22–24°C and humidity of 45% with a 12-h day and night cycle (lighting time 8:00–20:00). All animal experiments were reviewed and approved by the Ethics Committee of the Institute of Materia Medica, Chinese Academy of Medical Sciences (CAMS) and Peking Union Medical College (PUMC) (No. 00005787, No. 00005788, No. 00005789). After the experiments, all mice were anesthetized with 2% isoflurane inhalation and sacrificed with cervical dislocation to perform animal euthanasia. To protect animals used for scientific purposes, all animal procedures which were performed conformed to the guidelines from EU Directive 2010/63/EU for animal experiments.

Reagents and Kits

Sodium citrate tribasic dihydrate, prostaglandin E1 (PGE1), N-[2-Hydroxyethyl] piperazine-N'-[2-ethanesulfonic acid (HEPES), berberine chloride, ADP, 3,3′,5,5′-tetramethylbenzidine (TMB) liquid substrate (#T4444), aspirin (Asp), and a stop reagent for the TMB substrate (#S5814) were obtained from Sigma-Aldrich (St. Louis, MO, United States). Berberrubine chloride (M2) was obtained from Chengdu Herbpurify CO., LTD. (Chengdu, Sichuan, China). PE-labeled rat anti-mouse JON/A monoclonal antibody (#M023-2), PE-labeled rat IgG polyclonal antibody (#P190-2), FITC-labeled rat anti-mouse p-selectin (CD62P) monoclonal antibody (#M130-1), and FITC-labeled rat IgG polyclonal antibody (#P190-1) were purchased from Emfret Analytics (Würzburg, Germany). Eight-well chambered glass coverslips (#155411PK), FluoroNunc 96-well plates, Calcein-AM (#C3099), TRITC–phalloidin (#R415), the M-PER™ Mammalian Protein Extraction Reagent (#78501), the Mem-PER™ Plus Membrane Protein Extraction Kit (#89842), and the active Rap1 pull-down and detection kit (#16120) were purchased from Thermo Fisher Scientific Inc. (Waltham, MA, United States). Mouse fibrinogen (#CT15) was obtained from Oxford Biomedical Research (Oxford, United Kingdom). Human GPIIbIIIa (#GP2b3a) was obtained from Enzyme Research Laboratories (South Bend, IN, United States). Fibrinogen plasminogen-depleted (#341578) and rabbit anti-FcRγ polyclonal antibodies (#06–727) were purchased from Millipore (Billerica, MA, United States). Fibrinogen antibody (HRP) (#60R-1012) was purchased from Fitzgerald (Acton, MA, United States). Tirofiban hydrochloride monohydrate (#HY-17369) and clopidogrel (Clop) hydrogen sulfate were obtained from MedChemExpress (Shanghai, China). Rabbit anti-p-Akt (Ser^{473}) (#4058), rabbit anti-Akt (#9272), rabbit anti-ERK (#9102) antibodies, and wortmannin

(Wtm) were sourced from Cell Signaling Technology, Inc. (Danvers, MA, United States). Mouse anti-Rasa3 monoclonal antibody (#SC-398283) and integrin β3 antibody (B-7) (#SC-46655) were sourced from Santa Cruz Biotechnology, Inc. (Dallas, TX, United States). ADP-Glo lipid kinase systems (#V1691) were purchased from Promega Corporation (Madison, WI, United States). TGX221 was purchased from Cayman Chemical Company (Ann Arbor, MI, United States).

Preparation of Mouse Washed Platelets

Mouse washed platelets (WPs) were prepared as described previously (Blue et al., 2008). Briefly, mice were anaesthetized with 2% isoflurane inhalation, and retro-orbital blood samples were collected into the sodium citrate solution (blood volume: sodium citrate solution, 9:1). The anticoagulated whole blood sample was centrifuged at 22°C at 650 *g* for 4 min to obtain platelet-rich plasma (PRP). Then, PGE1 (final concentration 1 μM) was added to PRP and mixed well, and the PRP was centrifuged at 22°C at 1,200 *g* for 8 min to obtain the precipitation of WPs. Then, the WPs were resuspended in HEPES-modified Tyrode buffer (HBMT; 10 mM HEPES, 138 mM NaCl, 12 mM $NaHCO_3$, 2.7 mM KCl, 0.4 mM NaH_2PO_4, 0.1% glucose, 0.35% BSA, 2 mM $CaCl_2$, and 1 mM $MgCl_2$, pH = 7.4). The platelet concentration was adjusted to 3×10^8/ml by counting with a hemocytometer.

Flow Cytometry

The methods of flow cytometry were performed as described previously (Deng et al., 2016). Briefly, the suspension of the WPs was divided into several groups and treated with the vehicle control (0.1% DMSO) or different compounds at 37°C for 10 min and then stimulated with 10 μM of ADP for 10 min. After treatment, the WPs were fixed with 1% paraformaldehyde at room temperature for 15 min. The platelet suspension was centrifuged at 22°C at 1,200 *g* for 8 min, and then the precipitation was resuspended in HBMT. Each group was divided into four parts, and they were incubated with the PE-conjugated JON/A antibody (selectively binding to the high-affinity conformation of mouse integrin αIIbβ3), FITC-labeled rat anti-mouse P-selectin monoclonal antibody, or the negative control IgGs for 15 min. After terminating the reaction with 400 μl PBS, the platelets were analyzed using a BD FACSCalibur flow cytometer (BD-Biosciences, Heidelberg, Germany) or BD Accuri C6 flow cytometer (BD-Biosciences, Heidelberg, Germany). All data were analyzed using FlowJo software (BD-Biosciences, Heidelberg, Germany).

Immunofluorescence

Immunofluorescence was performed as described before with slight modifications (Blue et al., 2008). Briefly, eight-chambered glass coverslips (Nunc) were coated with 200 μl fibrinogen (50 μg/ml). After incubating at 4°C overnight, each chamber was washed three times with Tris/saline (100 mM sodium chloride, 50 mM Tris/HCl, pH = 7.4). And then, each chamber was blocked with HBMT at room temperature for 1 h and washed two times with Tris/saline. After treatment, WPs were added to the eight-well chambered glass coverslips coated with fibrinogen and incubated at room temperature for 1 h, then each chamber was washed with HBMT (containing 2 mM $CaCl_2$ and 1 mM $MgCl_2$) four times. The adherent platelets were fixed with 1% paraformaldehyde at room temperature for 15 min and washed with PBS three times. Then, the platelets were treated with 0.1% Triton X-100 for 15 min and washed with PBS for another three times. After being blocked with 1% BSA/PBS at room temperature for 1 h, the adherent platelets were incubated with the TRITC–phalloidin working solution at room temperature for 1 h and washed with PBS again three times. Finally, immunofluorescence images were taken using an Olympus IX71 fluorescent inverted microscope with a 40× objective and 10× eyepiece.

Platelet Adhesion Assay

Platelet adhesion to fibrinogen was performed as described before with slight modifications (Blue et al., 2008; Su et al., 2016). Briefly, human fibrinogen was diluted and dissolved into the fibrinogen solution with a final concentration of 50 g/ml. 200 μl of the fibrinogen solution (50 μg/ml) was added to FluoroNunc 96-well plates. After incubating at 4°C overnight, the plates were washed with 200 μl of Tris/saline three times. Then, the wells were blocked with 200 μl of HBMT containing 2% BSA for 1 h at room temperature and washed with Tris/saline two times. During the period, WPs were treated with different concentrations of BBR or M2 or the vehicle control (0.1% DMSO) at 37°C for 10 min and then stimulated with 10 μM ADP for 10 min. After treatment, WPs were labeled with calcein-AM at a final concentration of 16 μM at room temperature for 30 min in the absence of light. And then, 100 μl labeled platelets were added into coated FluoroNunc 96-well plates and incubated at room temperature for 1 h. After washing four times with 200 μl HBMT containing 2 mM $CaCl_2$ and 1 mM $MgCl_2$, 100 μl HBMT containing 2 mM $CaCl_2$ and 1 mM $MgCl_2$ was added. The fluorescence intensity was measured using the EnSpire Multimode Plate Reader (PerkinElmer, Waltham, MA, United States) to represent the relative number of adherent platelets (excitation wavelengths/emission wavelengths: 490 nm/515 nm).

Protein Extraction and Western Blot

After treatment, the WPs were centrifuged at 1,200 *g* at 22°C for 8 min to obtain the precipitation. The M-PER™ Mammalian Protein Extraction Reagent was added to obtain whole cell lysis, and the Mem-PER™ Plus Membrane Protein Extraction Kit was used to obtain membrane proteins and cytosolic proteins following the kit's instructions. Western blot was performed as described before (Wang et al., 2016). Briefly, 20 μl of the cell lysate was used for 10% sodium dodecyl sulfate polyacrylamide gel electrophoresis, and the proteins were transferred from the gels onto the PVDF membranes. After blocking, the blots of target proteins were detected with specific primary antibodies and appropriate secondary antibodies. The signals were developed using the ECL kit (EMD Millipore Corporation). After scanning and quantification, the levels of p-AKT (Ser^{473}) were normalized to those of AKT and plotted as indicated. The ratios of the Rasa3 protein in the membrane to FcRγ and those in the cytoplasm to ERK were calculated. The original scans of Western blot are shown in **Supplementary Figures S1–4**.

Rap1 Activation Assay

The Rap1 activation assay was performed following the kit's instructions; GTPγS (positive control) and GDP (negative control) were used to ensure that the pull-down procedures worked properly. Briefly, after treatment, the WPs precipitation was prepared and split with 300 μl lysis/binding/wash buffer on ice for 5 min. The supernatant was collected by centrifuging the lysate at 4°C for 15 min and added to the spin cup containing the glutathione resin and GST-RalGDS-RBD. The reaction mixture was vortexed and incubated at 4°C for 1 h with gentle rocking. The spin cups were centrifuged with collection tubes at 6,000 *g* for 1 min, and the resin was washed three times. After adding 50 μl 2× reducing sample buffer (1 part β-mercaptoethanol to 20 parts 2× SDS sample buffer), the samples were vortexed and incubated at room temperature for 2 min and then centrifuged at 6,000 *g* for 2 min. The spin cup containing the resin was removed and discarded. The eluted samples were heated for 5 min at 95–100°C. Western blot was used to detect the pull-down of GTP-Rap1 (Rap1 active form). The original scans of Western blot are shown in **Supplementary Figures S1, 3**.

Fibrinogen Binding to Purified Integrin αIIbβ3

The purified integrin αIIbβ3 binding assay was performed as described previously (Blue et al., 2008; Su et al., 2016). Briefly, 96-well plates were coated with the integrin β3 antibody (B-7) (10 μg/ml) at 4°C overnight and, then, were blocked with 3.5% BSA at room temperature for 1 h. Purified integrin αIIbβ3 was diluted in buffer A (50 mM Tris/HCl, 100 mM NaCl, 1 mM $CaCl_2$, 1 mM $MgCl_2$, 1% BSA, and 0.0035% Triton X-100) to 10 μg/ml, added to the wells, and captured by the integrin β3 antibody (B-7) for 2 h at 37°C. The wells were then washed three times with buffer A. Fibrinogen, prepared in buffer A (20 μg/ml), was incubated in the well plates for 2 h at 37°C with or without the studied compounds or control solutions. The wells were washed three times with buffer A and then incubated with a horseradish peroxidase (HRP)–conjugated polyclonal anti-fibrinogen antibody (1:1,000 in buffer A) for 1 h at room temperature. For color development, the wells were washed three times. 100 μl of a peroxidase substrate (TMB) was added, and the reaction was terminated after 30 min by adding 100 μl of the stop reagent for the TMB substrate. Finally, the absorbance value was determined by spectrophotometry at 450 nm.

Class I PI3K Activity Assays

The effects of BBR and M2 on different isoforms of class I PI3K were determined following the kit's instructions. Briefly, different isoforms of recombinant class I PI3K enzymes were mixed with the lipid kinase substrate which contained 1 mg of phosphoinositol-4, 5-bisphosphate (PIP2) and 3 mg of phosphatidylserine. Together with the studied compounds, the reactions were incubated at room temperature for 20 min. After incubation, the ATP solution (25 μM) was added to each well. The assay plate was covered and incubated at room temperature for 1 h. The ADP-Glo reagent containing 10 mM of $MgCl_2$ was used to stop the reaction and deplete the unconsumed ATP. Then, the kinase detection reagent was added to each well and incubated at room temperature for 40 min to convert ADP to ATP. The amount of newly synthesized ATP was detected with a coupled luciferin/luciferase reaction and used to represent class I PI3K activity.

For the ATP competition experiments, different isoforms of class I PI3K were incubated with the substrate and 1 μM of BBR or M2 for 20 min, and lipid kinase reactions were performed in the presence of different concentrations of ATP (6.25–400 μM).

Molecular Docking

The 2D structures of BBR and M2 were drawn using ChemBioDraw 2014 and converted to 3D structures in MOE through energy minimization. The 3D structure of the mouse protein PI3K p110β was downloaded from the RCSB Protein Data Bank (PDB ID was 2Y3A). Prior to docking, the force field of AMBER10:EHT and the implicit solvation model of the reaction field (R-field) were selected. MOE-Dock was used for molecular docking simulations of molecules with proteins. The docking workflow followed the "induced fit" protocol, in which the side chains of the receptor pocket were allowed to move according to ligand conformations, with a constraint on their positions. The weight used for tethering side chain atoms to their original positions was 10. For each ligand, all docked poses were ranked by London dG scoring first, then a force field refinement was carried out on the top 20 poses followed by the rescoring of GBVI/WSA dG. The conformations with the lowest free energies of binding were selected as the best (probable) binding modes. Molecular graphics were generated by PyMOL.

Determination of *Ex Vivo* Platelet Activation and Signaling Pathways

C57BL/6N mice were randomly divided into five groups (n = 5 each), and each group received the following treatment for 14 days: vehicle group—intragastric (i.g.) administration of normal saline (NS, 0.1 ml/10 g), and the WPs were incubated with the vehicle control (0.1% DMSO); vehicle + ADP group—i.g., administration of NS, and the WPs were stimulated with ADP (10 μM); BBR100 + ADP group—i.g., administration of BBR (100 mg/kg), and the WPs were stimulated with ADP; BBR200 + ADP group—i.g., administration of BBR (200 mg/kg), and the WPs were stimulated with ADP; Clop10 + ADP group—i.g., administration of Clop (10 mg/kg) and the WPs were stimulated with ADP.

After treatment, the PE-conjugated JON/A antibody and FITC-labeled P-selectin antibody binding of the platelets were determined by flow cytometry. The proteins were extracted, and p-Akt and GTP-Rap1 levels were determined by the pull-down assay and Western blot as described above.

Tail Bleeding Assay

The mice tail bleeding time was determined according to a method described previously with modifications (Song et al., 2019). Briefly, 30 C57BL/6N mice were randomly divided into

six groups (n = 5 each). Before drug administration, the mice were anaesthetized with 2% isoflurane inhalation, and then the tail bleeding time was determined. A 5-mm tail tip of each mouse was cut off using a surgical blade, and the transected tail tip was transferred onto a clean filter paper. The tail bleeding time was recorded every 30 s s until the bleeding completely stopped.

Twenty-five hours before the second measurement, the mice were orally administrated with BBR (200 mg/kg), Clop (10 mg/kg), Asp (100 mg/kg), BBR (200 mg/kg) + Clop (10 mg/kg), BBR (200 mg/kg) + Asp (100 mg/kg), or vehicle (1% carboxymethyl cellulose sodium). All mice were given the same volume at 0.1 ml/10 g. One hour before the second measurement, all groups' mice were given the studied compounds or the vehicle control once again in the same way as described above. One hour after the second dose administration, the mice were anaesthetized with 2% isoflurane inhalation, and then the tail bleeding time was measured again.

Carrageenan-Induced Thrombus Formation

The methods of carrageenan-induced thrombus formation in mice were performed as described previously with modifications (Li et al., 2019). Forty BALB/c mice were randomly divided into the following six groups: vehicle group (n = 5), which was i.g. administered with NS (0.1ml/10 g), vehicle + carrageenan group (n = 7), BBR 50 mg/kg + carrageenan group (n = 7), BBR 100 mg/kg + carrageenan group (n = 7), BBR 200 mg/kg + carrageenan group (n = 7), and Clop 10 mg/kg + carrageenan group (n = 7).

The treatment lasted for 12 days. On day 12, the mice in the vehicle control group were intraperitoneally (i.p.) injected with NS (50μl/10 g), while the mice in the other groups were i.p. injected with 0.5% carrageenan solution (50 μl/10 g, final dose 50 mg/kg). Two days after carrageenan injection, the mice were anaesthetized with 2% isoflurane inhalation. The tails of mice were photographed quickly; the original images of mice tail thrombosis are shown in **Supplementary Figure S4**, and both the length of thrombus in and the full length of the tails of the mice were measured using a steel ruler. The thrombosis rate of the tails of the mice was calculated by the following formula: thrombus length/whole tail length × 100.

After photography and measurement, the blood samples were collected through retro-orbital puncture, and the tails of the mice were harvested and fixed in 4% paraformaldehyde. For the tails of the mice, paraffin sections were prepared at 2, 4, and 6 cm away from the tail tips for hematoxylin and eosin (H&E) staining. The thrombus areas were calculated using Image-pro plus 6.0 (Media Cybernetics, Inc., Rockville, MD, United States) and presented as percentages of the whole mice tail vessels. The WPs were prepared, and the proteins were extracted for Western blot to detect the p-AKT/AKT level. The original scans of Western blot are shown in **Supplementary Figure S4**.

Statistical Analysis

For *in vitro* experiments, the values are expressed as mean ± standard deviation (SD) of three to five repeated experiments. For *ex vivo* and *in vivo* experiments, the values are expressed as mean ± SD of five or seven mice in each group. After validation of the test for homogeneity of variance, one-way ANOVA followed by the Newman–Keuls test for multiple comparisons was used to analyze significant differences among multiple studying groups. In all experiments, $p < 0.05$ was considered to be statistically significant.

RESULTS

BBR and M2 Inhibit Platelet Activation Induced by ADP *in vitro*

As shown in **Figure 2**, compared with the vehicle control group ($p < 0.05$, $p < 0.01$, or $p < 0.001$), the percentages of positive platelets with PE-conjugated JON/A antibody binding or FITC-conjugated P-selectin antibody binding on the surface increased significantly when platelets were stimulated by ADP. Compared with the ADP-treated platelets ($p < 0.05$ or $p < 0.01$), pretreatment with different concentrations of BBR (0.5–5.0 μM) (**Figures 2A–D**) or M2 (0.5–5.0 μM) (**Figures 2E–H**) significantly decreased the percentages of positive platelets.

The inhibitory effects of BBR and M2 on platelet activation at the same concentration were compared. Compared with the ADP group, 0.5 μM of BBR or M2 reduced the proportions of positive platelets binding to the PE-conjugated JON/A antibody by about 43.7% ($p < 0.001$) and 32.1% ($p < 0.01$), respectively (**Figures 2I,J**) and reduced the proportions of positive platelets binding to the FITC-conjugated P-selectin antibody by about 36.5% ($p < 0.001$) and 26.6% ($p < 0.01$), respectively (**Figures 2K,L**). These results indicated that both BBR and M2 could significantly inhibit platelet activation induced by ADP, and BBR has a stronger inhibitory effect on platelet activation than M2 at the same concentration ($p < 0.001$ or $p < 0.01$). As a positive control, TGX221 potently suppressed platelet activation induced by ADP, and the proportions of positive platelets almost returned to normal levels after TGX221 treatment (**Figures 2I–L**).

BBR and M2 Inhibit Fibrinogen Binding to Platelets but Have no Effect on Fibrinogen Binding to Purified Integrin αIIbβ3

As shown in **Figure 3A**, TRITC–phalloidin staining indicated that as compared to the vehicle control group, a large number of the WPs bound to coated fibrinogen after stimulation with ADP, as indicated by a significant increase of the red-stained area. BBR (0.5–5.0 μM) or M2 (0.5–5.0 μM) inhibited the binding of the platelets to fibrinogen, as indicated by an obvious reduction of the red-stained area after pretreatment. To quantitatively analyze the inhibitory effects of BBR and M2, the platelets were stained with calcein-AM, incubated with coated fibrinogen, and fluorescence intensities were determined. As shown in **Figure 3B**, as low as 0.5 μM of BBR or M2 was able to cause a significant reduction of the binding of platelets to fibrinogen ($p < 0.01$ vs ADP-induced platelets), and when the concentration of BBR or M2 reached

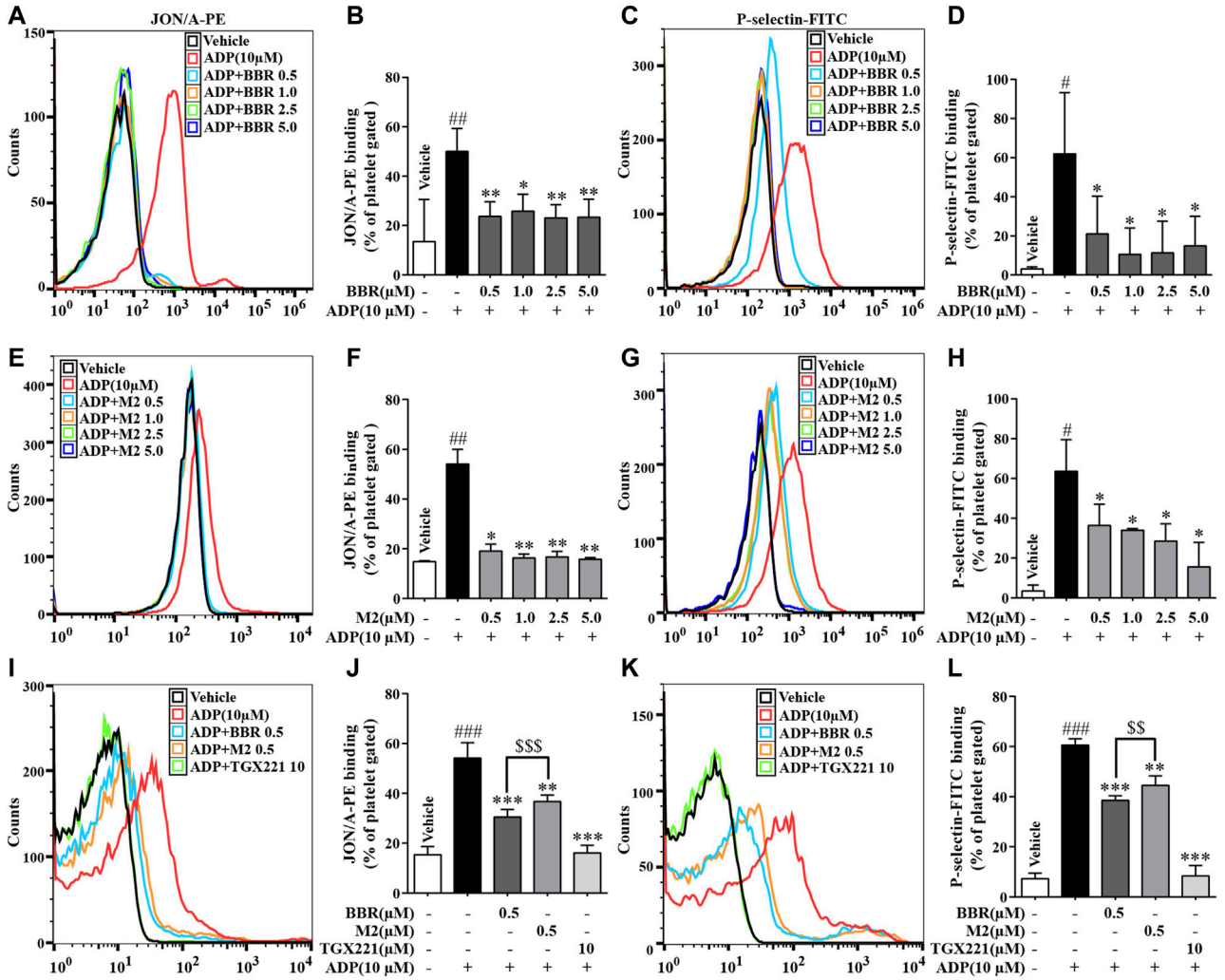

FIGURE 2 | Effects of BBR and M2 on platelet activation induced by ADP *in vitro*. The WPs were pretreated with different compounds or the vehicle control (0.1% DMSO) for 10 min and stimulated with 10 μM of ADP for 10 min. After treatment, the PE-conjugated JON/A antibody and the FITC-conjugated P-selectin antibody were used to detect the integrin αIIbβ3 active form and P-selectin expression on the platelet surface by flow cytometry. The positive platelet ratios in gated platelets were calculated and plotted as indicated. **(A-D)** The WPs were pretreated with BBR at indicated concentrations. **(E-H)** The WPs were pretreated with M2 at indicated concentrations. **(I-L)** The WPs were pretreated with BBR, M2, or TGX221 at indicated concentrations. The histograms **(A, C, E, G, I, K)** are representatives of four or five independent flow cytometry experiments, and the quantitative results **(B, D, F, H, J, L)** are expressed as their mean ± SD. Statistically significant differences compared with the vehicle control group are indicated by $^{\#}p < 0.05$, $^{\#\#}p < 0.01$, and $^{\#\#\#}p < 0.001$. Statistically significant differences compared with the ADP group are indicated by $^{*}p < 0.05$, $^{**}p < 0.01$, and $^{***}p < 0.001$, and statistically significant differences between the BBR and M2 groups are indicated by $^{\$\$}p < 0.01$, $^{\$\$\$}p < 0.001$.

5.0 μM, a greater extent of binding inhibition was observed ($p < 0.01$ or $p < 0.001$ vs ADP-induced platelets). Similar to the inhibitory effects on platelet activation, BBR exhibited a more potent effect to inhibit the binding of fibrinogen to the platelets than did M2 at the same concentration ($p < 0.05$) (**Figure 3B**).

To explore whether or not BBR and M2 could directly inhibit the binding of integrin αIIbβ3 to fibrinogen, purified αIIbβ3 was used in our experiments. As shown in **Figure 3C**, neither BBR nor M2 had any influence on the binding of fibrinogen to purified integrin αIIbβ3. For comparison, tirofiban, a positive control used in the experiments, suppressed the binding of fibrinogen to purified integrin αIIbβ3 significantly ($p < 0.001$ vs vehicle control) (**Figure 3C**).

BBR and M2 Suppress the PI3K/Akt Signaling Pathway and Inhibit Rap1 Activation Induced by ADP

As the activation of PI3K/Akt and Rap1 is crucial for ADP-induced platelet activation (Zhu et al., 2017; Stefanini and Bergmeier, 2019), the effects of BBR and M2 on these molecules were determined. As shown in **Figure 4**, compared with the vehicle control group ($p < 0.05$, $p < 0.01$, or $p < 0.001$), the phosphorylation of Akt, which reflected the activation of PI3K, and the level of GTP-Rap1 (Rap1 active form) in the platelets simultaneously increased after induction with 10 μM of ADP. BBR and M2 had no effect on the levels of total Akt and Rap1. However, compared with the ADP treatment group,

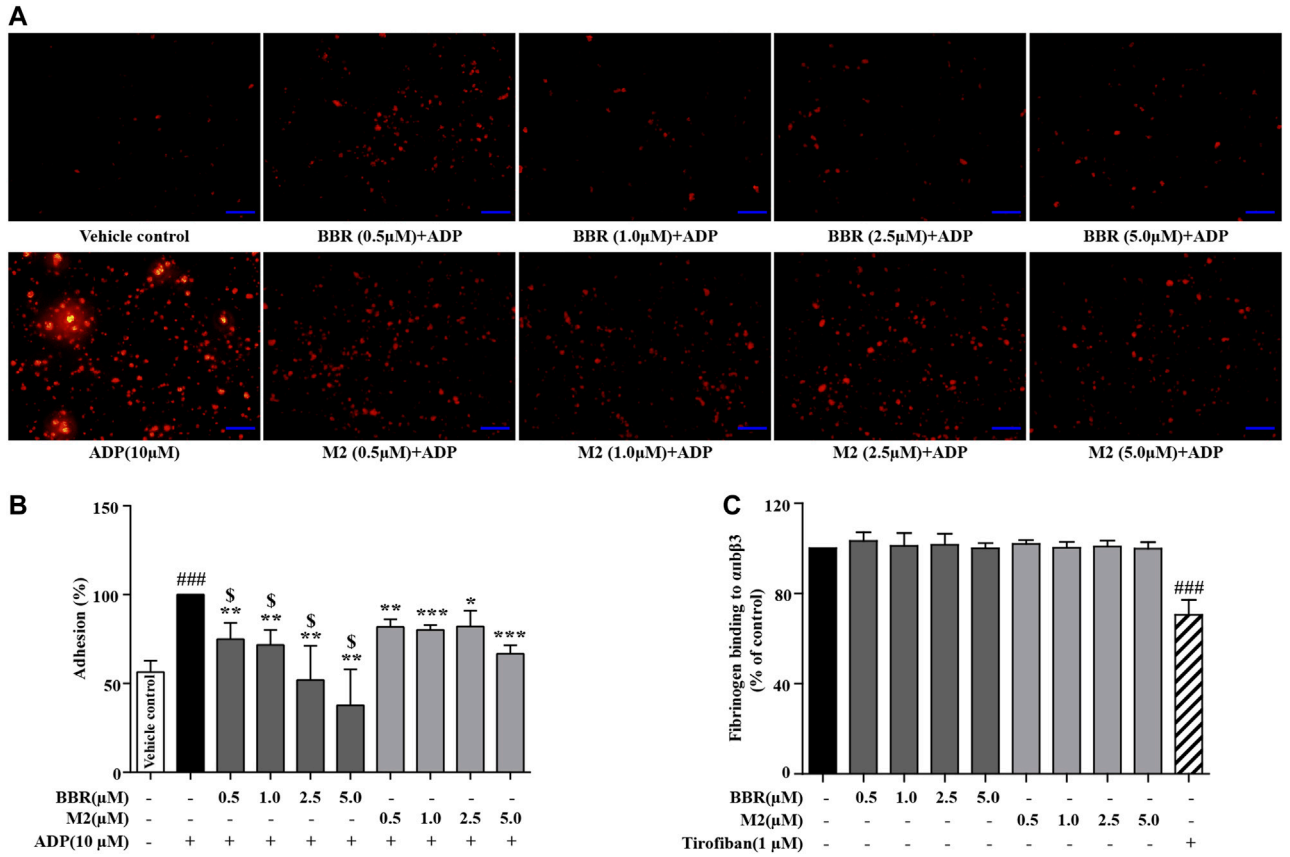

FIGURE 3 | Effects of BBR and M2 on the binding of fibrinogen to the platelets and purified αIIbβ3 *in vitro*. The WPs were pretreated with the vehicle control (0.1% DMSO), BBR, or M2 at indicated concentrations for 10 min and stimulated with 10 μM of ADP for 10 min. **(A)** The platelets were incubated with fibrinogen coated in glass coverslips and stained with TRITC–phalloidin. Images were taken using a fluorescence microscope and are presented as representative of three independent experiments (× 400, scale bar = 100 μm). **(B)** The platelets were stained with calcein-AM and incubated in glass coverslips coated with fibrinogen. The fluorescence intensities were measured for the quantification of platelet adhesion, which are plotted as percentages of the ADP group. The values are expressed as mean ± SD of three independent experiments. $^{###}p < 0.001$ vs that of the vehicle control group; $^{*}p < 0.05$, $^{**}p < 0.01$, and $^{***}p < 0.001$ vs that of the ADP group. $^{\$}p < 0.05$ vs that of the M2 group at the same concentration. **(C)** Fibrinogen was added to wells which were bound with purified αIIbβ3, together with the vehicle control, at different concentrations of BBR, M2, or 1 μM of tirofiban. After treatment, the residual fibrinogen was measured and plotted as percentages of the vehicle control. The values are expressed as mean ± SD of seven independent experiments. Statistically significant differences when compared with the vehicle control group are indicated by $^{###}p < 0.001$.

pretreatment with BBR (0.5–5.0 μM) ($p < 0.01$ or $p < 0.001$) (**Figures 4A–C**) or M2 (0.5–5.0 μM) ($p < 0.05$, $p < 0.01$, or $p < 0.001$) (**Figures 4D–F**) significantly inhibited Akt phosphorylation and reduced the GTP-Rap1 level upon ADP stimulation. Moreover, the effects of BBR were stronger than those of M2 ($p < 0.05$ or $p < 0.01$) when administered at the same concentration (**Figures 4G–I**). As a positive control, TGX221 had potent inhibitory effects on Akt phosphorylation and Rap1 activation stimulated by ADP ($p < 0.001$ vs ADP treatment group) (**Figures 4G–I**).

BBR and M2 Inhibit Rasa3 Membrane Translocation Upon ADP Stimulation

As the Rap1 GTPase-activating protein (GAP) Rasa3 was involved in the modulation of Rap1 activation in the platelets (Battram et al., 2017), the effects of BBR and M2 on Rasa3 were investigated in our experiments. As shown in **Figure 5**, compared with the vehicle control ($p < 0.05$ or $p < 0.01$), the membrane content of Rasa3 increased significantly, while that of cytosol decreased significantly after ADP stimulation, which indicated a membrane translocation of Rasa3. Different concentrations of BBR (**Figures 5A,B**) or M2 (**Figures 5C,D**) significantly inhibited the translocation of Rasa3 from the cytoplasm to membrane in the platelets upon ADP stimulation ($p < 0.05$ or $p < 0.01$ vs ADP treatment group). The inhibitory effect of BBR on Rasa3 membrane translocation was stronger than that of M2 when administered at the same concentration ($p < 0.05$) (**Figures 5E,F**). Actually, 0.5 μM of BBR showed an inhibitory effect similar to that of 100 nM of Wtm, which was used as a positive control in this experiment (**Figures 5E,F**).

BBR and M2 Are Isoform-Selective Class I PI3Kβ Inhibitors

The ADP-Glo lipid kinase systems were used to detect the influences of BBR and M2 on the activities of different class I

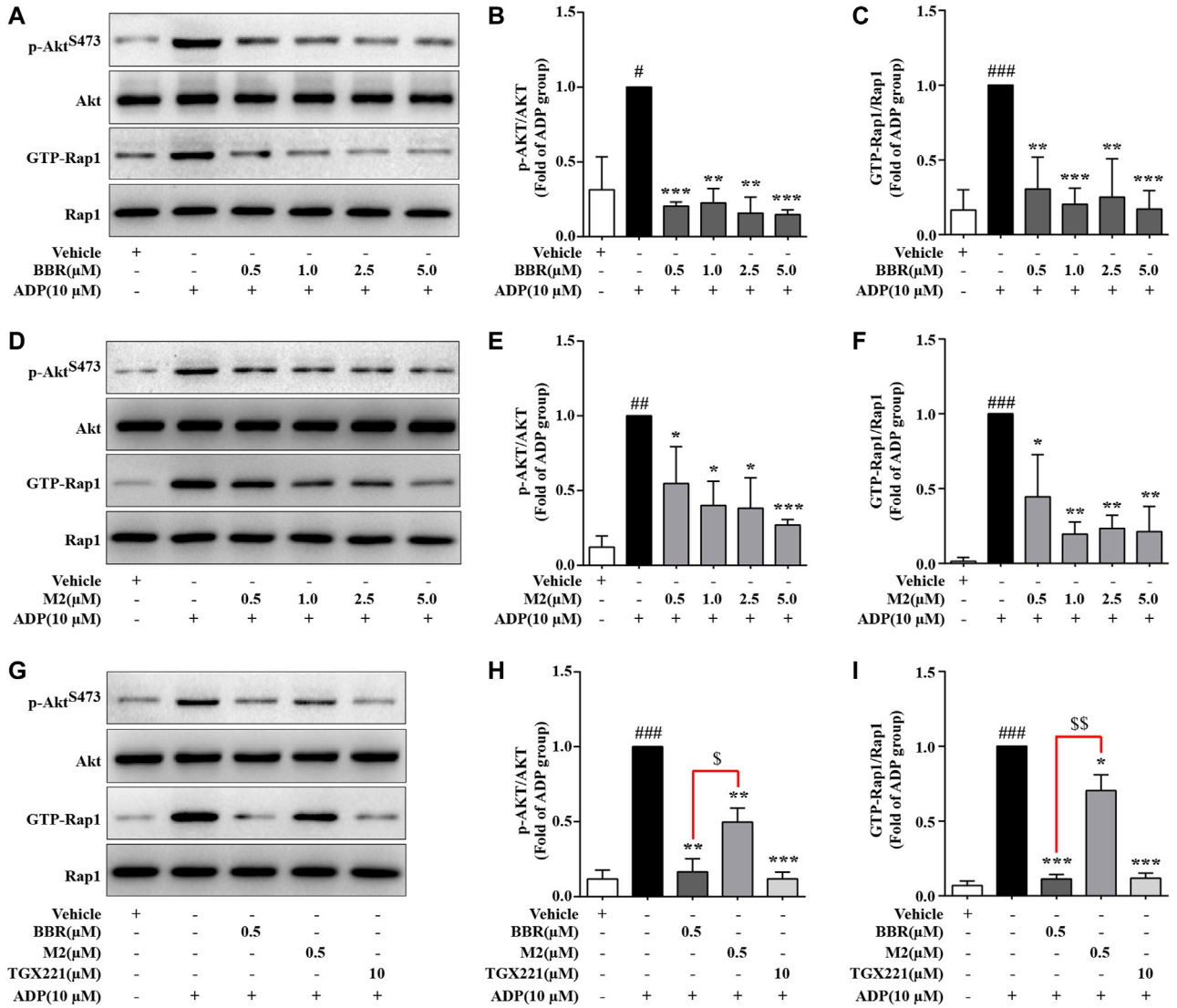

FIGURE 4 | Effects of BBR and M2 on Akt phosphorylation and Rap1 activation in ADP-stimulated platelets *in vitro*. The WPs were pretreated with the studied compounds or the vehicle control (0.1% DMSO) for 10 min and stimulated with 10 μM of ADP for 10 min. After treatment, the platelets were lysed for protein extraction and Western blot used to detect the levels of p-Akt^{S473}, Akt, and Rap1. In parallel experiments, platelet lysates were used to –pull down and detect GTP-Rap1. **(A-C)** The WPs were pretreated with BBR or the vehicle control as indicated. **(D-F)** The WPs were pretreated with M2 or the vehicle control as indicated. **(G-I)** The WPs were pretreated with BBR (0.5 μM), M2 (0.5 μM), TGX221 (10 μM), or the vehicle control as indicated. Representative blots are presented **(A, D, G)**. After quantification, the expression levels of p-Akt^{S473} and GTP-Rap1 were normalized to those of Akt and Rap1, respectively, and plotted as indicated **(B, C, E, F, H, I)**. Data are expressed as mean ± SD of three or four independent experiments. Statistically significant differences compared with the vehicle control group are indicated by $^{\#}p < 0.05$, $^{\#\#}p < 0.01$, and $^{\#\#\#}p < 0.001$. Statistically significant differences compared with the ADP group are indicated by $^{*}p < 0.05$, $^{**}p < 0.01$, and $^{***}p < 0.001$, and statistically significant differences between the BBR and M2 groups are indicated by $^{\$}p < 0.05$ and $^{\$\$}p < 0.01$.

PI3K isoforms. As shown in **Figure 6A**, both BBR and M2 significantly inhibited class I PI3Kβ activity ($p < 0.001$ vs vehicle control), and BBR had a stronger inhibitory effect than M2 when administered at the same concentration ($p < 0.05$ or $p < 0.01$). As a positive control, Wtm also potently inhibited class I PI3Kβ activity ($p < 0.001$ vs vehicle control) (**Figure 6A**).

Interestingly, neither BBR nor M2 inhibited the activities of class I PI3Kα, PI3Kγ, or PI3Kδ (**Figure 6B**), which were greatly inhibited by Wtm ($p < 0.01$ or $p < 0.001$ vs vehicle control). These results indicate that BBR and M2 are isoform-selective class I PI3Kβ inhibitors.

The class I PI3Kβ protein contains an active site and an ATP catalytic site (Zhang et al., 2011). To explore the mechanisms of BBR and M2 to inhibit class I PI3Kβ, we observed whether or not their inhibitory effects were competitively inhibited by increasing ATP concentrations. As shown in **Figures 6C,D**, the inhibitory effects of BBR and M2 on class I PI3Kβ activity were not influenced when ATP concentration increased from 6.25 to 400 μM ($p < 0.05$ or $p < 0.01$ vs vehicle control).

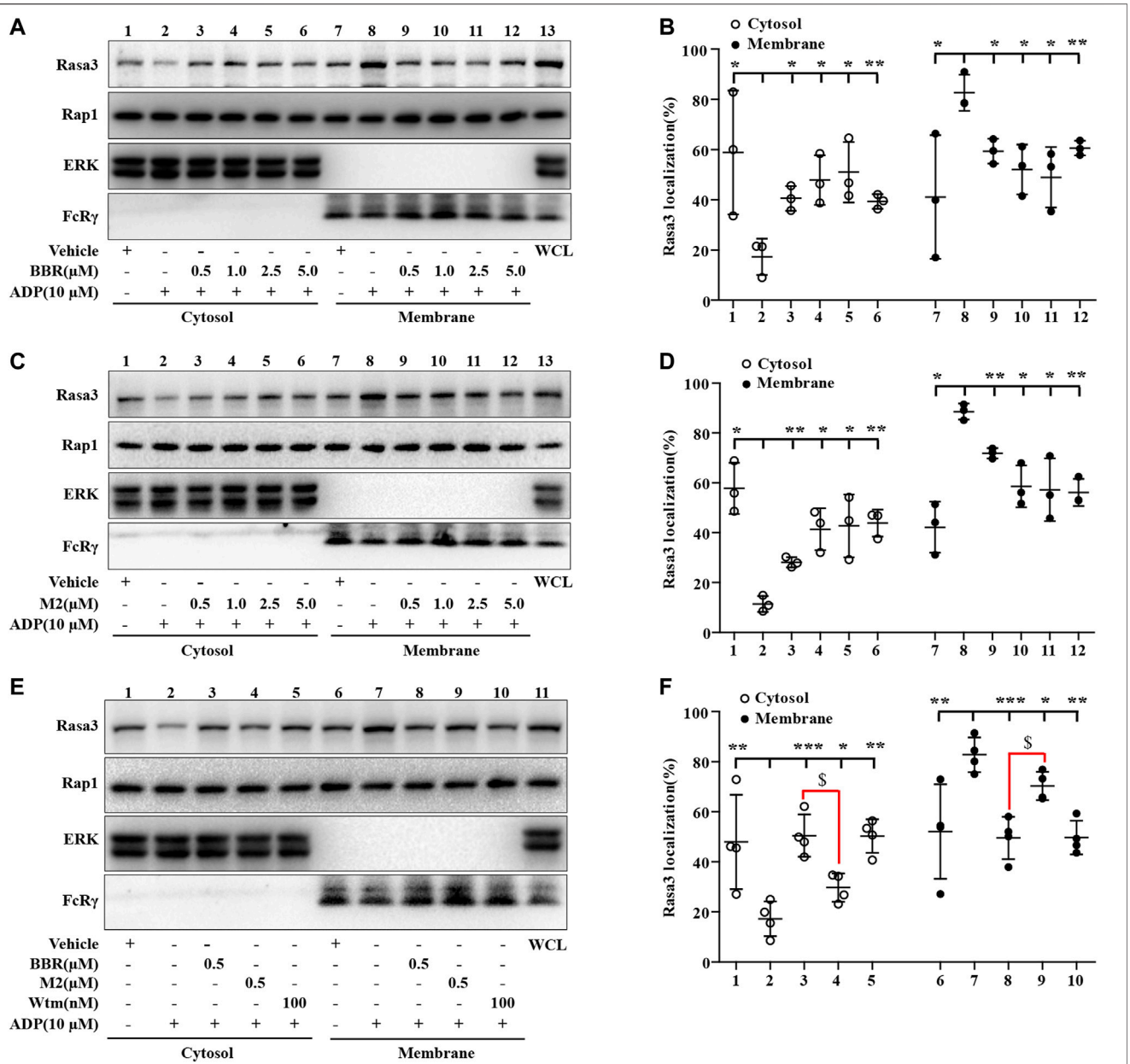

FIGURE 5 | Effects of BBR and M2 on Rasa3 membrane translocation upon ADP stimulation *in vitro*. The WPs were pretreated with the studied compounds or the vehicle control (0.1% DMSO) for 10 min, and stimulated with 10 μM of ADP for 10 min. After treatment, the cytosolic and membrane proteins were extracted for Western blot to detect Rasa3, Rap1, ERK (cytosolic control protein), and FcRγ (membrane control protein). **(A-B)** The WPs were pretreated with BBR or the vehicle control as indicated. **(C-D)** The WPs were pretreated with M2 or the vehicle control as indicated. **(E-F)** The WPs were pretreated with BBR (0.5 μM), M2 (0.5 μM), Wtm (100 nM), or the vehicle control as indicated. Representative blots are presented **(A, C, E)**. After quantification, the expression levels of cytosolic and membrane Rasa3 were normalized to those of ERK and FcRγ, respectively, and plotted as indicated **(B, D, F)**. Data are mean ± SD of three or four independent experiments. Statistically significant differences compared with ADP group are indicated by $^{*}p < 0.05$, $^{**}p < 0.01$, $^{***}p < 0.001$, and statistically significant differences between the BBR and M2 groups are indicated by $^{\$}p < 0.05$.

Then, docking simulation studies were carried out to investigate the binding modes of BBR and M2 with PI3K p110β. As known inhibitors of class I PI3Kβ, TGX211 and Wtm were used as positive controls for the active site (Marshall et al., 2015) and catalytic site (Yano et al., 1993) binding, respectively. The docking scores of BBR, M2, and TGX221 for the active site of PI3K p110β are shown in **Table 1**, which are −7.24, −6.93, and −7.88 kcal/mol, respectively. The binding mode of BBR with the active site of PI3K p110β is illustrated in **Figure 7A**. The oxygen atom of the methoxy radical of BBR, regarded as a hydrogen bond acceptor, forms a hydrogen bond with the nitrogen atom of the amino

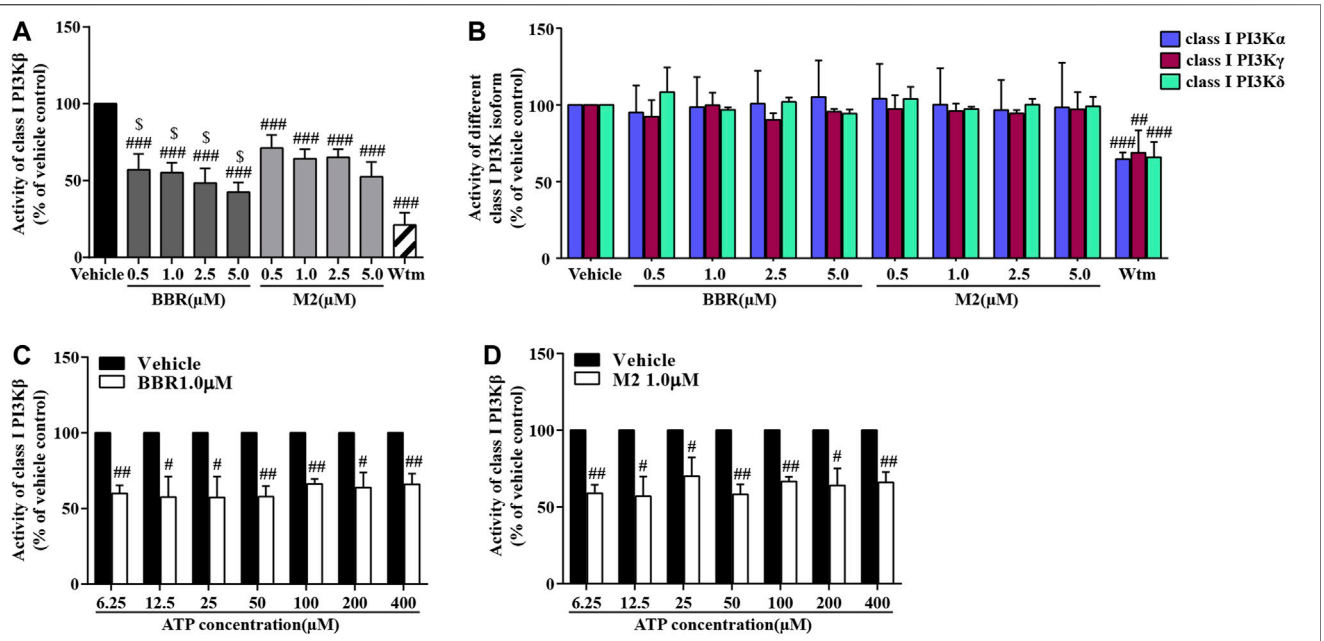

FIGURE 6 | Effects of BBR and M2 on class I PI3K activities. **(A)** After treatment with the vehicle control (0.1% DMSO), BBR, M2, or Wtm (100 nM) for 20 min, the activities of class I PI3Kβ were determined. **(B)** After treatment, the activities of class I PI3Kα, γ, and δ were determined. **(C)** After vehicle or BBR treatment, a class I PI3Kβ activity assay was performed with different concentrations of ATP for 1 h. **(D)** After the vehicle control or M2 treatment, the class I PI3Kβ activity assay was performed with different concentrations of ATP for 1 h. Data are expressed as mean ± SD of three–five independent experiments. Statistically significant differences compared with the vehicle control group are indicated by $^{\#}p < 0.05$, $^{\#\#}p < 0.01$, and $^{\#\#\#}p < 0.001$, and statistically significant differences between the BBR and M2 groups at the same concentration are indicated by $^{\$}p < 0.05$, $^{\$\$}p < 0.01$.

TABLE 1 | Docking scores of different ligands binding with PI3K p110β.

Ligand	Receptor	Docking score (kcal/mol)
BBR	PI3K p110β active site	−7.24
M2	PI3K p110β active site	−6.93
TGX211	PI3K p110β active site	−7.88
BBR	PI3K p110β catalytic site	−5.42
M2	PI3K p110β catalytic site	−5.14
Wtm	PI3K p110β catalytic site	−6.12

BBR, berberine; M2, berberrubine; Wtm, wortmannin.

group of Lys799 in the active site of PI3K p110β. The carbon atom of the dioxolane ring of BBR, regarded as a hydrogen-bond donor, forms a hydrogen bond with the sulfur atom of the thioether group of Met920 in the active site of PI3K p110β. The carbon atom of isoquinoline of BBR forms H-π conjugate with the benzene ring of Tyr833 in the active site of PI3K p110β. The binding mode of M2 with the active site of PI3K p110β is illustrated in **Figure 7B**. The carbon atom of the dioxolane ring of M2, regarded as a hydrogen-bond donor, forms a hydrogen bond with the sulfur atom of the thioether group of Met920 in the active site of PI3K p110β. The carbon atom of isoquinoline of M2 forms H-π conjugate with the benzene ring of Tyr833 in the active site of PI3K p110β. As a positive control, the binding mode of TGX211 with the active site of PI3K p110β is illustrated in **Figure 7C**. The oxygen atom of the six-membered heterocycles of TGX211, regarded as a hydrogen-bond acceptor, forms a hydrogen bond with the nitrogen atom of the amino group of Lys799 in the active site of PI3K p110β. The oxygen atom of carbonyl of TGX211, regarded as a hydrogen-bond acceptor, forms a hydrogen bond with the oxygen atom of the phenolic hydroxyl group of Tyr833 in the active site of PI3K p110β. The nitrogen atom of TGX211, regarded as a hydrogen-bond donor, forms a hydrogen bond with the sulfur atom of the thioether group of Met920 in the active site of PI3K p110β. The carbon atom TGX211 forms a H-π conjugate with the benzene ring of Tyr833 in the active site of PI3K p110β.

The docking scores of BBR, M2, and Wtm for the catalytic site of PI3K p110β are shown in **Table 1**, which are −5.42, −5.14, and −6.12 kcal/mol, respectively. The binding mode of BBR with the catalytic site of PI3K p110β is illustrated in **Figure 7D**. The carbon atom of the dioxolane ring of BBR, regarded as a hydrogen-bond donor, forms a hydrogen bond with the oxygen atom of the carboxyl group of Glu948 in the catalytic site of PI3K p110β. The binding mode of M2 with the catalytic site of PI3K p110β is illustrated in **Figure 7E**. Similar to BBR, the carbon atom of the dioxolane ring of M2, regarded as a hydrogen-bond donor, forms a hydrogen bond with the oxygen atom of the carboxyl group of Glu948 in the catalytic site of PI3K p110β. The binding mode of Wtm with the catalytic site of PI3K p110β is illustrated in **Figure 7F**. The oxygen atom of carbonyl of Wtm, regarded as a hydrogen-bond acceptor, forms hydrogen bonds with the nitrogen atoms of the backbone of Asp913 and Phe939 in the catalytic site of PI3K p110β. The carbon atom of Wtm, regarded as a hydrogen-bond donor, forms a hydrogen bond with the oxygen atom of the carboxyl group of Glu948 in the

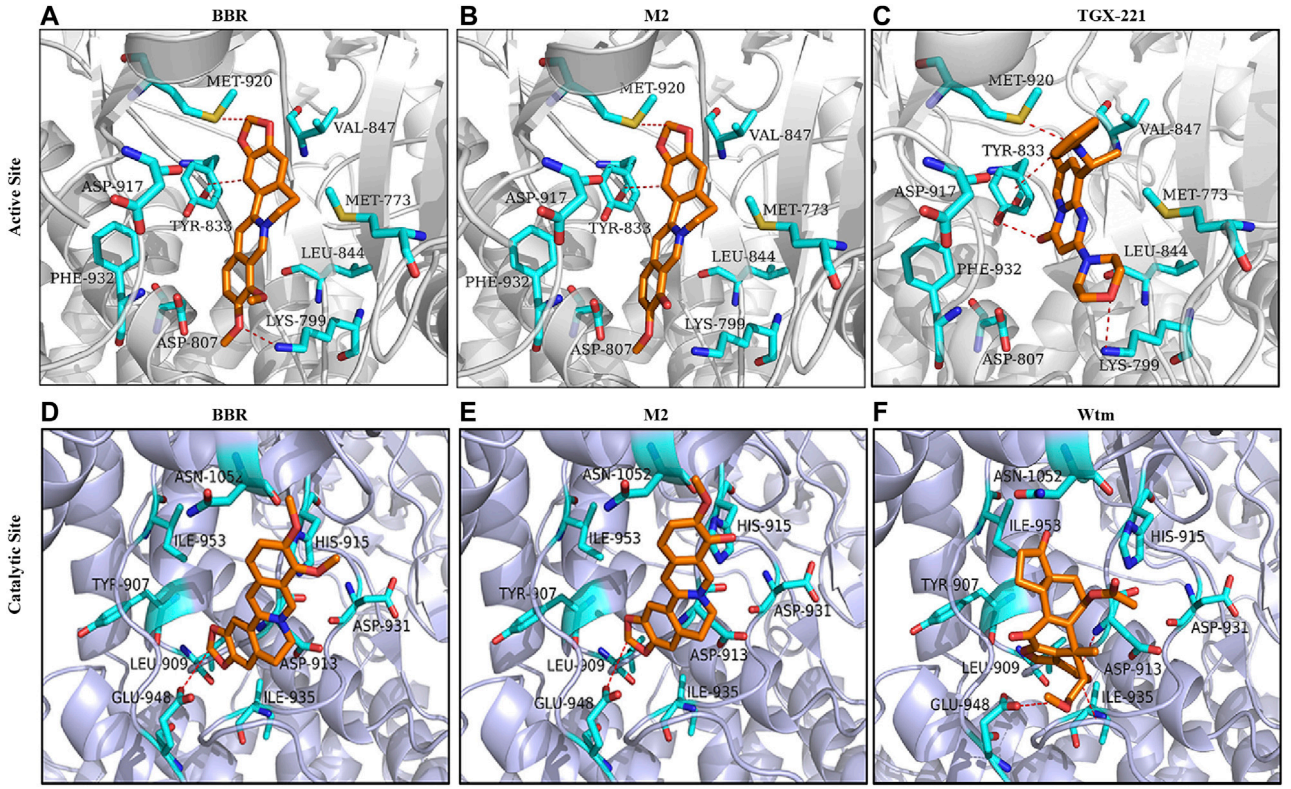

FIGURE 7 | Molecular docking. Molecular docking was performed to study the 3D binding modes of BBR and M2 with the active site **(A-B)** and the catalytic site **(D-E)** of class I PI3K p110β. The binding modes of TGX221 with the active site **(C)** and Wtm with the catalytic site **(F)** are also presented. All studied compounds are in orange, the surrounding residues in the binding pockets are in cyan, and the backbone of the receptor is depicted as grey or lavender cartoon.

catalytic site of PI3K p110β. Taken together, the computational results indicate that BBR and M2 are more likely to bind to the PI3K p110β active site rather than the catalytic site, which is in agreement with the results of the ATP competition experiment (**Figures 6C,D**).

BBR Inhibits Platelet Activation Through Suppressing the PI3K/Akt Pathway and Rap1 Activation *ex vivo*

To explore the suppressive effects of BBR on platelet activation *ex vivo*, the mice were orally administrated with 100 mg/kg or 200 mg/kg BBR for 14 days. After treatment, WPs were prepared and stimulated with 10 μM of ADP. Compared with the ADP-stimulated group ($p < 0.05$ or $p < 0.001$), 100 mg/kg and 200 mg/kg of BBR significantly reduced the process of positive platelets with PE-conjugated JON/A antibody binding (**Figures 8A,B**) or FITC-conjugated P-selectin antibody binding (**Figures 8C,D**) in a dose-dependent manner.

Compared with the ADP-stimulated group ($p < 0.01$ or $p < 0.001$), the oral treatment of BBR also inhibited the phosphorylation of Akt and suppressed Rap1 activation (**Figures 8E–G**) dose-dependently. The *ex vivo* inhibitory effects of BBR at 200 mg/kg on platelet activation (**Figures 8A–D**), Akt phosphorylation (**Figures 8E,F**), and Rap1 activation (**Figures 8E,G**) were similar to those of Clop at 10 mg/kg (Clop10), which was used as a positive control in this animal experiment.

BBR Does Not Prolong Tail Bleeding Time

As shown in **Figure 8I**, there was no statistically significant difference observed among the studied groups before treatment. After oral administration with 100 mg/kg of Asp or 10 mg/kg of Clop, the tail bleeding time in the mice was prolonged significantly as compared to the vehicle control group ($p < 0.01$). For comparison purposes, 200 mg/kg of BBR had no influence on the tail bleeding time in the mice. Moreover, when BBR was used in combination with Asp or Clop, it did not further prolong the tail bleeding time in the mice (**Figure 8I**).

BBR Suppresses Carrageenan-Induced Thrombosis

A carrageenan-induced thrombosis model was used to investigate the inhibitory effects of BBR on thrombus formation. The animal experimental scheme is shown in **Figure 9A**. After i.p. injection, carrageenan induced obvious thrombus formation in the tails of the mice (**Figure 9B**) with an average thrombosis rate of more than 80% ($p < 0.001$ vs vehicle control) (**Figure 9C**). The oral administration of BBR at 50, 100, or 200 mg/kg effectively

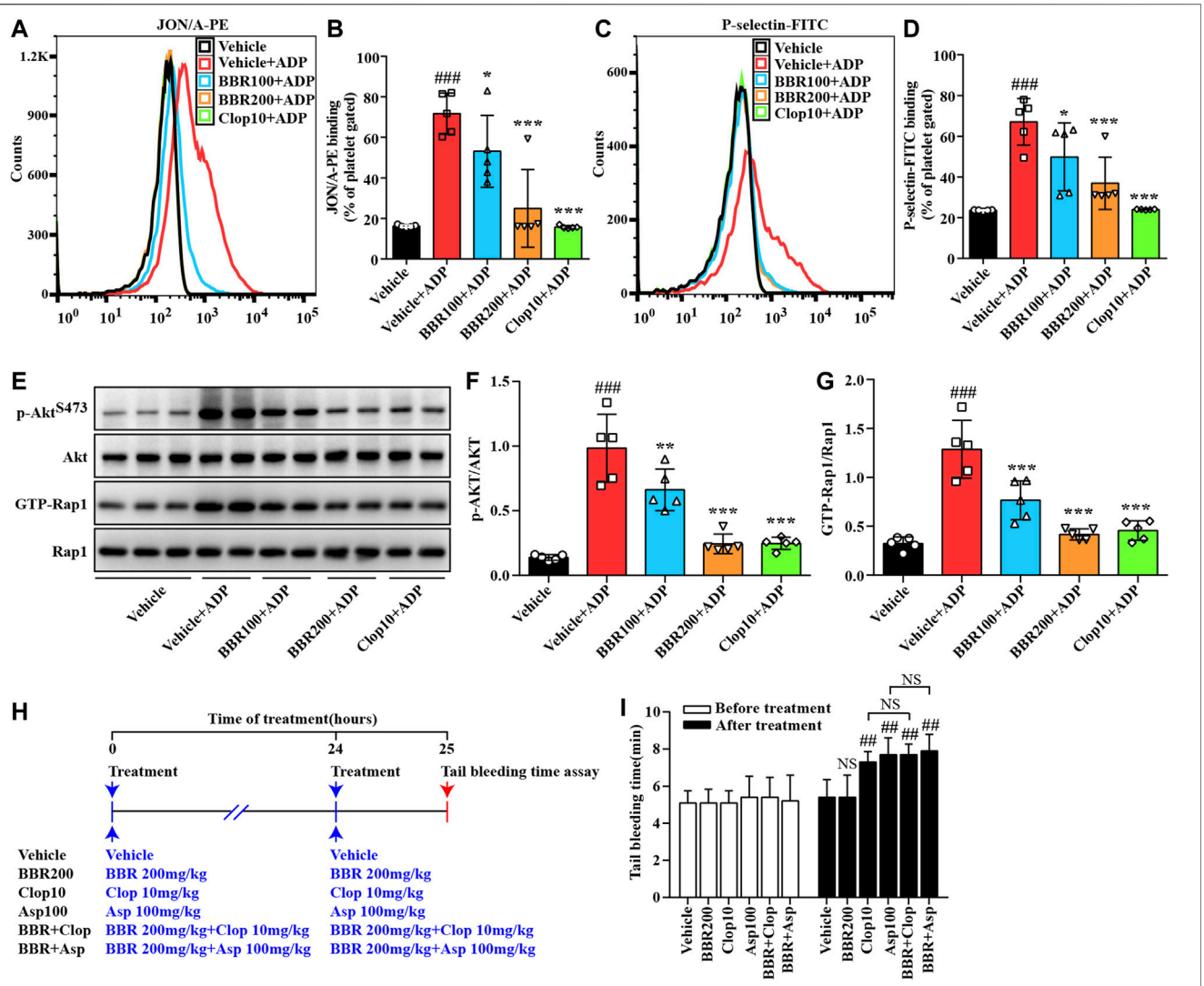

FIGURE 8 | Effects of BBR on platelet activation *ex vivo* and the tail bleeding time in mice. Twenty-five C57BL/6N mice were divided into five groups, and each group received the treatment as indicated. The WPs were prepared and treated with the vehicle control (0.1% DMSO) or ADP for 10 min, and the percent of JON/A-PE–positive platelets **(A-B)** and P-selectin-FITC–positive platelets **(C-D)** were determined by flow cytometry. Proteins were extracted for pull-down and Western blot analysis of p-Akt^{S473} and GTP-Rap1 levels **(E-G)**, which were normalized to Akt and Rap1, respectively, and plotted as indicated. Representative images of flow cytometry **(A, C)** and protein blots **(E)** are shown. For quantitative data **(B, D, F, G)**, values are expressed as mean ± SD of five mice in each group. Statistically significant differences compared with the vehicle control group are indicated by $^{###}p < 0.001$, and statistically significant differences compared with the vehicle control + ADP group are indicated by $^{*}p < 0.05$, $^{**}p < 0.01$, and $^{***}p < 0.001$. In a parallel experiment, 30 mice were divided into six groups and treated as indicated **(H)**. Before and after the treatment, the tail bleeding time was determined **(I)**. Values are expressed as mean ± SD of five mice in each group, and statistically significant differences compared with the vehicle control group are indicated by $^{##}p < 0.01$.

inhibited carrageenan-induced thrombosis (**Figure 9B**) and reduced the thrombosis rate in the tails of mice dose-dependently ($p < 0.001$ vs vehicle + carrageenan group) (**Figure 9C**). Clop at 10 mg/kg inhibited thrombus formation and reduced the thrombosis rate potently ($p < 0.001$ vs vehicle + carrageenan group), and the effects were similar to those of BBR at 200 mg/kg (**Figures 9B,C**).

The tails of the mice were subjected to pathological examination, and the results showed that in the vehicle + carrageenan group, the tail vessel lumen was almost completely occupied by thrombus (**Figure 9D**), and the percentages of the thrombus area exceeded 60% at 2, 4, and 6 cm from the tail tips ($p < 0.001$ vs vehicle control) (**Figures 9E–G**). BBR at different doses greatly reduced the thrombus area at different locations in the tails of the mice (**Figures 9D–G**). For instance, at 4-cm position from the tail tips, the thrombus area was reduced by about 29.6, 55.9, and 75.5% after receiving a low, middle, or high dose of BBR treatment, respectively ($p < 0.05$ or $p < 0.001$ vs vehicle + carrageenan group) (**Figure 9F**). Furthermore, there was no thrombus observed at the 6-cm position after different doses of BBR treatment ($p < 0.001$ vs vehicle + carrageenan group) (**Figures 9D,G**). As a positive

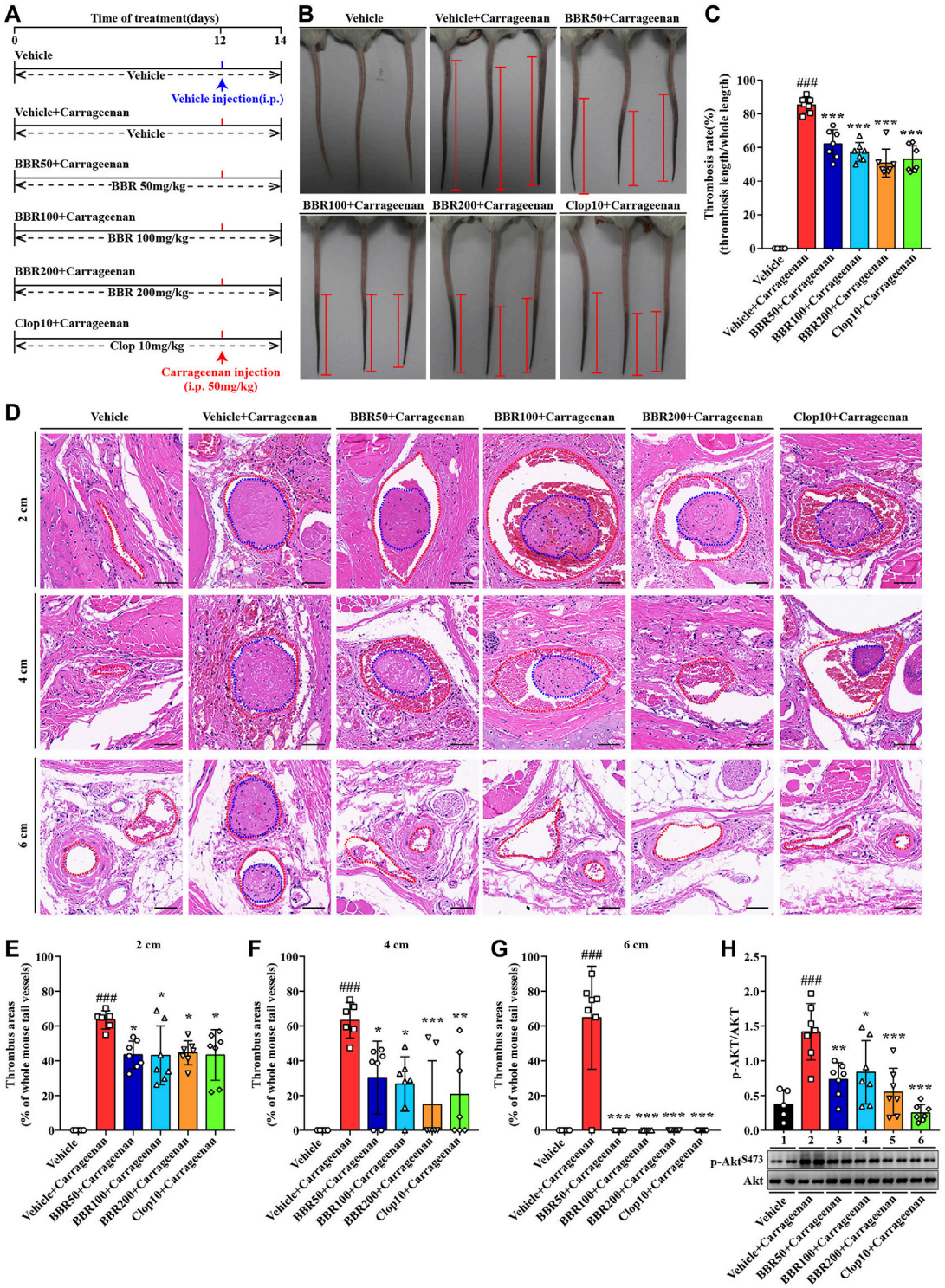

FIGURE 9 | Effects of BBR on carrageenan-induced thrombosis and Akt phosphorylation in mice. The experimental design **(A)**. Two days after carrageenan injection, the tails of the mice were photographed, and the representative images are presented **(B)**, in which the black parts in the tails of the mice are thrombus and the red segments indicate the length of thrombus. The thrombosis rate was calculated and plotted as indicated **(C)**. The mice were sacrificed, and their tails were subjected to paraffin sections at 2, 4, and 6 cm away from the tail tips. The sections were stained by H&E, and the typical images are presented **(D)** (×200, scale bar = 50 μm). The red dotted lines represent tail vessels and the blue dotted lines represent thrombi. Thrombus areas at 2, 4, and 6 cm away from the tail tips were quantified and are presented as the percentages of the whole tail vessels of the mice **(E-G)**. The WPs were used for protein extraction and Western blot analysis of the p-AKT^{S473} level **(H)**, which was normalized to Akt and plotted as indicated. Data are represented as mean ± SD of five or seven mice in each group. Statistically significant differences compared with the vehicle control group are indicated by $^{###}p < 0.001$, and statistically significant differences compared with the vehicle + carrageenan group are indicated by $^{*}p < 0.05$, $^{**}p < 0.01$, $^{***}p < 0.001$.

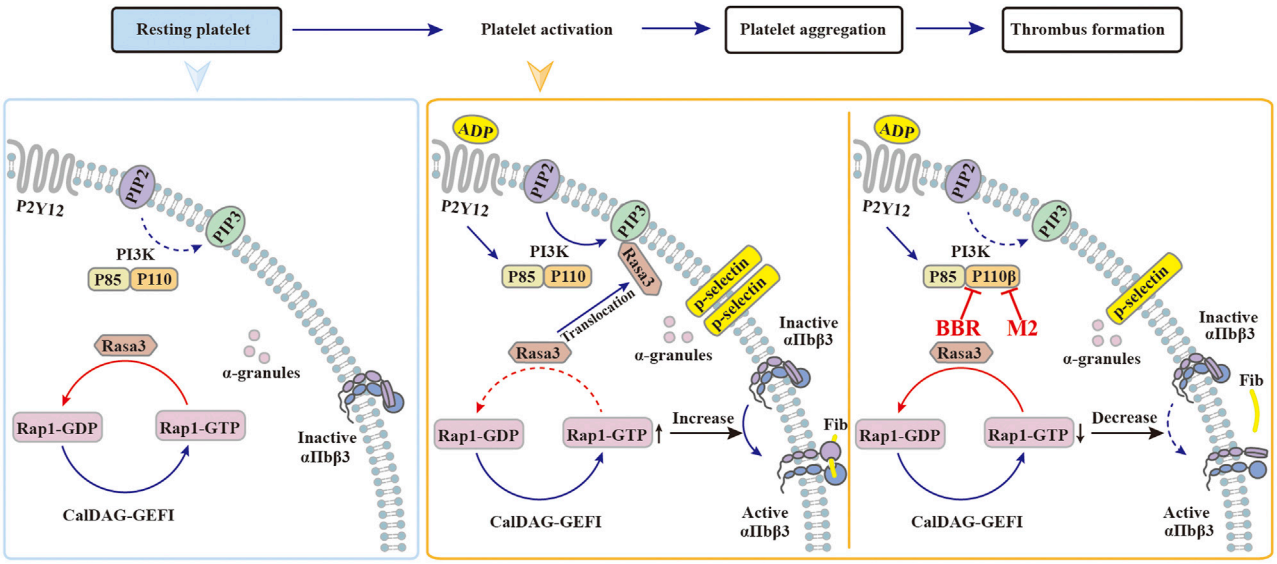

FIGURE 10 | Possible mechanisms of BBR to inhibit platelet activation. **(1)** In resting platelets, the majority of Rasa3 are located in the cytoplasm, while PI3K and CalDAG-GEFI jointly maintain the balance between GDP-Rap1 and GTP-Rap1. **(2)** When stimulated by agonists such as ADP, the PI3K signaling pathway is activated, and Rasa3 will translocate from the cytoplasm to the cell membrane, which is recruited by PIP3. As a result, the balance between GDP-Rap1 and GTP-Rap1 is broken, which causes the activation of integrin αIIbβ3 and the platelets. **(3)** When the platelets are pretreated with BBR or M2, the catalytic activity of class I PI3K p110β is inhibited. Rasa3 will not translocate to the cell membrane and will remain in the cytoplasm, which will help to maintain the balance between GDP-Rap1 and GTP-Rap1. In this manner, the integrin αIIbβ3 keeps an inactive form, and the platelet activation is inhibited by BBR or M2.

control, Clop reduced the thrombus area to an extent similar to that of BBR at 200 mg/kg (**Figures 9D–G**).

Accompanied by thrombus formation, carrageenan significantly activated the PI3K/Akt signaling pathway in the platelets, as indicated by a significant increase in the p-Akt level after injection ($p < 0.001$ vs vehicle control) (**Figure 9H**). The oral administration of BBR (50, 100, and 200 mg/kg) or Clop significantly inhibited the phosphorylation of Akt in platelets ($p < 0.05$, $p < 0.01$, or $p < 0.001$ vs vehicle + carrageenan group) (**Figure 9H**).

DISCUSSION

In this study, we report for the first time that BBR and its main metabolite M2 inhibit platelet activation through suppressing the class I PI3Kβ/Rasa3/Rap1 pathway.

The active forms of integrin αIIbβ3 and P-selectin on the platelet surface are two biomarkers of platelet activation (Bath et al., 2018; Huang et al., 2019). In our experiments, the direct evidence that BBR and M2 inhibit platelet activation was seen in the downregulation of their expression on the platelet surface upon ADP stimulation, both *in vitro* and *ex vivo*. In addition, upon stimulation with ADP or other agonists, the conformation of integrin αIIbβ3 changes from an inactive form to an active form, which lets it bind to fibrinogen in the blood and promote platelet aggregation and thrombosis. Therefore, the reduction of the binding ability of the platelets to fibrinogen is another evidence to support the inhibitory effects of BBR and M2 on platelet activation.

We found that BBR and M2 inhibited the binding of platelets to fibrinogen but did not affect the binding of purified αIIbβ3 to fibrinogen, which suggests that they might inhibit platelet activation through regulating certain intracellular signaling pathways rather than directly inhibiting integrin αIIbβ3. This inference was verified by experimental results that BBR and M2 blocked PI3K/Akt and Rap1 activation induced by ADP.

The PI3K/Akt signaling pathway is a common pathway for platelet activation and aggregation induced by a variety of agonists such as ADP, collagen, and arachidonic acid (Chu et al., 1989; Valet et al., 2016). There are many isoforms of PI3Ks which include class I PI3K (α, β, γ, δ), class II PI3Kα and β, and class III PI3K (Valet et al., 2016). Among these isoforms, only class I PI3K could catalyze the conversion of PIP2 to phosphatidylinositol-3,4,5-trisphosphate (PIP3), which is a second messenger and participated in platelet activation through binding with several target proteins (Valet et al., 2016). In this study, we found that BBR and M2 significantly inhibited the phosphorylation of Akt, both *in vitro* and *ex vivo*, which directly represented their suppressive activities on PI3K signaling. The kinase assay proved that BBR and M2 selectively inhibited class I PI3Kβ, and this was the most interesting and surprising finding in our study. In addition, the ATP competition experiment and computational simulation suggested that the target of BBR and M2 on class I PI3Kβ was probably its active site on the subunit of p100.

Upon activation, class I PI3Kβ plays a significant role in promoting Rasa3 membrane translocation, Rap1 activation, and the subsequent activation and adhesion of integrin αIIbβ3 (Su et al., 2016; Valet et al., 2016; Jackson et al., 2005), which will facilitate thrombus formation (**Figure 10**). In resting platelets, Rasa3 and the factor CalDAG-GEFI jointly balance the level of

GTP-Rap1 and GDP-Rap1 (Zhu et al., 2017). When the platelets are stimulated with agonists, Rasa3 is recruited from the cytoplasm to the cell membrane by PIP3, the dynamic balance of GTP-Rap1 and GDP-Rap1 is broken, and the level of GTP-Rap1 increases, which binds and activates integrin αIIbβ3 and finally activates platelets (**Figure 10**). Through selective inhibition of class I PI3Kβ, BBR and M2 can block Rasa3 membrane translocation, Rap1 activation, and integrin αIIbβ3 activation. Our results suggest that BBR and M2 inhibit platelet activation through suppressing the class I PI3Kβ/Rasa3/Rap1 pathway, which is summarized in **Figure 10**.

BBR is a multi-target drug, and it is proper to infer that it may suppress platelet activation through multiple mechanisms. For example, in addition to Rasa3 and Rap1, Akt (including AKT1, AKT2, and AKT3 isoforms) as a downstream molecule of PI3K may also participate in the antiplatelet activities of BBR. As previous reports have proved the deletion of the AKT1 (Chen et al., 2004) or AKT2 (Woulfe et al., 2004) gene could inhibit platelet activation and aggregation upon stimulation of various agonists *in vitro*, and the deletion of the Akt2 (Woulfe et al., 2004) or Akt3 (O'Brien et al., 2011) gene could inhibit (ferric chloride) $FeCl_3$-induced carotid artery thrombus formation *in vivo*.

In addition, according to a recent report, regulation of mitochondrial function may be a promising strategy to inhibit platelet activation (Fuentes et al., 2019). BBR is reported to have an influence on mitochondrial function (Kumar et al., 2015); therefore, its antiplatelet activities may be associated with the modulation of mitochondrial function, which merits further investigation.

We noticed that the inhibitory effects of BBR on platelet activation and the class I PI3Kβ/Rasa3/Rap1 pathway are stronger than those of M2, its main phase I metabolite. These findings agree with our previous studies, in which M2 had shown moderate BBR-like biological activities, such as low-density lipoprotein (LDLR) upregulation, insulin receptor (InsR) upregulation, and AMP-activated protein kinase (AMPK) activation (Li et al., 2010; Li et al., 2011; Wang et al., 2012). The activities of M2 on these molecular targets are approximately 59–68% of those of BBR (Li et al., 2010; Li et al., 2011; Wang et al., 2012). Due to the inner biological activities of M2, *in vivo* antiplatelet efficacies of BBR may be attributable to a combination of itself and M2, which needs further studying. In addition, whether or not other phase I metabolites of BBR have similar antiplatelet activities is unknown and needs further investigation. The clarification of the structure–activity relationship of BBR metabolites on inhibiting platelet activation is of scientific and practical significance, and relevant experiments are now ongoing in our laboratory.

The antiplatelet efficacy of BBR is translated into a suppressive activity on thrombus formation *in vivo*. In this study, we show that BBR greatly inhibits carrageenan-induced thrombosis in the tails of the mice after oral administration. Our findings are in agreement with previous reports, in which BBR suppressed thrombus formation in the inferior vena cava (Wang et al., 2018), cerebral artery (Wu and Liu, 1995), and lungs (Li et al., 1994). As a multi-target drug, BBR may suppress thrombus formation through multiple mechanisms in addition to the antiplatelet effect. For example, BBR is reported to have anticoagulant activities (Wang et al., 2017; Wang et al., 2018), and it also has protective activities on the vascular endothelium (Guo et al., 2016) and beneficial effects on hemodynamics (Xie et al., 2011). These effects of BBR may also contribute to its antithrombotic activity and support its future clinical application in the prevention or treatment of thrombotic diseases or cardiovascular/cerebrovascular events.

One of the major advantages of BBR is its good safety (Yao et al., 2015). In this study, BBR alone had no influence on the tail bleeding time in the mice, and when used in combination with Clop or Asp, it did not further prolong the tail bleeding time. This phenomenon may be explained as the following: first, the blood concentration of BBR is relatively low after oral administration and is not sufficient to cause bleeding, and second, rather than potently modulating a single target, such as other commonly used antiplatelet drugs, BBR has pleiotropic effects on a variety of targets, which will minimize its adverse effects (Kong et al., 2020). We consider that at this point, BBR may have an advantage over other antiplatelet drugs, and it is suitable for combination usage with other antiplatelet drugs in future clinical applications.

In conclusion, our studies reveal that the natural product BBR and its main metabolite M2 inhibit platelet activation through suppressing class I PI3Kβ, Rasa3 membrane translocation, and then Rap1 activation and that the antiplatelet activities of BBR are effectively converted to an antithrombotic efficacy *in vivo* without increasing the bleeding risk. These properties suggest that BBR may be a promising antiplatelet drug that can be used in the prevention or treatment of thrombotic diseases or cardiovascular/cerebrovascular events.

DATA AVAILABILITY STATEMENT

The original contributions presented in the study are included in the article/**Supplementary Material**; further inquiries can be directed to the corresponding authors.

ETHICS STATEMENT

The animal study was reviewed and approved by the Ethics Committee of the Institute of Materia Medica, Chinese Academy of Medical Sciences (CAMS) and Peking Union Medical College (PUMC).

AUTHOR CONTRIBUTIONS

CW performed the research and analyzed data. YC, YZ, HJ, ZZ, and AW participated in the animal experiments. JJ, WK, and JH conceived and designed the experiments. WK wrote the manuscript, and JJ proofread and edited the manuscript. All authors reviewed and approved the manuscript.

FUNDING

This study was supported by the CAMS Major Collaborative Innovation Project (No. 2016-I2M-1-011), the Fundamental

Research Funds for the Central Universities (2021-JYB-XJSJJ-003), and Science Fund for Creative Research Groups of the National Natural Science Foundation of China (81621064).

ACKNOWLEDGMENTS

We thank Haibo Liu from the Chinese Academy of Medical Sciences for providing the aforementioned modeling software and Wecomput Technology for providing computation consulting.

SUPPLEMENTARY MATERIAL

The Supplementary Material for this article can be found online at: https://www.frontiersin.org/articles/10.3389/fphar.2021.734603/full#supplementary-material

REFERENCES

Asada, Y., Yamashita, A., Sato, Y., and Hatakeyama, K. (2018). Thrombus Formation and Propagation in the Onset of Cardiovascular Events. *J. Atheroscler. Thromb.* 25, 653–664. doi:10.5551/jat.RV17022

Bath, P. M., May, J., and Heptinstall, S. (2018). Clinical Utility of Remote Platelet Function Measurement Using P-Selectin: Assessment of Aspirin, Clopidogrel, and Prasugrel and Bleeding Disorders. *Platelets* 29, 425–430. doi:10.1080/09537104.2018.1445839

Battram, A. M., Durrant, T. N., Agbani, E. O., Heesom, K. J., Paul, D. S., Piatt, R., et al. (2017). The Phosphatidylinositol 3,4,5-trisphosphate (PI(3,4,5)P3) Binder Rasa3 Regulates Phosphoinositide 3-kinase (PI3K)-dependent Integrin αIIbβ3 Outside-In Signaling. *J. Biol. Chem.* 292, 1691–1704. doi:10.1074/jbc.M116.746867

Binsaleh, N. K., Wigley, C. A., Whitehead, K. A., van Rensburg, M., Reynisson, J., Pilkington, L. I., et al. (2018). Thieno[2,3-b]pyridine Derivatives Are Potent Anti-platelet Drugs, Inhibiting Platelet Activation, Aggregation and Showing Synergy with Aspirin. *Eur. J. Med. Chem.* 143, 1997–2004. doi:10.1016/j.ejmech.2017.11.014

Blue, R., Murcia, M., Karan, C., Jirousková, M., and Coller, B. S. (2008). Application of High-Throughput Screening to Identify a Novel alphaIIb-specific Small-Molecule Inhibitor of alphaIIbbeta3-Mediated Platelet Interaction with Fibrinogen. *Blood* 111, 1248–1256. doi:10.1182/blood-2007-08-105544

Caron, F., and Anand, S. S. (2017). Antithrombotic Therapy in Aortic Diseases: A Narrative Review. *Vasc. Med.* 22, 57–65. doi:10.1177/1358863X16675229

Chen, Q. M., and Xie, M. Z. (1986). Studies on the Hypoglycemic Effect of Coptis Chinensis and Berberine. *Yao Xue Xue Bao* 21, 401–406. (Article in Chinese).

Chen, J., De, S., Damron, D. S., Chen, W. S., Hay, N., and Byzova, T. V. (2004). Impaired Platelet Responses to Thrombin and Collagen in AKT-1-Deficient Mice. *Blood* 104, 1703–1710. doi:10.1182/blood-2003-10-3428

Chu, Z. L., Jiang, Y. F., Wang, Z. H., Song, C. Q., and Xu, Z. P. (1989). Effects of Berberine on Platelet Aggregation and Release. *Acad. J. Second Mil. Med. Univ.* 10, 323–327. (Article in Chinese).

Deng, W., Xu, Y., Chen, W., Paul, D. S., Syed, A. K., Dragovich, M. A., et al. (2016). Platelet Clearance via Shear-Induced Unfolding of a Membrane Mechanoreceptor. *Nat. Commun.* 7, 12863. doi:10.1038/ncomms12863

Fuentes, E., Araya-Maturana, R., and Urra, F. A. (2019). Regulation of Mitochondrial Function as a Promising Target in Platelet Activation-Related Diseases. *Free Radic. Biol. Med.* 136, 172–182. doi:10.1016/j.freeradbiomed.2019.01.007

Guo, J., Wang, L., Wang, L., Qian, S., Zhang, D., Fang, J., et al. (2016). Berberine Protects Human Umbilical Vein Endothelial Cells against LPS-Induced Apoptosis by Blocking JNK-Mediated Signaling. *Evid. Based Complement. Alternat. Med.* 2016, 6983956. doi:10.1155/2016/6983956

Honda, Y., Kamisato, C., and Morishima, Y. (2016). Prevention of Arterial Thrombosis by Edoxaban, an Oral Factor Xa Inhibitor in Rats: Monotherapy and in Combination with Antiplatelet Agents. *Eur. J. Pharmacol.* 786, 246–252. doi:10.1016/j.ejphar.2016.06.011

Huang, W. M., Li, B. Z., and Yan, X. J. (1989). The Clinical and Basic Study on the Antiplatelet Aggregation Effect of Berberine. *Chin. J. Hematol.* 10, 228–230. (Article in Chinese).

Huang, Z. S., Zeng, C. L., Zhu, L. J., Jiang, L., Li, N., and Hu, H. (2010). Salvianolic Acid A Inhibits Platelet Activation and Arterial Thrombosis via Inhibition of Phosphoinositide 3-kinase. *J. Thromb. Haemost.* 8, 1383–1393. doi:10.1111/j.1538-7836.2010.03859.x

Huang, J., Li, X., Shi, X., Zhu, M., Wang, J., Huang, S., et al. (2019). Platelet Integrin αIIbβ3: Signal Transduction, Regulation, and its Therapeutic Targeting. *J. Hematol. Oncol.* 12, 26. doi:10.1186/s13045-019-0709-6

Jackson, S. P., Schoenwaelder, S. M., Goncalves, I., Nesbitt, W. S., Yap, C. L., Wright, C. E., et al. (2005). PI 3-kinase P110beta: a New Target for Antithrombotic Therapy. *Nat. Med.* 11, 507–514. doi:10.1038/nm1232

Jing, B. B., Li, Y. X., Zhang, H., Ren, S. T., Wang, M., Li, Y. P., et al. (2011). Antithrombotic Activity of Z4A5, a New Platelet Glycoprotein IIb/IIIa Receptor Antagonist Evaluated in a Rabbit Arteriovenous Shunt Thrombosis Model. *Thromb. Res.* 128, 463–469. doi:10.1016/j.thromres.2011.08.003

Kong, W., Wei, J., Abidi, P., Lin, M., Inaba, S., Li, C., et al. (2004). Berberine Is a Novel Cholesterol-Lowering Drug Working through a Unique Mechanism Distinct from Statins. *Nat. Med.* 10, 1344–1351. doi:10.1038/nm1135

Kong, W. J., Vernieri, C., Foiani, M., and Jiang, J. D. (2020). Berberine in the Treatment of Metabolism-Related Chronic Diseases: A Drug Cloud (dCloud) Effect to Target Multifactorial Disorders. *Pharmacol. Ther.* 209, 107496. doi:10.1016/j.pharmthera.2020.107496

Kumar, A., Ekavali, Chopra, K., Mukherjee, M., Pottabathini, R., and Dhull, D. K. (2015). Current Knowledge and Pharmacological Profile of Berberine: An Update. *Eur. J. Pharmacol.* 761, 288–297. doi:10.1016/j.ejphar.2015.05.068

Li, S. X., Zhu, Y. C., Liu, Y. H., Li, S. F., and Zhou, S. J. (1994). The Effects of Berberine on Experimental Mice Thrombosis. *Henan Med. Res.* 3, 43–45. (Article in Chinese).

Li, Y. H., Li, Y., Yang, P., Kong, W. J., You, X. F., Ren, G., et al. (2010). Design, Synthesis, and Cholesterol-Lowering Efficacy for Prodrugs of Berberrubine. *Bioorg. Med. Chem.* 18, 6422–6428. doi:10.1016/j.bmc.2010.06.106

Li, Y., Ren, G., Wang, Y. X., Kong, W. J., Yang, P., Wang, Y. M., et al. (2011). Bioactivities of Berberine Metabolites after Transformation through CYP450 Isoenzymes. *J. Transl. Med.* 9, 62. doi:10.1186/1479-5876-9-62

Li, Q., Chen, Y., Zhao, D., Yang, S., Zhang, S., Wei, Z., et al. (2019). LongShengZhi Capsule Reduces Carrageenan-Induced Thrombosis by Reducing Activation of Platelets and Endothelial Cells. *Pharmacol. Res.* 144, 167–180. doi:10.1016/j.phrs.2019.04.013

Marshall, A. J., Lill, C. L., Chao, M., Kolekar, S. V., Lee, W. J., Marshall, E. S., et al. (2015). Exploring the Isoform Selectivity of TGX-221 Related Pyrido[1,2-A] pyrimidinone-Based Class IA PI 3-kinase Inhibitors: Synthesis, Biological Evaluation and Molecular Modelling. *Bioorg. Med. Chem.* 23, 3796–3808. doi:10.1016/j.bmc.2015.03.073

Mega, J. L., and Simon, T. (2015). Pharmacology of Antithrombotic Drugs: an Assessment of Oral Antiplatelet and Anticoagulant Treatments. *Lancet* 386, 281–291. doi:10.1016/S0140-6736(15)60243-4

National Pharmacopoeia Committee (2015). "Berberine Hydrochloride and Berberine Hydrochloride Tablets," in *National Pharmacopoeia Committee, Pharmacopoeia of People's Republic of China/Part II*. Beijing: Chemical Industry Press, 875–876.

O'Brien, K. A., Stojanovic-Terpo, A., Hay, N., and Du, X. (2011). An Important Role for Akt3 in Platelet Activation and Thrombosis. *Blood* 118, 4215–4223. doi:10.1182/blood-2010-12-323204

Patrono, C., Morais, J., Baigent, C., Collet, J. P., Fitzgerald, D., Halvorsen, S., et al. (2017). Antiplatelet Agents for the Treatment and Prevention of Coronary Atherothrombosis. *J. Am. Coll. Cardiol.* 70, 1760–1776. doi:10.1016/j.jacc.2017.08.037

Pirillo, A., and Catapano, A. L. (2015). Berberine, a Plant Alkaloid with Lipid- and Glucose-Lowering Properties: From *In Vitro* Evidence to Clinical Studies. *Atherosclerosis* 243, 449–461. doi:10.1016/j.atherosclerosis.2015.09.032

Song, W., Ma, Y. Y., Miao, S., Yang, R. P., Zhu, Y., Shu, D., et al. (2019). Pharmacological Actions of Miltirone in the Modulation of Platelet Function. *Acta Pharmacol. Sin.* 40, 199–207. doi:10.1038/s41401-018-0010-1

Stefanini, L., and Bergmeier, W. (2019). RAP GTPases and Platelet Integrin Signaling. *Platelets* 30, 41–47. doi:10.1080/09537104.2018.1476681

Su, X. L., Su, W., Wang, Y., Wang, Y. H., Ming, X., and Kong, Y. (2016). The Pyrrolidinoindoline Alkaloid Psm2 Inhibits Platelet Aggregation and Thrombus Formation by Affecting PI3K/Akt Signaling. *Acta Pharmacol. Sin.* 37, 1208–1217. doi:10.1038/aps.2016.52

Tan, X. S., Ma, J. Y., Feng, R., Ma, C., Chen, W. J., Sun, Y. P., et al. (2013). Tissue Distribution of Berberine and its Metabolites after Oral Administration in Rats. *PLoS One* 8, e77969. doi:10.1371/journal.pone.0077969

Thomas, H., Diamond, J., Vieco, A., Chaudhuri, S., Shinnar, E., Cromer, S., et al. (2018). Global Atlas of Cardiovascular Disease 2000-2016: The Path to Prevention and Control. *Glob. Heart* 13, 143–163. doi:10.1016/j.gheart.2018.09.511

Valet, C., Severin, S., Chicanne, G., Laurent, P. A., Gaits-Iacovoni, F., Gratacap, M. P., et al. (2016). The Role of Class I, II and III PI 3-kinases in Platelet Production and Activation and Their Implication in Thrombosis. *Adv. Biol. Regul.* 61, 33–41. doi:10.1016/j.jbior.2015.11.008

Verma, D., Kumar, R., Pereira, R. S., Karantanou, C., Zanetti, C., Minciacchi, V. R., et al. (2019). Vitamin K Antagonism Impairs the Bone Marrow Microenvironment and Hematopoiesis. *Blood* 134, 227–238. doi:10.1182/blood.2018874214

Wang, Y. X., Kong, W. J., Li, Y. H., Tang, S., Li, Z., Li, Y. B., et al. (2012). Synthesis and Structure-Activity Relationship of Berberine Analogues in LDLR Up-Regulation and AMPK Activation. *Bioorg. Med. Chem.* 20, 6552–6558. doi:10.1016/j.bmc.2012.09.029

Wang, C., Jiang, J. D., Wu, W., and Kong, W. J. (2016). The Compound of Mangiferin-Berberine Salt Has Potent Activities in Modulating Lipid and Glucose Metabolisms in HepG2 Cells. *Biomed. Res. Int.* 2016, 8753436. doi:10.1155/2016/8753436

Wang, X., Zhang, Y., Yang, Y., Wu, X., Fan, H., and Qiao, Y. (2017). Identification of Berberine as a Direct Thrombin Inhibitor from Traditional Chinese Medicine through Structural, Functional and Binding Studies. *Sci. Rep.* 7, 44040. doi:10.1038/srep44040

Wang, C., Wu, Y.-B., Wang, A.-P., Jiang, J.-D., and Kong, W.-J. (2018). Evaluation of Anticoagulant and Antithrombotic Activities of Berberine: a Focus on the Ameliorative Effect on Blood Hypercoagulation. *Int. J. Pharmacol.* 14, 1087–1098. doi:10.3923/ijp.2018.1087.1098

Woulfe, D., Jiang, H., Morgans, A., Monks, R., Birnbaum, M., and Brass, L. F. (2004). Defects in Secretion, Aggregation, and Thrombus Formation in Platelets from Mice Lacking Akt2. *J. Clin. Invest.* 113, 441–450. doi:10.1172/JCI20267

Wu, J. F., and Liu, T. P. (1995). Effects of Berberine on Platelet Aggregation and Plasma Levels of TXB2 and 6-Keto-PGF1 Alpha in Rats with Reversible Middle Cerebral Artery Occlusion. *Yao Xue Xue Bao* 30, 98–102. (Article in Chinese).

Xie, X., Meng, X., Zhou, X., Shu, X., and Kong, H. (2011). Research on Therapeutic Effect and Hemorrheology Change of Berberine in New Diagnosed Patients with Type 2 Diabetes Combining Nonalcoholic Fatty Liver Disease. *Zhongguo Zhong Yao Za Zhi* 36, 3032–3035. (Article in Chinese). doi:10.4268/cjcmm20112127

Yano, H., Nakanishi, S., Kimura, K., Hanai, N., Saitoh, Y., Fukui, Y., et al. (1993). Inhibition of Histamine Secretion by Wortmannin through the Blockade of Phosphatidylinositol 3-kinase in RBL-2H3 Cells. *J. Biol. Chem.* 268, 25846–25856. doi:10.1016/s0021-9258(19)74466-4

Yao, J., Kong, W., and Jiang, J. (2015). Learning from Berberine: Treating Chronic Diseases through Multiple Targets. *Sci. China Life Sci.* 58, 854–859. doi:10.1007/s11427-013-4568-z

Zhang, H., Wei, J., Xue, R., Wu, J. D., Zhao, W., Wang, Z. Z., et al. (2010). Berberine Lowers Blood Glucose in Type 2 Diabetes Mellitus Patients through Increasing Insulin Receptor Expression. *Metabolism* 59, 285–292. doi:10.1016/j.metabol.2009.07.029

Zhang, X., Vadas, O., Perisic, O., Anderson, K. E., Clark, J., Hawkins, P. T., et al. (2011). Structure of Lipid Kinase P110β/p85β Elucidates an Unusual SH2-Domain-Mediated Inhibitory Mechanism. *Mol. Cel.* 41, 567–578. doi:10.1016/j.molcel.2011.01.026

Zhu, L., Yang, J., Bromberger, T., Holly, A., Lu, F., Liu, H., et al. (2017). Structure of Rap1b Bound to Talin Reveals a Pathway for Triggering Integrin Activation. *Nat. Commun.* 8, 1744. doi:10.1038/s41467-017-01822-8

Zou, K., Li, Z., Zhang, Y., Zhang, H. Y., Li, B., Zhu, W. L., et al. (2017). Advances in the Study of Berberine and its Derivatives: a Focus on Anti-inflammatory and Anti-tumor Effects in the Digestive System. *Acta Pharmacol. Sin.* 38, 157–167. doi:10.1038/aps.2016.125

Conflict of Interest: The authors declare that the research was conducted in the absence of any commercial or financial relationships that could be construed as a potential conflict of interest.

Publisher's Note: All claims expressed in this article are solely those of the authors and do not necessarily represent those of their affiliated organizations, or those of the publisher, the editors, and the reviewers. Any product that may be evaluated in this article, or claim that may be made by its manufacturer, is not guaranteed or endorsed by the publisher.

Copyright © 2021 Wang, Cheng, Zhang, Jin, Zuo, Wang, Huang, Jiang and Kong. This is an open-access article distributed under the terms of the Creative Commons Attribution License (CC BY). The use, distribution or reproduction in other forums is permitted, provided the original author(s) and the copyright owner(s) are credited and that the original publication in this journal is cited, in accordance with accepted academic practice. No use, distribution or reproduction is permitted which does not comply with these terms.

frontiers in Pharmacology

REVIEW
published: 15 October 2021
doi: 10.3389/fphar.2021.759220

Bioactivities and Structure–Activity Relationships of Fusidic Acid Derivatives: A Review

*Junjun Long, Wentao Ji, Doudou Zhang, Yifei Zhu and Yi Bi**

School of Pharmacy, Key Laboratory of Molecular Pharmacology and Drug Evaluation, Ministry of Education, Collaborative Innovation Center of Advanced Drug Delivery System and Biotech Drugs in Universities of Shandong, Yantai University, Yantai, China

Fusidic acid (FA) is a natural tetracyclic triterpene isolated from fungi, which is clinically used for systemic and local *staphylococcal* infections, including methicillin-resistant *Staphylococcus aureus* and coagulase-negative *staphylococci* infections. FA and its derivatives have been shown to possess a wide range of pharmacological activities, including antibacterial, antimalarial, antituberculosis, anticancer, tumor multidrug resistance reversal, anti-inflammation, antifungal, and antiviral activity *in vivo* and *in vitro*. The semisynthesis, structural modification and biological activities of FA derivatives have been extensively studied in recent years. This review summarized the biological activities and structure–activity relationship (SAR) of FA in the last two decades. This summary can prove useful information for drug exploration of FA derivatives.

Keywords: fusidic acid, biological activities, structure-activity relationship, tetracyclic triterpene, antimicrobial

OPEN ACCESS

Edited by:
Andres Trostchansky, Universidad de la República, Uruguay

Reviewed by:
Mohamed Abdo Rizk, Mansoura University, Egypt
Sadia Sultan, Universiti Teknologi MARA Puncak Alam, Malaysia

****Correspondence:***
Yi Bi
beeyee_413@163.com

Specialty section:
This article was submitted to Experimental Pharmacology and Drug Discovery, a section of the journal Frontiers in Pharmacology

Received: *16 August 2021*
Accepted: *27 September 2021*
Published: *15 October 2021*

Citation:
Long J, Ji W, Zhang D, Zhu Y and Bi Y (2021) Bioactivities and Structure–Activity Relationships of Fusidic Acid Derivatives: A Review. Front. Pharmacol. 12:759220. doi: 10.3389/fphar.2021.759220

1 INTRODUCTION

Over the past 40 years, more than half of the new chemical entities approved for the treatment of various diseases have originated from unmodified natural products, their semi-synthetic derivatives, or synthetic biological analogs (Newman and Cragg, 2020). Natural products are rich in structural types and have a wide range of biological activities, and are the main source for the discovery of new chemical entities and lead compounds (Chen et al., 2017; Agarwal et al., 2020). Thus, natural products have long been regarded as important sources in drug design, especially for drugs for cancer and infectious diseases (Brown et al., 2014; Rodrigues et al., 2016; Agarwal et al., 2020). Furthermore, almost all-important natural products, such as terpenes, alkaloids, sesquiterpenes, and sugars, can be produced by fungi (Aly et al., 2011; Singh et al., 2019).

Fusidic acid (FA) is a tetracyclic triterpenoids isolated from fungi, which was first isolated from *Fusidium coccineum* in 1960 (Godtfredsen WO. et al., 1962; Godtfredsen W. O. et al., 1962). FA binds to elongation factor G (EF-G) as an inhibitor of protein synthesis (Yamaki, 1965; Kinoshita et al., 1968). Since 1962, FA has been clinically used for systemic and local *staphylococcal* infections, including methicillin-resistant *Staphylococcus aureus* (MRSA) and coagulase-negative *staphylococci* infections (Godtfredsen WO. et al., 1962; Zhao et al., 2013). FA has been widely used throughout Europe, Australia, China, India, and other countries. There are many reasons why FA is not approved by USFDA, especially in funds and laws (Fernandes and Pereira, 2011). At present, FA is being promoted for approval in the United States market by Cempra Pharmaceuticals (ClinicalTrials.gov, 2020).

FA and its derivatives have been shown to possess a wide range of pharmacological activities, including antibacterial (Godtfredsen W. O. et al., 1962), antiparasitic (Gupta et al., 2013; Salama

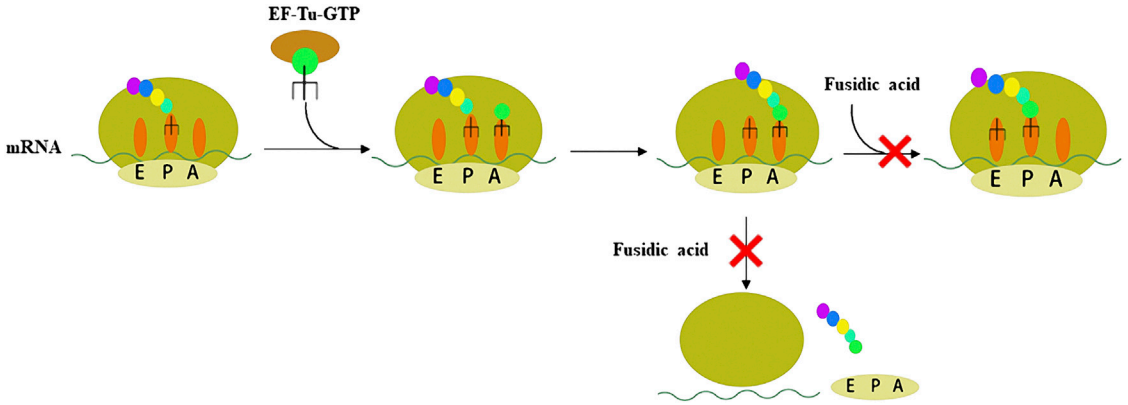

FIGURE 1 | Schematic representation of the two steps of peptide synthesis that FA blocks by binding to the EF-G-GDP complex.

et al., 2013), antituberculosis (Cicek-Saydam et al., 2001), anticancer (Ni et al., 2019), tumor multidrug resistance (MDR) reversal (Guo et al., 2019), anti-inflammation (Kilic et al., 2002), antifungal (Bi et al., 2020), and antiviral activity (Liu et al., 2019) *in vivo* and *in vitro*. However, there is no review on the semisynthesis, biological activities, and structure–activity relationship (SAR) studies of FA derivatives in the last 2 decades. This review summarized the semisynthesis, modification and bioactivities of FA derivatives. The SARs of FA and its derivatives in antibacterial, antiparasitic, antituberculosis, antitumor and tumor MDR reversal were summarized. This review provides useful information for the development of FA derivatives and gives a direction for further inspiration to enrich its structures with good pharmacological activities.

2 THE BIOLOGICAL ACTIVITIES AND STRUCTURE–ACTIVITY RELATIONSHIPS OF FA

2.1 Antimicrobial Activity

2.1.1 Anti-Gram-Positive Bacterial Activity

Resistance to antibiotic is a major obstacle to treating bacterial infection (Centers for Disease Control and Prevention, 2019). Therefore, antibiotics with novel mechanisms of action and low drug-resistance to bacteria are needed. FA acts on EF-G, which is the only antibiotic that acts on this target. There are four stages of protein synthesis in bacteria: initiation, extension, translocation, and recycling (**Figure 1**, Fernandes, 2016). Translocation is catalyzed by EF-G with GTPase activity. FA forms a stable complex with EF-G-GTP hydrolysate (EF-G-GDP), which causes the translocation to be blocked (Bodley et al., 1969; Belardinelli and Rodnina, 2017). Another function of EF-G is to split the terminated ribosome with the help of ribosome releasing factor, and then the next mRNA translation can occur, so FA also blocks the recycling stage (Savelsbergh et al., 2009; Wilson, 2014). In other words, FA blocks the translocation and recycling stages of protein synthesis, thereby killing bacteria through this mechanism. Additionally, FA lacks appreciable cross-resistance with other antibiotics, which is mainly attributed to the particular mechanism of action of FA (Borg et al., 2015).

According to previous metabolism studies of FA, the sodium salt of FA is well absorbed after oral administration with a bioavailability higher than 90%, and the FA binds highly and reversibly to protein (Turnidge, 1999; Still et al., 2011). Because of the high protein binding rate of FA, hyperbilirubinemia or jaundice is one of the main side effects of FA (Rieutord et al., 1995; Lapham et al., 2016). Many FA derivatives have been synthesized to develop antibiotics with better pharmacokinetic and pharmacodynamic profiles.

In 1979, Daehne et al. have synthesized more than 150 FA analogs, including modifications to the skeleton, the A, B, C, and D rings, and the side chains of FA, but the antibacterial activity of most of these derivatives was reduced or even completely abolished. The activity of a few compounds was maintained or enhanced, including derivatives with saturation of the delta-24 (25) double bond (**1**), substitution of the 16α-acetoxy by other groups (**2**), and conversion of the 11-OH to the corresponding ketone group (**3**) (Daehne et al., 1979).

Duvold et al. saturated the delta-17 (20) double bond of FA and obtained four stereoisomers, of which only 17(*S*),20(*S*)-dihydro-FA had the same potency as natural FA. This result indicated the necessity for the correct orientation and conformation of the side chains in a limited bioactive space for antimicrobial activity (Duvold et al., 2001). Subsequently, this group introduced a spiro-cyclopropane system in the delta-17 (20) double bond, and successfully synthesized 17(*S*),20(*S*)-methano-FA (**4**) (**Figure 2**), which exhibited the same activity against several Gram-positive bacteria as FA. This result further showed the importance of the side chains of FA for antimicrobial activity (Duvold et al., 2003).

In 2006, to clarify the interaction between FA and its receptor EF-G, Riber et al. developed three photoaffinity-labeled FA derivatives with the minimum inhibitory concentration (MIC) values of 0.016–4 μg/ml. (Riber et al., 2006). In 2007, Schou et al. have synthesized two radiolabeled photolabile FA analogs. These

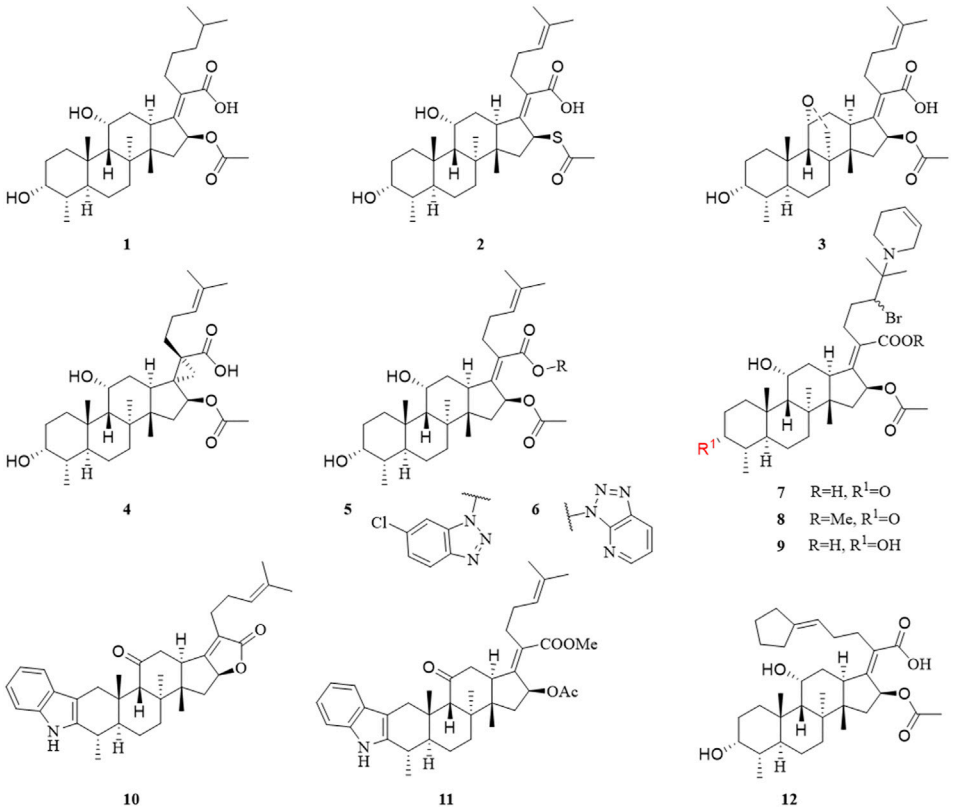

FIGURE 2 | Structural formulae of compounds **1–12**.

derivatives are potential tools for revealing the interaction between FA and EF-G (Schou et al., 2007).

In 2018, Salimova et al. synthesized some cyanoethyl derivatives of FA, which were screened primarily *in vitro*. Modification of FA with cyanoethyl fragments did not increase the activity, which is consistent with the previously summarized SAR (Salimova et al., 2018). Lu et al. have designed and synthesized 14 derivatives that blocked the metabolic sites (3-OH and 21-COOH) of FA, six of which had good antibacterial activity, MIC values of compounds **5** and **6** were less than 0.25 μg/ml; however, this result was contrary to previously SAR studies of the 21-COOH, as summarized by Daehne et al. Pharmacokinetic experiments were also performed, compounds **5** and **6** released FA *in vivo*, and their half-life was longer than that of FA. These derivatives provided a new concept for the structural modification of FA, with a triazole ring introduced at the 21-COOH. The activity of these FA derivatives was maintained, indicating that this was a new route to obtain long-lasting and effective antibiotics by structural modification (Daehne et al., 1979; Lu et al., 2019).

Shakurova et al. synthesized three quaternary pyridinium salts and tetrahydropyridine derivatives (**7**, **8**, and **9**) of FA using an effective one-pot method, but after antimicrobial screening, the results showed that there was no inhibitory activity against the tested strains when the concentration of the derivatives was 32 μg/ml (Shakurova et al., 2019). In 2020, Salimova et al. synthesized two new indole derivatives (**10** and **11**) of FA by the Fischer reaction. The antimicrobial activity of the derivatives was tested against MRSA (strain ATCC 43300), and the compounds showed comparable activity to FA (Salimova et al., 2020).

Chavez et al. have synthesized 14 FA analogs, compound **12** has equivalent potency against clinical isolates of *Staphylococcus aureus* and *Enterococcus faecium* as well as an improved resistance profile *in vitro* when compared to FA. Significantly, **12** displays efficacy against FA-resistant strain of *Staphylococcus aureus* in a soft-tissue murine infection model. This study indicated the structural features of FA necessary for potent antibiotic activity and demonstrates that the resistance profile can be improved for this target and scaffold (Chavez et al., 2021).

Since the marketing of FA, various structural modifications have been made, but only one derivative, l6-deacetoxy-l6β-acetylthio FA, is significantly more active than the parent antibiotic (Daehne et al., 1979). This review summarized the SAR of the antimicrobial activity of FA (**Figure 3**).

Recently, Hajikhani et al. used several international databases to discern studies addressing the prevalence of FA resistant *S. aureus* (FRSA), FA resistant MRSA (FRMRSA), and FA resistant methicillin-susceptible *S. aureus* (FRMSSA). The analyses manifested that the global prevalence of FRSA, FRMRSA, and FRMSSA was 0.5, 2.6, and 6.7%, respectively. These results

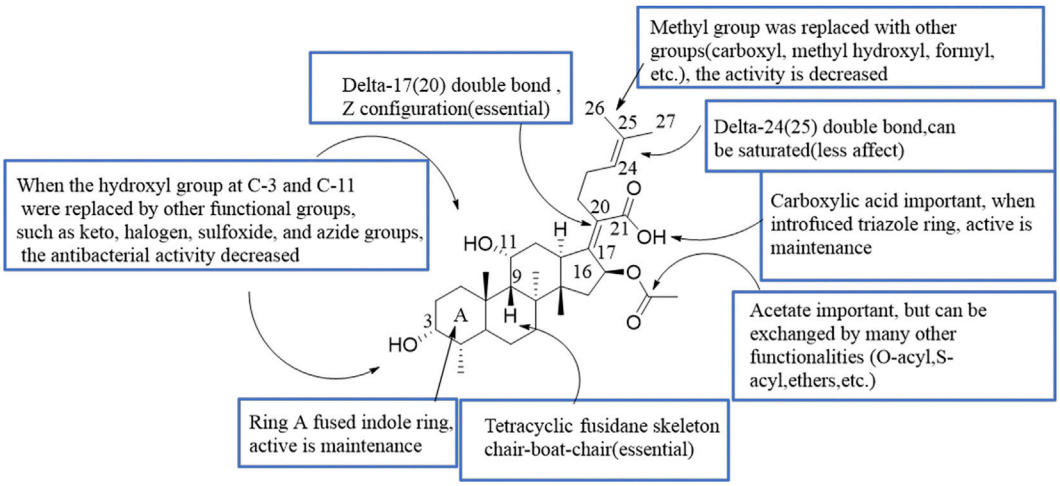

FIGURE 3 | SAR of the antibacterial activity of FA.

indicated the need for prudent prescription of FA to stop or diminish the incidence of FA resistance. (Hajikhani et al., 2021).

In conclusion, since the antibacterial activity of FA was found, many structural modifications have been made to FA. However, the antibacterial activity of only two compounds reached the level of FA activity, the antibacterial activity of other derivatives is worse than FA. At present, the SAR summarized according to the existing literature is not perfect and needs to be further enriched. In recent years, drug-resistant bacterial of FA has appeared. It is necessary to study FA derivatives with better activity against drug-resistant bacterial.

2.1.2 Anti-*M. tuberculosis* Activity

According to the WHO, tuberculosis remains the world's deadliest infectious killer. Worldwide, more than 4,000 people die of tuberculosis every day, and nearly 30,000 people are affected by this preventable and curable disease (World Health Organization, 2020b). In 1962, Godtfredsen et al. studied the antibacterial spectrum of FA and found that FA had some antituberculosis activity, but there was no further research performed (Godtfredsen WO. et al., 1962). In 1990, Hoffner et al. found that FA was effective against 30 clinically isolated *Mycobacterium tuberculosis* (*M. tuberculosis*) strains *in vitro* at concentrations of 32–64 mg/L, and was synergistic with ethambutol against *M. tuberculosis* (Hoffner et al., 1990). Fuursted et al. used a variety of tuberculosis bacilli (including drug-resistant tuberculosis bacilli) and determined the MIC values of FA against tuberculosis bacilli, which ranged from 8 to 32 mg/L (Fuursted et al., 1992; Fabry et al., 1996). Unlike the experimental results of Hoffner, Öztas did not observe either a synergistic or antagonistic effect when FA was used in combination with other standard antituberculosis drugs (Fuursted et al., 1992). The reason for this difference may be because the groups used different test methods. Previous studies have also found that FA was not cross-resistant with first-line drugs (Hoffner et al., 1990; Fuursted et al., 1992).

In 2008, Öztas et al. conducted susceptibility tests for FA in the sputum cultures of 728 tuberculosis patients. The results indicated that FA was effective at 32 mg/L *in vitro*, but resistance to FA was observed at 16 mg/L. This group suggested that FA might be an alternative antituberculosis drug (Öztas et al., 2008). FA was found to lack *in vivo* activity at doses of up to 200 mg/kg in a mouse model of tuberculosis (Shanika, 2017).

In 2014, to solve the problem that FA has no antituberculosis activity *in vivo*, Kigondu et al. adopted a repositioning strategy to determine whether FA could be used as an optional antituberculosis drug. They hope to synthesize and screen FA derivatives to study the antituberculosis activity and mechanism of action (Kigondu et al., 2014). In a recent study, Akinpelu et al. found that FA was a potential inhibitor of *M. tuberculosis* filamentous temperature sensitive mutant Z (FtsZ) by computer methods, including density function theory (DFT), molecular docking, and molecular dynamics simulations (Akinpelu et al., 2020).

Dziwornu et al. have synthesized 28 FA derivatives, which were amidated at the 21-COOH, including C-21 FA ethanamides, anilides, and benzyl amides. All the derivatives were evaluated for their antituberculosis activity using the H37RvMa strain and the minimum inhibitory concentration required to inhibit the growth of 90% of the bacterial population (MIC_{90}) values were determined. Compound **13** had the most potent antituberculosis activity with a MIC_{90} value of 2.71 μM, but not as good as FA with a MIC_{90} value of 0.24 μM (**Figure 4**) (Dziwornu et al., 2019).

Njoroge et al. synthesized 27 derivatives of FA by esterification at the 3-OH and 21-COOH, including C-3 alkyl, aryl, and silicate esters, and the Mtb H37RvMa strain was used to determine the antituberculosis activity of the derivatives *in vitro*. The activities of the C-3 silicate derivatives were similar to that of FA. The minimum concentration required to inhibit the growth of 99% of the bacterial population (MIC_{99}) values of compounds **14** and **15** against the Mtb H37RvMa strain were 0.2 and 0.3 μM,

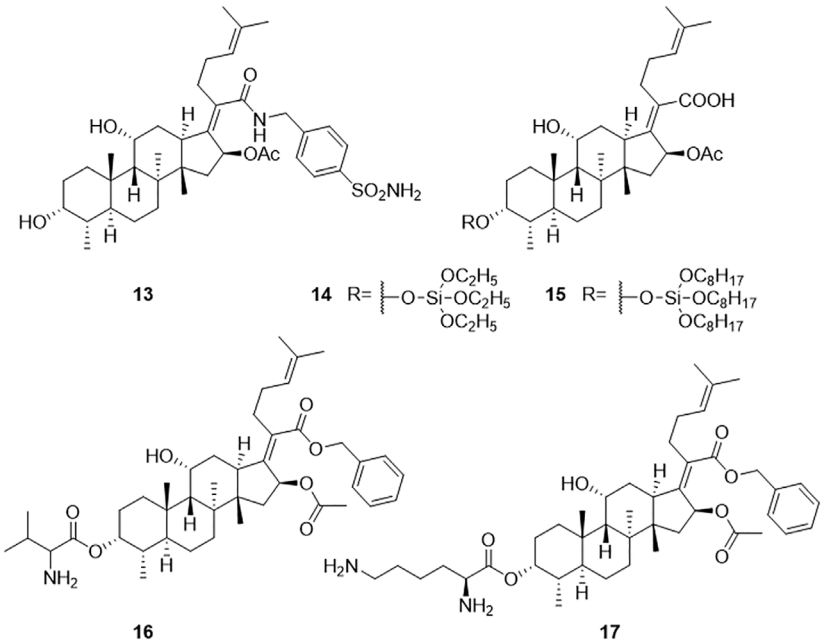

FIGURE 4 | Structural formulae of compounds **13–17**.

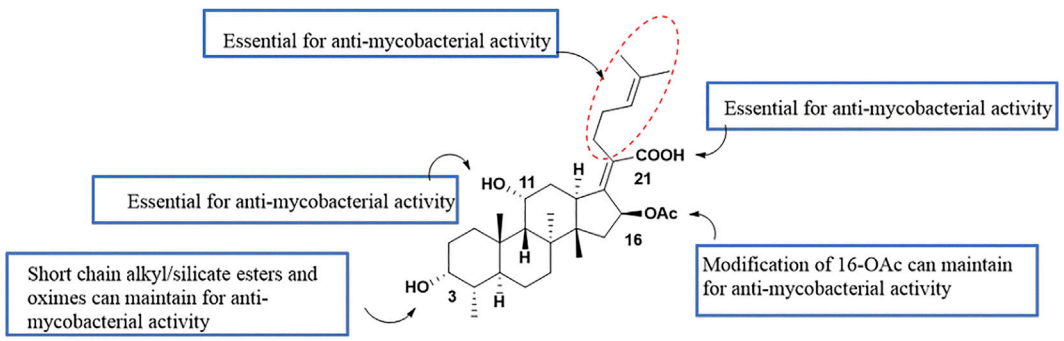

FIGURE 5 | SAR of the antituberculosis activity of FA.

respectively, while FA with a MIC_{99} value of <0.15 μM (Njoroge et al., 2019).

Singh et al. used chemical biology and genetics, showed essentiality of its encoding gene fusA1 in *M. tuberculosis* by demonstrating that the transcriptional silencing of fusA1 is bactericidal *in vitro* and in macrophages. Thus, this study identified EF-G as the target of FA in *M. tuberculosis*. (Singh et al., 2021).

Singh et al. have summarized the preliminary SAR of 58 antituberculosis FA derivatives (**Figure 5**). It was found that the 11-OH, 21-COOH, and lipid side chains were necessary for antituberculosis activity, while modification at the 3-OH with short chain alkyl or silicate esters and oximes could maintain the activity, and replacing the acetoxy group of C-16 with a propionyloxy group maintained the activity (Singh et al., 2020).

In conclusion, similar to the antibacterial modification of FA, the antituberculosis modification of FA has not made significant progress and needs to be further explored. And the reason why FA has no antituberculosis activity *in vivo* needs to be further clarified. It is also necessary to continue to study FA derivatives with antituberculosis activity *in vivo* and *in vitro*. If the above problems are solved, FA will be repositioned as an antituberculosis drug with novel mechanism of action.

2.1.3 Antifungal Activity

Many adults and pediatric patients use strong chemotherapy agents to treat hematological malignancies, thus increasing the incidence of invasive mycosis (Zając-Spychała et al., 2019; Malhotra, 2020). Because antifungal drugs are available in a limited number and are prone to drug resistance, there is a

view that the key to the future development of antifungal drugs is the repurposing of marketed drugs (Zida et al., 2017; Nicola et al., 2019).

FA itself has no antifungal activity, but recently it has been reported that FA derivatives have antifungal activity. Cao et al. inadvertently found that FA derivative **16** inhibited the growth of *Cryptococcus neoformans*. The inhibition rate of compound **16** against *C. neoformans* was 94.58% at a concentration of 32 μg/ml. Among the reported compounds, compound **17** had the strongest MIC value (4 μg/ml) against *C. neoformans* (Cao et al., 2020). In another study, Shakurova et al. synthesized quaternary pyridinium salts, and the tetrahydropyridine derivative **9** had moderate activity at a concentration of 32 μg/ml against *C. neoformans* (**Figure 4**) (Shakurova et al., 2019).

There are a limited number of antifungal FA derivatives reported in the literature, but the data provide insights for the development of FA antifungal activity. Furthermore, this information provides guidance for the future design of FA derivatives with good antifungal activity and selectivity.

2.2 Antiparasitic Activity

2.2.1 Antimalarial Activity

According to the World Health Organization (WHO) World Malaria Report 2020, it was estimated that there were 229 million new malaria infections, and 409,000 people died of malaria, worldwide in 2019 (World Health Organization, 2020a). *Plasmodium falciparum* is resistant to existing antimalarial drugs, including artemisinin, which poses a challenge for antimalarial treatment. Therefore, there is an urgent need for new antimalarial drugs, especially those with novel mechanisms of action and no cross-resistance to existing drugs (Biddau and Sheiner, 2019).

As early as 1985, FA was found to have antimalarial activity *in vitro* (Black et al., 1985). Johnson et al. found that FA killed malaria parasites (*P. falciparum* line D10) with an IC_{50} value of 52.8 μM, and then characterized the possible target of FA against malaria, which is EF-G in two organelles of *Plasmodium*, the apicoplast and mitochondria. It could be an effective lead compound because of its mechanism of action (Johnson et al., 2011). Compared with *P. falciparum* mitochondria EF-G, FA had a better effect on apicoplast EF-G. The reason for mitochondrial EF-G resistance is at least partly because there is a conservative three amino acid sequence (GVG motif) in the switch I loop, however this motif is not found in apicoplast EF-G (Gupta et al., 2013).

Kaur et al. synthesized a series of compounds in which the 21-COOH of FA was substituted with various bioisosteres, and evaluated the activity *in vitro* with the chloroquine-sensitive NF54 strain of the malaria parasite *P. falciparum*. Among these compounds, the antiplasmodial activity IC_{50}, CC_{50} and selection index of the most active compound **18** were 1.7, 77.4, and 46 μM, respectively. The IC_{50}, CC_{50}, and selection index of FA were 59.0, 194.0, and 3 μM, respectively. Compared with FA, compound 18 has a higher SI value. Furthermore, this group constructed apicoplast and mitochondrial EF-G homology structure models of *P. falciparum*, and compound **18** was docked with these two models. The docking results showed

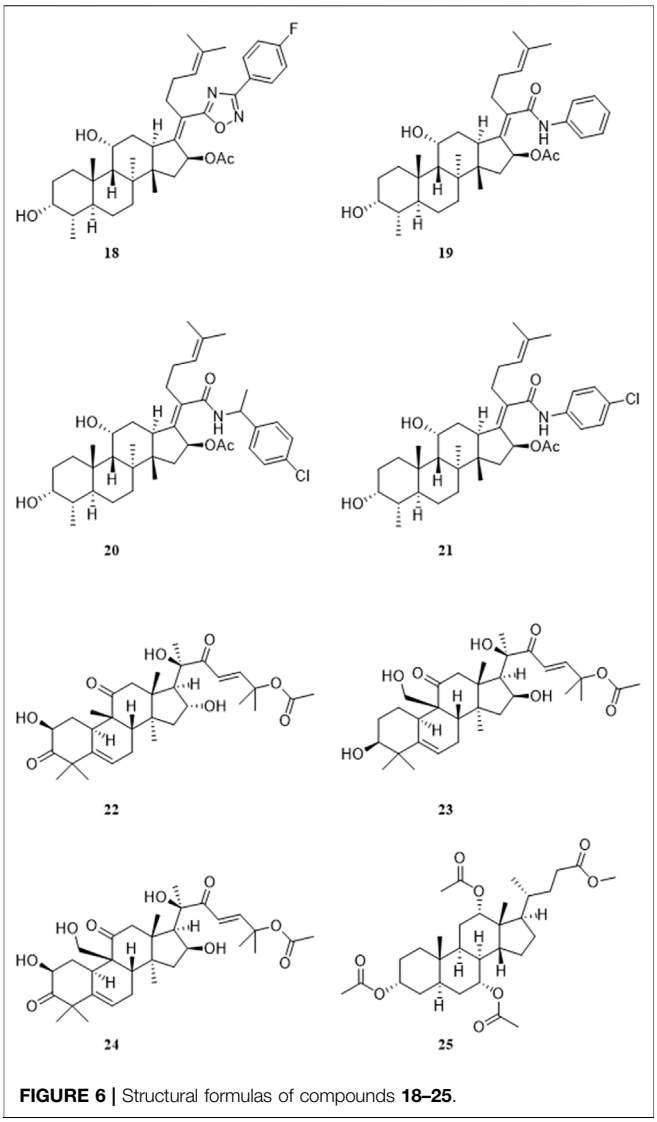

FIGURE 6 | Structural formulas of compounds **18–25**.

that the EF-G binding site of compound **18** and FA was consistent, but compound **18** had a higher binding score (**Figure 6**) (Kaur et al., 2015).

Espinoza-Moraga et al. amidated or esterified the 21-COOH in FA with various substituents, including ester chains and aromatic compounds, and evaluated the antiplasmodial activity of these compounds *in vitro* against the chloroquine-sensitive NF54 strains and multidrug-resistant K1 strains of the malarial parasite *P. falciparum*. Compound **19** had the best antiplasmodial activity, with IC_{50} values of 1.2 and 1.4 μM against the NF54 and K1 strains, respectively. Unfortunately, the mechanism of action was not explored (Espinoza-Moraga et al., 2016). Kaur et al. developed a 3D-QSAR model based on the antiplasmodial activity of 61 FA derivatives that they had synthesized previously. The verified Hypo2 model was used as a three-dimensional structure search query to screen combinatorial libraries based on FA. Eight virtual screening hit compounds were selected and synthesized, of which compounds **20** and **21** had IC_{50} values of 0.3 and 0.7 μM, respectively, for the NF54

strain of *P. falciparum*. The IC_{50} values of these two compounds for the drug-resistant K1 strain of *P. falciparum* were both 0.2 μM, and no appreciable cytotoxicity was detected (Kaur et al., 2018).

Pavadai et al. used FA as a search query, and adopted two-dimensional fingerprint- and three-dimensional shape-based virtual screening methods to obtain new inhibitors of *P. falciparum* from their in-house database, including 708 steroid-type natural products. After further screening, this group successfully identified nine compounds that inhibited the growth of the NF54 strain of *P. falciparum*, with IC_{50} values of less than 20 μM. The IC_{50} values of the four most active compounds **22–25** were 1.39, 1.76, 2.92, and 3.45 μM, respectively. Moreover, the predicted absorption, distribution, metabolism, and excretion (ADME) properties of these four compounds were comparable to FA (Pavadai et al., 2017).

To date, the chemical modification of FA for antimalarial activity has been mainly concentrated on the 21-COOH. Esterification or amidation is beneficial to the activity, and amidation is better than esterification for activity. The structural modification of other sites of FA needs to be further explored. FA derivatives have good inhibitory activity against *P. falciparum*, and apicoplast EF-G is the main action site of FA. It is necessary to modify FA to improve selectivity for apicoplast EF-G. Thus, FA derivatives have potential to be repositioned as an antimalarial drug.

2.2.2 Other Antiparasitic Activities

Rizk et al. described the inhibitory effects of FA on the *in vitro* growth of bovine and equine *Babesia* and *Theileria* parasites. The *in vitro* growth of four *Babesia* species that was significantly inhibited by micromolar concentrations of FA (IC_{50} values = 144.8, 17.3, 33.3, and 56.25 μM for *Babesia bovis*, *Babesia bigemina*, *Babesia caballi*, and *Theileria equi*, respectively). These results indicate that FA might be incorporated in treatment of *babesiosis* (Rizk et al., 2020).

Payne et al. investigated the therapeutic value of FA for *T. gondii* and found that the drug was effective in tissue culture, but not in a mouse model of infection. This work highlights the necessity of *in vivo* follow-up studies to validate *in vitro* drug investigations. (Payne et al., 2013).

2.3 Tumor Related Activity

2.3.1 Antitumor Activity

Malignant tumors are a health issue all over the world. There were an estimated 19.3 million new cases of cancer and almost 10.0 million deaths from cancer worldwide in 2020. (Ferlay et al., 2021). In 2019, Ni et al. accidentally discovered that FA derivatives have antitumor activity. Among the derivatives synthesized by this group, compounds where the 21-COOH was modified by a benzyl group, and with amino terminal modification at the C-3 position, had antitumor activity, of which compound **26** was the most active compound (Ni et al., 2019). Compound **26** had antitumor activity against various tumor cell lines including HeLa, U87, KBV, MKN45, and JHH-7, with IC_{50} values ranging from 1.26 to 3.57 μM. A preliminary mechanistic study was performed, which indicated that neo-synthesized proteins were decreased in HeLa cells under the action of compound **26**, and the ratio of cells in the Sub-G_0/G_1 phase was increased, as determined by flow cytometry monitoring, thus leading to HeLa cell apoptosis. Compound **26** also exhibited good antitumor activity *in vivo* against a xenograft tumor of HeLa cells in athymic nude mice (**Figure 7**).

Salimova et al. adopted different substituted amino groups to modify the 3-OH of FA, with or without esterification of the 21-COOH, to synthesize a series of 3-amino-substituted FA derivatives. To determine the antitumor activity of these derivatives, the researchers used nine different types of human tumor cell lines (sourced from the American Cancer Institute NCI-60) to study the antitumor activity of these compounds *in vitro*. Compound **27** had the highest cytotoxicity against leukemia cells and compound **28** had the broadest antitumor activity, including against leukemia, non-small cell lung cancer, colon cancer, neurological tumors, melanoma, ovarian cancer, and renal cancer (Salimova et al., 2019).

By analyzing the relationship between antitumor activity and structure of FA, the following preliminary SAR was obtained (**Figure 8**) (Ni et al., 2019; Salimova et al., 2019).

2.3.2 Tumor Multidrug Resistance Reversal Activity

MDR is the main cause of drug resistance in many tumors, and is the main factor leading to the failure of chemotherapy. MDR affects patients with a variety of hematological and solid tumors (Persidis, 1999). Drug-sensitive cells can be killed by chemotherapeutics, but there may be a proportion of drug-resistant tumor cells left behind, which grow later, resulting in resistance to chemotherapeutics, leading to treatment failure (Lage, 2008). Currently, it is considered that the most effective strategy to overcome MDR is to develop MDR reversal agents.

Several MDR reversal agents have failed in clinical trials because of inherent toxicity, low selectivity, or complex pharmacokinetic interactions (Palmeira et al., 2012). Therefore, a safe and effective MDR reversal agent with low toxicity is urgently needed. To date, many natural products with different structural types have been developed as potential MDR reversal agents (Kumar and Jaitak, 2019).

Guo et al. found that FA derivatives have tumor MDR reversal activity. The derivative **29**, which was modified with a benzyl group at the 21-COOH, had good MDR reversal activity *in vitro*. Further studies revealed that the combination of derivative **29** with paclitaxel re-sensitized the multidrug-resistant oral epidermoid carcinoma (KBV) cell line to paclitaxel. A mechanism study found that compound **29** enhanced the ATPase activity of P-glycoprotein (P-gp) by inhibiting the drug pump activity of P-gp, but did not affect the expression of P-gp (Guo et al., 2019).

According to the results for MDR reversal activity, the SAR of FA derivatives has been preliminarily summarized (**Figure 9**).

According to the existing literature, FA has certain potential in antitumor and tumor MDR reversal activity. However, there are few studies in antitumor and tumor MDR reversal activity of FA, which needs to be further explored.

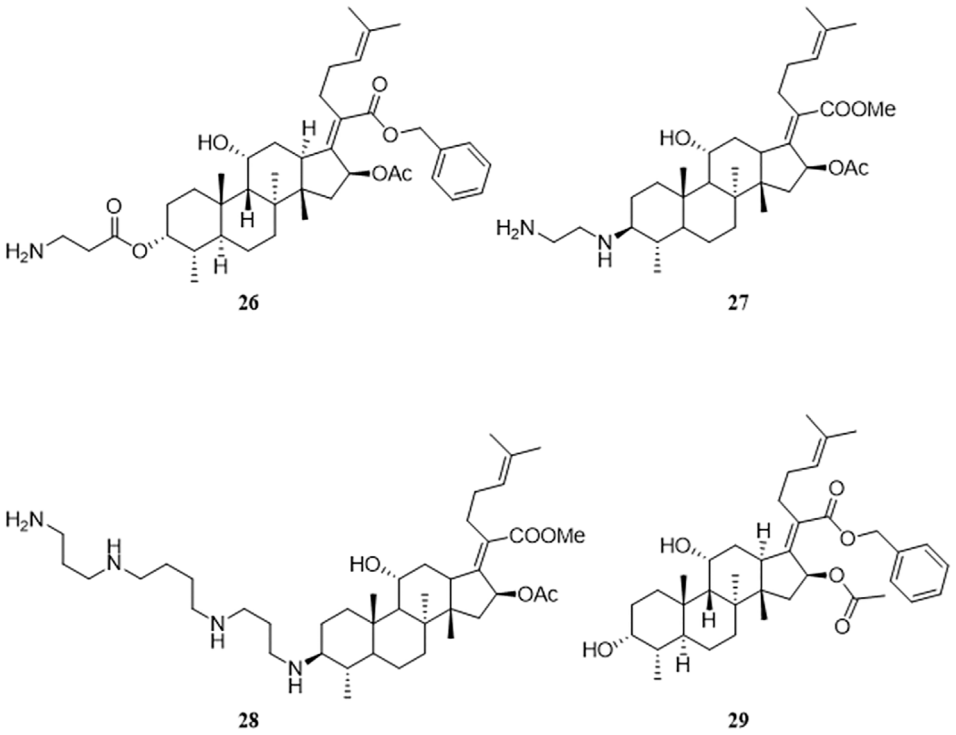

FIGURE 7 | Structural formulae of compounds **26–29**.

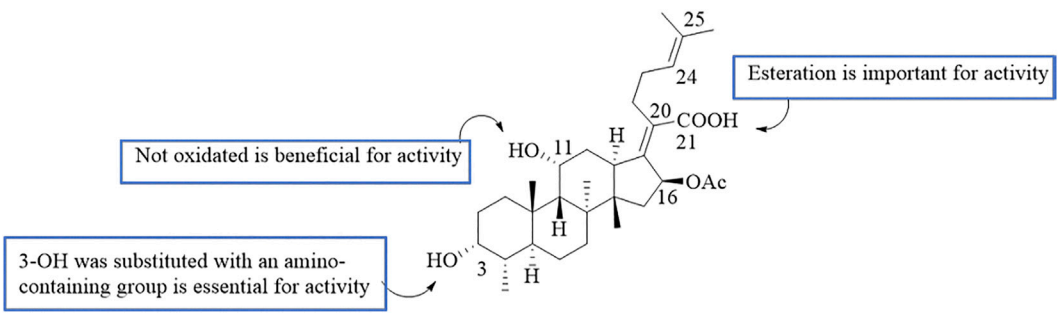

FIGURE 8 | SAR of the antitumor activity of FA.

2.4 Anti-Inflammatory Activity

Inflammation is a complex biological response to injury, and to attack pathogens as part of the body's immune response, which results in symptoms that include pain, fever, erythema, and edema (Ferrero-Miliani et al., 2007). The impact of antimicrobial agents on the immune and inflammatory systems and their possible clinical significance have greatly attracted the interest of scientists (Bosnar et al., 2019).

FA has been found to have some anti-inflammatory effects in mice and rats *in vivo*, especially by reducing the release of tumor necrosis factor alpha (TNF-α) (**Table 1**) (Bosnar et al., 2019). In 2018, Wu et al. saturated the delta-24 (25) double bond of FA and thus obtained the hydrogenated derivative **1**. The antimicrobial activity of FA and compound **1** were tested against six bacterial strains, and the results showed that both FA and **1** showed high levels of antimicrobial activity against Gram-positive strains. The anti-inflammatory activity of these compounds was evaluated using the 12-*O*-tetradecanoyl phorbol-13-acetate (TPA)-induced mouse ear edema model. The results showed that FA and **1** effectively reduced TPA-induced ear edema in a dose-dependent manner, and this inhibitory effect was associated with the inhibition of TPA-induced upregulation of the pro-inflammatory cytokines IL-1β, TNF-α, and COX-2. Furthermore, **1** significantly inhibited the expression levels of p65, IκB-α, and *p*-IκB-α in TPA-induced mouse ear edema models (**Figure 10**) (Wu PP. et al., 2018).

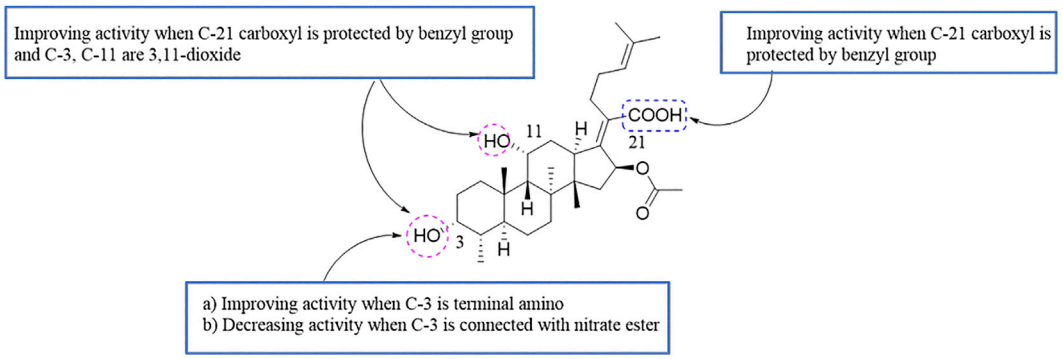

FIGURE 9 | SAR of the tumor multidrug resistance reversal activity of FA.

TABLE 1 | Experiments show that FA modulates immunity and the inflammatory process.

Pharmacological actions	References
FA decreased the plasma peak of TNF-α, improved the survival rate of neonatal mice, and decreased plasma TNF-α during endotoxic shock	Genovese et al. (1996)
FA protected mice from concanavalin-A-induced hepatitis. At the same time, the plasma levels of IL-2, IFN-γ, and TNF-α were significantly decreased, but the levels of IL-6 were increased	Nicoletti et al. (1998)
FA was beneficial for the treatment of experimental autoimmune neuritis in rats (a model of Guillain-Barre syndrome), where the serum levels of interferon-gamma, IL-10, and TNF-α were reduced	Marco et al. (1999)
FA could alleviate the tissue edema caused by local formalin injection in rats	Kilic et al. (2002)
The co-administration of FA and daptomycin significantly reduced the joint and tissue levels of systemic TNF-α, IL-6, IL-1β, and other pro-inflammatory cytokines in mice infected with multidrug-resistant group B streptococci	El-Shemi and Faidah (2011)

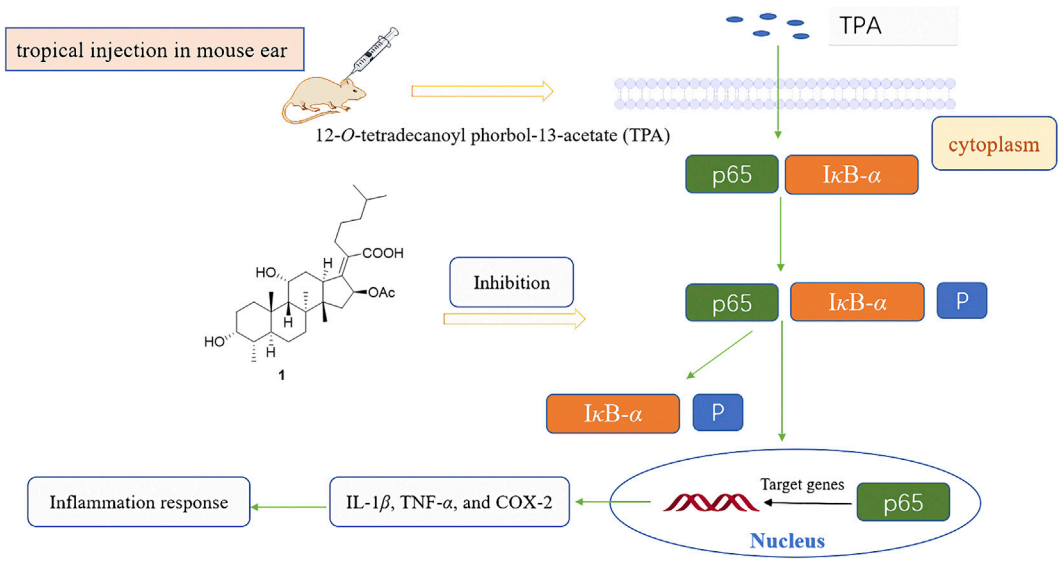

FIGURE 10 | Schematic representation of the anti-inflammation mechanism of compound **1** in TPA-induced mouse ear edema models.

According to current research, FA derivative has showed anti-inflammatory activity *in vivo* and *in vitro*. However, there is no literature yet reported the structural modification of anti-inflammatory of FA, which needs to be enriched. And other possible anti-inflammatory mechanisms need to be further studied.

2.5 Antiviral Activity

Severe Acute Respiratory Syndrome Coronavirus 2 (SARS-CoV-2), a new type of RNAβ coronavirus, has caused a pandemic worldwide (Gallelli et al., 2020). There is currently no effective treatment for the virus, and effective preventive and therapeutic drugs need to be identified (Sanders et al., 2020). There have been many reports of antibiotic agents that have antiviral activity. Minocycline, a tetracycline drug, can effectively inhibit human immunodeficiency viruses (HIV) (Zink et al., 2005). Aminoglycoside antibiotics can inhibit the replication of the herpes simplex virus, influenza A virus, and Zika virus *in vivo* and *in vitro* (Gopinath et al., 2018).

As early as 1967, the first antiviral research on FA appeared, FA was found to be ineffective against coxsackie A21 or rhinovirus infection, both orally and intranasally, and fifteen derivatives were found to be inactive or toxic (Acornley et al., 1967). There have been several reports regarding the effectiveness of FA toward human immunodeficiency virus (HIV), and the mechanism of action has also been studied. FA is an anionic surfactant that acts on the lipid molecular layer of infected cells, exposing the viral proteins to the host immune system to prevent the HIV from forming syncytium *in vitro* (Lloyd et al., 1988). Additionally, FA can directly inhibit reverse transcriptase and thus has anti-HIV activity (Famularo et al., 1993). Four clinical trials of FA in HIV-infected patients have been conducted, but the results were contradictory (Faber et al., 1987; Youle et al., 1989; Hørding et al., 1990; Famularo et al., 1993). Furthermore, a study has shown that human leukocyte interferon can enhance the anti-HIV effect of FA (Degre and Beck, 1994).

In recent years, it has been reported that FA was effective against John Cunningham virus (JCV) *in vivo* and *in vitro* (Brickelmaier et al., 2009; Chan et al., 2015). Liu et al. found that FA had good antiviral activity against enterovirus A71 (EV-A71) and coxsackievirus A16 (CV-A16). The potential antiviral mechanism is related to the inhibition of viral RNA replication and the synthesis of viral proteins (Liu et al., 2019). Kwofie et al. found that FA was the potential anti-SARS-CoV-2 compounds by antiviral activity predictions (Kwofie et al., 2021).

Although it has been found that FA has good *in vivo* and *in vitro* activity against a variety of viruses, there have been few studies on the antiviral effects of FA derivatives, which merit future exploration. Furthermore, whether FA has a therapeutic effect against SARS-CoV-2 is also a possible research direction.

2.6 Other Activities

Some antibiotics have been discovered to have the potential to treat neurological diseases, acting as neuroprotective agents via various pathways, including rifampicin, rapamycin, D-cycloserine, and ceftriaxone (Batson et al., 2017; Lin et al., 2017; Reglodi et al., 2017; Wu X. et al., 2018). Additionally, the property of easily crossing the blood-brain barrier is one of the necessary criteria for a neuroprotective agent, and researchers have found that FA has this characteristic (Mindermann et al., 1993).

Park et al. first discovered that FA had neuroprotective effects. This group used sodium nitroprusside (SNP) to pretreat C6 glial cells, and found that FA prevented SNP-induced cell death in a dose-dependent manner at 5–20 μM. Moreover, a mechanism study was performed, and the results indicated that FA had a neuroprotective effect against SNP-induced cytotoxicity through the 5′ adenosine monophosphate-activated protein kinase (AMPK) pathway and apoptotic events (Park et al., 2019).

Unfortunately, this research was only performed *in vitro*, not *in vivo*. Additionally, the mechanism of action of FA was not fully elucidated, and more studies are needed to clarify the mechanism. Nevertheless, the results of this study have provided a potential clinical strategy, suggesting that FA derivatives may be used for the treatment of neurological disease as neuroprotective agents.

3 CONCLUSION AND PERSPECTIVES

FA can be obtained by fermentation, and has attracted increasing attention in recent years. In summary, FA is a promising natural bioactive substance with a variety of pharmacological activities for the potential treatment of many diseases. Great progress has been achieved in the investigation of the pharmacological activity, SAR, and mechanism of action of FA. FA consists of a tetracyclic skeleton with several available sites for chemical modification, which enables the synthesis of novel compounds with potentially higher potency and selectivity, and with fewer side effects.

Despite extensive research and development into FA in recent years, considerable challenges still lie ahead because of the limited amount of studies on the pharmacological activities and mechanisms of action to date. FA has a very short half-life after oral absorption. Consequently, FA must be administered frequently, resulting in fluctuations in the plasma drug concentration and increasing the risk of poor clinical outcomes, including side effects and adverse reactions, limiting the application of FA in clinical use. Considering that triterpenes are known to possess a wide range of pharmacological activities, it is possible that other new pharmacological effects of FA still to be discovered. Much of the present research has been confined to *in vitro* rather than *in vivo* studies; hence, whether FA is effective or sufficiently efficient *in vivo* is questionable and must be validated.

In view of the above challenges, the following strategies will be of great value in future research into the drug development and clinical application of FA:

1) Extending the half-life of FA by adopting appropriate pharmaceutic or chemical methods. For example, FA is administered in liposomes or structural modifications that occlude the 21 COOH metabolic site.
2) From the view of the pharmacology and mechanism, further investigation of the potential pharmacological activities of FA expands the scope of its use. Meanwhile, more research into the mechanism of action will enable a better understanding of how FA works. Furthermore, a large number of *in vivo* studies should be conducted to validate its effectiveness, because a high sensitivity *in vitro* study does not necessarily represent the same result *in vivo*.
3) Synthesizing novel derivatives by structural modification at the confirmed modification sites, or other potentially available

sites of FA, to explore more promising agents with higher activity and better drug-like properties.

4) As a clinically used drug, FA has the possibility of repositioning as an antituberculous or antimalarial drug, which requires more research in these fields. The antitumor, tumor MDR reversal, anti-inflammatory, antifungal activities of FA are newly discovered biological activities in recent years, which have larger research value.

In conclusion, the knowledge regarding FA has been growing rapidly in recent years, but there is still room for improvement in the understanding of its pharmacology, mechanism of action, and structural modification.

AUTHOR CONTRIBUTIONS

JL, WJ and YB wrote the first draft and provided the organization and frame work of the article. DZ and YZ provided critical revisions. All authors approved the final version of the manuscript for submission.

FUNDING

This work was funded by the National Natural Science Foundation of China (No. 81773563), The Science and Technology Support Program for Youth Innovation in Universities of Shandong (No. 2020KJM003), Top Talents Program for One Case One Discussion of Shandong Province.

ACKNOWLEDGMENTS

We thank Victoria Muir, PhD, from Liwen Bianji, Edanz Group China (www.liwenbianji.cn/ac), edited the English text of a draft of this manuscript.

REFERENCES

Acornley, J. E., Bessell, C. J., Bynoe, M. L., Godtfredsen, W. O., and Knoyle, J. M. (1967). Antiviral Activity of Sodium Fusidate and Related Compounds. *Br. J. Pharmacol. Chemother.* 31, 210–220. doi:10.1111/j.1476-5381.1967.tb01992.x

Agarwal, G., Carcache, P. J. B., Addo, E. M., and Kinghorn, A. D. (2020). Current Status and Contemporary Approaches to the Discovery of Antitumor Agents from Higher Plants. *Biotechnol. Adv.* 38, 107337. doi:10.1016/j.biotechadv.2019.01.004

Akinpelu, O. I., Lawal, M. M., Kumalo, H. M., and Mhlongo, N. N. (2020). Drug Repurposing: Fusidic Acid as a Potential Inhibitor of *M. tuberculosis* FtsZ Polymerization - Insight from DFT Calculations, Molecular Docking and Molecular Dynamics Simulations. *Tuberculosis (Edinb)* 121, 101920. doi:10.1016/j.tube.2020.101920

Aly, A. H., Debbab, A., and Proksch, P. (2011). Fifty Years of Drug Discovery from Fungi. *Fungal Divers.* 50, 3–19. doi:10.1007/s13225-011-0116-y

Batson, S., De Chiara, C., Majce, V., Lloyd, A. J., Gobec, S., Rea, D., et al. (2017). Inhibition of D-Ala:D-Ala Ligase through a Phosphorylated Form of the Antibiotic D-Cycloserine. *Nat. Commun.* 8, 1939–1947. doi:10.1038/s41467-017-02118-7

Belardinelli, R., and Rodnina, M. V. (2017). Effect of Fusidic Acid on the Kinetics of Molecular Motions during EF-G-Induced Translocation on the Ribosome. *Sci. Rep.* 7, 10536–10538. doi:10.1038/s41598-017-10916-8

Bi, Y., Lu, J., Ni, J., and Cao, Y. (2020). *Application of Amino Substituted Fusidic Acid Derivatives in Preparing Antifungal Drugs*. Beijing: China National Intellectual Property Administration. CN Patent No ZL 2018 1 1 479612.8.

Biddau, M., and Sheiner, L. (2019). Targeting the Apicoplast in Malaria. *Biochem. Soc. Trans.* 47, 973–983. doi:10.1042/BST20170563

Black, F. T., Wildfang, I. L., and Borgbjerg, K. (1985). Activity of Fusidic Acid against Plasmodium Falciparum *In Vitro*. *Lancet* 1, 578–579. doi:10.1016/s0140-6736(85)91234-6

Bodley, J. W., Zieve, F. J., Lin, L., and Zieve, S. T. (1969). Formation of the Ribosome-G Factor-GDP Complex in the Presence of Fusidic Acid. *Biochem. Biophys. Res. Commun.* 37, 437–443. doi:10.1016/0006-291X(69)90934-6

Borg, A., Holm, M., Shiroyama, I., Hauryliuk, V., Pavlov, M., Sanyal, S., et al. (2015). Fusidic Acid Targets Elongation Factor G in Several Stages of Translocation on the Bacterial Ribosome. *J. Biol. Chem.* 290, 3440–3454. doi:10.1074/jbc.M114.611608

Bosnar, M., Haber, V. E., and Graham, G. G. (2019). "Influence of Antibacterial Drugs on Immune and Inflammatory Systems," in *Nijkamp and Parnham's Principles of Immunopharmacology*. Editors M. J. Parnham, F. P. Nijkamp, and A. G. Rossi (New York, NYCham: Springer), 589–611. doi:10.1007/978-3-030-10811-3_29

Brickelmaier, M., Lugovskoy, A., Kartikeyan, R., Reviriego-Mendoza, M. M., Allaire, N., Simon, K., et al. (2009). Identification and Characterization of Mefloquine Efficacy against JC Virus *In Vitro*. *Antimicrob. Agents Chemother.* 53, 1840–1849. doi:10.1128/AAC.01614-08

Brown, D. G., Lister, T., and May-Dracka, T. L. (2014). New Natural Products as New Leads for Antibacterial Drug Discovery. *Bioorg. Med. Chem. Lett.* 24, 413–418. doi:10.1016/j.bmcl.2013.12.059

Cao, Y., Ni, J., Ji, W., Shang, K., Liang, K., Lu, J., et al. (2020). Synthesis, Antifungal Activity and Potential Mechanism of Fusidic Acid Derivatives Possessing Amino-Terminal Groups. *Future Med. Chem.* 12, 763–774. doi:10.4155/fmc-2019-0289

Centers for Disease Control and Prevention (2019). Antibiotic Resistance Threats Report in the United States. Available at: https://www.cdc.gov/drugresistance/pdf/threats-report/2019-ar-threats-report-508.pdf (Accessed August 07, 2021).

Chan, J. F., Ma, M. K., Chan, G. S., Chan, G. C., Choi, G. K., Chan, K. H., et al. (2015). Rapid Reduction of Viruria and Stabilization of Allograft Function by Fusidic Acid in A Renal Transplant Recipient with JC Virus-Associated Nephropathy. *Infection* 43, 577–581. doi:10.1007/s15010-015-0721-x

Garcia Chavez, M., Garcia, A., Lee, H. Y., Lau, G. W., Parker, E. N., Komnick, K. E., et al. (2021). Synthesis of Fusidic Acid Derivatives Yields a Potent Antibiotic with an Improved Resistance Profile. *ACS. Infect. Dis.* 7, 493–505. doi:10.1021/acsinfecdis.0c00869

Chen, Y., de Bruyn Kops, C., and Kirchmair, J. (2017). Data Resources for the Computer-Guided Discovery of Bioactive Natural Products. *J. Chem. Inf. Model.* 57, 2099–2111. doi:10.1021/acs.jcim.7b00341

Cicek-Saydam, C., Cavusoglu, C., Burhanoglu, D., Hilmioglu, S., Ozkalay, N., and Bilgic, A. (2001). *In Vitro* Susceptibility of Mycobacterium Tuberculosis to Fusidic Acid. *Clin. Microbiol. Infect.* 7, 700–702. doi:10.1046/j.1469-0691.2001.00341.x

ClinicalTrials.gov (2020). Oral Sodium Fusidate (CEM-102) for the Treatment of Staphylococcal Bone or Joint Infections. Available at: https://clinicaltrials.gov/ct2/show/NCT02569541? term=fusidic+acid&cntry=US&draw=2&rank=1 (Accessed September 14, 2021).

Daehne, W. V., Godtfredsen, W. O., and Rasmussen, P. R. (1979). Structure-Activity Relationships in Fusidic Acid-type Antibiotics. *Adv. Appl. Microbiol.* 25, 95–146. doi:10.1016/S0065-2164(08)70148-5

Degré, M., and Beck, S. (1994). Anti-HIV Activity of Dideoxynucleosides, Foscarnet and Fusidic Acid Is Potentiated by Human Leukocyte Interferon in Blood-Derived Macrophages. *Chemotherapy* 40, 201–208. doi:10.1159/000239193

Duvold, T., Sørensen, M. D., Björkling, F., Henriksen, A. S., and Rastrup-Andersen, N. (2001). Synthesis and Conformational Analysis of Fusidic Acid Side Chain Derivatives in Relation to Antibacterial Activity. *J. Med. Chem.* 44, 3125–3131. doi:10.1021/jm010899a

Duvold, T., Jørgensen, A., Andersen, N. R., Henriksen, A. S., Dahl Sørensen, M., and Björkling, F. (2003). 17S,20S-Methanofusidic Acid, a New Potent Semi-synthetic Fusidane Antibiotic. *Bioorg. Med. Chem. Lett.* 12, 3569–3572. doi:10.1016/S0960-894X(02)00797-7

Dziwornu, G. A., Kamunya, S., Ntsabo, T., and Chibale, K. (2019). Novel Antimycobacterial C-21 Amide Derivatives of the Antibiotic Fusidic Acid: Synthesis, Pharmacological Evaluation and Rationalization of Media-dependent Activity Using Molecular Docking Studies in the Binding Site of Human Serum Albumin. *Med. Chem. Commun.* 10, 961–969. doi:10.1039/C9MD00161A

El-Shemi, A. G., and Faidah, H. S. (2011). Synergy of Daptomycin with Fusidin against Invasive Systemic Infection and Septic Arthritis Induced by Type IV Group B Streptococci in Mice. *Afr. J. Pharm. Pharmacol.* 5, 1125–1131. doi:10.5897/AJPP11.396

Espinoza-Moraga, M., Singh, K., Njoroge, M., Kaur, G., Okombo, J., De Kock, C., et al. (2016). Synthesis and Biological Characterisation of Ester and Amide Derivatives of Fusidic Acid as Antiplasmodial Agents. *Bioorg. Med. Chem. Lett.* 27, 658–661. doi:10.1016/j.bmcl.2016.11.077

Faber, V., Dalgleish, A. G., Newell, A., and Malkovsky, M. (1987). Inhibition of HIV Replication *In Vitro* by Fusidic Acid. *Lancet* 2, 827–828. doi:10.1016/S0140-6736(87)91016-6

Fabry, W., Schmid, E. N., and Ansorg, R. (1996). Comparison of the E Test and A Proportion Dilution Method for Susceptibility Testing of Mycobacterium Tuberculosis. *J. Med. Microbiol.* 44, 394–401. doi:10.1099/00222615-44-3-227

Famularo, G., De Simone, C., Tzantzoglou, S., Trinchieri, V., Moretti, S., and Tonietti, G. (1993). *In Vivo* and *In Vitro* Efficacy of Fusidic Acid in HIV Infection. *Ann. N. Y. Acad. Sci.* 685, 341–343. doi:10.1111/j.1749-6632.1993.tb35885.x

Ferlay, J., Colombet, M., Soerjomataram, I., Parkin, D. M., Piñeros, M., Znaor, A., et al. (2021). Cancer Statistics for the Year 2020: An Overview. *Int. J. Cancer* 149, 778–789. doi:10.1002/ijc.33588

Fernandes, P., and Pereira, D. (2011). Efforts to Support the Development of Fusidic Acid in the United States. *Clin. Infect. Dis.* 52, S542–S546. doi:10.1093/cid/cir170

Fernandes, P. (2016). Fusidic Acid: A Bacterial Elongation Factor Inhibitor for the Oral Treatment of Acute and Chronic Staphylococcal Infections. *Cold Spring Harb Perspect. Med.* 6, a025437. doi:10.1101/cshperspect.a025437

Ferrero-Miliani, L., Nielsen, O. H., Andersen, P. S., and Girardin, S. E. (2007). Chronic Inflammation: Importance of NOD2 and NALP3 in Interleukin-1beta Generation. *Clin. Exp. Immunol.* 147, 227–235. doi:10.1111/j.1365-2249.2006.03261.x

Fuursted, K., Askgaard, D., and Faber, V. (1992). Susceptibility of Strains of the Mycobacterium Tuberculosis Complex to Fusidic Acid. *APMIS* 100, 663–667. doi:10.1111/j.1699-0463.1992.tb03983.x

Gallelli, L., Zhang, L., Wang, T., and Fu, F. (2020). Severe Acute Lung Injury Related to COVID-19 Infection: A Review and the Possible Role for Escin. *J. Clin. Pharmacol.* 60, 815–825. doi:10.1002/jcph.1644

Genovese, F., Mancuso, G., Cuzzola, M., Cusumano, V., Nicoletti, F., Bendtzen, K., et al. (1996). Improved Survival and Antagonistic Effect of Sodium Fusidate on Tumor Necrosis Factor Alpha in A Neonatal Mouse Model of Endotoxin Shock. *Antimicrob. Agents Chemother.* 40, 1733–1735. doi:10.1128/AAC.40.7.1733

Godtfredsen, W. O., Jahnsen, S., Lorck, H., Roholt, K., and Tybring, L. (1962a). Fusidic Acid: A New Antibiotic. *Nature* 193, 987. doi:10.1038/193987a0

Godtfredsen, W. O., Roholt, K., and Tybring, L. (1962b). Fucidin, A New Antibiotic. *Can. Med. Assoc. J.* 86, 1122–1123. doi:10.1016/S0140-6736(62)91968-2

Gopinath, S., Kim, M. V., Rakib, T., Wong, P. W., Van Zandt, M., Barry, N. A., et al. (2018). Topical Application of Aminoglycoside Antibiotics Enhances Host Resistance to Viral Infections in a Microbiota-independent Manner. *Nat. Microbiol.* 3, 611–621. doi:10.1038/s41564-018-0138-2

Guo, M., Ren, Q., Wang, B., Ji, W., Ni, J., Feng, Y., et al. (2019). Discovery and Synthesis of 3- and 21-substituted Fusidic Acid Derivatives as Reversal Agents of P-Glycoprotein-Mediated Multidrug Resistance. *Eur. J. Med. Chem.* 182, 111668. doi:10.1016/j.ejmech.2019.111668

Gupta, A., Mir, S. S., Saqib, U., Biswas, S., Vaishya, S., Srivastava, K., et al. (2013). The Effect of Fusidic Acid on Plasmodium Falciparum Elongation Factor G (EF-G). *Mol. Biochem. Parasitol.* 192, 39–48. doi:10.1016/j.molbiopara.2013.10.003

Hajikhani, B., Goudarzi, M., Kakavandi, S., Amini, S., Zamani, S., van Belkum, A., et al. (2021). The Global Prevalence of Fusidic Acid Resistance in Clinical Isolates of *Staphylococcus aureus*: a Systematic Review and Meta-Analysis. *Antimicrob. Resist. Infect. Control.* 10, 75. doi:10.1186/s13756-021-00943-6

Hørding, M., Christensen, K. C., and Faber, V. (1990). Fusidic Acid Treatment of HIV Infection: No Significant Effect in A Pilot Trial. *Scand. J. Infect. Dis.* 22, 649–652. doi:10.3109/00365549009027116

Hoffner, S. E., Olsson-Liljequist, B., Rydgård, K. J., Svenson, S. B., and Källenius, G. (1990). Susceptibility of Mycobacteria to Fusidic Acid. *Eur. J. Clin. Microbiol. Infect. Dis.* 9, 294–297. doi:10.1007/BF01968066

Johnson, R. A., McFadden, G. I., and Goodman, C. D. (2011). Characterization of Two Malaria Parasite Organelle Translation Elongation Factor G Proteins: The Likely Targets of the Anti-malarial Fusidic Acid. *PLoS One* 6, e20633. doi:10.1371/journal.pone.0020633

Kaur, G., Singh, K., Pavadai, E., Njoroge, M., Espinoza-Moraga, M., De Kock, C., et al. (2015). Synthesis of Fusidic Acid Bioisosteres as Antiplasmodial Agents and Molecular Docking Studies in the Binding Site of Elongation Factor-G. *Med. Chem. Commun.* 6, 2023–2028. doi:10.1039/C5MD00343A

Kaur, G., Pavadai, E., Wittlin, S., and Chibale, K. (2018). 3D-QSAR Modeling and Synthesis of New Fusidic Acid Derivatives as Antiplasmodial Agents. *J. Chem. Inf. Model.* 58, 1553–1560. doi:10.1021/acs.jcim.8b00105

Kigondu, E. M., Wasuna, A., Warner, D. F., and Chibale, K. (2014). Pharmacologically Active Metabolites, Combination Screening and Target Identification-Driven Drug Repositioning in Antituberculosis Drug Discovery. *Bioorg. Med. Chem.* 22, 4453–4461. doi:10.1016/j.bmc.2014.06.012

Kilic, F. S., Erol, K., Batu, O., Yildirim, E., and Usluer, G. (2002). The Effects of Fusidic Acid on the Inflammatory Response in Rats. *Pharmacol. Res.* 45, 265–267. doi:10.1006/phrs.2001.0946

Kinoshita, T., Kawano, G., and Tanaka, N. (1968). Association of Fusidic Acid Sensitivity with G Factor in A Protein-Synthesizing System. *Biochem. Biophys. Res. Commun.* 33, 769–773. doi:10.1016/0006-291X(68)90226-X

Kumar, A., and Jaitak, V. (2019). Natural Products as Multidrug Resistance Modulators in Cancer. *Eur. J. Med. Chem.* 176, 268–291. doi:10.1016/j.ejmech.2019.05.027

Kwofie, S. K., Broni, E., Asiedu, S. O., Kwarko, G. B., Dankwa, B., Enninful, K. S., et al. (2021). Cheminformatics-Based Identification of Potential Novel Anti-SARS-CoV-2 Natural Compounds of African Origin. *Molecules* 26, 406. doi:10.3390/molecules26020406

Lage, H. (2008). An Overview of Cancer Multidrug Resistance: A Still Unsolved Problem. *Cell. Mol. Life Sci.* 65, 3145–3167. doi:10.1007/s00018-008-8111-5

Lapham, K., Novak, J., Marroquin, L. D., Swiss, R., Qin, S., Strock, C. J., et al. (2016). Inhibition of Hepatobiliary Transport Activity by the Antibacterial Agent Fusidic Acid: Insights into Factors Contributing to Conjugated Hyperbilirubinemia/Cholestasis. *Chem. Res. Toxicol.* 29, 1778–1788. doi:10.1021/acs.chemrestox.6b00262

Lin, D., Jing, X., Chen, Y., Liang, Y., Lei, M., Peng, S., et al. (2017). Rifampicin Pre-treatment Inhibits the Toxicity of Rotenone-Induced PC12 Cells by Enhancing Sumoylation Modification of α-synuclein. *Biochem. Biophys. Res. Commun.* 485, 23–29. doi:10.1016/j.bbrc.2017.01.100

Liu, J., Zeng, S., Meng, X., Jiang, X., and Guo, X. (2019). Antiviral Activity of Fusidate Sodium against Enterovirus A71. *China Trop. Med.* 19, 519–524. doi:10.13604/j.cnki.46-1064/r.2019.06.05

Lloyd, G., Atkinson, T., and Sutton, P. M. (1988). Effect of Bile Salts and of Fusidic Acid on HIV-1 Infection of Cultured Cells. *Lancet* 1, 1418–1421. doi:10.1016/s0140-6736(88)92236-2

Lu, J., Ni, J. X., Wang, J. A., Liu, Z. Y., Shang, K. L., and Bi, Y. (2019). Integration of Multiscale Molecular Modeling Approaches with the Design and Discovery of Fusidic Acid Derivatives. *Future Med. Chem.* 11, 1427–1442. doi:10.4155/fmc-2018-0567

Malhotra, P. (2020). "Mycoses in Hematological Malignancies," in *Clinical Practice of Medical Mycology in Asia*. Editor C. Arunaloke (Singapore: Springer Singapore), 119–134. doi:10.1007/978-981-13-9459-1_9

Di Marco, R., Khademi, M., Wallstrom, E., Muhallab, S., Nicoletti, F., and Olsson, T. (1999). Amelioration of Experimental Allergic Neuritis by Sodium Fusidate

(Fusidin): Suppression of IFN-γ and TNF-α and Enhancement of IL-10. *J. Autoimmun.* 13, 187–195. doi:10.1006/jaut.1999.0317

Mindermann, T., Zimmerli, W., Rajacic, Z., and Gratzl, O. (1993). Penetration of Fusidic Acid into Human Brain Tissue and Cerebrospinal Fluid. *Acta Neurochir (Wien)* 121, 12–14. doi:10.1007/BF01405176

Newman, D. J., and Cragg, G. M. (2020). Natural Products as Sources of New Drugs over the Nearly Four Decades from 01/1981 to 09/2019. *J. Nat. Prod.* 83, 770–803. doi:10.1021/acs.jnatprod.9b01285

Ni, J., Guo, M., Cao, Y., Lei, L., Liu, K., Wang, B., et al. (2019). Discovery, Synthesis of Novel Fusidic Acid Derivatives Possessed Amino-Terminal Groups at the 3-Hydroxyl Position with Anticancer Activity. *Eur. J. Med. Chem.* 162, 122–131. doi:10.1016/j.ejmech.2018.10.059

Nicola, A. M., Albuquerque, P., Paes, H. C., Fernandes, L., Costa, F. F., Kioshima, E. S., et al. (2019). Antifungal Drugs: New Insights in Research & Development. *Pharmacol. Ther.* 195, 21–38. doi:10.1016/j.pharmthera.2018.10.008

Nicoletti, F., Beltrami, B., Raschi, E., Di Marco, R., Magro, G., Grasso, S., et al. (1998). Protection from Concanavalin A (Con A)-Induced T Cell-dependent Hepatic Lesions and Modulation of Cytokine Release in Mice by Sodium Fusidate. *Clin. Exp. Immunol.* 110, 479–484. doi:10.1046/j.1365-2249.1997.4091423.x

Njoroge, M., Kaur, G., Espinoza-Moraga, M., Wasuna, A., Dziwornu, G. A., Seldon, R., et al. (2019). Semisynthetic Antimycobacterial C-3 Silicate and C-3/C-21 Ester Derivatives of Fusidic Acid: Pharmacological Evaluation and Stability Studies in Liver Microsomes, Rat Plasma, and Mycobacterium Tuberculosis Culture. *ACS Infect. Dis.* 5, 1634–1644. doi:10.1021/acsinfecdis.9b00208

Öztas, S., Kurutepe, M., Adigüzel, N., Acartürk, E., Saraç, S., Marasli, D., et al. (2008). Vitro Efficacy of Fusidic Acid on Drug Resistant Strains of Mycobacterium Tuberculosis. *Turk Toraks Dergisi* 9, 109–112.

Palmeira, A., Sousa, E., Vasconcelos, M. H., and Pinto, M. M. (2012). Three Decades of P-Gp Inhibitors: Skimming through Several Generations and Scaffolds. *Curr. Med. Chem.* 19, 1946–2025. doi:10.2174/092986712800167392

Park, E., Kim, D. K., Kim, C. S., Kim, J. S., Kim, S., Chun, H. S., et al. (2019). Protective Effects of Fusidic Acid against Sodium Nitroprusside-Induced Apoptosis in C6 Glial Cells. *NeuroReport* 30, 1222–1229. doi:10.1097/WNR.0000000000001354

Pavadai, E., Kaur, G., Wittlin, S., and Chibale, K. (2017). Identification of Steroid-like Natural Products as Antiplasmodial Agents by 2D and 3D Similarity-Based Virtual Screening. *Medchemcomm* 8, 1152–1157. doi:10.1039/C7MD00063D

Payne, A. J., Neal, L. M., and Knoll, L. J. (2013). Fusidic Acid Is an Effective Treatment against Toxoplasma Gondii and Listeria Monocytogenes *In Vitro*, but Not in Mice. *Parasitol. Res.* 112, 3859–3863. doi:10.1007/s00436-013-3574-1

Persidis, A. (1999). Cancer Multidrug Resistance. *Nat. Biotechnol.* 17, 94–95. doi:10.1038/5289

Reglodi, D., Renaud, J., Tamas, A., Tizabi, Y., Socías, S. B., Del-Bel, E., et al. (2017). Novel Tactics for Neuroprotection in Parkinson's Disease: Role of Antibiotics, Polyphenols and Neuropeptides. *Prog. Neurobiol.* 155, 120–148. doi:10.1016/j.pneurobio.2015.10.004

Riber, D., Venkataramana, M., Sanyal, S., and Duvold, T. (2006). Synthesis and Biological Evaluation of Photoaffinity Labeled Fusidic Acid Analogues. *J. Med. Chem.* 49, 1503–1505. doi:10.1021/jm050583t

Rieutord, A., Bourget, P., Troche, G., and Zazzo, J. F. (1995). *In Vitro* Study of the Protein Binding of Fusidic Acid: A Contribution to the Comprehension of its Pharmacokinetic Behaviour. *Int. J. Pharm.* 119, 57–64. doi:10.1016/0378-5173(94)00369-G

Rizk, M. A., El-Sayed, S. A. E., Nassif, M., Mosqueda, J., Xuan, X., and Igarashi, I. (2020). Assay Methods for *In Vitro* and *In Vivo* Anti-babesia Drug Efficacy Testing: Current Progress, Outlook, and Challenges. *Vet. Parasitol.* 279, 109013. doi:10.1016/j.vetpar.2019.109013

Rodrigues, T., Reker, D., Schneider, P., and Schneider, G. (2016). Counting on Natural Products for Drug Design. *Nat. Chem.* 8, 531–541. doi:10.1038/nchem.2479

Salama, A. A., AbouLaila, M., Moussa, A. A., Nayel, M. A., El-Sify, A., Terkawi, M. A., et al. (2013). Evaluation of *In Vitro* and *In Vivo* Inhibitory Effects of Fusidic Acid on Babesia and Theileria Parasites. *Vet. Parasitol.* 191, 1–10. doi:10.1016/j.vetpar.2012.08.022

Salimova, E. V., Mamaev, A. G., Tret'yakova, E. V., Kukovinets, O. S., Mavzyutov, A. R., Shvets, K. Y., et al. (2018). Synthesis and Biological Activity of Cyanoethyl Derivatives of Fusidic Acid. *Russ. J. Org. Chem.* 54, 1411–1418. doi:10.1134/S1070428018090245

Salimova, E. V., Tret'yakova, E. V., and Parfenova, L. V. (2019). Synthesis and Cytotoxic Activity of 3-amino Substituted Fusidane Triterpenoids. *Med. Chem. Res.* 28, 2171–2183. doi:10.1007/s00044-019-02445-y

Salimova, E. V., Magafurova, A. A., Tretyakova, E. V., Kukovinets, O. S., and Parfenova, L. V. (2020). Indole Derivatives of Fusidane Triterpenoids: Synthesis and the Antibacterial Activity. *Chem. Heterocycl Comp.* 56, 800–804. doi:10.1007/s10593-020-02733-1

Sanders, J. M., Monogue, M. L., Jodlowski, T. Z., and Cutrell, J. B. (2020). Pharmacologic Treatments for Coronavirus Disease 2019 (COVID-19): A Review. *JAMA* 323, 1824–1836. doi:10.1001/jama.2020.6019

Savelsbergh, A., Rodnina, M. V., and Wintermeyer, W. (2009). Distinct Functions of Elongation Factor G in Ribosome Recycling and Translocation. *RNA* 15, 772–780. doi:10.1261/rna.1592509

Schou, S. C., Riber, D., and Grue-Sørensen, G. (2007). Synthesis of Radiolabelled Photolabile Fusidic Acid Analogues. *J. Label Compd. Radiopharm.* 50, 1260–1261. doi:10.1002/jlcr.1458

Shakurova, E. R., Salimova, E. V., Mescheryakova, E. S., and Parfenova, L. V. (2019). One-pot Synthesis of Quaternary Pyridinium Salts and Tetrahydropyridine Derivatives of Fusidane Triterpenoids. *Chem. Heterocycl Comp.* 55, 1204–1210. doi:10.1007/s10593-019-02602-6

Shanika, P. S. (2017). Semi-synthesis and Evaluation of Fusidic Acid Derivatives as Potential Antituberculosis Agents. Dissertation/master's thesis. Cape Town (Western Cape): University of Cape Town.

Singh, A. K., Rana, H. K., and Pandey, A. K. (2019). "Fungal-Derived Natural Product: Synthesis, Function, and Applications," in *Recent Advancement in White Biotechnology through Fungi*. Editors A. N. Yadav, S. Singh, S. Mishra, and A. Gupta (New York, NY: Springer Cham), 229–248. doi:10.1007/978-3-030-14846-1_8

Singh, K., Kaur, G., Shanika, P. S., Dziwornu, G. A., Okombo, J., and Chibale, K. (2020). Structure-Activity Relationship Analyses of Fusidic Acid Derivatives Highlight Crucial Role of the C-21 Carboxylic Acid Moiety to its Anti-mycobacterial Activity. *Bioorg. Med. Chem.* 28, 115530. doi:10.1016/j.bmc.2020.115530

Singh, V., Dziwornu, G. A., Mabhula, A., and Chibale, K. (2021). Rv0684/fusA1, an Essential Gene, Is the Target of Fusidic Acid and its Derivatives in *Mycobacterium tuberculosis*. *ACS. Infect. Dis.* 7, 2437–2444. doi:10.1021/acsinfecdis.1c00195

Still, J. G., Clark, K., Degenhardt, T. P., Scott, D., Fernandes, P., and Gutierrez, M. J. (2011). Pharmacokinetics and Safety of Single, Multiple, and Loading Doses of Fusidic Acid in Healthy Subjects. *Clin. Infect. Dis.* 52, S504–S512. doi:10.1093/cid/cir174

Turnidge, J. (1999). Fusidic Acid Pharmacology, Pharmacokinetics and Pharmacodynamics. *Int. J. Antimicrob. Agents* 12, 23–34. doi:10.1016/S0924-8579(98)00071-5

Wilson, D. N. (2014). Ribosome-Targeting Antibiotics and Mechanisms of Bacterial Resistance. *Nat. Rev. Microbiol.* 12, 35–48. doi:10.1038/nrmicro3155

World Health Organization (2020a). World Malaria Report 2020. Available at: https://www.who.int/publications/i/item/9789240015791 (Accessed August 07, 2021).

World Health Organization (2020b). World Tuberculosis Day 2020. Available at: https://apps.who.int/iris/bitstream/handle/10665/336069/9789240013131-eng.pdf (Accessed August 07, 2021).

Wu, P. P., He, H., Hong, W. D., Wu, T. R., Huang, G. Y., Zhong, Y. Y., et al. (2018a). The Biological Evaluation of Fusidic Acid and its Hydrogenation Derivative as Antimicrobial and Anti-inflammatory Agents. *Infect. Drug Resist.* 11, 1945–1957. doi:10.2147/IDR.S176390

Wu, X., Liang, Y., Jing, X., Lin, D., Chen, Y., Zhou, T., et al. (2018b). Rifampicin Prevents SH-SY5Y Cells from Rotenone-Induced Apoptosis via the PI3K/Akt/GSK-3β/CREB Signaling Pathway. *Neurochem. Res.* 43, 886–893. doi:10.1007/s11064-018-2494-y

Yamaki, H. (1965). Inhibition of Protein Synthesis by Fusidic and Helvolinic Acids, Steroidal Antibiotics. *J. Antibiot.* 18, 228–232. doi:10.11554/antibioticsa.18.5_228

Youle, M. S., Hawkins, D. A., Lawrence, A. G., Tenant-Flowers, M., Shanson, D. C., and Gazzard, B. G. (1989). Clinical, Immunological, and Virological Effects of Sodium Fusidate in Patients with AIDS or AIDS-Related Complex (ARC): An

Open Study. *J. Acquired Immune Defic. Syndr.* 2, 59–62. doi:10.1007/BF01643625

Zając-Spychała, O., Skalska-Sadowska, J., Wachowiak, J., Szmydki-Baran, A., Hutnik, Ł., Matysiak, M., et al. (2019). Infections in Children with Acute Myeloid Leukemia: Increased Mortality in Relapsed/Refractory Patients. *Leuk. Lymphoma* 60, 3028–3035. doi:10.1080/10428194.2019.1616185

Zhao, M., Gödecke, T., Gunn, J., Duan, J. A., and Che, C. T. (2013). Protostane and Fusidane Triterpenes: A Mini-Review. *Molecules* 18, 4054–4080. doi:10.3390/molecules18044054

Zida, A., Bamba, S., Yacouba, A., Ouedraogo-Traore, R., and Guiguemdé, R. T. (2017). Anti-Candida Albicans Natural Products, Sources of New Antifungal Drugs: A Review. *J. Mycol. Med.* 27, 1–19. doi:10.1016/j.mycmed.2016.10.002

Zink, M. C., Uhrlaub, J., DeWitt, J., Voelker, T., Bullock, B., Mankowski, J., et al. (2005). Neuroprotective and Anti-human Immunodeficiency Virus Activity of Minocycline. *JAMA* 293, 2003–2011. doi:10.1001/jama.293.16.2003

Conflict of Interest: The authors declare that the research was conducted in the absence of any commercial or financial relationships that could be construed as a potential conflict of interest.

Publisher's Note: All claims expressed in this article are solely those of the authors and do not necessarily represent those of their affiliated organizations, or those of the publisher, the editors, and the reviewers. Any product that may be evaluated in this article, or claim that may be made by its manufacturer, is not guaranteed or endorsed by the publisher.

Copyright © 2021 Long, Ji, Zhang, Zhu and Bi. This is an open-access article distributed under the terms of the Creative Commons Attribution License (CC BY). The use, distribution or reproduction in other forums is permitted, provided the original author(s) and the copyright owner(s) are credited and that the original publication in this journal is cited, in accordance with accepted academic practice. No use, distribution or reproduction is permitted which does not comply with these terms.

frontiers in Pharmacology

ORIGINAL RESEARCH
published: 21 October 2021
doi: 10.3389/fphar.2021.746725

Photodynamic Therapy of Novel Photosensitizer Ameliorates TNBS-Induced Ulcerative Colitis *via* Inhibition of AOC_1

Yumei Rong[1], *Ge Hong*[1], *Na Zhu*[1], *Yang Liu*[1], *Yong Jiang*[2] *and Tianjun Liu*[1]*

[1]Tianjin Key Laboratory of Biomedical Material, Institute of Biomedical Engineering, Chinese Academy of Medical Sciences and Peking Union Medical College, Tianjin, China, [2]Department of Gastroenterology, The Second Hospital of Tianjin Medical University, Tianjin, China

Ulcerative colitis (UC), a chronic, nonspecific inflammatory bowel disease characterized by continuous and diffuse inflammatory changes in the colonic mucosa, requires novel treatment method. Photodynamic therapy (PDT), as a promising physico-chemical treatment method, were used to treat UC rats' model with novel photosensitizer LD_4 in this paper, the treatment effect and mechanism was investigated. LD_4-PDT could improve the survival rate of 2,4,6-trinitrobenzene sulfonic acid (TNBS)-induced UC model rats, decrease expression of interleukin (IL)-6, IL-1, tumor necrosis factor (TNF)-α, malondialdehyde (MDA), myeloperoxidase (MPO) and increase the expression of glutathione (GSH) and superoxide oxidase (SOD), while protecting the integrity of the intestinal epithelium. LD_4-PDT treatment could rebuild the intestinal microflora composition and reprogram the colonic protein profiles in TNBS-induced rats to almost the normal state. Proteomics analysis based upon TNBS-induced UC model rats revealed that Amine oxidase copper-containing 1 (AOC_1) was a potential target of LD_4-PDT. Novel photosensitizer agent LD_4-PDT represents an efficient treatment method for UC, and AOC_1 may be a promising target.

Keywords: ulcerative colitis, gut microbiota, photodynamic therapy, novel photosensitizer, AOC1

OPEN ACCESS

Edited by:
Andres Trostchansky, Universidad de la República, Uruguay

Reviewed by:
Hao-Sen Chiang, National Taiwan University, Taiwan
Mohamed Abdo Rizk, Mansoura University, Egypt

***Correspondence:**
Tianjun Liu
liutianjun@hotmail.com

Specialty section:
This article was submitted to Experimental Pharmacology and Drug Discovery, a section of the journal Frontiers in Pharmacology

Received: *24 July 2021*
Accepted: *01 October 2021*
Published: *21 October 2021*

Citation:
Rong Y, Hong G, Zhu N, Liu Y, Jiang Y and Liu T (2021) Photodynamic Therapy of Novel Photosensitizer Ameliorates TNBS-Induced Ulcerative Colitis via Inhibition of AOC_1. Front. Pharmacol. 12:746725. doi: 10.3389/fphar.2021.746725

INTRODUCTION

Ulcerative colitis (UC) is a chronic, nonspecific inflammatory disease of unknown etiology (Shivaji et al., 2020). The lesions are mainly located in the large intestine, mostly in the rectum and sigmoid colon, limited to the colonic mucosa and submucosa, showing continuous non-segmental distribution. The main acute clinical symptoms of UC are recurrent abdominal pain, diarrhea, and hematochezia. UC characterized by a wide range of lesions, complex pathogenesis, frequent recurrent attacks, and easy carcinogenesis, has been included in the list of modern refractory diseases by the World Health Organization (WHO). Its morbidity is related to infection, autoimmunity, heredity, and environment (Costello et al., 2019). With the development of economy and westernization of living habits and dietary composition, the incidence of UC in Asian countries is also increasing annually (Chow et al., 2009; Ng et al., 2017). Finding an effective treatment method of UC, to restore the patients' physical and mental health and relieve the heavy economic burden brought by the disease to the patients' families and society in general, has become a key scientific problem in clinical practice.

Currently, the clinical treatment of UC mainly focuses on anti-inflammatory, immune-regulatory or surgical treatments (Qiu et al., 2018; Ward et al., 2018), and pharmaceutical intervention has been the most adopted approach. Conventional therapeutic drugs mainly included amino salicylic acids, glucocorticoids, immunosuppressants, antibiotics and microecological agents. These drugs can only temporarily control and relieve symptoms, but cannot fundamentally cure the disease, and are accompanied by defects such as substantial toxicity and side effects, poor maintenance effect and frequent disease recurrence. Surgical treatment is mainly performed on patients with massive bleeding, intestinal perforation, canceration and toxic intestinal dilatation, and generally carries disadvantages such as large trauma, many complications, slow postoperative recovery and frequent disease recurrence (Hindryckx et al., 2015; Hirono et al., 2018; Ward et al., 2018). Therefore, development of an alternative therapy with good curative effect and fewer adverse reactions become a highly desire in UC research.

With the development of pharmaceutical biotechnology, many novel therapeutic methods have emerged, including biological targeted therapy, traditional Chinese medicine, stem cell therapy and photodynamic therapy (PDT) (Sands et al., 2019). Among them, PDT is a new technology being developed internationally. It can selectively act on target tissues and produce a photodynamic response *via* a photosensitizer (Mallidi et al., 2015). PDT has the advantages of rapid onset, strong targeting, low toxicity and side effects, and repeatable treatment. Recently, its clinical indications have been extended from malignant tumors to increasing numbers of benign diseases. The rapid development of endoscopy and fiber optics technology makes it possible to use PDT to treat gastrointestinal diseases and provides a new direction for the clinical treatment of UC. However, few reports regarding PDT treatment of UC (or inflammatory bowel disease). Favre and colleagues (Favre et al., 2011), using 5-aminolevulinic acid (5-ALA) as the photosensitizer to treat mice bearing Crohn's disease, found that low dose PDT can down-regulate the expression of proinflammatory cytokines and induction of T-cell apoptosis to improve T-cell-mediated colitis with no significant side effects. Reinhard et al. (2015) treated dextran sulfate sodium (DSS)-induced inflammatory bowel disease in mice with the photosensitizer temoporfin and found that PDT could effectively reduce the symptoms of colitis and prevent intestinal cancer.

Despite their potential, photosensitizers were crucial in PDT. However 5-ALA itself has no photosensitive activity; instead it is transformed to protoporphyrin IX upon activation by ALA dehydrase, the concentration remains low, with uneven distribution and low efficiency of photodynamic reaction (Maisch et al., 2011). The poor solubility of temoporfin in water tends to cause adverse reactions such as neuralgia and suppression of the central nervous system (Senge, 2012). Therefore, it is necessary to develop a better photosensitizer for the treatment of UC with good solubility in water, high bioavailability, high photo response efficiency and fewer adverse reactions.

We designed and synthesized a series of alkaline amino acid modified amino tetraphenyl porphyrin compounds, all of which showed good physical and chemical properties (Meng et al., 2015). One of the compounds, 5,10,15,20-tetra{4-[(S)-2,6-diamino-hexamide] phenyl} porphyrin (LD_4), with good water solubility, low toxicity and targeting characteristics, showed unique promotion of wound healing and immune regulation, as well inhibition of microbial pathogens in treatment of traumatic infection (Xu et al., 2016; Zhao et al., 2021). On the basis of these results, we sought to determine whether this photosensitizer could regulate the microflora and treat UC.

Amine oxidase copper-containing 1 (AOC_1), an amine oxidase containing copper, catalyzes the degradation of compounds such as propylamine and spermine. Some reports have indicated that AOC_1 was involved in allergy and immune responses, cell proliferation, tissue differentiation and cell apoptosis (Strolin Benedetti et al., 2007; Shepard and Dooley, 2015; Vakal et al., 2020). Although its mechanism of action *in vivo* is not fully understood, its role in immune cell transport makes it a target for autoimmune and inflammatory diseases (Peet et al., 2011). AOC_1 is mainly distributed in the intestines and kidneys. Clinically, plasma AOC_1 activity is used to diagnose intestinal integrity (DiSilvestro et al., 1997). Knockdown of AOC_1 could inhibit the activation of protein kinase B (*AKT*) and the epithelial-mesenchymal transition (EMT) process (Xu et al., 2020). The aim of this study was to investigate the photodynamic therapeutic efficacy and molecular mechanism of LD_4 in models of UC.

MATERIALS AND METHODS

LD_4 Synthesis and Characterization

Synthesis and characterization of LD_4 was previously reported by our laboratory (Meng et al., 2015). The structure of LD_4 is shown in **Supplementary Figure S1A**. The sample was excited by a 650 nm semiconductor laser (WSLS-650-500m-200M-H4; Wave spectrum Laser; China) through a columnar fiber. The energy density of the spot was measured using a light power meter (LM1; Carl Zeiss).

Experimental Animals

Male Sprague Dawley rats aged 6–8 weeks were purchased from HFK Biosciences Experimental Animals Company (SCXK 2019-0008, China) and raised in specific pathogen-free conditions. All animal experiments procedures were experimented according to the National Institutes of Health Guide for Care and Use of Laboratory Animals, and the protocol was approved by the Laboratory Animal Management Committee/Laboratory Animal Welfare Ethics Committee, Institute of Radiation Medicine, Chinese Academy of Medical Sciences (Approval No. IRM-DWLL-2017092). The ambient temperature was 22 ± 2°C, with relative air humidity of 40–70%, and food and sterile water were fed according to the experimental requirements.

Induction of Colitis

Rats were fasted for 24 h then anesthetized with 10% chloral hydrate before colitis induction. The UC model was induced using the method described by Morris et al. (1989), Wirtz et al. (2007). Briefly, 30 mg of TNBS (A28757; Innochem) in 0.25 ml of 50% ethanol was injected into rat colon through a 3 mm diameter polyethylene rubber catheter (inserted 8 cm into the proximal anal rectum). Rats were then maintained in a head low, tail high position for 1 min. Occult blood test paper was used to detect feces every day.

LD4-Photodynamic Therapy Treatment

The rats were randomly divided into six groups (10 rats per group) and treated as follows: 1, control group (normal saline); 2, TNBS group (TNBS enema); 3, LD_4-PDTL group [TNBS and low-dose LD_4 (60 μg/kg), both *via* enema]; 4, LD_4-PDTM group [TNBS and medium-dose LD_4 (120 μg/kg), both *via* enema]; 5, LD_4-PDTH group [TNBS and high-dose LD_4 (240 μg/kg), both *via* enema]; 6, SASP group [TNBS enema and positive control drug, SASP (500 mg/kg), gavage]. With the day of TNBS enema injection as day 0, treatment was initiated at day 7. LD_4 was administered *via* enema every other day, while SASP was administered *via* gavage at the same time points, for a total of four treatments. Thirty minutes after each treatment, the colon was irradiated with an intensive 650 nm PDT system at an energy density of 25 J/cm^2, excluding the SASP group, which was not irradiated. Body weight and food intake were daily measured. After all treatments were completed, fecal samples from each group were collected and stored at −80°C for further analysis of 16S rRNA. After 24 h of fasting, all rats were sacrificed and whole colons and blood were collected. The colon tissue was weighed, dissected and stored at −80°C. Parts of the tissue were also fixed with 4% paraformaldehyde. All rats in the experiment were treated according to guidelines set out in the National Institutes of Health's Laboratory Animal Care and Use Guidelines.

FITC-Dextran Fluorescence Intensity Test

Intestinal permeability can be semi-quantitatively measured by detecting fluorescence intensity in serum using fluorescent tracers. Two hundred micrograms of FITC-dextran (FD40S; Sigma-Aldrich) powder were weighed and dissolved in 5 ml rat serum, diluted by doubling dilution method for 10 dilutions, and then fluorescence intensity was detected with a Varioskan Flash 3001 enzyme plate analyzer (Thermo Fisher, Waltham, MA) to obtain a standard curve. The standard curve were shown in **Supplementary Figure S1C**. Following LD_4-PDT treatment, six rats from each group were fasted for 4 h before intragastric administration of FITC-dextran at a dose of 0.6 mg/g. Blood samples were collected before the animals were sacrificed and serum without hemolysis was collected. Sera were added to a 96-well plate, at 100 μl per well. Fluorescence intensity (Ex/Em: 488/520 nm) was measured with a Varioskan Flash 3001 enzyme plate analyzer. The FITC-dextran content in the rat sera was then calculated from the established standard curve.

Biochemical Analysis

Cytokines was correlated tightly with the occurrence of the infection, interleukin-6 (*IL-6*), tumor necrosis factor-*α* (*TNF-α*) and interleukin-1 (*IL-1*), while myeloperoxidase (*MPO*), malondialdehyde (*MDA*), glutathione (*GSH*) and superoxide dismutase (*SOD*) were correlated with oxidative stress reaction, which was often occurred in UC. So here we measured this cytokinesis to evaluate the efficacy of the treatment. *IL-6* (SEA079Ra; Cloud-Clone Corp) and *TNF-α* (SEA133Ra; Cloud-Clone Corp) were quantified using commercially available ELISA kits. Standard curves are shown in **Supplementary Figure S1D,E**. *MPO* (A044-1-1; Nanjing Jiancheng Bioengineering Institute), *GSH* (A006-1-1; Nanjing Jiancheng Bioengineering Institute), *MDA* (A003-1-2; Nanjing Jiancheng Bioengineering Institute) and *T-SOD* (A001-1-2; Nanjing Jiancheng Bioengineering Institute levels in sera were determined by ELISA assay kits according to the manufacturer's instructions.

Histopathological Analysis

Harvested colon tissue was dehydrated, embedded and sliced for histopathological analysis. Hematoxylin and eosin staining was performed as previously described (Zhang et al., 2020), and the extent of inflammation was scored according to the literature (Rong et al., 2018).

Bacterial Diversity Analysis

Fresh, uncontaminated feces were collected from six rats in different cages and stored at −80°C until use. DNA was extracted from feces and measured by Qubit Fluorometer. The mass concentration of the DNA library was greater than 1.0 ng/μl, which was of sufficient quality for use in subsequent experiments. Illumina MiSeq technology was used to amplify and sequence the V3–V4 region of the bacterial 16S rRNA gene. The bacterial 16S ribosomal (r) RNA forward primer sequence was 5′-CCTACGGGNGGCWGCAG-3′ and the reverse primer sequence was 5′-GACTACHVGGGTATCTAATCC-3′. USEARCH (http://www.drive5.com/usearch/7.0) was used to analyze the data. Bioinformatics analysis was performed according to the operational taxonomic unit (OTU). Similarity greater than 97% sequence clustering represented an OTU. The ribosomal database project (RDP) classifier was used to systematically classify OTU sequences with reference to the Silva database.

Protein Extraction and Quality Control

The colon tissue samples were lysed by addition of 600 μl of 8 M urea (lysate: protease inhibitor, 50:1), sonicated for 1 s, stopped for 2 s; this procedure was repeated for a total of 120 s. Samples were centrifuged at 14,000 × g for 20 min at 4°C. Protein was quantified by sodium dodecyl sulphate-polyacrylamide gel electrophoresis. The protein solution rapid prototype high performance liquid chromatograph (RP-HPLC) was separated using an RIGOL L-3000 system (Rigol Technologies, inc.; China) according to the manufacturer's protocol.

Peptide Identification by Liquid Chromatography Mass Spectrometry (LC–MS/MS)

The colon tissue samples were lyophilized and ground into powder before being dissolved in 10 μL of 0.1% formic acid solution, centrifuged at 14,000 × g for 20 min at 4°C, then a 1 μg sample was taken for LC–MS/MS measurement. The label-free mass spectrum was analyzed by MaxQuant software and the protein data were screened by Beijing QLBio Company using the Uniprot database.

Cell Culture

HCoEpiC was cultured in RPMI 1640 (C11875500BT; Gibco) and supplemented with 10% fetal bovine serum (S711-001S; Lonsera) at 37°C in a humidified atmosphere with 5% CO_2. The following viability experiment was performed in the same manner in all cell lines, with HCoEpiC cells described here as an example. HCoEpiC cells were divided into six groups randomly, marked as control, LPS (model), LD_4-PDTL, LD_4-PDTM, LD_4-PDTH and Dexamethasone (DXMS) groups. All groups were cultured with 2 ml serum-free 1640 medium. Except for the control group, 10 μg/ml LPS was added to each group, and the cells were cultured for another 24 h. The culture medium was replaced with fresh 1640 medium for the control and model groups, while 2 ml serum-free 1640 medium containing 1.9, 3.8, or 7.5 μM LD_4 was added to LD_4-PDTL, LD_4-PDTM and LD_4-PDTH groups, respectively; 2 ml serum-free 1640 medium containing 7.5 μM DXMS was added to the DXMS positive control group. Cells were cultured with LD_4 for 30 min. The time was sufficient for bacteria to take up LD_4, as demonstrated in the bacterial strain deactivation previously reported (Xu et al., 2016; Zhao et al., 2021), so we chose this time to investigate the cellular damage occurring under the same conditions. Cells were irradiated with an energy density of 6 J/cm^2 or kept in the dark for 30 min, following which the cells were cultured for a further 24 h before MTT assay.

Quantitative Real-Time PCR Assay

Total RNA in HCoEpiC cells was extracted using the TRIzol Reagent (15596018; Invitrogen) according to the manufacturer's protocol. qRT-PCR was performed using a UltraSYBR mixture kit (CW0957H; Kangwei Biotech) according to the manufacturer's instructions. The *IL-1β*, *IL-6*, *TNF-α*, *AOC_1*, *AKT*, and *NF-κB* gene sequences were synthesized by Sangon Biotech (Shanghai, China). Primers are shown in **Supplementary Table S1**. qRT-PCR was performed using a LightCycler® real-time PCR assay (Roche, China).

Immunofluorescence Staining

HCoEpiC cells were grown on glass bottomed cell culture dishes (801001; NEST) and treated with LPS for 24 h. HCoEpiC cells were then cultured with LD_4 for 30 min and irradiated with 650 nm laser light at an energy density of 6 J/cm^2. Follow-up experiments were conducted at 24 h. Anti-AOC_1(A6249; ABclonal) and fluorescein-conjugated goat anti-rabbit IgG (ZF-0311; ZSGB-BIO) at 1:100 dilution was added as previously described (Liu et al., 2019).

Western Blotting Analysis

RIPA (CW2333; CWBio) protein lysate was added to the culture plates containing treated cells as required to extract proteins. According to the molecular weight of the target protein, the corresponding prefabricated glue (C35502009; GenScript) was used, and the loading volume of the protein sample to be tested was 30–60 μg. Electrophoresis was performed at 150 V constant pressure for 50 min. A constant pressure of 100 V was set using the wet rotation method, and the film was transferred by ice bath for 2 h. The membrane was immersed in western blot blocking solution (232100; BD) and shaken gently at room temperature for 2 h. The following rabbit primary antibodies were diluted with TBST and prepared according to the manufacturer's instructions; *AOC_1* (16338-1-AP; Proteintech), *AOC_1* (A6249; ABclonal), *p-NF-κB* (3033; CST), *NF-κB* (8242; CST), p-*IκB* (2859S; CST), *IκB* (4812; CST), *IKK* (2697; CST), *AKT* (4691; CST), *p-AKT* (4060; CST), *p-IKK* (ab178870; Abcam), *IL-6* (WL02841; Wanleibio) and *TNF-α* (WL01581; Wanleibio).

Cell Transfection

HCoEpiC cells were cultured in six-well plates for 24 h and transfected with short hairpin (sh) RNA (**Supplementary Table S2**) and overexpressing plasmid vector. Sh-*AOC_1* inserted into the pGPU6/GFP/Neo vector and the total nucleotide sequence of *AOC_1* inserted into pEX-1 to obtain the plasmid. All plasmid were synthetized by Gene Pharma (Suzhou, China). Cells were cultured in Opti-mem medium (11058021; Gibco). All transfections were performed using lipofectamine 2000 (11668019; Invitrogen) according to the manufacturer's protocol.

Statistical Analysis

Data analysis were conducted using SPSS 18.0 and GraphPad Prism 6. SPSS 18.0 was data statistical analysis software, used to analyze the differences between data. GraphPad Prism 6 was used to plot the corresponding statistics. All data were expressed as mean ± standard deviation (SD). Significant differences were determined using one-way analysis of variance (ANOVA). Statistical differences in 16S rRNA high-throughput sequencing were assessed using Tukey's HSD (Li H. et al., 2020)' Chen et al., 2020). $p < 0.05$ was considered statistically significant.

RESULTS

LD_4-Photodynamic Therapy Reduces Inflammation in LPS-Induced HCoEpiC Cells

Intestinal epithelial cells were the first protective barrier for the intestinal, its weakness in function would cause the illness in intestinal. So here HCoEpiC cells and LPS-

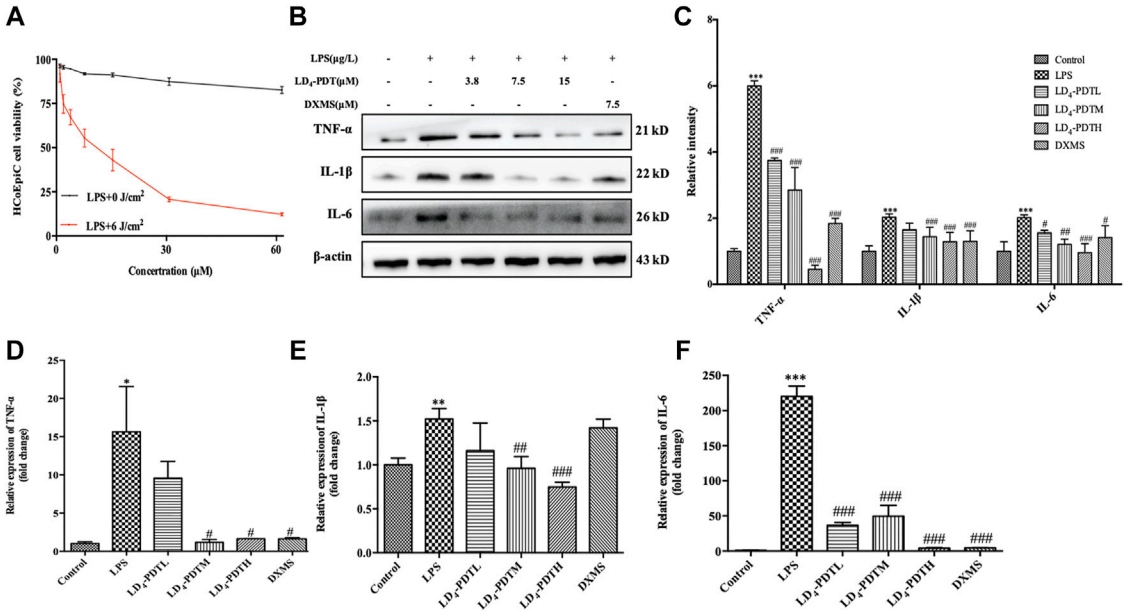

FIGURE 1 | LD_4-PDT reduced inflammation in LPS-induced HCoEpiC cells. **(A)** HCoEpiC cells were incubated with LPS for 24 h, LD_4 (0–60 μM) for 30 min, then irradiated (6 J/cm^2) or untreated. Cell viability was detected by MTT assay. Red line indicated the light reaction; black line indicated the dark reaction. **(B,C)** Protein expression of *TNF-α*, *IL-6* and *IL-1* was determined by western blot. **(D–F)** Expression levels of *TNF-α*, *IL-6* and *IL-1* in HCoEpiC cells were examined by qRT-PCR. $^{**}p < 0.01$, $^{***}p < 0.001$ vs control group; $^{\#}p < 0.05$, $^{\#\#}p < 0.01$, $^{\#\#\#}p < 0.001$ vs LPS model group. Data are representative of three independent experiments, expressed as mean ± SD.

stimulated HCoEpiC cells were chosen as normal and infectious cells *in vitro* model to evaluate the LD_4-PDT in IBD. DXMS a medicine with efficacy like anti-inflammatory, immunosuppressive and other pharmacological effects, is widely used in the treatment of autoimmune diseases, allergies, inflammation and other diseases in clinics. Therefore, DXMS is often selected as a positive control drug in UC *in vitro* and *in vivo*. Exposure to less than 30 μM LD_4 in either the dark or the light had no effect on the growth of HCoEpiC cells, indicating that LD_4-PDT had no obvious toxicity to intestinal tissue cells (**Supplementary Figure S1B**). While LPS-stimulated HCoEpiC cells were sensitive to LD_4-PDT, and their proliferation was inhibited in a LD_4 dose-dependent manner (**Figure 1A**). Proinflammatory cytokine expression is often changed with the progress of UC. We therefore determined the levels of *IL-6, TNF-α* and *IL-1* in HCoEpiC cells by western blotting and qRT-PCR. The protein and gene expressions of *IL-1*, *IL-6* and *TNF-α* were significantly decreased in the LD_4-PDT-treated group compared with control group (**Figures 1B–F**).

LD_4-Photodynamic Therapy Treatment of TNBS-Induced UC Model Rats

Our previous research has shown that LD_4 could inactivate microbial pathogens in traumatic infection ((Meng et al., 2015; Xu et al., 2016; Zhao et al., 2021). We have proved that the three different doses of LD_4 used in this paper have no significant effect on normal rats and PDT alone did not significantly relieve UC (**Supplementary Figure S1F,G**). The occurrence and development of IBD is also closely related to the change of gut microbes. On the basis of these results, we suggested LD_4-PDT could be used to treat UC. UC model was established using TNBS, and the treatment was started from day 7 post-induction, LD_4 at doses of 60, 120, and 240 μg/kg was administrated *via* enema every second day, 30 min later after which the colon was irradiated with an intensive 650 nm PDT system at an energy density of 25 J/cm^2, SASP, a standard UC drug as a positive control, was administered to the control group. The treatment was preformed four times. A steady increase in body weight in control group and body weight decrease in TNBS model group was observed, while body weight increasing in LD_4-PDT or SASP treated rats (**Figure 2A**). After LD_4-PDT treatment the animals were sacrificed and the colon was harvested. Its inner wall in the normal control group was complete, with regular folds and clear vascular texture, no obvious erosion, ulcers, or granuloma. In the TNBS model group, the colon intestine was shortened, the mucosa was marked with hyperemia and edema, scattered erosion or ulcers with hemorrhage, and large ulcerated areas. While the length of the colon and the thickness of the intestinal wall were improved to varying degrees in LD_4-PDT-treated or SASP control groups (**Figures 2B,C**). Colon histopathology showed that in TNBS group, epithelial cells shedding off, inflammatory cell infiltration in the sub-membrane, crypt abscess and ulcer formation were observed locally, mucosal glands were disorganized,

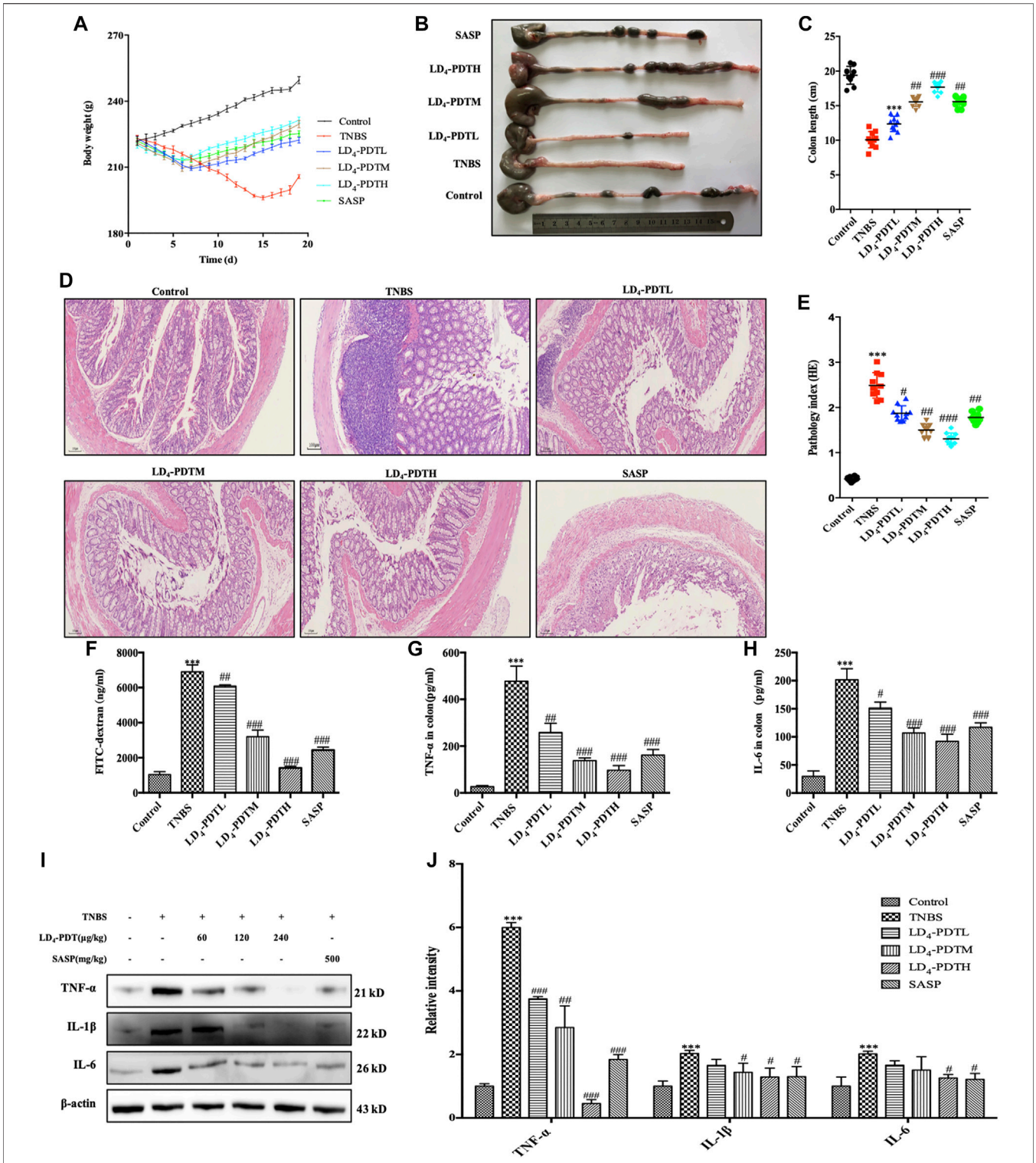

FIGURE 2 | LD_4-PDT alleviated TNBS-induced UC in model rats. **(A)** Body weight of UC model rats changed with time. **(B,C)** Length of colon. **(D,E)** Hematoxylin and eosin staining of colon tissue and inflammation score. **(F)** Serum fluorescent intensity of FITC-dextran. **(G,H)** *TNF-α* and *IL-6* levels determined by ELISA. **(I,J)** Protein expression of *TNF-α*, *IL-6* and *IL-1* were determined by western blot analysis. Each column represents the mean ± SD of 10 rats per group. $^{**}p < 0.01$, $^{***}p < 0.001$ vs control group; $^{\#}p < 0.05$, $^{\#\#}p < 0.01$, $^{\#\#\#}p < 0.001$ vs TNBS-treated group.

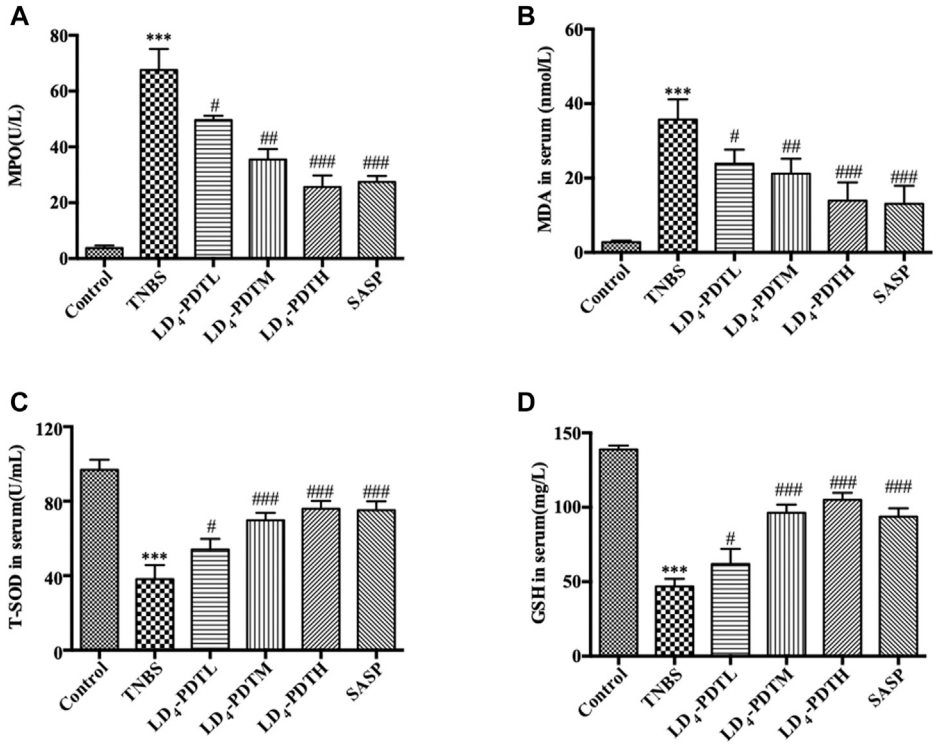

FIGURE 3 | LD_4-PDT regulated oxidative stress in TNBS-induced UC model rats. Concentrations of **(A)** *MPO*, **(B)** *MDA*, **(C)** *SOD* and **(D)** *GSH* in rat's serum were examined by ELISA. $^{**}p < 0.01$, $^{***}p < 0.001$ vs control group; $^{\#}p < 0.05$, $^{\#\#}p < 0.01$, $^{\#\#\#}p < 0.001$ vs TNBS model group. n = 10 rats per group.

destroyed or absent, goblet cells were reduced or absent, and histological injury score was significantly increased. Compared with the model group, LD_4-PDT-treated rats showed significantly alleviated pathological symptoms in the colon, and the colonic mucosal glands were arranged neatly, with few edemas and almost no ulcerative exudate (**Figures 2D,E**). The intestinal epithelial barrier is an important part of the intestinal innate immunity, and so measuring the permeability of the intestinal wall could determine disease activity. Following administration of FITC-dextran by intragastric gavage, the fluorescence intensity in serum indirectly reflects the intestinal permeability, the higher fluorescent intensity, the more severe the intestinal damage. Results showed that the levels of FITC-dextran in the serum of normal control rats were very low but significantly increased in TNBS groups, indicating that intestinal permeability was increased, and the intestinal wall was damaged following TNBS exposure. The content of FITC in serum of LD_4-PDT- and SASP-treated groups was significantly decreased, indicating that these drugs had a protective effect on intestinal integrity (**Figure 2F**). In accordance with the results above, the expression of *IL-1*, *IL-6* and *TNF-α* either in serum or in colon tissue were lower in LD_4-PDT-treated rats compared with the TNBS group (**Figures 2G–J**).

LD_4-Photodynamic Therapy Regulates Oxidative Stress in TNBS-Induced UC Model Rats

Because there is a close relationship between oxidative stress and UC (Morris et al., 1989), the level of *MPO* and *MDA* in serum as indicators of oxidative stress were investigated. *MPO* and *MDA* were significantly increased in the TNBS group but decreased in LD_4-PDT-treated rats in a dose dependent manner (**Figures 3A,B**), although levels in these animals remained higher than those of the normal control rats. Furthermore, the levels of two antioxidants *GSH* and *SOD* in serum were significantly decreased after TNBS exposure but increased significantly after LD_4-PDT treatment (**Figures 3C,D**). These changes all indicated that the LD4-PDT treatment could improve the living state of UC rats.

LD_4-Photodynamic Therapy Reprograms the Protein Profile of Colon Tissues in TNBS-Induced UC Model Rats

In order to investigate the mechanism of LD_4-PDT in the treatment of UC, the related protein profile was analyzed based upon proteomics. Label-free proteomics was used to detect the protein profiles in colon tissues of rats in the control, TNBS model and LD4-PDT treatment groups. A *t*-test

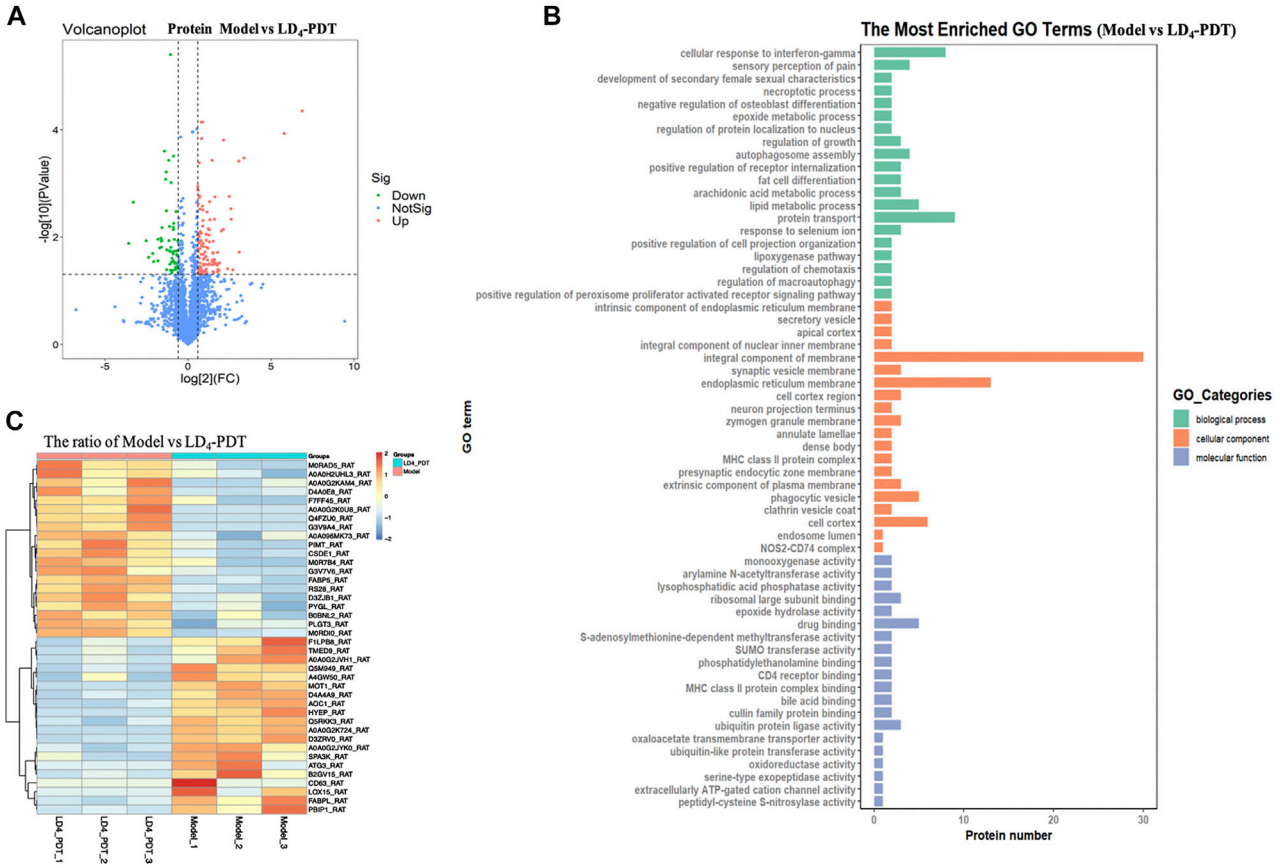

FIGURE 4 | LD_4-PDT reprogrammed the protein profile of colon tissues in TNBS-induced UC model rats. **(A)** Volcano plots showing the difference in protein expression among model and LD_4-PDT groups. **(B)** All identified proteins were classified according to the first 20 gene ontology ratios sorted by enrichment degree [–log10 (*p-value*)] and protein number according to biological process, cell composition and molecular function. Over-representation analysis was used for functional enrichment analysis, and the t-test based on hypergeometric distribution. **(C)** Heat map of 40 differentially expressed proteins among the model and LD_4-PDT groups. Each column represented a sample, and each row represented a factor; red indicated elevated protein expression, green indicated decreased protein expression.

was used directly for differential analysis, and the differentially expressed proteins meeting the criteria of $p \leq 0.05$ and fold change ≥1.5 times were screened. Scatter plots showed changes in protein expression between the TNBS model and LD_4-PDT groups (**Figure 4A**). Compared with LD_4-PDT-treated rats, there were 176 differentially expressed sites in the TNBS model group, among which 116 were highly expressed (**Figure 4A**, red) and 60 showed low expression (**Figure 4A**, green). Differentially expressed proteins are shown in **Supplementary Figure 2A** for comparison with other groups. Gene ontology (GO) is a standard vocabulary to describe the function, location and activity of genes, which covered three aspects of biology, namely biological process, cellular component, and molecular function. GO analysis of biological processes showed that differentially expressed proteins between the control and TNBS model groups were significantly related to collagen fibril organization, collagen biosynthesis, peptide acetyl threonine phosphorylation and negatively regulated biosynthesis by cell adhesion (**Supplementary Figure S2B**). However, treatment with LD_4-PDT changed the colonic protein expression profiles (**Figure 4B**). In terms of cellular component, the differentially expressed proteins were related to intracellular organelles, collagen and immunoglobulin complexes (**Supplementary Figure S2B**), indicating that treatment with LD_4-PDT resulted in changes in the cell cortex, intracellular organelles, and major histocompatibility complex class II proteins (**Figure 4B**). In terms of molecular function, the differentially expressed proteins were mainly derived from structural components of the extracellular matrix and the activities of ligase and transferase (**Supplementary Figure S2B**), while treatment with LD_4-PDT changed the activities of oxygenase and hydrolase (**Figure 4B**). We screened 40 significantly different proteins using heat maps to illustrate the differing protein expression profiles in the colon samples. The results showed that expression of AOC_1 in model rats was obviously increased (**Supplementary Figure S2C**), while this upregulation was eliminated following treatment with LD_4-PDT (**Figure 4C**). The role of AOC_1 in immune cell transport made it a target for autoimmune and inflammatory diseases, so we selected AOC_1 for further study (Peet et al., 2011).

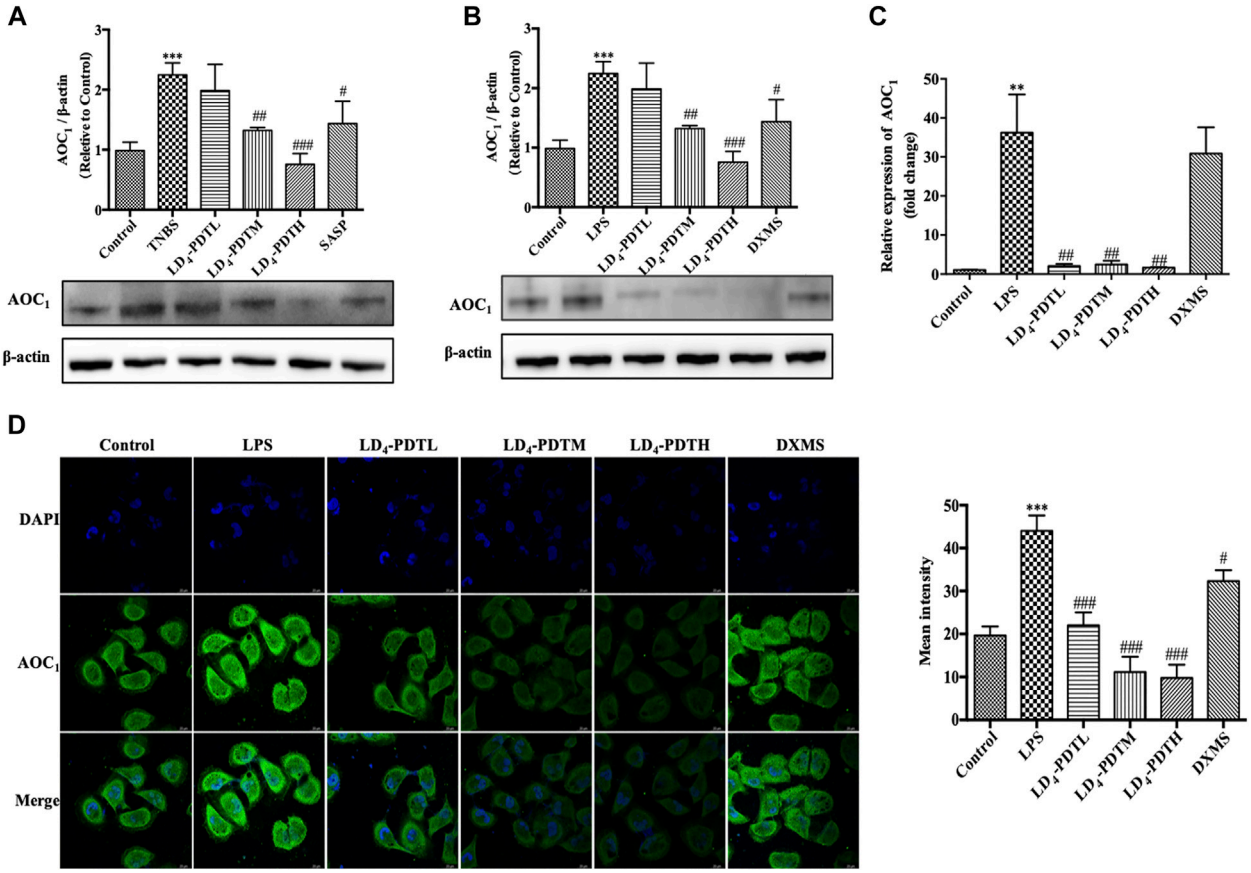

FIGURE 5 | LD_4-PDT suppressed the expression of *AOC_1*. **(A,B)** Protein expression of *AOC_1* in colon tissue and in HCoEpiC cells were determined by western blot analysis. **(C)** Gene expression of *AOC_1* in HCoEpiC cells was examined by qRT-PCR. **(D)** Protein expression of *AOC_1* was detected by immunofluorescence. Bars, 20 μm $^{**}p < 0.01$, $^{***}p < 0.001$ vs control group; $^{\#}p < 0.05$, $^{\#\#}p < 0.01$, $^{\#\#\#}p < 0.001$ vs TNBS model group. Data were representative of three independent experiments, expressed as mean ± SD.

LD_4-Photodynamic Therapy Suppresses the Expression of *AOC_1/AKT/IKK/NF-κB in vitro and in vivo*

Western blotting was used to further verify the expression of *AOC_1* protein. Compared with the control group, the expression of *AOC_1* was significantly increased in the TNBS model group but was significantly decreased after LD_4-PDT treatment (**Figure 5A**). The expression of *AOC_1* in HCoEpiC cells was detected by western blot (**Figure 5B**), qRT-PCR (**Figure 5C**) and immunofluorescence (**Figure 5D**). Consistent with the results of the animal experiments, *AOC_1* protein and gene expression were up-regulated after LPS treatment in HCoEpiC cells but were then reduced upon LD_4-PDT treatment. Because *AOC_1* can activate *AKT* and downstream pathways (Xu et al., 2020), the key factors interacting with *AOC_1* were screened. Western blotting showed that compared with the control group, the expression of *p-AKT*, *p-NF-κB*, *p-IKK,* and *p-IκB* was increased significantly in the TNBS group, while LD_4-PDT treatment significantly decreased the expressions of *p-AKT*, *p-NF-κB*, *p-IKK*, and *p-IκB* compared with the TNBS model group (**Figures 6A–D**). Similarly, the expressions of *p-AKT*, *p-NF-κB*, *p-IKK,* and *p-IκB* were significantly decreased after LD_4-PDT treatment compared with LPS stimulation alone in HCoEpiC cells (**Figures 6E–I**). Thus, our findings suggest that treatment with LD_4-PDT may decrease or block the expression of *AOC_1/AKT/IKK/NF-κB* in UC.

LD_4-Photodynamic Therapy Protects Intestine *via* Inhibition of *AOC_1*

The above results indicated that *AOC_1* played an important role in LD_4-PDT treatment of UC, so the impact of *AOC_1* protein in LD_4-PDT treatment was further investigated. We knocked down the *AOC_1* gene in HCoEpiC cells using a specific shRNA then induced the inflammatory model with LPS before treating the cells with LD_4-PDT. Western blot verified that more than 70% AOC_1 was silenced (**Supplementary Figure S3A**), and knockdown *AOC_1* led to reduce the levels of *IL-1*, *IL-6* and *TNF-α* in the cells to a varying degree compared with mock-transfected cells. Following LD_4-PDT treatment, the expression levels of these cytokines in all groups was reduced remarkably, and there was no obvious difference among knockdown *AOC_1* group and other group (**Figures 7A,B**). On the contrary,

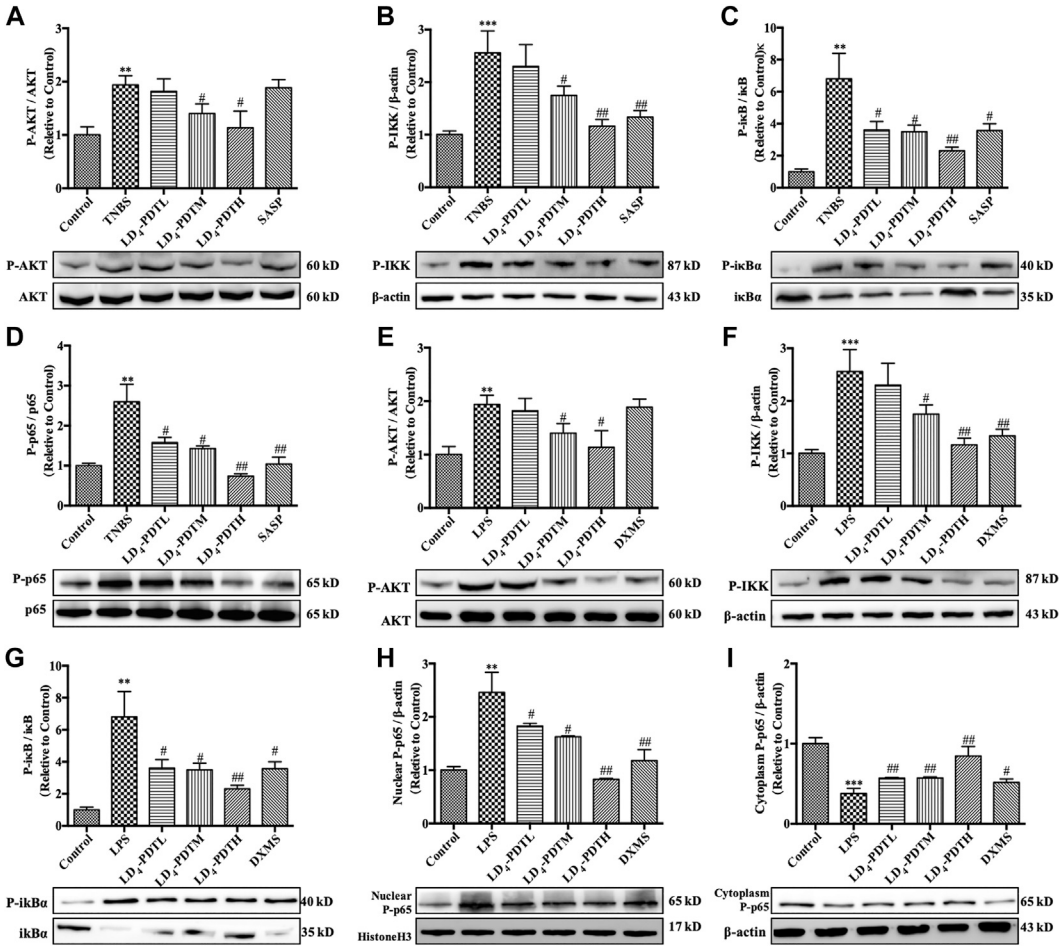

FIGURE 6 | LD_4-PDT inhibited the expression of *AOC_1/AKT/IKK/NF-κB*. **(A–D)** Protein expression of **(A)** *p-AKT*, **(B)** *p-IKK*, **(C)** *p-IκB* and **(D)** *p-p65* in colon tissue were determined by western blot. **(E–I)** Protein expression of **(E)** *p-AKT*, **(F)** *p-IKK*, **(G)** *p-IκB*, **(H)** *p-p65* (in nuclear), and **(I)** *p-p65* (in cytoplasm) in HCoEpiC cells were determined by western blot $^{**}p < 0.01$, $^{***}p < 0.001$ vs control group; $^{\#}p < 0.05$, $^{\#\#}p < 0.01$, $^{\#\#\#}p < 0.001$ vs TNBS model or LPS model group. Data are representative of three independent experiments, expressed as mean ± SD.

overexpressed *AOC_1* cells was also built, the same treatment was conducted as that of the down-regulated cells (**Supplementary Figure S3B**). Western blot assay showed that compared with mock-transfected cells, protein levels of IL-1, IL-6 and *TNF-α* in the *AOC_1* overexpression cells were increased, while these cytokines all reduced following LD_4-PDT treatment in all cells. Among all LD_4-PDT treatment cells, *AOC_1* overexpression HCoEpiC cells exhibited the higher protein levels of *IL-1, IL-6* and *TNF-α* (**Figures 7C,D**). We set AOC_1-knockdown group and AOC_1-overexpression group in HCoEpiC cells without LPS stimulation, as well as control cells group, to examine whether AOC_1 is critical for cytokine production at the basal conditions. Our results demonstrated that AOC_1 plays an important role in basal condition (**Supplementary Figure S3C,D**).Summary above, we found that the expression of *AOC_1* was up-regulated in the model group, while LD_4-PDT treatment reduced the expression of *AOC_1* at the gene and protein levels, indicating that LD_4-PDT exerted its effects in UC *via AOC_1*, thus mediating expression of downstream cytokines. These results suggested that LD_4-PDT treatment may work *via* inhibition of *AOC_1* to mediate *AKT/IKK/NF-κB* pathways, and thus knockdown of *AOC_1* protein either by LD_4-PDT treatment or other means could alleviate UC symptoms.

LD_4-Photodynamic Therapy Remodels the Gut Bacterial Composition Pattern in TNBS-Induced Ulcerative Colitis Model Rats

Effect of LD_4-PDT on the gut microbes among the control, TNBS and LD_4-PDT-treated groups were studied using the 16S rRNA method. The Venn diagram (**Figure 8A**) shows that a total of 2472 OTUs were obtained from all samples. A total of 589 OTUs were appeared in all three groups, while 990 OTUs were shared between the control and LD_4-PDT groups, 64 OTUs were shared between the TNBS model and control groups, the TNBS model and LD_4-PDT groups shared 60 (**Figure 8A**). The Shannon curve showed that sequencing depth covered rare new phylotypes, with both diversity and Shannon index in the TNBS model group

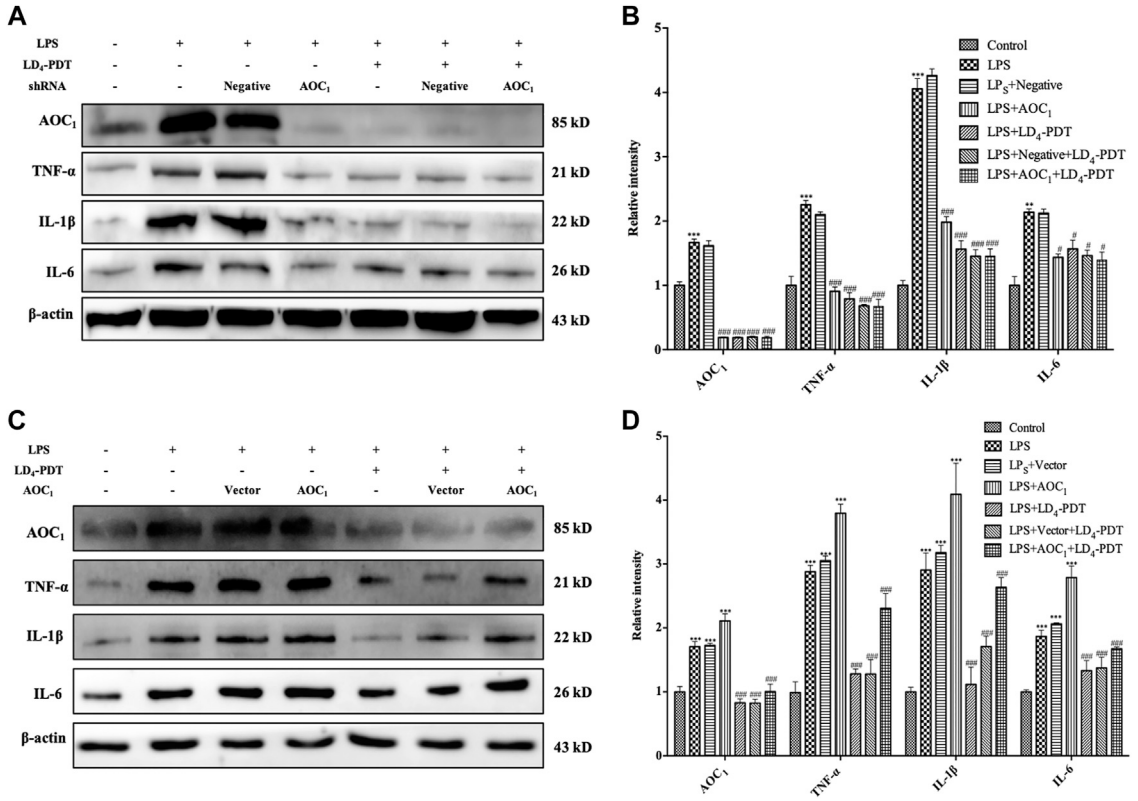

FIGURE 7 | LD_4-PDT protected intestine *via* inhibition of AOC_1. **(A,B)** LD_4-PDT effect on *TNF-α*, *IL-6* and *IL-1* expression in AOC_1 knockdown HCoEpiC cells. **(C,D)** LD_4-PDT effect on *TNF-α*, *IL-6* and *IL-1* expression in AOC_1 over-expression cells. $^{**}p < 0.01$, $^{***}p < 0.001$ vs control group; $^{\#}p < 0.05$, $^{\#\#}p < 0.01$, $^{\#\#\#}p < 0.001$ vs LPS groups. Data are representative of three independent experiments, expressed as mean ± SD.

being lower than those in the control and LD_4-PDT groups (**Supplementary Figure S4A**). Weighted UniFrac-based principal coordinates analysis (PCoA) indicated the unique intestinal microbiota composition clustering of individual groups (**Figure 8B**). The *α*-diversity of intestinal bacteria decreased significantly in TNBS model rats, but it was recovered to an almost normal state after LD_4-PDT treatment (**Figure 8C**, **Supplementary Figure S4B**). Unweighted pair group method with arithmetic mean analysis showed that there was a significant difference in intestinal flora between the TNBS model group and LD_4-PDT-treated rats, and LD_4-PDT treatment made the overall composition of intestinal flora in UC model rats return to a state similar with the control group (**Figure 8D**). Taxonomic bins at the phylum level indicated that gut bacterial composition patterns in model animals were obviously different from the control groups (**Figure 8E**): the proportions of Firmicutes in fecal stool of rats in the TNBS model group were higher than those in the normal control group (**Figure 8F**), while the abundance of Bacteroidetes (**Figure 8G**) and Verucomicrobia (**Figure 8H**) were lower than in control rats, the Firmicutes/Bacteroidetes (F/B) value in the TNBS model group was higher than that of the control group (**Figure 8I**); however, LD_4-PDT treatment reduced Firmicutes, increased Bacteroidetes and Verucomicrobia in fecal samples, the F/B value was reduced after LD_4-PDT treatment, and the gut bacterial composition pattern was comparable with that of the control group following LD_4-PDT treatment (**Figures 8F–I**).

DISCUSSION

In this study, we found that LD_4-PDT can effectively alleviate the inflammation both *in vitro and in vivo*. TNBS-induced UC model rats showed ruffled fur, loss of appetite, lethargy, blood in the stool, and weight loss, while LD_4-PDT treatment recovered their healthy appearance with no significant weight loss. Pathological observations revealed that the colonic mucosal barrier structure of the untreated group was destroyed with infiltration of inflammatory cells and obvious intestinal wall ulcers and adhesions, these illness characteristics was reduced in each LD_4-PDT-treated group. Neutrophils are rich in *MPO*, which can catalyze and oxidize chloride ions to produce hypochlorous acid to kill microorganisms in phagocytes, destroy a variety of target substances, and play a role in production and regulation of inflammation (Gu et al., 2017). *MDA* levels can reflect the degree of external damage to the body (Wang et al., 2019). Neutrophils in colitis model release *MPO,* which stimulates oxidative stress in the body, and increases the level of *MPO* and *MDA*. However, LD_4-PDT treatment significantly reduced both *MPO* and *MDA* levels. *SOD* which can remove the harmful substances produced

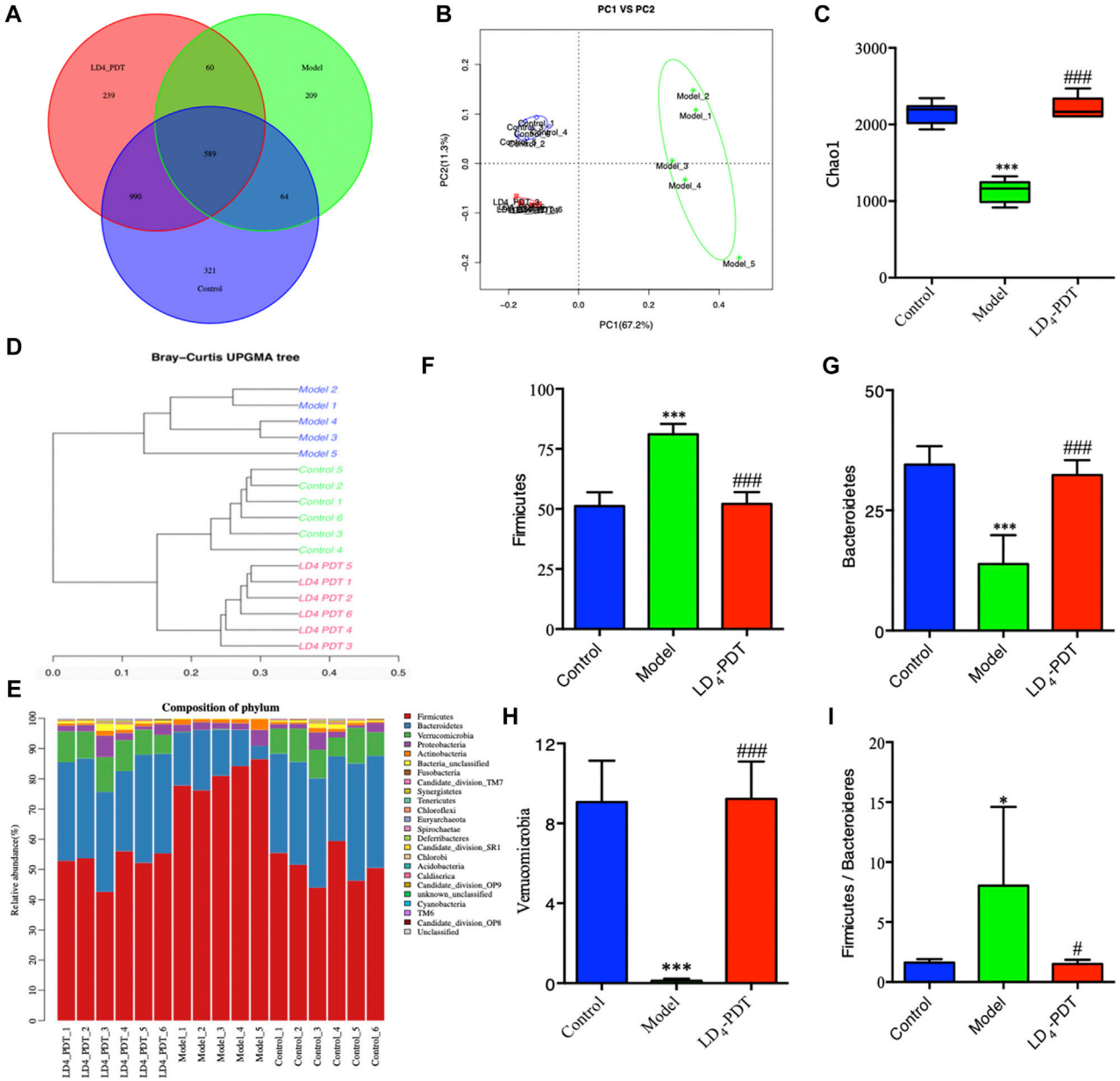

FIGURE 8 | LD_4-PDT treatment altered the gut microbiota in TNBS-induced UC model rats. **(A)** Venn diagram indicated the differential numbers of OTUs in each group. **(B)** PCoA score. **(C)** Chao1 index represented the α-diversity of the gut microbiota. **(D)** Hierarchical clustering of fecal microbiota in the control, model and LD_4-PDT groups. **(E)** Phylum-level distribution of fecal microbiota **(F–H)** Relative abundance of the **(F)** Firmicutes, **(G)** Bacteroidetes, **(H)** Verrucomicrobia **(I)** The Firmicutes/Bacteroidetes (F/B) value $^{**}p < 0.01$, $^{***}p < 0.001$ vs control group; $^{\#}p < 0.05$, $^{\#\#}p < 0.01$, $^{\#\#\#}p < 0.001$ vs model group; n = 6 rats per group.

in the process of metabolism (Gu et al., 2017; Wang et al., 2019), is the only enzyme that decomposes superoxide radicals into H_2O_2 in antioxidation. Another free radical scavenger, *GSH*, can also regulate oxidative stress (Gu et al., 2017; Wang et al., 2019). The levels of *GSH* and *SOD* were decreased in the colitis model, but were increased significantly after LD_4-PDT treatment, indicating that LD_4-PDT can regulate the level of oxidative stress during UC.

The inhibitory effect of amino salicylic acid drugs on *NF-κB* can improve the symptoms of UC (Murray et al., 2020). The role of *TNF-α* is mainly to regulate the function of immune cells and induce inflammation to produce *IL-1* and *IL-6*. Many studies have shown that the levels of *TNF-α, IL-1* and *IL-6* were elevated in the UC model (Wang et al., 2019; Zhai et al., 2020), while further studies have confirmed that inhibition of *TNF-α, IL-1* and *IL-6* could prevent the development of inflammation (Xu et al., 2017; Lee et al., 2020). In this study, LD_4-PDT treatment significantly inhibited *TNF-α*, *IL-1* and *IL-6* expression, and consequently reduced the severity of colitis in UC model (Huang et al., 2017; Lee et al., 2020; Li et al., 2020). Intestinal barrier function can be assessed by quantification of permeability,

so fluorescent tracers can be used to detect the degree of permeability by measuring the fluorescence intensity in serum. Many studies have shown that in UC models, the intestinal mucosal barrier function is impaired and so intestinal permeability increases, allowing harmful substances to invade the body and promoting development of the disease (Wang et al., 2019; Li H. et al., 2020). After LD_4-PDT treatment, the intestinal permeability was decreased and intestinal mucosal barrier function was recovered. The above results show that LD_4-PDT can not only restore the intestinal mucosal barrier function, but also reduce the damaging effects of mucosal injury factors on the intestinal mucosa, thus playing a key role in the treatment of UC.

The intestinal flora is the largest and most complex microecosystem in the human body. It is a dynamic community composed of bacteria, fungi, and viruses that regulate the homeostasis and physiological functions of the mucous membrane. There is a relatively balanced state between the body's intestinal microbes and the immune system. Abnormal immune responses to bacteria out of balance may disrupt this homeostasis and are related to human IBD (Le Chatelier et al., 2013). Several studies have shown that intestinal flora affects intestinal mucosal immune function, intestinal cell metabolism and renewal and other processes, which can cause obesity, diabetes, malignant tumors, toxemia and IBD (Chen et al., 2020; Ma et al., 2020; Wang et al., 2020). Therefore, exploring the role of the intestinal flora in the occurrence and development of UC, and restoring the balance of disordered flora is of great significance for the treatment of UC. 16S rRNA sequencing technology has shown that 90% of the dominant human intestinal flora consists of Firmicutes, Bacteroidetes, Proteobacteria and Verrucomicrobia (Nishino et al., 2018; Soltys et al., 2020; Wang et al., 2020; Zhu et al., 2020). Both UC patients and UC mice have serious flora imbalances, and the distribution of UC flora at different stages of disease is also significantly different. In our study, we found that Firmicutes and Bacteroidetes were dominant in the model group, followed by Verrucomicrobia. LD_4-PDT treatment increased the diversity of the flora and restored the flora composition towards normal. The F/B value, the ratio of the abundance of Firmicutes and *Bacteroides*, can effectively reflect the disorder of the intestinal flora and is usually significantly increased in the pathogenesis of UC (Wu et al., 2019; Zhu Y. et al., 2020). In our study, the F/B value in the TNBS model group was higher than that of the control group, and the F/B value was reduced after LD_4-PDT treatment, suggesting that LD_4-PDT can improve intestinal diseases to a certain extent. Verrucomicrobia, which gain energy from degradation of excess mucin produced in the lining of the gut and produce anti-inflammatory effects, are significantly more abundant in healthy persons than in patients with UC (Shah et al., 2016; Zakerska-Banaszak et al., 2021). In UC patients, the level of mucin is decreased resulting in reduced abundance of Verrucomicrobia (Shah et al., 2016; Zakerska-Banaszak et al., 2021). Consistent with previous reports, we found that at the phylum level, the relative content of Verrucomicrobia was reduced in the UC model compared with control rats, while LD_4-PDT treatment increased the abundance of this microbiota and protected the intestinal mucosa to produce an anti-inflammatory effect.

To further explore the biological mechanism of LD_4-PDT in UC, colonic protein assays were conducted using proteomics in model, control and LD_4-PDT groups. More than 176 proteins were detected and their differential expression were given between model and LD_4-PDT group. Although the first two protein changed large, however they were related to basic immunology and energy supply. AOC_1, whose abundance change was in third position and was correlated tightly with the inflammation, were identified as a potential target of LD_4-PDT. AOC_1 is known to be involved in allergic and immune responses, cell proliferation, tissue differentiation, and apoptosis (Strolin Benedetti et al., 2007; Shepard and Dooley, 2015; Vakal et al., 2020). Its role in the transport of immune cells has made it a target for autoimmune and inflammatory diseases (Peet et al., 2011). In addition, AOC_1 has the ability to regulate pathophysiological processes, such as cancer and EMT (Xu et al., 2020). Studies have reported that plasma AOC_1 activity can be used to diagnose intestinal integrity and play an important role in UC (DiSilvestro et al., 1997). In this study, we found that the expression of AOC_1 in the colon was up-regulated in the TNBS model group, while LD_4-PDT treatment reduced the expression of AOC_1 at the gene and protein levels, indicating that LD_4-PDT exerted its effects in UC *via* AOC_1, thus mediating expression of downstream cytokines. To test this hypothesis, AOC_1 was specifically knocked down or over-expressed *in vitro*. Consistent with our hypothesis, silencing of AOC_1 reduced the levels of *IL-1, IL-6* and *TNF-α*. These results suggested that AOC_1 protein may be a key protein in the treatment of UC, and that reducing its expression, either by LD_4-PDT treatment or by other means, could ameliorate UC symptoms. Studies have shown that AOC_1 can promote the expression of *AKT* and further regulate pro-inflammatory factors like *NF-κB* (Xu et al., 2020). The activated *NF-κB* signaling pathway can affect various biological processes, including innate and adaptive immunity, inflammation, stress responses, and B-cell development (Liu et al., 2020; Shamekhi et al., 2020). The AOC_1-AKT/IKK/ NF-κB pathway plays an important role in immune response and inflammatory response and is involved in the occurrence and development of various inflammatory diseases. Activation of NF-κB can promote the expression of various inflammatory factors such as IL-6, LI-1*β* and TNF-*α*, enhance the body's non-specific and specific immune responses, cause tissue damage and organ dysfunction, and further aggravate the symptoms of UC. Our research shows that when the UC model was established, the *AKT/IKK/NF-κB* pathway was activated to promote inflammation but following LD_4-PDT treatment, the *AKT/IKK/NF-κB* pathway was inhibited, thereby exerting a therapeutic effect on UC. In summary, our study indicates that LD_4-PDT treatment UC was effective, the working mechanism may be LD_4-PDT function *via* AOC_1 to mediate *AKT/IKK/NF-κB* pathways and downstream inflammatory cytokine expression. However, the mechanism of action behind LD_4-PDT function and whether AOC_1 is the sole

target of LD_4-PDT in the treatment of UC remain to be fully elucidated.

In conclusion, we have shown that LD_4-PDT treatment could promote healing of the colonic mucosa, regulation of intestinal flora, and improvement in the clinical symptoms of UC. LD_4-PDT can reduce the mucosal inflammatory response mediated by AOC_1, which we identified as a potential target for UC intervention. Novel photosensitizing agent, LD_4, was an efficient PDT treatment candidate for UC.

DATA AVAILABILITY STATEMENT

The original contributions presented in the study are publicly available. This data can be found here: http://proteomecentral.proteomexchange.org/cgi/GetDataset, submission number - 1-20210807-77236.

ETHICS STATEMENT

The animal study was reviewed and approved by the Laboratory Animal Management Committee/Laboratory Animal Welfare Ethics Committee, Institute of Radiation Medicine, Chinese Academy of Medical Sciences.

AUTHOR CONTRIBUTIONS

TL and YR designed and performed experiments, analyzed data, and wrote the paper. GH, YJ, NZ, and YL performed experiments. The final manuscript was reviewed and approved by all authors.

FUNDING

This work was supported by the national major science and technology special project for significant new drugs development under grant (2018ZX09711001-005-018/2019ZX09721001-006-001); The medical and health science and technology innovation project under grant (2017-I2M-3-021/2019-I2M-1-005); The key technologies R & D program of Tianjin under grant (20YFZCSY00570).

SUPPLEMENTARY MATERIAL

The Supplementary Material for this article can be found online at: https://www.frontiersin.org/articles/10.3389/fphar.2021.746725/full#supplementary-material

REFERENCES

Chen, J., Hu, S., Ji, D., Gao, Z., Wang, H., Yang, Y., et al. (2020). Hemolysin BL from Novel Bacillus Toyonensis BV-17 Induces Antitumor Activity Both *In Vitro* and *In Vivo*. *Gut Microbes* 12, 1782158. doi:10.1080/19490976.2020.1782158

Chow, D. K., Leong, R. W., Tsoi, K. K., Ng, S. S., Leung, W. K., Wu, J. C., et al. (2009). Long-Term Follow-Up of Ulcerative Colitis in the Chinese Population. *Am. J. Gastroenterol.* 104, 647–654. doi:10.1038/ajg.2008.74

Costello, S. P., Conlon, M. A., and Andrews, J. M. (2019). Fecal Microbiota Transplantation for Ulcerative Colitis-Reply. *JAMA* 321, 2240–2241. doi:10.1001/jama.2019.3950

DiSilvestro, R. A., Jones, A. A., Smith, D., and Wildman, R. (1997). Plasma Diamine Oxidase Activities in Renal Dialysis Patients, a Human with Spontaneous Copper Deficiency and Marginally Copper Deficient Rats. *Clin. Biochem.* 30, 559–563. doi:10.1016/s0009-9120(97)00102-1

Favre, L., Borle, F., Velin, D., Bachmann, D., Bouzourene, H., Wagnieres, G., et al. (2011). Low Dose Endoluminal Photodynamic Therapy Improves Murine T Cell-Mediated Colitis. *Endoscopy* 43, 604–616. doi:10.1055/s-0030-1256382

Gu, P., Zhu, L., Liu, Y., Zhang, L., Liu, J., and Shen, H. (2017). Protective Effects of Paeoniflorin on TNBS-Induced Ulcerative Colitis through Inhibiting NF-KappaB Pathway and Apoptosis in Mice. *Int. Immunopharmacol.* 50, 152–160. doi:10.1016/j.intimp.2017.06.022

Hindryckx, P., Baert, F., Hart, A., Magro, F., Armuzzi, A., Peyrin-Biroulet, L., et al. (2015). Clinical Trials in Ulcerative Colitis: A Historical Perspective. *J. Crohns Colitis* 9, 580–588. doi:10.1093/ecco-jcc/jjv074

Hirono, H., Watanabe, K., Hasegawa, K., Honma, T., Ajioka, Y., and Ohkoshi, S. (2018). A Case of Right-Sided Ulcerative Colitis with Mesalamine-Induced Hypersensitivity Reactions. *Am. J. Case Rep.* 19, 623–629. doi:10.12659/AJCR.909644

Huang, Y. F., Zhou, J. T., Qu, C., Dou, Y. X., Huang, Q. H., Lin, Z. X., et al. (2017). Anti-inflammatory Effects of Brucea Javanica Oil Emulsion by Suppressing NF-Kb Activation on Dextran Sulfate Sodium-Induced Ulcerative Colitis in Mice. *J. Ethnopharmacol* 198, 389–398. doi:10.1016/j.jep.2017.01.042

Le Chatelier, E., Nielsen, T., Qin, J., Prifti, E., Hildebrand, F., Falony, G., et al. (2013). Richness of Human Gut Microbiome Correlates with Metabolic Markers. *Nature* 500, 541–546. doi:10.1038/nature12506

Lee, C. L., Wang, C. M., Kuo, Y. H., Yen, H. R., Song, Y. C., Chou, Y. L., et al. (2020). IL-17A Inhibitions of Indole Alkaloids from Traditional Chinese Medicine Qing Dai. *J. Ethnopharmacol* 255, 112772. doi:10.1016/j.jep.2020.112772

Li, H., Fan, C., Lu, H., Feng, C., He, P., Yang, X., et al. (2020a). Protective Role of Berberine on Ulcerative Colitis through Modulating Enteric Glial Cells-Intestinal Epithelial Cells-Immune Cells Interactions. *Acta Pharm. Sin B* 10, 447–461. doi:10.1016/j.apsb.2019.08.006

Li, Y., Dong, J., Xiao, H., Zhang, S., Wang, B., Cui, M., et al. (2020b). Gut Commensal Derived-Valeric Acid Protects against Radiation Injuries. *Gut Microbes* 11, 789–806. doi:10.1080/19490976.2019.1709387

Liu, B., Rong, Y., Sun, D., Li, W., Chen, H., Cao, B., et al. (2019). Costunolide Inhibits Pulmonary Fibrosis via Regulating NF-kB and TGF-β1/Smad2/Nrf2-NOX4 Signaling Pathways. *Biochem. Biophys. Res. Commun.* 510, 329–333. doi:10.1016/j.bbrc.2019.01.104

Liu, Q., Zuo, R., Wang, K., Nong, F. F., Fu, Y. J., Huang, S. W., et al. (2020). Oroxindin Inhibits Macrophage NLRP3 Inflammasome Activation in DSS-Induced Ulcerative Colitis in Mice via Suppressing TXNIP-Dependent NF-Kb Pathway. *Acta Pharmacol. Sin.* 41, 771–781. doi:10.1038/s41401-019-0335-4

Ma, J., Hong, Y., Zheng, N., Xie, G., Lyu, Y., Gu, Y., et al. (2020). Gut Microbiota Remodeling Reverses Aging-Associated Inflammation and Dysregulation of Systemic Bile Acid Homeostasis in Mice Sex-Specifically. *Gut Microbes* 11, 1450–1474. doi:10.1080/19490976.2020.1763770

Maisch, T., Moor, A. C., Regensburger, J., Ortland, C., Szeimies, R. M., and Bäumler, W. (2011). Intense Pulse Light and 5-ALA PDT: Phototoxic Effects *In Vitro* Depend on the Spectral Overlap with Protoporphyrine IX but Do Not Match Cut-Off Filter Notations. *Lasers Surg. Med.* 43, 176–182. doi:10.1002/lsm.20970

Mallidi, S., Spring, B. Q., and Hasan, T. (2015). Optical Imaging, Photodynamic Therapy and Optically Triggered Combination Treatments. *Cancer J.* 21, 194–205. doi:10.1097/PPO.0000000000000117

Meng, S., Xu, Z., Hong, G., Zhao, L., Zhao, Z., Guo, J., et al. (2015). Synthesis, Characterization and *In Vitro* Photodynamic Antimicrobial Activity of Basic Amino Acid-Porphyrin Conjugates. *Eur. J. Med. Chem.* 92, 35–48. doi:10.1016/j.ejmech.2014.12.029

Morris, G. P., Beck, P. L., Herridge, M. S., Depew, W. T., Szewczuk, M. R., and Wallace, J. L. (1989). Hapten-Induced Model of Chronic Inflammation and

Ulceration in the Rat Colon. *Gastroenterology* 96, 795–803. doi:10.1016/s0016-5085(89)80079-4

Murray, A., Nguyen, T. M., Parker, C. E., Feagan, B. G., and MacDonald, J. K. (2020). Oral 5-Aminosalicylic Acid for Maintenance of Remission in Ulcerative Colitis. *Cochrane Database Syst. Rev.* 8, CD000544. doi:10.1002/14651858.CD000544.pub5

Ng, S. C., Shi, H. Y., Hamidi, N., Underwood, F. E., Tang, W., Benchimol, E. I., et al. (2017). Worldwide Incidence and Prevalence of Inflammatory Bowel Disease in the 21st Century: A Systematic Review of Population-Based Studies. *Lancet* 390, 2769–2778. doi:10.1016/S0140-6736(17)32448-0

Nishino, K., Nishida, A., Inoue, R., Kawada, Y., Ohno, M., Sakai, S., et al. (2018). Analysis of Endoscopic Brush Samples Identified Mucosa-Associated Dysbiosis in Inflammatory Bowel Disease. *J. Gastroenterol.* 53, 95–106. doi:10.1007/s00535-017-1384-4

Peet, G. W., Lukas, S., Hill-Drzewi, M., Martin, L., Rybina, I. V., Roma, T., et al. (2011). Bioluminescent Method for Assaying Multiple Semicarbazide-Sensitive Amine Oxidase (SSAO) Family Members in Both 96- and 384-Well Formats. *J. Biomol. Screen.* 16, 1106–1111. doi:10.1177/1087057111414897

Qiu, Y., Chen, B. L., Feng, R., Zhang, S. H., He, Y., Zeng, Z. R., et al. (2018). Prolonged Azathioprine Treatment Reduces the Need for Surgery in Early Crohn's Disease. *J. Gastroenterol. Hepatol.* 33, 664–670. doi:10.1111/jgh.14000

Reinhard, A., Bressenot, A., Dassonneville, R., Loywick, A., Hot, D., Audebert, C., et al. (2015). Photodynamic Therapy Relieves Colitis and Prevents Colitis-Associated Carcinogenesis in Mice. *Inflamm. Bowel Dis.* 21, 985–995. doi:10.1097/MIB.0000000000000354

Rong, Y., Cao, B., Liu, B., Li, W., Chen, Y., Chen, H., et al. (2018). A Novel Gallic Acid Derivative Attenuates BLM-Induced Pulmonary Fibrosis in Mice. *Int. Immunopharmacol.* 64, 183–191. doi:10.1016/j.intimp.2018.08.024

Sands, B. E., Peyrin-Biroulet, L., Loftus, E. V., Jr, Danese, S., Colombel, J. F., Törüner, M., et al. (2019). Vedolizumab versus Adalimumab for Moderate-To-Severe Ulcerative Colitis. *N. Engl. J. Med.* 381, 1215–1226. doi:10.1056/NEJMoa1905725

Senge, M. O. (2012). mTHPC--a Drug on its Way from Second to Third Generation Photosensitizer? *Photodiagnosis Photodyn Ther.* 9, 170–179. doi:10.1016/j.pdpdt.2011.10.001

Shah, R., Cope, J. L., Nagy-Szakal, D., Dowd, S., Versalovic, J., Hollister, E. B., et al. (2016). Composition and Function of the Pediatric Colonic Mucosal Microbiome in Untreated Patients with Ulcerative Colitis. *Gut Microbes* 7, 384–396. doi:10.1080/19490976.2016.1190073

Shamekhi, S., Abdolalizadeh, J., Ostadrahimi, A., Mohammadi, S. A., Barzegari, A., Lotfi, H., et al. (2020). Apoptotic Effect of *Saccharomyces cerevisiae* on Human Colon Cancer SW480 Cells by Regulation of Akt/NF-κb Signaling Pathway. *Probiotics Antimicrob. Proteins* 12, 311–319. doi:10.1007/s12602-019-09528-7

Shepard, E. M., and Dooley, D. M. (2015). Inhibition and Oxygen Activation in Copper Amine Oxidases. *Acc. Chem. Res.* 48, 1218–1226. doi:10.1021/ar500460z

Shivaji, U. N., Nardone, O. M., Cannatelli, R., Smith, S. C., Ghosh, S., and Iacucci, M. (2020). Small Molecule Oral Targeted Therapies in Ulcerative Colitis. *Lancet Gastroenterol. Hepatol.* 5, 850–861. doi:10.1016/S2468-1253(19)30414-5

Soltys, K., Stuchlikova, M., Hlavaty, T., Gaalova, B., Budis, J., Gazdarica, J., et al. (2020). Seasonal Changes of Circulating 25-Hydroxyvitamin D Correlate with the Lower Gut Microbiome Composition in Inflammatory Bowel Disease Patients. *Sci. Rep.* 10, 6024. doi:10.1038/s41598-020-62811-4

Strolin Benedetti, M., Tipton, K. F., and Whomsley, R. (2007). Amine Oxidases and Monooxygenases in the *In Vivo* Metabolism of Xenobiotic Amines in Humans: Has the Involvement of Amine Oxidases Been Neglected? *Fundam. Clin. Pharmacol.* 21, 467–480. doi:10.1111/j.1472-8206.2007.00498.x

Vakal, S., Jalkanen, S., Dahlström, K. M., and Salminen, T. A. (2020). Human Copper-Containing Amine Oxidases in Drug Design and Development. *Molecules* 25, 1293. doi:10.3390/molecules25061293

Wang, G., Xu, B., Shi, F., Du, M., Li, Y., Yu, T., et al. (2019). Protective Effect of Methane-Rich Saline on Acetic Acid-Induced Ulcerative Colitis via Blocking the TLR4/NF-Kb/MAPK Pathway and Promoting IL-10/JAK1/STAT3-Mediated Anti-Inflammatory Response. *Oxid Med. Cel Longev* 2019, 7850324. doi:10.1155/2019/7850324

Wang, Y., Li, J., Chen, C., Lu, J., Yu, J., Xu, X., et al. (2020). Targeting the Gut Microbial Metabolic Pathway with Small Molecules Decreases Uremic Toxin Production. *Gut Microbes* 12, 1–19. doi:10.1080/19490976.2020.1823800

Ward, M. G., Sparrow, M. P., and Roblin, X. (2018). Therapeutic Drug Monitoring of Vedolizumab in Inflammatory Bowel Disease: Current Data and Future Directions. *Therap Adv. Gastroenterol.* 11, 1756284818772786. doi:10.1177/1756284818772786

Wirtz, S., Neufert, C., Weigmann, B., and Neurath, M. F. (2007). Chemically Induced Mouse Models of Intestinal Inflammation. *Nat. Protoc.* 2, 541–546. doi:10.1038/nprot.2007.41

Wu, M., Li, P., An, Y., Ren, J., Yan, D., Cui, J., et al. (2019). Phloretin Ameliorates Dextran Sulfate Sodium-Induced Ulcerative Colitis in Mice by Regulating the Gut Microbiota. *Pharmacol. Res.* 150, 104489. doi:10.1016/j.phrs.2019.104489

Xu, B., Li, Y. L., Xu, M., Yu, C. C., Lian, M. Q., Tang, Z. Y., et al. (2017). Geniposide Ameliorates TNBS-Induced Experimental Colitis in Rats via Reducing Inflammatory Cytokine Release and Restoring Impaired Intestinal Barrier Function. *Acta Pharmacol. Sin.* 38, 688–698. doi:10.1038/aps.2016.168

Xu, F., Xu, Y., Xiong, J. H., Zhang, J. H., Wu, J., Luo, J., et al. (2020). AOC1 Contributes to Tumor Progression by Promoting the AKT and EMT Pathways in Gastric Cancer. *Cancer Manag. Res.* 12, 1789–1798. doi:10.2147/CMAR.S225229

Xu, Z., Gao, Y., Meng, S., Yang, B., Pang, L., Wang, C., et al. (2016). Mechanism and *In Vivo* Evaluation: Photodynamic Antibacterial Chemotherapy of Lysine-Porphyrin Conjugate. *Front. Microbiol.* 7, 242. doi:10.3389/fmicb.2016.00242

Zakerska-Banaszak, O., Tomczak, H., Gabryel, M., Baturo, A., Wolko, L., Michalak, M., et al. (2021). Dysbiosis of Gut Microbiota in Polish Patients with Ulcerative Colitis: a Pilot Study. *Sci. Rep.* 11, 2166. doi:10.1038/s41598-021-81628-3

Zhai, L., Huang, T., Xiao, H. T., Wu, P. G., Lin, C. Y., Ning, Z. W., et al. (2020). Berberine Suppresses Colonic Inflammation in Dextran Sulfate Sodium-Induced Murine Colitis Through Inhibition of Cytosolic Phospholipase A2 Activity. *Front. Pharmacol.* 11, 576496. doi:10.3389/fphar.2020.576496

Zhang, X. Y., Chen, J., Yi, K., Peng, L., Xie, J., Gou, X., et al. (2020). Phlorizin Ameliorates Obesity-Associated Endotoxemia and Insulin Resistance in High-Fat Diet-Fed Mice by Targeting the Gut Microbiota and Intestinal Barrier Integrity. *Gut Microbes* 12, 1–18. doi:10.1080/19490976.2020.1842990

Zhao, Z., Ma, J., Wang, Y., Xu, Z., Zhao, L., Zhao, J., et al. (2021). Antimicrobial Photodynamic Therapy Combined with Antibiotic in the Treatment of Rats with Third-Degree Burns. *Front. Microbiol.* 12, 622410. doi:10.3389/fmicb.2021.622410

Zhu, L., Xu, L. Z., Zhao, S., Shen, Z. F., Shen, H., and Zhan, L. B. (2020a). Protective Effect of Baicalin on the Regulation of Treg/Th17 Balance, Gut Microbiota and Short-Chain Fatty Acids in Rats with Ulcerative Colitis. *Appl. Microbiol. Biotechnol.* 104, 5449–5460. doi:10.1007/s00253-020-10527-w

Zhu, Y., Luo, J., Yang, Z., and Miao, Y. (2020b). High-Throughput Sequencing Analysis of Differences in Intestinal Microflora between Ulcerative Colitis Patients with Different Glucocorticoid Response Types. *Genes Genomics* 42, 1197–1206. doi:10.1007/s13258-020-00986-w

Conflict of Interest: The authors declare that the research was conducted in the absence of any commercial or financial relationships that could be construed as a potential conflict of interest.

Publisher's Note: All claims expressed in this article are solely those of the authors and do not necessarily represent those of their affiliated organizations, or those of the publisher, the editors and the reviewers. Any product that may be evaluated in this article, or claim that may be made by its manufacturer, is not guaranteed or endorsed by the publisher.

Copyright © 2021 Rong, Hong, Zhu, Liu, Jiang and Liu. This is an open-access article distributed under the terms of the Creative Commons Attribution License (CC BY). The use, distribution or reproduction in other forums is permitted, provided the original author(s) and the copyright owner(s) are credited and that the original publication in this journal is cited, in accordance with accepted academic practice. No use, distribution or reproduction is permitted which does not comply with these terms.

frontiers in Pharmacology

REVIEW
published: 03 November 2021
doi: 10.3389/fphar.2021.762807

A Comprehensive Account on Recent Progress in Pharmacological Activities of Benzimidazole Derivatives

Shejuti Rahman Brishty[1†], *Md. Jamal Hossain*[2†], *Mayeen Uddin Khandaker*[3], *Mohammad Rashed Iqbal Faruque*[4], *Hamid Osman*[5] *and S. M. Abdur Rahman*[1†*]

[1]Department of Clinical Pharmacy and Pharmacology, Faculty of Pharmacy, University of Dhaka, Dhaka, Bangladesh, [2]Department of Pharmacy, State University of Bangladesh, Dhaka, Bangladesh, [3]Centre for Applied Physics and Radiation Technologies, School of Engineering and Technology, Sunway University, Bandar Sunway, Malaysia, [4]Space Science Centre, Universiti Kebangsaan Malaysia, Bangi, Malaysia, [5]Department of Radiological Sciences, College of Applied Medical Sciences, Taif University, Taif, Saudi Arabia

OPEN ACCESS

Edited by:
Andres Trostchansky,
Universidad de la República, Uruguay

Reviewed by:
Alexander Spasov,
Volgograd State Medical University, Russia
Natalia Rios,
Universidad de la República, Uruguay

***Correspondence:**
S. M. Abdur Rahman
smarahman@du.ac.bd

†ORCID:
Shejuti Rahman Brishty
orcid.org/0000-0001-7794-6775
Md. Jamal Hossain
orcid.org/0000-0001-9706-207X
S. M. Abdur Rahman
orcid.org/0000-0002-9963-8885

Specialty section:
This article was submitted to Experimental Pharmacology and Drug Discovery, a section of the journal Frontiers in Pharmacology

Received: 22 August 2021
Accepted: 01 October 2021
Published: 03 November 2021

Citation:
Brishty SR, Hossain MJ, Khandaker MU, Faruque MRI, Osman H and Rahman SMA (2021) A Comprehensive Account on Recent Progress in Pharmacological Activities of Benzimidazole Derivatives. Front. Pharmacol. 12:762807. doi: 10.3389/fphar.2021.762807

Nowadays, nitrogenous heterocyclic molecules have attracted a great deal of interest among medicinal chemists. Among these potential heterocyclic drugs, benzimidazole scaffolds are considerably prevalent. Due to their isostructural pharmacophore of naturally occurring active biomolecules, benzimidazole derivatives have significant importance as chemotherapeutic agents in diverse clinical conditions. Researchers have synthesized plenty of benzimidazole derivatives in the last decades, amidst a large share of these compounds exerted excellent bioactivity against many ailments with outstanding bioavailability, safety, and stability profiles. In this comprehensive review, we have summarized the bioactivity of the benzimidazole derivatives reported in recent literature (2012–2021) with their available structure-activity relationship. Compounds bearing benzimidazole nucleus possess broad-spectrum pharmacological properties ranging from common antibacterial effects to the world's most virulent diseases. Several promising therapeutic candidates are undergoing human trials, and some of these are going to be approved for clinical use. However, notable challenges, such as drug resistance, costly and tedious synthetic methods, little structural information of receptors, lack of advanced software, and so on, are still viable to be overcome for further research.

Keywords: nitrogenous heterocyclic compounds, diverse pharmacological activities, structure-activity relationship (SAR), anti-infectious, anti-proliferative, cardiovascular agents

INTRODUCTION

Benzimidazole, alternatively known as 1*H*-benzimidazole and 1,3-benzodiazole, consists of benzene ring fused with a five-membered imidazole ring, and is an important heterocyclic pharmacophore. Benzimidazole is regarded as a "privileged structure" in heterocyclic chemistry due to its association with a wide range of biological activities (Barot et al., 2013; Alaqeel, 2017).

Back in 1940s, benzimidazole was speculated to act similarly as purines to provide biological responses and the first investigation on biological activity of benzimidazole nucleus was reported in 1944 (Woolley, 1944). Interest among the researchers about the synthetic procedure of benzimidazole and its derivatives escalated when Brink et al. (Brink and Folkers, 1949; Emerson et al., 1950) found that 5,6-dimethylbenzimidaozle was a degradation product of vitamin B_{12} and

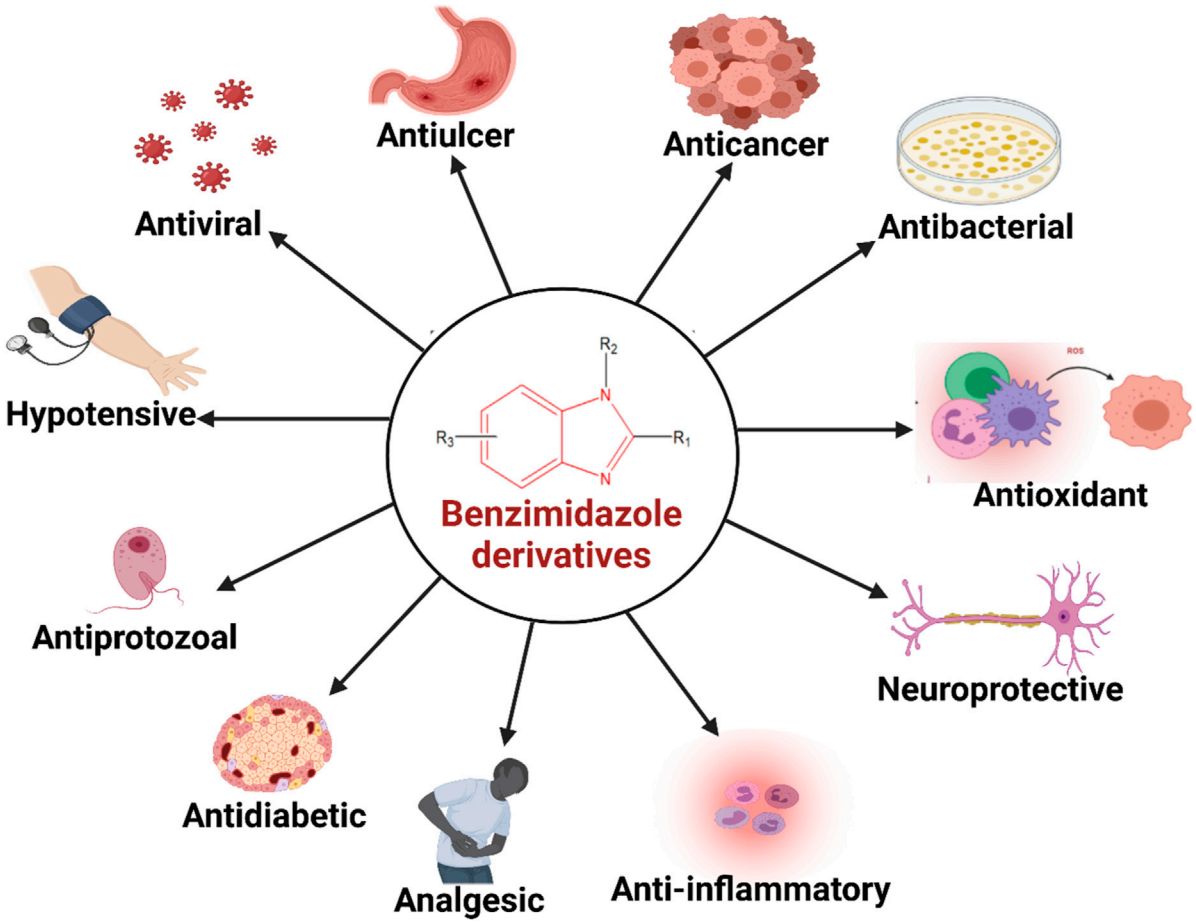

FIGURE 1 | Diverse biological activities of benzimidazole derivatives.

some of its derivatives also possessed vitamin B_{12} like activity. These early reports led researchers to the exploration of benzimidazole nucleus for numerous activities. Through the course of many years of research, benzimidazole has emerged as an important heterocyclic system because of its existence in diverse biologically active compounds, such as antiparasitics, antimicrobials, antivirals, antifungals, anticonvulsants, antihypertensives, antihistaminics, analgesics, anti-inflammatory agents, anticancers, anticoagulants and proton pump inhibitors (**Figure 1**) (Fei and Zhou, 2013; Wang et al., 2015). As a result of changing substituents around the core structure, many drugs of a wide variety of therapeutic lines have been developed such as albendazole, mebendazole, thiabendazole as antihelmintics; enviradine as antiviral; carbendazim as fungicidal; omeprazole, lansoprazole, pantoprazole as proton pump inhibitors; candesartan cilexitil and telmisartan as antihypertensives, and astemizole as antihistaminic agent (**Figure 2**) (Bansal and Silakari, 2012; Alaqeel, 2017). The high therapeutic potential of benzimidazole related drugs has inspired the medicinal chemists to carry out the synthesis of several novel chemotherapeutic agents containing benzimidazole moiety (Morais et al., 2017).

Numerous researches have been accomplished in the past couple of years which produced very intriguing results concerning the chemistry, structure-activity relationship and biological activities of different benzimidazole based compounds. The diverse biological activities displayed by compounds bearing benzimidazole moiety have prompted researchers all around the globe to design and synthesize various benzimidazole analogues. A number of recently published patents on the benzimidazole moiety are listed in **Table 1**. Several review articles have been published emphasizing on the contribution of benzimidazole nucleus in particular biological activity, e.g. anticancer, analgesic, anti-inflammatory, antimicrobial, antiviral, antitubercular, antiulcer, antihypertensive and antidiabetic property (Bansal and Silakari, 2012; Barot et al., 2013; Keri et al., 2015; Wang et al., 2015; Akhtar et al., 2017). To the best of our knowledge, there is no review article available in the literature which has focused on the most updated information of the diverse biological and therapeutic applications of benzimidazole derivatives. The present review gives a comprehensive account of all biological aspects of benzimidazole derivatives and has included information from the recent studies reported up to 2021. Apart from literature

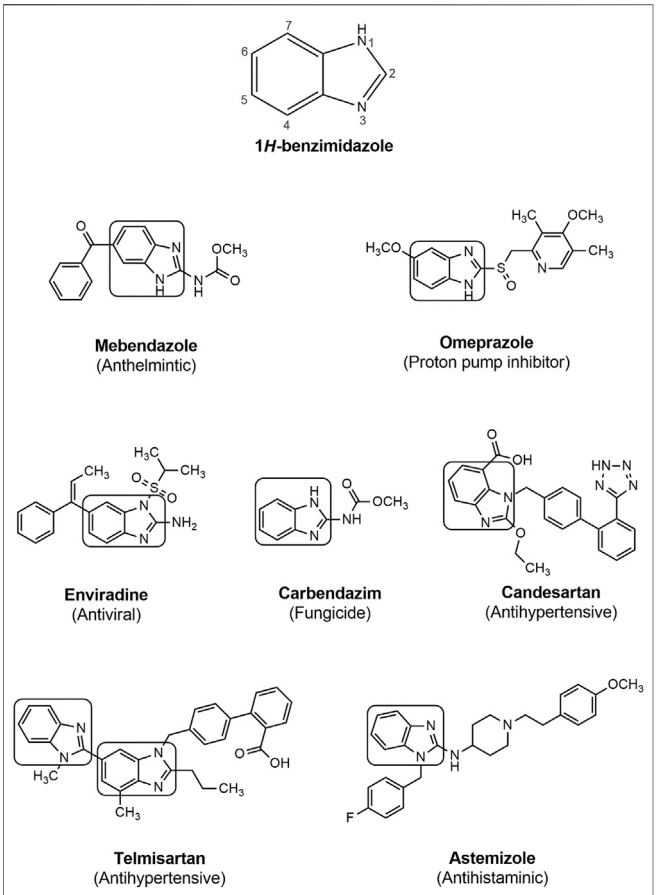

FIGURE 2 | 1*H*-benzimidazole and some benzimidazole containing drugs.

study, this review also provides a thoughtful insight into the latest ongoing research on benzimidazole derivatives in a variety of therapeutic fields.

BIOLOGICAL ACTIVITIES

The wide variety of benzimidazole derivatives synthesized during the last few years and their diverse biological applications are discussed in the following sections.

Antimicrobial Activity

Antimicrobial and Antifungal Activity

The antimicrobial potential of benzimidazole moiety has been explored notably since late 1990s and early 2000s (Özkay et al., 2011). Considering the huge dimension of research conducted on antimicrobial property of benzimidazole derivatives after 2012, the following section focuses on the up-to-date information on antibacterial and antifungal activities, while antiviral, antiulcer, antiprotozoal and antitubercular properties are discussed in separate sections. Different benzimidazole based compounds with antibacterial and antifungal activities are shown in **Figure 3**.

Kathrotiya and Patel (Kathrotiya and Patel, 2013) synthesized a series of indole-based pyrido [1,2-*a*] benzimidazole derivatives **(1–4)** and evaluated *in vitro* antimicrobial activity against some Gram-positive and Gram-negative bacteria and fungi using broth microdilution minimum inhibitory concentration (MIC) method. Compounds **1, 3** and **4** (MIC = 50, 62.5 and 12.5 μg/ml, respectively) displayed prominent antibacterial activity against *S. typhi* compared to standards ampicillin, chloramphenicol and ciprofloxacin (MIC = 100, 50 and 25 μg/ml, respectively). Compounds **2** and **3** exhibited notable antifungal activity against *C. albicans* (MIC = 250 μg/ml) in comparison with standard griseofulvin (MIC = 500 μg/ml). The derivatives with 4-methoxy **(1)** and cyano (**4**) group at 2-position of indole nucleus were found to possess excellent inhibitory activity against most of the tested organisms. Birajdar et al. (Birajdar et al., 2013) synthesized some amino alcohol derivatives of 2-methyl benzimidazole **(5–8)** by epoxide ring opening of 2-methyl benzimidazole with different substituted cyclic amines. Compounds **5–8** demonstrated moderate to good activity against Gram-positive (*S. aureus*) and Gram-negative (*E. coli*) pathogens in comparison with reference drugs ciprofloxacin and norfloxacin.

Several benzimidazole derivatives with imine functionality **(9–14)** were prepared by Kahveci et al. (Kahveci et al., 2014) using microwave irradiation as well as conventional method. Compounds **9–14** displayed notable antimicrobial property against the tested microorganisms. Desai et al. (Desai et al., 2014) synthesized a series of 2-pyridone based benzimidazole derivatives **(15–19)** and investigated *in vitro* antimicrobial potential against a number of bacterial and fungal strains using conventional broth dilution method. Compounds **15** and **18** (MIC = 12.5–25 μg/ml) showed better antibacterial activity, and **16** and **19** (MIC = 25–100 μg/ml) displayed comparable activity to standard chloramphenicol (MIC = 50 μg/ml). The presence of electron withdrawing groups, e.g. fluoro (**15, 16**) and nitro (**18, 19**) at the meta or para position might have contributed for their antimicrobial property. Compound **17** containing chloro group displayed the most remarkable antifungal activity, with MIC values in the range of 25–62.5 μg/ml against three fungal strains compared to standard ketoconazole (MIC = 50 μg/ml). A library of 1-methyl-*N*-[(substituted-phenylmethylidene)-1*H*-benzimidazol-2-amines **(20–24)** were synthesized and reported for notable antimicrobial activity against Gram-positive *S. aureus* (ATCC 6538), *B. pumilus* (ATCC 14884) and Gram-negative *E. coli* (NCTC 10418), *P. aeruginosa* (ATCC 25619) bacteria compared to reference drug ampicillin (Noolvi et al., 2014).

Luo et al. (Luo et al., 2015) synthesized a series of benzimidazole-based naphthalimide triazoles and triazolium compounds **(25–27)**. The derivatives were assessed for *in vitro* antibacterial activity against Gram-positive *S. aureus*, Methicillin-resistant *S. aureus*, *M. luteus* and *B. subtilis* and Gram-negative *B. proteus*, *E. coli*, *B. typhi*, and *P. aeruginosa* as well as for antifungal activity against *A. fumigatus*, *C. albicans*, *C. utilis*, *A. flavus*, and *S. cerevisiae*. The 2-chlorobenzyl triazolium compound **26** and octyl group-containing compound **27** showed the most potent antibacterial activity against *S. aureus* with an MIC of 2 μg/ml

TABLE 1 | Recently published patents of benzimidazole derivatives.

Sl. No	Patent No	Country	Patent title	Publication date	Current status	Inventors	Brief description
1	ES2807191T3 Berrebi-Bertrand et al. (2021)	Spain	Benzimidazole derivatives as dual ligands of the histamine H1 receptor and the histamine H4 receptor	Feb 22, 2021	Active	Isabelle Berrebi-Bertrand, Xavier Billot, Thierry Calmels, et al	The compounds are supposed to have pharmaceutically acceptable salt, tautomers, hydrates, and solvation properties
2	AU2017382436A1 Crew et al. (2021)	Australia	Compounds and methods for the targeted degradation of Rapidly Accelerated Fibrosarcoma polypeptides	Jan 28, 2021	Active	Andrew P. Crew, Craig M. Crews, Hanqing Dong et al	The compound showed a wide range of biological activities by inhibition/degradation of target protein
3	US10835488B2 Pevzner and Moses-Heller (2020)	United States	Stable orally disintegrating pharmaceutical compositions	Nov 17, 2020	Active	Victor Pevzner, Sheera Moses-Heller	The composition has proton pump inhibition property
4	US10787420B2 Liu et al. (2020)	United States	Benzimidazole compound and preparation method thereof	Sep 29, 2020	Active	Xuejing Liu, Ying Han, Liang Yang	Several benzimidazoles have been synthesized through SN2 and cyclization reactions by utilizing no toxic reagent and/or any metal catalyst
5	US20190322671A1 Bourque and Skerlj (2019)	United States	Cxcr4 inhibitors and uses thereof	Oct 24, 2019	Pending	Elyse Marie Josee Bourque, Renato Skerlj	Data supported that the inventions have been regarded as CXCR4 blockers and healers of many diseases induced by the receptors
6	CA3079081A1 Bartberger et al. (2019)	Canada	Benzimidazole derivatives and their uses	April 25, 2019	Pending	Michael D. Bartberger, Nagasree Chakka, Hua Gao, et al	The inventions have been considered as Transient Receptor Potential Channel 6 (TRPC6) protein inhibitors
7	AU2020104192A4 Adak et al. (2018)	Australia	Process of synthesis of benzimidazole derivatives against M.tb	Dec 20, 2018	Active	Vishal Sudam Adak, Pravin Baburao Awate, Vishwas Chandrakant Bhagat, et al	The present invention have been disclosed as inhibitors of M.tb (H37Rv strain/ATCC No- 27294)
8	WO2018057810A1 Chandrasekhar et al. (2018)	France	Benzimidazole derivatives and their use as phosphatidylinositol 3-kinase inhibitors	Mar 29, 2018	NA	Jayaraman Chandrasekhar, Stephane Perreault, Leena Patel	The present compounds are acceptable salts, isomers, or a mixture thereof, which showed efficacy against various conditions of inflammation and cancer
9	US8372987B2 Kolaczkowski (2013)	United States	2-{(R)-2-methylpyrrolidin-2-yl)-1H-benzimidazole-4-carboxamide crystalline form 1	Sep 13, 2013	Active	Lawrence, Kolaczkowski	The present invention has notable application in facilitating DNA repair and controlling RNA transcription
10	US20150361032A1 Pajouhesh et al. (2015)	United States	Benzimidazole inhibitors of the sodium channel	Dec 17, 2015	Active	Hassan Pajouhesh Richard Holland, Lingyun Zhang, et al	The current patent represents benzimidazole derivatives that showed inhibition of voltage gated sodium channel, which might be promising in the treatment of various

(Continued on following page)

TABLE 1 | (*Continued*) Recently published patents of benzimidazole derivatives.

Sl. No	Patent No	Country	Patent title	Publication date	Current status	Inventors	Brief description
							diseases and conditions
11	US 20150336967A1 Czardybon et al. (2015)	United States	Novel Benzimidazole Derivatives as Kinase Inhibitors	Nov 26, 2015	Active	Wojciech, Czardybon,Kraków Brzózka, Michal, Galezowski, et al	The patent describes benzimidazole derivatives as serine/ threonine and tyrosine kinase-inhibitors with useful application in the treatment of solid tumors, lymphomas, leukaemia, and autoimmune disorders
12	US 20150322065A1 Chappie et al. (2015)	United States	Azabenzimidazole Compounds	Nov 12, 2015	Active	Thomas Allen Chappie, Patrick Robert Verhoest, Nandini, Chaturbhai Patel, Matthew Merrill Hayward	The present invention depicts the role of azabenzimidazole derivatives in the treatment of metabolic, central nervous system (CNS), autoimmune and inflammatory disorders
13	US 20150307479A1 Kuduk et al. (2015)	United States	Cyclobutyl benzimidazoles as pde 10 inhibitors	Oct 29, 2015	Active	Scott D. Kuduk, Casey C. McComas, Thomas S. Reger	The patent describes the usefulness of cyclobutyl benzimidazole derivatives in treating CNS disorders related to phosphodiesterase 10 (PDE10)
14	US 20150265625A1 Brown and Matthews (2015)	United States	(alpha-substituted aralkylamino and heteroarylalkylamino) pyrimidinyl and 1,3,5-triazinyl benzimidazoles, pharmaceutical compositions thereof, and their use in treating proliferative diseases	Sep 24, 2015	Active	S. David Brown, David J. Matthews	The current invention has useful application as drugs or agents in the treatment of proliferative diseases
15	US 20150218149A1 Apgar et al. (2015)	United States	Novel benzimidazole tetrahydrofuran derivatives	Aug 06, 2015	Active	James M. Apgar, Tesfaye Biftu, Ping Chen, Danqing Feng, Jacqueline D. Hicks, et al	The present invention suggests that novel benzimidazole tetrahydrofuran derivatives are effective against diseases mediated by the AMPK-activated protein kinase
16	US 20150209259A1 Schade et al. (2015)	United States	Octocrylene-free sunscreen composition with low stickiness	July 30, 2015	Active	Tatjana Schade, Kerstin Skubsch, Sina Brinkmann, et al	The present invention suggests an octocrylene-free cosmetic sunscreen composition which has low stickiness
17	US 20150203455A1 Menet et al. (2015)	United States	Novel compounds and pharmaceutical compositions thereof for the treatment of inflammatory disorders	July 23, 2015	Active	Christel Jeanne, Marie Menet, Oscar Mammoliti, Javier Blanc, et al	The patent describes novel benzimidazole derivatives in treating and preventing a number of inflammatory, autoimmune and proliferative disorders
18	US 20150175608A1 Tahri et al. (2015)	United States	Novel 4-substituted 1,3-dihydro-2h-benzimidazol-2-one	June 25, 2015	NA	Abdellah Tahri, Tim Hugo Maria Jonckers, Pierre Jean-marie	The compounds have useful application as antiviral agents against

(Continued on following page)

TABLE 1 | (*Continued*) Recently published patents of benzimidazole derivatives.

Sl. No	Patent No	Country	Patent title	Publication date	Current status	Inventors	Brief description
			derivatives substituted with benzimidazoles as respiratory syncytial virus antiviral agents			Bernard, Raboisson, et al	respiratory syncytial virus (RSV)
19	US 20150175600A1 Atkinson et al. (2015)	United States	2-(azaindol-2-yl) benzimidazoles as pad4 inhibitors	June 25, 2015	Active	Stephen John, Atkinson, Michael David, Barker, Matthew, Campbell, et al	The patent describes the derivatives as PAD4 inhibitors with application against cystic fibrosis, rheumatoid arthritis, systemic lupus erythematosus, cancer, ulcerative colitis, asthma
20	US 20150158878A1 Leban and Zaja (2015)	United States	Bifluorodioxalane-amino-benzimidazole kinase inhibitors for the treatment of cancer, autoimmune inflammation and cns disorders	Jun 11, 2015	Active	Johann Leban, Mirko Zaja	The compounds are kinase inhibitors with notable role in the treatment of autoimmune inflammation, CNS disorders and cancer

to standard norfloxacin (MIC = 2 μg/ml) and better than standard chloromycin (MIC = 7 μg/ml). Compound **26** and 3-fluorobenzyl moiety bearing compound **25** appeared to be the most prominent antifungal agents, with MIC value in the range of 2–19 μg/ml against the tested fungal strains. Vasantha et al. (Vasantha et al., 2015) synthesized a series of *N*-arylidene-2-(2,4-dichlorophenyl)-1-propyl-1*H*-benzo [d]imidazole-5-carbohydrazides derivatives among which compounds **28–31** displayed notable inhibitory effect against *A. niger* with MIC value of 3.12 μg/ml. Compound **28** demonstrated a MIC value of 3.12 μg/ml against most bacterial and fungal strains and appeared to be a potent antibacterial and antifungal agent.

A series of benzimidazole derivatives were synthesized and evaluated by Padalkar et al. (Padalkar et al., 2016) (**32–34**) and Chandrika et al. (Chandrika et al., 2016) (**35–37**), where the compounds **32–34** showed prominent antibacterial activity against *S. aureus* strain and compounds **35–37** were found to be the most potent antifungal agents against azole-resistant fungal strain *C. albicans* ATCC 64124 (strain B). Another study reported that among the total 22 synthesized novel 2-substituted fluorinated benzimidazoles, compounds **38–40** showed antimicrobial activity. In contrast, compound **40** containing a trifluoromethyl substituent showed the highest antifungal activity against the fungus *C. albicans* (Shintre et al., 2017). Similarly, El-Gohary and Shaaban (El-Gohary and Shaaban, 2017) synthesized a series of benzimidazole derivatives **(41–43),** where compounds **41** and **43** showed notable activity against *S. aureus*, and compound **42** was found to be the most effective against *B. cereus*. Compound **41** displayed the highest antifungal potential against *C. albicans*, whereas **43** exhibited prominent activity against *A. fumigatus*.

Singh et al. (Singh LR. et al., 2017) prepared a library of coumarin-benzimidazole hybrids and screened them for antimicrobial activity. Compound **44** was found to be the promising broad-spectrum antibacterial agent against *P. aeruginosa*, *S. aureus*, *B. subtilis* and *P. vulgaris*. A series of *N*-(substitutedbenzylidene)-4-(1-((dimethylamino) methyl)-1*H*-benzimidazol-2-yl)thiazol-2-amine derivatives were investigated for antimicrobial activity using agar streak dilution test. Compound **45** appeared to be the most potent among the series. Notably, the presence of an electron-withdrawing group might have contributed to the improved antimicrobial property of the compound (Prasad and Sundararajan, 2017).

Recently, Yadav et al. (Yadav et al., 2018) synthesized 2-substituted benzimidazole derivatives (**46–47**), where compound **46** emerged as the most potent antibacterial agent against both Gram-positive and Gram-negative bacteria compared to standard cefadroxil. All derivatives exhibited better antifungal activity than the standard fluconazole, and compound **47** showed maximum activity against *A. niger* (MIC = 0.018 mM). Liu et al. (Liu et al., 2018) designed a series of novel aminopyrimidinyl benzimidazoles as potential antimicrobial agents. Among them, compound **48** showed effective growth inhibition of MRSA, *E. coli,* and fungus *A. flavus*, compared to standard drugs chloromycin, norfloxacin, and fluconazole.

Another study reported the evaluation of a series of 1-(3-(1*H*-benzoimidazol-2-yl)-5-aryl-4-5dihydro-1*H*-pyrazol-1-yl)-2-(napthalene-1-yloxy) ethanones (**49–52**), where the electron-withdrawing groups (compound **49** containing chloro group at ortho position and **50** with a nitro group at the para position) were the most effective against bacterial strains. On the contrary,

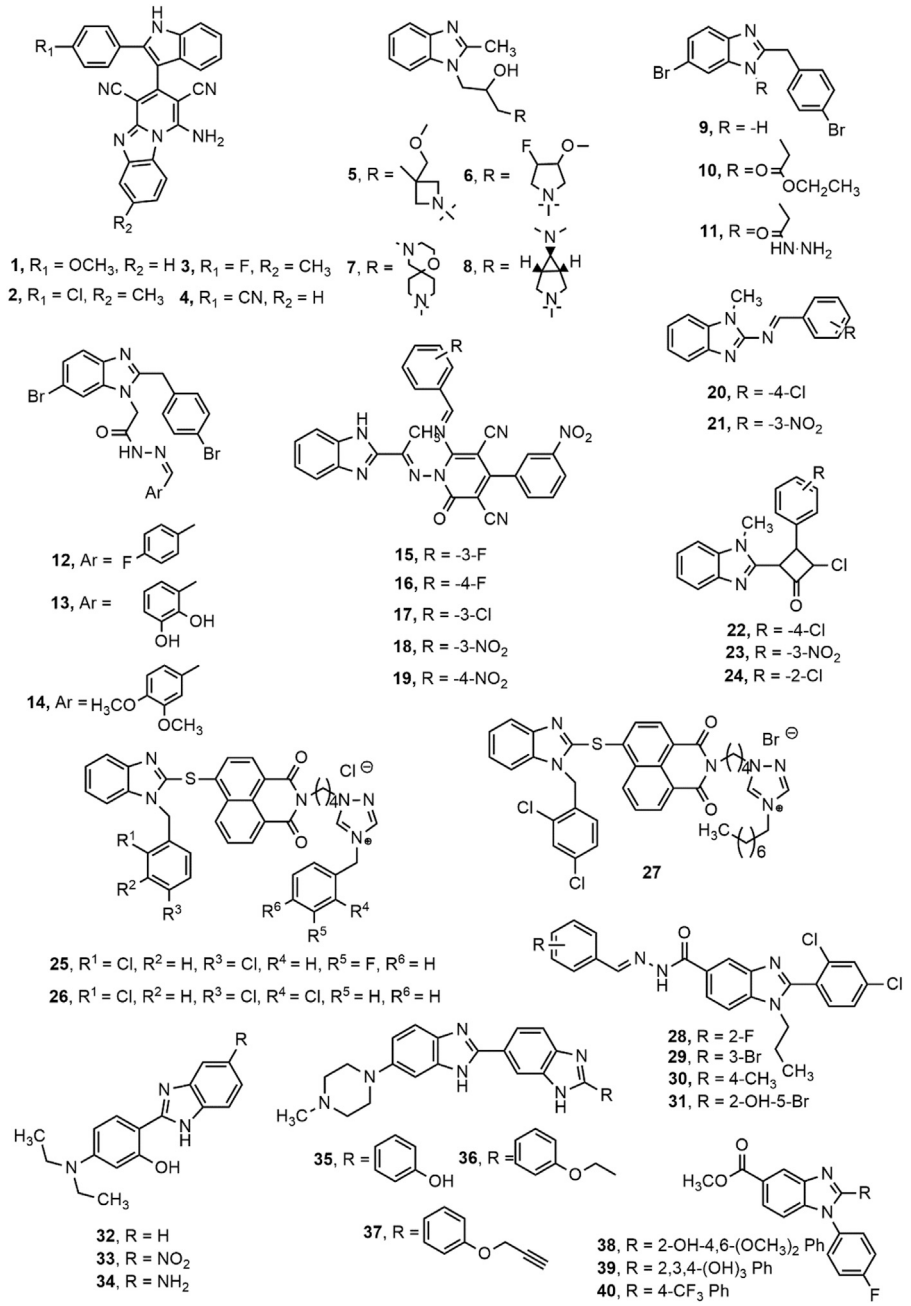

FIGURE 3 | Benzimidazole derivatives with antimicrobial activity.

electron releasing groups at the para position (compounds **51** and **52** carrying methyl and methoxy group, respectively) contributed to the most promising antifungal activity against the tested organisms (Desai et al., 2018). Wang et al. (Wang et al., 2018) synthesized a library of purine benzimidazole hybrids and assessed them for antimicrobial potency. Compound **53** exhibited prominent activity against most tested bacterial and fungal strains and multidrug-resistant strain *S. aureus*, 16 times more potent than the standard norfloxacin (MIC = 4 μg/ml vs. 64 μg/ml). Amongst a series of α-aminonitrile based benzimidazole derivatives (**54–57**), the compounds **55** and **56** were found to be the most potent antibacterial agents having MIC values ranging between 3.9 and 7.8 μg/ml against different bacterial species. All the compounds exerted illustrious antifungal activity against *C. albicans* (MIC = 3.9–7.8 μg/ml) compared to the reference drug fluconazole (MIC value <3.9 μg/ml) (Shaikh et al., 2018).

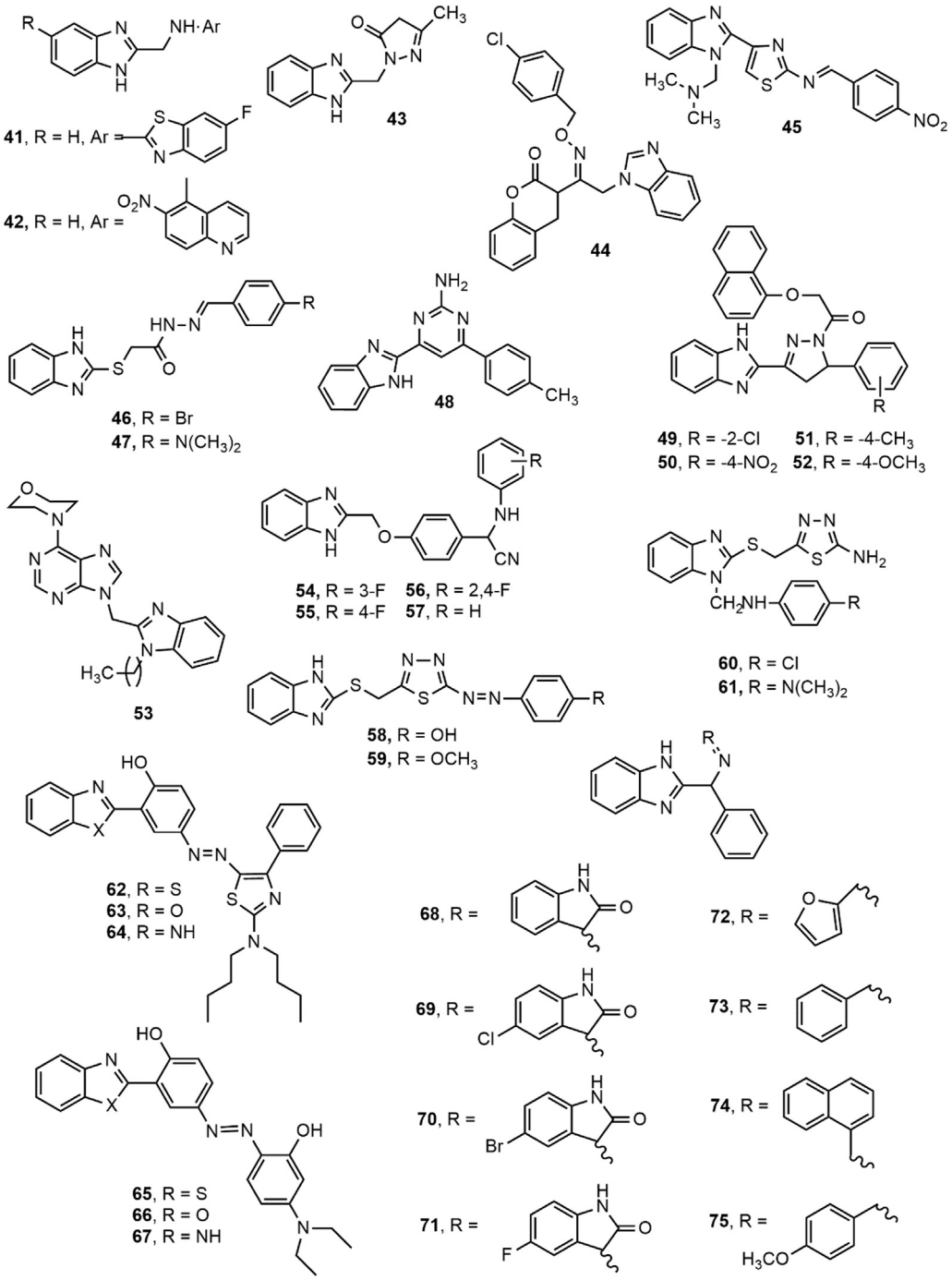

FIGURE 3 | Benzimidazole derivatives with antimicrobial activity.

Similarly, some recent publications also reported several potential antibacterial benzimidazole derivatives like compounds **58–61** containing the 1,3,4-thiadiazole ring and azo moiety showed excellent activity against *S. aureus, B. subtilis*, *E. coli*, and *p. aeruginosa* compared to amoxicillin and ciprofloxacin (Mahmoud et al., 2020). Also, the azo linked compounds **62–67** and novel Schiff bases of 2-(1-amino benzyl)-benzimidazole compounds **68–75** indicated moderate to high *in vitro* inhibition of both gram-positive (*S. aureus*) and gram-negative (*E. coli*) bacteria (Mishra et al., 2019; Singhal et al., 2019). Abdel-Motaal et al. (Abdel-Motaal et al., 2020) synthesized some substituted benzimidazole-2yl derivatives. Compounds **76** and **77** containing thiadiazole and thiazolone moieties, respectively, displayed antibacterial potency against

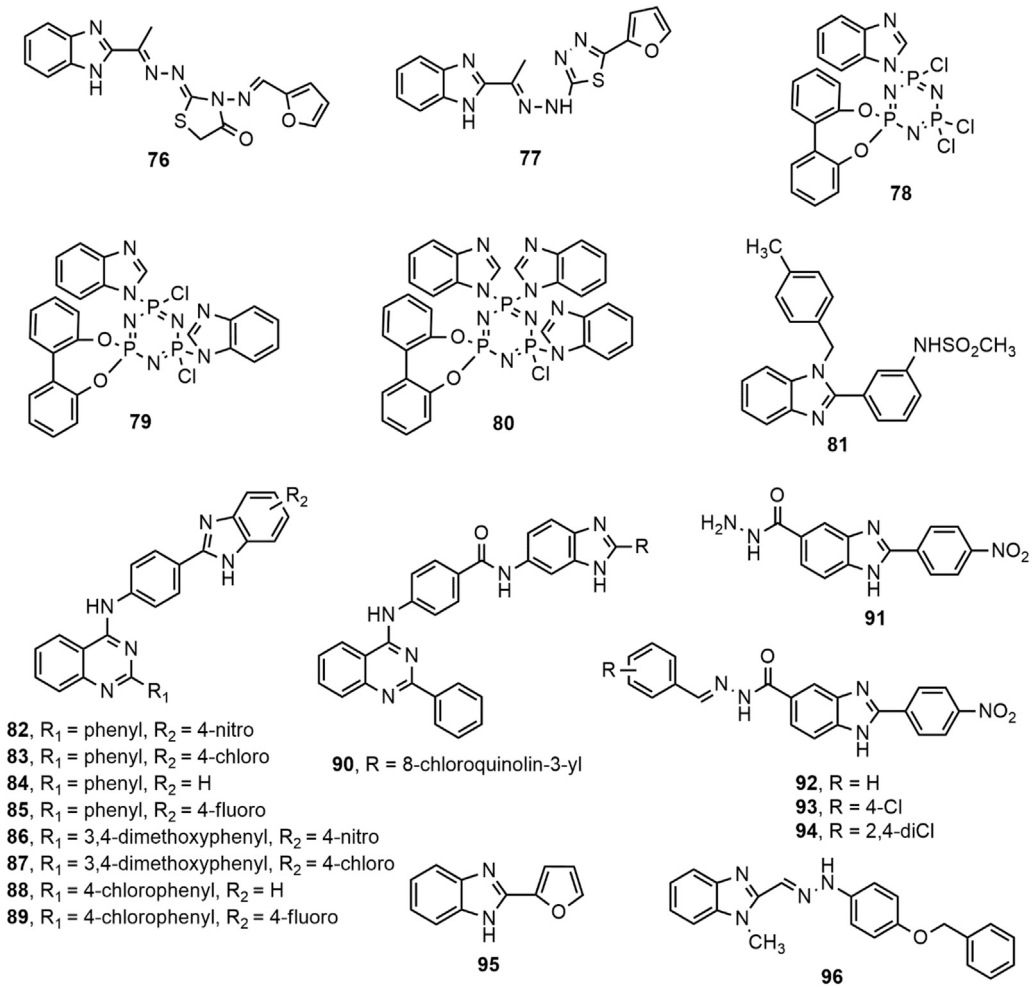

FIGURE 3 | Benzimidazole derivatives with antimicrobial activity.

S. aureus, E. coli, and *B. pumilus* comparable to standard gentamicin. Among the compounds **78–80**, the compound **80** highly inhibited the *B. subtilis* and *S. aureus* bacterial growth compared to the reference drug chloramphenicol (zone of inhibition, mm: 23 and 14 vs. 32 and 30) (İbişoğlu et al., 2020). Besides, co-treatment of compound **81** with colistin exhibited a promising synergistic effect against wild strains *E. coli*, *K. pneumoniae*, *A. baumannii*, and *P. aeruginosa* with MIC range = 8–16 μg/ml (Dokla et al., 2020). Malasala et al. (Malasala et al., 2021) reported nine more potent antibacterial agents **82–90** with MIC range 4–64 μg/ml against several resistant organisms, including methicillin and vancomycin-resistant *S. aureus*. The derivatives with 4-nitro, 4-chloro, 4-fluoro, 4-bromo, and unsubstituted exerted good to moderate inhibitory actions against *S. aureus and M. tuberculosis* H37Rv. Similarly, the analogues with phenyl, 3,4-dimethoxy, and 4-chloro exhibited moderate to good inhibitory property *S. aureus and M. tuberculosis* H37Rv (Malasala et al., 2021). Furthermore, compounds **91–94** inhibited *C. albicans* and *C. neoformans var. grubii* fungal growth with MIC values 4–16 μg/ml, and likewise, compounds **95** and **96** also exerted remarkable antifungal activity (Dhanamjayulu et al., 2019; Amine Khodja et al., 2020; Morcoss et al., 2020).

Antiviral Activity

The antiviral properties of benzimidazole derivatives have been tested against different viral strains; human immunodeficiency virus (HIV), hepatitis B and C virus (HBV and HCV), enteroviruses, respiratory syncytial virus (RSV), human cytomegalovirus (HCMV), bovine viral diarrhea virus (BVDV) and herpes simplex virus-1 (HSV-1) are some to mention (Abu-Bakr et al., 2012). This section focuses on the recent studies involving varied antiviral properties of different benzimidazole derivatives, and their structures are shown in **Figure 4**.

Benzimidazole Against HIV

A number of substituted benzimidazole derivatives were synthesized as reverse transcriptase inhibitors (RTIs) against

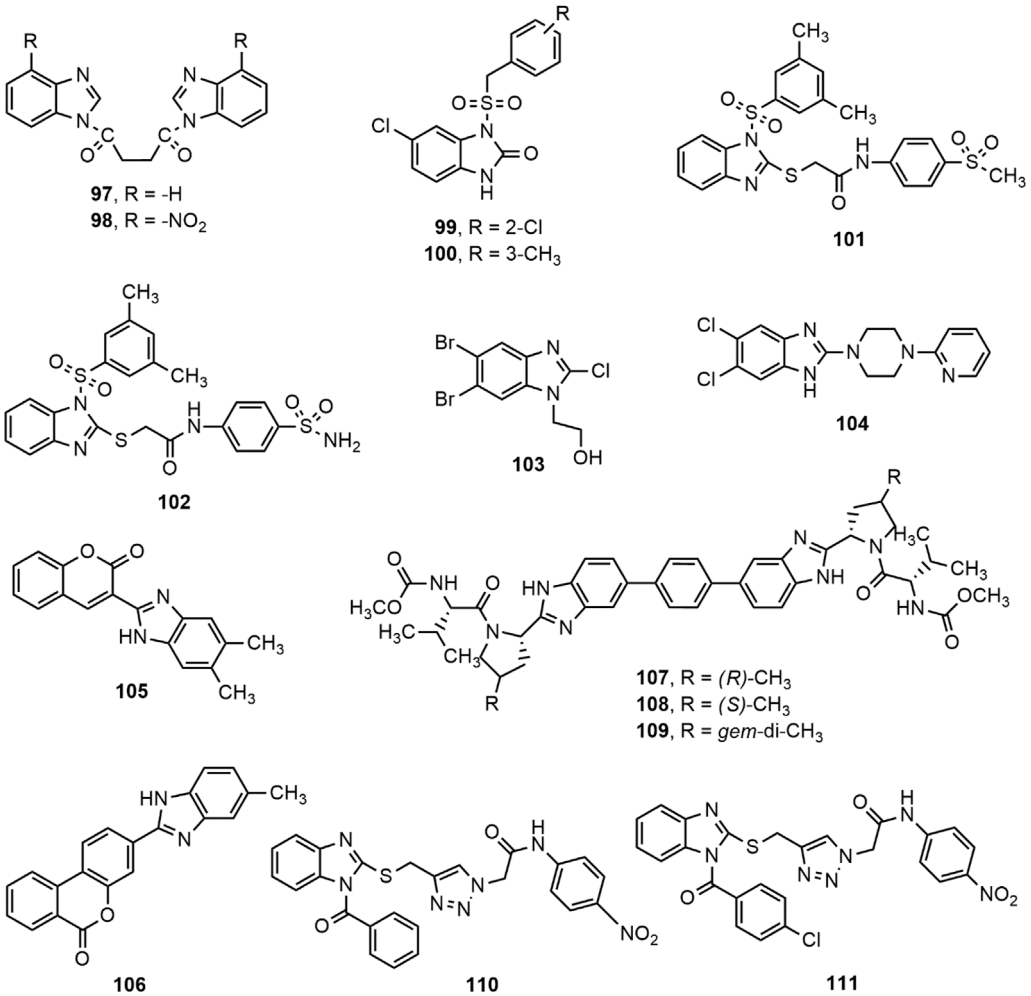

FIGURE 4 | Benzimidazole derivatives with antiviral activity.

HIV-1 replication, among them compounds **97–98** showed notable antiviral activity against laboratory-adapted strains HIV-1_{IIIB} and HIV-1_{Ada5} (EC_{50} = 15.4–40 μM) and primary isolates of HIV-1_{UG07O} and HIV-1_{VB59} strains (EC_{50} = 5.28–31.86 μM) (Singh et al., 2015). Besides, Ferro et al. (Ferro et al., 2017) synthesized two series of N_1-aryl-benzimidazol-2-one derivatives as non-nucleoside reverse transcriptase inhibitors (NNRTIs) against HIV-1, where the compounds **99–100** were more potent than the standard drug nevirapine (IC_{50}: 1.3 and 0.79 vs. 1.55 μM). The sulfone derivatives **101–102**, synthesized by the same research group were also found to be potent HIV-1 NNRTIs with IC_{50} values of 47 and 50 nM, respectively. The substitution at C-4 position of the arylacetamide portion of the compounds might have contributed for their notable activity against HIV-1_{IIIB} strain in cell-based assays (Monforte et al., 2018). Finally, Srivastava et al. (Srivastava et al., 2020) has recently reported a promising anti-HIV benzimidazole derivative **103** with a low IC_{50} value of 0.386×10^{-5} μM.

Benzimidazole Against Hepatitis B and C Viruses (HBV and HCV)

The hepatitis B surface antigen (HBsAg), an HBV surface protein is an important mediator of HBV life cycle (Wang et al., 2016). Xu et al. (Xu et al., 2014) carried out a high-throughput screening (HTS), and concluded that the compound **104** inhibited the secretion of HBsAg and HBV virions indicated by EC_{50} values of 1.5 and 0.6 μM, respectively, along with half cytotoxicity concentration (CC_{50}) value of 24.5 μM.

Moreover, Tsay et al. (Tsay et al., 2013) synthesized a library of hinged benzimidazole-coumarin hybrids and reported the potentiality of compounds **105–106** with EC_{50} values 3.0 and 5.5 nM, respectively, against hepatitis C virus (HCV), a prime cause of liver cirrhosis and hepatocellular carcinoma. Besides, Henderson et al. (Henderson et al., 2015) synthesized a series of 4-substituted pyrrolidine containing bis-benzimidazole analogues (**107–109**) and evaluated for their HCV non-structural 5A (NS5A) inhibitory effect with balanced Genotype

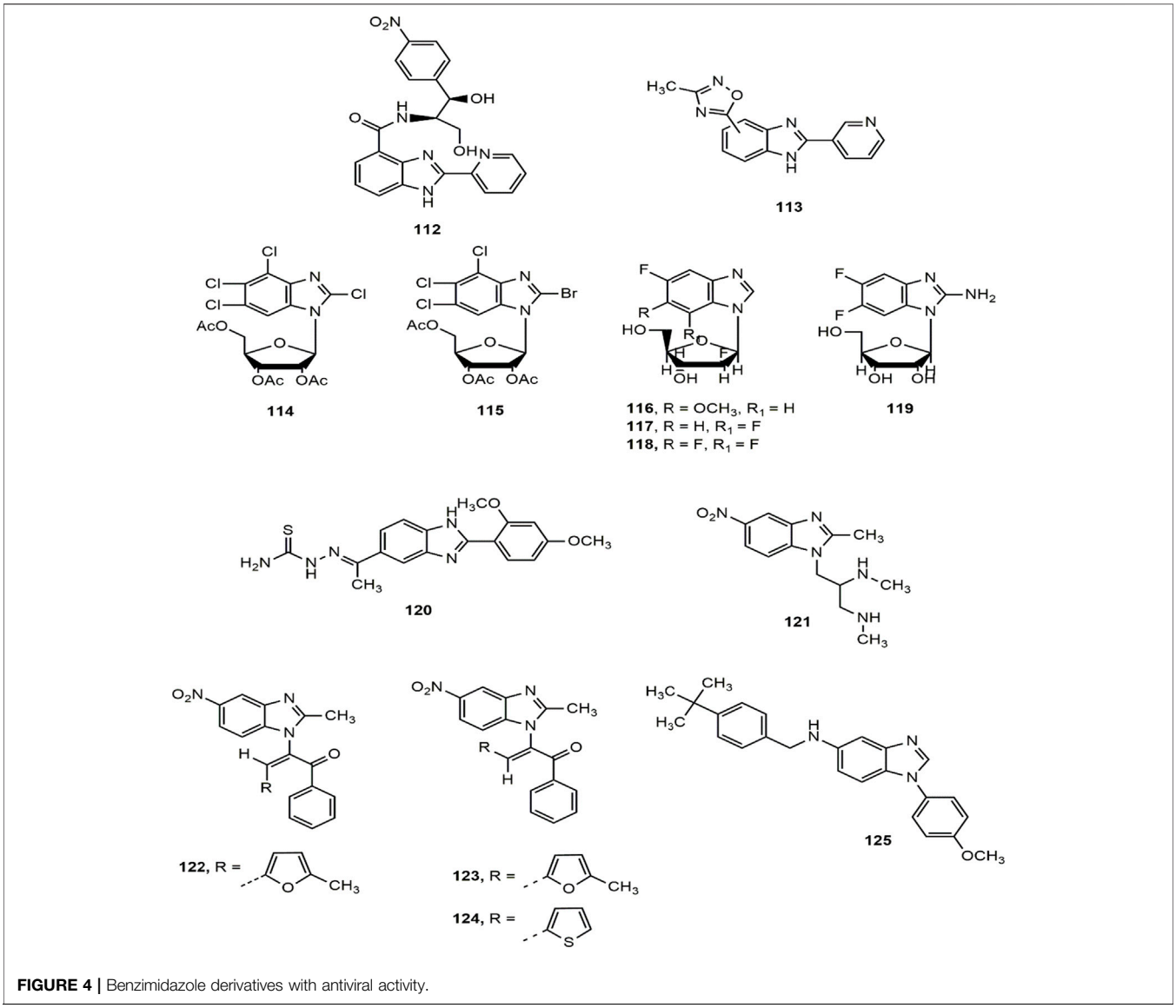

FIGURE 4 | Benzimidazole derivatives with antiviral activity.

1a (G1a) and Genotype 1b (G1b) potency. Compounds **107** (G1a EC_{50} = 0.028 nM, G1b EC_{50} = 0.007 nM), **108** (G1a EC_{50} = 0.026 nM, G1b EC_{50} = 0.037 nM) and **109** (G1a EC_{50} = 0.03 nM, G1b EC_{50} = 0.011 nM) appeared to be most active compounds from the series. Substitution of methyl group (**107–108**) and geminal dimethyl group (**109**) at 4-position of pyrrolidine nucleus was likely to contribute for G1a and G1b potency of the compounds. In another study, a set of 2-thiobenzimidazole analogues (**110–111**) containing triazole moiety were reported as promising HCV inhibitor, where the substituent at position-2 of benzimidazole nucleus played the crucial role to enhance the antiviral potency (Youssif et al., 2016).

Benzimidazole Against Enteroviruses, Cytomegalovirus and Herpes Simplex Virus (HSV)

Two distinct series of benzimidazole derivatives were synthesized, where the compounds **112–113** indicated potent enterovirus (Coxsackie) inhibition with the IC_{50} values of 1.76 and 1.08 μg/ml, respectively (Xue et al., 2011; Wubulikasimu et al., 2013). The benzimidazole D-ribonucleosides derivatives **114–115** exerted activity in rat cytomegalovirus infected cells, and prevented cleavage of concatemeric viral DNA and nuclear egress of mature viral capsids (Dittmer et al., 2017). In a pair consecutive studies (Kharitonova et al., 2016, 2017), Kharitonova et al. reported that several 2′-deoxy-2′-fluoro-β-D-arabinofuranosyl benzimidazole derivatives **(116–118)** and 2-amino-5,6-difluorobenzimidazole nucleosides **(119)** inhibited Herpes Simplex Virus-induced cytopathic effect (CPE). Impressively, the IC_{50} value of compound **119** was 104 μM, four times lower than that of ribavirin and eight times lower than that of maribavir.

Benzimidazole Against Bovine Viral Diarrhea Virus (BVDV), Rotavirus and Arenaviruses

Among a library of 5-acetyl-2-arylbenzimidazoles analogues, compound **120** appeared to be the most effective antiviral agent against Bovine Viral Diarrhea

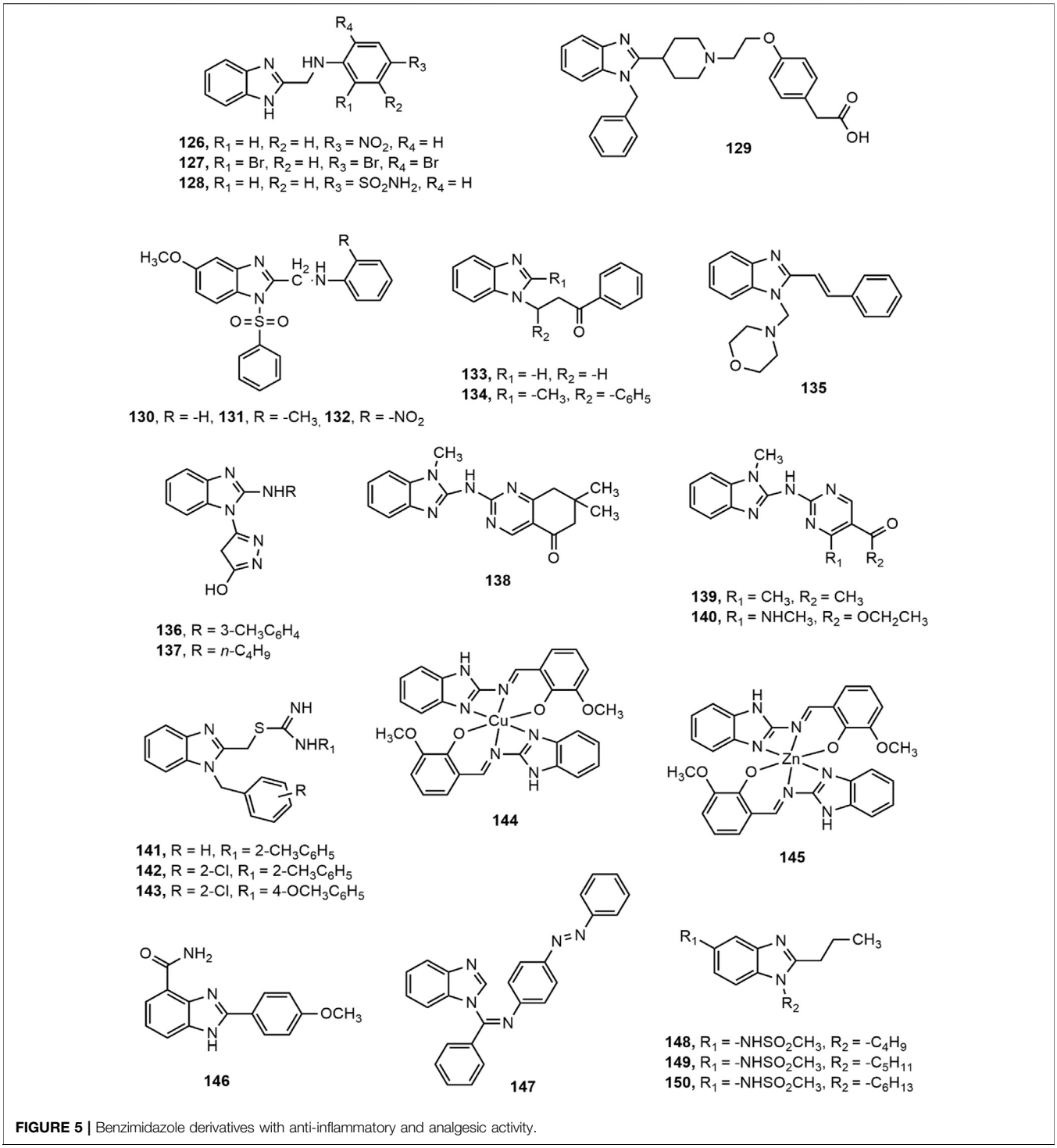

FIGURE 5 | Benzimidazole derivatives with anti-inflammatory and analgesic activity.

virus (BVDV, EC_{50} = 1.11 mM) due to the presence of 2,4-dimethoxy group in the phenyl moiety (Vitale et al., 2012). Shaker et al. (Shaker et al., 2015) synthesized a series of 5-nitro-1*H*-benzimidazole derivatives (**121–124**) bearing substitution of heterocyclic rings at position 1. Compounds **121** and **122** exhibited equal potency as standard doxorubicin against A-549, HCT-116, MCF-7 and human liver carcinoma HepG2 cell lines. Besides, compounds **122–124** showed great potential to be used as potent antiviral agents due to their inhibitory effect against rotavirus Wa strain. Finally, compound **125**, identified by Dai and co-workers, was found to be potent antiviral agent against Lassa virus envelope glycoprotein (LASV GP) pseudotypes with EC_{50} value of 1.1 nM (Dai et al., 2013).

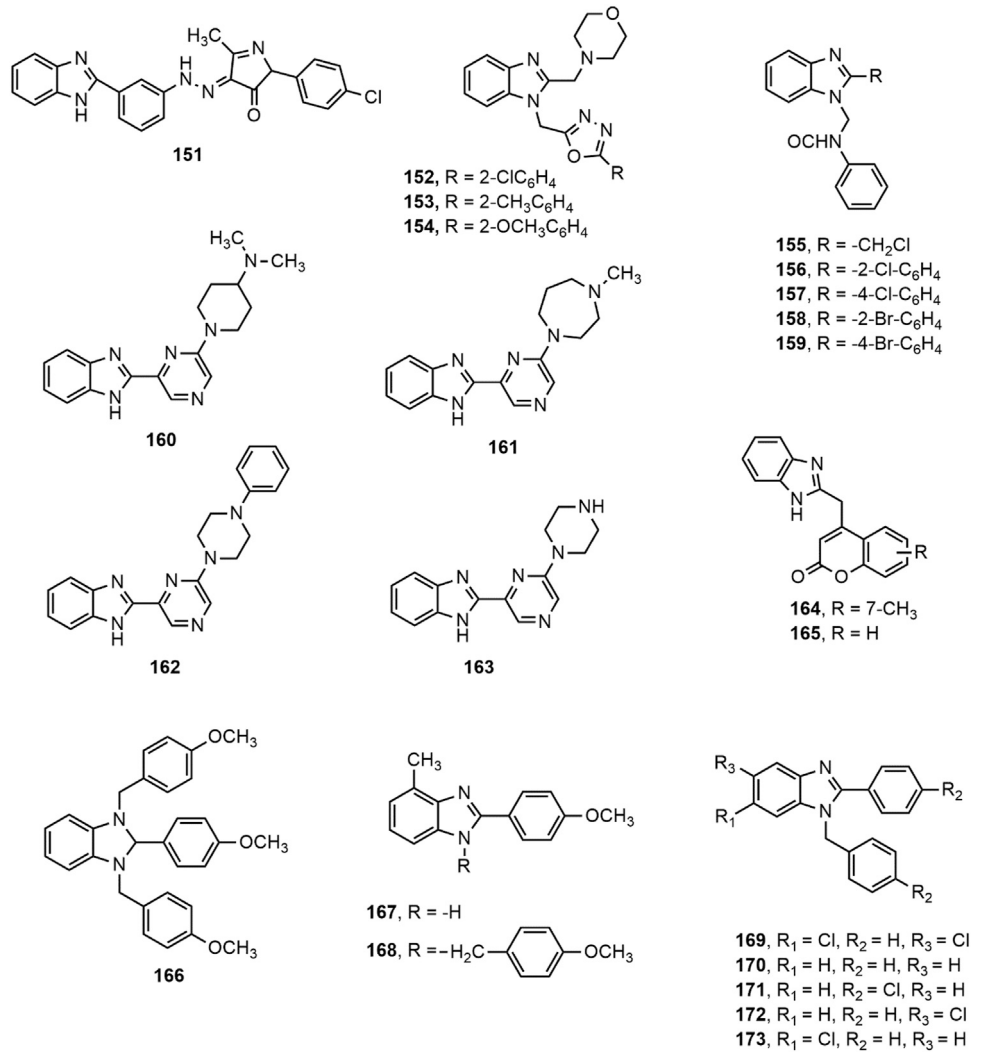

FIGURE 5 | Benzimidazole derivatives with anti-inflammatory and analgesic activity.

Anti-inflammatory and Analgesic Activity

Benzimidazole based compounds are of great importance as anti-inflammatory and analgesic agents because of their property to inhibit cyclooxygenases (COXs), enzymes involved in biosynthesis of important inflammatory mediators called prostaglandins (Akhtar et al., 2017). Apart from the cyclooxygenases (COX), the benzimidazole derivatives interact with transient receptor potential vanilloid-1, cannabinoid receptors, bradykinin receptors, specific cytokines, and 5-lipoxygenase (5-LOX) activating protein. Thus, the compounds derived from benzimidazole moiety show the anti-inflammatory property (Veerasamy et al., 2021). Different benzimidazole derivatives with analgesic and anti-inflammatory properties are shown in **Figure 5**.

Mariappan et al. (Mariappan et al., 2015) synthesized a set of 2-substituted benzimidazole derivatives and reported that compounds **126–128** were found to be the most promising agents among the series displaying significant ($p < 0.01$) analgesic and anti-inflammatory effect at a dose level of 100 mg/kg p.o. Li et al. (Li et al., 2015) assessed the synthesized two series of 2-(piperidin-4-yl)-1*H*-benzo[d] imidazole derivatives for anti-inflammatory activity and found that the compound **129** exhibited the most potent inhibitory activity on nitric oxide and TNF-α production (IC_{50} = 0.86 and 1.87 μM, respectively). Interestingly, the compound **129** also prevented 33.30 and 50.60% ear oedema in xylene-treated mice at doses of 4 and 12 mg/kg, respectively, compared to standard ibuprofen (26.77 and 39.34% inhibition at 4 and 12 mg/kg dose levels, respectively). Besides, compounds **130–132** showed the potentiality as gastroprotective lead compounds which can be developed into orally active analgesic and anti-inflammatory agents (Gaba and Mohan, 2015). Compounds **133–134,** synthesized by Kumar et al. displayed significant analgesic and anti-inflammatory properties, (Kumar et al., 2015) and compound **135** showed better inhibition of acetic acid induced writhing at 20 mg/kg

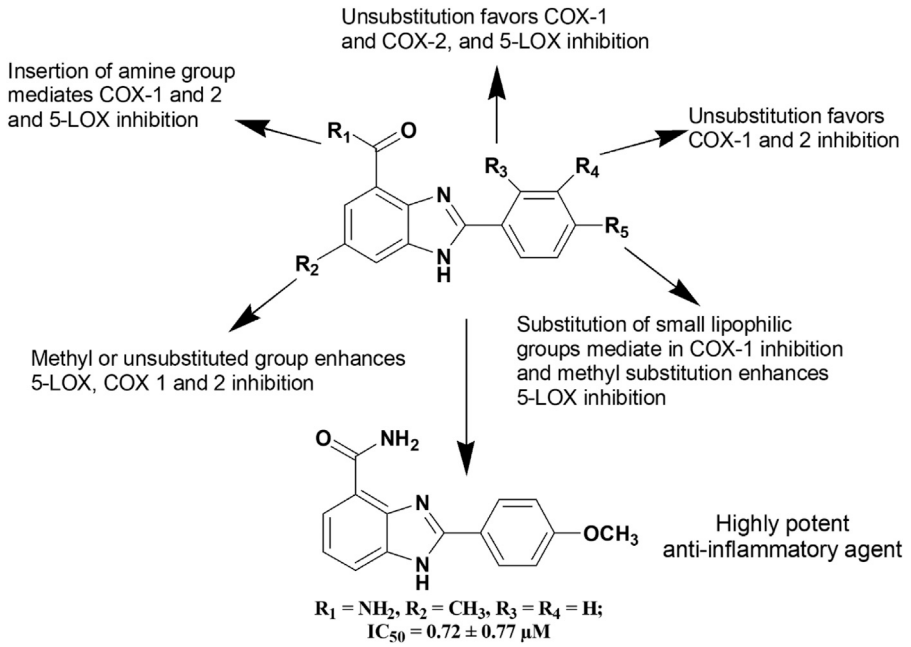

FIGURE 6 | Structure activity relationship (SAR) of benzimidazole derivatives having anti-inflammatory activity. The figure represents the SAR studies accomplished by Bukhari et al. (2016).

dose than the standard diclofenac (78.12 vs. 75%) (Datar and Limaye, 2015).

Moneer et al. (Moneer et al., 2016) synthesized a series of 5-[2-(substituted amino)-1*H*-benzimidazol-1-yl]-4*H*-pyrazol-3-ol derivatives (**136–137**) and investigated for *in vitro* cyclooxygenase inhibitory effect using Cayman's colorimetric COX (ovine) assay. Compounds **136–137** showed remarkable *in vitro* cyclooxygenase inhibition (IC_{50} on COX-1: 0.1664 and 0.2272 nM, respectively, and IC_{50} on COX-2: 0.0370 and 0.0469 nM, respectively) and significant ($p < 0.05$) reduction of edema volume compared to that of standard diclofenac at all time intervals. Prajapat and Talesara (Prajapat and Talesara, 2016) synthesized several alkoxyphthalimide based benzimidazole derivatives (**138–140**) and Siddiqui et al. (Siddiqui et al., 2016) prepared a series of 1-{(1-(2-substituted benzyl)-1*H*-benzo[d]imidazol-2-yl)methyl}-3-arylthioureas (**141–143**). All the compounds **(138–143)** exerted notable anti-inflammatory effect compared to standard diclofenac.

A series of Cu(II) and Zn(II) complexes of a 2-[(1*H*-benzoimidazol-2-ylimino)-methyl]-6-methoxy-phenol Schiff base ligands (**144–145**) were synthesized from condensation of 2-aminobenzimidazole and *o*-vanillin (AlAjmi et al., 2016). The both compounds (**144–145)** at 100 mg/kg b.w. showed around 55% inhibition of inflammation compared to standard diclofenac (65.4% inhibition). Furthermore, Bukhari et al. (Bukhari et al., 2016) reported about anti-inflammatory activity of a series of benzimidazole derivatives where compound **146** was found to be a potent inhibitor of 5-LOX, COX, TNF-α, IL-6 and cytokines among the series. **Figure 6** depicts a clear diagram for understanding the association of structural modifications with bioactivities of benzimidazole derivatives against inflammation.

Eswayah et al. (Eswayah et al., 2017) synthesized several *N*-substituted benzimidazole derivatives and concluded that compound **147** exhibited prominent analgesic activity indicated by decrease in number of writhing at 50 mg/kg dose compared to standard aspirin (17 vs. 12%). Besides, Sharma et al. (Sharma R. et al., 2017) stated that compounds **148–150** demonstrated notable reduction in edema ranging from 92.7 to 97.6% compared to the standard drugs rofecoxib and indomethacin (78.95 and 75%, respectively). Moreover, compound **151** displayed 72% analgesic activity and 67% protection of inflammation at 20 mg/kg dose in second hour in comparison with standard diclofenac (69% analgesic activity and 65% protection of inflammation) (Chikkula and Sundararajan, 2017). Similarly, Rathore et al. (Rathore et al., 2017) synthesized a series of 1-{(5-substituted-1,3,4-oxadiazol-2-yl)methyl}-2-(morpholinomethyl)-1*H*-benzimidazole derivatives (**152–154**) and reported that the compound **152** having chloro group at the ortho position of phenyl ring showed promising anti-inflammatory effect compared to standard indomethacin (74.17 ± 1.28% vs. 57.79 ± 1.71%). Besides, compounds **152–154** also produced remarkable COX-2 inhibition (IC_{50} range = 8–13.7 μM).

By applying Mannich reaction, Sethi et al. (Sethi et al., 2017) prepared a series of *N*-benzimidazol-1-yl methyl-benzamide derivatives (**155–159**), having electron-withdrawing groups chloro and bromo at ortho position of phenyl ring (**156–158**) and chloromethyl group at 2-position of benzimidazole nucleus (**155**), asserted significant analgesic and anti-inflammatory

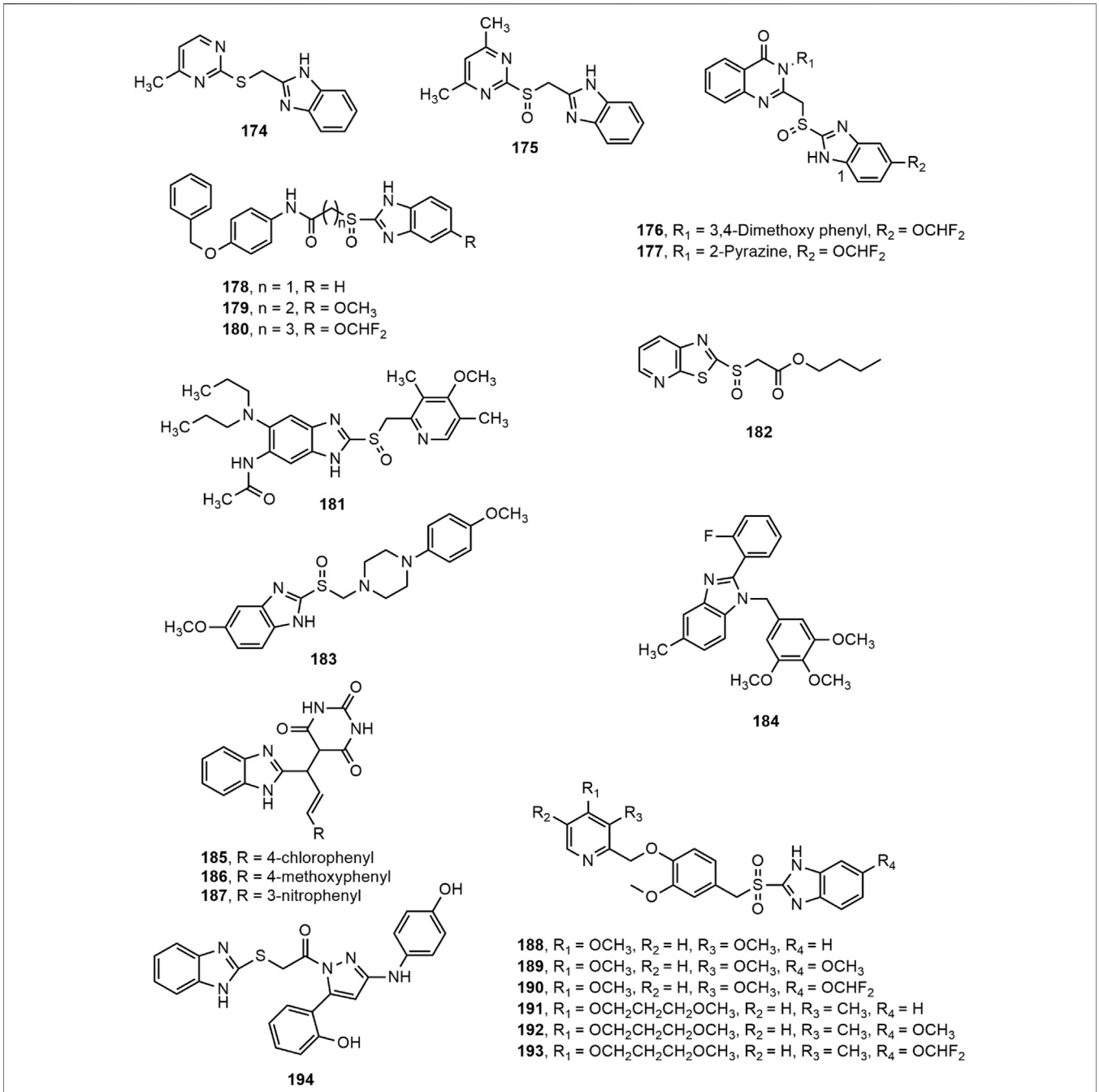

FIGURE 7 | Benzimidazole derivatives with antiulcer activity.

activities compared to vehicle control group (10% DMSO, $p < 0.05$). Moreover, Shankar et al. (Shankar et al., 2017) synthesized a series of 2-(6-alkyl-pyrazin-2-yl)-1*H*-benzo[d]imidazole derivatives (**160–163**), where the compound **162** showed maximum selectivity towards COX-2 enzyme among the series (% inhibition 78.68 ± 0.46 and selectivity ratio 3.71) and it might be due to the presence of *N*-phenyl piperzine moiety in the benzimidazole nucleus. Besides, compounds **160, 161** and **163** demonstrated notable activity against COX-2 enzyme (% inhibition 71.45 ± 0.65, 76.93 ± 0.84 and 58.27 ± 0.25, respectively).

Recently, Sethi et al. (Sethi et al., 2018) synthesized two series of benzimidazole based compounds from the coupling of coumarin and benzimidazole nuclei and narrated the anti-inflammatory activity of compounds **164–165** compared to the standard indomethacin (45 vs. 48%). Brishty et al. (Brishty et al., 2020) synthesized a group of substituted benzimidazole derivatives amongst which compounds **166, 167** and **168**

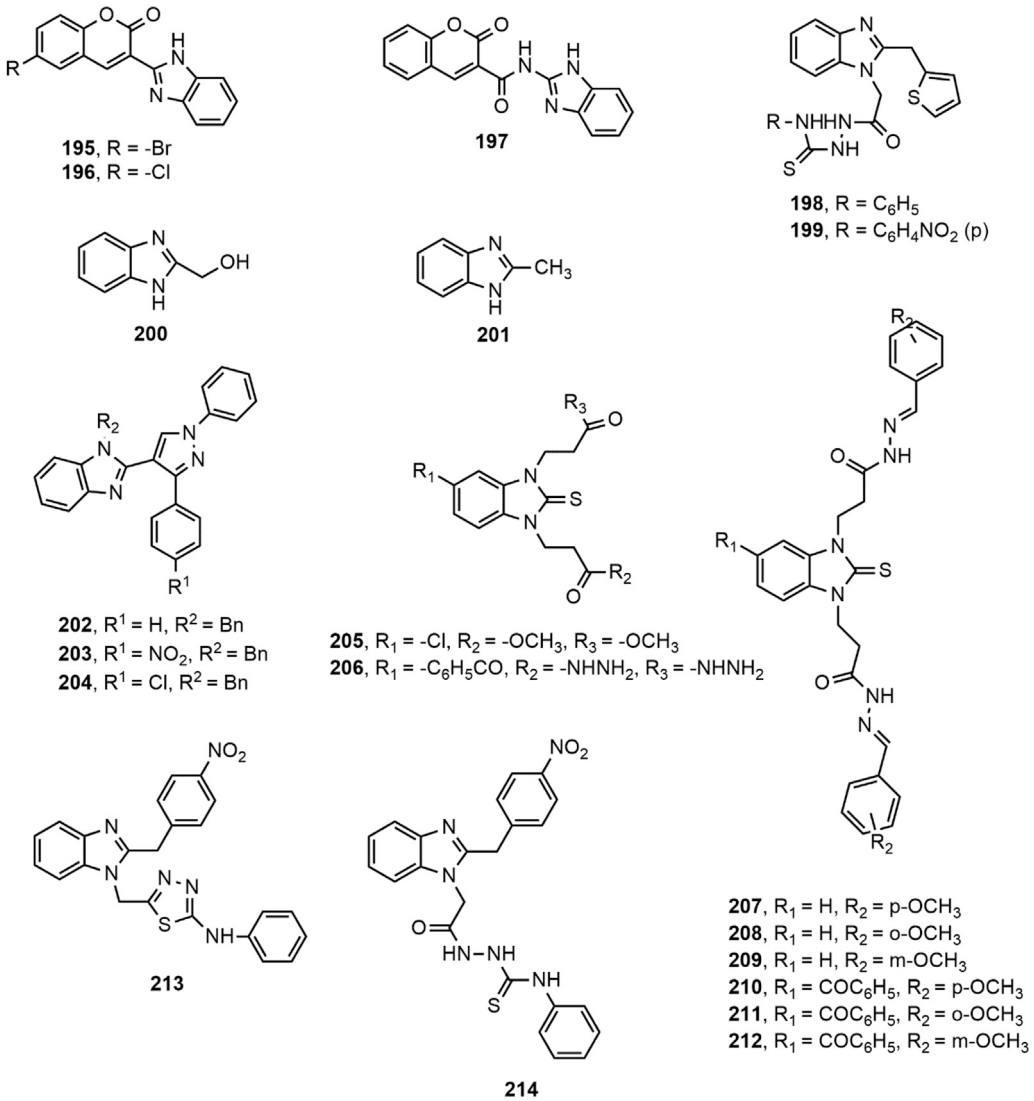

FIGURE 8 | Benzimidazole derivatives with antioxidant activity.

exhibited remarkable analgesic activity by inhibition of acetic acid induced writhing of mice compared to standard diclofenac (88.24, 84.03 and 85.71%, respectively, vs. 90.76%; $p < 0.001$). In continuation of the research by the group, Saha et al. (Saha et al., 2020) prepared a number of disubstituted benzimidazole derivatives. Compounds **169, 170** and **171** displayed notable analgesic property at a dose of 25 mg/kg by 88.81, 69.40 and 64.93% writhing inhibition, respectively ($p < 0.05$) in comparison with standard aceclofenac (88.81%). Very recently, the group reported the pharmacological investigation of some of their previously synthesized benzimidazoles (Saha et al., 2021). Compounds **170, 172** and **173** exhibited promising central analgesic potential in radiant heat tail flick method compared to standard morphine (% of elongation 58.07, 51.59, and 76.65, respectively vs. 87.17). Besides, **171, 172** and **173** displayed notable reduction in paw edema (81.75, 79.09 and 86.69%, respectively) comparable to standard aceclofenac (87.83) (Saha et al., 2021).

Antiulcer Activity

Many benzimidazole derivatives are known to possess potent antiulcer activity and H^+/K^+-ATPase inhibitory properties. During recent times, several new synthetic benzimidazole-based compounds were developed which exhibited similar or better antiulcerogenic potentials compared to the established market preparations. The benzimidazole derivatives with antiulcer activity are shown in **Figure 7**.

A series of pyrimidylthiomethyl benzimidazoles (e.g. **174**) and pyrimidylsulfinylmethyl benzimidazole derivatives (e.g. **175)** were developed and screened for antiulcer activity. Compounds **174–175** significantly reduced gastric acid secretion, free acidity and gastric ulcers in the pylorus-ligated

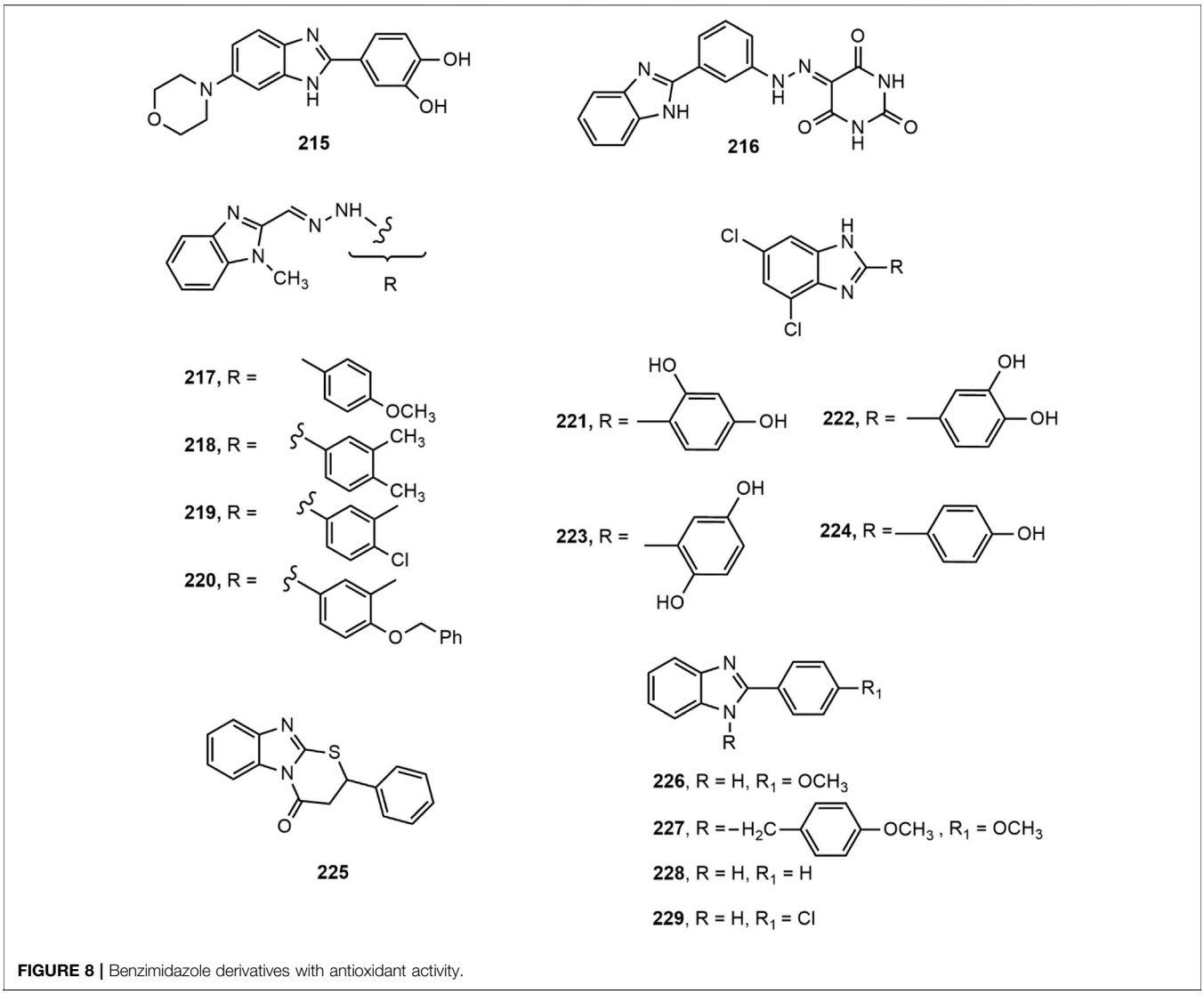

FIGURE 8 | Benzimidazole derivatives with antioxidant activity.

rats at 10 and 30 mg/kg doses, where the sulfinyl derivative (**175**) was found to be more effective than thio derivative (**174**) (Bariwal et al., 2008). In another study, compounds **176–177** exhibited most prominent antiulcer activity against pylorus ligation-induced, aspirin induced, and ethanol induced ulcer in rat model at a dose level of 10 and 20 mg/kg compared to omeprazole (Patil et al., 2010). Besides, Reddy et al. (Reddy et al., 2011) prepared a series of 2-substituted mercaptobenzimidazole derivatives and reported that compounds **178–180** produced notable antiulcer potentiality at a dose level of 10 mg/kg comparable to omeprazole. Furthermore, compound **181** prevented H^+/K^+-ATPase enzymatic activity with an IC_{50} value of 1.6×10^{-5} M and compound **182** displayed prominent effects on inhibition of gastric lesions and gastric acid secretion in a dose dependant manner (0.3–30 mg/kg) (Tanaka et al., 2011; Yan et al., 2011).

Moreover, some benzimidazole-piperazine conjugated analogues were assessed for their *in vivo* antiulcer property. The 4-methoxy phenyl piperazine substituted benzimidazole derivative **(183)** appeared to be the most effective agent (Patil et al., 2012). Chang et al. (Chang et al., 2012) developed a series of 3,4,5-trimethoxybenzylbenzimidazole derivatives among which compound **184** (2-fluorophenyl-5-methyl-1-(3,4,5-trimethoxybenzyl) benzimidazole) emerged as the most potent inhibitor of *Helicobacter pylori* growth and pathogenesis of host cells. The compound specifically inhibited *H. pylori* adhesion and invasion of gastric epithelial cells, as revealed by *in vitro H. pylori* infection model. Mathew et al. (Mathew et al., 2013) synthesized a series of substituted benzimidazole derivatives (**185–187**) and reported that derivatives **185–187** exerted remarkable protection of ulcer (69.58, 69.56 and 67.17%, respectively) at a dose of 50 mg/kg b.w compared to omeprazole (77.37%, 2 mg/kg b.w.). Amongst a series of substituted methoxybenzyl-sulfonyl-1*H*-benzo[d]imidazole derivatives, compounds **188–193** appeared to be the most potent H^+/K^+-ATPase inhibitors compared to omeprazole

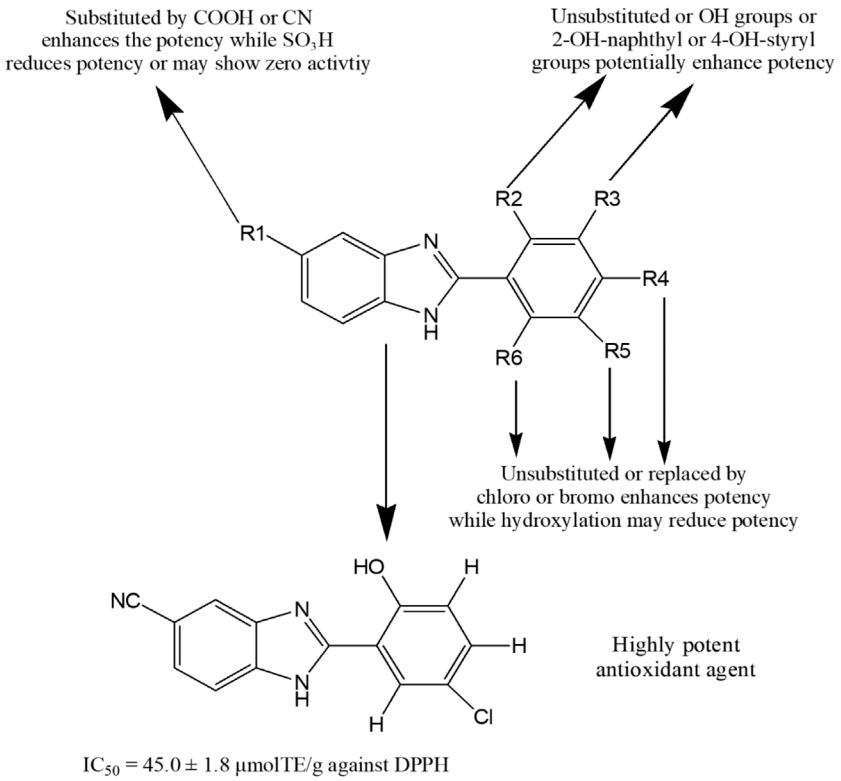

FIGURE 9 | Structure activity relationship (SAR) of benzimidazole derivatives having antioxidant potentiality. The figure represents the SAR studies accomplished by Baldisserotto et al. (2020).

(Rajesh et al., 2017). Finally, some new benzimidazole-pyrazole hybrids were evaluated for *in vivo* anti ulcerogenic activity using ethanol-induced gastric ulcer model in Albino rats. Compound **194** was found to be the most potent among the series with 83.1% ulcer inhibition at a dose level of 500 μg/kg (Noor et al., 2017).

Antioxidant Activity

Several benzimidazole derivatives have been explored through years for their capacity to act as antioxidants. Different benzimidazole derivatives with antioxidant activity are shown in **Figure 8**.

Two series of benzimidazole compounds made through coupling of coumarin derivatives with benzimidazole nucleus either directly or through amide linkage at 2-position were evaluated for antioxidant property (Arora et al., 2014). Compounds **195–197** demonstrated excellent antioxidant activity (IC_{50} values 19.7, 13.9 and 1.2 μmol/L, respectively) compared to standard butylated hydroxytoluene (BHT, IC_{50} = 23.4 μmol/L). Among the different benzimidazole derivatives with heterocyclic moieties developed by Mentese et al. (Menteşe et al., 2015), compound **198–199** with a thiophene ring exhibited remarkable antioxidant activity. Poddar et al. synthesized and evaluated the antioxidant property of substituted benzimidazoles by 1,1-diphenyl-2-picrylhydrazyl (DPPH) free radical scavenging method (Poddar et al., 2016). Compound **200** and **201** exhibited mild to moderate antioxidant potential (IC_{50} = 400.42 and 144.84 μg/ml, respectively) in comparison with standard BHT (IC_{50} = 51.56 μg/ml).

Among a library of *N*-substituted pyrazole-containing benzimidazoles, compounds **202–204** attributed prominent antioxidant activity in both DPPH and hydrogen peroxide assay supposed to the presence of benzyl substituent on imidazole nitrogen (Bellam et al., 2017). Besides, Anastassova et al. (Anastassova et al., 2018a) evaluated antioxidant property of compounds **205–206** using tert-butyl hydroperoxide (*tert*-BOOH) induced oxidative stress on rat hepatocytes, and reported that both compounds showed significant effect comparable to standard quercetin. Similarly, compounds **207–212** displayed notable cytoprotective effect on rat hepatocytes (Anastassova et al., 2018b).

Moreover, a library of 2-(4-nitrobenzyl)-1*H*-benzimidazole derivatives showed good antioxidant property where compounds **213** and **214** demonstrated prominent inhibitory effect against xanthine oxidase (IC_{50} = 12.30 ± 0.33 μg/ml) and urease (IC_{50} = 13.04 ± 0.89 μg/ml), respectively (Karaali et al., 2018). Furthermore, compound **215** had the most potency in the series of 2-(aryl)-6-morpholin-4-yl(or 4-methylpiperazin-1-yl)-1*H*-benzimidazoles (Özil et al., 2018).

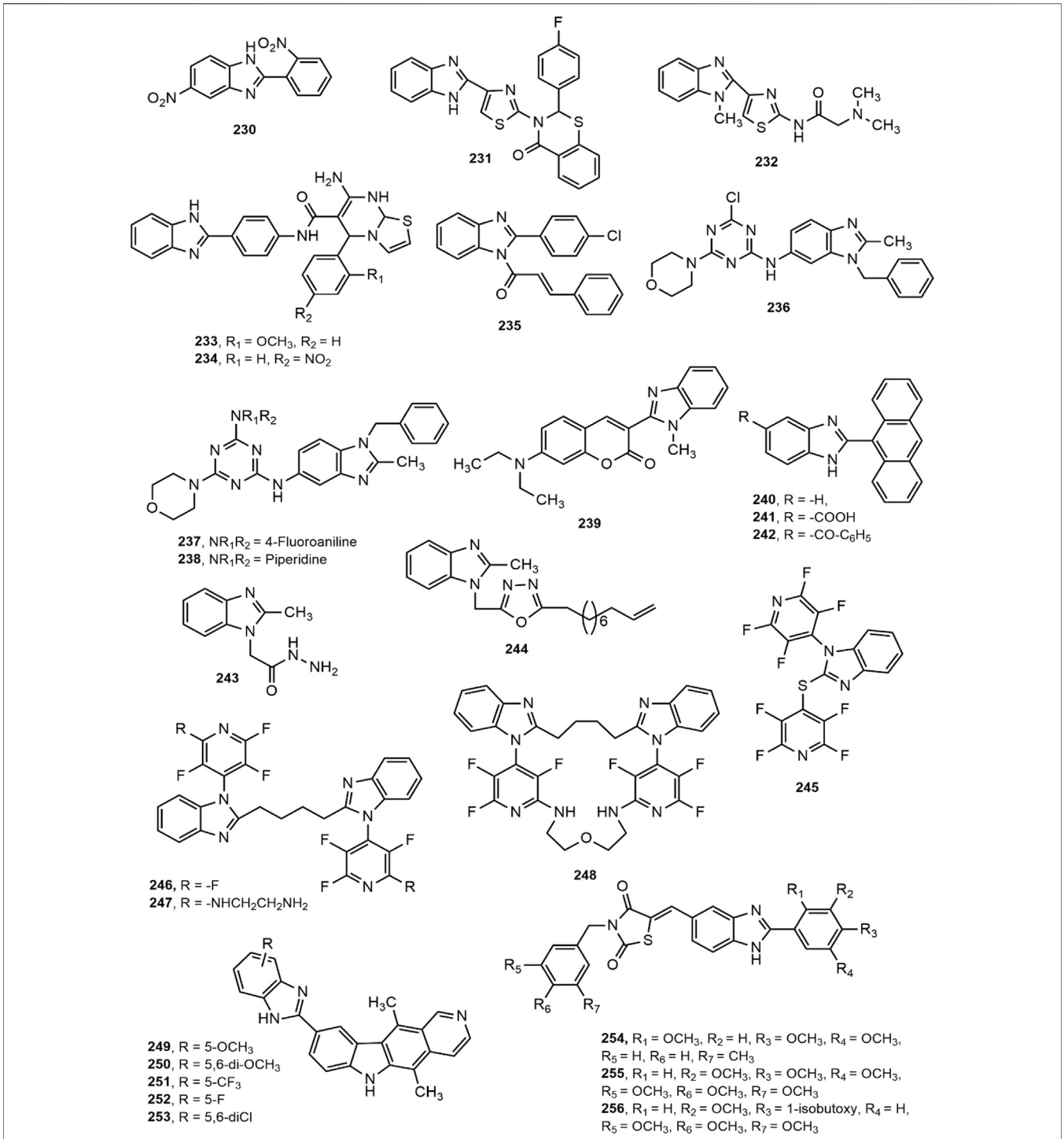

FIGURE 10 | Benzimidazole derivatives with anticancer activity.

Recently, Baldisserotto et al. (Baldisserotto et al., 2020) synthesized total 39 arylbenzimidazole derivatives and reported their remarkable potency against various free radicals. **Figure 9** represents a general structure for describing SAR of benzimidazoles possessing antioxidant activity. The addition of cyano or carboxyl group at 5-position (R_1) of the benzimidazole nucleus was responsible for exhibiting medium to high potency against several free radicals. In contrast, the derivatives containing the 5-sulfonic acid group showed poor or no antioxidant properties. Unsubstituted 2-aromatic ring or OH,

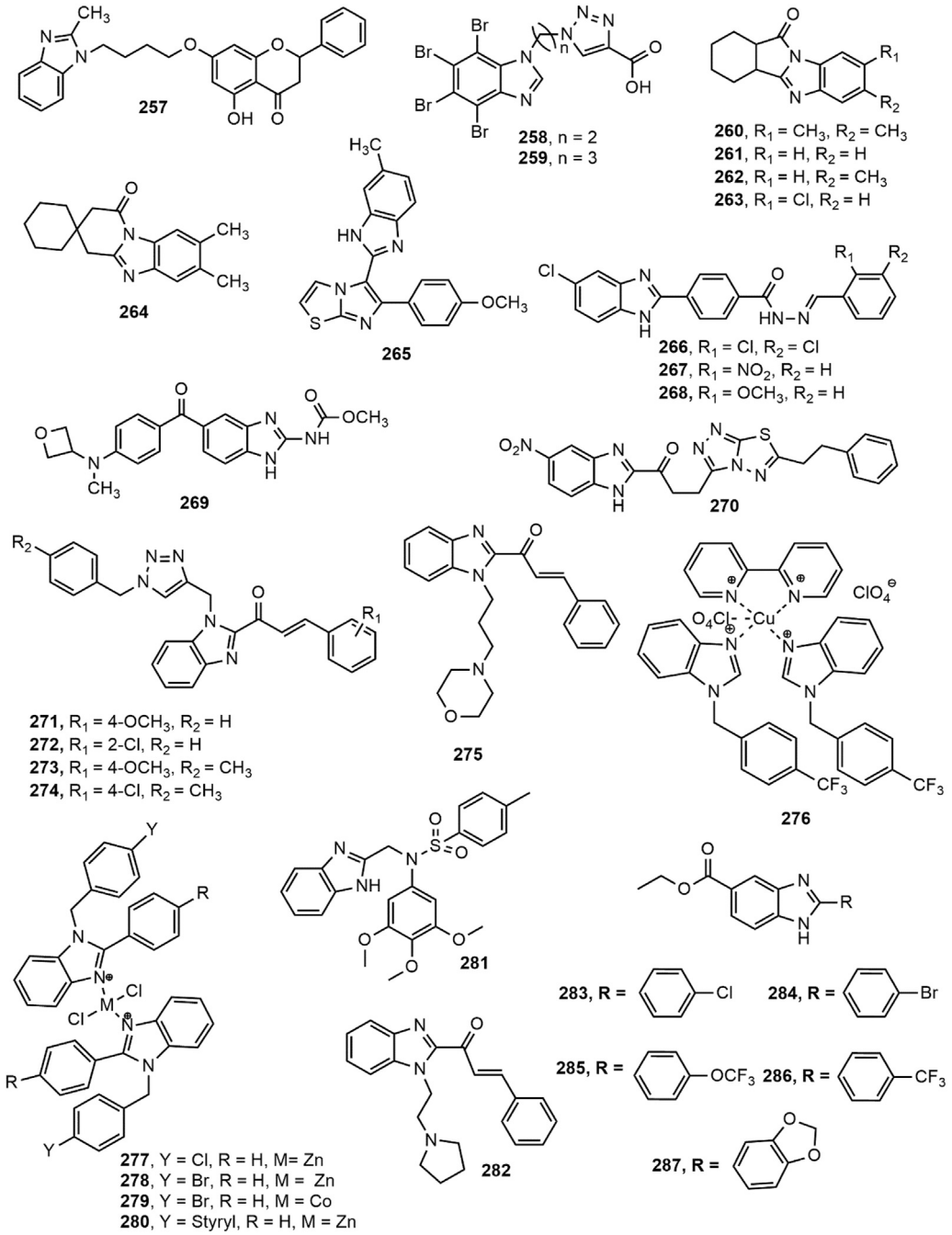

FIGURE 10 | Benzimidazole derivatives with anticancer activity.

Cl, Br, 2-OH-napthyl or 4-OH-steryl substitutions enhanced activity. In another study, compound **216** showed 40–80% antioxidant potential at different concentrations (10–100 μM) (Abdelgawad et al., 2019). Amine Khodja et al. reported that compounds **217–220** exerted promising inhibition capacity against various free radicals compared to BHT (IC_{50} (mean ± SD, μM) for DPPH assay: 40.4 ± 0.9 to 60.4 ± 1.9 vs. 70.8 ± 6.6) (Amine Khodja et al., 2020). Taha et al. (Taha et al., 2020) synthesized 20 benzimidazole derivates and found four potent antioxidant compounds **221–224** with IC_{50} values (mean ± SEM: 22.42 ± 0.26 to 40.60 ± 0.80) comparable to standard propyl gallate (29.20 ± 1.25). Interestingly, compound **225** exhibited more inhibition (%) of DPPH-free radical than the standard antioxidant Trolox (73% ± 2.42 vs. 70% ± 0.35) (Ramos Rodríguez et al., 2020). Furthermore, compounds **166, 168, 226** and **227** displayed prominent antioxidant property with lower

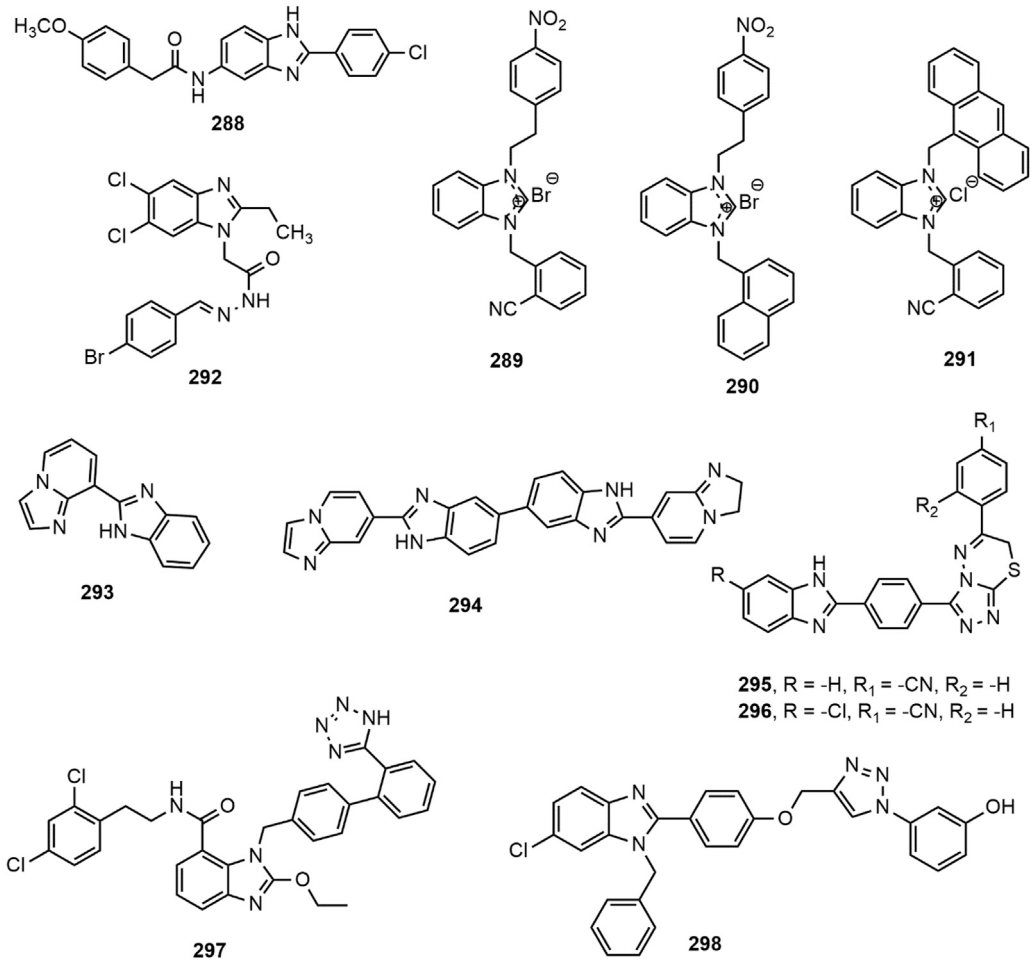

FIGURE 10 | Benzimidazole derivatives with anticancer activity.

IC_{50} values than the standard BHT (8.834, 7.519, 0.038 and 0.959 μg/ml, respectively vs. 14.44 μg/ml) (Brishty et al., 2020). Finally, compounds **228** and **229** demonstrated mild antioxidant potential in comparison with standard ascorbic acid (IC_{50} = 12.25 × 10^3 and 87.326 × 10^3 μg/ml, respectively vs. 2.19 μg/ml) (Saha et al., 2021).

Anticancer Activity

Among the anticancer drugs discovered in the recent years, different benzimidazole derivatives occupy an important place. The current review accounts the anticancer activity of benzimidazoles reported after 2013. The benzimidazole derivatives with anticancer activity are shown in **Figure 10**.

A series of substituted benzimidazole derivatives were evaluated for *in vitro* anticancer activity in human lung adenocarcinoma A549 cell line at normoxic and hypoxic conditions. Compound **230** was found to be the most cytotoxic agent with hypoxia/normoxia cytotoxic coefficient of 4.75, compared to standard tirapazamine (5.59) (Błaszczak-Świątkiewicz et al., 2014). The benzimidazole-thiazole derivatives **231–232** showed notable anticancer effect against human liver carcinoma cell line (HepG2: IC_{50} = 0.518 and 0.578 mM) and pheochromocytoma of the rat adrenal medulla cell line (PC12: IC_{50} = 0.309 and 0.298 mM) (Nofal et al., 2014). Compounds **233–234** with dual inhibition of Aurora A kinase and kinesin spindle protein were found to be the most prominent antitumor agents against various tested cell lines in comparison with standard drug CK0106023 (Abd El-All et al., 2015). Kalalbandi and Seetharamappa synthesized a series of 1-[(2*E*)-3-phenylprop-2-enoyl]-1*H*-benzimidazole derivatives among which compound **235** displayed notable antiproliferative activity against nine tumor subpanels, indicated by its selectivity ratios within the range of 0.79–1.53 and 0.47 to 1.69 at the GI_{50} (growth inhibitory 50%) and TGI level, respectively (Kalalbandi and Seetharamappa, 2015). Similarly, compounds **236–238** with GI_{50} values of 9.79, 2.58 and 3.81 μM, respectively exhibited broad spectrum antitumor activities, while the compound **236** was found to be the most potent DHFR inhibitor with IC_{50} value of 1.05 μM (Singla et al., 2015).

Among the derivatives identified by Liu et al. (Liu et al., 2015), compound **239** showed notable inhibition of PI3K-AKT-mTOR pathway having GI_{50} values in the range of 0.07–0.41 μmol/L

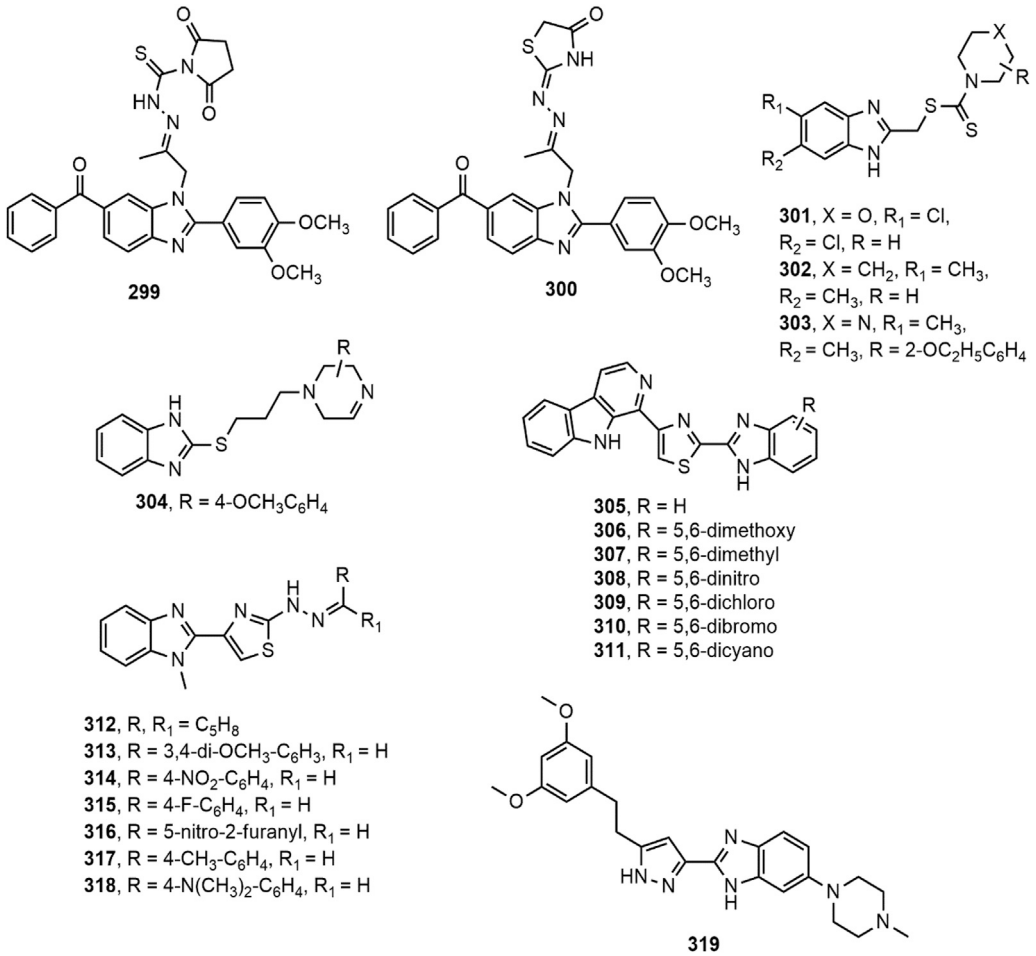

FIGURE 10 | Benzimidazole derivatives with anticancer activity.

against most of the tested cancer cell lines, signifying its potential to be used as anticancer agent. Sontakke and co-workers (Sontakke et al., 2015) synthesized 2-anthryl benzimidazole derivatives (**240–242**) bearing hydrogen, benzoyl and carboxyl substituents, respectively at 5th position. Compounds **241** and **242** showed anticancer potency against MCF-7 cell lines (IC_{50}: 16.18 and 19.21 μM, respectively) and HL-60 cell lines (IC_{50}: 15.15 and 18.29 μM, respectively) followed by compound **240** (MCF-7 IC_{50} = 20.48 μM and HL-60 IC_{50} = 23.23 μM). In another study, compound **243** displayed most notable activity against HeLa cell lines (IC_{50} = 05.34 ± 1.2 μM) compared to standards doxorubicin and 5-flurouracil (IC_{50} = 03.56 ± 2.7 and 02.78 ± 2.6 μM, respectively). On the other hand, compound **244** showed marked activity against Hep3B cell line with an IC_{50} value of 11.10 ± 1.1 μM (Varshney et al., 2015).

Bhambra et al. (Bhambra et al., 2016) synthesized a library of fluoroaryl benzimidazole derivatives (**245–248**) among which compounds **246–248** demonstrated inhibition against K-562 and MCF-7 cell lines in micromolar range. Compounds **246** and **248** were reported as activators of caspases, which play important role in apoptosis of cancerous cells. Bramhananda Reddy et al. designed and synthesized a library of benzimidazole fused ellipticine derivatives (**249–253**) and delineated antiproliferative potential against human cancer cell lines Zr-75–1, HeLa, MCF-7 and A-549 with GI_{50} values of <0.1–34.6 μM, compared to standard etopoxide (GI_{50} = 0.2–3.08 μM) (Bramhananda Reddy et al., 2016). Sharma et al. (Sharma P. et al., 2017) designed and synthesized a series of benzimidazole bearing thiazolidinedione derivatives, and proved remarkable cytotoxicity of these compounds (**254–256)** towards PC-3, HeLa, A549 and HT1080 cancer cell lines with IC_{50} values of 0.096–0.63 μM. In a different study, Compound **257** exhibited potent antiproliferative effect against MFC cells IC_{50} (mean ± SD) value of 25.72 ± 3.95 μM (Wang et al., 2017). Triazole containing 4,5,6,7-tetrabromo-1*H*-benzimidazole derivatives **258–259** bearing carboxyl substituent manifested the most prominent inhibitory effect against protein kinase 2 (CK2) with binding affinity value in the range of 1.96–0.91 μM (Chojnacki et al., 2017). Compounds **260–264** exerted antiproliferative property in MTT assay against five human cancer cell lines, breast (T47D), lung (NCl H-522), liver (HepG2), colon (HCT-15) and ovary (PA-1) with IC_{50} (mean ± SD) value of 7.5 ± 0.3 to 14.6 ± 0.4 μM

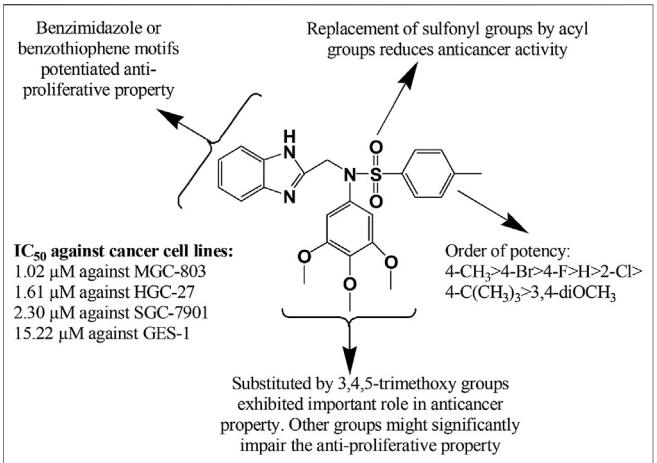

FIGURE 11 | Structure activity relationship (SAR) of benzimidazole derivatives having anticancer potentiality. The figure represents the SAR studies accomplished by Song, J. et al. (2019).

(Kumar et al., 2018). Upon assessment of antiproliferative property against four cancer cell lines (HeLa, MCF-7, A549 and DU-145 alongside normal HEK-293 cell line), Baig et al. (Baig et al., 2018) enumerated noteworthy IC_{50} (1.08 μM) of derivative **265** against A549 cell line. Compounds **266–268** displayed prominent cytotoxic activity against A549 and MCF-7 cancer cell lines in comparison with standard drug cisplatin with IC_{50} values of 0.03–0.06 μM. The presence of 2,4-dichlorobenzylidene (**266**), 2-nitrobenzylidene (**267**) and 2-methoxybenzylidene moiety (**268**) contributed for notable cytotoxic activity of these compounds (Acar Çevik et al., 2018). The oxetanyl substituted compound **269** exhibited cytotoxicity towards a wide range of cancer cell types, e. g. lung, prostate and ovarian cancers with prominent activity against highly aggressive cancer lines (IC_{50} = 0.9–3.8 μM) (Cheong et al., 2018). Besides, Ibrahim et al. synthesized 2-substituted-5-nitro-benzimidazole derivative **270** as dual inhibitors of c-Met and VEGFR-2 kinases which is important therapeutic target in the treatment of lung (IC_{50} 2.19 ± 0.09 against A549) and colorectal (IC_{50} 10.97 ± 0.09 μM against HCT116) cancers (Ibrahim et al., 2018).

Recently, Djemoui et al. (Djemoui et al., 2020) synthesized several triazole-benzimidazole-chalcone hybrid compounds **271–274** and narrated potential anti-proliferative property of these derivatives against two breast cancer (T47-D and MDA-MB-231) and one prostate cancer cell line (PC3) compared to standard Doxorubicin. It is mentionable here that the chloro substituent **274** at the chalcone ring proliferated the anticancer effects. In a distinct research, a total of 24 new molecules containing benzimidazole group, arene, and alkyl chain-bearing cyclic moieties were synthesized, where the compound **275** impeded the growth of MCF-7 and human ovarian carcinoma (OVCAR-3) cell lines manifesting superior effects to standard cisplatin (IC_{50} (mean ± SD, μM): 8.91 ± 0.07 vs. 11.7 ± 0.12 and 10.76 ± 0.12 vs. 16.04 ± 0.74, respectively) (Hsieh et al., 2019). A copper (II) complex (**276**) of benzimidazole derivatives showed excellent potency at 72 h post treatment against prostate cancer cell line (DU145) with IC_{50} 10 μM (Kacar et al., 2020). Besides, two zinc (II) complexes with 2-[2-(benzimidazol-2-yl)-phenyl]-1-methyl-benzimidazole and 1,2-bis(1-methyl-benzimidazol-2-yl)-benzene exerted both dose and time dependent cytotoxicity against breast cancer cell lines (MB-MDA-231) (Su et al., 2019). In another study (Yılmaz et al., 2019), 18 complexes of zinc (II) and cobalt (II) containing 1-benzyl and 2-phenyl moieties showed *in vitro* potency against human prostate (DU-145) and human ovarian (A-2780) cancer cell lines. Notably, compounds **277–280** at a concentration of 0.1 μM exhibited superior activity against A-2780 cell line in comparison with standard docetaxel. Jian-Song et al. (Jian-Song et al., 2019) synthesized a spectrum of unconventional BZD derivatives and reported their *in vitro* anticancer property, particularly against three genre of cell lines (MGC-803, PC-3, MCF-7). Notably, compound **281** inhibited predominately of all the three cancer cell lines compared to 5 Fluorouracil (IC_{50} (mean ± SD, μM): 1.02 ± 0.03 vs. 6.82 ± 1.17, 3.34 ± 0.09 vs. 18.42 ± 1.73, and 5.40 ± 0.51 vs. 17.11 ± 2.94, respectively). The structural modifications of the compound **281** might significantly influence its anti-proliferative property that has been illustrated in **Figure 11**. In another study (Suk et al., 2019), a benzimidazole derivative carrying a pyrrolidine side chain (**282**) significantly suppressed sorafenib-resistant cell lines growth in xenograft model by inhibiting the phosphorylation of AKT, p70S6 and the downstream molecule RPS6, has unlocked another milestone in the treatment of hepatocellular carcinoma. Yeong et al. (Yeong et al., 2019) synthesized several new benzimidazole derivatives **283–287** and screened them against sirtuin cancer lines (SIRT1, SIRT2, and SIRT3). Among them, compound **284** elicited significant inhibition of SIRT1-3 compared to tenovin-6 (IC_{50} (mean ± SD, μM): 7.7 ± 1.4 vs. 42.10, 5.6 ± 1.3 vs. 25.6, and 9.8 ± 2.0 vs. 82.65). Moreover, among 37 synthesized molecules, compound **288** exerted the most inhibition of angiogenesis (79%), and HUVEC and HepG2 cell lines (IC_{50}: 1.47 and 2.57 mM, respectively), and VEGFR-2 kinase inhibition (Yuan et al., 2019).

Akkoc et al. (Akkoç et al., 2020) synthesized three benzimidazole derivatives **289–291** and reported the most promising anti-breast cancer feature of compound **291** compared to standard cisplatin (IC_{50} (mean ± SD, μM): 1.26 ± 0.85 vs. 5.77 ± 0.40). In another study, Atmaca et al. (Atmaca et al., 2020) disclosed significant cytotoxicity of compound **292** against breast cancer (MCF-7), prostate cancer (DU-145), and lung cancer (H69AR) with IC50 values of 17.8 ± 0.24, 10.2 ± 1.4 and 49.9 ± 0.22 μg/ml, respectively, compared to 5-Fluorouracil. Compounds **293–294** showed stronger anticancer property against HepG2 (IC_{50}: 26.62 and 20.29, respectively) and DLD-1 cells (IC_{50}: 21.29 and 19.23 μM, respectively) than cisplatin (IC_{50}: 30.38 and 60.79 μM) (Caymaz et al., 2020). Particularly, compound **295–296** demonstrated potent anti-breast cancer effect by obstructing MCF-7 cell growth compared to standard cisplatin (IC_{50}: 0.016 ± 0.001 and 0.018 ± 0.001 vs. 0.020 ± 0.009 μM). Besides, compound **295** displayed efficiency for impeding estrogen-dependent breast cancer by inhibiting aromatase enzyme with IC_{50} 0.032 ± 0.042 μM, compared to IC_{50}

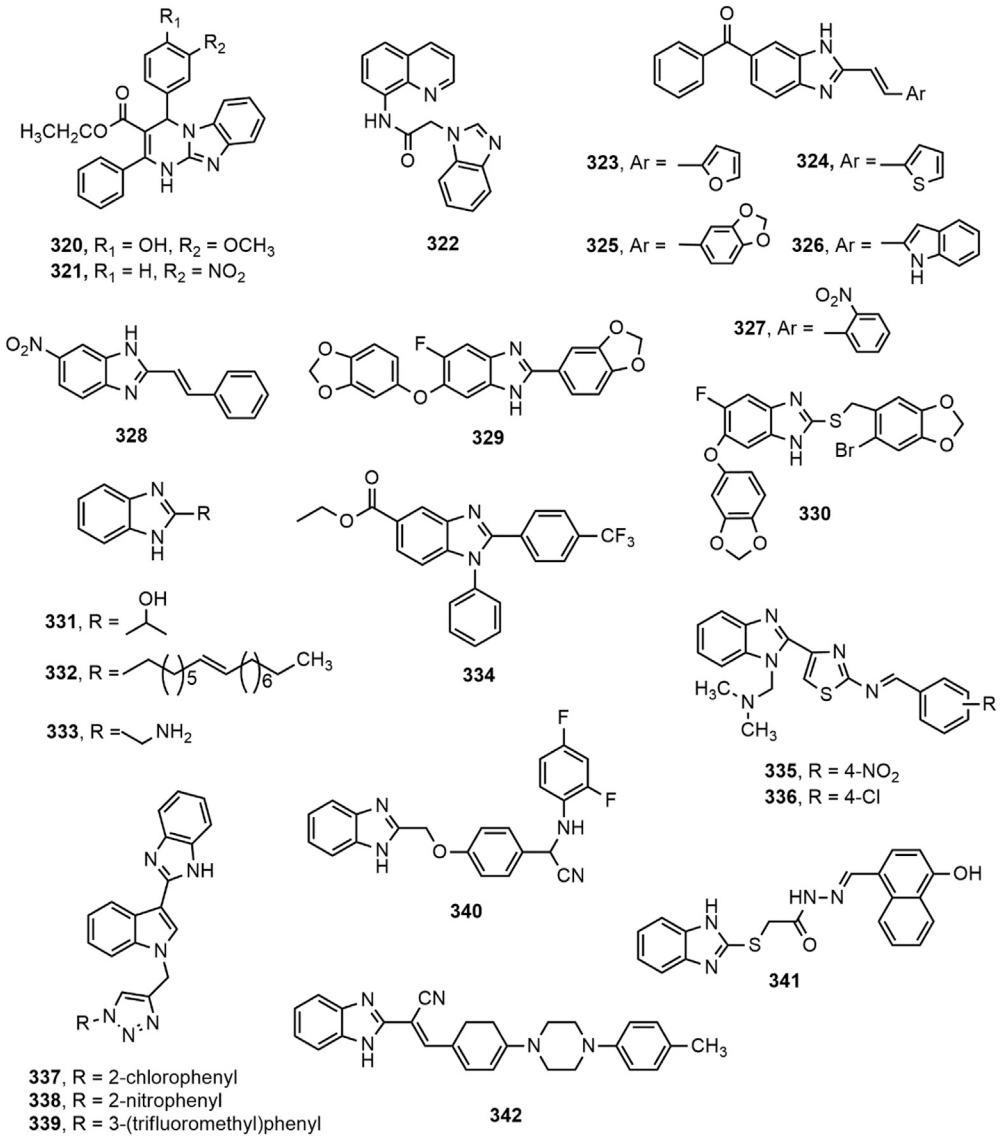

FIGURE 12 | Benzimidazole derivatives with antitubercular activity.

0.024 ± 0.001 μM for letrozole (Acar Çevik et al., 2020). Furthermore, compound **297** blocked neddylation process with superior anticancer property compared to candesartan cilexetil (IC_{50} 5.51 vs 16.43 mM) (Chen et al., 2021). Notably, compound **298** displayed excellent effect in the treatment of lung cancer by inhibiting A-549 and NCI-H460 cell lines growth with IC_{50} level of 0.63 ± 0.21 μM and 0.99 ± 0.01 μM, respectively, compared to 5-Fluorouracil (IC_{50} (μM): 1.69 ± 0.90 and 3.20 ± 0.50, respectively). Apart from, the compound **298** significantly suppressed the breast cancer cell lines MCF-7 and MDA-MB-23 with IC_{50} (μM) values, comparable to 5-Fluorouracil (1.3 ± 0.18 vs. 2.80 ± 0.12, and 0.94 ± 0.02 vs. 0.79 ± 0.09, respectively) (Sridhar Goud et al., 2020).

Meguid et al. (El-Meguid et al., 2020) synthesized an array of novel 6-benzoyl benzimidazole derivatives where most of the compounds exhibited promising anticancer activity with safety profile. Remarkably, compounds **299–300** exhibited superior inhibition of EGFR, HER2, PDGFR-β and VEGFR2, in comparison to erlotinib that opened several promising fighting tools against cervical cancer. In a distinct study, compounds **301–304** strongly prevented breast cancer cell lines manifesting IC_{50} values of 5.70 9.55, 5.58 and 6.84 μg/ml, respectively compared to standard doxurubucin (IC_{50} at 4.17 μg/ml) (Nashaat et al., 2020). Furthermore, Sireesha et al. (Sireesha et al., 2021) synthesized a library of hybrid *β*-carbolines **305–311** that were found to be effective against various cancer cell lines where compounds **306–307** exerted higher *in vitro*

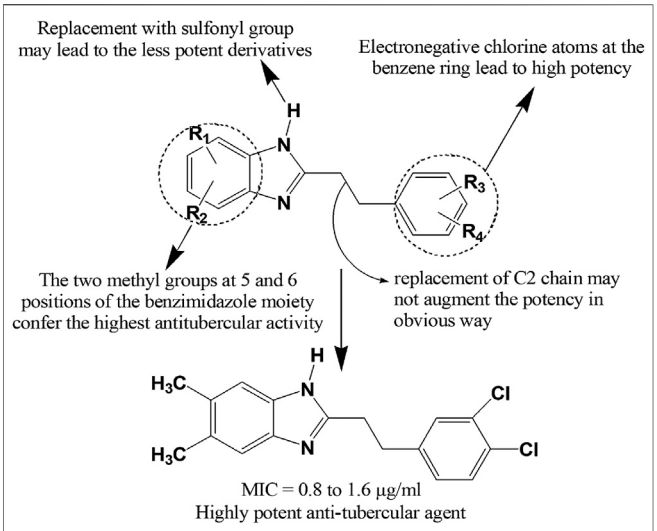

FIGURE 13 | Structure activity relationship (SAR) of benzimidazole derivatives having anti-tubercular effects. The figure represents the SAR studies accomplished by Gobis et al. (2015).

efficacy than the reference etoposide to prevent breast (IC_{50} against MCF-7: 0.092 ± 0.001 and 0.81 ± 0.062, vs. 2.11 ± 0.024), lung (IC_{50} against A549: 0.72 ± 0.042 and 1.90 ± 0.88, vs. 3.08 ± 0.135), colon (IC_{50} against Colo-205: 0.34 ± 0.071 and 0.41 ± 0.12, vs. 0.13 ± 0.017), and ovarian (IC_{50} against A2780: 1.23 ± 0.55 and 1.80 ± 0.59, vs. 1.31 ± 0.27) cancers. Similarly, Srour et al. (Srour et al., 2020) synthesized a series of benzimidazole derivatives **312–318** and reported promising anticancer potential of **312–316** against breast cancer (IC_{50} against MCF-7: 5.96–11.91 μM, vs. IC_{50} of erlotinib; 4.15 μM). Besides, compounds **312, 314, 316, 317** and **318** showed significant cytotoxicity against epidermal growth factor receptor tyrosine kinase with IC_{50} values of 71.67–152.59 nM compared to IC_{50} of standard erlotinib 152.59 nM. Finally, Yamani et al. (Yamani et al., 2021) applied scaffolds hybridization technique to formulate a total of 24 pyrazole-benzimidazole derivatives for blocking fibroblast growth factor receptors (FGFRs). Amongst the derivatives, compound **319** selectively inhibited FGFR (1–4) with IC_{50} values of 0.75, 0.50, 3.05, and 87.90 nM, respectively. Due to acceptable safety and pharmacokinetic profiles along with *in vivo* anti-tumor potency,

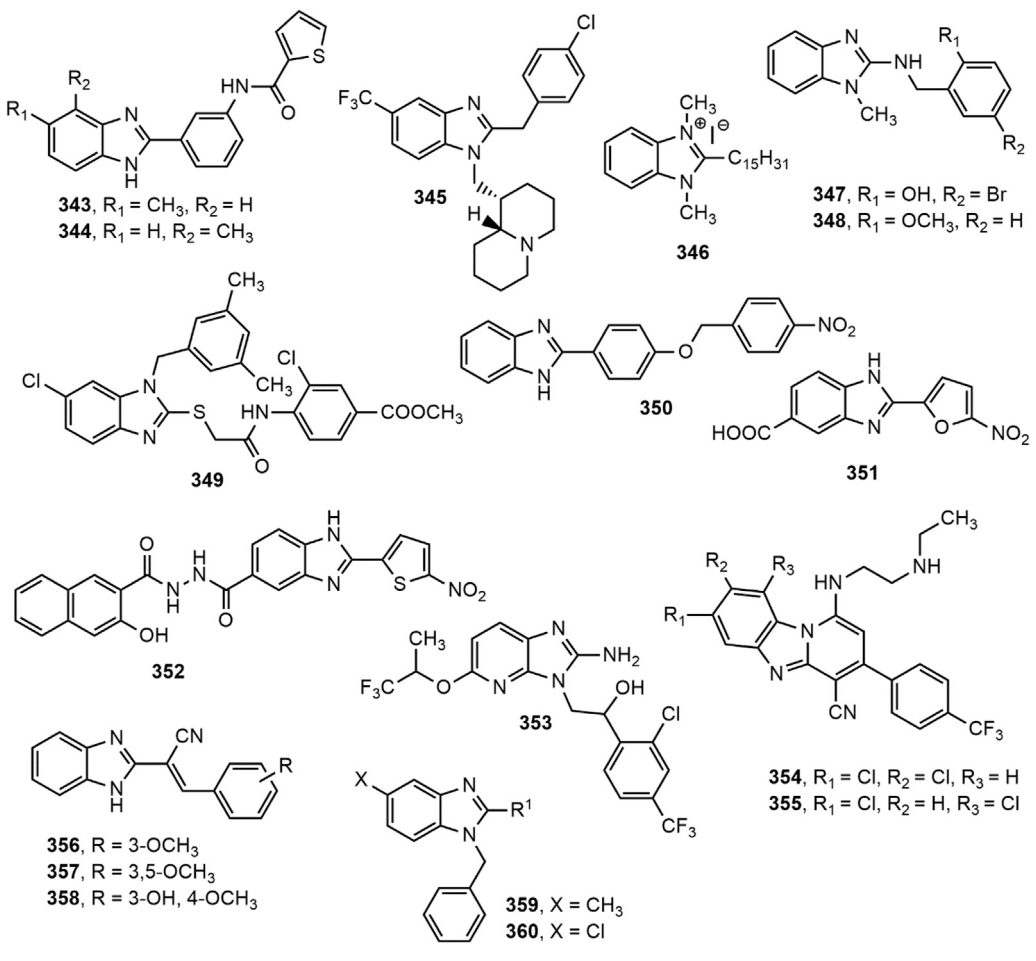

FIGURE 14 | Benzimidazole derivatives with antiprotozoal activity.

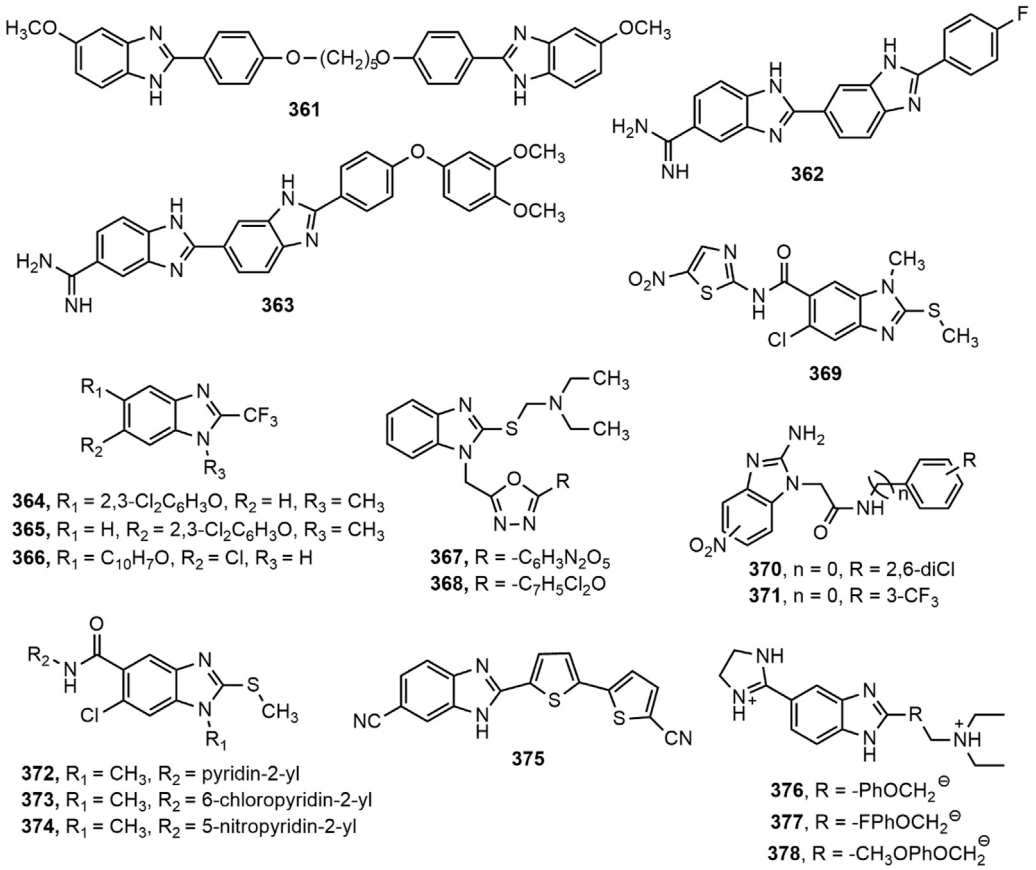

FIGURE 14 | Benzimidazole derivatives with antiprotozoal activity.

the compound **319** is now undergoing with an open-label, multicenter, dose-escalation phase I clinical trial for assessing the safety and tolerability against the adults patients with bladder, gastric, and squamous cell lung cancers (NCT04149691) (Yamani et al., 2021).

Antitubercular Activity

Compounds containing heterocyclic moieties, such as pyrrole, imidazole and benzimidazole have been reported to demonstrate excellent antitubercular properties (Wang et al., 2015). Benzimidazole scaffold has been on target of the scientists for producing novel antitubercular agents. Different benzimidazole derivatives with antitubercular property are shown in **Figure 12**.

Warekar et al. (Warekar et al., 2016) synthesized a series of 4-(4-nitro-phenyl)-2-phenyl-1,4-dihydro-benzo[4,5]imidazo[1,2-a]pyrimidine-3-carboxylic acid ethyl ester derivatives and reported that compounds **320–321** appeared to be the most promising antitubercular agents among the series with minimum inhibitory concentration (MIC) value of 25 μg/ml against *Mycobacterium tuberculosis* H37Rv strain. Compound **322** also displayed good activity against same strain under aerobic conditions, as indicated by its IC_{90} and MIC values (77 μg/ml and >100 μM, respectively) (Mantu et al., 2016). In a different study (Anguru et al., 2017), compounds **323–328** exhibited good activity against *M. tuberculosis* H37Rv strain while compound **325** emerged as the most promising agent with MIC value of 16 μg/ml.

A number of substituted fluorobenzimidazole derivatives (**329–330**) were synthesized and evaluated for *in vitro* antimycobacterial property against pathogenic *M. tuberculosis* H37Rv strain (ATCC 27294) using MABA method. Compounds **329–330** exhibited notable antitubercular activity against H37Rv strain and their activity was contributed by the incorporation of methylenedioxyphenyl moiety at 2- and 6-position of benzimidazole ring (Nandha et al., 2017). Harika et al. (Harika et al., 2017) synthesized a series of 2-substituted benzimidazole derivatives (**331–333**) using condensation of *o*-phenylenediamine with different aliphatic, aromatic, fatty acids, and amino acids, and depicted remarkable antitubercular property against *M. tuberculosis* H37Rv strain compared to reference drugs pyrazinamide, streptomycin and ciprofloxacin. In addition, Yeong et al. (Yeong et al., 2017) designed two series of benzimidazole derivatives among which compound **334** having trifluoromethyl group displayed antimycobacterial effect against both *M. tuberculosis* H37Rv strain and the drug-resistant-tuberculosis strain. Compounds **335–336**, synthesized by Prasad and Sundararajan, exhibited

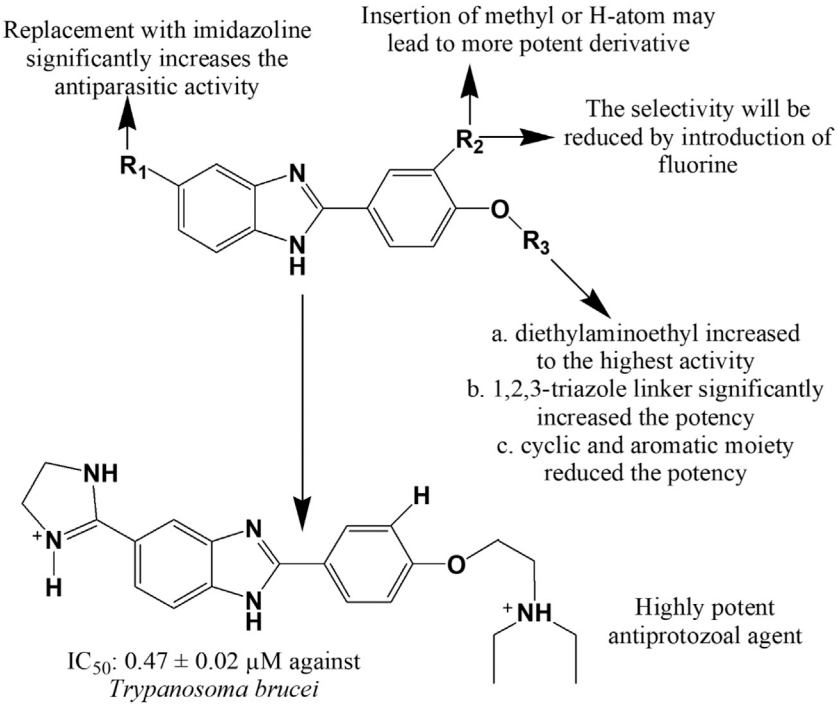

FIGURE 15 | Structure activity relationship (SAR) of benzimidazole derivatives effective against *Trypanosoma brucei*. The figure represents the SAR studies accomplished by Popov et al. (2020).

notable antitubercular activity against *M. tuberculosis* H37Rv strain with MIC value of 3.9 μg/ml compared to the standard isoniazid (Prasad and Sundararajan, 2017).

Recently, Ashok et al. (Ashok et al., 2018) synthesized a series of indole-benzimidazole-based 1,2,3-triazole hybrids (**337–339**) by conventional and microwave-assisted methods and evaluated for *in vitro* antitubercular activity against *M. tuberculosis* H37Rv strain. The derivatives **337–339** showed prominent antitubercular activity with MIC values in the range of 3.125–6.25 μg/ml. Compound **338** was the most potent among all (MIC = 3.125 μg/ml) which was likely due to the presence of nitro group at ortho position of phenyl ring. Compound **340** displayed notable activity (MIC = 0.05 μg/ml) and emerged as a promising antitubercular agent among the reported series (Shaikh et al., 2018). Compound **341** showing 67.56, 53.45, and 47.56% inhibition against mycobacterial enzymes isocitrate lyase, pantothenate synthetase and chorismate mutase, respectively appeared to be the most potent antitubercular agent among the series (Yadav et al., 2018). Very recently, compound **342** exerted excellent potency against *M. tuberculosis* H37Rv with IC_{50} value of 0.78 mg/ml compared to standard ethambutol (IC_{50} 1.56 mg/ml) (Sirim et al., 2020). Gobis et al. (Gobis et al., 2015) have prepared a series of compounds containing novel 2-(2-phenalkyl)-1*H*-benzo [d]imidazole where the compound bearing methyl groups at the benzimidazole system and phenethyl substituent at the C-2 position with electronegative chlorine atom at the phenyl ring exhibited prominent tuberculostatic property against *Mycobacterium tuberculosis* strains with MIC values ranging from 0.8 to 1.6 μg/ml (**Figure 13**).

Antiprotozoal Activity

The exploration of benzimidazole nucleus to discover new structural features required for the optimization of novel antiprotozoal agents is of utmost importance. Benzimidazole derivatives with antileishmanial, antimalarial, and antiprotozoal activities against different species are shown in **Figure 14**.

Benzimidazole Against *Leishmania* Species

Keurulainen et al. (Keurulainen et al., 2015) synthesized several 2-arylbenzimidazole derivatives and proclaimed extensive inhibitory property of compounds **343–344** against axenic amastigotes of *Leishmania donovani*. Tonelli and co-workers (Tonelli et al., 2018) reported *in vitro* antileishmanial activity of derivatives **345–346** with IC_{50} values of 3.70 and 0.19 μM, respectively against *L. tropica*, and 4.76 and 0.64 μM, respectively against *L. infantum*. In another research, a total of 28 *N*-benzyl-1*H*-benzimidazol-2-amine derivatives, where compounds **347–348** showed significant ($p < 0.05$) antileishmanial activity against the amastigote of *L. mexicana* and *L. braziliensis* with IC_{50} values of 2.62 and 3.21 μM, respectively, and their activity was 5.8 and 4.8 times better than standard miltefosine (IC_{50} = 15.34 μM) (Nieto-Meneses et al., 2018). Upon evaluation of *in vitro* antileishmanial activity against intracellular amastigotes of *L. infantum*, compound **349** displayed promising result with IC_{50} value of 6.8 μM. However, the compound possessed some degree of cytotoxicity with CC_{50} = 8.0 and 32.0 μM against primary peritoneal mouse macrophages PMM and human fetal lung fibroblasts MCR-5, respectively (De Luca et al., 2018).

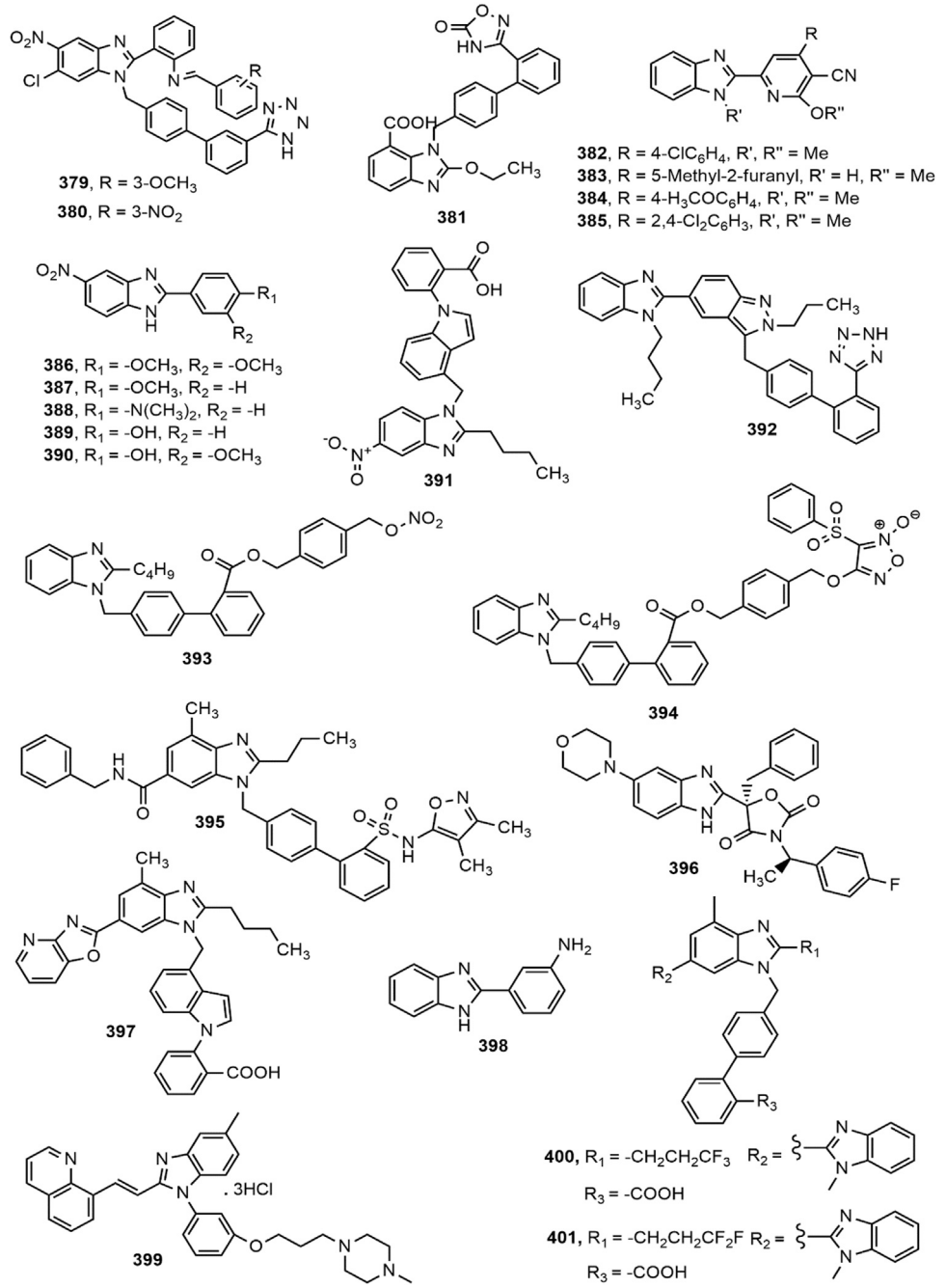

FIGURE 16 | Benzimidazole derivatives with antihypertensive activity.

Recently, compounds **350** exerted moderate antileishmanial effect by inhibiting *L. donovani* with IC_{50} value of 68 ± 2.8 μM compared to standard miltefosine (IC_{50} = 12 ± 0 μM) (Kapil et al., 2019).

Benzimidazole Against Malaria

Among the four *Plasmodium* species responsible for human malaria, *P. falciparum* has already started to show resistance to available antimalarial drugs, thus causing the urgency to develop drugs with novel drug targets and new mechanism of action (Singh et al., 2012). In search for compounds with comparable activity to chloroquine, Camacho et al. (Camacho et al., 2011) developed a series of benzimidazole-5-carbohydrazide derivatives and reported that the compounds **351–352** showed prominent *in vivo* antimalarial potential against rodent *P. berghei* and

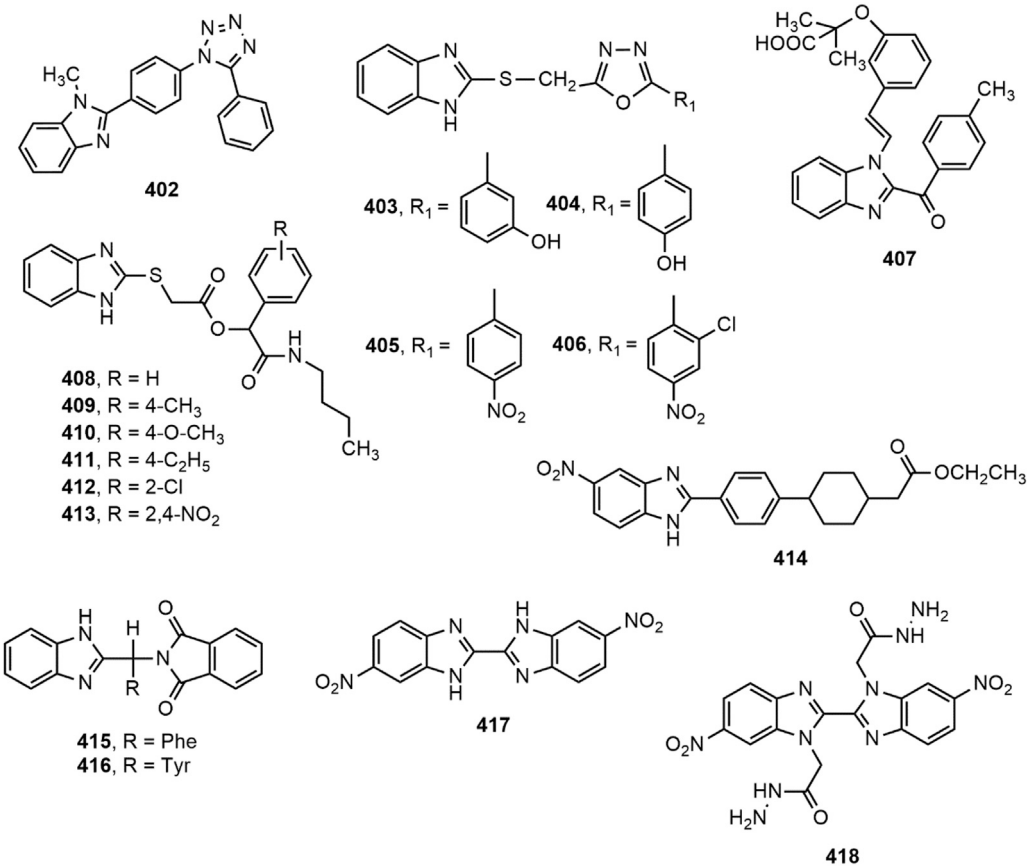

FIGURE 17 | Benzimidazole derivatives with antidiabetic activity.

appeared to be as effective as chloroquine. Based on structure-activity relationship studies and pharmacokinetics optimization, compound **353** was found to display noticeable efficacy in the humanized *P. falciparum* mouse model of malaria (*Pf*/SCID model) with ED_{90} value of 28.6 mg/kg. The attachment of the neutral hydrophobic group at position 6 of the benzimidazole moiety enhanced this excellent anti-malarial property (Hameed et al., 2014). Singh et al. (Singh K. et al., 2017) reported a series of pyrido [1,2-*a*]benzimidazole (PBI) antimalarial agents having *in vitro* anti-plasmodial activity with IC_{50} values of 0.02–0.95 μM against *Pf* NF54 strain, and 0.02–1.07 μM against multidrug-resistant *Pf* K1 strain of *P. falciparum*. Among which, compounds **354–355** exhibited most prominent *in vivo* efficacy in mouse *P. berghei* model due to the presence of chlorine group at C-7, C-8 and C-9 position of benzimidazole moiety. In another study, compounds **356–358** displayed excellent activity with IC_{50} values of 0.69, 1.60 and 1.61 μM, respectively against chloroquine-sensitive 3D7 strain compared to standard chloroquine (IC_{50} = 1.53 μM) (Sharma et al., 2018). Recently, compounds **359–360** were synthesized as highly potent antimalarial agents having IC_{50} values of 0.098 and 0.062 μM, respectively against NF54 strain of *P. falciparum* (Mueller et al., 2020).

Benzimidazole Against Different Protozoa

Torres-Gómez et al. (Torres-Gómez et al., 2008) synthesized a library of benzimidazole-pentamidine hybrids and evaluated them for antiprotozoal activity against *T. vaginalis*, *E. histolytica*, *G. lamblia*, *L. Mexicana* and *P. berghei*. Compound **361** was found to be the most potent from the series, showing 3- and 9- times more activity than standards metronidazole and pentamidine, respectively. Alp et al. (Alp et al., 2009) synthesized several 2'-arylsubstituted-1*H*,1'*H*-[2,5']-bisbenzimidazolyl-5-carboxamidine derivatives and found promising antiparasitic activity of compounds **362** and **363** against *P. falciparum, L. donovani, T. brucei rhodesiense* and *Trypanosoma cruzi.* The presence of 4-fluorophenyl (**362**) and 4-(3,4-dimethoxyphenoxy)phenyl groups (**363**) at the C-2' position of amidinobisbenzimidazole moiety contributed for the antiparasitic activity. Among a library of 2-(trifluoromethyl)-1*H*-benzimidazoles, compounds **364–366** displayed the most prominent *in vitro* antiparasitic activity against *E. histolytica*, *G. intestinalis*, *T. vaginalis* and *T. spiralis* (Hernández-Luis et al., 2010). Compounds **367–368** manifested notable activity against *Paramecium caudatum* and *Vorticella campanula* compared to standard metronidazole (Maske et al., 2012).

Matadamas-Martínez et al. (Matadamas-Martínez et al., 2016) designed and synthesized a novel nitazoxanide and N-methyl-

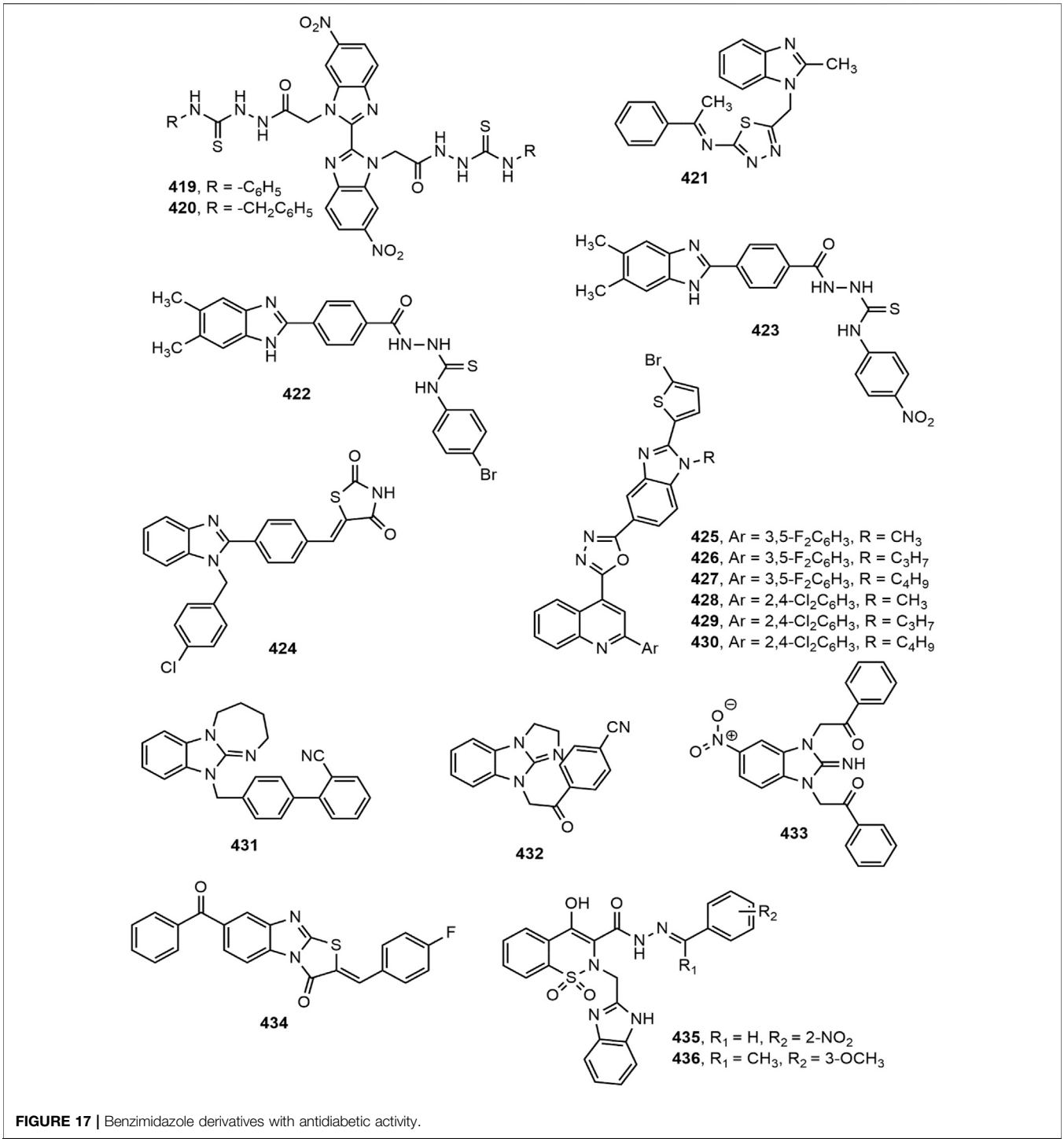

FIGURE 17 | Benzimidazole derivatives with antidiabetic activity.

1*H*-benzimidazole hybrid molecule **369** which displayed better activity with IC_{50} value of 0.010 μM than that of standards nitazoxanide, albendazole and metronidazole against *G. intestinalis* (IC_{50} = 0.015, 0.037 and 1.224 μM, respectively). Hernández-Núñez et al. (Hernández-Núñez et al., 2017) prepared a series of 2-(2-amino-5(6)-nitro-1*H*-benzimidazol-1-yl)-*N*-arylacetamide analogues and illustrated 7-fold more potency of compound **370** than the standard benznidazole against *G. intestinalis* with an IC_{50} of 3.95 μM, and 4-fold more activity of compounds **370–371** against *T. vaginalis* in comparison with benznidazole. Flores-Carrillo and co-workers (Flores-Carrillo et al., 2017) prepared a library of twelve 2-(methylthio)-1*H*-benzimidazole-5-carboxamide derivatives and investigated their *in vitro* antiparasitic

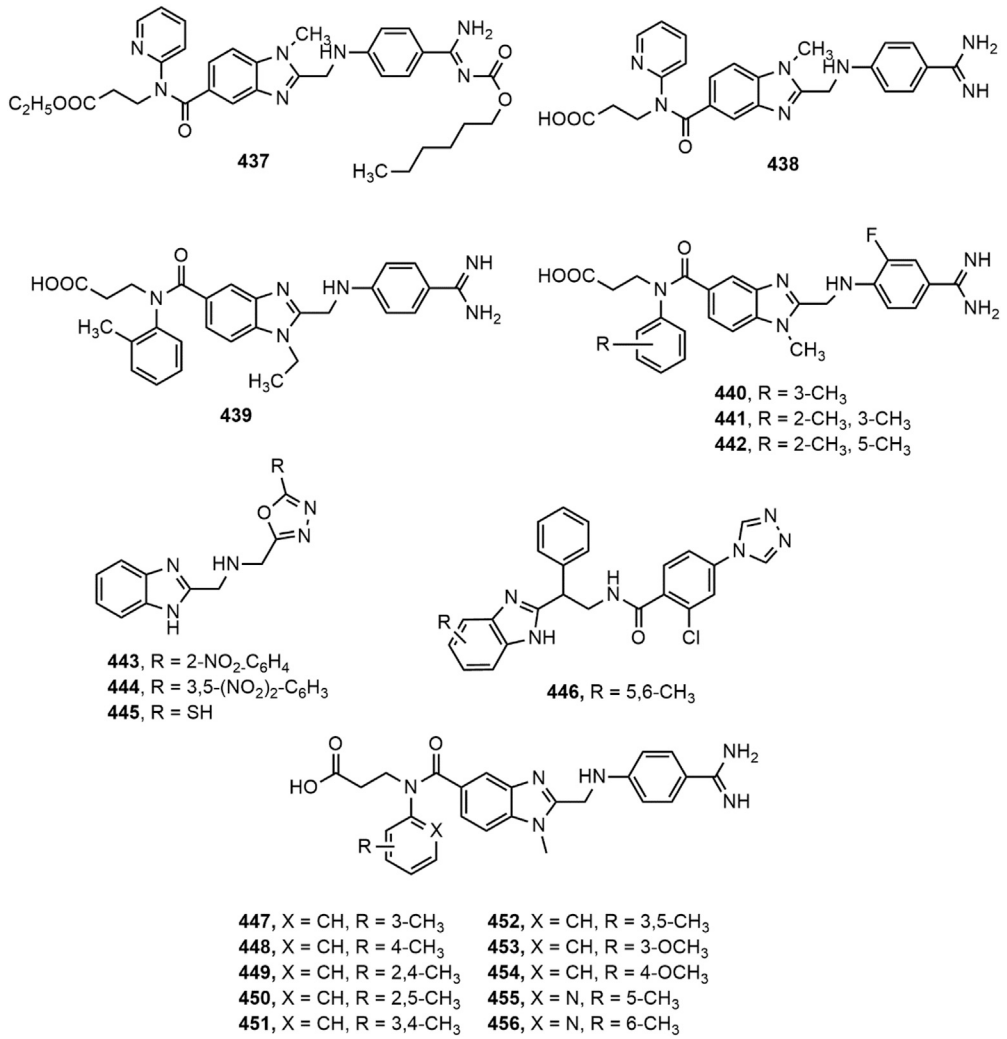

FIGURE 18 | Benzimidazole derivatives with anticoagulant activity.

activity against *G. intestinalis*, *E. histolytica* and *T. vaginalis*. Compounds **372** and **373** showed notable effect against *T. vaginalis* and *G. intestinalis*, respectively in comparison with standards albendazole and metronidazole, and compound **374** emerged as a broad-spectrum antiprotozoal agent with activity against all three tested protozoans. Farahat et al. (Farahat et al., 2018) synthesized a series of benzimidazole bichalcophene diamidine derivatives. Compound **375** showed prominent antiparasitic activity towards mice model infected with *T. brucei rhodesiense* at a dose of 4 × 5 mg/kg i.p. and was found to be more potent than pentamidine, the usual drug of choice to treat African sleeping sickness. Similarly, compounds **376–378** exerted superior efficacy against *T. brucei* in the treatment of human African trypanosomiasis with IC_{50} (mean ± SEM) values of 0.47 ± 0.02, 3.67 ± 0.30, and 0.71 ± 0.22, respectively compared to standard nifurtimox (IC_{50} = 2.0 ± 0.2). The presence of diethylaminoethyl group substantially augmented the antitrypanosomal property of the compounds (**376–378**). Unsubstituted or methyl substituted aromatic rings or inclusion of an imidazole ring at C-5 also potentiated the activity (**Figure 15**) (Popov et al., 2020).

Antihypertensive Activity

A number of marketed antihypertensive drugs comprise benzimidazole moiety, Candesartan cilexetil and Telmisartan are two major examples (**Figure 2**). Categorically they are the antagonists of angiotensin II receptor playing important role in managing hypertension (Keri et al., 2015). In recent years, a number of scientists have conducted research to prepare benzimidazole based novel antihypertensive agents which provided similar or even better efficacy than the conventional types of antihypertensive drugs. Different benzimidazole derivatives with antihypertensive activity are shown in **Figure 16**.

Sharma et al. (Sharma et al., 2010) synthesized a series of substituted benzimidazole derivatives and evaluated for their property as angiotensin II receptor antagonists or sartans

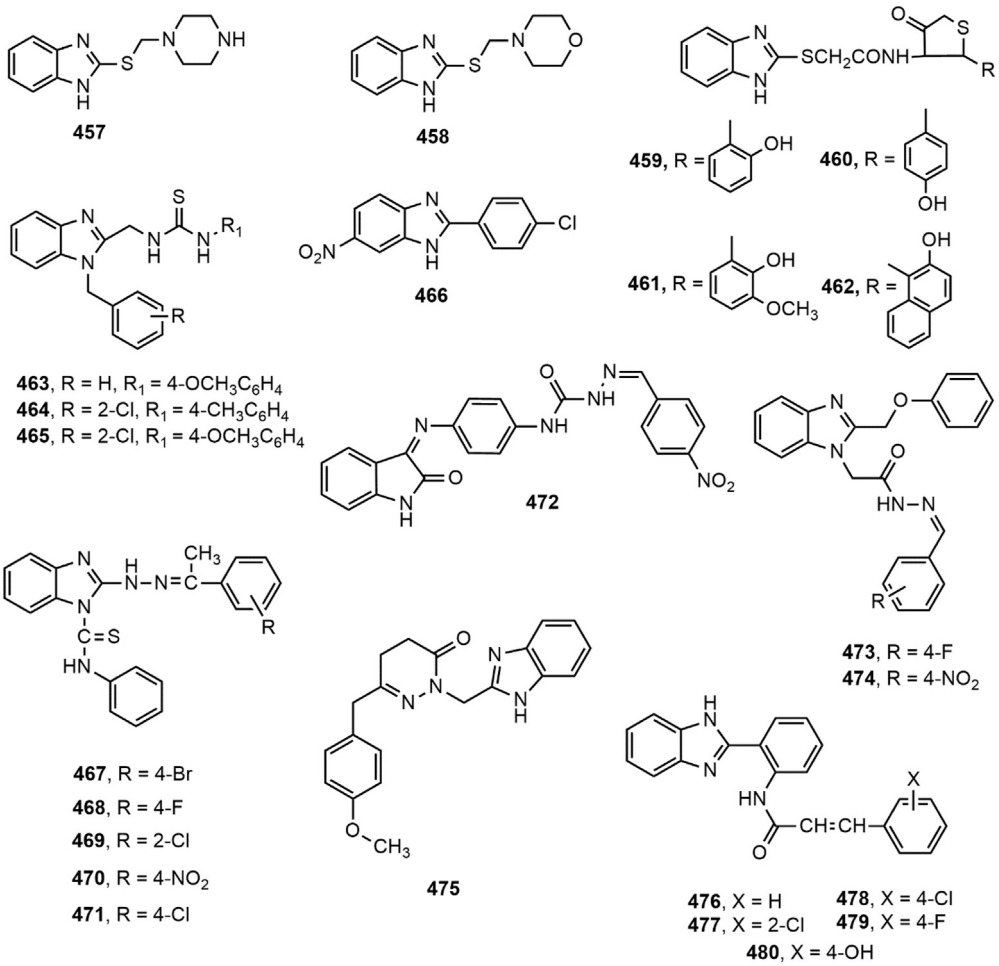

FIGURE 19 | Benzimidazole derivatives with anticonvulsant activity.

using invasive (direct) method in Wister rats. Compounds **379** and **380** appeared to be the most prominent antihypertensive agents from the series compared to standard losartan. Kusumoto et al. (Kusumoto et al., 2011) reported about a novel, long-lasting and potent AT_1 blocker azilsartan medoxomil and its active metabolite azilsartan (**381**) and investigated its pharmacological profile in rat and dog models. Oral administration of 0.1–1 mg/kg azilsartan medoxomil in spontaneously hypertensive rats (SHRs) and renal hypertensive dogs demonstrated better effect in reduction of blood pressure at all doses compared to standard drug olmesartan medoxomil. Abou-Seri et al. (Abou-Seri et al., 2011) synthesized a series of 2-alkoxy-4-aryl-6-(1*H*-benzimidazol-2-yl)-3-pyridinecarbonitrile derivatives. All compounds in the series displayed significant vasodilation properties. Compounds **382–385** showed most prominent activity (IC_{50} = 0.145, 0.202, 0.210, and 0.214 mM, respectively) compared to standard prazosin hydrochloride (IC_{50} = 0.487 mM).

Datani et al. (Datani et al., 2012) synthesized a series of twenty novel 5-nitro benzimidazole analogues and screened them for *ex vivo* vasorelaxant property in rat aorta rings pre-contracted with phenylephrine. Compounds **386–390** exhibited prominent vasorelaxant activity with EC_{50} value less than 30 μM. Among a new set of 5-nitro benzimidazole derivatives, compound **391** emerged as the most active agent against AT_1 with IC_{50} value of 1.03 ± 0.26 nM (Zhu et al., 2014). The presence of butyl chain on 2-position of benzimidazole moiety (**391**) helped the derivative to interact and bind tightly with lipophilic pocket of the receptor. Several benzimidazole derivatives containing indazole moiety were synthesized by Lamotte et al. (Lamotte et al., 2014) among which compound **392** displayed potent AT_1 receptor antagonism as indicated by IC_{50} value (0.006 mM).

Two series of nitric oxide (NO) releasing benzimidazole derivatives were synthesized by coupling benzimidazole biphenyl skeleton with nitro ester and furoxan NO-donor moieties, where compounds **393–394** were reported to possess comparable activity to positive control losartan (Zhang et al., 2015). Hao et al. (Hao et al., 2015) designed and synthesized a series of 4′-[(benzimidazol-1-yl)methyl]biphenyl-2-sulphonamide derivatives and reported that compound **395** was found to be the most potent AT_1 and Endothelin ET_A receptor antagonist with IC_{50} values 28 and 10 nM, respectively.

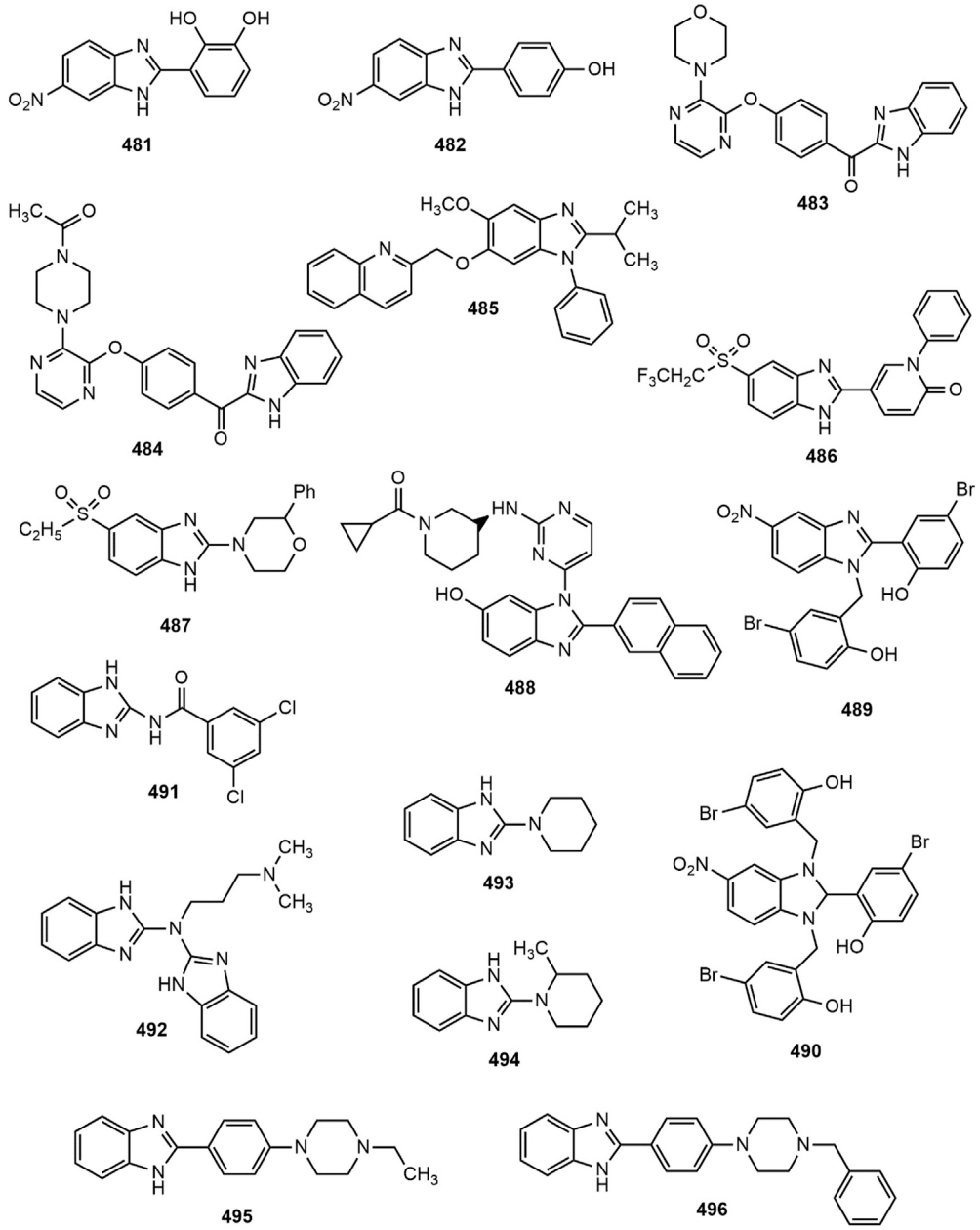

FIGURE 20 | Benzimidazole derivatives as neuro-protective agents.

Upon the identification of a new series of benzimidazole oxazolidinediones as mineralocorticoid receptor (MR) antagonists by high-throughput screening, compound **396** showed similar efficacy as standard drug spironolactone at a dose of 100 mg/kg (p.o.) in rat natriuresis model (Yang et al., 2015).

Bao et al. (Bao et al., 2017) synthesized a series of benzimidazole derivatives which reduced blood pressure in dose-dependent manner in spontaneously hypertensive rats. Among the series, compound **397** exhibited long-lasting efficiency in decreasing blood pressure, with a maximal lowered response of 35.82 ± 6.20 mmHg at 5 mg/kg and 55.98 ± 4.74 mmHg at 10 mg/kg. The compound also showed potent affinity towards AT_1 receptor compared to standard telmisartan with IC_{50} value of 1.13 ± 1.68 nM. In a separate study, Khan et al. (Khan et al., 2018) synthesized a series of 2-phenyl substituted benzimidazoles and assessed antihypertensive activity of these derivatives by using tail cuff method and confirmed excellent antihypertensive property of compound **398** in spontaneously hypertensive rats compared to

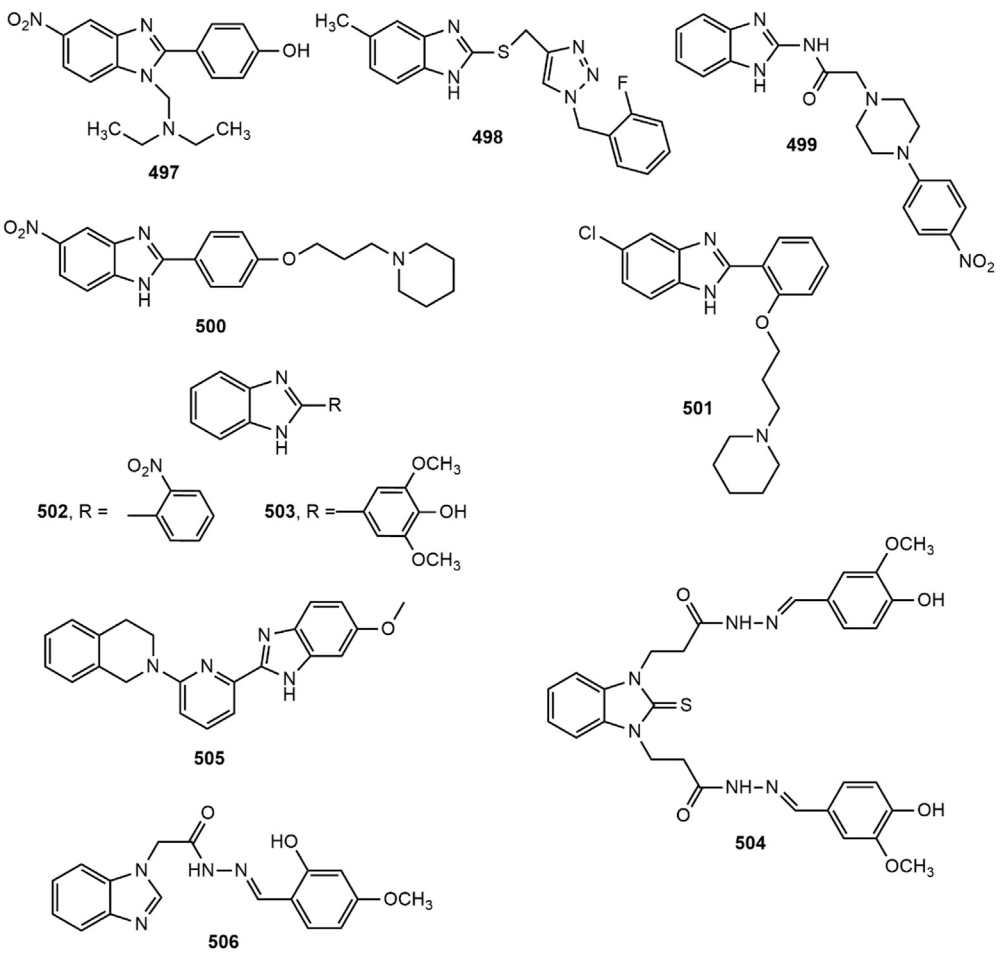

FIGURE 20 | Benzimidazole derivatives as neuro-protective agents.

standard losartan. A very recent report (Yang et al., 2020) ascertained the promising pulmonary hypotensive effect of compound **399** with excellent pharmacokinetic profile in comparison with tadalafil. Finally, compounds **400–401** showed superior inhibition of AT1 receptor (IC_{50} (mean ± SEM): 0.8 ± 0.1 and 2.3 ± 0.7, respectively) than the both standard losartan and telmisartan (Wu et al., 2020).

Antidiabetic Activity

Several benzimidazole based compounds have displayed promising antidiabetic activity by acting as targets of varied stages of carbohydrate metabolism and some of them have been marketed for the treatment of type 2 diabetes. The structure of benzimidazole derivatives with antidiabetic activity reported within recent years are shown in **Figure 17**.

Several 2-(pyridine-2-yl)-1*H*-benzimidazole derivatives were synthesized by Ishikawa et al. (Ishikawa et al., 2009) among which compound **402** emerged as the most potent and metabolically stable glucokinase activator. Besides, the compound proved its oral glucose lowering efficacy in rat oral glucose tolerance test (OGTT) model. A new series of 4-thiazolidinones and 1,3,4-oxadiazoles bearing 2-mercapto benzimidazole moiety were prepared by Shingalapur et al. (Shingalapur et al., 2010) among which compounds **403–406** produced notable results in OGTT model. All the potent derivatives contained hydroxyl group which might have contributed for their antidiabetic property. Some 2-benzoyl benzimidazole derivatives were assessed for antidiabetic and lipid-lowering effects (Ushiroda et al., 2011). Compound **407** appeared to be an effective peroxisome proliferator-activated receptor (PPARγ) partial agonist. Shaikh et al. (Shaikh et al., 2012) reported one-pot synthesis of carbonyl-amide linkage based benzimidazole derivatives (**408–413**) *via* Passerini reaction and demonstrated their antidiabetic potential using rat OGTT model compared to the standard drug glibenclamide.

Diacylglycerol O-acyltransferase-1 (DGAT-1) is an enzyme which catalyzes the formation of triglycerides from diacylglycerol and Acyl-CoA and thereby plays an important role in intestinal fat absorption. DGAT-1 has emerged as an important therapeutic target for the management of different metabolic disorders, such as obesity and diabetes (Birch et al., 2010). Kwak et al. (Kwak et al., 2013) prepared some benzimidazole derivatives as

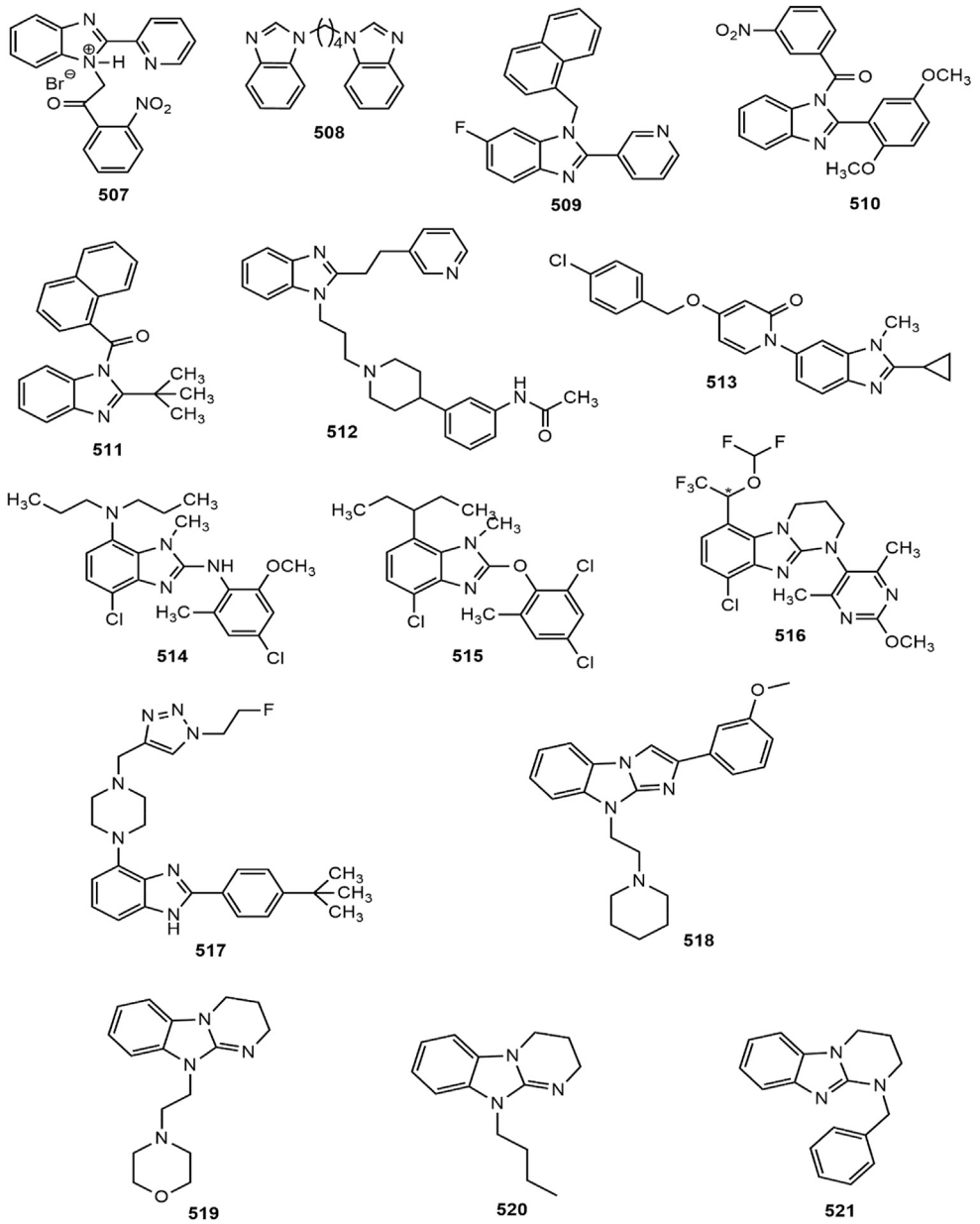

FIGURE 21 | Benzimidazole derivatives with miscellaneous activities.

inhibitors of DGAT-1 which contained a phenylcyclohexyl acetic acid group in benzimidazole moiety. Among the derivatives, compound **414** displayed potent *in vivo* antidiabetic potential in a 4-week study with diet-induced obesity (DIO) mouse model.

The α-glucosidase inhibitors are an important class of antidiabetic agents because of their property to reduce the postprandial glucose level in type-2 diabetic patients (Özil et al., 2016). Mobinikhaledi et al. (Mobinikhaledi et al., 2015) synthesized several new benzimidazole derivatives from amino acids in the presence of phosphorus oxychloride ($POCl_3$). Compounds **415** and **416**, upon evaluation of yeast and rat intestinal α-glucosidases inhibitory effect produced most notable results. The IC_{50} values for compound **416** against yeast and rat intestinal α-glucosidases were reported as 9.1 and 36.7 μM, respectively and thus it appeared to be the most potent benzimidazole among the series. Özil and co-workers (Özil et al., 2016) prepared a series of bis-benzimidazole derivatives by the reaction of *o*-phenylenediamine and 4-nitro-*o*-phenylenediamine with oxalic acid using both conventional and microwave techniques. Compounds **417–420** demonstrated prominent α-glucosidase inhibition with IC_{50} values of 0.54 ± 0.01, 0.44 ± 0.04, 1.24 ± 0.05 and 0.49 ± 0.01 μM, respectively compared to standard acarbose (IC_{50} 13.34 ± 1.26 μM).

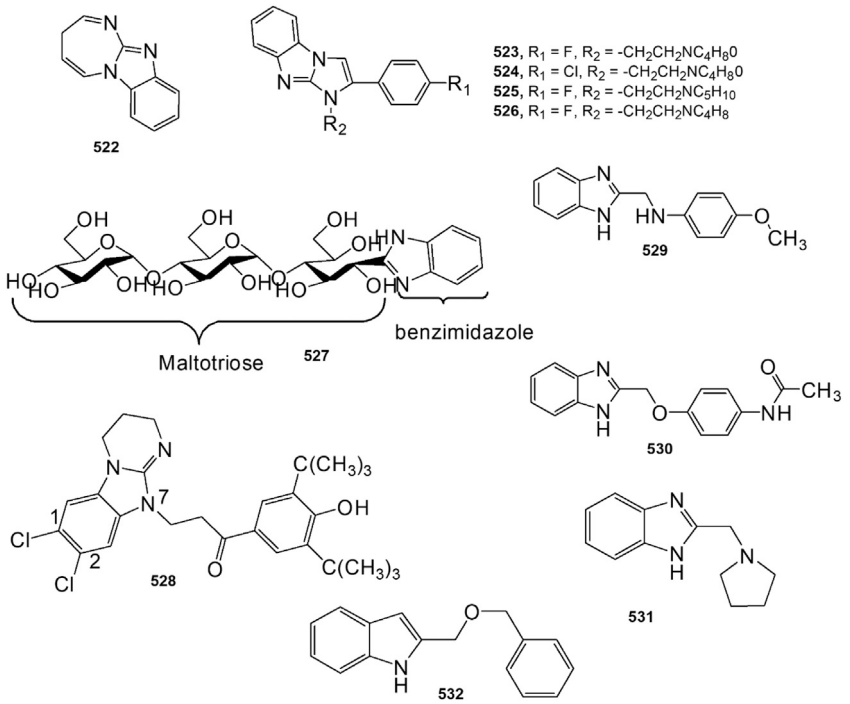

FIGURE 21 | (Continued) Benzimidazole derivatives with miscellaneous activities.

Some novel 1,3,4-thiadiazole substituted 2-methyl benzimidazole derivatives were synthesized by conventional methods among which compound **421** exhibited significant *in vitro* antidiabetic property (Nair et al., 2016). A series of hybrid benzimidazole-thiourea derivatives were synthesized by Zawawi et al. (Zawawi et al., 2017) and evaluated for α-glucosidases inhibitory potential. Compounds **422–423** displayed significant inhibitory properties with IC_{50} values of 50.57 ± 0.81 and 35.83 ± 0.66 μM, respectively. Besides, Singh et al. (Singh et al., 2018) synthesized a library of *N*-substituted-benzimidazolyl linked *para* substituted benzylidene derivatives. Compound **424** bearing 2,4-thiazolidinedione group at 4-position of phenyl ring exhibited pronounced *in vitro* α-amylase and α-glucosidase inhibitory properties (IC_{50} = 0.54 ± 0.01 μM) and appeared as a promising antidiabetic agent from the series.

Recently, Bharadwaj et al. (Bharadwaj et al., 2018) have developed several novel benzimidazole derivatives **(425–430)** and reported excellent antidiabetic activity by applying α-glucosidase inhibitory method with a range of IC_{50} = 0.66 ± 0.05 to 3.79 ± 0.46 μg/ml compared to standard IC_{50} value of acarbose (1460.28 ± 244.365). Besides, two potent AMP-activated protein kinase (AMPK) activators (**431–432**) with multi-target antidiabetic property were reported against LPS-activated murine peritoneal macrophages (Babkov et al., 2019). In another study, two molecules, 1,3-disubstituted-benzimidazole-2-imine (**433**) and 1,3-thiazolo[3,2-*a*] benzimidazolone derivative (**434**), exerted dual effects against dipeptidyl peptidase-IV (DPP-IV) and xanthine oxidase (XO) enzymes with IC_{50} values less than 200 μM (Tomovic et al., 2020). Finally, Kanwal et al. (Kanwal et al., 2020) prepared a library of benzimidazole-benzothiazine hybrid molecules by Gabriel–Colman rearrangement of methyl 2-(1,1-dioxido-3-oxobenzo[*d*]isothiazol-2(3*H*)-yl) acetate, and reported that compounds **435–436** exhibited potential antidiabetic property by inhibiting Ecto-nucleotide pyrophosphatases/phosphodiesterases 1 (ENPP1) 1 and -3.

Anticoagulant Activity

Different substituted benzimidazole derivatives have been explored for several years for their anticoagulant activity and potential use in clinical practice. Benzimidazole derivatives acting as anticoagulants are shown in **Figure 18**.

Thrombin (fIIa) is a multifunctional serine protease responsible for the proteolytic cleavage of fibrinogen. Inhibition of thrombin is a crucial mechanism for inhibition of coagulation. Benzimidazole moiety serves as a suitable template for placing a wide range of substituents required for interaction with thrombin (Hauel et al., 2002). Hauel et al. (Hauel et al., 2002) designed and synthesized a series of new benzimidazole derivatives bearing structural similarity to α-NAPAP (*N*-alpha-(2-naphthylsulfonylglycyl)-4-amidinophenylalanine piperidide), a benzamidine-based powerful inhibitor of thrombin, trypsin and other serine proteases. With the addition of ethyl ester and hexyloxycarbonyl carbamide hydrophobic side chains, improved pharmacokinetic profile was obtained leading to the invention of orally absorbed prodrug, **437** (Dabigatran etexilate).

The prodrug **437** reached clinical trials and its active form **438** (Dabigatran) was discovered with excellent thrombin inhibitory potency and tolerability.

Recently, Ren et al. (Ren et al., 2016) designed a series of benzimidazole derivatives and tested them for thrombin inhibitory effects. Compound **439** with IC_{50} value of 3.11 ± 0.21 nM appeared to be a potent thrombin inhibitor exhibiting better activity than the standard argatroban (IC_{50} 9.88 ± 2.26 nM). A series of 1,2,5-trisubstituted benzimidazole fluorinated derivatives (**440–442**) were also evaluated for *in vitro* inhibitory activity against thrombin (Yang et al., 2016). Compounds **440–442** with IC_{50} values of 2.26 ± 0.38, 1.54 ± 0.09 and 3.35 ± 0.87 nmol/L, respectively showed improved result compared to argatroban (IC_{50} 9.88 ± 2.26 nmol/L), thus showing their potential as thrombin inhibitors. A library of benzimidazole derived 1,3,4-oxadiazole derivatives (**443–445**) were assessed for *ex vivo* anticoagulant activity by determining the effect of compounds in increasing prothrombin time (PT) and activated partial thromboplastin time (aPTT) (Vishwanathan and Gurupadayya, 2015). Compounds **443–445** displayed significant increase in PT (32 ± 0.7, 36 ± 0.5 and 41 ± 0.4 s, respectively) compared to standard drug acenocoumarol (48 ± 0.5 s). The compounds, however, caused a slight increase in aPTT in comparison with the reference drug, unfractionated heparin (500 IU/kg).

Factor IXa (fIXa), an important coagulation factor, is a useful target for developing potent and selective antithrombotic agents. A research involving pharmacophore modelling of a new series of benzimidazole analogues presented the chemical features necessary for designing fIXa inhibitors and showed that benzimidazole derivatives have the potential to be developed into effective antithrombotic agents (Kumbhar et al., 2017). Compound **446** was found to be the most active compound from the series, indicated by fIXa binding affinity (K_i) value of 0.016 μM.

Recently, Zhang et al. (Zhang et al., 2020) designed and synthesized ten novel dabigatran derivatives **(447–456)** with high docking score. The study uncovered that all the compounds showed more than 50% *in vitro* thrombin inhibitory property at 1 mg/ml concentration, where the IC_{50} values of compounds **447, 450** and **456** were 1.92, 2.17 and 1.54 nM, respectively, comparable to the IC_{50} value of positive control dabigatran (1.20 nM). The derivatives **425** and **428,** previously reported in this review for antidiabetic property, exerted anticoagulant activity by augmenting the clotting duration. However, only compound **425** exhibited excellent inhibition (93.4%) of epinephrine-induced platelet aggregation (Bharadwaj et al., 2018).

Anticonvulsant Activity

Epilepsy is one of the most prevalent and serious neurological disorders, and recurrent seizures or convulsions are its characteristic syndrome. Around one-third of patients in the world show poor response to currently available antiepileptic drugs (Keri et al., 2015). In search of novel clinically effective anticonvulsant medications, benzimidazole nucleus has recently been explored by scientists with promising results. The benzimidazole derivatives with anticonvulsant property are shown in **Figure 19**.

A library of 2-mercaptobenzimidazole derivatives were evaluated for anticonvulsant activity using maximal electroshock seizure (MES) model. The synthesized compounds displayed anticonvulsant property at a dose of 20 mg/kg (i.p.) compared to standard phenytoin and compounds **457–458** appeared to be the most potent of all (Anandarajagopal et al., 2010). A series of 4-thiazolidinones and 1,3,4-oxadiazoles bearing 2-mercaptobenzimidazole moiety were assessed for *in vivo* anticonvulsant activity (Shingalapur et al., 2010). Compounds **459–462** emerged as the most promising anticonvulsants in MES model.

Siddiqui and co-workers described the synthesis of several 1-{(1-(2-substituted benzyl)-1*H*-benzo[d]imidazol-2-yl) methyl}-3-arylthioureas which have been mentioned earlier for their analgesic potential. The research group in a previous study reported about the anticonvulsant and cytotoxic effects of the same series of compounds. Compounds **463–465** were found to possess potent anticonvulsant property in comparison with standard drug phenytoin (Siddiqui and Alam, 2010). A series of nitro-benzimidazole derivatives were synthesized by Jain et al. and screened for anticonvulsant activity using MES and subcutaneous pentylenetetrazole (scPTZ) models. Compound **466** displayed the most promising result in inhibiting convulsion induced in mice by both methods (Jain et al., 2010). Bhrigu et al. synthesized a library of 2-[(1-substituted phenylethylidine) hydrazine]-*N*-phenyl-1*H*-benzo[d] imidazole-1-carbothioamides (**467–471**) from the reaction of 2-mercaptobenzimidazole with hydrazine hydrate, substituted acetophenones and phenylisothiocyanate. Compounds **467–471** were found to be active compounds in MES and scPTZ models, and devoid of neurotoxicity (Bhrigu et al., 2012).

A series of benzimidazole substituted semicarbazones were synthesized and tested for anticonvulsant activity using MES model. Compound **472** at a dose of 50 mg/kg (i.p.) appeared to be the most potent among the derivatives (Rajak, 2015). In another study, some oxadiazole bearing benzimidazoles and several derivatives of 2-[2-(phenoxymethyl)-1*H*-benzimidazol-1-yl]-N0-[(Z)-phenylmethylidene] acetohydrazide (**473–474**) were evaluated employing MES and scPTZ methods. Compounds **473–474** were found to be effective anticonvulsant agents (Shaharyar et al., 2016). A new series of hybrid benzimidazole containing pyridazinones were developed to assess anticonvulsant property. Compound **475** emerged as an effective and safe anticonvulsant in both MES and scPTZ models. The compound also exhibited notable increase in GABA level (1.7-fold) compared to control which was attributed to its good binding property with the $GABA_A$ receptor (Partap et al., 2017). Recently, Sahoo et al. (Sahoo et al., 2019) synthesized several benzimidazole derivatives and disclosed that compounds **476–480** exhibited notable anticonvulsant

potency (around 70–80%) in comparison to standard drug phenytoin.

Benzimidazole as Neuro-protective Agent

Neurological disorders comprise the disorders of central and peripheral nervous system. Alzheimer disease (AD), dementia, stroke, Parkinson's disease, multiple sclerosis, brain tumor etc. are the most common diseases affecting a large number of people. AD is a chronic neurodegenerative disorder and the most common form of dementia manifested by loss of memory, language, cognitive functions, behavior and emotion. The factors which mostly contribute in the development of AD include the levels of acetylcholine (ACh) and deposits of neurotoxic amyloid-β-peptide (Aβ) (Akhtar et al., 2017). A number of substituted benzimidazole derivatives have been developed for the management and treatment of neurological diseases. The benzimidazole derivatives explored recently as neuro-protective agents are shown in **Figure 20**.

Khan et al. synthesized a series of 6-nitrobenzimidazole derivatives and screened their phosphodiesterase inhibitory property. Among them, compounds **481** (IC_{50} = 1.5 ± 0.043 μM) and **482** (IC_{50} = 2.4 ± 0.049 μM) were found to possess better activity than the standard EDTA (IC_{50} = 274 ± 0.007 μM). The presence of 2,3-dihydroxyphenyl (**481**) and 4-hydroxyphenyl (**482**) moiety might have contributed for their notable property (Khan et al., 2012). Hu et al. designed and synthesized a series of keto-benzimidazole derivatives (**483–484**) as potent and selective inhibitors of Phosphodiesterase 10A (PDE10A). Compound **484** showed 55% receptor occupancy (RO) of PDE10A at 30 mg/kg p.o. in rat brain. Further research led to the identification of compound **484**, with improvements in *in vivo* efficacy (57% RO in rats at 10 mg/kg p.o.), rat clearance and oral bioavailability (Hu et al., 2013). Hamaguchi et al. (Hamaguchi et al., 2013) prepared a series of benzimidazole derivatives as PDE10A inhibitors with reduced CYP1A2 inhibition among which the compound **485** appeared to be the most prominent.

Tamura and co-workers synthesized a series of benzimidazole derivatives for neuropeptide Y (NPY) receptor antagonistic activity which is an important pharmacological target for the treatment of different neurodegenerative disorders. Compound **486** appeared to be the most promising agent (Tamura et al., 2012a). In another study by the same research group (Tamura et al., 2012b), compound **487** was reported to show high NPY Y5 receptor binding affinity along with good absorption, distribution, metabolism and elimination (ADME) profile resulting in notable *in vivo* efficacy as NPY Y5 receptor antagonist.

Kim et al. evaluated a series of 1-heteroaryl-2-aryl-1*H*-benzimidazole derivatives as inhibitors of c-Jun N-terminal kinases (JNK3), a group of degenerative signal transducers and potential target of neurodegenerative diseases, e.g. Alzheimer's and Parkinson's diseases. Majority of the compounds exhibited high affinity (K_d = 10 μM–46 nM) to JNK3 when investigated through SPR, JNK3 kinase assay and cell-viability of human neuroblastoma cells. The most potent compound **488** showed notable cell protective effect (IC_{50} = 1.09 μM) against toxicity induced by anisomycin (Kim et al., 2013).

Human Presequence Protease (hPreP) is a mitochondrial metalloprotease capable of degrading amyloid-β peptide and increasing its proteolysis in human neuronal cells. Identification of potential agonists of hPreP is of great importance for Alzheimer's drug design. Compounds **489–490** showed marked enhancement of hPreP-mediated proteolysis of Aβ, pF1β and fluorogenic-substrate V and thus presented great potential in the treatment of Alzheimer's disease (Vangavaragu et al., 2014).

Among the therapeutic agents used for the treatment of traumatic brain injury (TBI), positive allosteric modulators (PAMs) of metabotropic glutamate receptor 5 (mGluR5) are important. He et al. (He et al., 2015) designed and synthesized a series of acyl-2-aminobenzimidazole derivatives based on the chemical structure of a well-known mGluR5 PAM called 3,3'-difluorobenzaldazine (DFB). The compounds were tested for binding affinity to transmembrane domain of mGluR5 using nitric oxide (NO) production assay, among which compound **491** (IC_{50} = 6.4 μM) was found to be around 20 times more potent than DFB (IC_{50} = 136 μM) (He et al., 2015).

Zhu et al. synthesized a series of 2-aminobenzimidazole derivatives (**492–494**) under microwave irradiation and assessed their acetylcholinesterase (AChE) and butyrylcholinesterase (BuChE) inhibitory activities. Compounds **492–494** displayed more than 25-fold more selectivity towards BuChE than AChE (Zhu et al., 2013). In another study, the compounds **(495–496)** showed selective inhibition on BChE and appeared to be the most potent BuChE inhibitors (IC_{50} = 5.18 and 5.22 μM, respectively) (Ozadali-Sari et al., 2017). Besides, compound **497** was found to be the most potent AChE inhibitor (IC_{50} = 0.93 ± 0.04 μM) with marked selectivity ratio (13.68) (Alpan et al., 2017). Similarly, compound **498** carrying a methyl group at 5-position of benzimidazole ring and 2-fluorobenzyl group connected to 1,2,3-triazole system was found to be the most potent inhibitor of AChE displaying 84% inhibition at 100 μM concentration (Faraji et al., 2017). The nitrophenyl piperazine substituted derivative **499** showed 57.25 and 77.92% inhibition of Rho-associated protein kinase II (ROCK II) enzyme at a concentration of 0.5 and 1 mM, respectively and exerted prominent IOP lowering effect (51.56%) compared to the standard fasudil (Abbhi et al., 2017).

Recently, compounds **500–501** were reported as promising AChE and BuChE inhibitors (IC_{50} = 0.14 and 0.22 μM, respectively), highly neuroprotective against hydrogen peroxide mediated toxicity, metal chelators, and free radical scavengers in the treatment of Alzheimer's disease (Sarıkaya et al., 2018). Similarly, compounds **502–503** demonstrated duel effects as anti-Alzheimer agents by beta amyloid cleavage enzyme-1 (BACE1) inhibition and neuroprotection (Gurjar et al., 2020). In a 6-hydroxydopamine (6-OHDA)-induced oxidative stress *in vitro* model assay, compound **504** exerted neuroprotective action compared to melatonin, and reduced superoxide anion radical and hypochlorite level in a luminol-dependent chemiluminescent assay (Anastassova et al., 2020). In another

study, compound **505** displayed significant anti-neuroinflammatory property (IC_{50} = 5.07 mM to prevent nitric oxide generation) and 65.7% hBACE1 inhibition. Besides, the compound **(505)** increased glutathione (GSH) level, reduced ROS production, and subsequently opened a door for further development to be established as a promising treatment option against Alzheimer's disease (Fang et al., 2019). Finally, compound **506** exhibited promising neuroprotective role on SH-SY5Y cells by preserving the synaptosomal viability and minimizing GST level compared to the standards melatonin and rasagiline (Anastassova et al., 2021).

Miscellaneous Activities

Several other classes of benzimidazole derivatives have been prepared by different scientists during the last few years. Some of these novel benzimidazole based compounds are shown in **Figure 21**.

Saify et al. (Saify et al., 2014) synthesized a series of 2-(2'-pyridyl) benzimidazole derivatives and evaluated their urease inhibitory property. Compound **507** displayed significant urease inhibition compared to the standard thiourea (IC_{50} = 19.22 ± 0.49 μM and 21.00 ± 0.01 μM, respectively) and twofold more activity than another standard acetohydroxamic acid (IC_{50} = 42.00 ± 1.26 μM). Several 1-alkylbenzimidazoles and 1,3-dialkyl benzimidazolium salts were evaluated for their tyrosinase inhibitory activity among which compound **508** emerged as the most potent derivative (IC_{50} = 0.31 mM) (Karatas et al., 2014).

A series of 2-pyridylbenzimidazole derivatives were designed and synthesized as Cannabinoid 1 (CB1) receptor agonists amongst which compound **509** appeared to be the most potent with a binding affinity value (K_{iCB1}) of 0.53 nM (Mella-Raipán et al., 2013). The same research group synthesized a series of N-acyl-2,5-dimethoxyphenyl-1H-benzimidazole derivatives and assessed them for human CB1 receptor binding affinity using competitive binding assays (Espinosa-Bustos et al., 2015). Compound **510**, carrying 3-nitrophenyl group in the aroyl region of benzimidazole moiety was found to be the most promising agent (K_i = 1.2 nM). More recently, they synthesized a new series of benzimidazole derivatives which displayed more selectivity towards human Cannabinoid 2 (CB2) receptor than that towards CB1 receptor (Romero-Parra et al., 2016). Compound **511** demonstrated the best binding affinity (K_i = 0.08 μM), high selectivity index (K_iCB1/K_iCB2 >125) and low toxicity.

Lim et al. synthesized a series of 2-heteroaryl substituted benzimidazole derivatives bearing piperidinylphenyl acetamide group at 1-position and screened them for their effect on melanin-concentrating hormone (MCH), an attractive target for developing anti-obesity agents. Compound **512** displayed prominent MCH receptor 1(MCH-R1) binding affinity (IC_{50} = 1 nM), as well as low human ether-a-go-go-related gene (hERG) binding affinity thereby ensuring low risks of cardiovascular diseases, metabolic stability and preferable pharmacokinetic profile (Lim et al., 2013). Igawa et al. synthesized several 1-(1H-benzimidazol-6-yl) pyridin-2(1H)-one compounds among which compound **513** showed most prominent antagonistic property against MCH-R1 (Igawa et al., 2016).

Mochizuki and co-workers (Mochizuki et al., 2016) assessed several benzimidazole analogues for *in vivo* corticotropin releasing factor type 1 (CRF1) receptor antagonistic property. Compound **514** with an electron withdrawing cyano group at the 4-position of benzimidazole nucleus emerged as the most promising among the series. In continuation with their research to develop CRF1 receptor antagonists, compound **515** was reported as a potent CRF1 binding inhibitor (IC_{50} = 4.1 nM) and *in vitro* CRF1 antagonist (IC_{50} = 44 nM) (Mochizuki et al., 2017). More recently they designed a series of 1,2,3,4-tetrahydropyrimido[1,2-a]benzimidazole analogues as novel CRF1 receptor antagonists. Compound **516** displayed very prominent CRF1 receptor binding activity (IC_{50} = 58 nM) and oral bioavailability (F = 68% in rat model) indicating its potential in developing clinically effective CRF1 receptor antagonist in the future (Kojima et al., 2018).

A library of small molecules were tested for their property as human gonadotropin releasing hormone (GnRH) receptor antagonists. The derivative **517** (K_i = 13.8 nM) exhibited highest affinity towards human GnRH receptor and emerged as the most prominent GnRH receptor antagonist (Fjellaksel et al., 2017). Furthermore, a recent study reported several benzimidazole analogs **(518–521)** as intraocular pressure (IOP) reducer in the treatment of dexamethasone-induced ocular hypertension. Among these, compound **521** exerted the best anti-glaucoma action by the maximum IOP reduction of 22.32% from baseline following single drop administration (0.1%) (Marcus et al., 2019).

Maltsev et al. (Maltsev et al., 2020) evaluated a series of Diazepino[1,2-a]benzimidazole derivatives for their possible psychotropic properties. Compound **522** at a dose of 2.34 mg/kg showed prominent anxiolytic, antidepressant and anticonvulsant activities in both rat and mice models. Vasil'ev et al. (Vasil'ev et al., 2017) investigated a series of imidazo[1,2-a] benzimidazole derivatives using corazole-induced seizure model. The compounds **523–526** displayed notable anticonvulsive activity in comparison with standard valproic acid. The prominent activity is attributed to the presence of a 4-fluoro substituent in the 2-position and a dialkylaminoalkyl or cycloalkylaminoalkyl substituent in the 9-position of the fused ring.

Change et al. (Chang et al., 2017) investigated the antiplatelet activity of some novel saccharide-based benzimidazole derivatives. Compound **527** exhibited concentration-dependent inhibitory property against thrombin (0.01 U/ml) and collagen (1 μg/ml)-induced human platelet aggregation in an *in vitro* model. Its inhibitory effect might be attributed to the presence of 1-imidazolyl moiety at one end carrying a long chain of three sugar moieties. A series of benzimidazole derivatives bearing a sterically hindered phenolic group in their structures were evaluated for *in vitro* antiplatelet activity using the Adenosine diphosphate (ADP)-induced platelet aggregation model of rabbit's plasma (Spasov et al., 2020). Compound **528** showed notable antiplatelet activity by exceeding the standard acetylsalicylic acid by 21.8 times. In the *in vivo* study of inhibition of intravascular platelet aggregation, the same compound displayed 1.5 times superior activity than

acetylsalicylic acid and slightly inferior activity than another standard clopidogrel.

Idris and his co-workers (Idris et al., 2019) reported that benzimidazole derivatives **529** and **530** decreased repeated morphine administration-induced thermal hyperalgesia and tactile allodynia as well as the expression of spinal Tumor Necrosis Factor-alpha (TNF-α) in Balb-c mice. The compounds displayed PPARγ agonist activity, indicating their potential in the management of morphine-induced paradoxical pain. Akhtar et al. (Akhtar et al., 2021) evaluated the role of benzimidazole derivative **531** in managing nalbuphine-induced tolerance in cisplatin-induced neuropathic pain in mice. Cisplatin, a platinum-based anticancer medication, is often coupled with Nalbuphine, an opioid analgesic used for treating acute and chronic pain. The compound **531** attenuated the tolerance to the analgesic activity of nalbuphine developed due to its long-term use, as well as TNF-α expression in the spinal cord of mice.

Moreover, Raka et al. (Raka et al., 2021) reported a series of substituted benzimidazole derivatives and found a notable inhibitory property of compound **532** against the acetylcholinesterase enzyme with an IC_{50} value of 29.64 μg/ml compared to the standard drug donepezil (IC_{50} = 9.54 μg/ml).

EXPERT OPINION

Heterocyclic compounds possess versatile applications, such as antibacterial, antiviral, antitubercular, anticancer, anti-inflammatory, analgesics, herbicidal, fungicidal, insecticidal, antidiabetic, antihypertensive, and so on (Pathan et al., 2020). Some of these heterocyclic compounds, having several photochromic, solvatochromic, and biochemical luminescence characteristics, are widely distributed in natural sources as in plant alkaloids, hemoglobin, anthocyanins, flavones, etc., and play a vital role as drugs, vitamins, chlorophyll pigment, dyes, amino acids, and enzymes in human life (Pathan et al., 2020).

Among the heterocyclic compounds, benzimidazole derivatives have been playing the most pulsing and eye-catching pioneer role in synthetic pharmaceutical and agrochemical sectors for the last couple of decades (Pardeshi et al., 2021). As having the similarity of the benzimidazole nucleus with many naturally occurring nucleotides and its presence in several natural compounds, the benzimidazole derivatives can easily interact with various biomacromolecules or target proteins. Thus, the compounds derived from the benzimidazole ring system exert broad-spectrum efficacy against various human disorders like cancer, hypertension, diabetes, bacterial or viral infection, inflammation, gastritis, neurodegenerative disorders, and so on (Wang et al., 2015).

Moreover, the first effective therapy developed through benzimidazole moiety against the Ebola virus was an innovative breakthrough (De Clercq, 2019). Categorically, several approved drugs derived from benzimidazole are currently available in the market and they can be grouped as *1*) proton pump inhibitors (PPIs) exemplified by omeprazole, esomeprazole, lansoprazole, pantoprazole, etc., *2*) anthelmintic drugs demonstrated by mebendazole, albendazole, oxibendazole, etc., *3*) non-sedative H_1-receptor blockers or antihistamine presented by astemizole, norastemizole, emedastine, mizolastine, etc., *4*) angiotensin II receptor blocker illustrated by telmisartan, candesartan, azilsartan, and *5*) calcium sensitized cardiac agents instanced by isomazole (Tahlan et al., 2019).

As stated in the comprehensive review, there are diverse classes of benzimidazole derivatives synthesized by several groups, which showed prominent bioactivities even sometimes better than the existing drugs. Although several structure-activity relationship studies were accomplished by several groups in a particular area of bioactivities, it is challenging to draw any conclusion on the structural features needed for a specific activity. In many cases, further studies on specific benzimidazole derivatives leading to the development of potential drug candidates were not continued. The synthesis of a new library of benzimidazole structures is expanding day by day, with a unique spectrum of bioactivity being reported regularly. Despite having extensive biological and diagnostic applications with the lustrous futuristic potentiality of benzimidazole scaffolds, barriers and challenges are still viable in the clinical development process. Drug resistance is the major drawback of the antiviral, antifungal, antibacterial, antimalarial, anti-cancer, anti-hepatitis, and anti-HIV agents (Wang et al., 2015). Another notable concern is that several benzimidazole derivatives such as PPIs are showing *in vitro* and *in vivo* drug-drug interactions with several classes of therapeutics such as anti-cancer (Bezabeh et al., 2012) and antidiabetics (Hossain et al., 2020; Hossain et al., 2021).

Benzimidazole derivatives containing pyrrolidine side-chain exhibited a beacon of hope in malignancy treatment where several available drugs (for example, sorafenib) have become resistant due to long-term exposure against several cancers, such as hepatocellular carcinoma (Suk et al., 2019). It is a crucial fact that benzimidazole derivatives have been synthesized and screened against many disease conditions; among them, very few enter into clinical trials. For example, selumetinib (NCT01933932) and galeterone (NCT04098081) are two promising agents undergoing several clinical trials to be established as effective cancer agents. Besides, several ongoing clinical trials (For instance, NCT01611974) of various drugs (maribavir) bearing benzimidazole moiety showed promising effects against resistant cytomegalovirus (Maertens et al., 2019; Papanicolaou et al., 2019). Dexlansoprazole completed the phase IV trial (NCT01093755) and showed extensive effect against esophageal inflammation (Sharma et al., 2020). However, these reported trials are still very negligible compared to the preclinical status of the ample amount of benzimidazole drug candidates.

It is crystal clear that an exciting number of benzimidazole pharmacophore derivatives have become potential drug candidates to treat several disease conditions in ongoing clinical trials. However, this promising moiety is copious to be further investigated for designing a number of different target molecules, which might reveal some encouraging outcomes in medicinal research. It can easily be assumed at the current stage that several new strategies might be designed and developed for multi-target agents with the highest affinity,

specificity, and enhanced bioactivities. In the future, the benzimidazole scaffolds might be fused with another heterocyclic ring system to be explored several novel chemically stable and potent pharmacological agents against several rare or critical diseases or with better pharmacokinetic and pharmacodynamic profiles. This might be an outrageous and worldwide revolutionary achievement in the next century. Toxicity, drug resistance, and poor bioavailability are the significant concerns during drug development or the underlying reasons behind the compounds be untouched in the human trial. Structural modifications of the existing synthesized molecules might be an excellent technique to be brought about improved or novel activities with a better safety profile. Besides, the prodrug strategy can also be applied to ameliorate the bioavailability of the present derivatives. Furthermore, combinations of the benzimidazole derivatives with other existing drugs might be explored for finding synergistic effects or exciting pharmacological activities against multidrug-resistant microorganisms.

Moreover, several benzimidazole-containing clinically used medications, e.g., omeprazole, lansoprazole, pantoprazole, and rabeprazole, are actually in the form of prodrugs for which the onset of action is slower. Thus, there is an increased demand for producing the active form of drugs directly from benzimidazoles, and for this, researchers are paying attention to novel benzimidazole-derived therapeutics with lesser toxicity and better pharmacodynamic profile. In this case, PPIs containing benzimidazole ring might be modified, or the benzimidazole pharmacophore might be replaced by imidazole ring with the improved biological profile. The non-approved benzimidazole scaffolds for cancer therapy having eminent pharmacokinetics and safety profile might be repurposed to treat several life-threatening cancers with a lack of safe and effective treatment. Some anthelmintic drugs containing benzimidazole nuclei, such as flubendazole, albendazole, and mebendazole, could be considered to apply against various types of cancer in future investigations. Besides, stereochemistry could be regarded as to trace and explore more potent isomers of the existing approved benzimidazole derivatives because one enantiomer may exert distinct biochemical property than the other enantiomer.

CONCLUSION

Benzimidazole, an essential nitrogen-containing heterocyclic moiety, can be found in various therapeutically used compounds playing a vital role in treating many diseases. Many efforts have been given so far on the development of target-based benzimidazole derivatives, and the interest to produce new therapeutically active agents to treat different diseased conditions has grown noticeably during the last few years. However, this field has several challenges, especially to bring the numerous synthesized compounds into the clinical trial, which showed valuable pharmacological properties in different studies, and later to ensure their availability in the market and clinical practice. The present review has focused on the current status of benzimidazole moiety, emphasizing the SAR of different benzimidazole-based compounds explored by scientists around the world. So far this is the most inclusive and informative account about biological and therapeutic potential of benzimidazole derivatives. With a compilation of information from more than 250 latest pieces of literature, we aimed to aid the researchers, medicinal chemists, and drug designers with valuable and comprehensive knowledge and provide them the rationale to develop target-oriented and clinically useful benzimidazole-based molecules.

AUTHOR CONTRIBUTIONS

SMAR and SRB developed the idea of the article, SRB and MJH performed the literature search and data analysis. SRB and MJH wrote the original draft of the manuscript. MJH, MUK, MRIF, HO, and SMAR critically revised the work. All authors reviewed and approved the final manuscript.

FUNDING

This work was supported by the Research Universiti Grant, Universiti Kebangsaan Malaysia, Geran Universiti Penyelidikan (GUP), code: 2021-074.

REFERENCES

Abbhi, V., Saini, L., Mishra, S., Sethi, G., Kumar, A. P., and Piplani, P. (2017). Design and Synthesis of Benzimidazole-Based Rho Kinase Inhibitors for the Treatment of Glaucoma. *Bioorg. Med. Chem.* 25, 6071–6085. doi:10.1016/J.BMC.2017.09.045

Abd El-All, A. S., Magd-El-Din, A. A., Ragab, F. A., ElHefnawi, M., Abdalla, M. M., Galal, S. A., et al. (2015). New Benzimidazoles and Their Antitumor Effects with Aurora A Kinase and KSP Inhibitory Activities. *Arch. Pharm. (Weinheim)* 348, 475–486. doi:10.1002/ardp.201400441

Abdel-Motaal, M., Almohawes, K., and Tantawy, M. A. (2020). Antimicrobial Evaluation and Docking Study of Some New Substituted Benzimidazole-2yl Derivatives. *Bioorg. Chem.* 101, 103972. doi:10.1016/j.bioorg.2020.103972

Abdelgawad, M. A., Bakr, R. B., Ahmad, W., Al-Sanea, M. M., and Elshemy, H. A. H. (2019). New Pyrimidine-Benzoxazole/benzimidazole Hybrids: Synthesis, Antioxidant, Cytotoxic Activity, In Vitro Cyclooxygenase and Phospholipase A2-V Inhibition. *Bioorg. Chem.* 92, 103218. doi:10.1016/j.bioorg.2019.103218

Abou-Seri, S. M., Abouzid, K., and Abou El Ella, D. A. (2011). Molecular Modeling Study and Synthesis of Quinazolinone-Arylpiperazine Derivatives as α1-adrenoreceptor Antagonists. *Eur. J. Med. Chem.* 46, 647–658. doi:10.1016/J.EJMECH.2010.11.045

Abu-Bakr, S. M., Bassyouni, F. A., and Rehim, M. A. (2012). Pharmacological Evaluation of Benzimidazole Derivatives with Potential Antiviral and Antitumor Activity. *Res. Chem. Intermed.* 38, 2523–2545. doi:10.1007/s11164-012-0569-y

Acar Çevik, U., Kaya Çavuşoğlu, B., Sağlık, B. N., Osmaniye, D., Levent, S., Ilgın, S., et al. (2020). Synthesis, Docking Studies and Biological Activity of New Benzimidazole- Triazolothiadiazine Derivatives as Aromatase Inhibitor. *Molecules* 25, 1642. doi:10.3390/molecules25071642

Acar Çevik, U., Sağlık, B. N., Korkut, B., Özkay, Y., and Ilgın, S. (2018). Antiproliferative, Cytotoxic, and Apoptotic Effects of New Benzimidazole Derivatives Bearing Hydrazone Moiety. *J. Heterocyclic Chem.* 55, 138–148. doi:10.1002/jhet.3016

Adak, V. S., Awate, P. B., Bhagat, V. C., Bodake, V. S., Kardile, D. P., Kilaje, S. V., et al. (2018). *Process of Synthesis of Benzimidazole Derivatives against M.Tb.*

AU2020104192A4 https://patents.google.com/patent/AU2020104192A4/en?oq=AU2020104192A4.

Akhtar, S., Abbas, M., Naeem, K., Faheem, M., Nadeem, H., and Mehmood, A. (2021). Benzimidazole Derivative Ameliorates Opioid-Mediated Tolerance During Anticancer- Induced Neuropathic Pain in Mice. *Anticancer. Agents Med. Chem.* 21, 365–371. doi:10.2174/1871520620999200818155031

Akhtar, W., Khan, M. F., Verma, G., Shaquiquzzaman, M., Rizvi, M. A., Mehdi, S. H., et al. (2017). Therapeutic Evolution of Benzimidazole Derivatives in the Last Quinquennial Period. *Eur. J. Med. Chem.* 126, 705–753. doi:10.1016/J.EJMECH.2016.12.010

Akkoç, S., Tüzün, B., İlhan, İ. Ö., and Akkurt, M. (2020). Investigation of Structural, Spectral, Electronic, and Biological Properties of 1,3-disubstituted Benzimidazole Derivatives. *J. Mol. Struct.* 1219, 128582. doi:10.1016/j.molstruc.2020.128582

AlAjmi, M. F., Hussain, A., Alsalme, A., and Khan, R. A. (2016). In Vivo assessment of Newly Synthesized Achiral Copper(ii) and Zinc(ii) Complexes of a Benzimidazole Derived Scaffold as a Potential Analgesic, Antipyretic and Anti-inflammatory. *RSC Adv.* 6, 19475–19481. doi:10.1039/C5RA25071D

Alaqeel, S. I. (2017). Synthetic Approaches to Benzimidazoles from O-Phenylenediamine: A Literature Review. *J. Saudi Chem. Soc.* 21, 229–237. doi:10.1016/J.JSCS.2016.08.001

Alp, M., Göker, H., Brun, R., and Yildiz, S. (2009). Synthesis and Antiparasitic and Antifungal Evaluation of 2'-arylsubstituted-1H,1'H-[2,5']bisbenzimidazolyl-5-carboxamidines. *Eur. J. Med. Chem.* 44, 2002–2008. doi:10.1016/j.ejmech.2008.10.003

Alpan, A. S., Sarıkaya, G., Çoban, G., Parlar, S., Armagan, G., and Alptüzün, V. (2017). Mannich-Benzimidazole Derivatives as Antioxidant and Anticholinesterase Inhibitors: Synthesis, Biological Evaluations, and Molecular Docking Study. *Arch. Pharm. (Weinheim)* 350, e1600351. doi:10.1002/ardp.201600351

Amine Khodja, I., Boulebd, H., Bensouici, C., and Belfaitah, A. (2020). Design, Synthesis, Biological Evaluation, Molecular Docking, DFT Calculations and In Silico ADME Analysis of (Benz)imidazole-hydrazone Derivatives as Promising Antioxidant, Antifungal, and Anti-acetylcholinesterase Agents. *J. Mol. Struct.* 1218, 128527. doi:10.1016/j.molstruc.2020.128527

Anandarajagopal, K., Tiwari, R. N., Bothara, K. G., Sunilson, J. A. J., Dineshkumar, C., and Promwichit, P. (2010). 2-Mercaptobenzimidazole Derivatives: Synthesis and Anticonvulsant Activity. *Adv. Appl. Sci. Res.* 1, 132–138.

Anastassova, N., Aluani, D., Kostadinov, A., Rangelov, M., Todorova, N., Hristova-Avakumova, N., et al. (2021). Evaluation of the Combined Activity of Benzimidazole Arylhydrazones as New Anti-parkinsonian Agents: Monoamine Oxidase-B Inhibition, Neuroprotection and Oxidative Stress Modulation. *Neural Regen. Res.* 16, 2299–2309. doi:10.4103/1673-5374.309843

Anastassova, N., Yancheva, D., Hristova-Avakumova, N., Hadjimitova, V., Traykov, T., Aluani, D., et al. (2020). New Benzimidazole-Aldehyde Hybrids as Neuroprotectors with Hypochlorite and Superoxide Radical-Scavenging Activity. *Pharmacol. Rep.* 72, 846–856. doi:10.1007/s43440-020-00077-3

Anastassova, N. O., Mavrova, A. T., Yancheva, D. Y., Kondeva-Burdina, M. S., Tzankova, V. I., Stoyanov, S. S., et al. (2018a). Hepatotoxicity and Antioxidant Activity of Some New N,N′-disubstituted Benzimidazole-2-Thiones, Radical Scavenging Mechanism and Structure-Activity Relationship. *Arabian J. Chem.* 11, 353–369. doi:10.1016/J.ARABJC.2016.12.003

Anastassova, N. O., Yancheva, D. Y., Mavrova, A. T., Kondeva-Burdina, M. S., Tzankova, V. I., Hristova-Avakumova, N. G., et al. (2018b). Design, Synthesis, Antioxidant Properties and Mechanism of Action of New N,N′-disubstituted Benzimidazole-2-Thione Hydrazone Derivatives. *J. Mol. Struct.* 1165, 162–176. doi:10.1016/J.MOLSTRUC.2018.03.119

Anguru, M. R., Taduri, A. K., Bhoomireddy, R. D., Jojula, M., and Gunda, S. K. (2017). Novel Drug Targets for *Mycobacterium tuberculosis*: 2-heterostyrylbenzimidazoles as Inhibitors of Cell Wall Protein Synthesis. *Chem. Cent. J.* 11, 68. doi:10.1186/s13065-017-0295-z

Apgar, J. M., Biftu, T., Chen, P., Feng, D., Hicks, J. D., Kekec, A., et al. (2015). *Novel Benzimidazole Tetrahydrofuran Derivatives*. US20150218149A1 https://patents.google.com/patent/US20150218149A1/en?oq=US+20150218149+A1.

Arora, R. K., Kaur, N., Bansal, Y., and Bansal, G. (2014). Novel Coumarin-Benzimidazole Derivatives as Antioxidants and Safer Anti-inflammatory Agents. *Acta Pharm. Sin. B* 4, 368–375. doi:10.1016/J.APSB.2014.07.001

Ashok, D., Gundu, S., Aamate, V. K., and Devulapally, M. G. (2018). Conventional and Microwave-Assisted Synthesis of New Indole-Tethered Benzimidazole-Based 1,2,3-triazoles and Evaluation of Their Antimycobacterial, Antioxidant and Antimicrobial Activities. *Mol. Divers.* 22, 769–778. doi:10.1007/s11030-018-9828-1

Atkinson, S. J., Barker, M. D., Campbell, M., Diallo, H., Douault, C., Garton, N. S., et al. (2015). *2-(azaindol-2-yl)benzimidazoles as Pad4 Inhibitors*. US20150175600A1 https://patents.google.com/patent/US20150175600A1/en?oq=US+20150175600+A1.

Atmaca, H., İlhan, S., Batır, M. B., Pulat, Ç. Ç., Güner, A., and Bektaş, H. (2020). Novel Benzimidazole Derivatives: Synthesis, In Vitro Cytotoxicity, Apoptosis and Cell Cycle Studies. *Chem. Biol. Interact.* 327, 109163. doi:10.1016/j.cbi.2020.109163

Babkov, D. A., Zhukowskaya, O. N., Borisov, A. V., Babkova, V. A., Sokolova, E. V., Brigadirova, A. A., et al. (2019). Towards Multi-Target Antidiabetic Agents: Discovery of Biphenyl-Benzimidazole Conjugates as AMPK Activators. *Bioorg. Med. Chem. Lett.* 29, 2443–2447. doi:10.1016/j.bmcl.2019.07.035

Baig, M. F., Nayak, V. L., Budaganaboyina, P., Mullagiri, K., Sunkari, S., Gour, J., et al. (2018). Synthesis and Biological Evaluation of Imidazo[2,1-B]thiazole-Benzimidazole Conjugates as Microtubule-Targeting Agents. *Bioorg. Chem.* 77, 515–526. doi:10.1016/J.BIOORG.2018.02.005

Baldisserotto, A., Demurtas, M., Lampronti, I., Tacchini, M., Moi, D., Balboni, G., et al. (2020). Synthesis and Evaluation of Antioxidant and Antiproliferative Activity of 2-arylbenzimidazoles. *Bioorg. Chem.* 94, 103396. doi:10.1016/j.bioorg.2019.103396

Bansal, Y., and Silakari, O. (2012). The Therapeutic Journey of Benzimidazoles: A Review. *Bioorg. Med. Chem.* 20, 6208–6236. doi:10.1016/J.BMC.2012.09.013

Bao, X.-L., Zhu, W.-B., Shan, T.-L., Wu, Z., Zhang, R.-J., Liao, P.-Y., et al. (2017). Design, Synthesis and Evaluation of Novel Angiotensin II Receptor 1 Antagonists with Antihypertensive Activities. *RSC Adv.* 7, 26401–26410. doi:10.1039/C7RA03915H

Bariwal, J. B., Shah, A. K., Kathiravan, M. K., Somani, R. S., Jagtap, J. R., and Jain, K. S. (2008). Synthesis and Antiulcer Activity of Novel Pyrimidylthiomethyl-And Pyrimidylsulfinylmethyl Benzimidazoles as Potential Reversible Proton Pump Inhibitors. *Indian J. Pharm. Educ. Res.* 42, 225–231.

Barot, K. P., Nikolova, S., Ivanov, I., and Ghate, M. D. (2013). Novel Research Strategies of Benzimidazole Derivatives: A Review. *Mini Rev. Med. Chem.* 13, 1421–1447. doi:10.2174/13895757113139990072

Bartberger, M. D., Chakka, N., Gao, H., Guzman-Perez, A., Horne, D. B., Hua, Z., and Cirandur, S. R. (2019). *Benzimidazole Derivatives and Their Uses*. CA3079081A1 https://patents.google.com/patent/CA3079081A1/en?oq=CA3079081A1.

Bellam, M., Gundluru, M., Sarva, S., Chadive, S., Tartte, V., et al. (2017). Synthesis and Antioxidant Activity of Some New N-Alkylated Pyrazole-Containing Benzimidazoles. *Chem. Heterocycl Comp.* 53, 173–178. doi:10.1007/s10593-017-2036-6

Berrebi-Bertrand, I., Billot, X., Calmels, T., Capet, M., Krief, S., Labeeuw, O., et al. (2021). *Benzimidazole Derivatives as Dual Ligands of the Histamine H1 Receptor and the Histamine H4 Receptor*. ES2807191T3 https://patents.google.com/patent/ES2807191T3/en?oq=ES2807191T3.

Bezabeh, S., Mackey, A. C., Kluetz, P., Jappar, D., and Korvick, J. (2012). Accumulating Evidence for a Drug-Drug Interaction between Methotrexate and Proton Pump Inhibitors. *Oncologist* 17, 550–554. doi:10.1634/theoncologist.2011-0431

Bhambra, A. S., Edgar, M., Elsegood, M. R. J., Horsburgh, L., Kryštof, V., Lucas, P. D., et al. (2016). Novel Fluorinated Benzimidazole-Based Scaffolds and Their Anticancer Activity In Vitro. *J. Fluorine Chem.* 188, 99–109. doi:10.1016/J.JFLUCHEM.2016.06.009

Bharadwaj, S. S., Poojary, B., Nandish, S. K. M., Kengaiah, J., Kirana, M. P., Shankar, M. K., et al. (2018). Efficient Synthesis and In Silico Studies of the Benzimidazole Hybrid Scaffold with the Quinolinyloxadiazole Skeleton with Potential α-Glucosidase Inhibitory, Anticoagulant, and Antiplatelet Activities for Type-II Diabetes Mellitus Management and Treating Thrombotic Disorders. *ACS Omega* 3, 12562–12574. doi:10.1021/acsomega.8b01476

Bhrigu, B., Siddiqui, N., Pathak, D., Alam, M. S., Ali, R., and Azad, B. (2012). Anticonvulsant Evaluation of Some Newer Benzimidazole Derivatives: Design and Synthesis. *Acta Pol. Pharm.* 69, 53–62.

Birajdar, S. S., Hatnapure, G. D., Keche, A. P., and Kamble, V. M. (2013). Synthesis and Biological Evaluation of Amino Alcohol Derivatives of 2-methylbenzimidazole as Antitubercular and Antibacterial Agents. *J. Chem. Pharm. Res.* 5, 583–589.

Birch, A. M., Buckett, L. K., and Turnbull, A. V. (2010). DGAT1 Inhibitors as Anti-obesity and Anti-diabetic Agents. *Curr. Opin. Drug Discov. Devel.* 13, 489–496.

Bourque, E. M. J., and Skerlj, R. (2019). *Cxcr4 Inhibitors and Uses Thereof*. US20190322671A1 https://patents.google.com/patent/US20190322671A1/en?oq=US20190322671A1.

Bramhananda Reddy, N., Burra, V. R., Ravindranath, L. K., Naresh Kumar, V., Sreenivasulu, R., and Sadanandam, P. (2016). Synthesis and Biological Evaluation of Benzimidazole Fused Ellipticine Derivatives as Anticancer Agents. *Monatsh Chem.* 147, 599–604. doi:10.1007/s00706-016-1684-z

Brink, N. G., and Folkers, K. (1949). Vitamin B12. Vi. 5,6-Dimethylbenzimidazole, A Degradation Product of Vitamin B12. *J. Am. Chem. Soc.* 71, 2951. doi:10.1021/ja01176a532

Brishty, S. R., Saha, P., Mahmud, Z. A., and Rahman, S. A. (2020). Synthesis and Evaluation of Analgesic and Antioxidant Activities of Substituted Benzimidazole Derivatives. *Dhaka Univ. J. Pharm. Sci.* 19, 37–46. doi:10.3329/dujps.v19i1.47817

Brown, S. D., and Matthews, D. J. (2015). *(alpha-substituted Aralkylamino and Heteroarylalkylamino) Pyrimidinyl and 1,3,5-triazinyl Benzimidazoles, Pharmaceutical Compositions Thereof, and Their Use in Treating Proliferative Diseases*. US20150265625A1 https://patents.google.com/patent/US20150265625A1/en?oq=US+20150265625+A1.

Bukhari, S. N., Lauro, G., Jantan, I., Fei Chee, C., Amjad, M. W., Bifulco, G., et al. (2016). Anti-inflammatory Trends of New Benzimidazole Derivatives. *Future Med. Chem.* 8, 1953–1967. doi:10.4155/fmc-2016-0062

Błaszczak-Świątkiewicz, K., Olszewska, P., and Mikiciuk-Olasik, E. (2014). Biological Approach of Anticancer Activity of New Benzimidazole Derivatives. *Pharmacol. Rep.* 66, 100–106. doi:10.1016/J.PHAREP.2014.01.001

Camacho, J., Barazarte, A., Gamboa, N., Rodrigues, J., Rojas, R., Vaisberg, A., et al. (2011). Synthesis and Biological Evaluation of Benzimidazole-5-Carbohydrazide Derivatives as Antimalarial, Cytotoxic and Antitubercular Agents. *Bioorg. Med. Chem.* 19, 2023–2029. doi:10.1016/j.bmc.2011.01.050

Caymaz, B., Yıldız, U., Akkoç, S., Gerçek, Z., Şengül, A., and Coban, B. (2020). Synthesis, Characterization, and Antiproliferative Activity Studies of Novel Benzimidazole-Imidazopyridine Hybrids as DNA Groove Binders. *ChemistrySelect* 5, 8465–8474. doi:10.1002/slct.202001580

Chandrasekhar, J., Perreault, S., Patel, L., Phillips, G., Till, N. A., and Treiberg, J. A. (2018). *Benzimidazole Derivatives and Their Use as Phosphatidylinositol 3-kinase Inhibitors*. WO2018057810A1 https://patents.google.com/patent/WO2018057810A1/en?oq=WO2018057810A1.

Chandrika, N. T., Shrestha, S. K., Ngo, H. X., and Garneau-Tsodikova, S. (2016). Synthesis and Investigation of Novel Benzimidazole Derivatives as Antifungal Agents. *Bioorg. Med. Chem.* 24, 3680–3686. doi:10.1016/j.bmc.2016.06.010

Chang, C. S., Liu, J. F., Lin, H. J., Lin, C. D., Tang, C. H., Lu, D. Y., et al. (2012). Synthesis and Bioevaluation of Novel 3,4,5-trimethoxybenzylbenzimidazole Derivatives that Inhibit Helicobacter Pylori-Induced Pathogenesis in Human Gastric Epithelial Cells. *Eur. J. Med. Chem.* 48, 244–254. doi:10.1016/j.ejmech.2011.12.021

Chang, Y., Hsu, W. H., Yang, W. B., Jayakumar, T., Lee, T. Y., Sheu, J. R., et al. (2017). Structure-activity Relationship of Three Synthesized Benzimidazole-Based Oligosaccharides in Human Platelet Activation. *Int. J. Mol. Med.* 40, 1520–1528. doi:10.3892/IJMM.2017.3133

Chappie, T. A., Verhoest, P. R., Patel, N. C., and Hayward, M. M. (2015). *Azabenzimidazole Compounds*. US20150322065A1 https://patents.google.com/patent/US20150322065A1/en?oq=US+20150322065+A1.

Chen, X., Yang, X., Mao, F., Wei, J., Xu, Y., Li, B., et al. (2021). Development of Novel Benzimidazole-Derived Neddylation Inhibitors for Suppressing Tumor Growth Invitro and Invivo. *Eur. J. Med. Chem.* 210, 112964. doi:10.1016/j.ejmech.2020.112964

Cheong, J. E., Zaffagni, M., Chung, I., Xu, Y., Wang, Y., Jernigan, F. E., et al. (2018). Synthesis and Anticancer Activity of Novel Water Soluble Benzimidazole Carbamates. *Eur. J. Med. Chem.* 144, 372–385. doi:10.1016/J.EJMECH.2017.11.037

Chikkula, K. V., and Sundararajan, R. (2017). Analgesic, Anti-inflammatory, and Antimicrobial Activities of Novel Isoxazole/pyrimidine/pyrazole Substituted Benzimidazole Analogs. *Med. Chem. Res.* 26, 3026–3037. doi:10.1007/s00044-017-2000-0

Chojnacki, K., Wińska, P., Skierka, K., Wielechowska, M., and Bretner, M. (2017). Synthesis, In Vitro Antiproliferative Activity and Kinase Profile of New Benzimidazole and Benzotriazole Derivatives. *Bioorg. Chem.* 72, 1–10. doi:10.1016/J.BIOORG.2017.02.017

Crew, A. P., Crews, C. M., Dong, H., Hornberger, K. R., Jaime-Figueroa, S., Qian, Y., et al. (2021). *Compounds and Methods for the Targeted Degradation of Rapidly Accelerated Fibrosarcoma Polypeptides*. AU2017382436A1 https://patents.google.com/patent/AU2017382436A1/en?oq=AU2017382436A1.

Czardybon, W., Brzózka, K., Galezowski, M., Windak, R., Milik, M., Zawadzka, M., et al. (2015). *Novel Benzimidazole Derivatives as Kinase Inhibitors*. US20150336967A1 https://patents.google.com/patent/US20150336967A1/en?oq=US+20150336967+A1.

Dai, D., Burgeson, J. R., Gharaibeh, D. N., Moore, A. L., Larson, R. A., Cerruti, N. R., et al. (2013). Discovery and Optimization of Potent Broad-Spectrum Arenavirus Inhibitors Derived from Benzimidazole. *Bioorg. Med. Chem. Lett.* 23, 744–749. doi:10.1016/J.BMCL.2012.11.095

Datani, R. H., Kini, S. G., and Mubeen, M. (2012). Design, Synthesis and Vasorelaxant Activity of 5-Nitro Benzimidazole Derivatives. *J. Comput. Methods Mol. Des.* 2, 149–157.

Datar, P. A., and Limaye, S. A. (2015). Design and Synthesis of Mannich Bases as Benzimidazole Derivatives as Analgesic Agents. *Antiinflamm. Antiallergy. Agents Med. Chem.* 14, 35–46. doi:10.2174/1871523014666150312164625

De Clercq, E. (2019). New Nucleoside Analogues for the Treatment of Hemorrhagic Fever Virus Infections. *Chem. Asian J.* 14, 3962–3968. doi:10.1002/asia.201900841

De Luca, L., Ferro, S., Buemi, M. R., Monforte, A. M., Gitto, R., Schirmeister, T., et al. (2018). Discovery of Benzimidazole-Based Leishmania Mexicana Cysteine Protease CPB2.8ΔCTE Inhibitors as Potential Therapeutics for Leishmaniasis. *Chem. Biol. Drug Des.* 92 (3), 1585–1596. doi:10.1111/cbdd.13326

Desai, N. C., Pandya, D., and Vaja, D. (2018). Synthesis and Antimicrobial Activity of Some Heterocyclic Compounds Bearing Benzimidazole and Pyrazoline Motifs. *Med. Chem. Res.* 27, 52–60. doi:10.1007/s00044-017-2040-5

Desai, N. C., Shihory, N. R., and Kotadiya, G. M. (2014). Facile Synthesis of Benzimidazole Bearing 2-pyridone Derivatives as Potential Antimicrobial Agents. *Chin. Chem. Lett.* 25, 305–307. doi:10.1016/J.CCLET.2013.11.026

Dhanamjayulu, P., Boga, R. B., and Mehta, A. (2019). Inhibition of Aflatoxin B1 Biosynthesis and Down Regulation of aflR and aflB Genes in Presence of Benzimidazole Derivatives without Impairing the Growth of Aspergillus flavus. *Toxicon* 170, 60–67. doi:10.1016/j.toxicon.2019.09.018

Dittmer, A., Woskobojnik, I., Adfeldt, R., Drach, J. C., Townsend, L. B., Voigt, S., et al. (2017). Tetrahalogenated Benzimidazole D-Ribonucleosides Are Active against Rat Cytomegalovirus. *Antivir. Res* 137, 102–107. doi:10.1016/J.ANTIVIRAL.2016.11.012

Djemoui, A., Naouri, A., Ouahrani, M. R., Djemoui, D., Lahcene, S., Lahrech, M. B., et al. (2020). A Step-by-step Synthesis of Triazole-Benzimidazole-Chalcone Hybrids: Anticancer Activity in Human Cells+. *J. Mol. Struct.* 1204, 127487. doi:10.1016/j.molstruc.2019.127487

Dokla, E. M. E., Abutaleb, N. S., Milik, S. N., Li, D., El-Baz, K., Shalaby, M. W., et al. (2020). Development of Benzimidazole-Based Derivatives as Antimicrobial Agents and Their Synergistic Effect with Colistin against Gram-Negative Bacteria. *Eur. J. Med. Chem.* 186, 111850. doi:10.1016/j.ejmech.2019.111850

El-Gohary, N. S., and Shaaban, M. I. (2017). Synthesis and Biological Evaluation of a New Series of Benzimidazole Derivatives as Antimicrobial, Antiquorum-Sensing and Antitumor Agents. *Eur. J. Med. Chem.* 131, 255–262. doi:10.1016/j.ejmech.2017.03.018

El-Meguid, E. A. A., El-Deen, E. M. M., Nael, M. A., and Anwar, M. M. (2020). Novel Benzimidazole Derivatives as Anti-cervical Cancer Agents of Potential Multi-Targeting Kinase Inhibitory Activity. *Arabian J. Chem.* 13, 9179–9195. doi:10.1016/j.arabjc.2020.10.041

Emerson, G., Brink, N. G., Holly, F. W., Koniuszy, F., Heyl, D., and Folkers, K. (1950). Vitamin B12. VIII. Vitamin B12-like Activity of 5,6-Dimethylbenzimidazole and Tests on Related Compounds. *J. Am. Chem. Soc.* 72, 3084–3085. doi:10.1021/ja01163a078

Espinosa-Bustos, C., Lagos, C. F., Romero-Parra, J., Zárate, A. M., Mella-Raipán, J., Pessoa-Mahana, H., et al. (2015). Design, Synthesis, Biological Evaluation and Binding Mode Modeling of Benzimidazole Derivatives Targeting the

Cannabinoid Receptor Type 1. *Arch. Pharm. (Weinheim)* 348, 81–88. doi:10.1002/ardp.201400201

Eswayah, A., Khaliel, S., Saad, S., Shebani, N., Fhid, O., Belaid, A., et al. (2017). Synthesis and Analgesic Activity Evaluation of Some New Benzimidazole Derivatives. *Am. J. Chem. Appl.* 4, 30–35.

Fang, Y., Zhou, H., Gu, Q., and Xu, J. (2019). Synthesis and Evaluation of Tetrahydroisoquinoline-Benzimidazole Hybrids as Multifunctional Agents for the Treatment of Alzheimer's Disease. *Eur. J. Med. Chem.* 167, 133–145. doi:10.1016/j.ejmech.2019.02.008

Farahat, A. A., Ismail, M. A., Kumar, A., Wenzler, T., Brun, R., Paul, A., et al. (2018). Indole and Benzimidazole Bichalcophenes: Synthesis, DNA Binding and Antiparasitic Activity. *Eur. J. Med. Chem.* 143, 1590–1596. doi:10.1016/J.EJMECH.2017.10.056

Faraji, L., Shahkarami, S., Nadri, H., Moradi, A., Saeedi, M., Foroumadi, A., et al. (2017). Synthesis of Novel Benzimidazole and Benzothiazole Derivatives Bearing a 1,2,3-triazole Ring System and Their Acetylcholinesterase Inhibitory Activity. *J. Chem. Res.* 41, 30–35. doi:10.3184/174751917X14836231670980

Fei, F., and Zhou, Z. (2013). New Substituted Benzimidazole Derivatives: a Patent Review (2010 - 2012). *Expert Opin. Ther. Pat.* 23, 1157–1179. doi:10.1517/13543776.2013.800857

Ferro, S., Buemi, M. R., De Luca, L., Agharbaoui, F. E., Pannecouque, C., and Monforte, A. M. (2017). Searching for Novel N1-Substituted Benzimidazol-2-Ones as Non-nucleoside HIV-1 RT Inhibitors. *Bioorg. Med. Chem.* 25, 3861–3870. doi:10.1016/J.BMC.2017.05.040

Fjellaksel, R., Boomgaren, M., Sundset, R., Haraldsen, I. H., Hansen, J. H., and Riss, P. J. (2017). Small Molecule Piperazinyl-Benzimidazole Antagonists of the Gonadotropin-Releasing Hormone (GnRH) Receptor. *Medchemcomm* 8, 1965–1969. doi:10.1039/C7MD00320J

Flores-Carrillo, P., Velázquez-López, J. M., Aguayo-Ortiz, R., Hernández-Campos, A., Trejo-Soto, P. J., Yépez-Mulia, L., et al. (2017). Synthesis, Antiprotozoal Activity, and Chemoinformatic Analysis of 2-(methylthio)-1h-Benzimidazole-5-Carboxamide Derivatives: Identification of New Selective Giardicidal and Trichomonicidal Compounds. *Eur. J. Med. Chem.* 137, 211–220. doi:10.1016/J.EJMECH.2017.05.058

Gaba, M., and Mohan, C. (2015). Design, Synthesis and Biological Evaluation of Novel 1, 2, 5-Substituted Benzimidazole Derivatives as Gastroprotective Anti-inflammatory and Analgesic Agents. *Med. Chem.* 5, 58–63. doi:10.4172/2161-0444.1000243

Gobis, K., Foks, H., Suchan, K., Augustynowicz-Kopeć, E., Napiórkowska, A., and Bojanowski, K. (2015). Novel 2-(2-Phenalkyl)-1h-Benzo[d]imidazoles as Antitubercular Agents. Synthesis, Biological Evaluation and Structure-Activity Relationship. *Bioorg. Med. Chem.* 23 (9), 2112–2120. doi:10.1016/j.bmc.2015.03.008

Gurjar, A. S., Solanki, V. S., Meshram, A. R., and Vishwakarma, S. S. (2020). Exploring Beta Amyloid Cleavage Enzyme-1 Inhibition and Neuroprotective Role of Benzimidazole Analogues as Anti-alzheimer Agents. *J. Chin. Chem. Soc.* 67, 864–873. doi:10.1002/jccs.201900200

Hamaguchi, W., Masuda, N., Isomura, M., Miyamoto, S., Kikuchi, S., Amano, Y., et al. (2013). Design and Synthesis of Novel Benzimidazole Derivatives as Phosphodiesterase 10A Inhibitors with Reduced CYP1A2 Inhibition. *Bioorg. Med. Chem.* 21, 7612–7623. doi:10.1016/j.bmc.2013.10.035

Hameed, P. S., Chinnapattu, M., Shanbag, G., Manjrekar, P., Koushik, K., Raichurkar, A., et al. (2014). Aminoazabenzimidazoles, a Novel Class of Orally Active Antimalarial Agents. *J. Med. Chem.* 57, 5702–5713. doi:10.1021/jm500535j

Hao, L.-P., Xue, W.-Z., Han, X.-F., He, X., Zhang, J., and Zhou, Z.-M. (2015). Design, Synthesis and Biological Activity of 4′-[(benzimidazol-1-Yl) methyl]biphenyl-2-Sulphonamides as Dual Angiotensin II and Endothelin A Receptor Antagonists. *Med. Chem. Commun.* 6, 715–718. doi:10.1039/C4MD00499J

Harika, M. S., Bhargavi, S., Renukadevi, V., Karishma, S., Abbinaya, L., Ramya, L., et al. (2017). Synthesis and Pharmacological Screening of New Benzimidazole Derivatives. *Indian J. Heterocycl. Chem.* 27, 217–221.

Hauel, N. H., Nar, H., Priepke, H., Ries, U., Stassen, J. M., and Wienen, W. (2002). Structure-Based Design of Novel Potent Nonpeptide Thrombin Inhibitors. *J. Med. Chem.* 45, 1757–1766. doi:10.1021/jm0109513

He, X., Lakkaraju, S. K., Hanscom, M., Zhao, Z., Wu, J., Stoica, B., et al. (2015). Acyl-2-aminobenzimidazoles: A Novel Class of Neuroprotective Agents Targeting mGluR5. *Bioorg. Med. Chem.* 23, 2211–2220. doi:10.1016/J.BMC.2015.02.054

Henderson, J. A., Bilimoria, D., Bubenik, M., Cadilhac, C., Cottrell, K. M., Dietrich, E., et al. (2015). Benzimidazole-containing HCV NS5A Inhibitors: Effect of 4-substituted Pyrrolidines in Balancing Genotype 1a and 1b Potency. *Bioorg. Med. Chem. Lett.* 25, 944–947. doi:10.1016/J.BMCL.2014.12.045

Hernández-Luis, F., Hernández-Campos, A., Castillo, R., Navarrete-Vázquez, G., Soria-Arteche, O., Hernández-Hernández, M., et al. (2010). Synthesis and Biological Activity of 2-(trifluoromethyl)-1h-Benzimidazole Derivatives against Some Protozoa and *Trichinella spiralis*. *Eur. J. Med. Chem.* 45, 3135–3141. doi:10.1016/j.ejmech.2010.03.050

Hernández-Núñez, E., Tlahuext, H., Moo-Puc, R., Moreno, D., González-Díaz, M. O., Vázquez, G. N., et al. (2017). Design, Synthesis and Biological Evaluation of 2-(2-Amino-5(6)-nitro-1H-benzimidazol-1-yl)-N-arylacetamides as Antiprotozoal Agents. *Molecules* 22, 579. doi:10.3390/molecules22040579

Hossain, M. J., Sultan, M. Z., Rashid, M. A., and Kuddus, M. R. (2020). Does Rabeprazole Sodium Alleviate the Anti-diabetic Activity of Linagliptin? Drug-Drug Interaction Analysis by In Vitro and In Vivo Methods. *Drug Res. (Stuttg)* 70, 519–527. doi:10.1055/a-1233-3371

Hossain, M. J., Sultan, M. Z., Rashid, M. A., and Kuddus, M. R. (2021). Interactions of Linagliptin, Rabeprazole Sodium, and Their Formed Complex with Bovine Serum Albumin: Computational Docking and Fluorescence Spectroscopic Methods. *Anal. Sci. Adv.* 7, 202000153. doi:10.1002/ansa.202000153

Hsieh, C. Y., Ko, P. W., Chang, Y. J., Kapoor, M., Liang, Y. C., Lin, H. H., et al. (2019). Design and Synthesis of Benzimidazole-Chalcone Derivatives as Potential Anticancer Agents. *Molecules* 24, 3259. doi:10.3390/molecules24183259

Hu, E., Kunz, R. K., Chen, N., Rumfelt, S., Siegmund, A., Andrews, K., et al. (2013). Design, Optimization, and Biological Evaluation of Novel Keto-Benzimidazoles as Potent and Selective Inhibitors of Phosphodiesterase 10A (PDE10A). *J. Med. Chem.* 56, 8781–8792. doi:10.1021/jm401234w

Ibrahim, H. A., Awadallah, F. M., Refaat, H. M., and Amin, K. M. (2018). Molecular Docking Simulation, Synthesis and 3D Pharmacophore Studies of Novel 2-substituted-5-nitro-benzimidazole Derivatives as Anticancer Agents Targeting VEGFR-2 and C-Met. *Bioorg. Chem.* 77, 457–470. doi:10.1016/J.BIOORG.2018.01.014

Idris, Z., Abbas, M., Nadeem, H., and Khan, A. U. (2019). The Benzimidazole Derivatives, B1 (N-[(1H-Benzimidazol-2-yl)Methyl]-4-Methoxyaniline) and B8 (N-{4-[(1H-Benzimidazol-2-yl)Methoxy]Phenyl}Acetamide) Attenuate Morphine-Induced Paradoxical Pain in Mice. *Front. Neurosci.* 13, 101. doi:10.3389/FNINS.2019.00101

Igawa, H., Takahashi, M., Shirasaki, M., Kakegawa, K., Kina, A., Ikoma, M., et al. (2016). Amine-free Melanin-Concentrating Hormone Receptor 1 Antagonists: Novel 1-(1h-Benzimidazol-6-Yl)pyridin-2(1h)-One Derivatives and Design to Avoid CYP3A4 Time-dependent Inhibition. *Bioorg. Med. Chem.* 24, 2486–2503. doi:10.1016/j.bmc.2016.04.011

Ishikawa, M., Nonoshita, K., Ogino, Y., Nagae, Y., Tsukahara, D., Hosaka, H., et al. (2009). Discovery of Novel 2-(pyridine-2-Yl)-1h-Benzimidazole Derivatives as Potent Glucokinase Activators. *Bioorg. Med. Chem. Lett.* 19, 4450–4454. doi:10.1016/j.bmcl.2009.05.038

İbişoğlu, H., Erdemir, E., Atilla, D., Şahin Ün, Ş., Topçu, S., and Gül Şeker, M. (2020). Synthesis, Characterization and Antimicrobial Properties of Cyclotriphosphazenes Bearing Benzimidazolyl Rings. *Inorg. Chim. Acta* 509, 119679. doi:10.1016/j.ica.2020.119679

Jain, P., Sharma, P. K., Rajak, H., Pawar, R. S., Patil, U. K., and Singour, P. K. (2010). Design, Synthesis and Biological Evaluation of Some Novel Benzimidazole Derivatives for Their Potential Anticonvulsant Activity. *Arch. Pharm. Res.* 33, 971–980. doi:10.1007/s12272-010-0701-8

Kacar, S., Unver, H., and Sahinturk, V. (2020). A Mononuclear Copper(II) Complex Containing Benzimidazole and Pyridyl Ligands: Synthesis, Characterization, and Antiproliferative Activity against Human Cancer Cells. *Arabian J. Chem.* 13, 4310–4323. doi:10.1016/j.arabjc.2019.08.002

Kahveci, B., Yılmaz, F., Menteşe, E., Özil, M., and Karaoğlu, Ş. A. (2014). Microwave-Assisted Synthesis of Some Novel Benzimidazole Derivatives

Containing Imine Function and Evaluation of Their Antimicrobial Activity. *J. Heterocyclic Chem.* 51, 982–990. doi:10.1002/jhet.1593

Kalalbandi, V. K. A., and Seetharamappa, J. (2015). 1-[(2E)-3-Phenylprop-2-enoyl]-1H-benzimidazoles as Anticancer Agents: Synthesis, Crystal Structure Analysis and Binding Studies of the Most Potent Anticancer Molecule with Serum Albumin. *Med. Chem. Commun.* 6, 1942–1953. doi:10.1039/C5MD00293A

Kanwal, A., Ullah, S., Ahmad, M., Pelletier, J., Aslam, S., Sultan, S., et al. (2020). Synthesis and Nucleotide Pyrophosphatase/Phosphodiesterase Inhibition Studies of Carbohydrazides Based on Benzimidazole-Benzothiazine Skeleton. *ChemistrySelect* 5, 14399–14407. doi:10.1002/slct.202003479

Kapil, S., Singh, P. K., Kashyap, A., and Silakari, O. (2019). Structure Based Designing of Benzimidazole/benzoxazole Derivatives as Anti-leishmanial Agents. *SAR QSAR Environ. Res.* 30, 919–933. doi:10.1080/1062936X.2019.1684357

Karaali, N., Baltaş, N., and Menteşe, E. (2018). Synthesis and Antioxidant, Antiurease and Anti-xanthine Oxidase Activities of Some New Benzimidazoles Bearing Triazole, Oxadiazole, Thiadiazole and Imin Function. *Indian J. Chem. - Sect. B Org. Med. Chem.* 57, 374–384.

Karatas, M. O., Alici, B., Çetinkaya, E., Bilen, C., Gençer, N., and Arslan, O. (2014). Synthesis, Characterization, and Tyrosinase Inhibitory Properties of Benzimidazole Derivatives. *Bioorg. Khim* 40, 497–502. doi:10.1134/S1068162014040049

Kathrotiya, H. G., and Patel, M. P. (2013). An Efficient Synthesis of 3′-indolyl Substituted Pyrido[1,2-A]benzimidazoles as Potential Antimicrobial and Antioxidant Agents. *J. Chem. Sci.* 125, 993–1001. doi:10.1007/s12039-013-0468-9

Keri, R. S., Hiremathad, A., Budagumpi, S., and Nagaraja, B. M. (2015). Comprehensive Review in Current Developments of Benzimidazole-Based Medicinal Chemistry. *Chem. Biol. Drug Des.* 86, 19–65. doi:10.1111/cbdd.12462

Keurulainen, L., Siiskonen, A., Nasereddin, A., Kopelyanskiy, D., Sacerdoti-Sierra, N., Leino, T. O., et al. (2015). Synthesis and Biological Evaluation of 2-arylbenzimidazoles Targeting Leishmania Donovani. *Bioorg. Med. Chem. Lett.* 25, 1933–1937. doi:10.1016/j.bmcl.2015.03.027

Khan, K. M., Shah, Z., Ahmad, V. U., Ambreen, N., Khan, M., Taha, M., et al. (2012). 6-Nitrobenzimidazole Derivatives: Potential Phosphodiesterase Inhibitors: Synthesis and Structure-Activity Relationship. *Bioorg. Med. Chem.* 20, 1521–1526. doi:10.1016/J.BMC.2011.12.041

Khan, M. T., Razi, M. T., Jan, S. U., Mukhtiar, M., Gul, R., IzharUllah, S., et al. (2018). Synthesis, Characterization and Antihypertensive Activity of 2-phenyl Substituted Benzimidazoles. *Pak. J. Pharm. Sci.* 31, 1067–1074.

Kharitonova, M. I., Denisova, A. O., Andronova, V. L., Kayushin, A. L., Konstantinova, I. D., Kotovskaya, S. K., et al. (2017). New Modified 2-aminobenzimidazole Nucleosides: Synthesis and Evaluation of Their Activity against Herpes Simplex Virus Type 1. *Bioorg. Med. Chem. Lett.* 27, 2484–2487. doi:10.1016/J.BMCL.2017.03.100

Kharitonova, M., Antonov, K., Fateev, I., Berzina, M., Kaushin, A., Paramonov, A., et al. (2016). Chemoenzymatic Synthesis of Modified 2′-Deoxy-2′-Fluoro-β-D-Arabinofuranosyl Benzimidazoles and Evaluation of Their Activity against Herpes Simplex Virus Type 1. *Synthesis* 49, 1043–1052. doi:10.1055/s-0036-1588625

Kim, M. H., Lee, J., Jung, K., Kim, M., Park, Y. J., Ahn, H., et al. (2013). Syntheses and Biological Evaluation of 1-Heteroaryl-2-Aryl-1h-Benzimidazole Derivatives as C-Jun N-Terminal Kinase Inhibitors with Neuroprotective Effects. *Bioorg. Med. Chem.* 21, 2271–2285. doi:10.1016/J.BMC.2013.02.021

Kojima, T., Mochizuki, M., Takai, T., Hoashi, Y., Morimoto, S., Seto, M., et al. (2018). Discovery of 1,2,3,4-Tetrahydropyrimido[1,2-A]benzimidazoles as Novel Class of Corticotropin Releasing Factor 1 Receptor Antagonists. *Bioorg. Med. Chem.* 26, 2229–2250. doi:10.1016/J.BMC.2018.01.020

Kolaczkowski, L. (2013). *2-{(R)-2-methylpyrrolidin-2-yl)-1H-benzimidazole-4-carboxamide Crystalline Form 1*. US8372987B2 https://patents.google.com/patent/US8372987B2/en?oq=US8372987+B2.

Kuduk, S. D., McComas, C. C., and Reger, T. S. (2015). *Cyclobutyl Benzimidazoles as Pde 10 Inhibitors*. US20150307479A1 https://patents.google.com/patent/US20150307479A1/en?oq=US+20150307479+A1.

Kumar, A., Banerjee, S., Roy, P., Sondhi, S. M., and Sharma, A. (2018). Solvent-free Synthesis and Anticancer Activity Evaluation of Benzimidazole and Perimidine Derivatives. *Mol. Divers.* 22, 113–127. doi:10.1007/s11030-017-9790-3

Kumar, N., Sharma, C. S., Ranawat, M. S., Singh, H. P., Chauhan, L. S., and Dashora, N. (2015). Synthesis, Analgesic and Anti-inflammatory Activities of Novel Mannich Bases of Benzimidazoles. *J. Pharm. Invest.* 45, 65–71. doi:10.1007/s40005-014-0145-0

Kumbhar, S. S., Choudhari, P. B., and Bhatia, M. S. (2017). 3D QSAR and Pharmacophore Modelling of Selected Benzimidazole Derivatives as Factor IXa Inhibitors. *pharmaceutical-sciences* 79, 813–819. doi:10.4172/pharmaceutical-sciences.1000295

Kusumoto, K., Igata, H., Ojima, M., Tsuboi, A., Imanishi, M., Yamaguchi, F., et al. (2011). Antihypertensive, Insulin-Sensitising and Renoprotective Effects of a Novel, Potent and Long-Acting Angiotensin II Type 1 Receptor Blocker, Azilsartan Medoxomil, in Rat and Dog Models. *Eur. J. Pharmacol.* 669, 84–93. doi:10.1016/J.EJPHAR.2011.07.014

Kwak, H. J., Pyun, Y. M., Kim, J. Y., Pagire, H. S., Kim, K. Y., Kim, K. R., et al. (2013). Synthesis and Biological Evaluation of Aminobenzimidazole Derivatives with a Phenylcyclohexyl Acetic Acid Group as Anti-obesity and Anti-diabetic Agents. *Bioorg. Med. Chem. Lett.* 23, 4713–4718. doi:10.1016/J.BMCL.2013.05.081

Lamotte, Y., Faucher, N., Sançon, J., Pineau, O., Sautet, S., Fouchet, M. H., et al. (2014). Discovery of Novel Indazole Derivatives as Dual Angiotensin II Antagonists and Partial PPARγ Agonists. *Bioorg. Med. Chem. Lett.* 24, 1098–1103. doi:10.1016/J.BMCL.2014.01.004

Leban, J., and Zaja, M. (2015). *Bifluorodioxalane-amino-benzimidazole Kinase Inhibitors for the Treatment of Cancer, Autoimmuneinflammation and Cns Disorders*. US20150158878A1 https://patents.google.com/patent/US20150158878A1/en?oq=US+20150158878+A1.

Li, Q., Hu, Q., Wang, X., Zong, Y., Zhao, L., Xing, J., et al. (2015). Discovery of Novel 2-(piperidin-4-Yl)-1h-Benzo[d]imidazole Derivatives as Potential Anti-inflammatory Agents. *Chem. Biol. Drug Des.* 86, 509–516. doi:10.1111/cbdd.12513

Lim, C. J., Kim, J. Y., Lee, B. H., Oh, K.-S., and Yi, K. Y. (2013). 2-Heteroaryl Benzimidazole Derivatives as Melanin Concentrating Hormone Receptor 1 (MCH-R1) Antagonists. *Bull. Korean Chem. Soc.* 34, 2305–2310. doi:10.5012/bkcs.2013.34.8.2305

Liu, H., Wang, Y., Sharma, A., Mao, R., Jiang, N., Dun, B., et al. (2015). Derivatives Containing Both Coumarin and Benzimidazole Potently Induce Caspase-dependent Apoptosis of Cancer Cells through Inhibition of PI3K-AKT-mTOR Signaling. *Anticancer. Drugs* 26, 667–677. doi:10.1097/CAD.0000000000000232

Liu, H. B., Gao, W. W., Tangadanchu, V. K. R., Zhou, C. H., and Geng, R. X. (2018). Novel Aminopyrimidinyl Benzimidazoles as Potentially Antimicrobial Agents: Design, Synthesis and Biological Evaluation. *Eur. J. Med. Chem.* 143, 66–84. doi:10.1016/J.EJMECH.2017.11.027

Liu, X., Han, Y., and Yang, L. (2020). *Benzimidazole Compound and Preparation Method Thereof*. US10787420B2 https://patents.google.com/patent/US10787420B2/en?oq=US10787420B2.

Luo, Y.-L., Baathulaa, K., Kannekanti, V. K., Zhou, C.-H., and Cai, G.-X. (2015). Novel Benzimidazole Derived Naphthalimide Triazoles: Synthesis, Antimicrobial Activity and Interactions with Calf Thymus DNA. *Sci. China Chem.* 58, 483–494. doi:10.1007/s11426-014-5296-3

Maertens, J., Cordonnier, C., Jaksch, P., Poiré, X., Uknis, M., Wu, J., et al. (2019). Maribavir for Preemptive Treatment of Cytomegalovirus Reactivation. *N. Engl. J. Med.* 381, 1136–1147. doi:10.1056/nejmoa1714656

Mahmoud, M. A., Ibrahim, S. K., and Rdaiaan, M. A. (2020). Antibacterial Evaluation of Some New Benzimidazole Derivatives. *Ijpr* 12, 282–287. doi:10.31838/ijpr/2020.12.01.050

Malasala, S., Ahmad, M. N., Akunuri, R., Shukla, M., Kaul, G., Dasgupta, A., et al. (2021). Synthesis and Evaluation of New Quinazoline-Benzimidazole Hybrids as Potent Anti-microbial Agents against Multidrug Resistant *Staphylococcus aureus* and *Mycobacterium tuberculosis*. *Eur. J. Med. Chem.* 212, 112996. doi:10.1016/j.ejmech.2020.112996

Maltsev, D. V., Spasov, A. A., Miroshnikov, M. V., Skripka, M. O., and Divaeva, L. N. (2020). Influence of Diazepino[1,2-A]benzimidazole Derivative (DAB-19) on Behavioral Aspects of Animals. *Rrp* 6, 9–14. doi:10.3897/RRPHARMACOLOGY.6.55142

Mantu, D., Antoci, V., Moldoveanu, C., Zbancioc, G., and Mangalagiu, I. I. (2016). Hybrid Imidazole (Benzimidazole)/pyridine (Quinoline) Derivatives and Evaluation of Their Anticancer and Antimycobacterial Activity. *J. Enzyme Inhib. Med. Chem.* 31, 96–103. doi:10.1080/14756366.2016.1190711

Marcus, A. J., Iezhitsa, I., Agarwal, R., Vassiliev, P., Spasov, A., Zhukovskaya, O., et al. (2019). Intraocular Pressure-Lowering Effects of Imidazo[1,2-A]- and Pyrimido[1,2-A]benzimidazole Compounds in Rats with Dexamethasone-Induced Ocular Hypertension. *Eur. J. Pharmacol.* 850, 75–87. doi:10.1016/j.ejphar.2019.01.059

Mariappan, G., Hazarika, R., Alam, F., Karki, R., Patangia, U., and Nath, S. (2015). Synthesis and Biological Evaluation of 2-substituted Benzimidazole Derivatives. *Arabian J. Chem.* 8, 715–719. doi:10.1016/J.ARABJC.2011.11.008

Maske, P. P., Lokapure, S. G., Nimbalkar, D., and Disouza, J. I. (2012). Synthesis and Antiprotozoal Activity of Nitro and Halogeno Substituted Some Novel Mercaptobenzimidazole Derivatives. *Der Pharma Chem.* 4, 1283–1287.

Matadamas-Martínez, F., Castillo, R., Hernández-Campos, A., Méndez-Cuesta, C., de Souza, W., Gadelha, A. P., et al. (2016). Proteomic and Ultrastructural Analysis of the Effect of a New Nitazoxanide-N-Methyl-1h-Benzimidazole Hybrid against Giardia Intestinalis. *Res. Vet. Sci.* 105, 171–179. doi:10.1016/J.RVSC.2016.02.006

Mathew, B., Suresh, J., and Anbazhagan, S. (2013). Synthesis and PASS-Assisted In Silico Approach of Some Novel 2-substituted Benzimidazole Bearing a Pyrimidine-2, 4, 6(trione) System as Mucomembranous Protector. *J. Pharm. Bioallied Sci.* 5, 39–43. doi:10.4103/0975-7406.106563

Mella-Raipán, J. A., Lagos, C. F., Recabarren-Gajardo, G., Espinosa-Bustos, C., Romero-Parra, J., Pessoa-Mahana, H., et al. (2013). Design, Synthesis, Binding and Docking-Based 3D-QSAR Studies of 2-Pyridylbenzimidazoles-Aa New Family of High Affinity CB1 Cannabinoid Ligands. *Molecules* 18, 3972–4001. doi:10.3390/molecules18043972

Menet, C. J. M., Mammoliti, O., Blanc, J., Orsulic, M., and Roscic, M. (2015). *Novel Compounds and Pharmaceutical Compositions Thereof for the Treatment of Inflammatory Disorders*. US20150203455A1 https://patents.google.com/patent/US20150203455A1/en?oq=US+20150203455+A1.

Menteşe, E., Yılmaz, F., Baltaş, N., Bekircan, O., and Kahveci, B. (2015). Synthesis and Antioxidant Activities of Some New Triheterocyclic Compounds Containing Benzimidazole, Thiophene, and 1,2,4-triazole Rings. *J. Enzyme Inhib. Med. Chem.* 30, 435–441. doi:10.3109/14756366.2014.943203

Mishra, V. R., Ghanavatkar, C. W., Mali, S. N., Qureshi, S. I., Chaudhari, H. K., and Sekar, N. (2019). Design, Synthesis, Antimicrobial Activity and Computational Studies of Novel Azo Linked Substituted Benzimidazole, Benzoxazole and Benzothiazole Derivatives. *Comput. Biol. Chem.* 78, 330–337. doi:10.1016/j.compbiolchem.2019.01.003

Mobinikhaledi, A., Asghari, B., and Jabbarpour, M. (2015). Design and Synthesis of New Benzimidazole and Pyrimidine Derivatives as α-glucosidase Inhibitor. *Iran J. Pharm. Res.* 14, 723–731.

Mochizuki, M., Kojima, T., Kobayashi, K., Kotani, E., Ishichi, Y., Kanzaki, N., et al. (2017). Discovery of 4-Chloro-2-(2,4-Dichloro-6-Methylphenoxy)-1-Methyl-7-(pentan-3-Yl)-1h-Benzimidazole, a Novel CRF1 Receptor Antagonist. *Bioorg. Med. Chem.* 25, 1556–1570. doi:10.1016/j.bmc.2016.11.011

Mochizuki, M., Kori, M., Kobayashi, K., Yano, T., Sako, Y., Tanaka, M., et al. (2016). Design and Synthesis of Benzimidazoles as Novel Corticotropin-Releasing Factor 1 Receptor Antagonists. *J. Med. Chem.* 59, 2551–2566. doi:10.1021/acs.jmedchem.5b01715

Moneer, A. A., Mohammed, K. O., and El-Nassan, H. B. (2016). Synthesis of Novel Substituted Thiourea and Benzimidazole Derivatives Containing a Pyrazolone Ring as Anti-inflammatory Agents. *Chem. Biol. Drug Des.* 87, 784–793. doi:10.1111/cbdd.12712

Monforte, A. M., De Luca, L., Buemi, M. R., Agharbaoui, F. E., Pannecouque, C., and Ferro, S. (2018). Structural Optimization of N1-Aryl-Benzimidazoles for the Discovery of New Non-nucleoside Reverse Transcriptase Inhibitors Active against Wild-type and Mutant HIV-1 Strains. *Bioorg. Med. Chem.* 26, 661–674. doi:10.1016/J.BMC.2017.12.033

Morais, G. R., Palma, E., Marques, F., Gano, L., Oliveira, M. C., Abrunhosa, A., et al. (2017). Synthesis and Biological Evaluation of Novel 2-Aryl Benzimidazoles as Chemotherapeutic Agents. *J. Heterocyclic Chem.* 54, 255–267. doi:10.1002/jhet.2575

Morcoss, M. M., Abdelhafez, E. S. M. N., Ibrahem, R. A., Abdel-Rahman, H. M., Abdel-Aziz, M., and Abou El-Ella, D. A. (2020). Design, Synthesis, Mechanistic Studies and In Silico ADME Predictions of Benzimidazole Derivatives as Novel Antifungal Agents. *Bioorg. Chem.* 101, 103956. doi:10.1016/j.bioorg.2020.103956

Mueller, R., Reddy, V., Nchinda, A. T., Mebrahtu, F., Taylor, D., Lawrence, N., et al. (2020). Lerisetron Analogues with Antimalarial Properties: Synthesis, Structure-Activity Relationship Studies, and Biological Assessment. *ACS Omega* 5, 6967–6982. doi:10.1021/acsomega.0c00327

Nair, S. M., Beevi, J., Nj, M., Emmanuel, B. D., Dharan, S. S., and Cr, R. (2016). Insilico Design, Synthesis and In Vitro Antidiabetic and Anti-inflammatory Activities of 1,3,4-Thiadiazole Substituted 2-Methyl Benzimidazole Derivatives. *J. Pharm. Res. Clin. Pract.* 6, 27–36. doi:10.21817/ijpsr/2020/v11i6/201106011

Nandha, B., Nargund, L. G., Nargund, S. L., and Bhat, K. (2017). Design and Synthesis of Some Novel Fluorobenzimidazoles Substituted with Structural Motifs Present in Physiologically Active Natural Products for Antitubercular Activity. *Iran J. Pharm. Res.* 16, 929–942.

Nashaat, S., Henen, M. A., El-Messery, S. M., and Eisa, H. (2020). Synthesis, State-Of-The-Art NMR-Binding and Molecular Modeling Study of New Benzimidazole Core Derivatives as Pin1 Inhibitors: Targeting Breast Cancer. *Bioorg. Med. Chem.* 28, 115495. doi:10.1016/j.bmc.2020.115495

Nieto-Meneses, R., Castillo, R., Hernández-Campos, A., Maldonado-Rangel, A., Matius-Ruiz, J. B., Trejo-Soto, P. J., et al. (2018). In Vitro Activity of New N-Benzyl-1h-Benzimidazol-2-Amine Derivatives Against Cutaneous, Mucocutaneous and Visceral Leishmania Species. *Exp. Parasitol.* 184, 82–89. doi:10.1016/J.EXPPARA.2017.11.009

Nofal, Z. M., Soliman, E. A., Abd El-Karim, S. S., El-Zahar, M. I., Srour, A. M., Sethumadhavan, S., et al. (2014). Synthesis of Some New Benzimidazole-Thiazole Derivatives as Anticancer Agents. *J. Hetercyclic Chem.* 51, 1797–1806. doi:10.1002/jhet.1886

Noolvi, M., Agrawal, S., Patel, H., Badiger, A., Gaba, M., and Zambre, A. (2014). Synthesis, Antimicrobial and Cytotoxic Activity of Novel Azetidine-2-One Derivatives of 1H-Benzimidazole. *Arabian J. Chem.* 7, 219–226. doi:10.1016/J.ARABJC.2011.02.011

Noor, A., Qazi, N. G., Nadeem, H., Khan, A. U., Paracha, R. Z., Ali, F., et al. (2017). Synthesis, Characterization, Anti-ulcer Action and Molecular Docking Evaluation of Novel Benzimidazole-Pyrazole Hybrids. *Chem. Cent. J.* 11, 85. doi:10.1186/s13065-017-0314-0

Ozadali-Sari, K., Tüylü Küçükkılınç, T., Ayazgok, B., Balkan, A., and Unsal-Tan, O. (2017). Novel Multi-Targeted Agents for Alzheimer's Disease: Synthesis, Biological Evaluation, and Molecular Modeling of Novel 2-[4-(4-Substitutedpiperazin-1-Yl)phenyl]benzimidazoles. *Bioorg. Chem.* 72, 208–214. doi:10.1016/J.BIOORG.2017.04.018

Özil, M., Emirik, M., Beldüz, A., and Ülker, S. (2016). Molecular Docking Studies and Synthesis of Novel Bisbenzimidazole Derivatives as Inhibitors of α-glucosidase. *Bioorg. Med. Chem.* 24, 5103–5114. doi:10.1016/J.BMC.2016.08.024

Özil, M., Parlak, C., and Baltaş, N. (2018). A Simple and Efficient Synthesis of Benzimidazoles Containing Piperazine or Morpholine Skeleton at C-6 Position as Glucosidase Inhibitors with Antioxidant Activity. *Bioorg. Chem.* 76, 468–477. doi:10.1016/j.bioorg.2017.12.019

Özkay, Y., Tunalı, Y., Karaca, H., and Işıkdağ, I. (2011). Antimicrobial Activity of a New Series of Benzimidazole Derivatives. *Arch. Pharm. Res.* 34, 1427–1435. doi:10.1007/s12272-011-0903-8

Padalkar, V. S., Borse, B. N., Gupta, V. D., Phatangare, K. R., Patil, V. S., Umape, P. G., et al. (2016). Synthesis and Antimicrobial Activity of Novel 2-substituted Benzimidazole, Benzoxazole and Benzothiazole Derivatives. *Arabian J. Chem.* 9, S1125–S1130. doi:10.1016/J.ARABJC.2011.12.006

Pajouhesh, H., Holland, R., Zhang, L., Pajouhesh, H., Lamontagne, J., and Whelan, B. (2015). *Benzimidazole Inhibitors of the Sodium Channel*. US20150361032A1 https://patents.google.com/patent/US20150361032A1/en?oq=US20150361032A1.

Papanicolaou, G. A., Silveira, F. P., Langston, A. A., Pereira, M. R., Avery, R. K., Uknis, M., et al. (2019). Maribavir for Refractory or Resistant Cytomegalovirus Infections in Hematopoietic-Cell or Solid-Organ Transplant Recipients: A Randomized, Dose-Ranging, Double-Blind, Phase 2 Study. *Clin. Infect. Dis.* 68, 1255–1264. doi:10.1093/cid/ciy706

Pardeshi, V. A. S., Chundawat, N. S., Pathan, S. I., Sukhwal, P., Chundawat, T. P. S., and Singh, G. P. (2021). A Review on Synthetic Approaches of Benzimidazoles. *Synth. Commun.* 51, 485–513. doi:10.1080/00397911.2020.1841239

Partap, S., Yar, M. S., Hassan, M. Z., Akhtar, M. J., and Siddiqui, A. A. (2017). Design, Synthesis, and Pharmacological Screening of Pyridazinone Hybrids as Anticonvulsant Agents. *Arch. Pharm. (Weinheim)* 350, 1700135. doi:10.1002/ardp.201700135

Pathan, S. I., Chundawat, N. S., Chauhan, N. P. S., and Singh, G. P. (2020). A Review on Synthetic Approaches of Heterocycles via Insertion-Cyclization Reaction. *Synth. Commun.* 50, 1251–1285. doi:10.1080/00397911.2020.1712609

Patil, A., Ganguly, S., Hundiwale, J., and Tayade, S. (2012). Synthesis and Study of Some Novel Benzimidazole Analogs as Potential Antiulcer Agents. *Int. J. Pharm. Chem.* 2, 89–92. doi:10.7439/ijpc.v2i3.679

Patil, A., Ganguly, S., and Surana, S. (2010). Synthesis and Antiulcer Activity of 2-[5-Substituted-1-H-Benzo(d) Imidazol-2-Yl Sulfinyl]methyl-3-Substituted quinazoline-4-(3H) Ones. *J. Chem. Sci.* 122, 443–450. doi:10.1007/s12039-010-0052-5

Pevzner, V., and Moses-Heller, S. (2020). *Stable Orally Disintegrating Pharmaceutical Compositionsns*. US10835488B2 https://patents.google.com/patent/US10835488B2/en?oq=US10835488B2.

Poddar, S. K., Saqueeb, N., and Rahman, S. A. (2016). Synthesis and Biological Evaluation of 2-methyl-1Hbenzimidazole and 1H-Benzimidazol-2-Yl-Methanol. *Dhaka Univ. J. Pharm. Sci.* 15, 83–87. doi:10.3329/dujps.v15i1.29201

Popov, A. B., Krstulović, L., Koštrun, S., Jelić, D., Bokulić, A., Stojković, M. R., et al. (2020). Design, Synthesis, Antitrypanosomal Activity, DNA/RNA Binding and In Vitro ADME Profiling of Novel Imidazoline-Substituted 2-arylbenzimidazoles. *Eur. J. Med. Chem.* 207, 112802. doi:10.1016/j.ejmech.2020.112802

Prajapat, P., and Talesara, G. L. (2016). Synthesis and Anti-inflammatory Screening of Some Mono and Bis-Alkoxyphthalimide Linked Benzimidazole and Their Quinazoline and Pyrimidine Derivatives. *J. Heterocyclic Chem.* 53, 1603–1610. doi:10.1002/jhet.2471

Prasad, P. M. K., and Sundararajan, R. (2017). Design, Synthesis, Antitubercular and Antimicrobial Activities of Novel Thiazole Substituted Benzimidazole Derivatives. *Der Pharm. Lett.* 9, 270–284.

Rajak, H. (2015). Synthesis and Evaluation of Some Novel Semicarbazones Based Benzimidazole Derivatives as Anticonvulsant Agent. *Ijcea* 6, 142–145. doi:10.7763/IJCEA.2015.V6.469

Rajesh, R., Manikandan, A., Sivakumar, A., Ramasubbu, C., and Nagaraju, N. (2017). Substituted Methoxybenzyl-Sulfonyl-1h-Benzo[d]imidazoles Evaluated as Effective H+/K+-ATPase Inhibitors and Anti-ulcer Therapeutics. *Eur. J. Med. Chem.* 139, 454–460. doi:10.1016/J.EJMECH.2017.08.001

Raka, S. C., Rahman, A., Hussain, F., and Rahman, S. M. A. (2021). Synthesis, Characterization and In Vitro, In Vivo, In Silico Biological Evaluations of Substituted Benzimidazole Derivatives. *Saudi J. Biol. Sci.* 9, 2. doi:10.1016/j.sjbs.2021.08.082

Ramos Rodríguez, O. A., Magaña Vergara, N. E., Mojica Sánchez, J. P., Sumaya Martínez, M. T., Gómez Sandoval, Z., Cruz, A., et al. (2020). Synthesis, crystal Structure, Antioxidant Activity and Dft Study of 2-Aryl-2,3-Dihydro-4h-[1,3]thiazino[3,2-A]benzimidazol-4-One. *J. Mol. Struct.* 1199, 127036. doi:10.1016/j.molstruc.2019.127036

Rathore, A., Sudhakar, R., Ahsan, M. J., Ali, A., Subbarao, N., Jadav, S. S., et al. (2017). In Vivo Anti-inflammatory Activity and Docking Study of Newly Synthesized Benzimidazole Derivatives Bearing Oxadiazole and Morpholine Rings. *Bioorg. Chem.* 70, 107–117. doi:10.1016/J.BIOORG.2016.11.014

Ren, W., Ren, Y., Dong, M., and Gao, Y. (2016). Design, Synthesis, and Thrombin Inhibitory Activity Evaluation of Some Novel Benzimidazole Derivatives. *Helv. Chim. Acta* 99, 325–332. doi:10.1002/hlca.201500527

Romero-Parra, J., Mella-Raipán, J., Palmieri, V., Allarà, M., Torres, M. J., Pessoa-Mahana, H., et al. (2016). Synthesis, Binding Assays, Cytotoxic Activity and Docking Studies of Benzimidazole and Benzothiophene Derivatives with Selective Affinity for the CB2 Cannabinoid Receptor. *Eur. J. Med. Chem.* 124, 17–35. doi:10.1016/J.EJMECH.2016.08.005

Saha, P., Brishty, S. R., and Rahman, S. A. (2021). Pharmacological Screening of Substituted Benzimidazole Derivatives. *Dhaka Univ. J. Pharm. Sci.* 20, 95–102. doi:10.3329/dujps.v20i1.54037

Saha, P., Brishty, S. R., and Rahman, S. M. A. (2020). Synthesis and Evaluation of Disubstituted Benzimidazole Derivatives as Potential Analgesic and Antidiarrheal Agents. *pharmaceutical-sciences* 82, 222–229. doi:10.36468/pharmaceutical-sciences.642

Sahoo, B. M., Banik, B. K., Mazaharunnisa, N. S., and Rao, B. (2019). Microwave Assisted Green Synthesis of Benzimidazole Derivatives and Evaluation of Their Anticonvulsant Activity. *Cmic* 6, 23–29. doi:10.2174/2213335606666190429124745

Saify, Z. S., Kamil, A., Akhtar, S., Taha, M., Khan, A., Khan, K. M., et al. (2014). 2-(2′-Pyridyl) Benzimidazole Derivatives and Their Urease Inhibitory Activity. *Med. Chem. Res.* 23, 4447–4454. doi:10.1007/s00044-014-1015-z

Sarıkaya, G., Çoban, G., Parlar, S., Tarikogullari, A. H., Armagan, G., Erdoğan, M. A., et al. (2018). Multifunctional Cholinesterase Inhibitors for Alzheimer's Disease: Synthesis, Biological Evaluations, and Docking Studies of O/p -propoxyphenylsubstituted-1H -benzimidazole Derivatives. *Arch. Pharm. Chem. Life Sci.* 351, 1800076. doi:10.1002/ardp.201800076

Schade, T., Skubsch, K., Brinkmann, S., Bleckmann, A., and Schlenker, D. (2015). *Octocrylene-free Sunscreen Composition with Low Stickiness*. US20150209259A1 https://patents.google.com/patent/US20150209259A1/en?oq=US+20150209259+A1.

Sethi, P., Bansal, Y., and Bansal, G. (2018). Synthesis and PASS-Assisted Evaluation of Coumarin-Benzimidazole Derivatives as Potential Anti-inflammatory and Anthelmintic Agents. *Med. Chem. Res.* 27, 61–71. doi:10.1007/s00044-017-2036-1

Sethi, R., Arora, S., Saini, D., Singh, T. G., and Jain, S. (2017). Design and Synthesis of N-(benzimidazol-1-yl Methyl)-Benzamide Derivatives Anti-inflammatory and Analgesic Agents. *ACTA Pol. Pharm.* 74, 1413–1425.

Shaharyar, M., Mazumder, A., Salahuddin, R., and Garg, R. D. (2016). Synthesis, Characterization and Pharmacological Screening of Novel Benzimidazole Derivatives. *Arabian J. Chem.* 9, S342–S347. doi:10.1016/J.ARABJC.2011.04.013

Shaikh, I. N., Hosamani, K. M., and Kurjogi, M. M. (2018). Design, Synthesis, and Evaluation of New α-aminonitrile-based Benzimidazole Biomolecules as Potent Antimicrobial and Antitubercular Agents. *Arch. Pharm. (Weinheim)* 351, 1700205. doi:10.1002/ardp.201700205

Shaikh, I. N., Hosamani, K. M., Seetharamareddy, H. R., and Hugar, M. H. (2012). Synthesis and In-Vivo Evaluation of Carbonyl-Amide Linkage Based New Benzimidazole Derivatives. *Arch. Pharm. (Weinheim)* 345, 65–72. doi:10.1002/ardp.201100068

Shaker, Y. M., Omar, M. A., Mahmoud, K., Elhallouty, S. M., El-Senousy, W. M., Ali, M. M., et al. (2015). Synthesis, In Vitro and In Vivo Antitumor and Antiviral Activity of Novel 1-substituted Benzimidazole Derivatives. *J. Enzyme Inhib. Med. Chem.* 30, 826–845. doi:10.3109/14756366.2014.979344

Shankar, B., Jalapathi, P., Valeru, A., Kishor Kumar, A., Saikrishna, B., and Kudle, K. r. (2017). Synthesis and Biological Evaluation of New 2-(6-Alkyl-Pyrazin-2-Yl)-1h-Benz[d]imidazoles as Potent Anti-inflammatory and Antioxidant Agents. *Med. Chem. Res.* 26, 1835–1846. doi:10.1007/s00044-017-1897-7

Sharma, K., Shrivastava, A., Mehra, R. N., Deora, G. S., Alam, M. M., Zaman, M. S., et al. (2018). Synthesis of Novel Benzimidazole Acrylonitriles for Inhibition of *Plasmodium Falciparum* Growth by Dual Target Inhibition. *Arch. Pharm. (Weinheim)* 351, 1700251. doi:10.1002/ardp.201700251

Sharma, M. C., Kohli, D. V., and Sharma, S. (2010). Benzimidazoles Derivatives with (2-{6-Chloro-5-nitro-1-[2-(1H-tetrazol-5-yl) Biphenyl-4-Ylmethyl] 1H-Benzoimidazol-2-Yl}-Phenyl)-(substituted-Benzylidene)-Amine with Potential Angiotensin II Receptor Antagonists as Antihypertensive Activity. *Int. J Drug Delivery* 2, 228–237. doi:10.5138/ijdd.2010.0975.0215.02033

Sharma, P., Reddy, T. S., Kumar, N. P., Senwar, K. R., Bhargava, S. K., and Shankaraiah, N. (2017a). Conventional and Microwave-Assisted Synthesis of New 1H-Benzimidazole-Thiazolidinedione Derivatives: A Potential Anticancer Scaffold. *Eur. J. Med. Chem.* 138, 234–245. doi:10.1016/J.EJMECH.2017.06.035

Sharma, R., Bali, A., and Chaudhari, B. B. (2017b). Synthesis of Methanesulphonamido-Benzimidazole Derivatives as Gastro-Sparing Antiinflammatory Agents with Antioxidant Effect. *Bioorg. Med. Chem. Lett.* 27, 3007–3013. doi:10.1016/J.BMCL.2017.05.017

Sharma, S., Kumar, D., Singh, G., Monga, V., and Kumar, B. (2020). Recent Advancements in the Development of Heterocyclic Anti-inflammatory Agents. *Eur. J. Med. Chem.* 200, 112438. doi:10.1016/j.ejmech.2020.112438

Shingalapur, R. V., Hosamani, K. M., Keri, R. S., and Hugar, M. H. (2010). Derivatives of Benzimidazole Pharmacophore: Synthesis, Anticonvulsant, Antidiabetic and DNA Cleavage Studies. *Eur. J. Med. Chem.* 45, 1753–1759. doi:10.1016/J.EJMECH.2010.01.007

Shintre, S. A., Ramjugernath, D., Singh, P., Mocktar, C., and Koorbanally, N. A. (2017). Microwave Synthesis, Biological Evaluation and Docking Studies of 2-substituted Methyl 1-(4-Fluorophenyl)-1h-Benzimidazole-5-Carboxylates. *Med. Chem. Res.* 26, 484–498. doi:10.1007/s00044-016-1763-z

Siddiqui, N., and Alam, M. S. (2010). Anticonvulsant and Toxicity Evaluation of Newer 1-{(1-(2-substituted Benzyl)-1h-Benzo [d] Imidazol-2-Yl) Methyl}-3-Arylthioureas. *Der Pharma Chem.* 2, 163–171.

Siddiqui, N., Alam, M. S., Sahu, M., Yar, M. S., Alam, O., and Siddiqui, M. J. A. (2016). Antidepressant, Analgesic Activity and SAR Studies of Substituted Benzimidazoles. *Asian Jour. Pharmac. Rese.* 6, 170–174. doi:10.5958/2231-5691.2016.00024.1

Singh, A., Yadav, D., Yadav, M., Dhamanage, A., Kulkarni, S., and Singh, R. K. (2015). Molecular Modeling, Synthesis and Biological Evaluation of N-Heteroaryl Compounds as Reverse Transcriptase Inhibitors against HIV-1. *Chem. Biol. Drug Des.* 85, 336–347. doi:10.1111/cbdd.12397

Singh, G., Singh, A., Verma, R. K., Mall, R., and Azeem, U. (2018). Synthesis, Biological Evaluation and Molecular Docking Studies of Novel Benzimidazole Derivatives. *Comput. Biol. Chem.* 72, 45–52. doi:10.1016/J.COMPBIOLCHEM.2017.12.010

Singh, K., Okombo, J., Brunschwig, C., Ndubi, F., Barnard, L., Wilkinson, C., et al. (2017a). Antimalarial Pyrido[1,2-A]benzimidazoles: Lead Optimization, Parasite Life Cycle Stage Profile, Mechanistic Evaluation, Killing Kinetics, and In Vivo Oral Efficacy in a Mouse Model. *J. Med. Chem.* 60, 1432–1448. doi:10.1021/acs.jmedchem.6b01641

Singh, L. R., Avula, S. R., Raj, S., Srivastava, A., Palnati, G. R., Tripathi, C. K. M., et al. (2017b). Coumarin-benzimidazole Hybrids as a Potent Antimicrobial Agent: Synthesis and Biological Elevation. *J. Antibiot. (Tokyo)* 70, 954–961. doi:10.1038/ja.2017.70

Singh, N., Pandurangan, A., Rana, K., Anand, P., Ahamad, A., and Tiwari, A. K. (2012). Benzimidazole: A Short Review of Their Antimicrobial Activities. *Int. Curr. Pharm. J.* 1, 110–118. doi:10.3329/icpj.v1i5.10284

Singhal, S., Khanna, P., and Khanna, L. (2019). Synthesis, DFT Studies, Molecular Docking, Antimicrobial Screening and UV Fluorescence Studies on Ct-DNA for Novel Schiff Bases of 2-(1-aminobenzyl) Benzimidazole. *Heliyon* 5, e02596. doi:10.1016/j.heliyon.2019.e02596

Singla, P., Luxami, V., and Paul, K. (2015). Triazine-benzimidazole Hybrids: Anticancer Activity, DNA Interaction and Dihydrofolate Reductase Inhibitors. *Bioorg. Med. Chem.* 23, 1691–1700. doi:10.1016/J.BMC.2015.03.012

Sireesha, R., Sreenivasulu, R., Chandrasekhar, C., Jadav, S. S., Pavani, Y., Rao, M. V. B., et al. (2021). Design, Synthesis, Anti-cancer Evaluation and Binding Mode Studies of Benzimidazole/benzoxazole Linked β-carboline Derivatives. *J. Mol. Struct.* 1226, 129351. doi:10.1016/j.molstruc.2020.129351

Sirim, M. M., Krishna, V. S., Sriram, D., and Unsal Tan, O. (2020). Novel Benzimidazole-Acrylonitrile Hybrids and Their Derivatives: Design, Synthesis and Antimycobacterial Activity. *Eur. J. Med. Chem.* 188, 112010. doi:10.1016/j.ejmech.2019.112010

Song, J., Gao, Q. L., Wu, B. W., Li, D., Shi, L., Zhu, T., et al. (2019). Novel Tertiary Sulfonamide Derivatives Containing Benzimidazole Moiety as Potent Anti-gastric Cancer Agents: Design, Synthesis and SAR Studies. *Eur. J. Med. Chem.* 183, 111731. doi:10.1016/j.ejmech.2019.111731

Sontakke, V. A., Kate, A. N., Ghosh, S., More, P., Gonnade, R., Kumbhar, N. M., et al. (2015). Synthesis, DNA Interaction and Anticancer Activity of 2-anthryl Substituted Benzimidazole Derivatives. *New J. Chem.* 39, 4882–4890. doi:10.1039/C4NJ02415J

Spasov, A. A., Kucheryavenko, A. F., Gaidukova, K. A., Kosolapov, V. A., and Zhukovskaya, O. N. (2020). Antiplatelet Activity of New Derivatives of Benzimidazole Containing Sterically Hindered Phenolic Group in Their Structure. *Rrp* 6, 1–9. doi:10.3897/RRPHARMACOLOGY.6.50373

Sridhar Goud, N., Pooladanda, V., Muni Chandra, K., Lakshmi Soukya, P. S., Alvala, R., Kumar, P., et al. (2020). Novel Benzimidazole-Triazole Hybrids as Apoptosis Inducing Agents in Lung Cancer: Design, Synthesis, 18F-Radiolabeling & Galectin-1 Inhibition Studies. *Bioorg. Chem.* 102, 104125. doi:10.1016/j.bioorg.2020.104125

Srinivas Reddy, M., Nath Anisetti, R., Durga Prasad, K., Sannigrahi, S., and Arvinda Reddy, P. (2011). Synthesis, Characterization and Biological Evaluation of Some Novel 2-substituted Mercaptobenzimidazole Derivatives. *Pharm. Chem. J.* 44, 642–645. doi:10.1007/s11094-011-0537-7

Srivastava, R., Gupta, S. K., Naaz, F., Sen Gupta, P. S., Yadav, M., Singh, V. K., et al. (2020). Alkylated Benzimidazoles: Design, Synthesis, Docking, DFT Analysis, ADMET Property, Molecular Dynamics and Activity Against HIV and YFV. *Comput. Biol. Chem.* 89, 107400. doi:10.1016/j.compbiolchem.2020.107400

Srour, A. M., Ahmed, N. S., Abd El-Karim, S. S., Anwar, M. M., and El-Hallouty, S. M. (2020). Design, Synthesis, Biological Evaluation, QSAR Analysis and Molecular Modelling of New Thiazol-Benzimidazoles as EGFR Inhibitors. *Bioorg. Med. Chem.* 28, 115657. doi:10.1016/j.bmc.2020.115657

Su, W.-Y., Pan, R.-K., Song, J.-L., Li, G.-B., and Liu, S.-G. (2019). Synthesis, Crystal Structures and Cytotoxic Activity of Two Zinc(II) Complexes Derived from Benzimidazole Derivatives. *Polyhedron* 161, 268–275. doi:10.1016/j.poly.2019.01.012

Suk, F. M., Liu, C. L., Hsu, M. H., Chuang, Y. T., Wang, J. P., and Liao, Y. J. (2019). Treatment with a New Benzimidazole Derivative Bearing a Pyrrolidine Side Chain Overcomes Sorafenib Resistance in Hepatocellular Carcinoma. *Sci. Rep.* 9, 17259. doi:10.1038/s41598-019-53863-2

Taha, M., Mosaddik, A., Rahim, F., Ali, S., Ibrahim, M., and Almandil, N. B. (2020). Synthesis, Antiglycation and Antioxidant Potentials of Benzimidazole Derivatives. *J. King Saud Univ. - Sci.* 32, 191–194. doi:10.1016/j.jksus.2018.04.003

Tahlan, S., Kumar, S., and Narasimhan, B. (2019). Pharmacological Significance of Heterocyclic 1H-Benzimidazole Scaffolds: A Review. *BMC Chem.* 13, 101. doi:10.1186/s13065-019-0625-4

Tahri, A., Jonckers, T. H. M., Raboisson, P. J.-M. B., Vendeville, S. M. H., and Hu, L. (2015). *Novel 4-substituted 1,3-Dihydro-2h-Benzimidazol-2-One Derivatives Substituted with Benzimidazoles as Respiratory Syncytial Virus Antiviral Agents*. US20150175608A1 https://patents.google.com/patent/US20150175608A1/en?oq=US+20150175608+A1.

Tamura, Y., Omori, N., Kouyama, N., Nishiura, Y., Hayashi, K., Watanabe, K., et al. (2012a). Design, Synthesis and Identification of Novel Benzimidazole Derivatives as Highly Potent NPY Y5 Receptor Antagonists with Attractive In Vitro ADME Profiles. *Bioorg. Med. Chem. Lett.* 22, 5498–5502. doi:10.1016/J.BMCL.2012.07.020

Tamura, Y., Omori, N., Kouyama, N., Nishiura, Y., Hayashi, K., Watanabe, K., et al. (2012b). Identification of a Novel and Orally Available Benzimidazole Derivative as an NPY Y5 Receptor Antagonist with In Vivo Efficacy. *Bioorg. Med. Chem. Lett.* 22, 6554–6558. doi:10.1016/J.BMCL.2012.09.025

Tanaka, J., Iida, H., Abe, M., Yuda, Y., Inoue, S., and Okabe, S. (2011). Gastric Antisecretory and Anti-ulcer Effect of ME3407, A New Benzimidazole Derivative, in Rats. *Arzneimittelforschung* 54, 221–229. doi:10.1055/s-0031-1296963

Tomovic, K., Ilic, B. S., Smelcerovic, Z., Miljkovic, M., Yancheva, D., Kojic, M., et al. (2020). Benzimidazole-based Dual Dipeptidyl Peptidase-4 and Xanthine Oxidase Inhibitors. *Chem. Biol. Interact.* 315, 108873. doi:10.1016/j.cbi.2019.108873

Tonelli, M., Gabriele, E., Piazza, F., Basilico, N., Parapini, S., Tasso, B., et al. (2018). Benzimidazole Derivatives Endowed with Potent Antileishmanial Activity. *J. Enzyme Inhib. Med. Chem.* 33, 210–226. doi:10.1080/14756366.2017.1410480

Torres-Gómez, H., Hernández-Núñez, E., León-Rivera, I., Guerrero-Alvarez, J., Cedillo-Rivera, R., Moo-Puc, R., et al. (2008). Design, Synthesis and In Vitro Antiprotozoal Activity of Benzimidazole-Pentamidine Hybrids. *Bioorg. Med. Chem. Lett.* 18, 3147–3151. doi:10.1016/j.bmcl.2008.05.009

Tsay, S. C., Hwu, J. R., Singha, R., Huang, W. C., Chang, Y. H., Hsu, M. H., et al. (2013). Coumarins Hinged Directly on Benzimidazoles and Their Ribofuranosides to Inhibit Hepatitis C Virus. *Eur. J. Med. Chem.* 63, 290–298. doi:10.1016/J.EJMECH.2013.02.008

Ushiroda, K., Maruta, K., Takazawa, T., Nagano, T., Taiji, M., Kohno, T., et al. (2011). Synthesis and Pharmacological Evaluation of Novel Benzoylazole-Based PPAR α/γ Activators. *Bioorg. Med. Chem. Lett.* 21, 1978–1982. doi:10.1016/j.bmcl.2011.02.032

Vangavaragu, J. R., Valasani, K. R., Gan, X., and Yan, S. S. (2014). Identification of Human Presequence Protease (hPreP) Agonists for the Treatment of Alzheimer's Disease. *Eur. J. Med. Chem.* 76, 506–516. doi:10.1016/J.EJMECH.2014.02.046

Varshney, H., Ahmad, A., Rauf, A., Sherwani, A., and Owais, M. (2015). Multistep Synthesis of 1-[{(5-Alkenyl/hydroxyalkenylsubstituted)-1,3,4-Oxadiazol-2-Yl}-Methyl]-2-Methyl-1h-Benzimidazole Series and In Vitro Anticancer Screening, SAR Studies. *Med. Chem. Res.* 24, 944–953. doi:10.1007/s00044-014-1162-2

Vasantha, K., Basavarajaswamy, G., Vaishali Rai, M., Boja, P., Pai, V. R., Shruthi, N., et al. (2015). Rapid 'one-Pot' Synthesis of a Novel Benzimidazole-5-Carboxylate and its Hydrazone Derivatives as Potential Anti-inflammatory

and Antimicrobial Agents. *Bioorg. Med. Chem. Lett.* 25, 1420–1426. doi:10.1016/J.BMCL.2015.02.043

Vasil'ev, P. M., Kalitin, K. Y., Spasov, A. A., Grechko, O. Y., Poroikov, V. V., Filimonov, D. A., et al. (2017). Prediction and Study of Anticonvulsant Properties of Benzimidazole Derivatives. *Pharm. Chem. J.* 50, 775–780. doi:10.1007/S11094-017-1530-6

Veerasamy, R., Roy, A., Karunakaran, R., and Rajak, H. (2021). Structure-Activity Relationship Analysis of Benzimidazoles as Emerging Anti-inflammatory Agents: An Overview. *Pharmaceuticals* 14 (7), 663. doi:10.3390/ph14070663

Vishwanathan, B., and Gurupadayya, B. (2015). Anticoagulant Evaluation of 1,3,4-oxadiazole Derivatives Derived from Benzimidazole. *World J. Pharm. Sci.* 3, 154–157.

Vitale, G., Corona, P., Loriga, M., Carta, A., Paglietti, G., Giliberti, G., et al. (2012). 5-Acetyl-2-arylbenzimidazoles as Antiviral Agents. Part 4. *Eur. J. Med. Chem.* 53, 83–97. doi:10.1016/J.EJMECH.2012.03.038

Wang, M., Han, X., and Zhou, Z. (2015). New Substituted Benzimidazole Derivatives: A Patent Review (2013 - 2014). *Expert Opin. Ther. Pat.* 25, 595–612. doi:10.1517/13543776.2015.1015987

Wang, Y. J., Yang, L., and Zuo, J. P. (2016). Recent Developments in Antivirals against Hepatitis B Virus. *Virus. Res.* 213, 205–213. doi:10.1016/J.VIRUSRES.2015.12.014

Wang, Y. N., Bheemanaboina, R. R. Y., Cai, G. X., and Zhou, C. H. (2018). Novel Purine Benzimidazoles as Antimicrobial Agents by Regulating ROS Generation and Targeting Clinically Resistant *Staphylococcus aureus* DNA Groove. *Bioorg. Med. Chem. Lett.* 28, 1621–1628. doi:10.1016/J.BMCL.2018.03.046

Wang, Z., Deng, X., Xiong, S., Xiong, R., Liu, J., Zou, L., et al. (2017). Design, Synthesis and Biological Evaluation of Chrysin Benzimidazole Derivatives as Potential Anticancer Agents. *Nat. Product. Res.* 32, 2900–2909. doi:10.1080/14786419.2017.1389940

Warekar, P. P., Patil, P. T., Patil, K. T., Jamale, D. K., Kolekar, G. B., and Anbhule, P. V. (2016). Ecofriendly Synthesis and Biological Evaluation of 4-(4-nitrophenyl)-2-phenyl-1,4-dihydro-benzo[4,5]imidazo[1,2-a]pyrimidine-3-carboxylic Acid Ethyl Ester Derivatives as an Antitubercular Agents. *Synth. Commun.* 46, 2022–2030. doi:10.1080/00397911.2016.1244273

Woolley, D. W. (1944). Some Biological Effects Produced by Benzimidazole and Their Reversal by Purines. *J. Biol. Chem.* 152, 225–232. doi:10.1016/s0021-9258(18)72045-0

Wu, Z., Xia, M. B., Bertsetseg, D., Wang, Y. H., Bao, X. L., Zhu, W. B., et al. (2020). Design, Synthesis and Biological Evaluation of Novel Fluoro-Substituted Benzimidazole Derivatives with Anti-hypertension Activities. *Bioorg. Chem.* 101, 104042. doi:10.1016/j.bioorg.2020.104042

Wubulikasimu, R., Yang, Y., Xue, F., Luo, X., Shao, D., Li, Y., et al. (2013). Synthesis and Biological Evaluation of Novel Benzimidazole Derivatives Bearing a Heterocyclic Ring at 4/5 Position. *Bull. Korean Chem. Soc.* 34, 2297–2304. doi:10.5012/bkcs.2013.34.8.2297

Xu, Y. B., Yang, L., Wang, G. F., Tong, X. K., Wang, Y. J., Yu, Y., et al. (2014). Benzimidazole Derivative, BM601, a Novel Inhibitor of Hepatitis B Virus and HBsAg Secretion. *Antivir. Res* 107, 6–15. doi:10.1016/J.ANTIVIRAL.2014.04.002

Xue, F., Luo, X., Ye, C., Ye, W., and Wang, Y. (2011). Inhibitory Properties of 2-Substituent-1h-Benzimidazole-4-Carboxamide Derivatives Against Enteroviruses. *Bioorg. Med. Chem.* 19, 2641–2649. doi:10.1016/J.BMC.2011.03.007

Yadav, S., Narasimhan, B., Lim, S. M., Ramasamy, K., Vasudevan, M., Shah, S. A. A., et al. (2018). Synthesis and Evaluation of Antimicrobial, Antitubercular and Anticancer Activities of Benzimidazole Derivatives. *Egypt. J. Basic Appl. Sci.* 5, 100–109. doi:10.1016/J.EJBAS.2017.11.001

Yamani, A., Zdżalik-Bielecka, D., Lipner, J., Stańczak, A., Piórkowska, N., Stańczak, P. S., et al. (2021). Discovery and Optimization of Novel Pyrazole-Benzimidazole CPL304110, as a Potent and Selective Inhibitor of Fibroblast Growth Factor Receptors FGFR (1-3). *Eur. J. Med. Chem.* 210, 112990. doi:10.1016/j.ejmech.2020.112990

Yan, Y., Liu, Z., Zhang, J., Xu, R., Hu, X., and Liu, G. (2011). A Reverse Method for Diversity Introduction of Benzimidazole to Synthesize H(+)/K(+)-ATP Enzyme Inhibitors. *Bioorg. Med. Chem. Lett.* 21, 4189–4192. doi:10.1016/J.BMCL.2011.05.080

Yang, C., Balsells, J., Chu, H. D., Cox, J. M., Crespo, A., Ma, X., et al. (2015). Discovery of Benzimidazole Oxazolidinediones as Novel and Selective Nonsteroidal Mineralocorticoid Receptor Antagonists. *ACS Med. Chem. Lett.* 6, 461–465. doi:10.1021/acsmedchemlett.5b00010

Yang, H., Ren, Y., Gao, X., and Gao, Y. (2016). Synthesis and Anticoagulant Bioactivity Evaluation of 1,2,5-trisubstituted Benzimidazole Fluorinated Derivatives. *Chem. Res. Chin. Univ.* 32, 973–978. doi:10.1007/s40242-016-6205-4

Yang, Y., Zhang, S., Zhou, Q., Zhang, C., Gao, Y., Wang, H., et al. (2020). Discovery of Highly Selective and Orally Available Benzimidazole-Based Phosphodiesterase 10 Inhibitors with Improved Solubility and Pharmacokinetic Properties for Treatment of Pulmonary Arterial Hypertension. *Acta Pharm. Sin. B* 10, 2339–2347. doi:10.1016/j.apsb.2020.04.003

Yeong, K. Y., Nor Azizi, M. I. H., Berdigaliyev, N., Chen, W. N., Lee, W. L., Shirazi, A. N., et al. (2019). Sirtuin Inhibition and Anti-cancer Activities of Ethyl 2-Benzimidazole-5-Carboxylate Derivatives. *Medchemcomm* 10, 2140–2145. doi:10.1039/c9md00323a

Yeong, K. Y., Ang, C. W., Ali, M. A., Osman, H., and Tan, S. C. (2017). Antituberculosis Agents Bearing the 1,2-disubstituted Benzimidazole Scaffold. *Med. Chem. Res.* 26, 770–778. doi:10.1007/s00044-017-1784-2

Youssif, B. G., Mohamed, Y. A., Salim, M. T., Inagaki, F., Mukai, C., and Abdu-Allah, H. H. (2016). Synthesis of Some Benzimidazole Derivatives Endowed with 1,2,3-triazole as Potential Inhibitors of Hepatitis C Virus. *Acta Pharm.* 66, 219–231. doi:10.1515/acph-2016-0014

Yuan, X., Yang, Q., Liu, T., Li, K., Liu, Y., Zhu, C., et al. (2019). Design, Synthesis and In Vitro Evaluation of 6-Amide-2-Aryl Benzoxazole/benzimidazole Derivatives Against Tumor Cells by Inhibiting VEGFR-2 Kinase. *Eur. J. Med. Chem.* 179, 147–165. doi:10.1016/j.ejmech.2019.06.054

Yılmaz, Ü., Tekin, S., Buğday, N., Yavuz, K., Küçükbay, H., and Sandal, S. (2019). Synthesis and Evaluation of Anticancer Properties of Novel Benzimidazole Ligand and Their Cobalt(II) and Zinc(II) Complexes Against Cancer Cell Lines A-2780 and DU-145. *Inorg. Chim. Acta* 495, 118977. doi:10.1016/j.ica.2019.118977

Zawawi, N. K., Taha, M., Ahmat, N., Ismail, N. H., Wadood, A., and Rahim, F. (2017). Synthesis, Molecular Docking Studies of Hybrid Benzimidazole as α-glucosidase Inhibitor. *Bioorg. Chem.* 70, 184–191. doi:10.1016/J.BIOORG.2016.12.009

Zhang, T., Liu, Q., and Ren, Y. (2020). Design, Synthesis and Biological Activity Evaluation of Novel Methyl Substituted Benzimidazole Derivatives. *Tetrahedron* 76, 131027. doi:10.1016/j.tet.2020.131027

Zhang, Y., Xu, J., Li, Y., Yao, H., and Wu, X. (2015). Design, Synthesis and Pharmacological Evaluation of Novel NO-Releasing Benzimidazole Hybrids as Potential Antihypertensive Candidate. *Chem. Biol. Drug Des.* 85, 541–548. doi:10.1111/cbdd.12442

Zhu, J., Wu, C. F., Li, X., Wu, G. S., Xie, S., Hu, Q. N., et al. (2013). Synthesis, Biological Evaluation and Molecular Modeling of Substituted 2-aminobenzimidazoles as Novel Inhibitors of Acetylcholinesterase and Butyrylcholinesterase. *Bioorg. Med. Chem.* 21, 4218–4224. doi:10.1016/J.BMC.2013.05.001

Zhu, W., Da, Y., Wu, D., Zheng, H., Zhu, L., Wang, L., et al. (2014). Design, Synthesis and Biological Evaluation of New 5-nitro Benzimidazole Derivatives as AT1 Antagonists with Anti-hypertension Activities. *Bioorg. Med. Chem.* 22, 2294–2302. doi:10.1016/J.BMC.2014.02.008

Conflict of Interest: The authors declare that the research was conducted in the absence of any commercial or financial relationships that could be construed as a potential conflict of interest.

Publisher's Note: All claims expressed in this article are solely those of the authors and do not necessarily represent those of their affiliated organizations, or those of the publisher, the editors and the reviewers. Any product that may be evaluated in this article, or claim that may be made by its manufacturer, is not guaranteed or endorsed by the publisher.

Copyright © 2021 Brishty, Hossain, Khandaker, Faruque, Osman and Rahman. This is an open-access article distributed under the terms of the Creative Commons Attribution License (CC BY). The use, distribution or reproduction in other forums is permitted, provided the original author(s) and the copyright owner(s) are credited and that the original publication in this journal is cited, in accordance with accepted academic practice. No use, distribution or reproduction is permitted which does not comply with these terms.

frontiers in Pharmacology

ORIGINAL RESEARCH
published: 16 November 2021
doi: 10.3389/fphar.2021.773204

Antinociceptive and Antipruritic Effects of HSK21542, a Peripherally-Restricted Kappa Opioid Receptor Agonist, in Animal Models of Pain and Itch

Xin Wang[1†], Xiaoli Gou[2†], Xiaojuan Yu[2], Dongdong Bai[2], Bowei Tan[2], Pingfeng Cao[2], Meilin Qian[2], Xiaoxiao Zheng[2], Hairong Wang[2], Pingming Tang[2], Chen Zhang[2], Fei Ye[2] and Jia Ni[2]**

[1]Intensive Care Unit, First Affiliated Hospital of Xinjiang Medical University, Urumqi, China, [2]Center for Drug Research and Development, Haisco Pharmaceutical Group Co., Ltd., Chegdu, China

OPEN ACCESS

Edited by:
Andres Trostchansky,
Universidad de la República, Uruguay

Reviewed by:
Saadet Inan,
Temple University, United States
Marta Valenza,
Sapienza University of Rome, Italy

***Correspondence:**
Fei Ye
yef@haisco.com
Jia Ni
njia@haisco.com

†These authors have contributed equally to this work and share first authorship

Specialty section:
This article was submitted to Experimental Pharmacology and Drug Discovery, a section of the journal Frontiers in Pharmacology

Received: 09 September 2021
Accepted: 28 October 2021
Published: 16 November 2021

Citation:
Wang X, Gou X, Yu X, Bai D, Tan B, Cao P, Qian M, Zheng X, Wang H, Tang P, Zhang C, Ye F and Ni J (2021) Antinociceptive and Antipruritic Effects of HSK21542, a Peripherally-Restricted Kappa Opioid Receptor Agonist, in Animal Models of Pain and Itch. Front. Pharmacol. 12:773204. doi: 10.3389/fphar.2021.773204

Kappa opioid receptor (KOR) agonists have been promising therapeutic candidates, owing to their potential for relieving pain and treating intractable pruritus. Although lacking morphine-like central nervous system (CNS) effects, KOR agonists do elicit sedation, dysphoria and diuresis which seriously impede their development. Peripherally-restricted KOR agonists have a poor ability to penetrate into the CNS system, so that CNS-related adverse effects can be ameliorated or even abolished. However, the only approved peripherally-restricted KOR agonist CR845 remains some frequent CNS adverse events. In the present study, we aim to address pharmacological profiles of HSK21542, with an expectation to provide a safe and effective alternative for patients who are suffering from pain and pruritus. The *in vitro* experimental results showed that HSK21542 was a selective and potent KOR agonist with higher potency than CR845, and had a brain/plasma concentration ratio of 0.001, indicating its peripheral selectivity. In animal models of pain, HSK21542 significantly inhibited acetic acid-, hindpaw incision- or chronic constriction injury-induced pain-related behaviors, and the efficacy was comparable to CR845 at 15 min post-dosing. HSK21542 had a long-lasting analgesic potency with a median effective dose of 1.48 mg/kg at 24 h post-drug in writhing test. Meanwhile, the antinociceptive activity of HSK21542 was effectively reversed by a KOR antagonist nor-binaltorphimine. In addition, HSK21542 had powerful antipruritic activities in compound 48/80-induced itch model. On the other hand, HSK21542 had a weak ability to produce central antinociceptive effects in a hot-plate test and fewer effects on the locomotor activity of mice. HSK21542 didn't affect the respiratory rate of mice. Therefore,

Abbreviations: BSA, bovine serum albumin; CCI, chronic constriction injury; CI, onfidence interval; CNS, central nervous system; DOR, delta opioid receptor; EC_{50}, half maximal effective concentration; ED_{50}, median effective dose; FBS, fetal bovine serum; GPCR, G-protein coupled receptor; HBSS, hank's balanced salt solution; HEPES, hydroxyethyl piperazineethanesulfonic acid; IBMX, 3-Isobutyl-1-methylxanthine; IC_{50}, 50% inhibitory concentration; KOR, kappa opioid receptor; MED, minimum effective dose; MOR, mu opioid receptor; MPE, maximum possible effect; PWT, paw withdrawal threshold; SD, standard deviation; TR-FRET, time-resolved fluorescence resonance energy transfer.

HSK21542 might be a safe and effective KOR agonist and promising candidate for treating pain and pruritus.

Keywords: HSK21542, kappa opioid receptor, pain, pruritus, animal models

INTRODUCTION

Kappa opioid receptor (KOR), one of the classical opioid receptors, is an inhibitory G-protein coupled receptor (GPCR) that is distributed in both the central nervous system (CNS) and the peripheral tissues (Ragen et al., 2015; Snyder et al., 2018). Due to the wide distribution and associated physiological functions of KOR, it has been used in exploring as a potential target for drug development in many diseases, including pain, inflammation, pruritus and addiction (Kieffer and Gaveriaux-Ruff, 2002; Bailey and Ribeiro-da-Silva, 2006; Chavkin, 2011; Kardon et al., 2014). Since the cloning of KOR in 1993 (Chen et al., 1993; Yasuda et al., 1993), the centrally penetrating KOR agonists have become the main focus of research for a long time. Unfortunately, although the undesirable side effects induced by mu opioid receptor (MOR) agonists are lacking, the centrally penetrating KOR agonists are frequently accompanied by certain side effects such as sedation, dysphoria and diuresis. The development of centrally penetrating KOR agonists is severely limited due to its unpleasant adverse events, and only one centrally penetrating KOR agonist nalfurafine has been approved so far for the treatment of pruritus in Japan (Inui, 2015).

To avoid these adverse side effects, other approaches have been attempted for developing the KOR agonists, and the biased KOR agonists and peripherally-restricted KOR agonists among these have gained much attention. The development of biased KOR agonists was based on the concept that G-protein coupled receptors (GPCRs) can selectively signal in different contexts (Violin et al., 2014). It is evident that opioid receptors-mediated GPCRs have the ability to interact with both G proteins and β-arrestins simultaneously. Previous studies have revealed that the side effects associated with opioid receptor activation are mediated by β-arrestin-mediated signaling pathway (Schmid et al., 2017; Hill et al., 2018b). Therefore, developing G protein-biased agonists of opioid receptors is considered as a promising strategy to bypass the CNS-mediated side effects. The biased KOR agonists were shown to be effective in treating pain and pruritus in animal models (Brust et al., 2016; Gupta et al., 2016). However, the results from two phase 3 clinical trials showed that the performance of oliceridine (TRV130), which is a biased MOR agonist, is not obviously superior to morphine, especially for reducing the respiratory depression (Singla et al., 2019; Viscusi et al., 2019). Since then, the concept of biased opioid receptor agonist has met with less enthusiasm.

The actions of peripherally-restricted KOR agonists are restricted to peripheral sites due to their low penetration into the brain, and the CNS-associated side effects associated with this can be significantly ameliorated or even completely abolished. The peripherally-restricted KOR agonists had analgesic, anti-inflammatory and antipruritic effects (Naser and Kuner, 2018). Till now, some peripherally-restricted KOR agonists, including ICI-204448, GR-94839, asimadoline, ADL-10-0116, FE200665 (CR665) and difelikefalin (CR845), have been successfully identified (Barber et al., 1994; Binder et al., 2001; Vanderah et al., 2004; Negus et al., 2012). However, the development of other compounds, except for asimadoline and CR845, has been discontinued. Originally, asimadoline was studied in treating pain and found to be ineffective. Subsequently, asimadoline has been shown to be an effective treatment for pruritus associated with atopic dermatitis (Bishop et al., 2015; Vakharia and Silverberg, 2018), but no further development of it has been reported after that. CR845, a peptide-based peripherally-restricted KOR agonist, exhibited excellent analgesic and antipruritic effects in clinical trials with limited side effects (Menzaghi et al., 2015; Fishbane et al., 2020; Steele, 2020). At present, CR845 has been approved for the treatment of moderate-to-severe pruritus associated with chronic kidney disease (CKD-aP) in adults undergoing hemodialysis. However, CR845 is only available in the United States and has some frequent adverse events, such as diarrhea, dizziness, vomiting and nasopharyngitis (Fishbane et al., 2020).

With the aim to develop more effective and safer peripherally-restricted KOR agonist, HSK21542 [7-(D-phenylalanyl-D-phenylalanyl-D-leucyl-D-lysyl)-2-acetyl-2,7-diazaspiro (3.5) nonane], was synthesized. Several studies were conducted to comprehensively address the pharmacological profiles of HSK21542. The biological activity and selectivity of HSK21542 were examined using *in vitro* assays, including [^{3}H] diprenorphine binding assay, cAMP accumulation assay, and a SafetyScreen panel. Its ability to penetrate into CNS tissues was detected with a brain/plasma distribution study. Four different animal models of pain and compound 48/80-induced scratching mouse model of pruritus were used to evaluate the *in vivo* pharmacological activities of HSK21542, and the CNS side effects associated with it were also detected. Further, pharmacological profiles of HSK21542 and CR845 were compared.

MATERIALS AND METHODS

Animals

ICR mice weighing 18–22 g and Sprague Dawley (SD) rats weighing 160–180 g were purchased from Beijing Vital River Laboratory Animal Technology Co., Ltd. (China). C57BL/6J mice weighing 18–22 g were obtained from Chengdu DOSSY Laboratory Animal Technology Co., Ltd. (China). All animals were aged between 8 and 10 weeks at the start of the experiments. Animals were maintained on a standard 12 h light/12 h dark cycle in a temperature-and humidity-controlled facility with free access to food and water. The investigators were blinded to the treatment conditions. All animal care and experimental

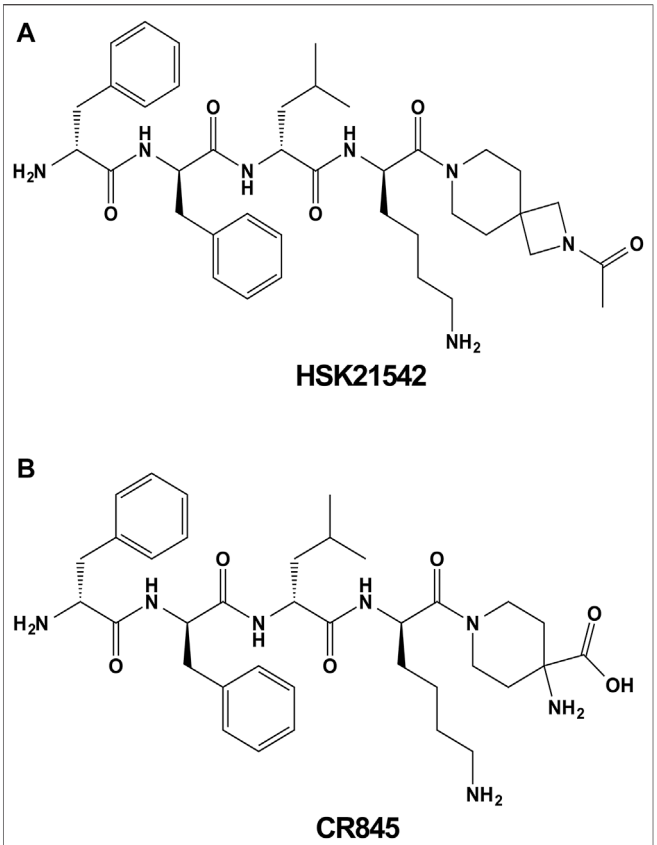

FIGURE 1 | Chemical structures of HSK21542 **(A)** and CR845 **(B)**.

procedures were performed in accordance with the guidelines of National Institutes of Health for the handling and use of laboratory animals and approved by the Guideline of the Institutional Animal Care and Use Committee of Haisco Pharmaceutical Group Co., Ltd. [HSK-(HEISCO-I-17)-2-1-2001-01].

Chemicals and Reagents

HSK21542 and CR845 were synthesized in Sichuan Haisco Pharmaceutical Co., Ltd. (China). The synthesis and physicochemical characteristics of HSK21542 have been described in a patent (WO2019015644). The chemical structures of HSK21542 and CR845 are shown in **Figure 1**. The sources of chemicals were as follows: [^{3}H]diprenorphine (Perkin Elmer, United States), U69593 (Sigma-Aldrich, United States), morphine sulfate (National Institutes for Food and Drug Control, China), nor-binaltorphimine (Abcam, United Kingdom), nalfurafine hydrochloride (MedChem Express, United States) and compound 48/80 (Sigma-Aldrich, United States). For *in vivo* experiments, all the test compounds were solubilized in normal saline, and intravenously administered with a volume of 10 μL/g, except for morphine and nor-binaltorphimine (subcutaneously) when the animals were not under anesthesia and were awake. All other reagents used were of analytical grade unless otherwise stated.

[^{3}H]Diprenorphine Binding Assay

HEK-293 cells (ATCC) were maintained in Eagle's Minimum Essential Medium with 10% FBS, and incubated at 37°C in humidified air containing 5% CO_2. HEK-293 cells that stably express human κ opioid receptor were established in our laboratory and used in this assay. The cell membranes were prepared in 50 mM Tris-HCl buffer (pH 7.4). An equivalent of 30 μg of membranes was incubated with compounds and 0.6 nM [^{3}H]diprenorphine (an opioid antagonist) at 25°C for 60 min (inhibitory effect) or the multiple time points (binding kinetics). Nonspecific binding was estimated in the presence of 10 μM naloxone. The bound and free fractions were separated by vacuum filtration through a GF/B filter that was pretreated with 0.3% polyetherimide. The filters were washed with ice-cold buffer and then were counted to specifically determine the bound radioligand (Olianas et al., 2006). The percentage inhibition of [^{3}H]diprenorphine binding was calculated as follows: inhibition rate (%) = (CPM_{total}–$CPM_{compound}$)/(CPM_{total}–$CPM_{non\text{-}specific}$) × 100, where CPM_{total} = total [^{3}H] diprenorphine bound (membrane +0.6 nM [^{3}H]diprenorphine) and $CPM_{non\text{-}specific}$ = non-specific [^{3}H]diprenorphine bound (membrane +0.6 nM [^{3}H]diprenorphine + 10 μM naloxone). For the unlabeled compounds, the association/dissociation constants were calculated by fitting the data using equations as described by Motulsky and Mahan (Motulsky and Mahan, 1984).

cAMP Accumulation Assay

PathHunter® U2OS OPRK1 β-Arrestin cell line (DiscoverX) was maintained in McCoy's 5A with 10% FBS, 250 μg/ml Hygromycin B and 500 μg/ml G418. When the cells reached to 80–90% confluence, they were collected and resuspended in HBSS (1X) containing 50 mM HEPES, 5 mM IBMX and 1% BSA stabilizer (lance® UltracAMP Kit, PerkinElmer) by adjusting the cell density to 3×10^5 cells/mL. The cells were divided into 384-well white plate (Corning®3572) at a volume of 5 μL, and were treated with compounds and 2 μM forskolin (an inducer of intracellular cAMP formation) for 30 min at room temperature. Subsequently, 5 μL of Eu-cAMP Tracer Working Solution and 5 μL of Ulight-anti-cAMP Working Solution per well were added to reach a final volume of 20 μL. The plate was incubated for 1 h at room temperature in the dark. The cAMP levels were then determined by using a microplate reader with TR-FRET assay (Wang et al., 2014). The results was expressed as (1–$Signal_{[compound]}$/$Signal_{[control]}$) × 100.

In vitro SafetyScreen Panel

In vitro off-target pharmacological activities of HSK21542 were evaluated on 86 targets using a SafetyScreen panel (Item PP223, target selectivity panel) and the corresponding methods could be found at https://www.eurofinsdiscoveryservices.com/.

In vivo Brain/Plasma Distribution of HSK21542 in Rats

SD rats (half male and half female) were intravenously given a single dose of 0.3 mg/kg HSK21542. The samples were collected at 0.083, 0.5, 1.5 and 4 h after dosing. The rats were anesthetized

with isoflurane and then sacrificed by taking blood from the abdominal aorta. The whole brains were rapidly removed from the crania. The plasma (~100 μL) was separated from the blood by centrifugating at 2000 ×g for 10 min at 4°C. The brains were rinsed with ice-cold normal saline, blotted dry, weighted and placed into a plastic tube. For 1.0 g of brain sample, 4 ml of acetonitrile-ultrapure water solution (1:4, v/v) was added to the tube. The brain samples were then homogenized for 120 s at 50 Hz and ultrasound was performed for 5 min. The plasma and the brain samples were analyzed using a LC-MS/MS assay as detailed in supplementary materials.

LC-MS/MS Assay

The plasma or brain homogenate was ice thawed. After 30 μL of plasma or brain homogenate was transferred into a centrifuge tube, 50 μL of internal standard (D4-HSK21542, 50 ng/ml) and 120 μL of acetonitrile were added. The mixture was vortexed for 10 min and centrifuged at 2000 ×g for 10 min at 4°C. The collected supernatant (150 μL) was placed in a 96-well plate and dried under nitrogen. The residue was reconstituted with 150 μL of ultrapure water and vortexed for 10 min. The resulting solution was then analyzed to determine the concentrations of HSK21542 on a LC-MS/MS system, which consisted of a DGU-20A5R degasser, a LC-30AD pump, a SIL-30AC autosampler, a CTO-20A column oven (Shimadzu, Japan) and an AB Sciex Triple Quad 5500 mass spectrometer (Sciex, Canada). The LC system was coupled to mass spectrometer by using an electrospray ionization (ESI) source (Yang et al., 2011; Dong et al., 2018). Chromatographic separation was performed on a reverse phase column (Venusil ASB C18, 4.6 mm × 50 mm) under a ternary gradient elution. The temperatures of autosampler and column were maintained at 4 and 40°C, respectively. The mobile phase A consisted of 0.3% formic acid in 2 mM acetic acid solution and the mobile phase B consisted of 0.2% formic acid in acetonitrile. The flow rate was held constant (0.7 ml/min) and the injection volume was set to 20 μL. Quantification was conducted in positive ion mode. The MRM transition of m/z 704.4→295.2 was used to quantify HSK21542.

Writhing Test

ICR mice (half male and half female) were used in this assay. Fifteen or 30 min (only for morphine) after test compounds were given, each mouse was intraperitoneally injected with 0.6% acetic acid at a volume of 0.4 ml. Subsequently, each animal was individually maintained in a Plexiglas chamber and the pain-induced writhing behaviors were observed for 15 min (Abdollahi et al., 2003; Bourgeois et al., 2014). A writhe was defined as a wave of contraction of the abdominal musculature followed by extension of the hind limbs (Wang et al., 2018). The percentage inhibition of writhes was calculated by the following formula: % antinociception = (Nv–Nt)/Nv × 100, where Nv is the number of writhes in vehicle group and Nt is the number of writhes in treatment groups.

Hindpaw Incision Model

The surgery was conducted as reported previously (Brennan et al., 1996; Whiteside et al., 2004; Biddlestone et al., 2007). Male SD rats were anesthetized with isoflurane inhalation (3–5%) and the plantar surface of the left hindpaw was sterilized using iodophor solution. A 1-cm longitudinal incision was made on the plantar surface with no. Eleven scalpel blade, starting at 0.5 cm from the heel and extending toward the toes. The deep fascia was cut to expose the flexor digitorum brevis muscle. The muscle was elevated with curved forceps and incised longitudinally with the tip of a scalpel blade without disturbing the origin and insertion. Following hemostasis with gentle pressure, the skin was closed with silk thread using two mattress sutures. After surgery, antibiotic ointment was applied on the incision site and the animals were returned to their home cages with clean bedding to prevent further damage to the injured hindpaw. The responses to mechanical stimulation of the hindpaws were recorded at 2 h post-surgery and the mechanical pain thresholds were defined as pre-dose values. After dividing into different groups according to the pre-dose values, the animals were administered vehicle (normal saline) or test compounds and the mechanical pain thresholds were measured at 15 min and 24 h post-dose.

Chronic Constriction Injury Model

The CCI surgery was performed as described previously with slight modifications (Bennett and Xie, 1988). Male SD rats were used in the CCI model. After isoflurane inhalation anesthesia, the femoral skin of the left hindlimb was incised and the sciatic nerve was exposed by blunt dissection of the biceps femoris muscle with a pair of forceps (Chen et al., 2018). A 2 mm-long polyethylene cuff was successively implanted around the nerve and the incision was then closed with skin stapler (Bailey and Ribeiro-da-Silva, 2006; Balasubramanyan et al., 2006). Animals were returned to their cages after recovering from anesthesia. Seventeen days after the surgery, the responses to mechanical stimulation of the hindpaws were measured before the compounds were administered. The rats were then divided into different groups according to the pre-administration values. After the animals were given vehicle or test compounds, the mechanical pain thresholds were taken at multiple time points.

Mechanical Allodynia Testing

The rats were placed individually in Plexiglas chambers on a metallic mesh floor and allowed to acclimatize for 30–60 min (Tsuda et al., 2011). Mechanical allodynia was determined by probing the plantar surface of the hindpaw from below the mesh floor with a series of calibrated von Frey filaments (Stoelting) in log increments of force (Lai et al., 2006). The interval between two neighboring stimulations was more than 5 s in order to eliminate the effects of the previous stimulation, and the bending angle of von Frey filaments was controlled at 15–30°. Followed by, Dixon's up-down procedure was done to present the series of hairs and calculate the 50% paw withdrawal threshold (PWT) (Chaplan et al., 1994; Weir et al., 2017). The area under the curve (AUC, 50% PWT *vs.* time) was calculated using a trapezoid rule.

Compound 48/80-Induced Scratching Test

After acclimatization for 30–60 min in Plexiglas chambers, the male ICR mice were given vehicle or test compounds. Compound 48/80 (50 μg, 0.1 ml) was subcutaneously injected into the back of

the neck at 15 min after drug administration (Salaga et al., 2015). The mice were immediately placed back into the chambers and the scratching behaviors were recorded for 30 min (Kobayashi et al., 2003; Inan et al., 2009; Hachisuka et al., 2010). One bout of scratching was defined as the mouse lifting its hindpaw towards the injection site to scratch until it either licked or bite the hindpaw or placed it back down on the floor (Nojima and Carstens, 2003). The percentage inhibition of scratching was calculated by the following formula: % antipruritis = (Bv−Bt)/Bv × 100, where Bv is the bouts of scratching in vehicle group and Bt is the bouts of scratching in treatment groups.

Hot-Plate Test

The hot-plate test was performed according to previous reports (DeWire et al., 2013; Hill et al., 2018a; Wang et al., 2018). Female C57BL/6J mice were individually placed on a hot plate at 56°C and the latency to licking or jumping was then recorded. A cut-off time of 30 s was imposed in order to prevent tissue damage. Before drug administration, the latency of each mouse was measured and defined as the pre-drug value. The animals with a pre-drug value of greater than 20 s were excluded. Fifteen or 30 min (only for morphine) after drug administration, the post-drug values were taken, and the percentage of maximum possible effect (% MPE) was determined as follows: [(post-drug value−pre-drug value)/(30−pre-drug value)] × 100.

Locomotor Activity Test

The locomotor activity test was applied to analyze sedation in rats (half male and half female). Experiments were performed after animals were acclimatized to a rectangular experimental cage (35 × 35 × 35 cm^3) for 2 days. 15 or 30 min (only for morphine) after either vehicle or test compounds were administered, each rat was returned to the cage, and then allowed to explore the field for 1 h. The data were collected using an ANY-maze video tracking system and the total distance traveled was analyzed (Gou et al., 2021).

Measurement of Respiration

A whole body plethysmography (DSI, US) was used to measure respiration in freely moving ICR mice (half male and half female) as described previously (Manglik et al., 2016; Hill et al., 2018a; Hill et al., 2018b) with some modifications. The respiratory frequency was recorded and then averaged for over 5-min period. The baseline values were recorded for 10 min before dosing. The mice were then removed from the chambers and given drugs, and respiration was then measured for 45 min.

Data and Statistical Analysis

All study endpoints were expressed as means ± SD and no data have been excluded. Statistical comparisons were made using GraphPad Prism 8.3.0 software (San Diego, CA, United States). No statistical methods were used to predetermine the sample sizes, but the choice of sample sizes was based on our previous studies and the sample sizes are similar to those that are typically used in the field. For *in vitro* experiments, the IC_{50} or EC_{50} value was determined by non-linear, least squares regression analysis. The binding kinetic curves were fitted by a competitive binding model. In this model, the K1 (the association rate of [^{3}H]diprenorphine) and K2 (the dissociation rate of [^{3}H]diprenorphine) were constrained to $1.44 \times 10^8\ M^{-1}\ min^{-1}$ and $0.0257\ min^{-1}$, respectively. The association kinetic curves of [^{3}H]diprenorphine are shown in **Supplementary Figure S1**. For most of the *in vivo* experiments, a parametric analysis (one-way analysis of variance) was performed if the Bartlett's test for variance homogeneity showed no significance at 1% level, and the treated groups were compared to the vehicle group using Dunnett's test when F achieves the necessary level of statistical significance (the null hypothesis: there was no difference among the treated groups and the vehicle group). Otherwise, a non-parametric analysis (Kruskal-Wallis test) was performed, and the treated groups were compared to the vehicle group using Dunn's test when necessary. Planned comparison was done between the two groups using student's t-test (with same variance) or Mann-Whitney test. The original data from chronic constriction injury model and the measurement of respiration in mice were analyzed by two-way analysis of variance (ANOVA) using the treatment conditions and time as factors. Then, *post-hoc* Dunnett's test was performed at different time points if there was an interaction effect. The criterion for statistical significance was set at $p < 0.05$.

RESULTS

HSK21542 is a Peripherally-Restricted Kappa Opioid Receptor Agonist

To unravel the pharmacological profiles of HSK21542 at KOR, [^{3}H]diprenorphine binding assay was performed to investigate the inhibitory effects of HSK21542 on [^{3}H]diprenorphine competition binding and determine the binding kinetics of unlabeled HSK21542. U69593, a positive control, obviously prevented [^{3}H]diprenorphine binding to KOR with an IC_{50} value of 14.72 nM (95% CI: 9.08–22.38 nM). As anticipated, HSK21542 significantly inhibited [^{3}H]diprenorphine binding to KOR with an IC_{50} value of 0.54 nM (95% CI: 0.38–0.75 nM), while CR845 had an IC_{50} value of 1.16 nM (95% CI: 0.85–1.57 nM, **Figure 2A**). The results of the binding kinetics study revealed that HSK21542 and CR845 bound to KOR with K_d values of 0.068 nM (95% CI: 0.028–0.092 nM) and 0.23 nM (95% CI: 0.17–0.26 nM), respectively (**Figures 2B,C**). Meanwhile, HSK21542 had a $t_{1/2}$ value of 90.6 min (95% CI: 53.6–292.7 min), which was found to be longer than that of CR845 (42.0 min, 95% CI: 28.6–79.4 min). On the other hand, HSK21542 significantly inhibited forskolin-induced cAMP accumulation in HEK-293 cells that stably expressed human κ opioid receptor with an EC_{50} value of 2.41 pM (95% CI: 1.43–4.67 pM), which was 12.4-fold and 747-fold lower than those of CR845 and U69593, respectively (**Figure 2D**).

To investigate the specificity, the *in vitro* profile of HSK21542 was observed against a broad panel of receptors, ion channels, transporters and enzymes, including MOR and DOR. At a concentration of 10 μM, HSK21542 was shown to bind to cannabinoid CB_1 receptor with an inhibitory rate of 47%, and no obvious activity was observed at the remaining 85 targets (**Supplementary Table S1**).

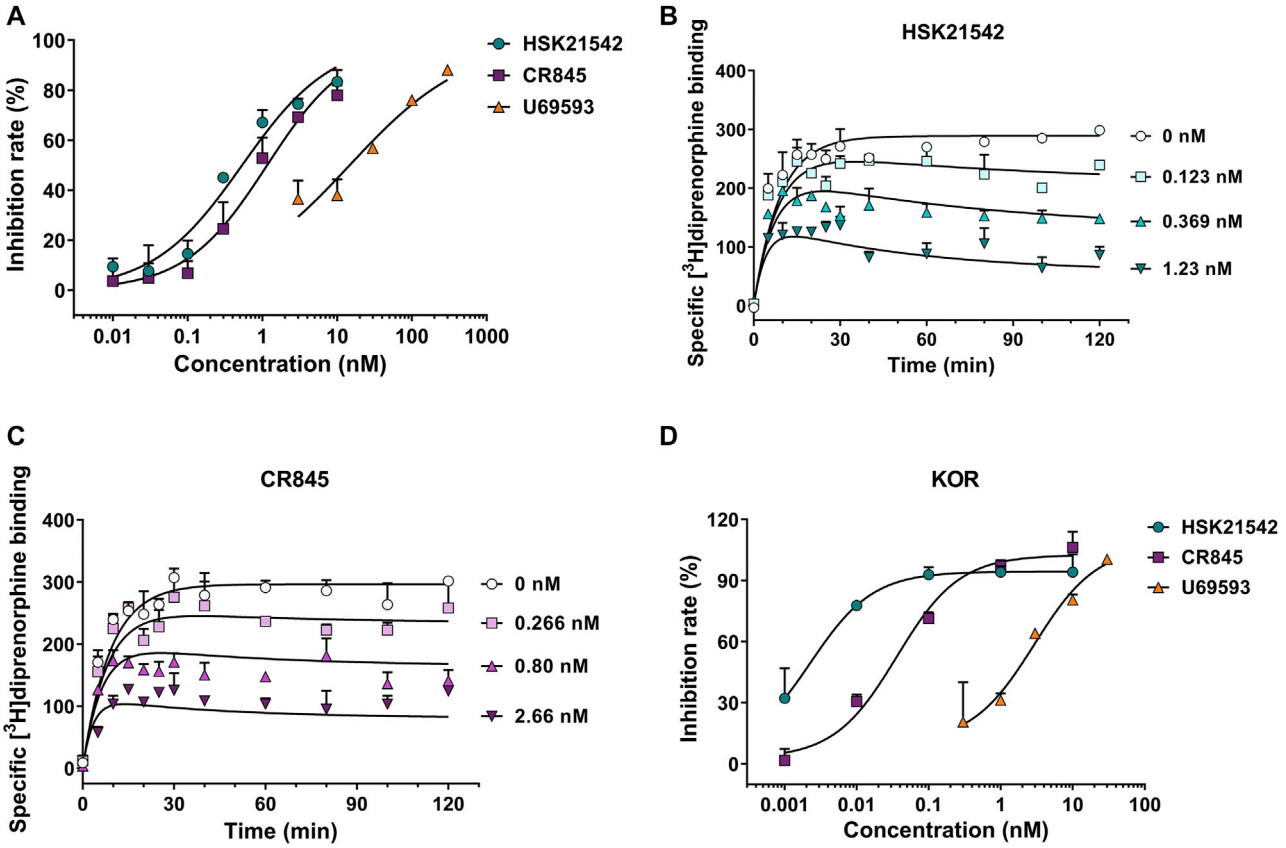

FIGURE 2 | Kappa opioid receptor binding affinity and the effects on forskolin-induced cAMP accumulation of HSK21542 and CR845. **(A)** Concentration-effect curves of the inhibitory rates induced by HSK21542, CR845 or U69593 (the positive control) on [^{3}H]diprenorphine binding to KOR. **(B)** The binding kinetic curves of HSK21542 binding to KOR. **(C)** The binding kinetic curves of CR845 binding to KOR. **(D)** Concentration-effect curves of the inhibitory rates induced by HSK21542, CR845 or U69593 (the positive control) on forskolin-induced cAMP accumulation. Data are presented as means ± SD of triple determinations.

Furthermore, it was extremely hard for HSK21542 to penetrate into the brain tissues with a brain/plasma concentration ratio of 0.001 (**Supplementary Figure S2**).

HSK21542 Causes Potent Antinociceptive Effects

The antinociceptive effects of HSK21542 were evaluated using a writhing test in mice, which is an animal model of inflammatory pain. Both male and female mice were used to investigate any sex differences in this assay. Morphine (10 mg/kg), a positive control, completed suppressed acetic acid-induced pain behaviors at 30 min post-dosing ($p < 0.001$, Mann-Whitney test). However, the efficacy of 10 mg/kg morphine had vanished at 24 h post-dosing ($t_{(18)} = 1.25$, $p = 0.30$), which was corresponding to the pharmacological profile of morphine. Fifteen minutes after drug administration, HSK21542 inhibited acetic acid-induced writhing response in a dose-dependent manner (**Figure 3A**, $F_{(7, 72)} = 41.18$, $p < 0.001$), and there was no obvious sex difference (**Supplementary Figure S3A**, $F_{(1, 32)} = 3.40$, $p = 0.075$). HSK21542 at a dose of 0.03 mg/kg induced an inhibitory rate of 27.46% on writhing behaviors, and there was a statistically significant difference in writhing responses between 0.03 mg/kg HSK21542-treated group and vehicle group ($p = 0.023$). Therefore, the dose of 0.03 mg/kg was defined as the minimum effective dose (MED), which was 3.33-fold lower than that of CR845 (0.1 mg/kg). Moreover, the ED_{50} values of HSK21542 and CR845 were both 0.09 mg/kg (95% CI: 0.06–0.12 mg/kg), and the inhibitory activity of HSK21542 on writhing response was comparable to that produced by CR845 at the same doses. Finally, nor-binaltorphimine (32 mg/kg, s.c.), a kappa opioid receptor antagonist which was given at 24 h before drug administation, reversed the antinociceptive effects produced by 0.3 or 1 mg/kg HSK21542 (**Figure 3B**).

To explore the duration of action of a single dose of HSK21542, the antinociceptive effects of HSK21542 were detected at 24 h post-drug. Surprisingly, 0.3 mg/kg of HSK21542 still significantly inhibited the writhing responses with an inhibitory rate of 32.75% (**Figure 3C**, $p = 0.02$). At the doses of 1, 3, 10 and 30 mg/kg, HSK21542 induced inhibitory rates of 49.67, 55.60, 68.12 and 75.16%, respectively. However, as for CR845, a dose of 30 mg/kg was needed to maintain the antinociceptive effects at 24 h post-drug ($p < 0.001$). The ED_{50} values of HSK21542 and CR845 were 1.48 mg/kg (95% CI:

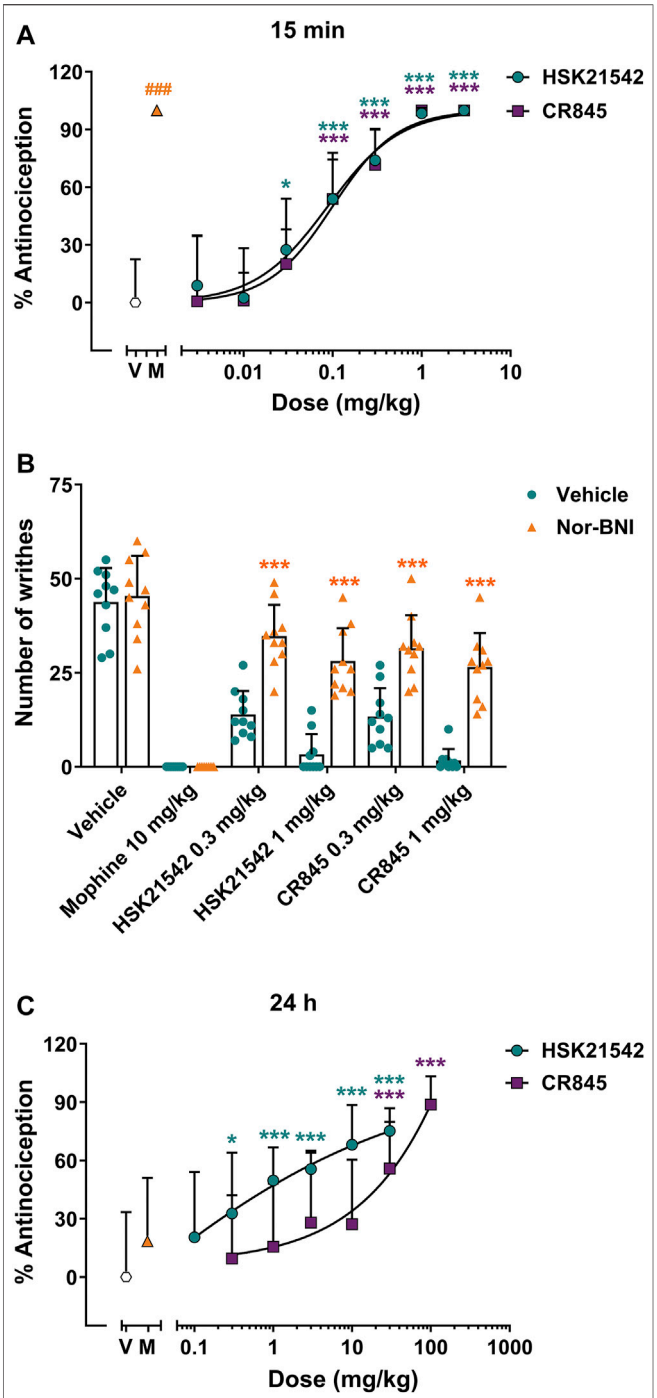

FIGURE 3 | Antinociceptive effects of HSK21542 and CR845 in acetic acid-induced writhing response in mice. **(A)** The writhing tests were conducted at 15 min post-dosing. **(B)** Nor-binaltorphimine (Nor-BNI, 32 mg/kg, s.c.), a KOR antagonist, was given at 24 h before drug administration, and the antinociceptive effects of HSK21542 and CR845 were examined at 15 min post-dosing. **(C)** The writhing tests were performed at 24 h post-dosing. Data are presented as means ± SD (n = 10/group). **(A, C)** $^{*}p < 0.05$, $^{***}p < 0.001$ vs. vehicle, one-way ANOVA followed by Dunnett's test; **(B)** $^{***}p < 0.001$ *vs.* vehicle, Student's t-test; $^{###}p < 0.001$ vs. vehicle, Mann-Whitney test. V, Vehicle; M, Morphine (10 mg/kg, a positive control).

0.62–2.45 mg/kg) and 24.62 mg/kg (95% CI: 13.90–42.55 mg/kg), respectively.

HSK21542 Produces Significant Antiallodynic Effects

The hindpaw incision model and chronic constriction injury (CCI) model in rats, which were widely used for evaluating the analgesic property, were employed to determine the antiallodynic effects of HSK21542. Morphine, a potent analgesic, was given as a positive control. Obviously, morphine (10 mg/kg) completely inhibited hindpaw incision- or CCI-induced mechanical allodynia at 15 min after dosing ($p < 0.001$, Mann-Whitney test), while morphine had no any effect on pain behaviors at 24 h post-dosing ($p = 0.30$, Mann-Whitney test).

In the hindpaw incision model, systemic HSK21542 (0.1–10 mg/kg) exerted a dose-dependent inhibitory effect on incision-induced mechanical allodynia ($p < 0.001$, Kruskal-Wallis test). At a dose of 1 mg/kg, HSK21542 induced a 10.5-fold increase of 50% PWT (7.51 g vs. 0.72 g in the vehicle group, $p = 0.001$) at 15 min post-dosing. The MED value of HSK21542 was 1 mg/kg, which was comparable to that achieved by CR845 at 15 min after dosing, and 10 mg/kg HSK21542 induced the maximum antiallodynic activity (**Figure 4A**). It is noteworthy that the effects of HSK21542 were still statistically significant at 24 h after drug administration at the doses of 3 mg/kg ($p = 0.01$) and 10 mg/kg ($p < 0.001$), which were similar to those of CR845 (**Figure 4B**).

In the chronic constriction injury model, intravenous injection of HSK21542 (0.1–3 mg/kg) suppressed CCI-induced mechanical allodynia in rats in a dose-dependent manner ($F_{(5, 316)} = 245.0$, $p < 0.001$). At a dose of 0.3 mg/kg, HSK21542 induced a 5.15-fold increase of 50% PWT (6.62 g vs. 1.29 g in the vehicle group) at 15 min post-dosing. In 1 or 3 mg/kg HSK21542-treated group, the 50% PWT value reached a peak at 2 h post-dosing, and then gradually faded (**Figure 4C**). Furthermore, when given at a dose of 1 or 3 mg/kg, the mechanical pain threshold in HSK21542-treated groups was significantly higher than that in the vehicle-treated group at 24 h post-dosing. The results showed that the treatment with 0.3 mg/kg HSK21542 induced a statistically significant increase on the AUC value (50% PWT vs. time, **Figure 4D**, $p < 0.001$). Therefore, the dose of 0.3 mg/kg was defined as the MED value of HSK21542. On the other hand, there was no obvious difference in mechanical pain thresholds between 0.1 mg/kg HSK21542-treated group and vehicle-treated group at any time points post-dosing. Moreover, although the antiallodynic effects of CR845 could still persist until 24 h post-administration at a dose of 3 mg/kg ($p < 0.001$), the effects of CR845 had completely vanished at a dose of 1 mg/kg (**Figure 4E**, $p = 0.13$).

HSK21542 Attenuates Compound 48/80-Induced Itch

KOR agonist has been validated as an effective therapy for pathological itch (Kardon et al., 2014; Cowan et al., 2015; Inui,

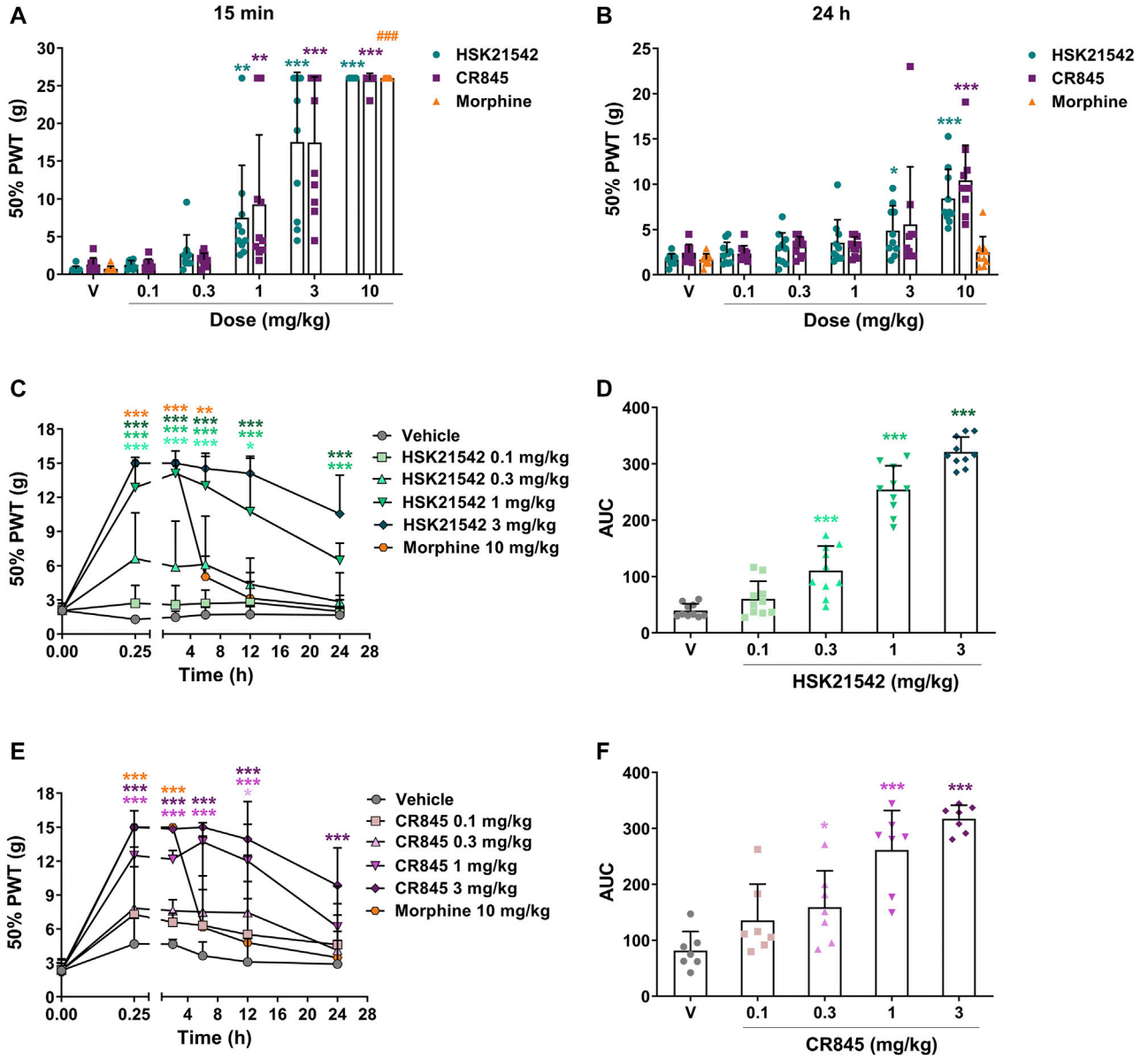

FIGURE 4 | Antiallodynic effects of HSK21542 and CR845 in hindpaw incision- or CCI-induced mechanical pain. In hindpaw incision model, the mechanical allodynia testing (von Frey) was performed at 15 min **(A)** and 24 h **(B)** after drug administration. In CCI model, mechanical allodynia testing was performed at 0.25, 2, 6, 12 and 24 h post-drug **(C, E)**, and the area under the curve (AUC) was calculated using a trapezoidal method **(D, F)**. Morphine was presented as a positive control. Data are presented as means ± SD (n = 7–10/group). (A and B) $^{*}p < 0.05$, $^{**}p < 0.01$, $^{***}p < 0.001$ vs. vehicle, Kruskal-Wallis test followed by Dunn's post-hoc test; **(C, E)** $^{*}p < 0.05$, $^{**}p < 0.01$, $^{***}p < 0.001$ vs. vehicle, two-way ANOVA followed by Dunnett's test; **(D, F)** $^{*}p < 0.05$, $^{***}p < 0.001$ vs. vehicle, one-way ANOVA followed by Dunnett's test; $^{\#\#\#}p < 0.05$ vs. vehicle, Mann-Whitney test. V, Vehicle.

2015). The antipruritic effects of HSK21542 were then determined with compound 48/80-induced scratching test in mice. In the compound 48/80-induced scratching test, when given at a dose of 0.02 mg/kg, nalfurafine (a positive control) effectively suppressed the scratching responses with an inhibitory rate of 94.30% ($p < 0.001$, Mann-Whitney test). HSK21542 (0.01–3 mg/kg) inhibited the scratching responses to a similar extent as did CR845 in a dose-dependent manner at 15 min post-drug (**Figure 5**, $F_{(6,\ 63)} = 27.82$, $p < 0.001$). At a dose of 0.03 mg/kg, HSK21542 induced an inhibitory rate of 34.89%, and the number of scratching bouts was statistically less than that in the vehicle-treated group ($p = 0.015$). Therefore, the MED value of HSK21542 was designated as 0.03 mg/kg. At a dose of 1 mg/kg, the antipruritic activity of HSK21542 reached a peak with an inhibitory rate of 99.78%. In the 0.1 and 0.3 mg/kg HSK21542-treated groups, the inhibitory rates of 53.02 and 73.75% were observed, respectively. Furthermore, the analysis of dose-response curve showed that HSK21542 had an ED_{50} value

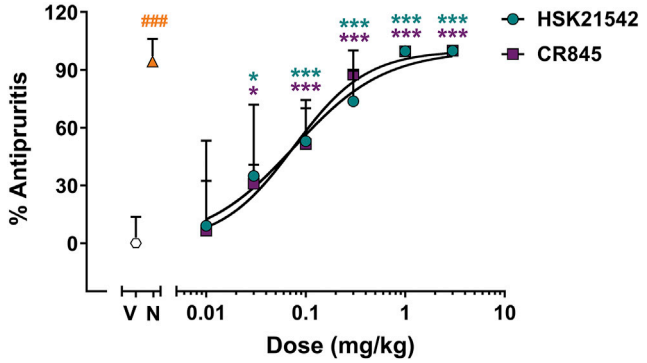

FIGURE 5 | Antipruritic effects of HSK21542 and CR845 in compound 48/80-induced itch model. Data are presented as means ± SD (n = 10/group). $^{*}p < 0.05$, $^{***}p < 0.001$ vs. vehicle, one-way ANOVA followed by Dunnett's test; $^{###}p < 0.001$ vs. vehicle, Mann-Whitney test. V, Vehicle; N, Nalfurafine (0.02 mg/kg, a positive control).

of 0.09 mg/kg (95% CI: 0.04–0.16 mg/kg), and this was comparable to that of CR845 (0.10 mg/kg, 95% CI: 0.04–0.23 mg/kg, p = 0.91, Extra sum-of-squares F test).

HSK21542 Showed Fewer CNS Side Effects

As a supraspinal model for acute pain, the hot-plate test is considered as one of the experimental methods for differentiating the central and peripheral antinociceptive effects (Le Bars et al., 2001). To validate whether the *in vivo* pharmacological effects of HSK21542 are mediated by a peripheral mechanism, a hot-plate test was employed in mice to evaluate the central antinociceptive effects of HSK21542 at 15 min post-drug. As one of central analgesics, 10 mg/kg morphine (a positive control) showed an almost complete efficacy. HSK21542 at 3.75 mg/kg did not evoke significant antinociceptive effects (p = 0.12), although 7.5 mg/kg HSK21542 induced a percent maximum possible effect (% MPE) of 29.60%, which was statistically higher than that in the vehicle-treated group (p = 0.007). However, CR845 displayed significant antinociceptive effects at a dose of 3.75 mg/kg (**Figure 6A**, p = 0.008). In addition, the effects of HSK21542 at 7.5 mg/kg were comparable to that of CR845 at 3.75 mg/kg (29.60% *vs.* 21.67%, $t_{(18)}$ = 0.42, p = 0.68). The ED_{50} values of HSK21542 and CR845 were 10.49 mg/kg (95% CI: 7.58–15.37 mg/kg) and 6.76 mg/kg (95% CI: 4.70–8.69 mg/kg), respectively (p = 0.026, Extra sum-of-squares F test).

To directly explore the CNS effects of HSK21542, its effects on sedation and respiration rate were measured. The sedative effects of HSK21542 and CR845 at 15 min post-dosing were evaluated using a locomotor activity test. The results showed that 10 mg/kg morphine reduced remarkedly the distance traveled by mice (p < 0.001) and there was no sex difference (**Supplementary Figure S4**, $F_{(1, 24)}$ = 4.19, p = 0.052). Although HSK21542 at 2 mg/kg induced an obvious sedative effect (p = 0.005), the lower dose of HSK21542 (0.4 mg/kg) did not significantly affect the locomotor activity of mice (**Figure 6B**, p = 0.16). On the other hand, 0.4 mg/kg CR845 induced an obvious decrease in the total distance traveled by mice (p < 0.001) with comparable efficacy to the higher dose of HSK21542 or CR845 (p > 0.05, Student's t-test). As shown in **Figure 6C**, 10 mg/kg morphine significantly reduced the respiratory rate (p < 0.001). There were no obvious effects on respiration when HSK21542 was given at a dose of as high as 2 mg/kg (p > 0.05). In contrast, CR845 caused significant decrease in the respiratory rate at a dose of 2 mg/kg at 25 min post-administration and the effects reached a peak at 45 min post-drug (**Figure 6D**, p < 0.01).

DISCUSSION

The current work provided significant findings, validating that HSK21542 is a peripherally-restricted KOR agonist and has an outstanding translational potential. These studies revealed that the combination of radioligand [^{3}H]diprenorphine and KOR was significantly inhibited by HSK21542, which could bind to KOR with high affinity, and HSK21542 inhibited cAMP accumulation induced by KOR activation. On the other hand, HSK21542 had no obvious biological effects on the remaining 86 targets. Meanwhile, the brain/plasma concentration ratio of HSK21542 remained extremely low, suggesting its peripheral selectivity. Furthermore, HSK21542 produced powerful analgesic and antipruritic effects in animal models. HSK21542 attenuated acetic acid-induced writhing response and the therapeutic efficacy was maintained for over 24 h by a single intravenous dose of 0.1–3 mg/kg. Meanwhile, the analgesic activity of HSK21542 could be reversed by the KOR antagonist nor-BNI, indicating its on-target activity. HSK21542 also suppressed hindpaw incision- or CCI-induced mechanical allodynia and the effects were still able to be detected at 24 h post-drug within a certain range of doses. Moreover, HSK21542 inhibited compound 48/80-induced scratching response. Finally, HSK21542 lacked obvious antinociceptive effects in hot-plate test, and had weaker effects on the locomotor activity and respiratory rate in mice.

CR845 is a peripherally-restricted KOR agonist that has been originally developed by Ferring Pharmaceuticals SA, and has been approved for treating pruritus. To validate if HSK21542 would be a better alternative for patients who are suffering from pain or pruritus, its pharmacological profiles were compared to those of CR845. In [^{3}H]diprenorphine binding assay, the IC_{50} and K_d values of HSK21542 were much smaller than those of CR845, and HSK21542 had a longer $t_{1/2}$ value for disassociating from KOR. These results indicated that HSK21542 acts as a ligand of KOR with higher affinity. Moreover, HSK21542 reversed forskolin-induced cAMP accumulation in HEK-293 cells that stably express human κ opioid receptor with subnanomolar potency, and was superior to CR845.

In 0.6% acetic acid-induced writhing test, HSK21542 induced potent antinociceptive effects at 15 min after systemic administration. The profile of HSK21542 was similar to that of CR845. Although the ED_{50} value of HSK21542 was completely identical to that of CR845 at 15 min post-dose, the ED_{50} value of HSK21542 was 16.6-fold lower than that of CR845 at 24 h post-drug. In addition, the MED of HSK21542 was 3.33–100 times lower than that of CR845. Therefore, HSK21542 is considered as a more promising candidate than CR845 for treating pain. To

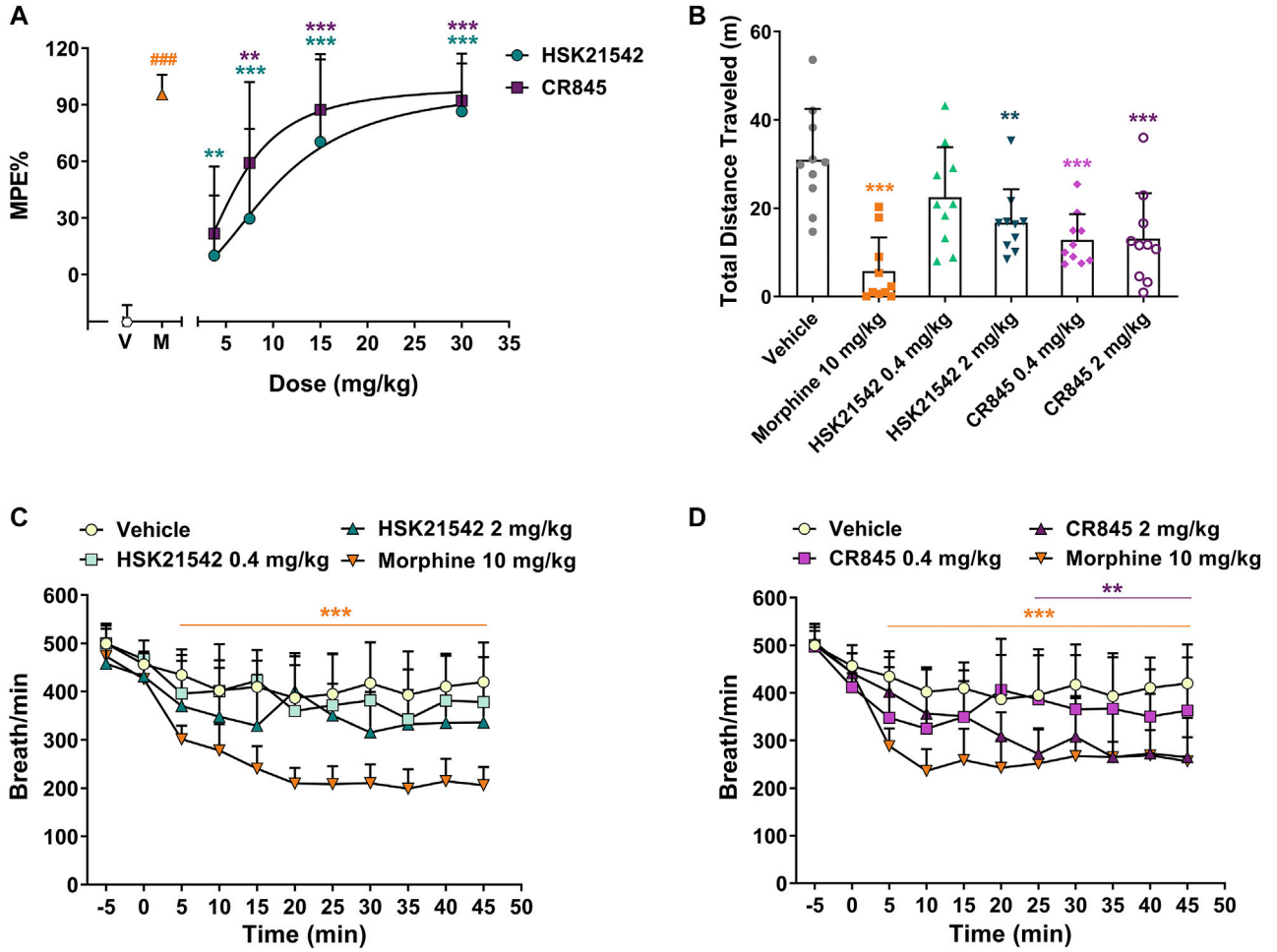

FIGURE 6 | Central antinociceptive activities, and effects on locomotor activity and respiratory rate of HSK21542 and CR845 in mice. **(A)** The central antinociceptive activities were evaluated using a hot-plate test in mice at 15 min post-drug. **(B)** The sedative effects at 15 min post-dosing were detected using a locomotor activity test. **(C, D)** The effects on respiratory rate in mice were measured with whole body plethysmography. Data are presented as means ± SD (n = 10/group). **(A, B)** $^{**}p < 0.01$, $^{***}p < 0.001$ vs. vehicle, one-way ANOVA followed by Dunnett's test; **(C, D)** $^{**}p < 0.01$, $^{***}p < 0.001$ vs. vehicle, two-way ANOVA followed by Dunnett's test; $^{\#\#\#}p < 0.001$ vs. vehicle, Mann-Whitney test. V, Vehicle; M, Moprhine (10 mg/kg, a positive control).

verify this conclusion, the antiallodynic effects of HSK21542 and CR845 were also evaluated in a hindpaw incision model and a CCI model. As predicted, HSK21542 achieved outstanding antiallodynic effects, which were comparable or even superior to CR845. The more potent analgesic effects of HSK21542 are attributed to its excellent *in vitro* biological activities. It is undeniable that HSK21542 might be a more potent and longer-acting analgesic than CR845. To further address the *in vivo* pharmacological profiles of HSK21542 and CR845, their antipruritic activities were measured in an animal model of compound 48/80-induced itch, wherein HSK21542 presented remarkable antipruritic effects, similar to that of CR845.

To validate HSK21542 as a safer candidate drug for treating pain and pruritus, the central antinociceptive effects of HSK21542 and CR845 were assessed with a hot-plate test, and the effects on locomotor activity and respiration in mice were observed. In the hot-plate test, the MED value (7.5 mg/kg) of HSK21542 was higher than the dose (1 mg/kg) needed to produce maximum antinociceptive effects in writhing test. The ED_{50} value of HSK21542 was 10.49 mg/kg, suggesting that HSK21542 has a therapeutic index of 116.6 (**Supplementary Table S2**). In contrast, CR845 has a smaller therapeutic index (75.1). Furthermore, HSK21542 at a dose of 2 mg/kg did not affect the locomotor activity and respiratory rate in mice, which was obviously higher than the doses needed to produce analgesic and antipruritic effects. However, CR845 suppressed the respiratory rate in mice at the same dose. Morphine, a typical representative of MOR agonist, highly inhibited the respiratory rate in mice at a dose of 10 mg/kg, at which the antinociceptive effects of morphine was comparable to that achieved by HSK21542 or CR85 (**Supplementary Figure S5**). Therefore, HSK21542 does not produce obvious CNS effects, which are typical profiles of centrally penetrating KOR agonists and MOR agonist. In view of all these results, HSK21542 might have a larger translational potential than CR845.

However, it is noteworthy that there is a huge challenge in preclinical-to-clinical translation for analgesic and antipruritic

candidates. One of the main causes is the discordance in endpoints between animal and human studies. In animals, the pain- or itch-stimulated behaviors are recorded to label analgesic or antipruritic candidates, making it unavoidable that the false-positive effects might exist, resulting from non-selective drug effects such as sedation and paralysis (Lazenka et al., 2018). Therefore, it is important to look forward to the results of clinical trials that will validate if HSK21542 could be a safe and effective analgesic and antipruritic drug. At present, HSK21542 is under Phase II clinical development for treating pain or pruritis (CTR20201702, CTR20201210, CTR20200371; http://www.chinadrugtrials.org.cn/clinicaltrials.searchlist.dhtml).

In conclusion, the *in vitro* findings revealed that HSK21542 is a selective KOR agonist with a higher potency than CR845. The brain/plasma distribution study showed that HSK21542 has an extremely poor ability to penetrate into the CNS system. The *in vivo* pharmacological activities supported the translational potential of HSK21542 as a safe and effective analgesic and antipruritic candidate. Generally, HSK21542 has the ability to avoid adverse CNS effects that are associated with centrally penetrating KOR agonists and MOR agonist, and might provide an effective alternative for treating patients with pain or pruritus.

DATA AVAILABILITY STATEMENT

The original contributions presented in the study are included in the article/**Supplementary Material**, further inquiries can be directed to the corresponding authors.

ETHICS STATEMENT

The animal study was reviewed and approved by Institutional Animal Care and Use Committee of Haisco Pharmaceutical Group Co., Ltd.

AUTHOR CONTRIBUTIONS

Conceptualization: XW, XG, FY and JN; Methodology: XG, FY and JN; Software: XG and XY; Validation: XG, XY, DB, BT, PC, MQ, XZ and HW; Formal analysis: XG and PT; Resources: CZ; Visualization: XG; Supervision: FY and JN; Project administration: FY and JN; Roles/Writing–original draft: XG; Writing–review and editing: XW, FY and JN. All authors have read and agreed to the published version of the manuscript.

ACKNOWLEDGMENTS

The authors are grateful to Eurofins Panlabs Discovery Services Taiwan, Ltd for their assistance with the experiments.

SUPPLEMENTARY MATERIAL

The Supplementary Material for this article can be found online at: https://www.frontiersin.org/articles/10.3389/fphar.2021.773204/full#supplementary-material

REFERENCES

Abdollahi, M., Karimpour, H., and Monsef-Esfehani, H. R. (2003). Antinociceptive Effects of Teucrium Polium L Total Extract and Essential Oil in Mouse Writhing Test. *Pharmacol. Res.* 48 (1), 31–35. doi:10.1016/s1043-6618(03)00059-8

Bailey, A. L., and Ribeiro-da-Silva, A. (2006). Transient Loss of Terminals from Non-peptidergic Nociceptive Fibers in the Substantia Gelatinosa of Spinal Cord Following Chronic Constriction Injury of the Sciatic Nerve. *Neuroscience* 138 (2), 675–690. doi:10.1016/j.neuroscience.2005.11.051

Balasubramanyan, S., Stemkowski, P. L., Stebbing, M. J., and Smith, P. A. (2006). Sciatic Chronic Constriction Injury Produces Cell-type-specific Changes in the Electrophysiological Properties of Rat Substantia Gelatinosa Neurons. *J. Neurophysiol.* 96 (2), 579–590. doi:10.1152/jn.00087.2006

Barber, A., Bartoszyk, G. D., Bender, H. M., Gottschlich, R., Greiner, H. E., Harting, J., et al. (1994). A Pharmacological Profile of the Novel, Peripherally-Selective Kappa-Opioid Receptor Agonist, EMD 61753. *Br. J. Pharmacol.* 113 (4), 1317–1327. doi:10.1111/j.1476-5381.1994.tb17142.x

Bennett, G. J., and Xie, Y. K. (1988). A Peripheral Mononeuropathy in Rat that Produces Disorders of Pain Sensation like Those Seen in Man. *Pain* 33 (1), 87–107. doi:10.1016/0304-3959(88)90209-6

Biddlestone, L., Corbett, A. D., and Dolan, S. (2007). Oral Administration of Ginkgo Biloba Extract, EGb-761 Inhibits thermal Hyperalgesia in Rodent Models of Inflammatory and post-surgical Pain. *Br. J. Pharmacol.* 151 (2), 285–291. doi:10.1038/sj.bjp.0707220

Binder, W., Machelska, H., Mousa, S., Schmitt, T., Rivière, P. J., Junien, J. L., et al. (2001). Analgesic and Antiinflammatory Effects of Two Novel Kappa-Opioid Peptides. *Anesthesiology* 94 (6), 1034–1044. doi:10.1097/00000542-200106000-00018

Bishop, K., Visonneau, S., and McGuire, D. (2015). Development of Asimadoline, a Selective Kappa Opioid Receptor Agonist, for the Treatment of Pruritus. In: Presented at: 8th World Congress on Itch (WCI), Nara, Japan, September 27–29.

Bourgeois, C., Werfel, E., Galla, F., Lehmkuhl, K., Torres-Gómez, H., Schepmann, D., et al. (2014). Synthesis and Pharmacological Evaluation of 5-pyrrolidinylquinoxalines as a Novel Class of Peripherally Restricted κ-opioid Receptor Agonists. *J. Med. Chem.* 57 (15), 6845–6860. doi:10.1021/jm500940q

Brennan, T. J., Vandermeulen, E. P., and Gebhart, G. F. (1996). Characterization of a Rat Model of Incisional Pain. *Pain* 64 (3), 493–501. doi:10.1016/0304-3959(95)01441-1

Brust, T. F., Morgenweck, J., Kim, S. A., Rose, J. H., Locke, J. L., Schmid, C. L., et al. (2016). Biased Agonists of the Kappa Opioid Receptor Suppress Pain and Itch without Causing Sedation or Dysphoria. *Sci. Signal.* 9 (456), ra117. doi:10.1126/scisignal.aai8441

Chaplan, S. R., Bach, F. W., Pogrel, J. W., Chung, J. M., and Yaksh, T. L. (1994). Quantitative Assessment of Tactile Allodynia in the Rat Paw. *J. Neurosci. Methods* 53 (1), 55–63. doi:10.1016/0165-0270(94)90144-9

Chavkin, C. (2011). The Therapeutic Potential of κ-opioids for Treatment of Pain and Addiction. *Neuropsychopharmacology* 36 (1), 369–370. doi:10.1038/npp.2010.137

Chen, Y., Mestek, A., Liu, J., and Yu, L. (1993). Molecular Cloning of a Rat Kappa Opioid Receptor Reveals Sequence Similarities to the Mu and delta Opioid Receptors. *Biochem. J.* 295 (Pt 3), 625–628. doi:10.1042/bj2950625

Chen, J. Y., Chu, L. W., Cheng, K. I., Hsieh, S. L., Juan, Y. S., and Wu, B. N. (2018). Valproate Reduces Neuroinflammation and Neuronal Death in a Rat Chronic Constriction Injury Model. *Sci. Rep.* 8 (1), 16457. doi:10.1038/s41598-018-34915-5

Cowan, A., Kehner, G. B., and Inan, S. (2015). Targeting Itch with Ligands Selective for κ Opioid Receptors. *Handb Exp. Pharmacol.* 226, 291–314. doi:10.1007/978-3-662-44605-8_16

DeWire, S. M., Yamashita, D. S., Rominger, D. H., Liu, G., Cowan, C. L., Graczyk, T. M., et al. (2013). A G Protein-Biased Ligand at the μ-opioid Receptor Is Potently Analgesic with Reduced Gastrointestinal and Respiratory Dysfunction Compared with Morphine. *J. Pharmacol. Exp. Ther.* 344 (3), 708–717. doi:10.1124/jpet.112.201616

Dong, S., Gu, Y., Wei, G., Si, D., and Liu, C. (2018). Determination of Liraglutide in Rat Plasma by a Selective Liquid Chromatography-Tandem Mass Spectrometry Method: Application to a Pharmacokinetics Study. *J. Chromatogr. B Analyt Technol. Biomed. Life Sci.* 1091, 29–35. doi:10.1016/j.jchromb.2018.05.020

Fishbane, S., Jamal, A., Munera, C., Wen, W., Menzaghi, F., and Investigators, K.-T. (2020). A Phase 3 Trial of Difelikefalin in Hemodialysis Patients with Pruritus. *N. Engl. J. Med.* 382 (3), 222–232. doi:10.1056/NEJMoa1912770

Gou, X., Yu, X., Bai, D., Tan, B., Cao, P., Qian, M., et al. (2021). Pharmacology and Mechanism of Action of HSK16149, a Selective Ligand of α2δ Subunit of Voltage-Gated Calcium Channel with Analgesic Activity in Animal Models of Chronic Pain. *J. Pharmacol. Exp. Ther.* 376 (3), 330–337. doi:10.1124/jpet.120.000315

Gupta, A., Gomes, I., Bobeck, E. N., Fakira, A. K., Massaro, N. P., Sharma, I., et al. (2016). Collybolide Is a Novel Biased Agonist of κ-opioid Receptors with Potent Antipruritic Activity. *Proc. Natl. Acad. Sci. U S A.* 113 (21), 6041–6046. doi:10.1073/pnas.1521825113

Hachisuka, J., Furue, H., Furue, M., and Yoshimura, M. (2010). Responsiveness of C Neurons in Rat Dorsal Root Ganglion to 5-Hydroxytryptamine-Induced Pruritic Stimuli *In Vivo*. *J. Neurophysiol.* 104 (1), 271–279. doi:10.1152/jn.00938.2009

Hill, R., Dewey, W. L., Kelly, E., and Henderson, G. (2018a). Oxycodone-induced Tolerance to Respiratory Depression: Reversal by Ethanol, Pregabalin and Protein Kinase C Inhibition. *Br. J. Pharmacol.* 175 (12), 2492–2503. doi:10.1111/bph.14219

Hill, R., Disney, A., Conibear, A., Sutcliffe, K., Dewey, W., Husbands, S., et al. (2018b). The Novel μ-opioid Receptor Agonist PZM21 Depresses Respiration and Induces Tolerance to Antinociception. *Br. J. Pharmacol.* 175 (13), 2653–2661. doi:10.1111/bph.14224

Inan, S., Dun, N. J., and Cowan, A. (2009). Nalfurafine Prevents 5'-guanidinonaltrindole- and Compound 48/80-induced Spinal C-Fos Expression and Attenuates 5'-Guanidinonaltrindole-Elicited Scratching Behavior in Mice. *Neuroscience* 163 (1), 23–33. doi:10.1016/j.neuroscience.2009.06.016

Inui, S. (2015). Nalfurafine Hydrochloride to Treat Pruritus: a Review. *Clin. Cosmet. Investig. Dermatol.* 8, 249–255. doi:10.2147/CCID.S55942

Kardon, A. P., Polgár, E., Hachisuka, J., Snyder, L. M., Cameron, D., Savage, S., et al. (2014). Dynorphin Acts as a Neuromodulator to Inhibit Itch in the Dorsal Horn of the Spinal Cord. *Neuron* 82 (3), 573–586. doi:10.1016/j.neuron.2014.02.046

Kieffer, B. L., and Gavériaux-Ruff, C. (2002). Exploring the Opioid System by Gene Knockout. *Prog. Neurobiol.* 66 (5), 285–306. doi:10.1016/s0301-0082(02)00008-4

Kobayashi, Y., Nakano, Y., Inayama, K., Sakai, A., and Kamiya, T. (2003). Dietary Intake of the Flower Extracts of German Chamomile (Matricaria Recutita L.) Inhibited Compound 48/80-induced Itch-Scratch Responses in Mice. *Phytomedicine* 10 (8), 657–664. doi:10.1078/0944-7113-00283

Lai, J., Luo, M. C., Chen, Q., Ma, S., Gardell, L. R., Ossipov, M. H., et al. (2006). Dynorphin A Activates Bradykinin Receptors to Maintain Neuropathic Pain. *Nat. Neurosci.* 9 (12), 1534–1540. doi:10.1038/nn1804

Lazenka, M. L., Moerke, M. J., Townsend, E. A., Freeman, K. B., Carroll, F. I., and Negus, S. S. (2018). Dissociable Effects of the Kappa Opioid Receptor Agonist Nalfurafine on Pain/itch-Stimulated and Pain/itch-Depressed Behaviors in Male Rats. *Psychopharmacology (Berl)* 235 (1), 203–213. doi:10.1007/s00213-017-4758-7

Le Bars, D., Gozariu, M., and Cadden, S. W. (2001). Animal Models of Nociception. *Pharmacol. Rev.* 53 (4), 597–652.

Manglik, A., Lin, H., Aryal, D. K., McCorvy, J. D., Dengler, D., Corder, G., et al. (2016). Structure-based Discovery of Opioid Analgesics with Reduced Side Effects. *Nature* 537 (7619), 185–190. doi:10.1038/nature19112

Menzaghi, F., Spencer, R. H., Stauffer, J. W., Tiseo, P. J., and Abrouk, N. E. D. (2015). CR845, a Peripheral Kappa Opioid Receptor Agonist, Provides Better Pain Relief with Less Nausea and Vomiting Than Placebo in Patients after Bunionectomy. *Present. Am. Acad. Phys. Med. Rehabil.* 7, S140, 2015 . October. doi:10.1016/j.pmrj.2015.06.185

Motulsky, H. J., and Mahan, L. C. (1984). The Kinetics of Competitive Radioligand Binding Predicted by the Law of Mass Action. *Mol. Pharmacol.* 25 (1), 1–9. doi:10.1007/978-1-4613-2399-0_1

Naser, P. V., and Kuner, R. (2018). Peripheral Kappa Opioid Receptor Signaling Takes on a Central Role. *Neuron* 99 (6), 1102–1104. doi:10.1016/j.neuron.2018.09.006

Negus, S. S., O'Connell, R., Morrissey, E., Cheng, K., and Rice, K. C. (2012). Effects of Peripherally Restricted κ Opioid Receptor Agonists on Pain-Related Stimulation and Depression of Behavior in Rats. *J. Pharmacol. Exp. Ther.* 340 (3), 501–509. doi:10.1124/jpet.111.186783

Nojima, H., and Carstens, E. (2003). Quantitative Assessment of Directed Hind Limb Scratching Behavior as a Rodent Itch Model. *J. Neurosci. Methods* 126 (2), 137–143. doi:10.1016/s0165-0270(03)00074-8

Olianas, M. C., Concas, D., and Onali, P. (2006). Agonist Activity of Naloxone Benzoylhydrazone at Recombinant and Native Opioid Receptors. *Br. J. Pharmacol.* 147 (4), 360–370. doi:10.1038/sj.bjp.0706601

Ragen, B. J., Freeman, S. M., Laredo, S. A., Mendoza, S. P., and Bales, K. L. (2015). μ and κ Opioid Receptor Distribution in the Monogamous Titi Monkey (*Callicebus cupreus*): Implications for Social Behavior and Endocrine Functioning. *Neuroscience* 290, 421–434. doi:10.1016/j.neuroscience.2015.01.023

Salaga, M., Polepally, P. R., Zielinska, M., Marynowski, M., Fabisiak, A., Murawska, N., et al. (2015). Salvinorin A Analogues PR-37 and PR-38 Attenuate Compound 48/80-induced Itch Responses in Mice. *Br. J. Pharmacol.* 172 (17), 4331–4341. doi:10.1111/bph.13212

Schmid, C. L., Kennedy, N. M., Ross, N. C., Lovell, K. M., Yue, Z., Morgenweck, J., et al. (2017). Bias Factor and Therapeutic Window Correlate to Predict Safer Opioid Analgesics. *Cell* 171 (5), 1165–1175.e13. doi:10.1016/j.cell.2017.10.035

Singla, N. K., Skobieranda, F., Soergel, D. G., Salamea, M., Burt, D. A., Demitrack, M. A., et al. (2019). APOLLO-2: A Randomized, Placebo and Active-Controlled Phase III Study Investigating Oliceridine (TRV130), a G Protein-Biased Ligand at the μ-Opioid Receptor, for Management of Moderate to Severe Acute Pain Following Abdominoplasty. *Pain Pract.* 19 (7), 715–731. doi:10.1111/papr.12801

Snyder, L. M., Chiang, M. C., Loeza-Alcocer, E., Omori, Y., Hachisuka, J., Sheahan, T. D., et al. (2018). Kappa Opioid Receptor Distribution and Function in Primary Afferents. *Neuron* 99 (6), 1274–1288.e6. doi:10.1016/j.neuron.2018.08.044

Steele, D. J. R. (2020). Difelikefalin for the Treatment of Uremic Pruritus. *N. Engl. J. Med.* 382 (3), 289–290. doi:10.1056/NEJMe1916598

Tsuda, M., Kohro, Y., Yano, T., Tsujikawa, T., Kitano, J., Tozaki-Saitoh, H., et al. (2011). JAK-STAT3 Pathway Regulates Spinal Astrocyte Proliferation and Neuropathic Pain Maintenance in Rats. *Brain* 134 (Pt 4), 1127–1139. doi:10.1093/brain/awr025

Vakharia, P. P., and Silverberg, J. I. (2018). New Therapies for Atopic Dermatitis: Additional Treatment Classes. *J. Am. Acad. Dermatol.* 78 (3 Suppl. 1), S76–S83. doi:10.1016/j.jaad.2017.12.024

Vanderah, T. W., Schteingart, C. D., Trojnar, J., Junien, J. L., Lai, J., and Riviere, P. J. (2004). FE200041 (D-Phe-D-Phe-D-Nle-D-Arg-NH2): A Peripheral Efficacious Kappa Opioid Agonist with Unprecedented Selectivity. *J. Pharmacol. Exp. Ther.* 310 (1), 326–333. doi:10.1124/jpet.104.065391

Violin, J. D., Crombie, A. L., Soergel, D. G., and Lark, M. W. (2014). Biased Ligands at G-Protein-Coupled Receptors: Promise and Progress. *Trends Pharmacol. Sci.* 35 (7), 308–316. doi:10.1016/j.tips.2014.04.007

Viscusi, E. R., Skobieranda, F., Soergel, D. G., Cook, E., Burt, D. A., and Singla, N. (2019). APOLLO-1: a Randomized Placebo and Active-Controlled Phase III Study Investigating Oliceridine (TRV130), a G Protein-Biased Ligand at the μ-Opioid Receptor, for Management of Moderate-To-Severe Acute Pain Following Bunionectomy. *J. Pain Res.* 12, 927–943. doi:10.2147/jpr.s171013

Wang, Y., Yan, M., Zheng, G. Y., He, L., and Yang, H. (2014). A Cell-Based, High-Throughput Homogeneous Time-Resolved Fluorescence Assay for the Screening of Potential κ-opioid Receptor Agonists. *Acta Pharmacol. Sin* 35, 957–966. doi:10.1038/aps.2014.21

Wang, Y. H., Chai, J. R., Xu, X. J., Ye, R. F., Zan, G. Y., Liu, G. Y., et al. (2018). Pharmacological Characterization of Dezocine, a Potent Analgesic Acting as a κ Partial Agonist and μ Partial Agonist. *Sci. Rep.* 8 (1), 14087. doi:10.1038/s41598-018-32568-y

Weir, G. A., Middleton, S. J., Clark, A. J., Daniel, T., Khovanov, N., McMahon, S. B., et al. (2017). Using an Engineered Glutamate-Gated Chloride Channel to Silence Sensory Neurons and Treat Neuropathic Pain at the Source. *Brain* 140 (10), 2570–2585. doi:10.1093/brain/awx201

Whiteside, G. T., Harrison, J., Boulet, J., Mark, L., Pearson, M., Gottshall, S., et al. (2004). Pharmacological Characterisation of a Rat Model of Incisional Pain. *Br. J. Pharmacol.* 141 (1), 85–91. doi:10.1038/sj.bjp.0705568

Yang, S. H., Cho, Y. A., and Choi, J. S. (2011). Effects of Ticlopidine on Pharmacokinetics of Losartan and its Main Metabolite EXP-3174 in Rats. *Acta Pharmacol. Sin* 32, 967–972. doi:10.1038/aps.2011.32

Yasuda, K., Raynor, K., Kong, H., Breder, C. D., Takeda, J., Reisine, T., et al. (1993). Cloning and Functional Comparison of Kappa and delta Opioid Receptors from Mouse Brain. *Proc. Natl. Acad. Sci. U S A.* 90 (14), 6736–6740. doi:10.1073/pnas.90.14.6736

Conflict of Interest: Authors XG, XY, DB, BT, PC, MQ, XZ, HW, PT, CZ, FY, and JN are employed by Haisco Pharmaceutical Group Co., Ltd.

The remaining author declares that the research was conducted in the absence of any commercial or financial relationships that could be construed as a potential conflict of interest.

Publisher's Note: All claims expressed in this article are solely those of the authors and do not necessarily represent those of their affiliated organizations, or those of the publisher, the editors and the reviewers. Any product that may be evaluated in this article, or claim that may be made by its manufacturer, is not guaranteed or endorsed by the publisher.

Copyright © 2021 Wang, Gou, Yu, Bai, Tan, Cao, Qian, Zheng, Wang, Tang, Zhang, Ye and Ni. This is an open-access article distributed under the terms of the Creative Commons Attribution License (CC BY). The use, distribution or reproduction in other forums is permitted, provided the original author(s) and the copyright owner(s) are credited and that the original publication in this journal is cited, in accordance with accepted academic practice. No use, distribution or reproduction is permitted which does not comply with these terms.

frontiers in Pharmacology

ORIGINAL RESEARCH
published: 06 December 2021
doi: 10.3389/fphar.2021.781856

Protective Effects and Mechanisms of Polyethylene Glycol Loxenatide Against Hyperglycemia and Liver Injury in *db/db* diabetic Mice

Yu Zhang[1,2], *Yufeng Li*[3], *Junjun Zhao*[4], *Cong Wang*[1,2], *Bin Deng*[1,2], *Qilin Zhang*[1,2]* and *Chen Shi*[1,2]*

[1]*Department of Pharmacy, Union Hospital, Tongji Medical College, Huazhong University of Science and Technology, Wuhan, China,* [2]*Hubei Province Clinical Research Center for Precision Medicine for Critical Illness, Wuhan, China,* [3]*Preclinical Development Department, Shanghai Hansoh Biomedical Co., Ltd., Shanghai, China,* [4]*Pharmaceutical Research Institute, Jiangsu Hansoh Pharmaceutical Group Co. Ltd., Lianyungang, China*

Background: Type 2 diabetes mellitus (T2DM) is a metabolic disorder with insulin resistance and impaired insulin secretion that can cause complications, including liver injury. Polyethylene glycol loxenatide (PEG-Loxe), a glucagon-like peptide-1 (GLP-1) analog, is widely used to treat T2DM. However, its specific glucose-lowering and hepatoprotective mechanisms of action have not been established yet.

METHODS: Using a high glucose-induced hepatocyte injury model and a type 2 diabetic *db/db* mouse model, we assessed PEG-Loxe's impact on reducing blood glucose and improving liver injury in T2DM and revealed its mechanism.

RESULTS: PEG-Loxe treatment significantly reduced body weight and fasting glucose, increased glucose tolerance, improved serum and liver biochemical parameters (glycated hemoglobin, serum insulin, triglycerides, total cholesterol, high-density lipoprotein cholesterol, low-density lipoprotein cholesterol, alanine aminotransferase, and aspartate aminotransferase), and attenuated hepatic steatosis and liver and pancreatic tissue damages in *db/db* mice. Additionally, PEG-Loxe considerably inhibited oxidative stress, decreased pro-inflammatory factor (TNF-α, IL-6, and MCP-1) levels, and increased anti-inflammatory factor IL-10 levels. PEG-Loxe possibly inhibits hepatic lipid synthesis, oxidative stress, and inflammatory response by upregulating Sirt1, p-AMPK, and p-ACC expressions in the Sirt1/AMPK/ACC pathway of lipid metabolism, thereby improving T2DM liver injury. PEG-Loxe most likely also promotes GLP-1R expression by inhibiting β-cell apoptosis, which in turn activates the insulin PI3K/AKT pathway to promote insulin synthesis and secretion, thereby exerting hypoglycemic effects. *In vitro* cellular experiments further confirmed that PEG-Loxe possibly exerts hypoglycemic effects by activating the insulin PI3K/AKT pathway.

Conclusion: PEG-Loxe improved liver injury in T2DM probably by activating Sirt1/AMPK/ACC lipid metabolism pathway, and exerted hypoglycemic effects through activation of insulin PI3K/AKT pathway.

Keywords: GLP-1 receptor agonists, polyethylene glycol loxenatide, type 2 diabetes, liver injury, AMPK/ACC, PI3K/AKT

OPEN ACCESS

Edited by:
Andres Trostchansky,
Universidad de la República, Uruguay

Reviewed by:
Tom L Broderick,
Midwestern University, United States
Guoping Yang,
Central South University, China

***Correspondence:**
Qilin Zhang
qilinzhang88@163.com
Chen Shi
whxhchen@163.com

Specialty section:
This article was submitted to Experimental Pharmacology and Drug Discovery, a section of the journal Frontiers in Pharmacology

Received: *23 September 2021*
Accepted: *22 November 2021*
Published: *06 December 2021*

Citation:
Zhang Y, Li Y, Zhao J, Wang C, Deng B, Zhang Q and Shi C (2021) Protective Effects and Mechanisms of Polyethylene Glycol Loxenatide Against Hyperglycemia and Liver Injury in db/db *diabetic Mice. Front. Pharmacol. 12:781856. doi: 10.3389/fphar.2021.781856*

INTRODUCTION

Type 2 diabetes mellitus (T2DM) is a metabolic disorder with insulin resistance (IR) and impaired insulin secretion. An estimated 642 million people in the world are projected to have diabetes by 2040 (Zheng et al., 2018). Long-term T2DM can lead to a variety of complications, including damage to the liver, kidney, cardiovascular system, and retina, and these are often huge economic and medical burdens on healthcare systems across the world (Regensteiner et al., 2015; Afkarian et al., 2016; Zheng et al., 2018). T2DM is currently treated primarily with oral hypoglycemic drugs and insulin. While traditional hypoglycemic drugs, including metformin, sulfonylureas, thiazolidinediones, α-glucosidase inhibitors, and insulin, may exert hypoglycemic effects through different mechanisms, they are prone to adverse effects, including hypoglycemia, weight gain, severe ketonuria, and lactic acidemia (Kohlroser et al., 2000; Monami et al., 2014; Fadini et al., 2017; Flory et al., 2020). Therefore, clinically, there is an urgent need for drugs with stable glucose-lowering effects and a low incidence of adverse effects.

Glucagon-like peptide-1 (GLP-1) is the most potent intestinal peptide hormone for insulin secretion that has been identified so far, and it is secreted primarily by L cells in the ileum and colon. It is now widely used to treat T2DM (Drucker et al., 2017). GLP-1 promotes intracellular insulin synthesis and secretion, inhibit glucagon secretion through binding to the GLP-1 receptor (GLP-1R) to facilitate the cellular signal transduction pathway (Madhu et al., 2020). Because GLP-1R is also expressed in the kidney, gastrointestinal tract, pancreas, nervous system, and heart, in addition to exerting hypoglycemic effects on the pancreas, GLP-1 can, hence, also suppress appetite, delay gastric emptying, increase insulin sensitivity in peripheral tissues and the liver, and protect the heart, brain, kidney, and liver (Drucker, 2018; Rowlands et al., 2018).

PEG-Loxe is a long-acting hypoglycemic agent derived from Exenatide via amino acid modification and PEGylation. PEG modification can reduce the toxicity, prolong the half-life and action time *in vivo*, thus improving bioavailability and the therapeutic effect. PEG-Loxe can effectively prolong GLP-1 activity and can be injected once a week due to its improved resistance to dipeptidyl peptidase-IV (DPP-IV) (Chen et al., 2017; Shuai et al., 2021). It is the first long-acting glucagon-like peptide-1 receptor agonist (GLP-1RA) in China, and can improve blood glucose in a glucose-concentration-dependent manner, making it less likely to trigger hypoglycemia. Results of a meta-analysis of 54 randomized controlled trials showed that PEG-Loxe reduced HbA1c in a similar way as exenatide, dulaglutide or liraglutide, and had an advantage in reducing the incidence of hypoglycemia (Jiang et al., 2021). PEG-Loxe was the only GLP-1RA to enhance the therapeutic dose without increasing the risk of hypoglycemia. Recently, GLP-1RA has been shown to effectively reduce lipid load and free fatty acid (FFA)-induced hepatic steatosis. However, their specific mechanisms of action for glucose-lowering and hepatoprotection are not well understood (Pan et al., 2021).

Islet dysfunction is an important factor in the development of hyperglycemia in patients with T2DM. Insufficient insulin secretion is caused by β-cell dysfunction, resulting in elevated blood glucose. Hyperglycemia, in turn, causes further damage to β-cells associated with a decrease in β-cell numbers due to apoptosis (Huang et al., 2007; Costes, 2018). Indeed, GLP-1 and its analogs can reduce β-cell endoplasmic reticulum (ER) stress and inhibit β-cell apoptosis (Ferdaoussi et al., 2008; Campbell and Drucker, 2013). The PI3K/AKT pathway is a key insulin signaling pathway that promotes glucose absorption and glycogen synthesis, thereby reducing blood glucose levels (Kuang et al., 2017; Wang et al., 2018). The Sirt1/AMPK/ACC axis, as demonstrated previously, is the master switch that controls the hepatic glucolipid metabolic pathway (Gruzman et al., 2009; Mottillo et al., 2016; Woods et al., 2017). However, the potential regulation of these signals by GLP-1 analogs or PEG-Loxe remains poorly understood.

All these data highlight the importance of PI3K/AKT, Sirt1/AMPK/ACC, and apoptosis in T2DM and the possible beneficial role of GLP-1 analogs in modulating these cellular response pathways to lower blood glucose and attenuate diabetes-related liver injury. In this study, we assessed PEG-Loxe's pharmacological effects and its potential mechanisms of action on long-acting hypoglycemia, weight control, and improvement of liver complications by constructing animal and cellular models of diabetes mellitus. PEG-Loxe's impact was also compared with the impact of short-acting GLP-1R agonists liraglutide and loxenatide to provide experimental evidence for the clinical application of PEG-Loxe.

MATERIALS AND METHODS

Chemicals and Reagents

Insulin receptor substrate-1 (IRS-1, #2382), p-IRS-1 (#2384), p-AKT (#4060), AKT (#9272), p-GSK-3β (#9322), GSK-3β (#12456), p-AMPK (#50081), AMPK (#5832), p-ACC (#11818), ACC (#3676), and Bax (#2772) were obtained from Cell Signaling Technology, Inc. (Danvers, MA, United States). PI3K (#ab133595), p-PI3K p85 (#ab182651), GLP-1R (#ab218532), Bcl-2 (#ab196495), carnitine palmitoyl transferase-1 (CPT1, #ab234111) and fatty acid translocase (FAT/CD36, #ab64014) were purchased from Abcam (Cambridge, MA, United States). GLUT4 (#AF5386), Caspase-3 (#AF6311), and Cleaved caspase-3 (#AF7022) were acquired from Affinity Biosciences (United States). Sirt1 (#13161-1-AP) was purchased from Proteintech Group (Wuhan, China). LY294002 (PI3K inhibitor, #1105) was obtained from Selleck Chemicals (United States). Horseradish peroxidase-conjugated goat anti-rabbit IgG, goat anti-mouse IgG, and β-actin were procured from Sigma-Aldrich (St Louis, MO, United States). Enzyme-linked immunosorbent assay (ELISA) kits for insulin were obtained from R&D Systems (Minneapolis, MN, United States). Biochemical analysis kits for glycosylated hemoglobin (HbA1c, H464-1), triacylglycerol (TG, A110-1), total cholesterol (TC, A111-1), high-density lipoprotein cholesterol (HDL-C, A112-1), low-density lipoprotein cholesterol (LDL-C, A113-1), alanine aminotransferase (ALT, C009-2), aspartate aminotransferase (AST, C010-2), reactive

oxygen species (ROS, E004-1-1), glutathione (GSH, A006-2), malondialdehyde (MDA, A003-1), superoxide dismutase (SOD, A001-3), and catalase (CAT, A007-1) were bought from the Nanjing Jiancheng Bioengineering Institute (Nanjing, China). ELISA kits for interleukin-10 (IL-10, ELK1143), interleukin-6 (IL-6, ELK1157), tumor necrosis factor-α (TNF-α, ELK1395), and monocyte chemotactic protein-1 (MCP-1, ELK7694) were obtained from ELK Biotechnology (Wuhan, China).

Experimental Animals

Male mice on C57BL/6.BKS.Cg-Dock7m +/+ Lepr$^{db/J(000697)}$ (C57BL/6-*db/db*) and C57BL/6-*m/m* background (8 weeks) were purchased from the Changzhou Cavins Experimental Animal Co., LTD. The mice were bred in a 12-h dark-light cycle SPF room in standard cages (5 mice/cage) at a temperature of 22 ± 1°C. All animals had *ad libitum* access to water and standard chow. All animal experiments were approved by the Institutional Animal Care and Use Committee of Tongji Medical College, Huazhong University of Science and Technology. Animal care and experimental procedures were conducted under the Guidelines of the Institutional Animal Care and Use Committee of Tongji Medical College and the National Institutes of Health Guide for the Care and Use of Laboratory Animals.

After 1 week of adaptive feeding, 10 healthy *m/m* mice and 50 *db/db* mice were divided into six groups of 10 each. Group I (control, NC): healthy mice. Group II (T2DM): *db/db* mice. Mice in the NC and T2DM groups were subcutaneously injected with an equal volume of saline every 3 days. Group III (PEG-Loxe-L): *db/db* mice, subcutaneous injection of PEG-Loxe (0.3 mg/kg) every 3 days. Group IV (PEG-Loxe-H): *db/db* mice, subcutaneous injection of PEG-Loxe (1 mg/kg) every 3 days. Group V (Lira): *db/db* mice, subcutaneous injection of Lira (0.4 mg/kg) once a day. Group VI (Loxe): *db/db* mice, subcutaneous injection of Loxe (0.3 mg/kg) once a day. Treatment lasted four consecutive weeks for all groups.

Determination of Body Weight, Fasting Blood Glucose, and Oral Glucose Tolerance Test

Mice body weight and fasting blood glucose (FBG) were measured once a week. The oral glucose tolerance test (OGTT) was performed at the end of the experiment. Briefly, all mice were subjected to fasting for 12 h and then given glucose (2 g/kg) through gavage (American Diabetes Association, 2021). Blood glucose samples were collected from the tail tip at 0, 30, 60, 90, 120, and 150 min after gavage, and their levels were measured with a glucometer (Bayer, Germany) according to the manufacturer's instructions.

Sample Collection and Serum Biochemical Parameter Detection

The FBG of all mice was tested after 4 weeks before the mice were anesthetized with pentobarbital. Blood samples were then collected from the eye orbits of mice, and the mice were euthanized. Liver and pancreatic tissues were subsequently harvested and weighed. Some of the liver and pancreatic tissues were fixed with 10% paraformaldehyde and stored at −80°C for further analysis. Blood specimens were immediately centrifuged (1,200 g, 4°C, 15 min) to obtain serum from which the levels of TC, TG, HDL-C, LDL-C, HbA1c, and insulin were quantified using a fully automatic biochemical analyzer (BS-420, Mindray, China).

Biochemical Analysis of Liver

Liver tissues were homogenized in 9× (wt/vol) ice-cold phosphate-buffered saline and centrifuged at 3,500 rpm for 15 min to collect the supernatants. Lipid (TC and TG), AST, ALT, oxidative factors (ROS, MDA, SOD, GSH, and CAT), and inflammatory factors (IL-10, TNF-α, IL-6, and MCP-1) in liver tissues were measured using ELISA kits according to the manufacturer's instructions.

Detection of Reactive Oxygen Species in the Liver

Detection of reactive oxygen species in the liver was performed as described previously (Zhang et al., 2021). Briefly, 10 μm-thick frozen liver tissue sections were obtained using a freezing microtome (CM 1900, Leica, Germany), incubated with 5 mmol/L fluorescently-labeled DHE for 30 min at 37 °C in a light-proof environment (the DHE was diluted at 1:1,000), and then stained with 4′,6′-diamidino-2-phenylindole (DAPI, AS1075, Aspen Biological, Wuhan, China). Images were taken using a fluorescent microscope (MicroPublisher, MP3.3-RTV-CLR-10, Q-IMAGING, Canada) at ×200 magnification. The average fluorescence intensity of DHE was quantified using Image-Pro Plus 6.0 (IPP, Media Cybernetics, Rockville, MD, United States). Results were expressed by the ratio of the fluorescence intensity of DHE-positive area to the DAPI.

Liver and Pancreas Histopathological Analysis

Liver and pancreas tissues were fixed in 10% formalin solution, dehydrated, and embedded with paraffin. Embedded liver and pancreas sections (3–5 μm thick) were stained with hematoxylin and eosin (H&E) for histopathological analysis (Wang et al., 2016). Besides, liver sections were stained with Sirius red and oil red O (ORO) (Wang et al., 2016). All sections were observed and imaged at ×400 magnification using an Olympus B×51 microscope (Tokyo, Japan).

Immunohistochemistry

Paraffin-embedded pancreatic tissues (4 μm thick) were dewaxed, hydrated, and sealed with 5% bovine serum albumin (BSA) solution for 30 min at room temperature. The samples were then incubated with anti-insulin or anti-GLP-1R overnight and horseradish peroxidase (HRP)-conjugated anti-rabbit secondary antibody for 30 min the following day, stained with stable diaminobenzidine (DAB) solution, re-stained with hematoxylin, dehydrated, blocked,

and observed and imaged using an Olympus BX51 microscope (Tokyo, Japan) (Zhou et al., 2020).

Cell Culture and Treatment

Human hepatocellular carcinoma HepG2 cells were obtained from Tongji Medical College and cultured in DMEM medium containing 10% fetal bovine serum (FBS) and 1% penicillin-streptomycin in a 5% CO_2 incubator at 37 °C. After growing and fusing to 70%, the HepG2 cells were randomly seeded in 6-well plates and grouped. Subsequently, they were exposed to 30 mM high glucose (HG) for 24 h, then to PEG-Loxe (100, 200 nM), Lira (100, 200 nM), or Loxe (100, 200 nM) with and without the addition of a PI3K inhibitor (LY294002, 20 μM), and treated for another 24 h. Cellular proteins were extracted to assay p-PI3K, PI3K, p-AKT, and AKT using Western blot.

Western Blot Analysis

Western blot was performed as described previously (Zhou et al., 2020). Liver or pancreatic tissues were homogenized with RIPA lysate containing 1% PMSF protease inhibitor and phosphatase inhibitor, and total tissue protein was extracted via centrifugation for 10 min. Protein concentration was determined using the BCA kit. Equal amounts of proteins were separated with electrophoresis using 10–15% SDS-PAGE and then transferred to PVDF membranes where they were incubated with 5% BSA at room temperature for 3 h: liver tissues were incubated with primary antibodies p-IRS-1, IRS-1, p-PI3K, PI3K, p-AKT, AKT, p-GSK-3β, GSK-3β, GLUT4, p-AMPK, AMPK, p-ACC, ACC, Sir1, CPT1 and FAT/CD36 while pancreatic tissues were incubated with primary antibodies Bcl-2, Bax, Cleaved Caspase-3, and Caspase-3. After incubation, the membranes were washed three times with TBST solution, incubated with secondary antibodies at room temperature for 1 h, visualized with a chemically enhanced luminescence solution, and imaged using an automated imaging system (Gene Gnome5, Synoptics Ltd, United Kingdom). We assumed that β-actin was present at equal levels in all samples and served as a control.

Statistical Analysis

All data were analyzed using GraphPad Prism version 7.0 (GraphPad Software, San Diego, CA, United States). Data are presented as the mean ± standard deviation, and their normal distribution was verified using the nonparametric Kolmogorov-Smirnov test. Differences between groups were analyzed using one-way ANOVA followed by Dunnett's test. p-values < 0.05 were considered statistically significant.

RESULTS

PEG-Loxe Reduces Body Weight and Hyperglycemia in T2DM Mice

As shown in **Figure 1A**, the body weights of mice in the T2DM group and Loxe groups did not change significantly before and after treatment. T2DM mice given PEG-Loxe-L, PEG-Loxe-H, and Lira had considerably reduced body weights. Of all the treatments, PEG-Loxe-H was most potent in reducing body weight.

FBG changes in mice were monitored weekly, and at the end of the experiment, FBG was markedly higher in T2DM group mice (26.51 mmol/L) than in NC group mice (5.39 mmol/L) (**Figure 1B**). However, treatment with PEG-Loxe-L, PEG-Loxe-H, Lira, and Loxe, the FBG of diabetic mice were significantly lower than that of T2DM group mice by 35.87, 36.51, 55.30, and 63.37%, respectively. Lira and Loxe showed more pronounced hypoglycemic effects than PEG-Loxe, probably because Lira and Loxe were administered daily while PEG-Loxe, as a long-acting formulation, was administered only once every 3 days. In addition, HbA1c was substantially increased in diabetic mice compared to healthy mice ($p < 0.001$). However, PEG-Loxe-H and Loxe reversed this increase ($p < 0.01$, **Table 1**).

OGTT was performed at the end of the experiment and revealed that diabetic mice given 2 g/kg of glucose via gavage had significantly higher plasma glucose levels at 30, 60, 90, 120, and 150 min (**Figure 1C**) compared to NC group mice, indicating a decrease in oral glucose tolerance in diabetic mice. In contrast, PEG-Loxe, Lira, and Loxe prevented the increase in blood glucose levels in diabetic mice, pointing to an improvement in impaired glucose tolerance (**Figure 1C**). The OGTT curve reflects the changes in glucose. The area under the curve (AUC) in T2DM mice was significantly greater than that in the NC group, but it was considerably reduced after PEG-Loxe, Lira, and Loxe treatments (**Figure 1D**).

PEG-Loxe Improves Lipid Disorders in T2DM Mice

The effects of PEG-Loxe on serum and liver lipids were shown in **Table 1**. Compared to normal mice, T2DM mice had significantly higher ($p < 0.001$) levels of TC and TG in their serum and considerably higher levels of lipids in their livers (TC and TG). However, the changes in hepatic TC, TG and serum TG were markedly reversed after 4 weeks of treatment with PEG-Loxe-L, PEG-Loxe-H, Lira, and Loxe ($p < 0.05$). PEG-Loxe treatment, particularly the 1 mg/kg dose, also drastically elevated serum HDL-C levels and decreased LDL-C levels in T2DM mice.

PEG-Loxe Improves Hepatic Steatosis and Liver Injury in T2DM Mice

The H&E staining of liver sections of mice in the NC group revealed regular morphology, uniform distribution, and tight hepatocyte arrangements. T2DM mice exhibited cytoplasmic vacuolation and hepatocyte necrosis. However, PEG-Loxe-L, PEG-Loxe-H, Lira, and Loxe significantly reduced liver lesions after 4 weeks of treatment (**Figure 2A**). Measurements of the levels of hepatic ALT and AST to evaluate liver damage in T2DM mice established that T2DM mice had severe liver damage compared to normal controls, as evidenced by the significantly increased levels of ALT and AST ($p < 0.001$). However, PEG-Loxe, Lira, and Loxe treatments considerably alleviated these abnormal levels (**Table 1**).

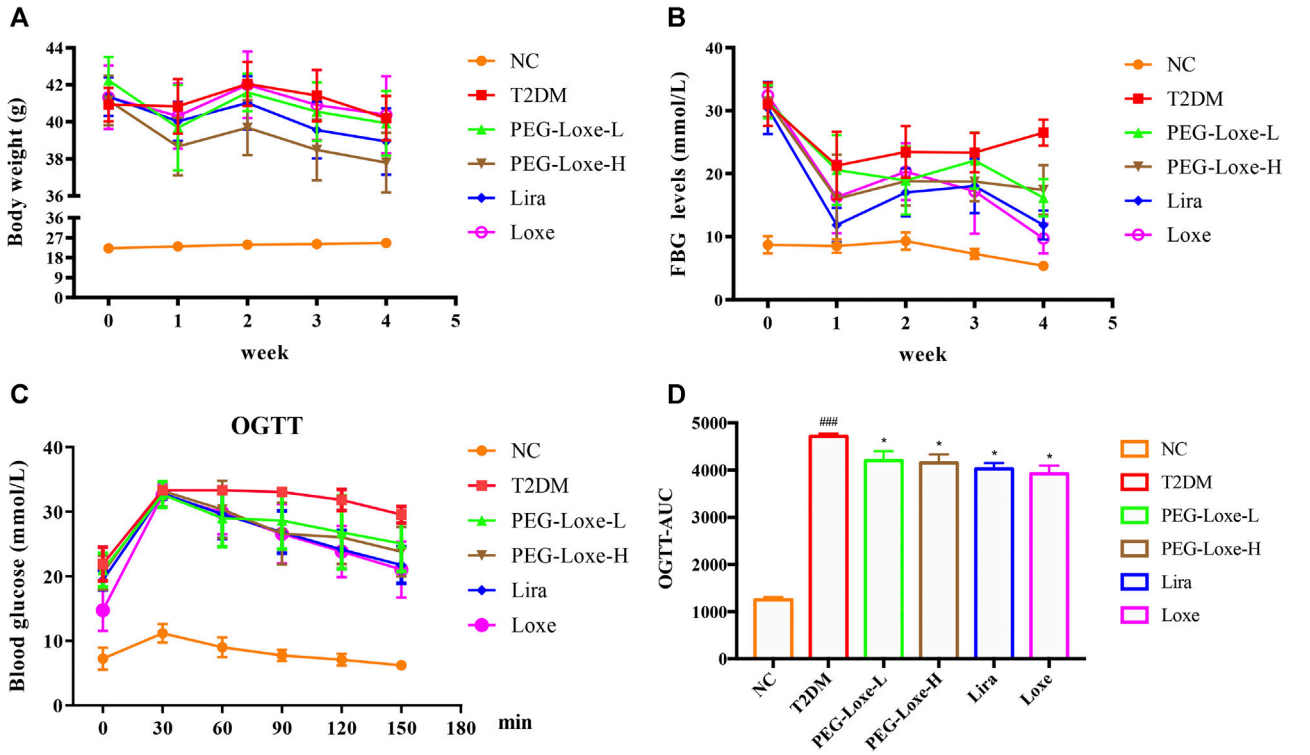

FIGURE 1 | Polyethylene glycol loxenatide (PEG-Loxe) reduces body weight and hyperglycemia in *db/db* mice **(A)** Changes in body weight after PEG-Loxe treatment over 4 weeks **(B)** Changes in fasting blood glucose (FBG) levels after PEG-Loxe treatment over 4 weeks **(C)** Oral glucose tolerance test (OGTT) test **(D)** The area under the curve (AUC) of OGTT. Data are expressed as the mean ± SD (n = 8). $^{###}p < 0.001$ compared to the normal control group; $^{*}p < 0.05$ compared to the T2DM group.

TABLE 1 | PEG-Loxe improved the levels of various biochemical parameters in *db/db* mice.

	NC	T2DM	PEG-Loxe-L	PEG-Loxe-H	Lira	Loxe
Serum TC (mmol/L)	1.08 ± 0.18	1.58 ± 0.26$^{###}$	1.76 ± 0.21	1.50 ± 0.27	1.57 ± 0.26	1.37 ± 0.19
Serum TG (mmol/L)	0.62 ± 0.11	1.70 ± 0.33$^{###}$	1.94 ± 0.34	1.26 ± 0.20*	1.31 ± 0.26*	0.98 ± 0.26***
Serum HDL-C (mmol/L)	1.38 ± 0.24	1.57 ± 0.09	1.84 ± 0.13*	1.84 ± 0.24*	1.77 ± 0.18	1.56 ± 0.10
Serum LDL-C (mmol/L)	0.35 ± 0.83	0.47 ± 0.14	0.51 ± 0.17	0.29 ± 0.08*	0.35 ± 0.06	0.44 ± 0.10
HbA1c (%)	4.44 ± 0.45	11.16 ± 1.12$^{###}$	12.89 ± 1.62**	9.19 ± 0.93**	11.30 ± 0.80	9.03 ± 0.84***
Serum insulin (mIU/L)	6.52 ± 0.43	12.91 ± 0.40$^{###}$	14.58 ± 1.70*	16.37 ± 0.90***	14.49 ± 0.63*	11.41 ± 2.02
Liver TC (mmol/gprot)	0.59 ± 0.26	6.55 ± 1.19$^{###}$	4.18 ± 0.51***	1.40 ± 0.21***	3.02 ± 0.54***	3.76 ± 0.38***
Liver TG (mmol/gprot)	0.32 ± 0.19	2.74 ± 0.13$^{###}$	1.84 ± 0.21***	0.81 ± 0.09***	1.35 ± 0.13***	1.88 ± 0.34***
Liver ALT (U/gprot)	3.48 ± 1.31	32.62 ± 3.35$^{###}$	20.81 ± 3.46***	9.33 ± 0.72***	16.08 ± 2.18***	21.21 ± 1.86***
Liver AST (U/gprot)	9.75 ± 2.52	37.19 ± 3.84$^{###}$	27.86 ± 2.23***	16.16 ± 1.89***	22.18 ± 3.23***	28.93 ± 3.68***

NC, denotes normal control group; T2DM, denotes type 2 diabetes group. Data are expressed as the mean ± SD (n = 8).
###p < 0.001 compared to the normal control group.
**p < 0.05.*
***p < 0.01, and.*
****p < 0.001 compared to the T2DM, group.*

In addition, Sirius red- and ORO-stained liver sections showed large lipid droplet depositions and liver fibrosis in the hepatocytes of T2DM mice, which were substantially reduced after 4 weeks of treatment with PEG-Loxe, Lira, and Loxe (**Figures 2A,B**). These results suggested that PEG-Loxe, Lira, and Loxe were protective against T2DM-induced liver injury.

PEG-Loxe Attenuates Hepatic Oxidative Stress and Inflammatory Response in T2DM Mice

Our further exploration of the potential mechanism of PEG-Loxe's protection against liver damage revealed that T2DM mice had significantly higher liver ROS and MDA levels and pro-

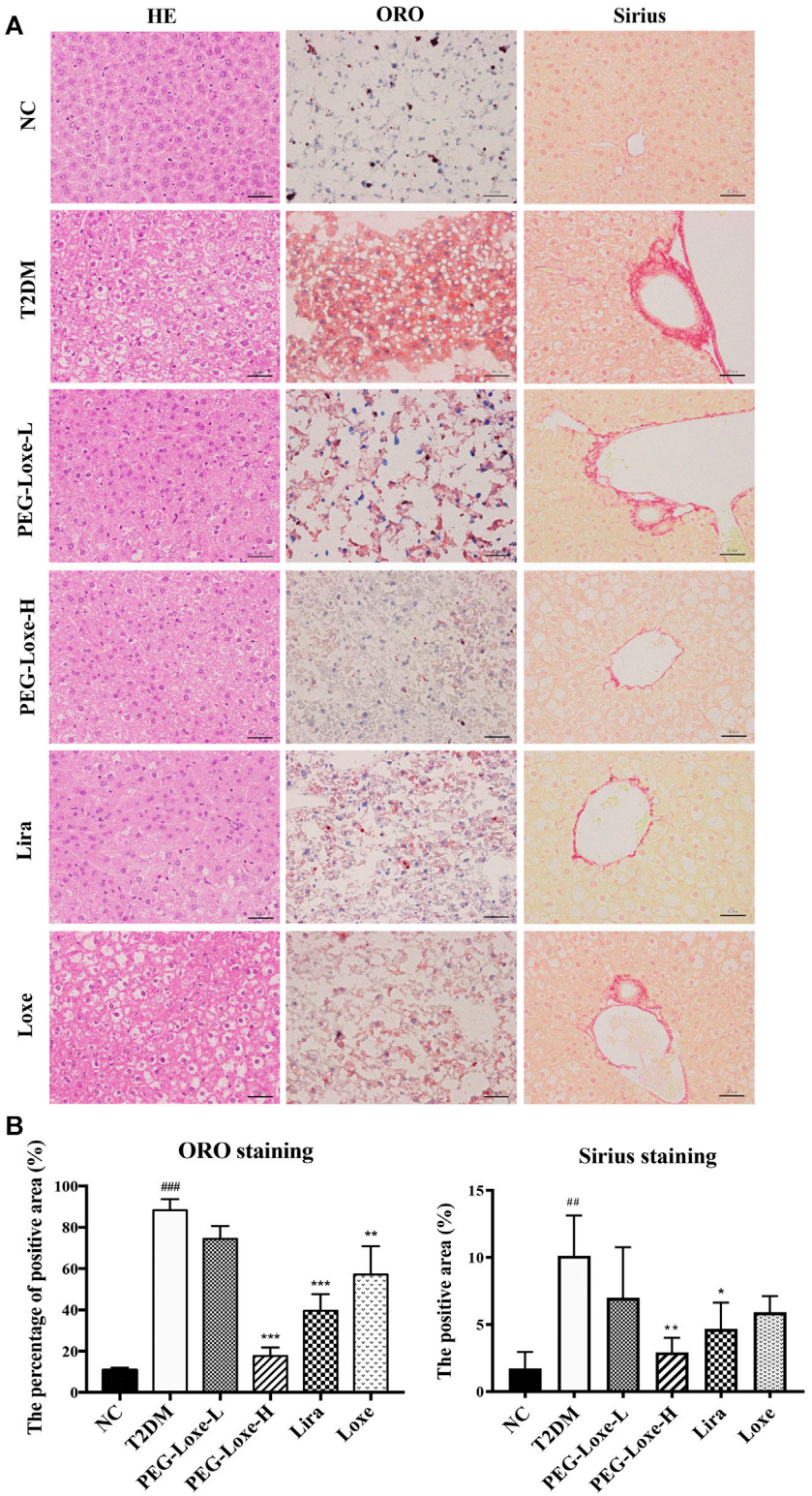

FIGURE 2 | Effects of polyethylene glycol loxenatide (PEG-Loxe) on the histopathological changes in the liver of *db/db* mice **(A)** Representative images of the hematoxylin and eosin (H&E), oil red O (ORO), and Sirius staining of liver tissues (400×) **(B)** Quantitative analysis of liver injury using ORO and Sirius staining. Data are presented as the mean ± SD; n = 3; $^{\#\#}p < 0.01$ and $^{\#\#\#}p < 0.001$ compared to the normal control group; $^{*}p < 0.05$, $^{**}p < 0.01$, and $^{***}p < 0.001$ compared to the T2DM group.

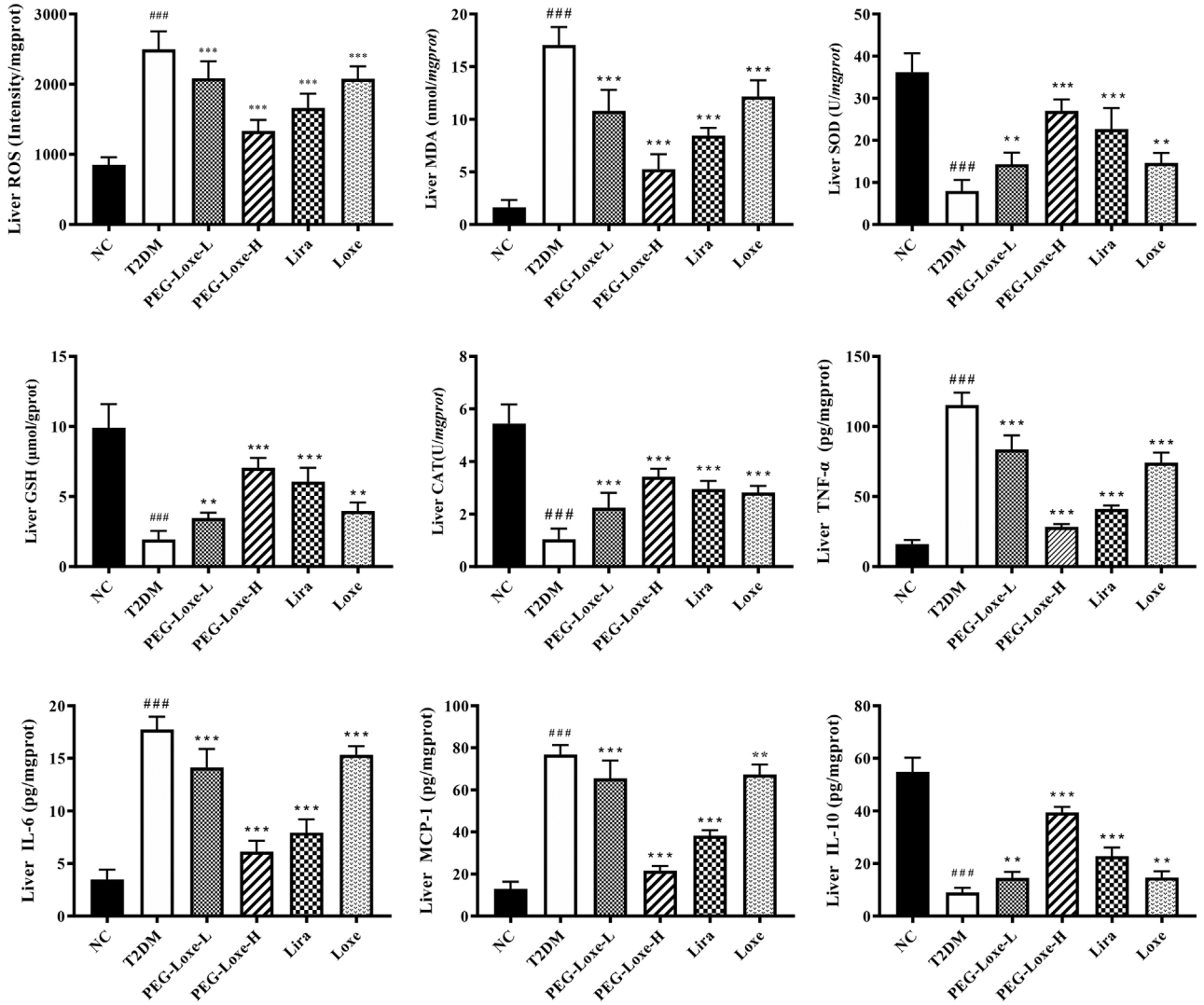

FIGURE 3 | Polyethylene glycol loxenatide (PEG-Loxe) improved oxidative stress and the production of inflammatory factors in the liver of *db/db* mice. Oxidative stress parameters, including reactive oxygen species (ROS), malondialdehyde (MDA), glutathione (GSH), superoxide dismutase (SOD), and catalase (CAT), and inflammatory factors, including tumor necrosis factor-α (TNF-α), interleukin-6 (IL-6), monocyte chemotactic protein-1 (MCP-1), and interleukin-10 (IL-10), were detected using the ELISA assay. Data are presented as the mean ± SD; n = 8; $^{###}p < 0.001$ compared to the normal control group; $^{**}p < 0.01$ and $^{***}p < 0.001$ compared to the T2DM group.

inflammatory factors TNF-α, IL-6, and MCP-1 levels than normal mice and markedly lower levels of liver antioxidant enzymes SOD, GSH, and CAT and anti-inflammatory cytokine IL-10 (**Figure 3**), indicating that oxidative stress and inflammation possibly occur with long-term hyperglycemic stimulation of the liver. **Figure 4** shows significantly enhanced ROS fluorescence intensity and drastically elevated ROS content in the liver tissues of T2DM mice, consistent with the results of our biochemical experiments. In contrast, PEG-Loxe, Lira, and Loxe reversed the above changes, indicating that PEG-Loxe protected the liver by reducing hepatic oxidative stress and inflammatory damage in T2DM mice.

PEG-Loxe Regulates Lipid Metabolism Through the Sirt1-AMPK Pathway to Improve Liver Damage in T2DM Mice

The Sirt1-AMPK signaling pathway is crucial to glucolipid metabolism in the body, but it also causes oxidative stress and inflammation (Jung et al., 2015). We assessed the effect of PEG-Loxe on the hepatic Sirt1-AMPK pathway in T2DM mice. As shown in **Figure 5B**, hepatic Sirt1, p-AMPK, p-ACC and CPT1 expressions decreased and FAT increased significantly in T2DM mice compared to normal mice ($p < 0.001$). However, treatment with PEG-Loxe and Lira improved markedly, suggesting that PEG-Loxe can inhibit hepatic lipid synthesis and oxidative stress,

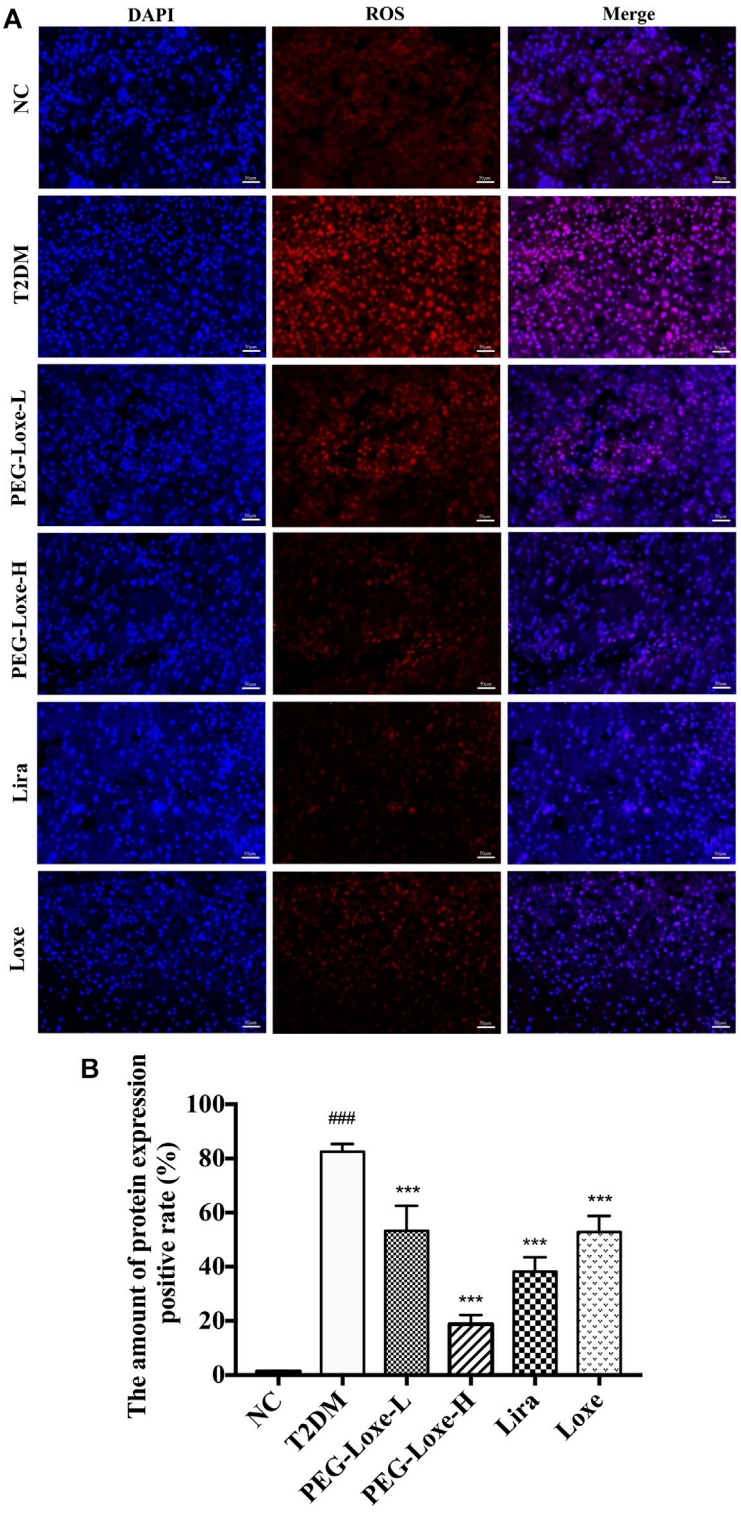

FIGURE 4 | Polyethylene glycol loxenatide (PEG-Loxe) reduced ROS levels in *db/db* mice (A) Representative images of reactive oxygen species (ROS) levels after dihydroethidium (DHE) staining (200×) (B) ROS levels expressed as the ratio of the fluorescence intensity of the DHE-positive area to 4′,6′-diamidino-2-phenylindole (DAPI). Data are presented as the mean ± SD; n = 3; $^{\#\#}p < 0.01$ and $^{\#\#\#}p < 0.001$ compared to the normal control group; $^{*}p < 0.05$, $^{**}p < 0.01$, and $^{***}p < 0.001$ compared to the T2DM group.

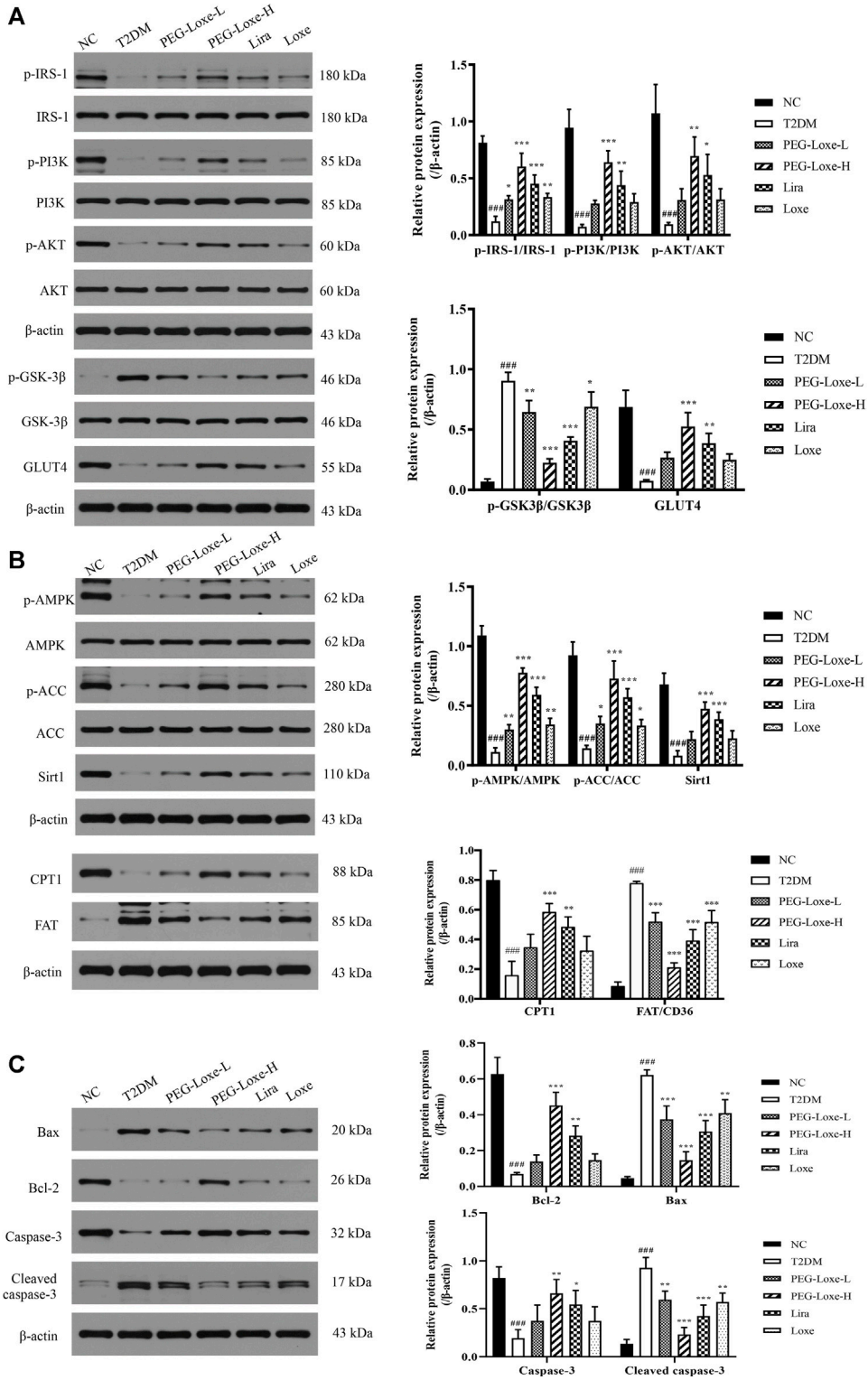

FIGURE 5 | Polyethylene glycol loxenatide (PEG-Loxe) regulates the expressions of the Sirt1-AMPK pathway-, insulin PI3K/AKT pathway- and apoptosis-related proteins. Protein expression levels were normalized to the levels of β-actin. Data are presented as the mean ± SD; n = 3; $^{###}p < 0.001$ compared to the normal control group; $^{*}p < 0.05$, $^{**}p < 0.01$, and $^{***}p < 0.001$ compared to the T2DM group.

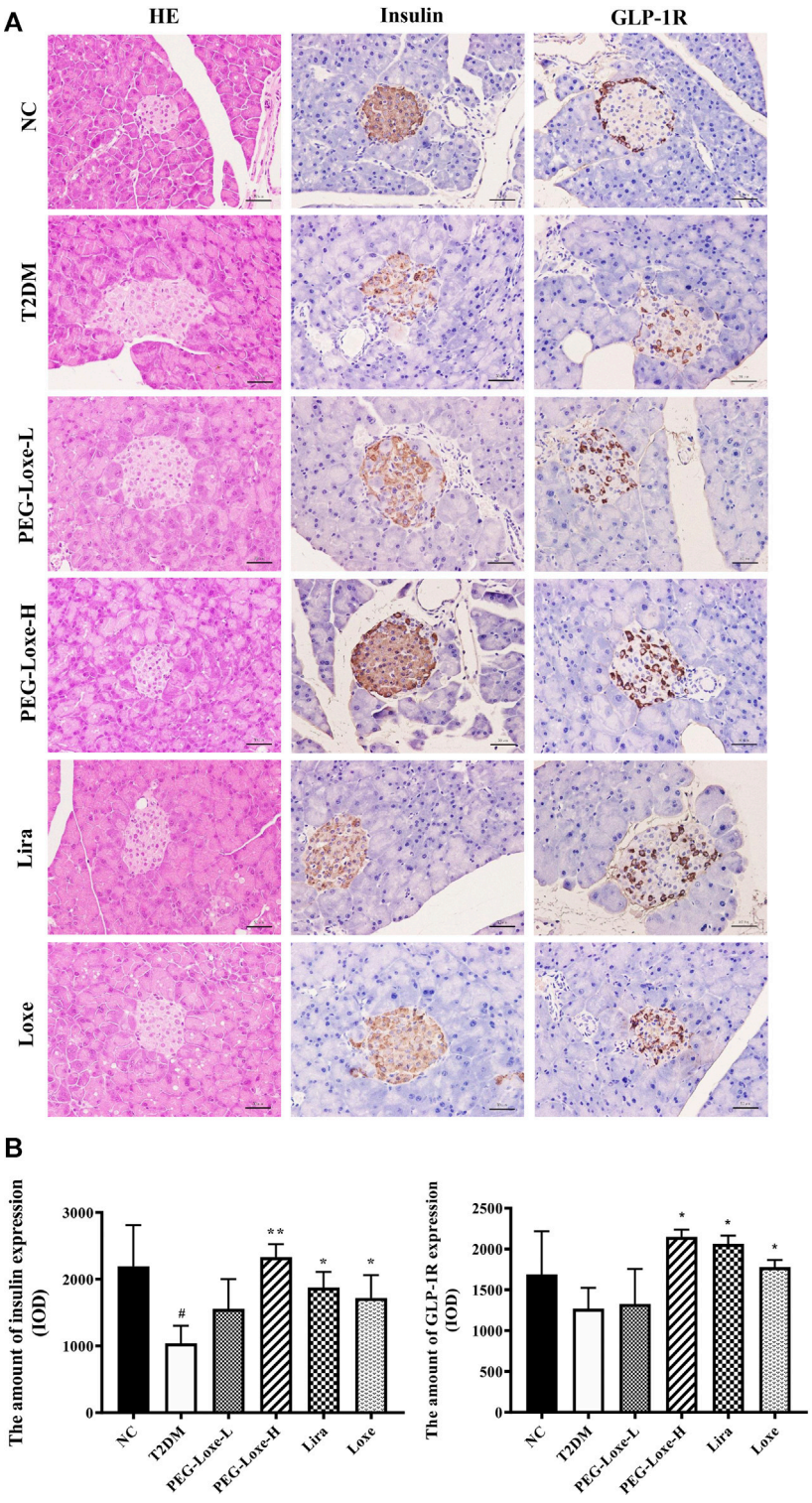

FIGURE 6 | Polyethylene glycol loxenatide (PEG-Loxe) prevents injury to pancreatic islets and promotes insulin secretion and GLP-1R production in *db/db* mice **(A)** Histological examination of pancreatic islet slices with hematoxylin and eosin (H&E) staining (400×) and representative images of islet insulin and glucagon-like peptide-1 receptor (GLP-1R) staining by the immunohistochemistry test (400×) **(B)** Quantitative immunohistochemical analysis of insulin and GLP-1R levels in islets. Data are presented as the mean ± SD; n = 3; $^{\#}p < 0.05$ compared to the normal control group; $^{*}p < 0.05$ and $^{**}p < 0.01$ compared to the T2DM group.

and promote fatty acid oxidation by regulating lipid metabolism via the Sirt1-AMPK pathway, thereby improving liver damage in T2DM.

PEG-Loxe Improves Pancreatic Islet Damage, Increases Pancreatic GLP-1R Expression, and Promotes Pancreatic Insulin Secretion in T2DM Mice

As shown in **Figure 6A**, the H&E staining revealed that the islets of the pancreatic tissues of mice in the NC group had regular morphology (round and oval) with clear borders and uniform distribution of islet cells (at ×400 magnification). On the other hand, the islets of mice in the T2DM group were swollen, irregular in morphology (polygonal), and had blurred borders. The morphologies of the islets of mice in the PEG-Loxe, Lira, and Loxe treatment groups showed improvement compared to those of T2DM group mice. PEG-Loxe is an agonist of GLP-1R, capable of promoting the synthesis and release of insulin by binding to GLP-1R. As shown in **Figures 6A,B**, PEG-Loxe-H, Lira, and Loxe significantly increased pancreatic GLP-1R levels in T2DM mice compared to T2DM mice, thereby promoting insulin secretion. Consistently, the islet insulin levels in the T2DM group were significantly lower than those in the NC group, indicating that the islet β-cells of T2DM mice had a reduced ability to secrete insulin and an impaired islet function. PEG-Loxe-H, Lira, and Loxe markedly increased insulin levels in T2DM mice (**Figure 6B**, $p < 0.05$). These results suggest that PEG-Loxe-H, Lira, and Loxe can repair damaged islet cells and promote insulin secretion from pancreatic β-cells, thus exerting hypoglycemic effects.

PEG-Loxe Inhibits Pancreatic β-Cell Apoptosis in T2DM Mice

To understand whether the damage of pancreatic islets was caused by β-cell apoptosis, we determined the expression of apoptosis-related proteins in pancreatic tissues using western blot. Our findings showed that the anti-apoptotic protein, Bcl-2, was significantly lower and the pro-apoptotic proteins, Bax and Cleaved-caspase-3, were considerably higher in the T2DM group of mice than in the NC group, pointing to increased apoptosis of islet cells in T2DM mice. PEG-Loxe, Lira, and Loxe drastically decreased Bax and Cleaved-caspase-3 levels while stimulating Bcl-2 expression, effectively inhibiting β-cell apoptosis (**Figure 5C**).

PEG-Loxe Activates the Insulin Signaling Pathway and Increases Serum Insulin Levels in T2DM Mice

As shown in **Table 1**, serum insulin levels were significantly higher in T2DM mice than in normal mice (about 2-fold higher), and treatment with PEG-Loxe-L, PEG-Loxe-H, and Lira further significantly increased serum insulin levels by 12.94, 26.80, 12.24%, respectively ($p < 0.05$).

To further investigate the impact of PEG-Loxe on insulin signaling, the expressions of proteins associated with the hepatic PI3K/AKT pathway were determined using western blot. The hepatic insulin signaling pathway is initiated when insulin binds to insulin receptor-β and is then activated by insulin receptor substrate (IRS)-1, followed by the triggering of the PI3K/AKT pathway, prompting the transfer of glucose transporter protein (GLUT) from the cytoplasm to the cell membrane to promote glucose absorption and glycogen synthesis (Wang et al., 2018). Proteins p-IRS-1, p-PI3K, p-AKT, and GLUT4 expression in the liver were significantly lower while p-GSK-3β expression was considerably higher in T2DM mice compared to the NC group, indicating that the insulin pathway in T2DM mice was impeded. PEG-Loxe, Lira, and Loxe activated the hepatic insulin signaling pathway in T2DM mice, as evidenced by pointedly elevated p-IRS-1, p-PI3K, p-AKT, and GLUT4 levels and considerably diminished p-GSK-3β expression (**Figure 5A**).

In vitro experiments were performed to further verify whether PEG-Loxe activated the PI3K/AKT signaling pathway. Results were shown in **Figures 7A–C** p-PI3K/PI3K and p-AKT/AKT in HepG2 cells were significantly lowered after high glucose culture ($p < 0.001$), indicating that the PI3K/AKT signaling pathway was impeded. HepG2 cells in the PEG-Loxe, Lira, and Loxe groups had significantly higher levels of each protein compared to the high glucose group ($p < 0.01$). In the presence of the PI3K inhibitor LY294002, p-PI3K/PI3K and p-AKT/AKT protein levels decreased substantially ($p < 0.05$). The addition of LY294002 offset the activation of the insulin pathway by PEG-Loxe, Lira, and Loxe, further confirming that PEG-Loxe can activate the PI3K/AKT insulin signaling pathway.

DISCUSSION

GLP-1RAs are novel hypoglycemic agents that have emerged in recent years and are now the focus of clinical studies for the treatment of T2DM because they have specific outstanding advantages (Müller et al., 2019). Our results suggest that PEG-Loxe can effectively lower blood glucose and improve glucolipid disorders in *db/db* mice. However, the underlying mechanisms had not been explored. Therefore, in the present study, we sought to establish the mechanism of the hypoglycemic and hypolipidemic effects of PEG-Loxe using T2DM as a model.

The liver is the central organ for glycogen synthesis and glucose metabolism. Insulin resistance, hyperglycemia, and disorders of fatty acid metabolism are important causes of dyslipidemia after meals in diabetic patients. In 2020, an international panel of 30 experts from 22 countries published a consensus that the diagnostic criteria for metabolic dysfunction-associated fatty liver disease (MAFLD) is based on hepatic fat accumulation in combination with one of the following three conditions: overweight/obesity, type 2 diabetes, or metabolic dysfunction. Among them, triacylglycerol (TAG) accumulation was a risk factor for metabolic abnormalities (Eslam et al., 2020). Studies have shown that liraglutide, exenatide, and lixisenatide reduce TG, TC, and LDL-C in the blood of diabetic patients

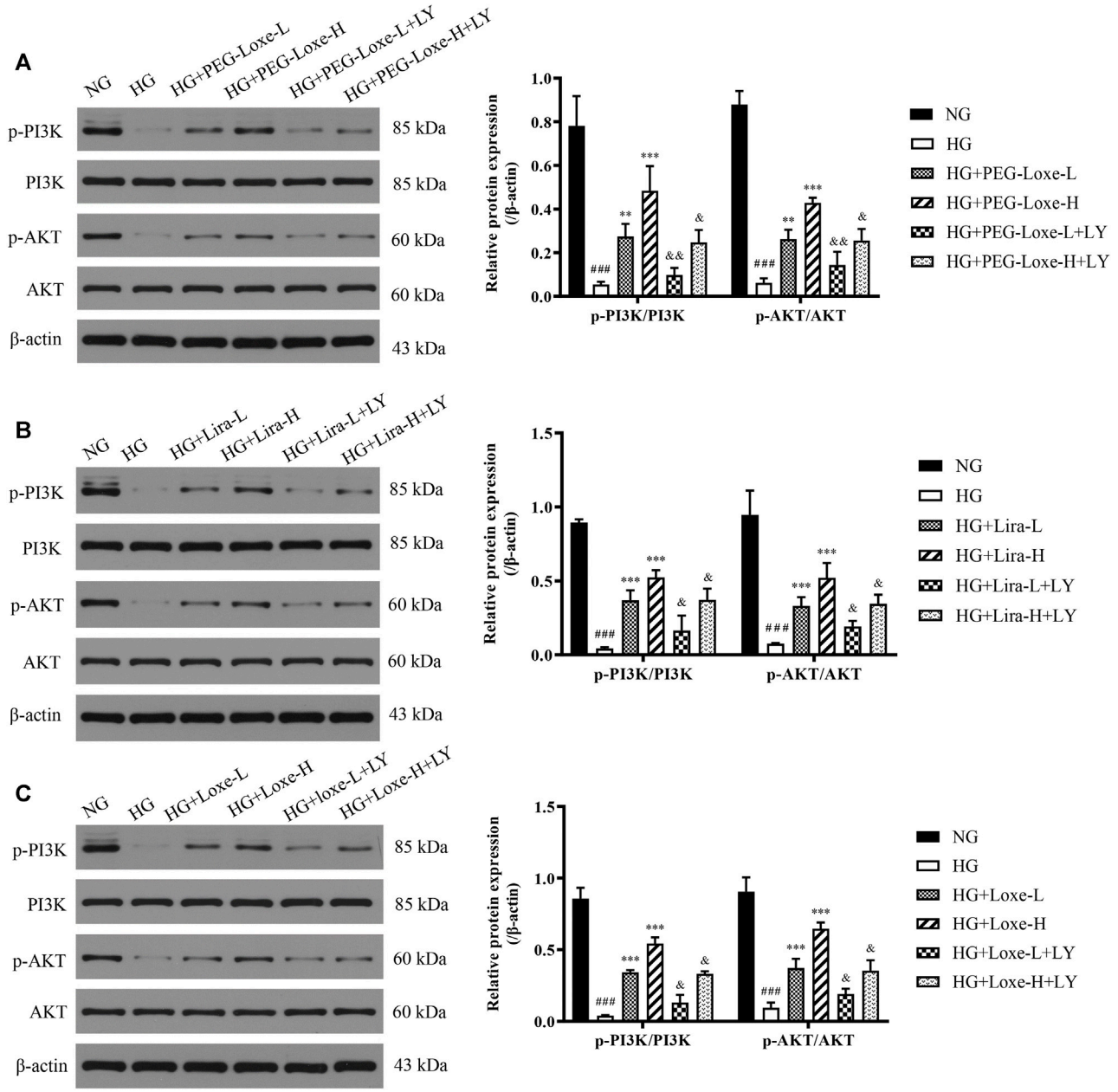

FIGURE 7 | The expressions of phospho-phosphoinositol 3 kinase (p-PI3K), PI3K, phospho-protein kinase B (p-AKT), and AKT in HepG2 cells treated with normal glucose (NG), high glucose (HG), HG + PEG-Loxe, HG + PEG-Loxe + LY (PI3K inhibitor), HG + Lira, HG + Lira + LY, HG + Loxe, and HG + Loxe + LY. Protein expression levels were normalized to the levels of β-actin. Data are presented as the mean ± SD; n = 3; $^{###}p < 0.001$ compared to the NG group; $^{**}p < 0.01$ and $^{***}p < 0.001$ compared to the HG group; $^{&}p < 0.05$ and $^{&&}p < 0.01$ compared to the HG + PEG-Loxe/HG + Lira/HG + Loxe group.

during T2DM treatment (Voukali et al., 2014; Sun et al., 2015; Roca-Rodríguez et al., 2017). In the meanwhile, these drugs also protect against T2DM-induced hepatic steatosis and liver damage by inhibiting oxidative stress and various inflammatory responses, and promoting body mass reduction in patients. Consistent with previous reports, we also observed a significant reduction in hepatic TC, TG and serum TG levels in *db/db* mice after 4 weeks of treating mice with PEG-Loxe, Lira, and Loxe in the present study. Furthermore, we also assessed and observed a significant increase in liver AST and ALT levels in T2DM mice, pointing to liver tissue damage. Histopathological evaluations also revealed steatosis, cytoplasmic vacuolation, massive lipid droplet deposition, and slight fibrosis in liver tissue sections, further confirming the accumulation of fat in the liver and the impaired structure and function of the liver. However, treatment with PEG-Loxe, Lira, and Loxe reversed these pathological changes. PEG-Loxe-L exhibited comparable effects to those of Lira in lowering blood glucose and regulating

lipid levels, suggesting that PEG-Loxe could also improve diabetes-induced hepatic lipid disorders and liver damage, which is corresponding to previous literature reports (Trevaskis et al., 2012; Liu et al., 2015).

Oxidative stress and inflammatory response are critical for abnormal glucolipid metabolism in T2DM and are also the main reason behind the progression of diabetes and its complications. Chronic high-sugar and high-fat diets lead to excessive hepatic lipid deposition, oxidative stress, and inflammatory response (Zhou et al., 2019). In this study, we observed similar changes in the levels of oxidative and inflammatory factors in diabetic mice, with ROS fluorescence intensity in liver tissues significantly enhanced, suggesting that chronic hyperglycemia stimulates peroxidative and inflammatory damages in the liver. Treatment with PEG-Loxe, Lira, and Loxe notably repaired these abnormal changes, as shown by the decline in ROS, MDA, TNF-α, IL-6, and MCP-1 levels and the increase in SOD, GSH, CAT, and IL-10 levels. Of these treatments, PEG-Loxe modulations on the above factors were dose-dependent, and PEG-Loxe-L and Loxe had comparable weaker remediation impact on hepatic oxidative stress and inflammatory response than Lira. In line with these findings, one investigation established that GLP-1 effectively improved endothelial dysfunction and enhanced antioxidant and anti-inflammatory levels in T2DM patients (Ceriello et al., 2014). Overall, our results suggest that PEG-Loxe possibly reduces lipid metabolism disorders in T2DM and protects against diabetes-induced liver damage by activating antioxidant defense systems and attenuating inflammatory responses.

Lipid metabolism disorder can cause the deposition of TAG and fatty acids in hepatocytes, and then promote the occurrence and development of fatty liver. In clinical practice, GLP-1RAs reduce body weight and liver fat accumulation. However, there is limited research on the underlying mechanisms. AMPK is an important signaling molecule involved in glucolipid metabolism and is widely distributed in tissues with excited metabolisms, such as the liver, adipose tissues, and skeletal muscles. ACC is a downstream target of AMPK regulation, with the AMPK/ACC pathway playing a key role as a regulator of energy homeostasis, including mitochondrial biogenesis, cellular lipolysis, fatty acid synthesis and oxidation (Hardie et al., 2012). In the liver, GLP-1 stimulated the phosphorylation of AMPK and expression of Sirt1, then activated AMPK can phosphorylate ACC and reduce the production of malonyl-coA, thus up-regulating CPT1 expression, reducing FAT level, promoting fatty acid oxidation and reducing lipid deposition (Mottillo et al., 2016; Liu et al., 2015; Wan et al., 2021; O'Neill et al., 2013; Ben-Shlomo et al., 2011). Lira, as demonstrated in recent years, improves insulin resistance and hepatic lipid deposition in T2DM rats fed with a high-fat diet and promotes lipid degradation in liver and adipose tissues through activation of the AMPK pathway (He et al., 2016; He et al., 2020; Zhou et al., 2020). Similarly, our study demonstrated that PEG-Loxe, Lira, and Loxe notably upregulated the levels of Sirt1, p-AMPK, and p-ACC in the liver. Activation of AMPK signaling pathway promoted the oxidation of liver fatty acids, which in turn increased CPT1 protein expression, reduced FAT level, and decreased lipid accumulation, with the most significant effect observed in the PEG-Loxe-H group. A previous study demonstrated that the activation of the Sirt1-AMPK pathway inhibits hepatic oxidative stress and inflammatory responses (Jung et al., 2015). Consistent with that observation, our findings suggest that PEG-Loxe possibly inhibits hepatic lipid synthesis, oxidative stress, and inflammatory response, and promote fatty acid oxidation by regulating lipid metabolism via the Sirt1/AMPK/ACC pathway, thereby remedying T2DM liver damage.

The development of T2DM is due in part to damage to the islet β-cells, which results in failure to secrete sufficient insulin (Eizirik et al., 2020). As observed in this study, T2DM mice had swollen islets with irregular morphology and significantly reduced serum insulin levels. Additionally, immunohistochemical measurements of insulin revealed that islet insulin levels were considerably lower in diabetic mice than in normal mice. Therefore, the islets of T2DM mice are damaged and unable to regulate the rise in blood glucose levels. Treatment with PEG-Loxe and Lira could significantly increase pancreatic GLP-1R expression and increase insulin stores, as demonstrated here. Mounting evidence suggests that the reduced number and increased apoptosis of islet β-cells are the primary causes of the impaired structure and function of islets in T2DM (Meier, 2012; Eizirik et al., 2020). GLP-1 promotes islet β-cell proliferation and inhibits β-cell apoptosis (Drucker, 2018). In line with this, PEG-Loxe and Lira could block the pancreatic apoptotic pathway by regulating the expression of apoptotic proteins. As expected, PEG-Loxe treatment markedly increased the expression of the anti-apoptotic protein Bcl-2 and decreased the level of the pro-apoptotic protein Bax, which led to an increase in the Bcl-2/Bax ratio, resulting in the inhibition of the apoptosis enforcer Cleaved-caspase-3/Caspase-3 ratio and the blockage of the β-cell apoptosis program. PEG-Loxe tellingly inhibits β-cell apoptosis arguably by restoring the Bcl-2/Bax balance, blocking the endogenous apoptotic pathway, promoting the recovery of islet structural breakdowns and functional defects, and increasing insulin secretion for the effective treatment of T2DM.

The impairment of the PI3K/AKT signaling pathway is the key to causing glucose metabolism disorders. GLP-1R, which belongs to the G protein-coupled receptor family, exerts biological effects mainly through the activation of phosphoinositide 3 kinase (PI3K), protein kinase A (PKA), and extracellular signal-regulated kinase (ERK) 1/2 (He et al., 2019; Li et al., 2019). GLP-1RAs activate the PI3K/AKT and AMPK signaling pathways in T2DM rats, protecting against T2DM-related learning memory impairment and lowering blood glucose (Yang et al., 2018). Here, T2DM mice harbored an impaired hepatic insulin pathway and had reduced serum insulin levels, which led to an increase in blood glucose. However, PEG-Loxe, Lira, and Loxe significantly increased serum insulin levels, and the expression of hepatic proteins p-IRS-1, p-PI3K, p-AKT, and

GLUT4 in T2DM mice. *In vitro* cellular experiments confirmed that the activation of the insulin pathway by PEG-Loxe, Lira, and Loxe was offset by the presence of the PI3K inhibitor, further demonstrating that PEG-Loxe, Lira, and Loxe promote insulin secretion and stimulate the hepatic insulin pathway, thereby improving insulin sensitivity and promoting glucose uptake, which eventually reduces blood glucose.

CONCLUSION

In summary, we have shown that PEG-Loxe has hypoglycemic and hepatoprotective effects in db/db mice. PEG-Loxe inhibited hepatic lipid synthesis, oxidative stress, and inflammatory response by activating lipid metabolism through the Sirt1/AMPK/ACC pathway, thereby improving T2DM-associated liver damage. PEG-Loxe also subdued β-cell apoptosis, increased pancreatic GLP-1R expression, and activated the insulin PI3K/AKT pathway, promoting the synthesis and secretion of insulin and providing hypoglycemic effects.

DATA AVAILABILITY STATEMENT

The original contributions presented in the study are included in the article/supplementary material, further inquiries can be directed to the corresponding authors.

ETHICS STATEMENT

The animal study was reviewed and approved by Institutional Animal Care and Use Committee of Tongji Medical College, Huazhong University of Science and Technology.

AUTHOR CONTRIBUTIONS

YZ, YL, JZ, QZ, and CS contributed to experimental design. QZ, CW and BD contributed to animal experiments and biochemical analysis. YZ, QZ and CS contributed to manuscript writing, critical review of results and revising. All authors have read, revised, and approved the final manuscript.

REFERENCES

Afkarian, M., Zelnick, L. R., Hall, Y. N., Heagerty, P. J., Tuttle, K., Weiss, N. S., et al. (2016). Clinical Manifestations of Kidney Disease Among US Adults with Diabetes, 1988-2014. *Jama* 316 (6), 602–610. doi:10.1001/jama.2016.10924

American Diabetes Association (2021). 2. Classification and Diagnosis of Diabetes: Standards of Medical Care in Diabetes-2021. *Diabetes care.* 44 (Suppl. 1), S15–s33. doi:10.2337/dc21-S002

Ben-Shlomo, S., Zvibel, I., Shnell, M., Shlomai, A., Chepurko, E., Halpern, Z., et al. (2011). Glucagon-like Peptide-1 Reduces Hepatic Lipogenesis via Activation of AMP-Activated Protein Kinase. *J. Hepatol.* 54 (6), 1214–1223. doi:10.1016/j.jhep.2010.09.032

Campbell, J. E., and Drucker, D. J. (2013). Pharmacology, Physiology, and Mechanisms of Incretin Hormone Action. *Cell Metab* 17 (6), 819–837. doi:10.1016/j.cmet.2013.04.008

Ceriello, A., Novials, A., Canivell, S., La Sala, L., Pujadas, G., Esposito, K., et al. (2014). Simultaneous GLP-1 and Insulin Administration Acutely Enhances Their Vasodilatory, Antiinflammatory, and Antioxidant Action in Type 2 Diabetes. *Diabetes care* 37 (7), 1938–1943. doi:10.2337/dc13-2618

Chen, X., Lv, X., Yang, G., Lu, D., Piao, C., Zhang, X., et al. (2017). Polyethylene Glycol Loxenatide Injections Added to Metformin Effectively Improve Glycemic Control and Exhibit Favorable Safety in Type 2 Diabetic Patients. *J. Diabetes* 9 (2), 158–167. doi:10.1111/1753-0407.12397

Costes, S. (2018). Targeting Protein Misfolding to Protect Pancreatic Beta-Cells in Type 2 Diabetes. *Curr. Opin. Pharmacol.* 43, 104–110. doi:10.1016/j.coph.2018.08.016

Drucker, D. J., Habener, J. F., and Holst, J. J. (2017). Discovery, Characterization, and Clinical Development of the Glucagon-like Peptides. *J. Clin. Invest.* 127 (12), 4217–4227. doi:10.1172/jci97233

Drucker, D. J. (2018). Mechanisms of Action and Therapeutic Application of Glucagon-like Peptide-1. *Cel Metab* 27 (4), 740–756. doi:10.1016/j.cmet.2018.03.001

Eizirik, D. L., Pasquali, L., and Cnop, M. (2020). Pancreatic β-cells in Type 1 and Type 2 Diabetes Mellitus: Different Pathways to Failure. *Nat. Rev. Endocrinol.* 16 (7), 349–362. doi:10.1038/s41574-020-0355-7

Eslam, M., Newsome, P. N., Sarin, S. K., Anstee, Q. M., Targher, G., Romero-Gomez, M., et al. (2020). A New Definition for Metabolic Dysfunction-Associated Fatty Liver Disease: An International Expert Consensus Statement. *J. Hepatol.* 73 (1), 202–209. doi:10.1016/j.jhep.2020.03.039

Fadini, G. P., Bonora, B. M., and Avogaro, A. (2017). SGLT2 Inhibitors and Diabetic Ketoacidosis: Data from the FDA Adverse Event Reporting System. *Diabetologia* 60 (8), 1385–1389. doi:10.1007/s00125-017-4301-8

Ferdaoussi, M., Abdelli, S., Yang, J. Y., Cornu, M., Niederhauser, G., Favre, D., et al. (2008). Exendin-4 Protects Beta-Cells from Interleukin-1 Beta-Induced Apoptosis by Interfering with the C-Jun NH2-terminal Kinase Pathway. *Diabetes* 57 (5), 1205–1215. doi:10.2337/db07-1214

Flory, J. H., Hennessy, S., Bailey, C. J., and Inzucchi, S. E. (2020). Reports of Lactic Acidosis Attributed to Metformin, 2015-2018. *Diabetes care* 43 (1), 244–246. doi:10.2337/dc19-0923

Gruzman, A., Babai, G., and Sasson, S. (2009). Adenosine Monophosphate-Activated Protein Kinase (AMPK) as a New Target for Antidiabetic Drugs: A Review on Metabolic, Pharmacological and Chemical Considerations. *Rev. Diabet Stud.* 6 (1), 13–36. doi:10.1900/rds.2009.6.13

Hardie, D. G., Ross, F. A., and Hawley, S. A. (2012). AMPK: a Nutrient and Energy Sensor that Maintains Energy Homeostasis. *Nat. Rev. Mol. Cel Biol* 13 (4), 251–262. doi:10.1038/nrm3311

He, Q., Sha, S., Sun, L., Zhang, J., and Dong, M. (2016). GLP-1 Analogue Improves Hepatic Lipid Accumulation by Inducing Autophagy via AMPK/mTOR Pathway. *Biochem. Biophys. Res. Commun.* 476 (4), 196–203. doi:10.1016/j.bbrc.2016.05.086

He, S., Wu, W., Wan, Y., Nandakumar, K. S., Cai, X., Tang, X., et al. (2019). GLP-1 Receptor Activation Abrogates β-Cell Dysfunction by PKA Cα-Mediated Degradation of Thioredoxin Interacting Protein. *Front. Pharmacol.* 10, 1230. doi:10.3389/fphar.2019.01230

He, Y., Ao, N., Yang, J., Wang, X., Jin, S., and Du, J. (2020). The Preventive Effect of Liraglutide on the Lipotoxic Liver Injury via Increasing Autophagy. *Ann. Hepatol.* 19 (1), 44–52. doi:10.1016/j.aohep.2019.06.023

Huang, Q., Bu, S., Yu, Y., Guo, Z., Ghatnekar, G., Bu, M., et al. (2007). Diazoxide Prevents Diabetes through Inhibiting Pancreatic Beta-Cells from Apoptosis via Bcl-2/Bax Rate and P38-Beta Mitogen-Activated Protein Kinase. *Endocrinol.* 148 (1), 81–91. doi:10.1210/en.2006-0738

Jiang, Y., Liu, J., Chen, X., Yang, W., Jia, W., and Wu, J. (2021). Efficacy and Safety of Glucagon-like Peptide 1 Receptor Agonists for the Treatment of Type 2 Diabetes Mellitus: A Network Meta-Analysis. *Adv. Ther.* 38 (3), 1470–1482. doi:10.1007/s12325-021-01637-6

Jung, T. W., Hwang, H. J., Hong, H. C., Yoo, H. J., Baik, S. H., and Choi, K. M. (2015). BAIBA Attenuates Insulin Resistance and Inflammation Induced by

Palmitate or a High Fat Diet via an AMPK-pparδ-dependent Pathway in Mice. *Diabetologia* 58 (9), 2096–2105. doi:10.1007/s00125-015-3663-z

Kohlroser, J., Mathai, J., Reichheld, J., Banner, B. F., and Bonkovsky, H. L. (2000). Hepatotoxicity Due to Troglitazone: Report of Two Cases and Review of Adverse Events Reported to the United States Food and Drug Administration. *Am. J. Gastroenterol.* 95 (1), 272–276. doi:10.1111/j.1572-0241.2000.01707.x

Kuang, J. R., Zhang, Z. H., Leng, W. L., Lei, X. T., and Liang, Z. W. (2017). Dapper1 Attenuates Hepatic Gluconeogenesis and Lipogenesis by Activating PI3K/Akt Signaling. *Mol. Cel Endocrinol* 447, 106–115. doi:10.1016/j.mce.2017.02.028

Li, R., Shan, Y., Gao, L., Wang, X., Wang, X., and Wang, F. (2019). The Glp-1 Analog Liraglutide Protects against Angiotensin II and Pressure Overload-Induced Cardiac Hypertrophy via PI3K/Akt1 and AMPKa Signaling. *Front. Pharmacol.* 10, 537. doi:10.3389/fphar.2019.00537

Liu, J., Wang, G., Jia, Y., and Xu, Y. (2015). GLP-1 Receptor Agonists: Effects on the Progression of Non-alcoholic Fatty Liver Disease. *Diabetes Metab. Res. Rev.* 31 (4), 329–335. doi:10.1002/dmrr.2580

Madhu, D., Khadir, A., Hammad, M., Kavalakatt, S., Dehbi, M., Al-Mulla, F., et al. (2020). The GLP-1 Analog Exendin-4 Modulates HSP72 Expression and ERK1/2 Activity in BTC6 Mouse Pancreatic Cells. *Biochim. Biophys. Acta Proteins Proteom* 1868 (7), 140426. doi:10.1016/j.bbapap.2020.140426

Meier, J. J. (2012). GLP-1 Receptor Agonists for Individualized Treatment of Type 2 Diabetes Mellitus. *Nat. Rev. Endocrinol.* 8 (12), 728–742. doi:10.1038/nrendo.2012.140

Monami, M., Dicembrini, I., Kundisova, L., Zannoni, S., Nreu, B., and Mannucci, E. (2014). A Meta-Analysis of the Hypoglycaemic Risk in Randomized Controlled Trials with Sulphonylureas in Patients with Type 2 Diabetes. *Diabetes Obes. Metab.* 16 (9), 833–840. doi:10.1111/dom.12287

Mottillo, E. P., Desjardins, E. M., Crane, J. D., Smith, B. K., Green, A. E., Ducommun, S., et al. (2016). Lack of Adipocyte AMPK Exacerbates Insulin Resistance and Hepatic Steatosis through Brown and Beige Adipose Tissue Function. *Cel Metab* 24 (1), 118–129. doi:10.1016/j.cmet.2016.06.006

Müller, T. D., Finan, B., Bloom, S. R., D'Alessio, D., Drucker, D. J., Flatt, P. R., et al. (2019). Glucagon-like Peptide 1 (GLP-1). *Mol. Metab.* 30, 72–130. doi:10.1016/j.molmet.2019.09.010

O'Neill, H. M., Holloway, G. P., and Steinberg, G. R. (2013). AMPK Regulation of Fatty Acid Metabolism and Mitochondrial Biogenesis: Implications for Obesity. *Mol. Cel Endocrinol* 366 (2), 135–151. doi:10.1016/j.mce.2012.06.019

Pan, Q., Lin, S., Li, Y., Liu, L., Li, X., Gao, X., et al. (2021). A Novel GLP-1 and FGF21 Dual Agonist Has Therapeutic Potential for Diabetes and Non-alcoholic Steatohepatitis. *EBioMedicine* 63, 103202. doi:10.1016/j.ebiom.2020.103202

Regensteiner, J. G., Golden, S., Huebschmann, A. G., Barrett-Connor, E., Chang, A. Y., Chyun, D., et al. (2015). Sex Differences in the Cardiovascular Consequences of Diabetes Mellitus: A Scientific Statement from the American Heart Association. *Circulation* 132 (25), 2424–2447. doi:10.1161/cir.0000000000000343

Roca-Rodríguez, M. M., Muros de Fuentes, M. T., Piédrola-Maroto, G., Quesada-Charneco, M., Maraver-Selfa, S., Tinahones, F. J., et al. (2017). Lixisenatida en pacientes con diabetes tipo 2 y obesidad: más allá del control glucémico. *Atención Primaria* 49 (5), 294–299. doi:10.1016/j.aprim.2016.06.009

Rowlands, J., Heng, J., Newsholme, P., and Carlessi, R. (2018). Pleiotropic Effects of GLP-1 and Analogs on Cell Signaling, Metabolism, and Function. *Front. Endocrinol. (Lausanne)* 9, 672. doi:10.3389/fendo.2018.00672

Shuai, Y., Yang, G., Zhang, Q., Li, W., Luo, Y., Ma, J., et al. (2021). Efficacy and Safety of Polyethylene Glycol Loxenatide Monotherapy in Type 2 Diabetes Patients: A Multicentre, Randomized, Double-blind, Placebo-controlled Phase 3a Clinical Trial. *Diabetes Obes. Metab.* 23 (1), 116–124. doi:10.1111/dom.14198

Sun, F., Wu, S., Wang, J., Guo, S., Chai, S., Yang, Z., et al. (2015). Effect of Glucagon-like Peptide-1 Receptor Agonists on Lipid Profiles Among Type 2 Diabetes: a Systematic Review and Network Meta-Analysis. *Clin. Ther.* 37 (1), 225–241.e8. doi:10.1016/j.clinthera.2014.11.008

Trevaskis, J. L., Griffin, P. S., Wittmer, C., Neuschwander-Tetri, B. A., Brunt, E. M., Dolman, C. S., et al. (2012). Glucagon-like Peptide-1 Receptor Agonism Improves Metabolic, Biochemical, and Histopathological Indices of Nonalcoholic Steatohepatitis in Mice. *Am. J. Physiol. Gastrointest. Liver Physiol.* 302 (8), G762–G772. doi:10.1152/ajpgi.00476.2011

Voukali, M., Kastrinelli, I., Stragalinou, S., Tasiopoulou, D., Paraskevopoulou, P., Katsilambros, N., et al. (2014). Study of Postprandial Lipaemia in Type 2 Diabetes Mellitus: Exenatide versus Liraglutide. *J. Diabetes Res.* 2014, 304032. doi:10.1155/2014/304032

Wan, J., Zhang, Y., Yang, D., Liang, Y., Yang, L., Hu, S., et al. (2021). Gastrodin Improves Nonalcoholic Fatty Liver Disease through Activation of the Adenosine Monophosphate-Activated Protein Kinase Signaling Pathway. *Hepatol.* doi:10.1002/hep.32068

Wang, K., Tang, Z., Zheng, Z., Cao, P., Shui, W., Li, Q., et al. (2016). Protective Effects of Angelica Sinensis Polysaccharide against Hyperglycemia and Liver Injury in Multiple Low-Dose Streptozotocin-Induced Type 2 Diabetic BALB/c Mice. *Food Funct.* 7 (12), 4889–4897. doi:10.1039/c6fo01196a

Wang, K., Wang, H., Liu, Y., Shui, W., Wang, J., Cao, P., et al. (2018). Dendrobium Officinale Polysaccharide Attenuates Type 2 Diabetes Mellitus via the Regulation of PI3K/Akt-Mediated Glycogen Synthesis and Glucose Metabolism. *J. Funct. Foods* 40, 261–271. doi:10.1016/j.jff.2017.11.004

Woods, A., Williams, J. R., Muckett, P. J., Mayer, F. V., Liljevald, M., Bohlooly-Y, M., et al. (2017). Liver-Specific Activation of AMPK Prevents Steatosis on a High-Fructose Diet. *Cell Rep* 18 (13), 3043–3051. doi:10.1016/j.celrep.2017.03.011

Yang, Y., Fang, H., Xu, G., Zhen, Y., Zhang, Y., Tian, J., et al. (2018). Liraglutide Improves Cognitive Impairment via the AMPK and PI3K/Akt Signaling Pathways in Type 2 Diabetic Rats. *Mol. Med. Rep.* 18 (2), 2449–2457. doi:10.3892/mmr.2018.9180

Zhang, Q., Liu, X., Sullivan, M. A., Shi, C., and Deng, B. (2021). Protective Effect of Yi Shen Pai Du Formula against Diabetic Kidney Injury via Inhibition of Oxidative Stress, Inflammation, and Epithelial-To-Mesenchymal Transition in Db/db Mice. *Oxidative Med. Cell Longevity* 2021, 7958021. doi:10.1155/2021/7958021

Zheng, Y., Ley, S. H., and Hu, F. B. (2018). Global Aetiology and Epidemiology of Type 2 Diabetes Mellitus and its Complications. *Nat. Rev. Endocrinol.* 14 (2), 88–98. doi:10.1038/nrendo.2017.151

Zhou, J. Y., Poudel, A., Welchko, R., Mekala, N., Chandramani-Shivalingappa, P., Rosca, M. G., et al. (2019). Liraglutide Improves Insulin Sensitivity in High Fat Diet Induced Diabetic Mice through Multiple Pathways. *Eur. J. Pharmacol.* 861, 172594. doi:10.1016/j.ejphar.2019.172594

Zhou, R., Lin, C., Cheng, Y., Zhuo, X., Li, Q., Xu, W., et al. (2020). Liraglutide Alleviates Hepatic Steatosis and Liver Injury in T2MD Rats via a GLP-1R Dependent AMPK Pathway. *Front. Pharmacol.* 11, 600175. doi:10.3389/fphar.2020.600175

Conflict of Interest: YL was employed by the company Shanghai Hansoh Biomedical Co. Ltd. JZ was employed by the company Jiangsu Hansoh Pharmaceutical Group Co. Ltd.

The remaining authors declare that the research was conducted in the absence of any commercial or financial relationships that could be construed as a potential conflict of interest.

Publisher's Note: All claims expressed in this article are solely those of the authors and do not necessarily represent those of their affiliated organizations, or those of the publisher, the editors and the reviewers. Any product that may be evaluated in this article, or claim that may be made by its manufacturer, is not guaranteed or endorsed by the publisher.

Copyright © 2021 Zhang, Li, Zhao, Wang, Deng, Zhang and Shi. This is an open-access article distributed under the terms of the Creative Commons Attribution License (CC BY). The use, distribution or reproduction in other forums is permitted, provided the original author(s) and the copyright owner(s) are credited and that the original publication in this journal is cited, in accordance with accepted academic practice. No use, distribution or reproduction is permitted which does not comply with these terms.

frontiers in Pharmacology

BRIEF RESEARCH REPORT
published: 24 December 2021
doi: 10.3389/fphar.2021.809541

Antioxidant Activity of Fluoxetine and Vortioxetine in a Non-Transgenic Animal Model of Alzheimer's Disease

Giuseppe Caruso[1†], Margherita Grasso[1,2†], Annamaria Fidilio[1,3], Sebastiano Alfio Torrisi[3], Nicolò Musso[3], Federica Geraci[3], Maria Rosaria Tropea[3], Anna Privitera[1], Fabio Tascedda[4,5], Daniela Puzzo[2,3], Salvatore Salomone[3], Filippo Drago[3], Gian Marco Leggio[3‡] and Filippo Caraci[1,2‡]*

[1]Department of Drug and Health Sciences, University of Catania, Catania, Italy, [2]Oasi Research Institute—IRCCS, Troina, Italy, [3]Department of Biomedical and Biotechnological Sciences, University of Catania, Catania, Italy, [4]Center for Neuroscience and Neurotechnology, University of Modena and Reggio Emilia, Modena, Italy, [5]Department of Life Sciences, University of Modena and Reggio Emilia, Modena, Italy

OPEN ACCESS

Edited by:
Maria Grazia Morgese,
University of Foggia, Italy

Reviewed by:
Rosalia Crupi,
University of Messina, Italy
Cristina Lanni,
University of Pavia, Italy

***Correspondence:**
Giuseppe Caruso
forgiuseppecaruso@gmail.com

†These authors share first authorship

‡These authors share last authorship

Specialty section:
This article was submitted to Experimental Pharmacology and Drug Discovery, a section of the journal Frontiers in Pharmacology

Received: 05 November 2021
Accepted: 17 November 2021
Published: 24 December 2021

Citation:
Caruso G, Grasso M, Fidilio A, Torrisi SA, Musso N, Geraci F, Tropea MR, Privitera A, Tascedda F, Puzzo D, Salomone S, Drago F, Leggio GM and Caraci F (2021) Antioxidant Activity of Fluoxetine and Vortioxetine in a Non-Transgenic Animal Model of Alzheimer's Disease. Front. Pharmacol. 12:809541. doi: 10.3389/fphar.2021.809541

Depression is a risk factor for the development of Alzheimer's disease (AD). A neurobiological and clinical continuum exists between AD and depression, with neuroinflammation and oxidative stress being involved in both diseases. Second-generation antidepressants, in particular selective serotonin reuptake inhibitors (SSRIs), are currently investigated as neuroprotective drugs in AD. By employing a non-transgenic AD model, obtained by intracerebroventricular (i.c.v.) injection of amyloid-β (Aβ) oligomers in 2-month-old C57BL/6 mice, we recently demonstrated that the SSRI fluoxetine (FLX) and the multimodal antidepressant vortioxetine (VTX) reversed the depressive-like phenotype and memory deficits induced by Aβ oligomers rescuing the levels of transforming growth factor-β1 (TGF-β1). Aim of our study was to test FLX and VTX for their ability to prevent oxidative stress in the hippocampus of Aβ-injected mice, a brain area strongly affected in both depression and AD. The long-term intraperitoneal (i.p.) administration of FLX (10 mg/kg) or VTX (5 and 10 mg/kg) for 24 days, starting 7 days before Aβ injection, was able to prevent the over-expression of inducible nitric oxide synthase (iNOS) and NADPH oxidase 2 (Nox2) induced by Aβ oligomers. Antidepressant pre-treatment was also able to rescue the mRNA expression of glutathione peroxidase 1 (Gpx1) antioxidant enzyme. FLX and VTX also prevented Aβ-induced neurodegeneration in mixed neuronal cultures treated with Aβ oligomers. Our data represent the first evidence that the long-term treatment with the antidepressants FLX or VTX can prevent the oxidative stress phenomena related to the cognitive deficits and depressive-like phenotype observed in a non-transgenic animal model of AD.

Keywords: oxidative stress, Alzheimer's disease, depression, amyloid-β, vortioxetine, fluoxetine, TGF-β1, neuroprotection

INTRODUCTION

Alzheimer's disease (AD) represents a type of dementia affecting memory, global cognitive function, and behavior, severe enough to interfere with activities of daily living (Kumar et al., 2021). This disease also presents neuropsychiatric symptoms, such as depression, along with neurodegeneration, neuroinflammation, and oxidative stress phenomena (Caruso et al., 2021). The latter occurs when the homeostatic equilibrium between pro-oxidants species and antioxidants is missing, with the pro-oxidants being in excess (Caruso et al., 2019a). With regard to depression, a neurobiological and clinical continuum has been demonstrated between this disease and AD (Caraci et al., 2018b). In fact, depression represents a risk factor for AD development, while the occurrence of depressive symptoms significantly increases the conversion from mild cognitive impairment (MCI) into AD (Petersen et al., 2014).

It is now well-known that amyloid-β (Aβ), the peptide involved in the pathogenesis of AD, can undergo aggregation, starting with soluble monomers and forming species characterized by higher molecular weight such as oligomers, protofibrils, and mature fibrils (Brorsson et al., 2010). Among the above species, oligomers represent the most toxic species of Aβ, leading to synaptic loss and neuronal death in AD brain (Klein, 2013). It has been shown that oxidative stress plays a crucial role in mediating the toxicity of Aβ oligomers; in fact, neurodegeneration and neuroinflammation as well as the impairment of synaptic plasticity are, at least in part, due to the oxidative stress Aβ oligomers-induced (Varadarajan et al., 2000; Gelain et al., 2012). Oxidative stress is able to promote Aβ oligomerization (Zhao and Zhao, 2013) and β- and γ-secretase activation, the two enzymes involved in the formation of the different Aβ species (Zhao and Zhao, 2013). Markers of oxidative stress have been found in AD animal models before plaques deposition as well as in brain, plasma, and erythrocytes from MCI and AD patients (Glenner and Wong, 1984; Minati et al., 2009), suggesting that redox imbalance and oxidative damage play a key role in an early stage of AD pathophysiology, as well as in the disease progression (Cheignon et al., 2018).

Different groups are currently studying antidepressants in AD (Lozupone et al., 2018). Second-generation antidepressants have been associated with a reduced risk of developing AD, but there are still no clear findings demonstrating the ability of these drugs to counteract the progression of this disease (Correia and Vale, 2021). Positive outcomes have been observed by using selective serotonin reuptake inhibitors (SSRIs) (Dafsari and Jessen, 2020). Long-term SSRI treatment (>4 years) was significantly associated with a delayed progression from MCI to AD (Bartels et al., 2018). The immune regulatory effect of antidepressants observed in depressed patients is attributable to their ability to decrease the levels of pro-inflammatory cytokines (e.g., tumor necrosis factor-α (TNF-α)) and increase those of anti-inflammatory cytokines, such as transforming growth factor-β1 (TGF-β1) (Szałach et al., 2019). Antidepressant drugs could also exert their therapeutic effect by suppressing the production of reactive oxygen and nitrogen species, ROS and RNS respectively, and/or rescuing the antioxidant defense (Behr et al., 2012; Wu et al., 2013). The SSRI fluoxetine (FLX) is able to revert the brain oxidative damage by reducing lipid peroxidation at hippocampal level, also increasing the activity of antioxidant enzymes, such as superoxide dismutase (SOD) and catalase (CAT), in different animal models of depression (Chung et al., 2010; Moretti et al., 2012). Evidence also exists that FLX prevents amyloid pathology, also reverting memory impairment in different animal models of AD (Wang et al., 2014; Jin et al., 2017). Furthermore, FLX exerts neuroprotection in an established *in vitro* model of Aβ-induced neurodegeneration *via* a paracrine signaling mediated by TGF-β1 (Caraci et al., 2016). Acute and long-term treatments with the new multimodal antidepressant vortioxetine (VTX) improve cognitive function in preclinical models of depression (Bennabi et al., 2019). This drug also exhibits an increased efficacy, compared to FLX, in aged mice in counteracting depressive-like behavior and memory deficits (Li et al., 2017; Bennabi et al., 2019). At clinical level, VTX has proven more effective than SSRIs in the treatment of specific clinical domains, such as cognitive deficits in elderly depressed patients (McIntyre et al., 2016; Thase et al., 2016), underlining its therapeutic potential for the treatment of cognitive impairment in depression (Bennabi et al., 2019). Interestingly, VTX exerts antioxidant activity and anti-inflammatory effects in human monocytes/macrophages stimulated with phorbol 12-myristate 13-acetate (PMA), also inducing the shift of macrophages from M1 (pro-inflammatory) to M2 (anti-inflammatory) phenotype (Talmon et al., 2018).

Intracerebroventricular (i.c.v.) injection of Aβ oligomers in mice has been used to obtain a non-transgenic (non-Tg) AD model characterized by memory deficits and depressive-like phenotype (Ledo et al., 2016; Ledo et al., 2020). An equivalent outcome has been observed in rats that underwent i.c.v. injection of Aβ oligomers (Colaianna et al., 2010; Schiavone et al., 2017). By using this non-Tg AD model, we have recently demonstrated that FLX or VTX revert the behavioral and memory alterations induced by Aβ oligomers (Torrisi et al., 2019). In the same study we also detected a significant reduction of the synaptic proteins synaptophysin and PSD-95 paralleled by a significant deficit of TGF-β1 at hippocampal level that was completely rescued by the long-term treatment with FLX or VTX.

Starting from these grounds, we hypothesized that the i.c.v. injection of Aβ oligomers could also induce oxidative stress in the hippocampus of our non-Tg model of AD and that a long-term treatment with FLX or VTX could prevent this phenomenon by regulating the subtle equilibrium between pro- and antioxidant factors.

MATERIALS AND METHODS

Materials

All chemicals and reagents used in this study were of analytical grade and obtained from Sigma-Aldrich Inc. (St. Louis, MO, United States) or Thermo Fisher Scientific Inc. (Pittsburgh, PA, United States) unless specified otherwise.

TABLE 1 | List of primers used for quantitative real-time PCR (qRT-PCR).

Official name[a]	Official symbol	Alternative titles/symbols	Detected transcript	Amplicon length	Cat. No.[b]
Nitric oxide synthase 2, inducible	Nos2	iNOS; Nos-2; Nos2a; i-NOS; NOS-II; MAC-NOS	NM_010927	118 bp	QT00100275
Cytochrome b-245, beta polypeptide	Cybb	Cgd; Cyd; Nox2; C88302; gp91-1; gp91phox; CGD91-phox	NM_007807 XM_006527565	146 bp	QT00139797
Glutathione peroxidase 1	Gpx1	Gpx; CGPx; GPx-1; GSHPx-1; AI195024; AL033363	NM_008160	133 bp	QT01195936
Glyceraldehyde-3-phosphate dehydrogenase	Gapdh	Gapd	NM_008084 XM_001003314 XM_990238 NM_001289726	144 bp	QT01658692

[a]*https://www.ncbi.nlm.nih.gov/gene/.*
[b]*https://www.qiagen.com/it/shop/pcr/real-time-pcr-enzymes-and-kits/two-step-qrt-pcr/quantitect-primer-assays/.*

Establishment of the Non-Tg AD Mouse Model

The cohorts of animals whose tissues were used for gene and protein analysis are the same described in Torrisi et al. (2019).

Eight-week-old male C57BL/6 mice, obtained from Envigo RMS s.r.l. laboratories (San Pietro al Natisone, Italy), were maintained and used as previously described (Torrisi et al., 2019), following procedures in accordance with the U.K. Animals (Scientific Procedures) Act, 1986 and associated guidelines, EU Directive 2010/63/EU for animal experiments.

As previously described, in order to obtain the non-Tg AD mouse model, 2 μL of the 10 μM Aβ oligomers solution (Bachem Distribution Services GmbH, Weil am Rhein, Germany), prepared according to the original protocol of Klein's group (Gong et al., 2003), were i.c.v. injected by using a microsyringe with a 28-gauge stainless-steel needle 3.0-mm-long (Hamilton). The injection of this Aβ solution corresponds to 20 pmol of Aβ monomer equivalent, giving a final concentration of approximately 0.18 μg/g tissue.

Drug Treatment

Vortioxetine hydrobromide [purity > 98.0% (HPLC)] was obtained from H. Lundbeck A/S (Denmark) according to the MTA N.417394 signed by University of Catania (Department of Drug and Health Sciences) and H. Lundbeck A/S and Lundbeck Italia S.p.A. FLX and VTX were prepared and administered i.p. (FLX at 10 mg/kg; VTX at 5 or 10 mg/kg) daily for a total of 21 to 26 days starting from 7 days before Aβ i.c.v injection as previously described in details (Torrisi et al., 2019). Control animals received the vehicle i.p. A total of five groups of animals were employed in this study and are indicated as follows: 1) control group (phosphate-buffered saline [PBS + vehicle (VEH)]; 2) Aβ group (Aβ + VEH); 3) FLX10 group (Aβ + FLX 10 mg/kg); 4) VTX5 group (Aβ + VTX 5 mg/kg); 5) VTX10 group (Aβ + VTX 10 mg/kg). PBS and VEH were injected i.c.v. and i.p., respectively, while to test the drug activity *per se*, so in absence of Aβ, drugs were administered i.p. for a total of 21 days.

Gene Expression Analysis by Quantitative Real-Time PCR (qRT-PCR)

Gene expression analysis by qRT-PCR was carried out on hippocampal samples. The protocol employed for these experiments is the same previously described (Caruso et al., 2019c; Fidilio et al., 2021) with slight modifications. Briefly, NanoDrop® ND-1000 (Thermo Fisher Scientific, Waltham, MA, United States) was used to determine the RNA concentrations, while Qubit® 3.0 Fluorometer (Thermo Fisher Scientific) was employed to assess the quality of RNA (Fresta et al., 2020a). The reverse transcription was obtained by using the SuperScript III First-Strand Synthesis SuperMix kit. The quantification of all the cDNA samples obtained and loaded in a 384-well plate was measured through a LightCycler® 480 System (Roche Molecular Systems, Inc., Pleasanton, CA, United States). The information relative to the Quanti Tect Primer Assays (Qiagen, Hilden, Germany) used is reported in **Table 1**. Sample amplification, fluorescence data collection, and sample quantification is the same previously described elsewhere (Caruso et al., 2019c; Fidilio et al., 2021). The relative RNA expression level for each sample was calculated using the $2^{-\Delta\Delta CT}$ method in which the threshold cycle (CT) value of the target gene is compared to the CT value of the selected internal control (GAPDH gene in our case). The number of samples analyzed obtained by each animal group is indicated in the pertinent Figure legend.

Protein Expression Analysis by Western Blot (WB)

WB analysis was performed on hippocampal samples following the previously described procedure (Caraci et al., 2015). Briefly, once the protein concentration in tissue homogenate was determined (Pierce™ BCA protein assay kit), 30 μg of total proteins were denatured, separated by gel electrophoresis, and transferred to nitrocellulose membranes. The membranes were incubated overnight (4°C) with the following primary antibodies: rabbit anti-iNOS (Abcam ab136918, 1:1,000), rabbit anti-Nox2/gp91phox (Abcam ab80508, 1:4,000), rabbit anti-Gpx1 (Cell Signaling Technology 3206, 1:500), mouse anti-β-actin (Sigma Aldrich A4700, 1:1,000). Secondary goat anti-rabbit labeled with IRDye 800 (Li-COR Biosciences; 1:15,000) and goat anti-mouse labeled with IRDye 680 (Li-COR Biosciences; 1:15,000) were used at room temperature in the dark for 1 h after three washes in tris-buffered saline (TBS)/Tween 20× 0.1%. Hybridization signals were detected by the Odyssey Infrared Imaging System (LI-COR

Biosciences) and the densitometry analysis was performed by using ImageJ software. The number of samples analyzed obtained by each animal group is indicated in the pertinent Figure legend.

Mixed Neuronal Cultures

Mixed neuronal cultures consisting of 35–40% neurons and 60–65% glial cells (astrocytes and microglia) were obtained from rats at embryonic day 15 (Harlan Laboratories, Italy) as previously described (Caraci et al., 2016). Cells were grown into DMEM/F12 (1:1) (American Type Culture Collection (ATCC), Manassas, VA, United States) supplemented with 10% horse serum, 10% fetal calf serum, 2 mM glutamine, and 6 mg/ml glucose. After 7–10 days *in vitro*, to avoid the proliferation of non-neuronal elements, cytosine-D-arabinoside (10 μM) was added, for a total of 3 days. Cells were then moved into a maintenance medium in absence of serum. Mixed neuronal cultures were treated with Aβ oligomers (2 μM) for 48 h both in absence or presence of FLX (1 μM) or increasing concentrations of VTX (100 nM, 250 nM, or 1 μM) (pre-treatment of 1 h). The Aβ oligomers-induced toxicity was quantitatively assessed by trypan blue exclusion assay. Cell counts were performed in three to four random microscopic fields/well.

Statistics

Data are reported as mean ± standard error of the mean (S.E.M.) except in the case of cell experiments in which standard deviation (S.D.) was showed. One-way analysis of variance (ANOVA) followed by Tukey's *post hoc* test were used for multiple comparisons. The version 8.0 of GraphPad Prism software® (GraphPad, La Jolla, CA, United States) was used to perform all the analyses. Only two-tailed p values < 0.05 were considered statistically significant.

Study Approval

The study was authorized by the Institutional Animal Care and Use Committee (IACUC) of the University of Catania and by the Italian Ministry of Health (DDL 26/2014 and previous legislation; OPBA Project #266/2016). Animal care followed Italian (D.M. 116192) and EEC (O.J. of E.C.L 358/1 12/18/1986) regulations on protection of animals used for experimental and scientific purposes.

RESULTS

Fluoxetine and Vortioxetine Decreased the Expression of iNOS and Nox2 mRNAs

Oxidative stress and neuroinflammation play a significant role in the pathogenesis of depression (Bhattacharya and Drevets, 2017; Caruso et al., 2019a) and AD (Huang et al., 2016; Knezevic and Mizrahi, 2018). During the inflammation process, both inducible nitric oxide synthase (iNOS), responsible for nitric oxide production (Aktan, 2004; Metto et al., 2013), and NADPH oxidase 2 (Nox2), responsible for superoxide production (de Campos et al., 2015), are over-activated in immune cells including microglia (Siegel et al., 2019). When the above-mentioned enzymes are simultaneously activated, they synergistically promote neuronal cell death by generating peroxynitrite (Beckman and Crow, 1993). We therefore examined the effects of Aβ oligomers on the mRNAs levels of the pro-oxidant enzymes iNOS and Nox2 in the hippocampus (**Figure 1**), a brain area strongly affected in depression and AD (Villa et al., 2016; Setti et al., 2017). The i.c.v. injection of Aβ oligomers induced a statistically significant increase in the expression level of iNOS mRNA in the hippocampus compared with vehicle-treated controls ($p < 0.05$ vs. PBS + VEH; **Figure 1A**). Long-term i.p. treatment with FLX or VTX, administered at the same dose of 10 mg/kg, was able to abolish the over-expression of iNOS Aβ-induced ($p < 0.05$ vs. Aβ oligomers), whereas the lower dose of VTX (5 mg/kg) did not reach a statistically significant difference, even though a trend in iNOS mRNA enzyme expression decrease was observed. More robust effects were observed when measuring the variation of Nox2 mRNA expression levels under our experimental conditions. In fact, as shown in **Figure 1B**, the expression level of Nox2 mRNA was significantly increased in the hippocampus of Aβ-injected mice compared with vehicle-treated controls ($p < 0.001$ vs. PBS + VEH). Long-term i.p. treatment with FLX (10 mg/kg) or VTX, at both doses (5 or 10 mg/kg), was able to completely counteract the over-expression of this enzyme ($p < 0.001$ vs. Aβ oligomers for all of them). It is worth mentioning that treatment with FLX or VTX *per se* did not significantly modify the mRNA expression levels of iNOS and Nox2 enzymes (**Supplementary Figure S1**).

Fluoxetine and Vortioxetine Decreased the Expression of iNOS and Nox2 Proteins

We then carried out WB experiments in order to corroborate with protein data the results obtained by using qRT-PCR in which the expression levels of iNOS and Nox2 mRNA were measured. WB analysis confirmed that the i.c.v. injection of Aβ oligomers is able to induce a significant increase of iNOS protein expression at hippocampal level ($p < 0.05$ vs. PBS + VEH) and, most importantly, that the treatment with FLX and VTX is able to completely abolish Aβ-induced iNOS expression ($p < 0.001$ vs. Aβ oligomers for both of them; **Figure 2A**). A very similar profile was observed when measuring the variation of Nox2 protein levels. **Figure 2B** shows that the expression level of Nox2 protein was significantly increased in the hippocampus of Aβ-injected mice compared with vehicle-treated controls ($p < 0.05$ vs. PBS + VEH). Treatment with FLX at the dose of 10 mg/kg or with the lower dose of VTX (5 mg/kg) abolished Aβ oligomers induction ($p < 0.05$ vs. Aβ oligomers), while a stronger decrease was observed in the case of the higher dose of VTX (10 mg/kg) ($p < 0.01$ vs. Aβ oligomers). As expected based on the qRT-PCR results, the treatment with FLX or VTX *per se* did not significantly modify the protein expression levels of iNOS and Nox2 enzymes (**Supplementary Figure S2**).

Fluoxetine or Vortioxetine Rescued the Expression of Gpx1 at Gene but Not at Protein Level

As previously mentioned, oxidative stress, a key factor in the progression of AD (Zhao and Zhao, 2013; Bajpai et al., 2014), reflects the imbalance between the production and quenching of reactive species in the biological system. This imbalance could also depend on the reduced activity of antioxidant enzymes such

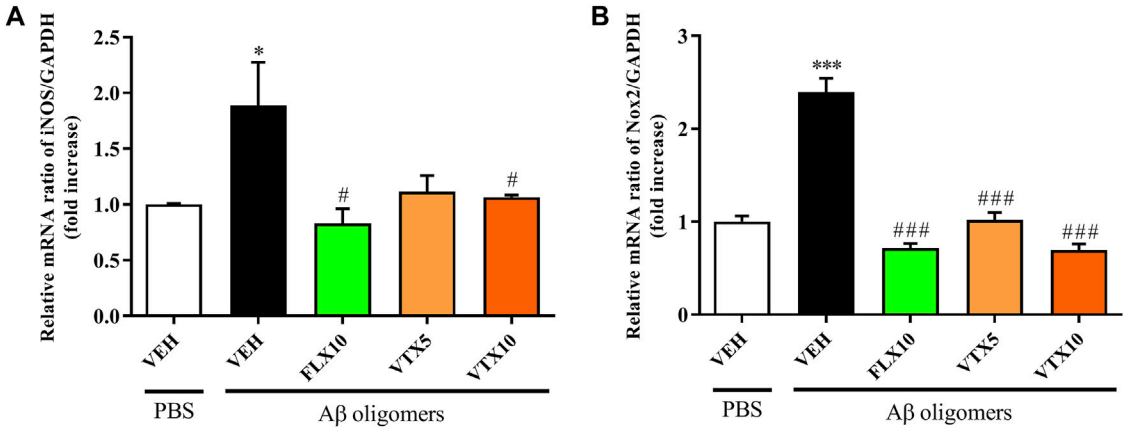

FIGURE 1 | Fluoxetine and vortioxetine decrease the expression of iNOS and Nox2 mRNAs. Effects induced by i.c.v. administration of Aβ oligomers (Aβ + VEH) in absence or presence of FLX10, VTX5, or VTX10 on **(A)** iNOS and **(B)** Nox2 mRNAs expression measured by qRT-PCR. The abundance of each mRNA of interest was expressed relative to the abundance of GAPDH-mRNA, as an internal control. As a negative control, a reaction in absence of cDNA (no template control, NTC) was performed. qRT-PCR amplifications were performed at least in triplicate (mean of three to six determinations). Data are shown as mean ± S.E.M. $^{*}p < 0.05$ vs. PBS + VEH, $^{***}p < 0.001$ vs. PBS + VEH, $^{\#}p < 0.05$ vs. Aβ oligomers + VEH, $^{\#\#\#}p < 0.001$ vs. Aβ oligomers + VEH.

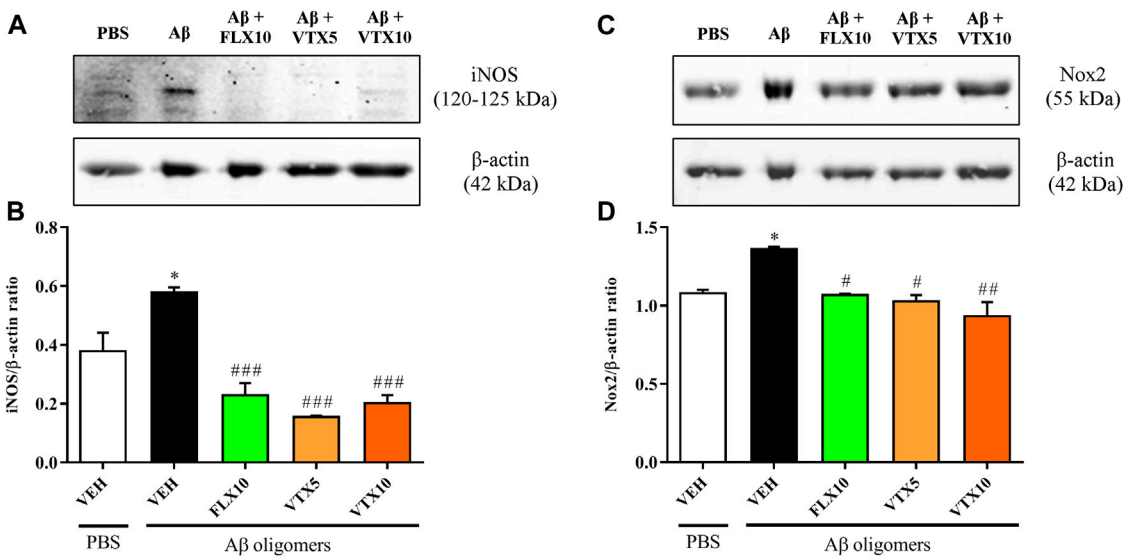

FIGURE 2 | Fluoxetine and vortioxetine decrease the expression of iNOS and Nox2 proteins. Effects induced by i.c.v. administration of Aβ oligomers (Aβ + VEH) in absence or presence of FLX10, VTX5, or VTX10 on **(B)** iNOS and **(D)** Nox2 protein levels measured by WB. **(A, C)** show the representative immunoblots of iNOS (120–125 kDa) and Nox2 (55 kDa), respectively, in total protein extracts from hippocampal tissue. Histograms refer to the means ± S.E.M. of the densitometric values of iNOS or Nox2 bands normalized against β-actin (42 kDa). Each experiment was repeated three times. $^{*}p < 0.05$ vs. PBS + VEH, $^{\#}p < 0.05$ vs. Aβ oligomers + VEH. $^{\#\#}p < 0.01$ vs. Aβ oligomers + VEH, $^{\#\#\#}p < 0.001$ vs. Aβ oligomers + VEH.

as glutathione peroxidase 1 (Gpx1) (Marcus et al., 1998; Katrenčíková et al., 2021). The lack of Gpx1 has been related to the exacerbation of Aβ-mediated neurotoxicity in cortical neurons (Crack et al., 2006). With this in mind, we investigated the effects of Aβ oligomers, in absence or presence of FLX10, VTX5, or VTX10, on the mRNA levels of Gpx1 in the hippocampus. The results depicted in **Figure 3A** show that the expression level of Gpx1 mRNA was significantly decreased in the hippocampus of Aβ-injected mice compared with vehicle-treated controls ($p < 0.05$ vs. PBS + VEH), while the treatment with FLX was able to completely restore Gpx1 mRNA levels ($p < 0.05$ vs. Aβ oligomers). A more significant effect was observed in the case of both doses of VTX ($p < 0.001$ vs. Aβ oligomers). Since it has been shown that oxidative stress can induce multimerization of Gpx1 enzyme by forming complexes via oxidative linkage between subunits (Park et al., 2004; Sultan et al., 2018), we performed WB analysis by measuring both monomeric and dimeric forms. However, the results obtained

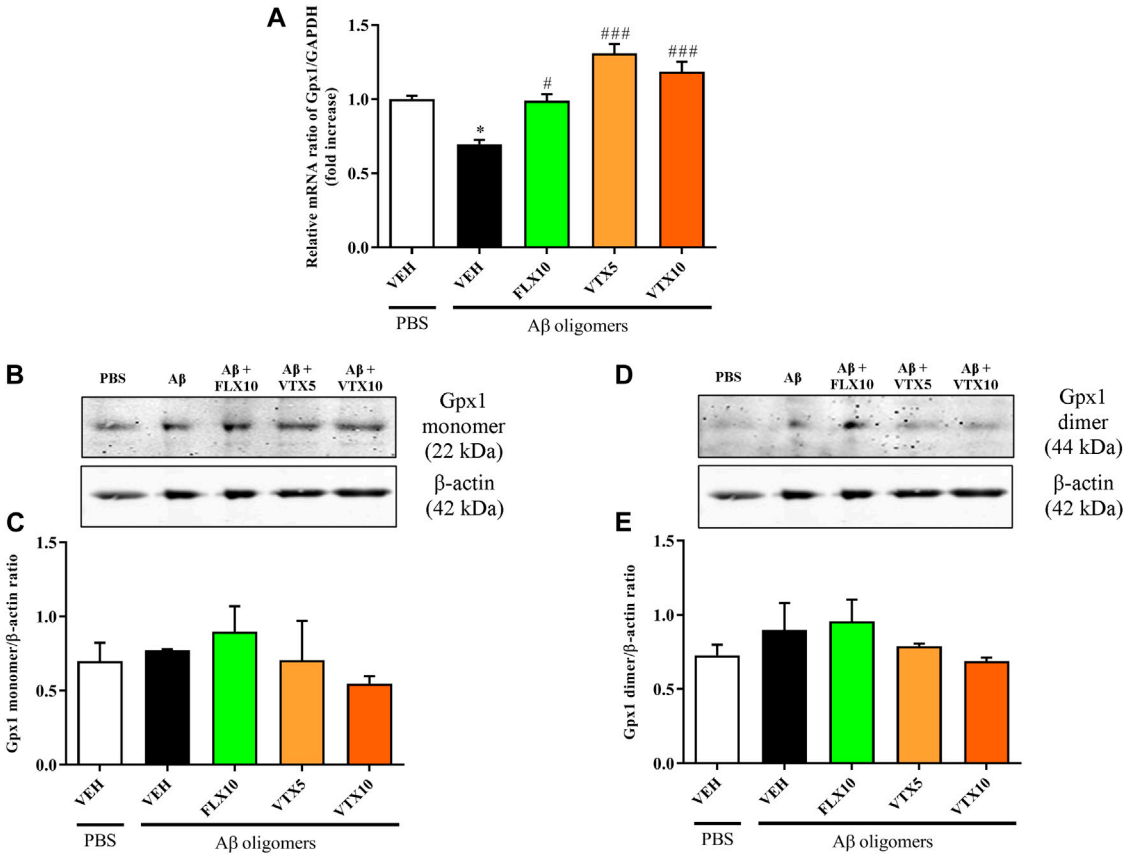

FIGURE 3 | The treatment with fluoxetine or vortioxetine is needed to rescue the expression of Gpx1 at gene but not at protein level. Effects induced by i.c.v. administration of Aβ oligomers (Aβ + VEH) in absence or presence of FLX10, VTX5, or VTX10 on **(A)** Gpx1 mRNA expression measured by qRT-PCR; **(C)** monomer and **(E)** dimer of Gpx1 protein levels measured by WB. **(B, D)** show the representative immunoblots of Gpx1 monomer (22 kDa) and Gpx1 dimer (44 kDa) in total protein extracts from hippocampal tissue. In the case of gene expression measurements, the abundance of Gpx1 mRNA was expressed relative to the abundance of GAPDH-mRNA, as an internal control. As a negative control, a reaction in absence of cDNA (no template control, NTC) was performed. qRT-PCR amplifications were performed at least in triplicate (mean of three to five determinations). In the case of protein expression measurements, histograms refer to the means ± S.E.M. of the densitometric values of Gpx1 monomer or Gpx1 dimer bands normalized against β-actin (42 kDa). Each experiment was repeated three times. $^{*}p < 0.05$ vs. PBS + VEH, $^{\#}p < 0.05$ vs. Aβ oligomers + VEH, $^{\#\#\#}p < 0.001$ vs. Aβ oligomers + VEH.

by WB showed that either the monomeric nor the dimeric form of Gpx1 protein in the hippocampus were significantly affected by Aβ treatment as compared to vehicle-treated controls (**Figures 3B,C**). The presence of antidepressants during Aβ treatment did not modulate the expression levels of either enzyme isoforms. The treatment with FLX or VTX *per se*, in the absence of Aβ treatment, did not significantly modify the mRNA (**Supplementary Figure S1**) and protein (**Supplementary Figure S2**) levels of Gpx1 enzyme.

Fluoxetine and Vortioxetine Exert Neuroprotection Against the Toxicity Induced by Aβ Oligomers

The neuroprotective activity of FLX in mixed cultures of cortical cells treated with Aβ oligomers, representing an established experimental model of Aβ-induced neurodegeneration (Caruso et al., 2019c), has been already reported (Caraci et al., 2016). However, it is presently unknown whether a treatment with VTX can prevent the neuronal cell death due to Aβ treatment. We then investigated the neuroprotective activity of increasing concentrations of VTX in mixed cultures of cortical cells treated with Aβ oligomers (2 μM) for 48 h. In this set of experiments, FLX at the concentration of 1 μM was used as a gold standard. Since Aβ is known to promote glutamate release and toxicity (Caraci et al., 2011), the experiments were performed in the presence of a cocktail of ionotropic glutamate receptor antagonists [MK-801 (10 μM) and DNQX (30 μM)] to exclude the contribution of endogenous excitotoxicity to the overall process of neuronal death. The treatment of mixed cultures of cortical cells with Aβ oligomers for 48 h led to a significant increase (about 300%) in the number of trypan blue positive cells (dead neurons) compared to untreated (CTRL) cells ($p < 0.001$) (**Figure 4**). VTX, starting at a concentration of 250 nM, significantly prevented Aβ toxicity in mixed neuronal cultures ($p < 0.05$ vs. Aβ), though not completely. The maximal neuroprotective effect was observed in the case of VTX 1 μM ($p < 0.001$ vs. Aβ), with a number of dead cells comparable to that

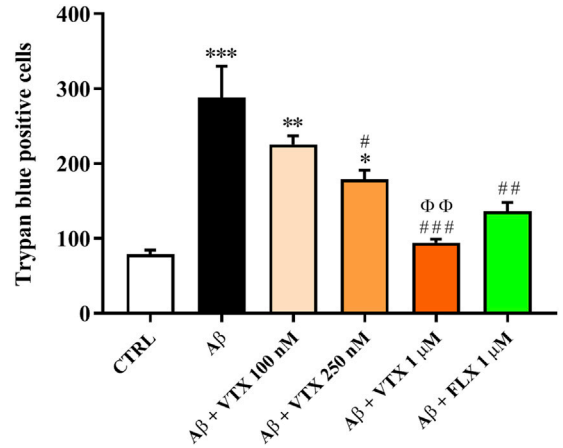

FIGURE 4 | Fluoxetine and vortioxetine exert neuroprotection against the toxicity induced by Aβ oligomers. Primary mixed neuronal cultures were treated with Aβ oligomers (2 μM) for 48 h both in absence or presence of FLX (1 μM) or increasing concentrations of VTX (100 nM, 250 nM, and 1 μM) (pre-treatment of 1 h). The toxicity of Aβ oligomers in mixed neuronal cultures was assessed by cell counting after trypan blue staining. Cell counts was performed in three random microscopic fields/well. Data are the mean of three to four determinations. S.D. are represented by vertical bars. $^{*}p < 0.05$ vs. CTRL, $^{**}p < 0.01$ vs. CTRL, $^{***}p < 0.001$ vs. CTRL, $^{\#}p < 0.05$ vs. Aβ, $^{\#\#}p < 0.01$ vs. Aβ, $^{\#\#\#}p < 0.001$ vs. Aβ, $^{\Phi\Phi}p < 0.01$ vs. VTX 100 nM.

observed for untreated cells or for FLX-treated cells (positive control).

DISCUSSION

Reactive species such as reactive oxygen species (ROS) and reactive nitrogen species (RNS) play a crucial role in numerous human pathophysiological processes. These species, when produced at physiological concentration, are able to regulate growth, apoptosis, and complex functions such as blood pressure, immune and cognitive functions. When overproduced, they can contribute to a well-known and deleterious phenomenon called oxidative stress (Estévez and Jordán, 2002). During acute oxidative stress, the components of the antioxidant system are able to counteract the increased levels of pro-oxidants, such as ROS and RNS, resetting them to the physiological levels. Whenever ROS and RNS levels overcome the antioxidant defense, chronic oxidative stress takes place, as it has been observed in neuropsychiatric disorders such as depression and AD (Caruso et al., 2019d). Both ROS and RNS are involved in the pathogenesis of depression by influencing neuronal processes such as neurogenesis and neuroplasticity, also inducing neuroinflammation and neurodegeneration (Cheignon et al., 2018; Solleiro-Villavicencio and Rivas-Arancibia, 2018). When considering AD, the over-production of ROS and RNS, and then oxidative stress, has been related to increased Aβ production and/or aggregation, which in turn exacerbates neuronal oxidative damage, contributing to neuronal death in AD brain (Cheignon et al., 2018).

In the present work we employed a non-Tg model of AD, obtained by i.c.v. injection of Aβ oligomers, allowing to investigate the molecular mechanisms through which the oligomeric form of Aβ causes cognitive dysfunction, and finally to test novel pharmacological approaches (Balducci and Forloni, 2014). As previously demonstrated, this non-Tg AD model is characterized by cerebral concentrations of soluble Aβ oligomers comparable to those observed in the AD brain, sufficient to induce a memory deficit that persists for 2–3 weeks (Leggio et al., 2016). By adopting this model, we have recently demonstrated that both FLX and VTX possess the ability to reverse the depressive-like phenotype and memory deficits induced by the i.c.v. injection of Aβ oligomers in mice, also rescuing the levels of the synaptic proteins synaptophysin and PSD-95 as well as of TGF-β1, the deficit of which has been shown to contribute to inflammation and cognitive decline both in depression and AD (Caraci et al., 2018b; Torrisi et al., 2019). In order to correlate the above-mentioned preclinical efficacy of these two second-generation antidepressants with an antioxidant activity of these drugs, we examined the mRNA levels of iNOS and Nox2, two pro-oxidant enzymes synergistically able to promote neuronal death through the production of ROS and RNS (Beckman and Crow, 1993), in the hippocampus of Aβ-injected mice, a brain area strongly affected in both depression and AD (Villa et al., 2016; Setti et al., 2017). Our results show that the i.c.v. injection of Aβ oligomers in mice induced a significant increase in iNOS and Nox2 enzymes in the hippocampus, both at mRNA (**Figure 1**) and protein (**Figure 2**) level, compared with vehicle-treated controls. These findings are in agreement with an *in vivo* study carried out by Medeiros et al. (2007) in which the i.c.v. injection of Aβ1–40 induced iNOS protein expression in hippocampus and prefrontal cortex of mice that was paralleled by marked deficits of learning and memory, emphasizing the deleterious effects of aberrant expression of NOS isoforms in AD brain (Lüth et al., 2002). Our findings are also in line with other studies showing that AD is characterized by inflammatory processes in which the production of nitric oxide from iNOS and/or superoxide from Nox2 is strongly increased (Murphy, 2000; Brown and Bal-Price, 2003; Zekry et al., 2003). In the present study we showed for the first time that a long-term i.p. treatment with FLX or VTX was able to abolish the over-expression of iNOS and Nox2 induced by Aβ oligomers (**Figures 1**, **2**). These results are also consistent with previous findings, showing the ability of antidepressant drugs to exert immune-regulatory effects by reducing the levels of pro-inflammatory cytokines, also decreasing the production of reactive species and/or enhancing key elements of the antioxidant machinery. Along this line, FLX has been shown to revert brain oxidative damage by reducing lipid peroxidation and increasing the activity of the antioxidant enzymes (i.e., CAT and SOD) in the hippocampus of an animal model of depression (Moretti et al., 2012). In a study carried out by Talmon et al. (2018) the multimodal antidepressant VTX was able to reduced the oxidative burst induced by PMA in monocytes and in macrophages (M1 and M2), also leading to a shift of macrophage polarization from the pro-inflammatory (M1) to the anti-inflammatory (M2) phenotype. The above reduction of oxidative stress was also paralleled by a decrease of nuclear

factor kappa-light-chain-enhancer of activated B cells (NF-kB) translocation and TNF-α release. The present data on the antioxidant activity of FLX and VTX *in vivo* reinforce the above-described previous findings obtained in translational models of inflammation. Our findings on the antioxidant activity of FLX and VTX might be therapeutically relevant in the context of depression and AD, when considering that depression acts as a risk factor for AD and, most importantly, that oxidative stress processes play a key role in the pathophysiology of cognitive deficits in depression (Scapagnini et al., 2012).

About 30% of depressed patients show a poor response to conventional antidepressants associated with a significant cognitive impairment and a poor quality of life, a clinical phenotype classified as treatment-resistant depression (TRD) (Caraci et al., 2018a). It has been recently shown how TRD is characterized by increased oxidative stress coupled to inflammation (Sowa-Kućma et al., 2018). Furthermore, plasma levels of Coenzyme Q10 (CoQ10), a strong antioxidant with anti-inflammatory activity, are lower in TRD patients compared to responders depressed patients (Maes et al., 2009) and CoQ10 (200 mg/die) has been proposed as an adjuvating agent for the treatment of depression (Mehrpooya et al., 2018). According to this scenario second-generation antidepressant drugs, endowed with antioxidant activity, may display an increased clinical efficacy in TRD patients; studies in animal models are useful to test this hypothesis. As previously mentioned, antioxidants play a significant role in maintaining redox homeostasis. It is also worth mentioning that an increase in Nox2 protein expression and the related oxidative stress have also been observed in sleep deprivation known to induce memory impairments, serotoninergic system dysfunction, and depression in mice (Wang et al., 2020). In our experimental model of amyloid-related depression the presence of depressive-like behavior and memory deficit was paralleled by an increase in Nox2 protein levels in Aβ-injected mice that was rescued by the long-term treatment with FLX at 10 mg/kg and more significantly by VTX, being effective at the lowest dose of 5 mg/kg, suggesting that the antidepressant activity of these drugs is not simply related to the inhibition of serotonin transporter (SERT), but it is also includes antioxidants effects.

In our study we also measured the mRNA and protein levels of Gpx1, an antioxidant enzyme known to play a protective role against Aβ-toxicity and the related ROS accumulation at intracellular level (Barkats et al., 2000), and the deficit of which has been related to increased Aβ-mediated neurotoxicity (Crack et al., 2006). Our data show that the treatment with FLX or VTX is needed to rescue the expression of Gpx1 at mRNA, but not at protein level. We cannot exclude a post-trascriptional regulation of Gpx1 gene expression. In our case, the discrepancy observed when comparing mRNA and protein levels within the same time frame might be due to a compensatory response of the antioxidant system with an additional role played by FLX or VTX, which remains to be elucidated.

We know from our previous work in the non-Tg model of AD that FLX and VTX not only counteract oxidative stress, but also rescue the hippocampal TGF-β1 levels. This neurobiological link could be of utmost importance since it has already been demonstrated that other multimodal drugs that counteract oxidative stress can also rescue TGF-β1 levels (Caruso et al., 2019b; Fresta et al., 2020b). In two very recent research studies it has also demonstrated the ability of TGF-β1 to protect retinal ganglion cells against oxidative stress through the modulation of the HO-1/Nrf2 pathway (Chen et al., 2020) and chondrocytes *via* FOXO1-autophagy axis (Kurakazu et al., 2021), strongly suggesting a key role of TGF-β1 in counteracting oxidative stress induced by Aβ.

In the AD brain, oxidative stress promotes the generation of ROS that contribute to neurodegeneration (Shimohama et al., 2000; Abramov and Duchen, 2005). During the last decade, based on their ability to exert neuroprotection, the use of antidepressants to reduce the risk to develop AD has been proposed (Kessing et al., 2009; Kessing, 2012; Yuste et al., 2015; Bartels et al., 2018). By using a well-established *in vitro* model of Aβ-induced neurodegeneration consisting of mixed cultures of cortical cells challenged with Aβ oligomers, we were able to compare, for the first time, the well-known neuroprotective activity of FLX (Caraci et al., 2016) with the protective effects of VTX. Interestingly we found that VTX pre-treatment started to exert significant neuroprotective effects at nanomolar concentrations (250 nM) with a maximal effect at 1 μM, similar to that observed for FLX pre-treatment and untreated cells (**Figure 4**). The neuroprotective effects exerted *in vitro*, as well as the antidepressant effects exerted *in vivo* by FLX and VTX could be related to the anti-amyloidogenic and anti-aggregant activity of these drugs. In particular, SSRIs including FLX have shown the potential to prevent Aβ aggregation by direct binding and could be beneficial to AD patients (Tin et al., 2019). FLX also possesses a recognized ability to revert soluble Aβ-induced depressive phenotype with a specific "Aβ-lowering" effect (Schiavone et al., 2017). Furthermore, it cannot be excluded that both FLX and VTX could exert their therapeutic potential by enhancing the release of TGF-β1 from microglial cells, as observed in our *in vivo* experiments, then rescuing the antioxidant system through the activation of TGF-β1 signaling. The results observed in our experimental models with therapeutic concentrations of VTX also stimulate further studies both in rodents and MCI patients with amyloid-related depression.

All together the data presented in this study, obtained by using a non-Tg model of AD, demonstrated that oxidative stress, taking place as a consequence of pro-oxidant enzymes (i.e., iNOS and Nox2) activation, along with the previously showed deficit of TGF-β1, represents one of the neurobiological links between depression and AD. We also showed for the first time how a long-term administration of the antidepressants fluoxetine and vortioxetine, able to rescue the TGF-β1 pathway, can also contribute to prevent amyloid-induced depression and cognitive decline by counteracting Aβ-induced oxidative stress.

DATA AVAILABILITY STATEMENT

All datasets generated for this study are included in the article and the **Supplementary Material**. Further inquiries can be directed to the corresponding author.

ETHICS STATEMENT

The animal study was reviewed and approved by the Institutional Animal Care and Use Committee (IACUC) of the University of Catania and by the Italian Ministry of Health (DDL 26/2014 and previous legislation; OPBA Project #266/2016).

AUTHOR CONTRIBUTIONS

GC and FC gave substantial contributions to the conception and design of the work. GC, MG, AF, ST, NM, FG, MT, and AP performed the experiments. GC, MG, AF, and FC analyzed the data. FT, DP, SS, GL, FD, and FC participated in the design and coordination of the study. GC, MG, AF, and GL drafted the work. All authors revised the work and approved the version to be published.

FUNDING

This research was funded by University of Catania, PIAno InCEntivi per la RIcerca di Ateneo UniCT 2020–2022-Linea 3 Project Asclepio and also conducted with a partial unrestricted support of Lundbeck. This research was also supported by PRIN 2017 (Program of Relevant National interest-2017AY8BP4_004) from the Italian Ministry of University and Research.

ACKNOWLEDGMENTS

The authors would like to thank the BRIT laboratory at the University of Catania (Italy) for the valuable technical assistance and use of their laboratories.

SUPPLEMENTARY MATERIAL

The Supplementary Material for this article can be found online at: https://www.frontiersin.org/articles/10.3389/fphar.2021.809541/full#supplementary-material

REFERENCES

Abramov, A. Y., and Duchen, M. R. (2005). The Role of an Astrocytic NADPH Oxidase in the Neurotoxicity of Amyloid Beta Peptides. *Philos. Trans. R. Soc. Lond. B Biol. Sci.* 360 (1464), 2309–2314. doi:10.1098/rstb.2005.1766

Aktan, F. (2004). iNOS-mediated Nitric Oxide Production and its Regulation. *Life Sci.* 75 (6), 639–653. doi:10.1016/j.lfs.2003.10.042

Bajpai, A., Verma, A. K., Srivastava, M., and Srivastava, R. (2014). Oxidative Stress and Major Depression. *J. Clin. Diagn. Res.* 8 (12), Cc04–7. doi:10.7860/jcdr/2014/10258.5292

Balducci, C., and Forloni, G. (2014). *In Vivo* application of Beta Amyloid Oligomers: a Simple Tool to Evaluate Mechanisms of Action and New Therapeutic Approaches. *Curr. Pharm. Des.* 20 (15), 2491–2505. doi:10.2174/13816128113199990497

Barkats, M., Millecamps, S., Abrioux, P., Geoffroy, M. C., and Mallet, J. (2000). Overexpression of Glutathione Peroxidase Increases the Resistance of Neuronal Cells to Abeta-Mediated Neurotoxicity. *J. Neurochem.* 75 (4), 1438–1446. doi:10.1046/j.1471-4159.2000.0751438.x

Bartels, C., Wagner, M., Wolfsgruber, S., Ehrenreich, H., and Schneider, A. (2018). Impact of SSRI Therapy on Risk of Conversion from Mild Cognitive Impairment to Alzheimer's Dementia in Individuals with Previous Depression. *Am. J. Psychiatry* 175 (3), 232–241. doi:10.1176/appi.ajp.2017.17040404

Beckman, J. S., and Crow, J. P. (1993). Pathological Implications of Nitric Oxide, Superoxide and Peroxynitrite Formation. *Biochem. Soc. Trans.* 21 (2), 330–334. doi:10.1042/bst0210330

Behr, G. A., Moreira, J. C., and Frey, B. N. (2012). Preclinical and Clinical Evidence of Antioxidant Effects of Antidepressant Agents: Implications for the Pathophysiology of Major Depressive Disorder. *Oxid Med. Cel Longev* 2012, 609421. doi:10.1155/2012/609421

Bennabi, D., Haffen, E., and Van Waes, V. (2019). Vortioxetine for Cognitive Enhancement in Major Depression: From Animal Models to Clinical Research. *Front. Psychiatry* 10, 771. doi:10.3389/fpsyt.2019.00771

Bhattacharya, A., and Drevets, W. C. (2017). Role of Neuro-Immunological Factors in the Pathophysiology of Mood Disorders: Implications for Novel Therapeutics for Treatment Resistant Depression. *Curr. Top. Behav. Neurosci.* 31, 339–356. doi:10.1007/7854_2016_43

Brorsson, A. C., Kumita, J. R., MacLeod, I., Bolognesi, B., Speretta, E., Luheshi, L. M., et al. (2010). Methods and Models in Neurodegenerative and Systemic Protein Aggregation Diseases. *Front. Biosci. (Landmark Ed.* 15, 373–396. doi:10.2741/3626

Brown, G. C., and Bal-Price, A. (2003). Inflammatory Neurodegeneration Mediated by Nitric Oxide, Glutamate, and Mitochondria. *Mol. Neurobiol.* 27 (3), 325–355. doi:10.1385/mn:27:3:325

Caraci, F., Calabrese, F., Molteni, R., Bartova, L., Dold, M., Leggio, G. M., et al. (2018a). International Union of Basic and Clinical Pharmacology CIV: The Neurobiology of Treatment-Resistant Depression: From Antidepressant Classifications to Novel Pharmacological Targets. *Pharmacol. Rev.* 70 (3), 475–504. doi:10.1124/pr.117.014977

Caraci, F., Gulisano, W., Guida, C. A., Impellizzeri, A. A., Drago, F., Puzzo, D., et al. (2015). A Key Role for TGF-B1 in Hippocampal Synaptic Plasticity and Memory. *Sci. Rep.* 5, 11252. doi:10.1038/srep11252

Caraci, F., Molinaro, G., Battaglia, G., Giuffrida, M. L., Riozzi, B., Traficante, A., et al. (2011). Targeting Group II Metabotropic Glutamate (mGlu) Receptors for the Treatment of Psychosis Associated with Alzheimer's Disease: Selective Activation of mGlu2 Receptors Amplifies Beta-Amyloid Toxicity in Cultured Neurons, whereas Dual Activation of mGlu2 and mGlu3 Receptors Is Neuroprotective. *Mol. Pharmacol.* 79 (3), 618–626. doi:10.1124/mol.110.067488

Caraci, F., Spampinato, S. F., Morgese, M. G., Tascedda, F., Salluzzo, M. G., Giambirtone, M. C., et al. (2018b). Neurobiological Links between Depression and AD: The Role of TGF-B1 Signaling as a New Pharmacological Target. *Pharmacol. Res.* 130, 374–384. doi:10.1016/j.phrs.2018.02.007

Caraci, F., Tascedda, F., Merlo, S., Benatti, C., Spampinato, S. F., Munafò, A., et al. (2016). Fluoxetine Prevents Aβ1-42-Induced Toxicity via a Paracrine Signaling Mediated by Transforming-Growth-Factor-B1. *Front. Pharmacol.* 7, 389. doi:10.3389/fphar.2016.00389

Caruso, G., Benatti, C., Blom, J. M. C., Caraci, F., and Tascedda, F. (2019a). The Many Faces of Mitochondrial Dysfunction in Depression: From Pathology to Treatment. *Front. Pharmacol.* 10, 995. doi:10.3389/fphar.2019.00995

Caruso, G., Benatti, C., Musso, N., Fresta, C. G., Fidilio, A., Spampinato, G., et al. (2021). Carnosine Protects Macrophages against the Toxicity of Aβ1-42

Oligomers by Decreasing Oxidative Stress. *Biomedicines* 9 (5), 477. doi:10.3390/biomedicines9050477

Caruso, G., Fresta, C. G., Fidilio, A., O'Donnell, F., Musso, N., Lazzarino, G., et al. (2019b). Carnosine Decreases PMA-Induced Oxidative Stress and Inflammation in Murine Macrophages. *Antioxidants (Basel)* 8 (8), 281. doi:10.3390/antiox8080281

Caruso, G., Fresta, C. G., Musso, N., Giambirtone, M., Grasso, M., Spampinato, S. F., et al. (2019c). Carnosine Prevents Aβ-Induced Oxidative Stress and Inflammation in Microglial Cells: A Key Role of TGF-B1. *Cells* 8 (1), 64. doi:10.3390/cells8010064

Caruso, G., Spampinato, S. F., Cardaci, V., Caraci, F., Sortino, M. A., and Merlo, S. (2019d). β-Amyloid and Oxidative Stress: Perspectives in Drug Development. *Curr. Pharm. Des.* 25 (45), 4771–4781. doi:10.2174/1381612825666191209115431

Cheignon, C., Tomas, M., Bonnefont-Rousselot, D., Faller, P., Hureau, C., and Collin, F. (2018). Oxidative Stress and the Amyloid Beta Peptide in Alzheimer's Disease. *Redox Biol.* 14, 450–464. doi:10.1016/j.redox.2017.10.014

Chen, H. Y., Ho, Y. J., Chou, H. C., Liao, E. C., Tsai, Y. T., Wei, Y. S., et al. (2020). TGF-β1 Signaling Protects Retinal Ganglion Cells from Oxidative Stress via Modulation of the HO-1/Nrf2 Pathway. *Chem. Biol. Interact* 331, 109249. doi:10.1016/j.cbi.2020.109249

Chung, E. S., Chung, Y. C., Bok, E., Baik, H. H., Park, E. S., Park, J. Y., et al. (2010). Fluoxetine Prevents LPS-Induced Degeneration of Nigral Dopaminergic Neurons by Inhibiting Microglia-Mediated Oxidative Stress. *Brain Res.* 1363, 143–150. doi:10.1016/j.brainres.2010.09.049

Colaianna, M., Tucci, P., Zotti, M., Morgese, M. G., Schiavone, S., Govoni, S., et al. (2010). Soluble Beta Amyloid(1-42): a Critical Player in Producing Behavioural and Biochemical Changes Evoking Depressive-Related State. *Br. J. Pharmacol.* 159 (8), 1704–1715. doi:10.1111/j.1476-5381.2010.00669.x

Correia, A. S., and Vale, N. (2021). Antidepressants in Alzheimer's Disease: A Focus on the Role of Mirtazapine. *Pharmaceuticals (Basel)* 14 (9), 930. doi:10.3390/ph14090930

Crack, P. J., Cimdins, K., Ali, U., Hertzog, P. J., and Iannello, R. C. (2006). Lack of Glutathione Peroxidase-1 Exacerbates Abeta-Mediated Neurotoxicity in Cortical Neurons. *J. Neural Transm. (Vienna)* 113 (5), 645–657. doi:10.1007/s00702-005-0352-y

Dafsari, F. S., and Jessen, F. (2020). Depression-an Underrecognized Target for Prevention of Dementia in Alzheimer's Disease. *Transl Psychiatry* 10 (1), 160. doi:10.1038/s41398-020-0839-1

de Campos, R. P., Siegel, J. M., Fresta, C. G., Caruso, G., da Silva, J. A., and Lunte, S. M. (2015). Indirect Detection of Superoxide in RAW 264.7 Macrophage Cells Using Microchip Electrophoresis Coupled to Laser-Induced Fluorescence. *Anal. Bioanal. Chem.* 407 (23), 7003–7012. doi:10.1007/s00216-015-8865-1

Estévez, A. G., and Jordán, J. (2002). Nitric Oxide and Superoxide, a Deadly Cocktail. *Ann. N. Y Acad. Sci.* 962, 207–211. doi:10.1111/j.1749-6632.2002.tb04069.x

Fidilio, A., Grasso, M., Turnaturi, R., Caruso, G., Spitale, F. M., Vicario, N., et al. (2021). The Multimodal MOPr/DOPr Agonist LP2 Reduces Allodynia in Chronic Constriction Injured Rats by Rescue of TGF-B1 Signalling. *Front. Pharmacol.* 12, 749365. doi:10.3389/fphar.2021.749365

Fresta, C. G., Caruso, G., Fidilio, A., Platania, C. B. M., Musso, N., Caraci, F., et al. (2020a). Dihydrotanshinone, a Natural Diterpenoid, Preserves Blood-Retinal Barrier Integrity via P2X7 Receptor. *Int. J. Mol. Sci.* 21 (23), 9305. doi:10.3390/ijms21239305

Fresta, C. G., Fidilio, A., Lazzarino, G., Musso, N., Grasso, M., Merlo, S., et al. (2020b). Modulation of Pro-oxidant and Pro-inflammatory Activities of M1 Macrophages by the Natural Dipeptide Carnosine. *Int. J. Mol. Sci.* 21 (3), 776. doi:10.3390/ijms21030776

Gelain, D. P., Antonio Behr, G., Birnfeld de Oliveira, R., and Trujillo, M. (2012). Antioxidant Therapies for Neurodegenerative Diseases: Mechanisms, Current Trends, and Perspectives. *Oxid Med. Cel Longev* 2012, 895153. doi:10.1155/2012/895153

Glenner, G. G., and Wong, C. W. (1984). Alzheimer's Disease: Initial Report of the Purification and Characterization of a Novel Cerebrovascular Amyloid Protein. *Biochem. Biophys. Res. Commun.* 120 (3), 885–890. doi:10.1016/s0006-291x(84)80190-4

Gong, Y., Chang, L., Viola, K. L., Lacor, P. N., Lambert, M. P., Finch, C. E., et al. (2003). Alzheimer's Disease-Affected Brain: Presence of Oligomeric A Beta Ligands (ADDLs) Suggests a Molecular Basis for Reversible Memory Loss. *Proc. Natl. Acad. Sci. U S A.* 100 (18), 10417–10422. doi:10.1073/pnas.1834302100

Huang, W. J., Zhang, X., and Chen, W. W. (2016). Role of Oxidative Stress in Alzheimer's Disease. *Biomed. Rep.* 4 (5), 519–522. doi:10.3892/br.2016.630

Jin, L., Gao, L. F., Sun, D. S., Wu, H., Wang, Q., Ke, D., et al. (2017). Long-term Ameliorative Effects of the Antidepressant Fluoxetine Exposure on Cognitive Deficits in 3×TgAD Mice. *Mol. Neurobiol.* 54 (6), 4160–4171. doi:10.1007/s12035-016-9952-910.1007/s12035-016-9952-9

Katrenčíková, B., Vaváková, M., Paduchová, Z., Nagyová, Z., Garaiova, I., Muchová, J., et al. (2021). Oxidative Stress Markers and Antioxidant Enzymes in Children and Adolescents with Depressive Disorder and Impact of Omega-3 Fatty Acids in Randomised Clinical Trial. *Antioxidants* 10 (8), 1256. doi:10.3390/antiox10081256

Kessing, L. V. (2012). Depression and the Risk for Dementia. *Curr. Opin. Psychiatry* 25 (6), 457–461. doi:10.1097/YCO.0b013e328356c368

Kessing, L. V., Søndergård, L., Forman, J. L., and Andersen, P. K. (2009). Antidepressants and Dementia. *J. Affect Disord.* 117 (1-2), 24–29. doi:10.1016/j.jad.2008.11.020

Klein, W. L. (2013). Synaptotoxic Amyloid-β Oligomers: a Molecular Basis for the Cause, Diagnosis, and Treatment of Alzheimer's Disease. *J. Alzheimers Dis.* 33 (Suppl. 1), S49–S65. doi:10.3233/jad-2012-129039

Knezevic, D., and Mizrahi, R. (2018). Molecular Imaging of Neuroinflammation in Alzheimer's Disease and Mild Cognitive Impairment. *Prog. Neuropsychopharmacol. Biol. Psychiatry* 80 (Pt B), 123–131. doi:10.1016/j.pnpbp.2017.05.007

Kumar, A., Sidhu, J., Goyal, A., and Tsao, J. W. (2021). "Alzheimer Disease," in *StatPearls* (Treasure Island (FL): StatPearls Publishing LLC.).

Kurakazu, I., Akasaki, Y., Tsushima, H., Sueishi, T., Toya, M., Kuwahara, M., et al. (2021). TGFβ1 Signaling Protects Chondrocytes against Oxidative Stress via FOXO1-Autophagy axis. *Osteoarthritis Cartilage* 29 (11), 1600–1613. doi:10.1016/j.joca.2021.07.015

Ledo, J. H., Azevedo, E. P., Beckman, D., Ribeiro, F. C., Santos, L. E., Razolli, D. S., et al. (2016). Cross Talk between Brain Innate Immunity and Serotonin Signaling Underlies Depressive-like Behavior Induced by Alzheimer's Amyloid-β Oligomers in Mice. *J. Neurosci.* 36 (48), 12106–12116. doi:10.1523/jneurosci.1269-16.2016

Ledo, J. H., Azevedo, E. P., Clarke, J. R., Ribeiro, F. C., Figueiredo, C. P., Foguel, D., et al. (2020). Correction: Amyloid-β Oligomers Link Depressive-like Behavior and Cognitive Deficits in Mice. *Mol. Psychiatry*. doi:10.1038/s41380-020-00873-6

Leggio, G. M., Catania, M. V., Puzzo, D., Spatuzza, M., Pellitteri, R., Gulisano, W., et al. (2016). The Antineoplastic Drug Flavopiridol Reverses Memory Impairment Induced by Amyloid-SS1-42 Oligomers in Mice. *Pharmacol. Res.* 106, 10–20. doi:10.1016/j.phrs.2016.02.007

Li, Y., Sanchez, C., and Gulinello, M. (2017). Distinct Antidepressant-like and Cognitive Effects of Antidepressants with Different Mechanisms of Action in Middle-Aged Female Mice. *Int. J. Neuropsychopharmacol.* 20 (6), 510–515. doi:10.1093/ijnp/pyx004

Lozupone, M., La Montagna, M., D'Urso, F., Piccininni, C., Sardone, R., Dibello, V., et al. (2018). Pharmacotherapy for the Treatment of Depression in Patients with Alzheimer's Disease: a Treatment-Resistant Depressive Disorder. *Expert Opin. Pharmacother.* 19 (8), 823–842. doi:10.1080/14656566.2018.1471136

Lüth, H. J., Münch, G., and Arendt, T. (2002). Aberrant Expression of NOS Isoforms in Alzheimer's Disease Is Structurally Related to Nitrotyrosine Formation. *Brain Res.* 953 (1-2), 135–143. doi:10.1016/s0006-8993(02)03280-8

Maes, M., Mihaylova, I., Kubera, M., Uytterhoeven, M., Vrydags, N., and Bosmans, E. (2009). Lower Plasma Coenzyme Q10 in Depression: a Marker for Treatment Resistance and Chronic Fatigue in Depression and a Risk Factor to Cardiovascular Disorder in that Illness. *Neuro Endocrinol. Lett.* 30 (4), 462–469.

Marcus, D. L., Thomas, C., Rodriguez, C., Simberkoff, K., Tsai, J. S., Strafaci, J. A., et al. (1998). Increased Peroxidation and Reduced Antioxidant Enzyme Activity in Alzheimer's Disease. *Exp. Neurol.* 150 (1), 40–44. doi:10.1006/exnr.1997.6750

McIntyre, R. S., Harrison, J., Loft, H., Jacobson, W., and Olsen, C. K. (2016). The Effects of Vortioxetine on Cognitive Function in Patients with Major Depressive Disorder: A Meta-Analysis of Three Randomized Controlled Trials. *Int. J. Neuropsychopharmacol.* 19 (10), pyw055. doi:10.1093/ijnp/pyw055

Medeiros, R., Prediger, R. D., Passos, G. F., Pandolfo, P., Duarte, F. S., Franco, J. L., et al. (2007). Connecting TNF-Alpha Signaling Pathways to iNOS Expression in a Mouse Model of Alzheimer's Disease: Relevance for the Behavioral and Synaptic Deficits Induced by Amyloid Beta Protein. *J. Neurosci.* 27 (20), 5394–5404. doi:10.1523/jneurosci.5047-06.2007

Mehrpooya, M., Yasrebifar, F., Haghighi, M., Mohammadi, Y., and Jahangard, L. (2018). Evaluating the Effect of Coenzyme Q10 Augmentation on Treatment of Bipolar Depression: A Double-Blind Controlled Clinical Trial. *J. Clin. Psychopharmacol.* 38 (5), 460–466. doi:10.1097/jcp.0000000000000938

Metto, E. C., Evans, K., Barney, P., Culbertson, A. H., Gunasekara, D. B., Caruso, G., et al. (2013). An Integrated Microfluidic Device for Monitoring Changes in Nitric Oxide Production in Single T-Lymphocyte (Jurkat) Cells. *Anal. Chem.* 85 (21), 10188–10195. doi:10.1021/ac401665u

Minati, L., Edginton, T., Bruzzone, M. G., and Giaccone, G. (2009). Current Concepts in Alzheimer's Disease: a Multidisciplinary Review. *Am. J. Alzheimers Dis. Other Demen.* 24 (2), 95–121. doi:10.1177/1533317508328602

Moretti, M., Colla, A., de Oliveira Balen, G., dos Santos, D. B., Budni, J., de Freitas, A. E., et al. (2012). Ascorbic Acid Treatment, Similarly to Fluoxetine, Reverses Depressive-like Behavior and Brain Oxidative Damage Induced by Chronic Unpredictable Stress. *J. Psychiatr. Res.* 46 (3), 331–340. doi:10.1016/j.jpsychires.2011.11.009

Murphy, S. (2000). Production of Nitric Oxide by Glial Cells: Regulation and Potential Roles in the CNS. *Glia* 29 (1), 1–13. doi:10.1002/(sici)1098-1136(20000101)29:1<1:aid-glia1>3.0.co;2-n

Park, S. J., Ciccone, S. L., Beck, B. D., Hwang, B., Freie, B., Clapp, D. W., et al. (2004). Oxidative Stress/damage Induces Multimerization and Interaction of Fanconi Anemia Proteins. *J. Biol. Chem.* 279 (29), 30053–30059. doi:10.1074/jbc.M403527200

Petersen, R. C., Caracciolo, B., Brayne, C., Gauthier, S., Jelic, V., and Fratiglioni, L. (2014). Mild Cognitive Impairment: a Concept in Evolution. *J. Intern. Med.* 275 (3), 214–228. doi:10.1111/joim.12190

Scapagnini, G., Davinelli, S., Drago, F., De Lorenzo, A., and Oriani, G. (2012). Antioxidants as Antidepressants: Fact or Fiction. *CNS Drugs* 26 (6), 477–490. doi:10.2165/11633190-000000000-00000

Schiavone, S., Tucci, P., Mhillaj, E., Bove, M., Trabace, L., and Morgese, M. G. (2017). Antidepressant Drugs for Beta Amyloid-Induced Depression: A New Standpoint. *Prog. Neuropsychopharmacol. Biol. Psychiatry* 78, 114–122. doi:10.1016/j.pnpbp.2017.05.004

Setti, S. E., Hunsberger, H. C., and Reed, M. N. (2017). Alterations in Hippocampal Activity and Alzheimer's Disease. *Transl Issues Psychol. Sci.* 3 (4), 348–356. doi:10.1037/tps0000124

Shimohama, S., Tanino, H., Kawakami, N., Okamura, N., Kodama, H., Yamaguchi, T., et al. (2000). Activation of NADPH Oxidase in Alzheimer's Disease Brains. *Biochem. Biophys. Res. Commun.* 273 (1), 5–9. doi:10.1006/bbrc.2000.2897

Siegel, J. M., Schilly, K. M., Wijesinghe, M. B., Caruso, G., Fresta, C. G., and Lunte, S. M. (2019). Optimization of a Microchip Electrophoresis Method with Electrochemical Detection for the Determination of Nitrite in Macrophage Cells as an Indicator of Nitric Oxide Production. *Anal. Methods* 11 (2), 148–156. doi:10.1039/c8ay02014k

Solleiro-Villavicencio, H., and Rivas-Arancibia, S. (2018). Effect of Chronic Oxidative Stress on Neuroinflammatory Response Mediated by CD4+T Cells in Neurodegenerative Diseases. *Front Cel Neurosci* 12, 114. doi:10.3389/fncel.2018.00114

Sowa-Kućma, M., Styczeń, K., Siwek, M., Misztak, P., Nowak, R. J., Dudek, D., et al. (2018). Lipid Peroxidation and Immune Biomarkers Are Associated with Major Depression and its Phenotypes, Including Treatment-Resistant Depression and Melancholia. *Neurotox Res.* 33 (2), 448–460. doi:10.1007/s12640-017-9835-5

Sultan, C. S., Saackel, A., Stank, A., Fleming, T., Fedorova, M., Hoffmann, R., et al. (2018). Impact of Carbonylation on Glutathione Peroxidase-1 Activity in Human Hyperglycemic Endothelial Cells. *Redox Biol.* 16, 113–122. doi:10.1016/j.redox.2018.02.018

Szałach, Ł. P., Lisowska, K. A., and Cubała, W. J. (2019). The Influence of Antidepressants on the Immune System. *Arch. Immunol. Ther. Exp. (Warsz)* 67 (3), 143–151. doi:10.1007/s00005-019-00543-8

Talmon, M., Rossi, S., Pastore, A., Cattaneo, C. I., Brunelleschi, S., and Fresu, L. G. (2018). Vortioxetine Exerts Anti-inflammatory and Immunomodulatory Effects on Human Monocytes/macrophages. *Br. J. Pharmacol.* 175 (1), 113–124. doi:10.1111/bph.14074

Thase, M. E., Mahableshwarkar, A. R., Dragheim, M., Loft, H., and Vieta, E. (2016). A Meta-Analysis of Randomized, Placebo-Controlled Trials of Vortioxetine for the Treatment of Major Depressive Disorder in Adults. *Eur. Neuropsychopharmacol.* 26 (6), 979–993. doi:10.1016/j.euroneuro.2016.03.007

Tin, G., Mohamed, T., Shakeri, A., Pham, A. T., and Rao, P. P. N. (2019). Interactions of Selective Serotonin Reuptake Inhibitors with β-Amyloid. *ACS Chem. Neurosci.* 10 (1), 226–234. doi:10.1021/acschemneuro.8b00160

Torrisi, S. A., Geraci, F., Tropea, M. R., Grasso, M., Caruso, G., Fidilio, A., et al. (2019). Fluoxetine and Vortioxetine Reverse Depressive-like Phenotype and Memory Deficits Induced by Aβ1-42 Oligomers in Mice: A Key Role of Transforming Growth Factor-B1. *Front. Pharmacol.* 10, 693. doi:10.3389/fphar.2019.00693

Varadarajan, S., Yatin, S., Aksenova, M., and Butterfield, D. A. (2000). Review: Alzheimer's Amyloid Beta-Peptide-Associated Free Radical Oxidative Stress and Neurotoxicity. *J. Struct. Biol.* 130 (2-3), 184–208. doi:10.1006/jsbi.2000.4274

Villa, R. F., Ferrari, F., Gorini, A., Brunello, N., and Tascedda, F. (2016). Effect of Desipramine and Fluoxetine on Energy Metabolism of Cerebral Mitochondria. *Neuroscience* 330, 326–334. doi:10.1016/j.neuroscience.2016.05.051

Wang, J., Zhang, Y., Xu, H., Zhu, S., Wang, H., He, J., et al. (2014). Fluoxetine Improves Behavioral Performance by Suppressing the Production of Soluble β-amyloid in APP/PS1 Mice. *Curr. Alzheimer Res.* 11 (7), 672–680. doi:10.2174/1567205011666140812114715

Wang, W., Yang, L., Liu, T., Ma, Y., Huang, S., He, M., et al. (2020). Corilagin Ameliorates Sleep Deprivation-Induced Memory Impairments by Inhibiting NOX2 and Activating Nrf2. *Brain Res. Bull.* 160, 141–149. doi:10.1016/j.brainresbull.2020.03.010

Wu, J. Q., Kosten, T. R., and Zhang, X. Y. (2013). Free Radicals, Antioxidant Defense Systems, and Schizophrenia. *Prog. Neuropsychopharmacol. Biol. Psychiatry* 46, 200–206. doi:10.1016/j.pnpbp.2013.02.015

Yuste, J. E., Tarragon, E., Campuzano, C. M., and Ros-Bernal, F. (2015). Implications of Glial Nitric Oxide in Neurodegenerative Diseases. *Front. Cel Neurosci* 9, 322. doi:10.3389/fncel.2015.00322

Zekry, D., Epperson, T. K., and Krause, K. H. (2003). A Role for NOX NADPH Oxidases in Alzheimer's Disease and Other Types of Dementia. *IUBMB Life* 55 (6), 307–313. doi:10.1080/1521654031000153049

Zhao, Y., and Zhao, B. (2013). Oxidative Stress and the Pathogenesis of Alzheimer's Disease. *Oxid Med. Cel Longev* 2013, 316523. doi:10.1155/2013/316523

Conflict of Interest: The authors declare that the research was conducted in the absence of any commercial or financial relationships that could be construed as a potential conflict of interest.

Publisher's Note: All claims expressed in this article are solely those of the authors and do not necessarily represent those of their affiliated organizations, or those of the publisher, the editors and the reviewers. Any product that may be evaluated in this article, or claim that may be made by its manufacturer, is not guaranteed or endorsed by the publisher.

Copyright © 2021 Caruso, Grasso, Fidilio, Torrisi, Musso, Geraci, Tropea, Privitera, Tascedda, Puzzo, Salomone, Drago, Leggio and Caraci. This is an open-access article distributed under the terms of the Creative Commons Attribution License (CC BY). The use, distribution or reproduction in other forums is permitted, provided the original author(s) and the copyright owner(s) are credited and that the original publication in this journal is cited, in accordance with accepted academic practice. No use, distribution or reproduction is permitted which does not comply with these terms.

frontiers in Pharmacology

ORIGINAL RESEARCH
published: 03 January 2022
doi: 10.3389/fphar.2021.799561

Precision Medicine in Alzheimer's Disease: Investigating Comorbid Common Biological Substrates in the Rat Model of Amyloid Beta-Induced Toxicity

Maria Grazia Morgese[1]†, Maria Bove[1]†, Lorenzo Di Cesare Mannelli[2], Stefania Schiavone[1], Anna Laura Colia[1], Stefania Dimonte[1], Emanuela Mhillaj[1], Vladyslav Sikora[1,3], Paolo Tucci[1], Carla Ghelardini[2] and Luigia Trabace[1]*

[1]Department of Clinical and Experimental Medicine, University of Foggia, Foggia, Italy, [2]Pharmacology and Toxicology Section, Department of Neuroscience, Psychology, Drug Research and Child Health (NEUROFARBA), University of Firenze, Firenze, Italy, [3]Department of Pathology, Sumy State University, Sumy, Ukraine

OPEN ACCESS

Edited by:
Salvatore Salomone,
University of Catania, Italy

Reviewed by:
Shaoqiu He,
Johns Hopkins Medicine,
United States
Fabio Tascedda,
University of Modena and Reggio Emilia, Italy

***Correspondence:**
Maria Grazia Morgese
mariagrazia.morgese@unifg.it

†These authors share first authorship

Specialty section:
This article was submitted to Experimental Pharmacology and Drug Discovery, a section of the journal Frontiers in Pharmacology

Received: 21 October 2021
Accepted: 01 December 2021
Published: 03 January 2022

Citation:
Morgese MG, Bove M, Di Cesare Mannelli L, Schiavone S, Colia AL, Dimonte S, Mhillaj E, Sikora V, Tucci P, Ghelardini C and Trabace L (2022) Precision Medicine in Alzheimer's Disease: Investigating Comorbid Common Biological Substrates in the Rat Model of Amyloid Beta-Induced Toxicity. Front. Pharmacol. 12:799561. doi: 10.3389/fphar.2021.799561

Alzheimer's disease (AD), one of the most widespread neurodegenerative disorder, is a fatal global burden for the elder population. Although many efforts have been made, the search of a curative therapy is still ongoing. Individuating phenotypic traits that might help in investigating treatment response is of growing interest in AD research. AD is a complex pathology characterized by many comorbidities, such as depression and increased susceptibility to pain perception, leading to postulate that these conditions may rely on common biological substrates yet to be determined. In order to investigate those biological determinants to be associable with phenotypic traits, we used the rat model of amyloid beta-induced toxicity. This established model of early phase of AD is obtained by the intracerebroventricular injection of soluble amyloid beta1-42 (Aβ) peptide 7 days before performing experiments. In this model, we have previously reported increased immobility in the forced swimming test, reduced cortical serotonin levels and subtle alterations in the cognitive domain a depressive-like phenotype associated with subtle alteration in memory processes. In light of evaluating pain perception in this animal model, we performed two different behavioral tests commonly used, such as the paw pressure test and the cold plate test, to analyze mechanical hyperalgesia and thermal allodynia, respectively. Behavioural outcomes confirmed the memory impairment in the social recognition test and, compared to sham, Aβ-injected rats showed an increased selective susceptibility to mechanical but not to thermal stimulus. Behavioural data were then corroborated by neurochemical and biochemical biomarker analyses either at central or peripheral level. Data showed that the peptide injection evoked a significant increase in hypothalamic glutamate, kynurenine and dopamine content, while serotonin levels were reduced. Plasma Cystatin-C, a cysteine protease, was increased while serotonin and melatonin levels were decreased in Aβ-injected rats. Urinary levels paralleled plasma quantifications, indicating that Aβ-induced deficits in pain perception, mood and cognitive domain may also depend on these biomarkers. In conclusion, in the present study, we demonstrated that this animal

model can mimic several comorbid conditions typical of the early phase of AD. Therefore, in the perspective of generating novel therapeutic strategies relevant to precision medicine in AD, this animal model and the biomarkers evaluated herein may represent an advantageous approach.

Keywords: pain, amyloid beta, depression, serotonin, kynurenine, melatonin, glutamate, precision medicine

INTRODUCTION

Alzheimer's disease (AD) is the most common form of dementia in the elderly. It is nowadays becoming more evident that AD is heterogeneous in many aspects, ranging from biomolecular or clinical manifestations, thus indicating that AD cannot be explained with a single pathological process (Ferrari and Sorbi, 2021). In this light, studying differences in disease symptomatology, treatment responses may represent an innovative field of study for supporting and implementing precision medicine in AD. Indeed, this complex neurological disorder is often accompanied by a variety of comorbidities. Among these, depression is highly frequent in the way that some Authors have hypothesized that depressive symptoms may represent an early manifestation of this neurodegenerative disease (Pomara and Sidtis, 2010). Interestingly, the prevalence of chronic pain in dementia is quite elevated and it is esteemed to be between 30 and 80% (Defrin et al., 2015). On the other hand, several lines of evidence have reported alterations of pain perception in different psychiatric disorders (Lautenbacher and Krieg, 1994; Malejko et al., 2020). In particular, the pain experience has been frequently associated with emotional and cognitive dysfunctions, as well as to depressive states (Moriarty et al., 2011; Bushnell et al., 2013). Indeed, the comorbidity of pain and depression has been described as the "pain-depression syndrome or pain-depression dyad" (Thompson et al., 2016). More specifically, depression may induce a reduction of the pain threshold (Torta and Munari, 2010). This suggests a possible overlapping of neurobiological and molecular mechanisms underlying this comorbidity (Li, 2015), whose understanding may be crucially provided by preclinical investigations using animal models of depressive-like state. In this regard, we have previously reported that rats receiving an intracerebroventricular (icv) injection of soluble amyloid beta1-42 (Aβ) peptide showed increased immobility frequency in the forced swimming test, mimicking a behavioral despair state, also accompanied by neurochemical alterations, as well as changes in neurotrophin levels (Colaianna et al., 2010; Schiavone et al., 2017). Furthermore, in this animal model, depressive like symptoms are accompanied by subtle changes in spatial memory, mimicking the early manifestation of AD onset, featured by higher Aβ levels and alterations in emotional and cognitive domains. In this regard, we have previously fully validated this model. Immunohistochemical analyses were also previously carried out after the peptide injection (Trabace et al., 2007), and the peptide solution was fully evaluated by atomic force and transmission electron microscopy (Morgese et al., 2015). In particular, systemic soluble Aβ levels were still highier in treated injected rats 7 days after central administration of the peptide, while immunohistochemical analyses reveiled no gross signs of neurodegeneration within the area of Aβ diffusion in the periventricular parenchyma (Trabace et al., 2007; Morgese et al., 2015; Schiavone et al., 2017; Morgese et al., 2018). Therefore, in this model we generally assume that the supraphysiological levels of the peptide lead to profound unbalance in several brain circuitries (see (Trabace et al., 2007; Preda et al., 2008; Mura et al., 2010) for reference). Thus, from a behavioral and neurobiological point of view, this model can be considered as a valid animal model of early AD phase.

A key brain region involved in pain perception, particularly in its descending modulation, is the hypothalamus (Puopolo, 2019), which has also been reported to play key functions in the development of different depressive symptoms, acting as a crucial hub in a network of neurocircuits modulating these two comorbidities (Bao and Swaab, 2019). Interestingly, alteration in the hypothalamic area has also been reported in the early AD phase (Vercruysse et al., 2018). Of note, neurotransmitter systems implicated in pain perception, transmission and control physiologically overlap with those underlying the development of depressive disorders and cognition (Yang and Chang, 2019). Among them, dopaminergic pathways have been implicated in the central regulation and modulation of pain (Li C. et al., 2019). Conversely, nociceptive stimuli have been described to disrupt dopamine homeostasis in the central nervous system (Wood, 2008; Kim et al., 2015). Moreover, it has been reported that soluble Aβ could determine alterations in dopamine content in the rodent brain (Wu et al., 2007; Morgese and Trabace, 2019). Together with its crucial role in pain perception (Paredes et al., 2019), decreased central levels of serotonin (5-HT) have been widely described in depressive-like states induced by soluble Aβ (Colaianna et al., 2010; Schiavone et al., 2017; Morgese et al., 2018). In addition, drugs able to increase 5-HT levels can improve cognitive function in AD patients (Xie et al., 2019) and in rodent AD models (Ma et al., 2017). Increased levels of glutamate (GLU), a key player in the perception of pain and pain transmission from peripheral to central districts (Pereira and Goudet, 2018), were found in rodent brain following icv injection of soluble Aβ able to cause spatial memory impairment (Tucci et al., 2014), and whose accumulation might also lead to synaptic failure through disruption of the glutamatergic pathways (Findley et al., 2019). Of note, ketamine, an antagonist of the glutamatergic NMDA receptor, is able to reduce pain perception as well as depressive symptoms (Dowben et al., 2013; Hayley and Litteljohn, 2013), and in this model we

have demonstrated that ketamine is able to prevent depressive-like phenotype in Aβ-treated rats (Schiavone et al., 2017).

Together with neuropathological dysfunctions at central levels, depression and AD have been described to be also associated with peripheral alterations. In particular, decreased plasma 5-HT levels have been detected in patients with major depression (Paul-Savoie et al., 2011). The 5-HT content in plasma has also been considered as a predictor of antidepressant treatment outcomes (Blardi et al., 2002; Holck et al., 2019; Sun et al., 2020). In addition, it has been suggested that the peripheral serotonergic system is negatively implicated in AD (Kumar et al., 1995). Moreover, a negative association has been found between peripheral 5-HT amount and pain perception after different noxious stimuli (Ernberg et al., 2000; Farhanchi et al., 2018). On the other hand, melatonin (MEL), a circadian rhythm–regulated hormone, has been shown to be protective in neurodegeneration associated with AD (Savaskan et al., 2005). Indeed, anti-amyloidogenic as well as free radical–scavenging properties have been reported for MEL leading to hypothesize that this molecule might represent a therapeutic candidate to inhibit AD progression (Rosales-Corral et al., 2012; Lin et al., 2013) or a valid biomarker for defining disease progression or therapeutic success (Nous et al., 2021).

Depressive symptoms have also been associated with increased peripheral levels of Cystatin-C (Cys-C), a low-molecular-weight protein, synthesized at a constant rate in all nucleated cells (Li H. et al., 2019; Huang et al., 2021). Cys-C has been thought to be crucially implicated in the development of soluble Aβ neuronal dysfunctions, also relating to cognitive impairment (Zeng et al., 2019). Of note, central and peripheral enhanced amount of this protein has been described as a pain biomarker (Mannes et al., 2003). Hence, in our animal model of early phase AD, we investigated possible alterations of pain threshold as possible comorbidity in the early AD phase and in the depressive-like state.

In addition, involvement of noradrenergic, dopaminergic, serotonergic, including the tryptophan derivate kynurenine (KYN), glutamatergic and gamma-aminobutyric acid (GABA)-ergic systems was assessed in the hypothalamus, an area whose dysfunction has been considered a putative driver of AD pathology (Ishii and Iadecola, 2015). Furthermore, possible alterations in peripheral, such as in plasma and in urine levels, of 5-HT, KYN, MEL and Cys-C amounts were also evaluated.

In this light, the establishment of an animal model that can allow to study different aspects of this neuropathology could represent a valid advantage in the perspective of building tailored treatment for AD patients, thus pursuing the goal of precision medicine for this complex neurologic and neuropsychiatric disorder.

MATERIALS AND METHODS

Animals

Experiments were performed on a total number of 47 seven week-old male Wistar rats (Envigo, San Pietro al Natisone, Italy). Animals were constantly maintained under controlled conditions, with a room temperature of 22 ± 1°C, relative humidity of 55 ± 5% and a light/dark cycle of 12 h (light on from 7:00 a.m. to 7:00 p.m.). Rats were group-housed and food and water were provided *ad libitum*. We carried out all experimental procedures involving animals in conformity with the institutional guidelines of the Italian Ministry of Health (D.L. 26/2014), the Guide for the Care and Use of Mammals in Neuroscience and Behavioral Research (National Research Council 2004), the Directive 2010/63/EU of the European Parliament and of the Council of September 22, 2010, on the protection of animals used for scientific purposes, as well as the ARRIVE guidelines. The Italian Ministry of Health approved our experimental protocol (protocol number: B2EF8.15-aut.737-2017-PR). Animal welfare was daily monitored in order to detect any signs of animal suffering or distress during the entire experimental procedure. All efforts to reduce the number of animals used and their suffering were conducted.

Aβ Administration

The human Aβ1–42 peptide (Tocris, Bristol, United Kingdom) was freshly prepared by using sterile double distilled water as vehicle (final concentration 4 μM), as previously described (Bove et al., 2018). An anesthetic cocktail solution (0.85 ml/kg) containing ketamine (100 mg/ml), xylazine (100 mg/ml) and acepromazine (10 mg/ml), dissolved in saline, was injected intraperitoneally in seven week-old rats. Rats were then secured in a stereotaxic frame (David Kopf Instruments, Tujunga, CA, United States) and underwent an icv infusion based on the following coordinates from bregma according to Paxinos and Watson rat brain atlas (Paxinos, 1986): AP = −0.5, ML = +1.2 and DV = −3.2. The incisor bar was set at −3.3 mm. A Hamilton micro-syringe was used to infuse 5 μl of soluble Aβ peptide, with an infusion rate of 2 μl/min over 2.5 min. Subsequently, the needle was left in place for 5 min in order to avoid elapsing. Vehicle was delivered to sham animals used as controls. Once dissecting the brain, it was verified whether the needle was placed in the correct way. Seven days after icv administration, experimental procedures were carried out.

Behavioural Tests

Paw Pressure Test

The test was performed according to Di Cesare Mannelli et al. (Di Cesare Mannelli et al., 2015), by using an analgesimeter (Ugo Basile, Varese, Italy) to determine the nociceptive threshold in rats. This test is widely used as a test for hyperalgesia-like measurement (Deuis et al., 2017). Briefly, a blunt conical mechanical probe was used to apply an increasing pressure to the dorsal surface of the hind paw of slightly restrained rats. The constantly increasing pressure was applied until rats vocalized or showed a withdrawal reflex. Results were expressed in grams of tolerated mechanical pressure. The arbitrary cut-off value was set at 100 g and a blind observer collected the data.

Cold Plate Test

The test was performed by using a cold plate kept at a constant temperature (4 ± 1°C) as floor in a stainless steel box (12 cm × 20 cm × 10 cm), as reported by Pacini et al. (Pacini et al., 2016).

This test is widely used as a test for allodynia-like measurement (Deuis et al., 2017). Each animal was placed in the box and the latency to first lick the hind paw, expressed in seconds, was recorded as a measure of pain-related behaviour. A cut-off time of 60 s was adopted.

Social Recognition Test

This test was used to analyze short-term memory by using a natural animal behaviour as social interacting with a similar (Mathiasen and Dicamillo, 2010) Briefly, rats were housed individually in plastic cages 3 days before the test. Juvenile rats used as stimulus animals were isolated in individual cages 30 min prior the beginning of the experiment. The social recognition test consisted in two trials of 5 min each, separated by an inter-trial of 30 min. During the first trial (T1) the stimulus animal is placed in the test animal home cage for 5 min. Then, an inter-trial of 30 min in which the stimulus returned to its cage was carried out. Subsequently, the trial 2 (T2) took place and the test animal was re-exposed to the stimulus animal. Time spent sniffing and social interacting, expressed in seconds, was scored by a blind observer. In order to exclude exploratory impairments, the time spent exploring the environment was also recorded.

Post-mortem Analyses

At the end of the behavioural experiments, rats were euthanized, plasma was collected and brains were dissected by using a chilled rat brain matrix (World Precision Instruments, Inc. FL, United States) according to Paxinos and Watson rats brain atlas (Paxinos, 1986). The hypothalamus was weighed, frozen in liquid nitrogen and stored at − 80°C until *ex vivo* quantifications were performed.

High-Performance Liquid Chromatography (HPLC) Quantifications

Neurochemical analyses were performed by using HPLC. Hypothalamic samples were homogenized in 10 volumes (w/V) of 0.1 N perchloric acid, stored on ice for 30 min and then centrifuged at 10.000 × g for 10 min at 4°C, as previously described (Zotti et al., 2013). Plasma and urine samples were homogenized with 0.1 volumes (V/V) of 8% perchloric acid and centrifuged at 10.000 × g for 15 min at 4°C. Supernatants were then collected and HPLC analyses were carried out. Hypothalamic noradrenaline (NA), dopamine (DA) and 5-HT concentrations, plasma and urine 5-HT and 5-hydroxy-indole acetic acid (5-HIAA) levels were determined by using a LC18 reverse phase column (Kinetex, 150 mm × 4.2 mm, ODS 5 µm; Phenomenex, Castel Maggiore-Bologna, Italy). An electrochemical detector with a thin-layer amperometric cell (Ultimate 3000RS–ECD, Dionex, ThermoScientifics, Milan, Italy) at a working potential of 0.400 V was used. As previously described, KYN (Morgese et al., 2021b) and MEL were quantified with the same method by applying a working potential of 0.550 V. The flow rate was maintained at 0.7 ml/min by an isocratic pump (Shimadzu LC-10 AD, Kyoto, Japan). The mobile phase consisted of an aqueous solution of 75 mM NaH_2PO_4, 1.7 mM octane sulfonic acid, 0.3 mM EDTA, acetonitrile 10%, buffered at pH 3.0. Chemicals and reagents were purchased from Sigma Aldrich (Sigma Aldrich Milan Italy). Chromeleon software (version 6.80, Thermo Scientific Dionex, San Donato Milanese, Italy) was used for data analyses. The 5-HT turnover was calculated as 5-HIAA/5-HT ratio. Sample concentrations were expressed as fmol/mg of tissue. A fluorescence detector (emission length, 460 nm; excitation length, 340 nm, Jasco, Tokyo, Japan), after derivatization with *o*-phthalaldehyde/mercaptopropionic acid, was used to determine GLU, glutamine and GABA hypothalamic concentrations, as previously described (Bove et al., 2018). Chromatographic evaluation was accomplished by using an ODS-3 column (Kinetex 150 mm × 3 mm, ODS 5 µm; Phenomenex, Castel Maggiore-Bologna, Italy) with a gradient mobile phase (50 mM sodium acetate buffer, pH 6.95, with methanol increasing linearly from 2 to 30% (v/v) over 40 min. The flow rate was set at 0.5 ml/min. Data were acquired and integrated by using Borwin software (version 1.50; Jasco). Results are expressed as µM/mg of tissue.

Enzyme-Linked Immunosorbent Assays (ELISA) Quantifications

Cys-C levels were quantified in plasmatic samples by using Rat Cys-C (Enzyme-Linked Immunosorbent Assays) ELISA kit (Fine Test, Wuhan Fine Biotech Co., Ltd., Wuhan, Hubei, China), according to manufacturers' instructions. In order to avoid intra-assay variations, both standards and samples were analyzed in duplicate.

Statistical Analyses

Statistical analyses were performed by using Two-way ANOVA for repeated measures followed by Šídák's multiple comparisons test or Unpaired Student's t-test, as required. Welch's correction was applied to Unpaired Student's t-test when F test indicated unequal variances. The statistical software used was GraphPad 9.0 for Windows (GraphPad Software, San Diego, CA, United States). For all tests, p-value was set at 0.05. Results are expressed as means ± standard error of the mean (S.E.M.).

RESULTS

Effects of Aβ Administration on Pain-Related Behavioural Tests

In order to evaluate the effects of Aβ administration in response to a noxious mechanical stimulus, we performed the paw pressure test (hyperalgesia-like measurement). **Figure 1A** showed that the pain threshold, expressed as grams of tolerated weight, was significantly decreased in Aβ-treated rats compared to sham rats (**Figure 1A**, Two-Way ANOVA for repeated measures, followed by Šídák's multiple comparisons test, $F_{(3,\ 42)} = 5.039$, $p < 0.05$, time 0: Aβ vs sham). Moreover, we assessed the thermal pain sensitivity in Aβ-treated and sham rats by performing the cold plate test, based on a non-noxious cold stimulation (allodynia-like measurement). Our results showed no differences in cold hypersensitivity, expressed as latency to lick the paws, between the two experimental groups, although a slight trend

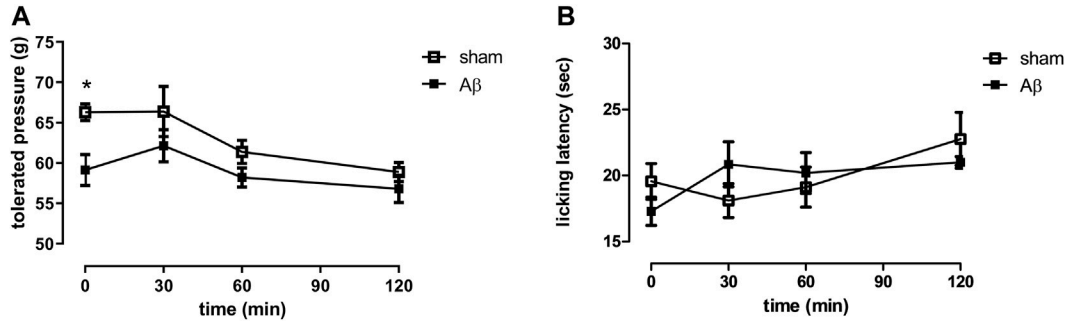

FIGURE 1 | Effects of Aβ administration on paw pressure and cold plate tests. **(A)** Tolerated weight (g) in sham (n = 9) and Aβ-treated (n = 7) animals. Two-way ANOVA for repeated measures followed by Šídák's multiple comparisons test, $^{*}p < 0.05$ Aβ vs sham. **(B)** Licking latency (sec) in sham (n = 10) and Aβ-treated (n = 7) animals. Two-way ANOVA for repeated measures followed by Šídák's multiple comparisons test, $p > 0.05$.

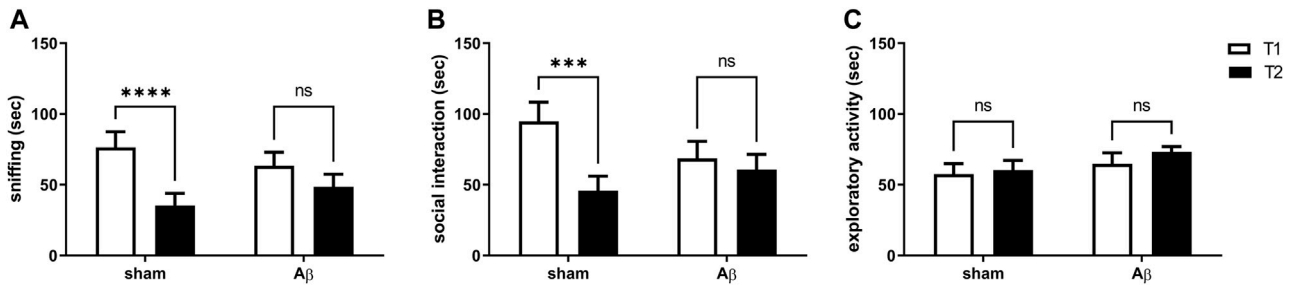

FIGURE 2 | Effects of Aβ administration on social recognition paradigm. **(A)** Sniffing time (sec) in sham (n = 7) and Aβ-treated (n = 7) animals. Two-Way ANOVA for repeated measures followed by Šídák's multiple comparisons test, $^{****}p < 0.0001$ Aβ vs sham. **(B)** Social interaction time (sec) in sham (n = 7) and Aβ-treated (n = 7) animals. Two-way ANOVA for repeated measures followed by Šídák's multiple comparisons test, $^{***}p < 0.001$ Aβ vs sham. **(C)** Exploratory activity time (sec) in sham (n = 7) and Aβ-treated (n = 7) animals. Two-way ANOVA for repeated measures followed by Šídák's multiple comparisons test, $p > 0.05$.

to reduction could be appreciated (**Figure 1B**, Two-Way ANOVA for repeated measures, followed by Šídák's multiple comparisons test, $F_{(3, 36)} = 1.599$, $p > 0.05$ n. s., Aβ vs sham).

Effects of Aβ Administration on Social Memory

Here, we tested the effects of Aβ administration on social memory by carrying out the social recognition test. We found that sham rats reported a significant decrease in time spent sniffing and performing social interaction in the second exposition to a juvenile rats compared to first presentation, while no difference in both sniffing and social interaction between first and second encounter were retrieved in Aβ-treated rats (**Figure 2A**, Two-Way ANOVA for repeated measures followed by Šídák's multiple comparisons test, $F_{(1,12)} = 41.13$, $p < 0.0001$ sham T2 vs sham T1, **Figure 2B**, Two-Way ANOVA for repeated measures followed by Šídák's multiple comparisons test, $F_{(1,12)} = 18.85$, $p < 0.001$ sham T2 vs sham T1). In order to evaluate whether the results in time spent performing social exploration might depend from exploratory deficits, we scored total exploratory behaviours and we found no differences between trial 1 and trial 2 in both Aβ-treated and sham groups (**Figure 2C**, Two-Way ANOVA for repeated measures followed by Šídák's multiple comparisons test, $F_{(1,12)} = 1.109$, n. s sham T2 vs sham T1).

Effects of Aβ Administration on Hypothalamic Monoamines

In order to corroborate behavioural results with neurochemical analyses, we quantified NA, DA and 5-HT content in the hypothalamus. Our results show no difference in NA content between the two experimental groups (**Figure 3A**, Unpaired Student's t-test with Welch's correction, n. s., $\eta^2 = 0.005560$ Aβ vs sham), while DA was significantly increased in Aβ injected rats (**Figure 3B**, Unpaired Student's t-test with Welch's correction, $p < 0.01$ $\eta^2 = 0.7808$, Aβ vs sham). In addition, rats injected with Aβ showed a significant decrease in 5-HT levels (**Figure 3C**, Unpaired Student's t-test with Welch's correction, $p < 0.05$ $\eta^2 = 0.5795$, Aβ vs sham), while KYN levels were significantly increased (**Figure 3D**, Unpaired Student's t-test, $p < 0.001$ $\eta^2 = 0.7456$, Aβ vs sham) compared to controls.

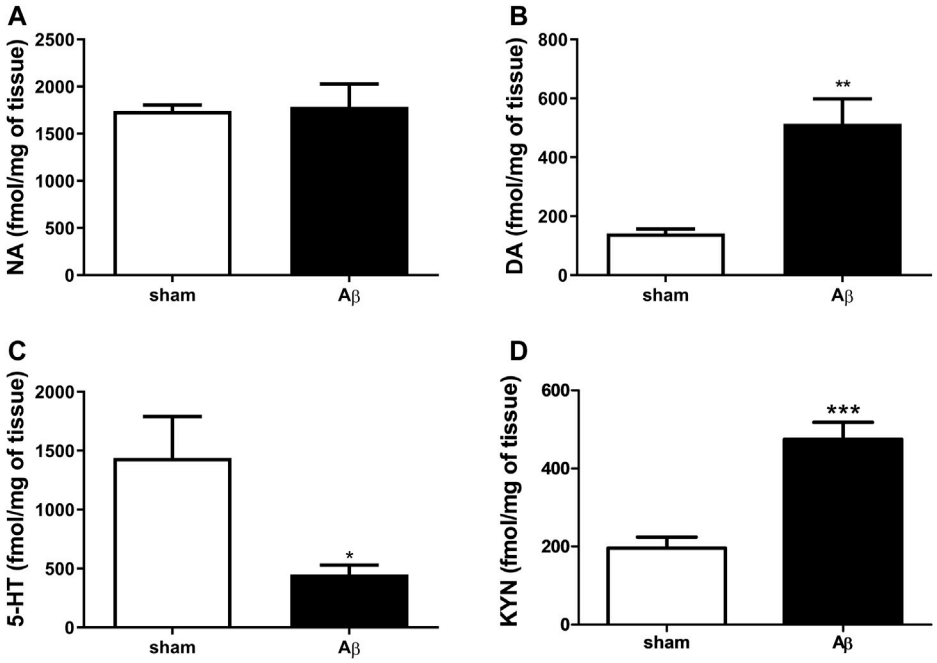

FIGURE 3 | Effects of Aβ administration on hypothalamic NA, DA and 5-HT levels. **(A)** NA (fmol/mg of tissue) in sham (n = 5) and Aβ-treated (n = 6) animals. Unpaired Student's t-test, $p > 0.05$. **(B)** DA (fmol/mg of tissue) in sham (n = 5) and Aβ-treated (n = 6) animals. Unpaired Student's t-test, $^{**}p < 0.01$ Aβ vs sham. **(C)** 5-HT (fmol/mg of tissue) in sham (n = 6) and Aβ-treated (n = 6) animals. Unpaired Student's t-test, $^{*}p < 0.05$ Aβ vs sham. **(D)** KYN (fmol/μl) in sham (n = 5) and Aβ-treated (n = 5) animals. Unpaired Student's t-test, $^{***}p < 0.001$ Aβ vs sham.

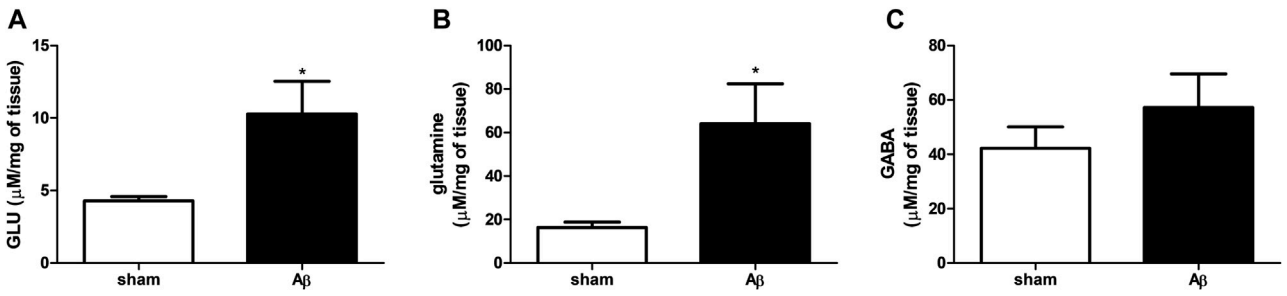

FIGURE 4 | Effects of Aβ administration on hypothalamic GLU, glutamine and GABA levels. **(A)** GLU (μM/mg of tissue) in sham (n = 5) and Aβ-treated (n = 6) animals. Unpaired Student's t-test, $^{*}p < 0.05$. **(B)** Glutamine (μM/mg of tissue) in sham (n = 5) and Aβ-treated (n = 6) animals. Unpaired Student's t-test, $^{*}p < 0.05$. **(C)** GABA (μM/mg of tissue) in sham (n = 5) and Aβ-treated (n = 6) animals. Unpaired Student's t-test, $p > 0.05$ Aβ vs sham.

Effects of Aβ Administration on Excitatory-Inhibitory Neurotransmission in the Hypothalamus

We evaluated the effect of Aβ administration on hypothalamic GLU, glutamine and GABA levels. We found an increase in GLU and glutamine contents in Aβ-treated rats (**Figures 4A,B**, Unpaired Student's t-test with Welch's correction, $\eta^2 = 0.5718$ and 0.5628, respectively, $p < 0.05$ Aβ vs sham). As regarding GABA quantifications, rats administrated with Aβ did not show any difference compared to sham rats (**Figure 4C**, Unpaired Student's t-test with Welch's correction, n. s. $\eta^2 = 0.1124$, Aβ vs sham).

Effects of Aβ Administration on Plasma 5-HT, 5-HT Turnover, KYN, MEL and Cys-C Levels

In **Figure 5**, peripheral alterations after Aβ injection have been determined. In particular, we measured 5-HT and its turnover in plasma samples of Aβ-injected and sham rats, together with KYN, MEL and Cys-C content. Concerning 5-HT, rats treated with Aβ showed a significant decrease in plasmatic levels compared to sham (**Figure 5A**, Unpaired Student's t-test with Welch's correction, $\eta^2 = 0.6862$, $p < 0.05$ Aβ vs sham). In addition, an increased 5-HT turnover was found in Aβ-treated rats compared

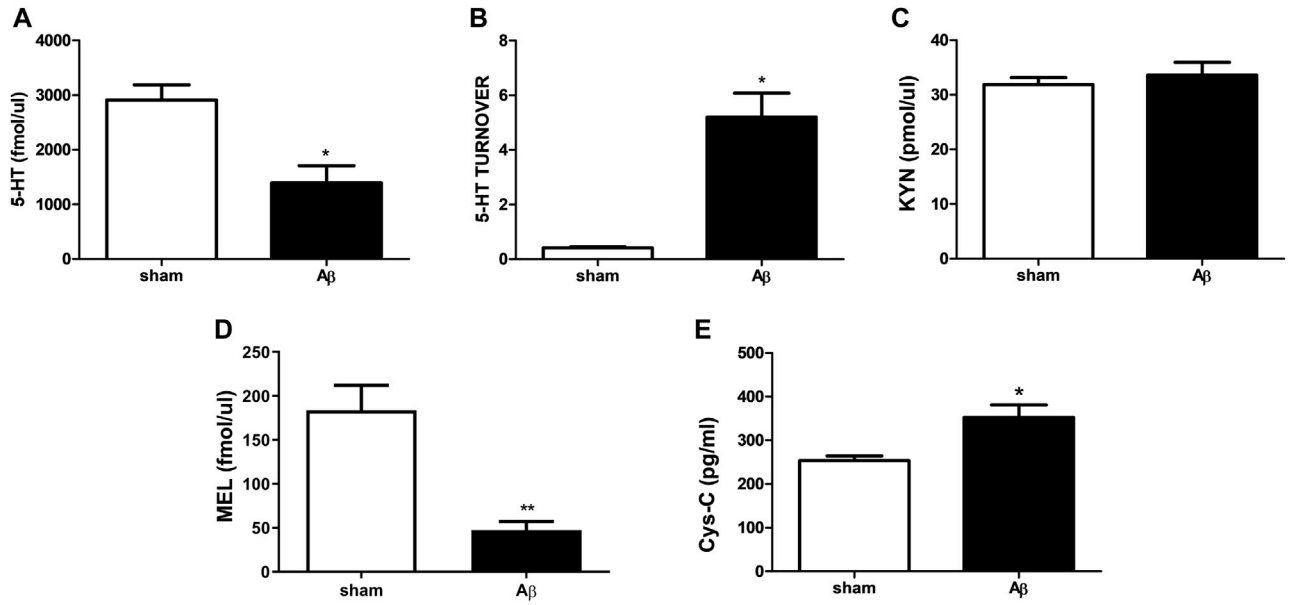

FIGURE 5 | Effects of Aβ administration on plasma 5-HT, 5-HT turnover, KYN, MEL and Cys-C levels. **(A)** 5-HT (fmol/μl) in sham (n = 4) and Aβ-treated (n = 4) animals. Unpaired Student's t-test, $^{*}p < 0.05$ Aβ vs sham. (B) 5-HT turnover in sham (n = 4) and Aβ-treated (n = 4) animals. Unpaired Student's t-test with Welch's correction, $^{*}p < 0.05$ Aβ vs sham. **(C)** KYN (pmol/μl) in sham (n = 5) and Aβ-treated (n = 5) animals. Unpaired Student's t-test, $p > 0.05$ Aβ vs sham. **(D)** MEL (fmol/μl) in sham (n = 5) and Aβ-treated (n = 5) animals. Unpaired Student's t-test, $^{**}p < 0.01$ Aβ vs sham. **(E)** Cys-C (pg/ml) in sham (n = 5) and Aβ-treated (n = 5) animals. Unpaired Student's t-test, $^{*}p < 0.05$ Aβ vs sham.

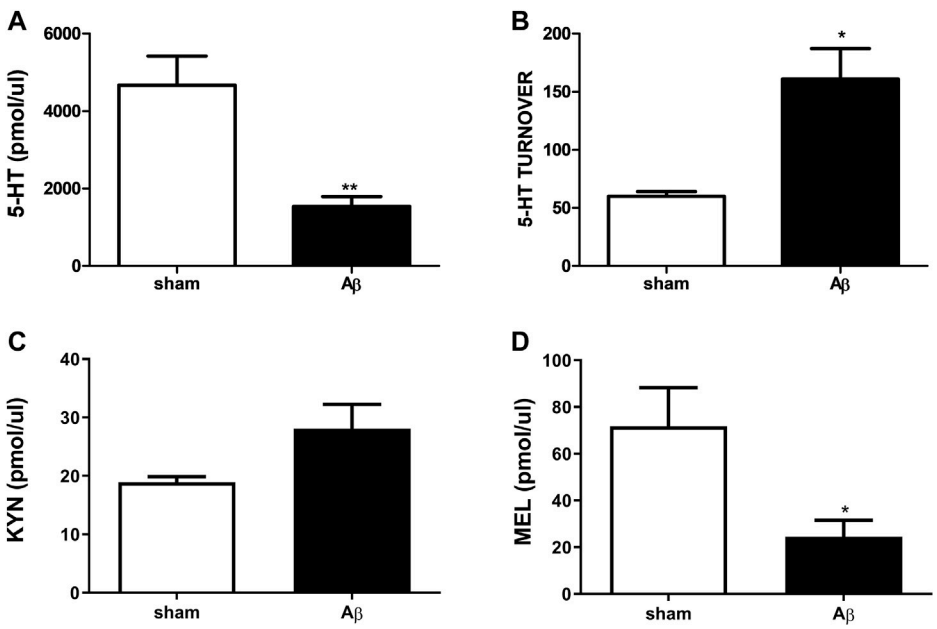

FIGURE 6 | Effects of Aβ administration on urinary 5-HT, 5-HT turnover, KYN and MEL. **(A)** 5-HT (pmol/μl) in sham (n = 4) and Aβ-treated (n = 4) animals. Unpaired Student's t-test, $^{**}p < 0.01$ Aβ vs sham. **(B)** 5-HT turnover in sham (n = 4) and Aβ-treated (n = 4) animals. Unpaired Student's t-test with Welch's correction, $^{*}p < 0.05$ Aβ vs sham. **(C)** KYN (pmol/μl) in sham (n = 5) and Aβ-treated (n = 5) animals. Unpaired Student's t-test, $p > 0.05$ Aβ vs sham. **(D)** MEL (pmol/μl) in sham (n = 5) and Aβ-treated (n = 5) animals. Unpaired Student's t-test, $^{*}p < 0.05$ Aβ vs sham.

to sham ones (**Figure 5B**, Unpaired Student's t-test with Welch's correction, $\eta^2 = 0.9085$, $p < 0.05$ Aβ vs sham). No difference was found between groups in KYN levels (**Figure 5C**, Unpaired Student's t-test, $\eta^2 = 0.03343$, $p > 0.05$ n. s.), while MEL was significantly reduced in Aβ-treated rats (**Figure 5D**, Unpaired Student's t-test, $\eta^2 = 0.7742$, $p < 0.01$ Aβ vs sham). As regarding plasma Cys-C content, our results reported a significant increase in animals administrated with Aβ compared to sham rats (**Figure 5E**, Unpaired Student's t-test, $\eta^2 = 0.5641$, $p < 0.05$ Aβ vs sham).

Effects of Aβ Administration on Urinary 5-HT, 5-HT Turnover, KYN, and MEL Levels

As shown in **Figure 6**, urinary concentrations of 5-HT and its turnover, KYN and MEL after Aβ or its vehicle injection were determined. Concerning 5-HT, rats treated with Aβ showed a significant decrease in its plasmatic levels compared to sham (**Figure 6A**, Unpaired Student's t-test with Welch's correction, $\eta^2 = 0.7247$, $p < 0.05$ Aβ vs sham). In addition, an increased 5-HT turnover was found in Aβ-treated rats compared to control (**Figure 6B**, Unpaired Student's t-test with Welch's correction, $\eta^2 = 0.8237$, $p < 0.05$ Aβ vs sham). No difference was found between groups in KYN levels (**Figure 6C**, Unpaired Student's t-test, $\eta^2 = 0.5078$, $p > 0.05$ n. s.), while MEL was significantly reduced in Aβ-treated rats (**Figure 6D**, Unpaired Student's t-test, $\eta^2 = 0.4647$, $p < 0.05$ Aβ vs sham).

DISCUSSION

In the present work, we aimed at evaluating if the rat model of Aβ-induced toxicity might represent a nonclinical model able to provide reliably probabilistic estimates of translation into human biology, according to the need of precision medicine.

Here, we demonstrated showed that in rats exposed to central administration of Aβ peptide, a rodent model we have previously shown validated useful for mimicking the symptomatology of early phase AD (Colaianna et al., 2010; Morgese et al., 2014), also showed impairment in social memory, along with reduced 5-HT content and enhanced GLU, DA and KYN at hypothalamic level. In addition, increased mechanonociception, but not thermal nociception, was evident after central Aβ administration.

This event might likely be due to increased inflammation caused by the peptide. Indeed, mechanonociception seems to be specifically dependent on phospholipase A2 (PLA2) activation, arachidonic acid release and production of pro-inflammatory cyclooxygenase (COX) derivatives (Meller, 1994). In keeping with this hypothesis, we have previously shown, in the same animal model, that the icv injection of Aβ peptide increased the expression of the inducible COX-2 enzyme (Mhillaj et al., 2018). Furthermore, it has been shown that expression of COX-2 as well as prostaglandin E2, can be enhanced after phosphorylation of MAPKs and NF-κB induced by oxidative stress (Onodera et al., 2015). In our experience, we have found that Aβ-induced toxicity is also occurring through the increased oxidative biomarker production and NF-κB expression (Morgese et al., 2021a; Morgese et al., 2021b), therefore we can speculate that alterations in oxidative and inflammatory status migh represent putative factors that predispose Aβ-treated rats to increased mechanical pain susceptibility.

Over the past few decades, a pivotal role for GLU in pain sensation and transmission has been increasingly proposed, and, in this regard, novel pain medications targeting this excitatory system are in the spotlight. Thus, the role played by supraspinal mGluRs to pain modulation, including the descending pain pathway that involves also the hypothalamus, is an emerging field of study (Pereira and Goudet, 2018). In this regard, it is well known that neural populations of the descending inhibitory pain pathway originate in the amygdala and in the hypothalamus and project to the spinal cord and other relevant areas (Rea et al., 2007). Glutamate and glutamatergic receptor activation in this area exerts a fine tune on the release of hypothalamic factors, including Substance P, crucial for pain chronicity (Zieglgansberger, 2019), and GABA. Thus, this model may be also suitable for the evaluation of novel drugs acting on these targets, future investigations are surely warranted.

Interestingly, hypothalamic dopaminergic tone was increased in Aβ-treated rats. Previous reports have evaluted hypothalamic-spinal dopaminergic system on pain modulation, however the role played by this neurotrasmitter in such a context has not been completely unravelled. Indeed, activation of DA receptors seems to differently interact with nociception and in particular, D2-like agonism has been linked to analgesia specific to mechanonociception, but not thermonociception (Almanza et al., 2015). It is worth to note that, in patients early diagnosed with AD, reduction of D2 receptors has been reported in brain areas associated with emotional control, such as the hippocampus, but also in brain areas deputed to control motor coordination such as the nigrostriatal pathways (Pan et al., 2019). Therefore, we can speculate that such an increase in DA can be related to reduced D2 receptors, leading to enhanced DA tone and higher D1 activation. On the other hand, Aβ has been shown to modulate the release of factors implicated in the response to stress, such as corticotropin releasing factor (CRF) (Lv et al., 2020). Elevated glucocorticoids can trigger dopamine release (Czyrak et al., 2003; Belujon and Grace, 2017), while GLU can induce CRF release (Herman et al., 2004). In addition, stress response is correlated with Aβ release and the peptide, in turn, controls HPA functioning (Morgese et al., 2017). In addition, along with the well defined decline of cognitive and emotional domains, also functions under hypothalamic control are dysfunctional in these patients, such as the disruption of circadian rhythms (Baloyannis et al., 2018). Indeed, reduced levels of MEL were identified at both plasma and urine in our model. This evaluation, in the light of individuating novel peripheral biomarkers useful for monitoring AD progression or efficacy of used AD

medications might represents a valid advantage also for the purpose of precision medicine. In particular, MEL is a multifunctional hormone involved not only in the regulation of circadian rhythm, but also with recognized anti-oxidant and anti-amyloidogenic (He et al., 2010) properties, proposed as a possible factor for contrasting AD progression (Hossain et al., 2019). Indeed, MEL has been suggested as an early biomarker for detecting the first stages of AD (Wu et al., 2003; Hossain et al., 2019). Furthermore, MEL was shown to suppressed NF-κB, an ubiquitary located transcriptional effector of inflammatory mediators, whose activation lead to higher prostaglandin and nitric oxide levels contributing to the development of hyperalgesia (Petho and Reeh, 2012). In this regard, we have very recently shown, in mice, that the icv injection of Aβ led to increased expression of this factor (Morgese et al., 2021b). In addition, MEL can prevent IL-6 release NF-κB-induced in Aβ-treated brain slices (Lau et al., 2012) and memory loss secondary to NF-κB activation (Shen et al., 2007). Pro-inflammatory biomarkers, such as cytokines, are able of modulating neuronal activity by promoting the release of neuroactive molecules from glia or the endothelium, including GLU (Vezzani and Viviani, 2015). Furthermore, chronic inflammation is able to decrease central 5-HT tone (Couch et al., 2013) also in condition of pseudoinflammation, an inflammatory state in absence of pathogens, associated with enhanced Aβ production and depressive-like behavior in rats (Morgese et al., 2020). Lower cerebral 5-HT levels leads to alteration in functioning of descending pain pathways, indicating that impairment in mood and emotions mediated by brainstem areas are important in determining the levels of pain. In particular, the emotional and autonomic aspects of nociceptive processing crucially implicated the parabrachial area. This important supraspinal target relays to the hypothalamus and amygdala, thus driving the descending modulatory pathways through the rostroventral medulla, resulting in a spino–bulbo–spinal loop. Indeed, the effectiveness of pain relievers depends on 5-HT levels and represents a mechanism whereby emotions can alter pain perception (Suzuki et al., 2004). As confirmation, pharmacological modulation that correspond to higher 5-HT tone has been shown to be useful for reverting pain-like behaviors in pertinent animal models (Bobinski et al., 2015). Indeed, in our model, we found that 5-HT was reduced in the hypothalamus of treated rats. Therefore, such different outcomes, retrieved in the behavioral paradigms used, might depend on the selective activation of glutamatergic and serotonergic pathways associated with inflammatory state. In this regard, it has been reported that inflammation (Tu et al., 2005), as well as increased corticosterone levels (Luo et al., 2017), can lead to enhaced metabolism of tryptophan toward KYN production at hypothalamic level. Moreover, it has been reported that KYN metabolites can directly act on GLU receptors, thus influencing excitatory neurotransmission and stimulating an increase in GLU release (Schwarcz, 2016). In addition, plasma and urinary content of 5-HT and 5-HT turnover were reduced in our model. This kind of alterations have been reported also in depressed patients (Mitani et al., 2006) and might represent a possible non invasive biomarkers for monitoring drug efficacy.

In keeping with this hypothesis, Aβ administration was able to alter other relevant biological peripheral parameters, such as Cys-C (Zhai et al., 2016), involved in both depression and AD (Sundelof et al., 2008; Minev et al., 2010). This molecule is a cysteine protease inhibitor, expressed either centrally (Lofberg and Grubb, 1979) or peripherally. This enzyme has been proposed as a biomarker of renal insufficiency and it has been shown to correlate with depressive symptoms in the elderly with normal renal function (Minev et al., 2010). Accordingly, a greater Cys-C levels were associated with an increased risk of new diagnosis of depression in subjects with normal renal function (Li H. et al., 2019). Furthermore, cognitive decline and AD are associated with renal impairment in human (Zhang et al., 2020) and in animal model of AD (Nakagawa et al., 2017). In further support of this evidence, it has been shown that Cys-C and Aβ peptide co-localize in brains of AD patients (Sastre et al., 2004) and polymorphisms of the Cys-C gene are associated with an increased risk for AD (Finckh et al., 2000; Chuo et al., 2007). Furthermore Cys-C levels directly correlate with cognitive impairment in the elderly (Yaffe et al., 2008). Our data are in line with these clinical evidences, considering that higher systemic Cys-C levels were found here and impairment of memory were previuosly shown in our model (Mhillaj et al., 2018). Cys-C was reported to be higher also in chronic pain patients and persistent pain can induce the synthesis and the release of Cys-C in dorsal spinal cord able to outflow to the brain (Mannes et al., 2003).

In conclusion, we found that in our model of depressive-like phenotype, induced by central administration of Aβ peptide, a state of enhanced pain perception was present. This increased susceptibility to mechanical pain was accompanied by impaired central and peripheral neurotransmission. In turn, also alterations in peripheral biomarkers, both linked to depression and AD, were evidenced. These outcomes also support the hypothesis that this animal model can be a suitable tool for investigating comorbid conditions associated with the early phase AD.

After a long search for new drugs for this condition, AD is still a fatal global epidemic. However, research in recent decades has focused its attention on the development of drugs capable of counteracting this complex pathology without seeking specific treatments for specific symptoms. This animal model could therefore result in a useful tool displaying some AD endophenotypes on which a targeted pharmacological strategy could be pursued in a tailored manner.

DATA AVAILABILITY STATEMENT

The raw data supporting the conclusion of this article will be made available by the authors, without undue reservation.

ETHICS STATEMENT

The animal study was reviewed and approved by The Italian Ministry of Health, experimental protocol B2EF8.18-aut.954-2017-PR.

AUTHOR CONTRIBUTIONS

MGM, LDCM, MB, SS, PT, CG and LT designed the research. MB, LDCM, SD, EM, VS, ALC, SS, PT and MGM performed the research. MB, PT, SS, LDCM, EM, VS, ALC and MGM analyzed the data. MGM, LCDM, MB, PT, CG, SS and LT wrote the manuscript. All authors revised and contributed to the article and approved the submitted version.

FUNDING

This research was funded by PRIN 2017 code 2017YZF7MA to LT from Italian Ministry of Education, University and Research (MIUR), PRIN 2017 code 2017AY8BP4 to SS from MIUR and Research for Innovation (REFIN) from Apulia Region code OE9C2692 to MB.

REFERENCES

Almanza, A., Simón-Arceo, K., Coffeen, U., Fuentes-García, R., Contreras, B., Pellicer, F., et al. (2015). A D2-like Receptor Family Agonist Produces Analgesia in Mechanonociception but Not in Thermonociception at the Spinal Cord Level in Rats. *Pharmacol. Biochem. Behav.* 137, 119–125. doi:10.1016/j.pbb.2015.08.013

Baloyannis, S. J., Mavroudis, I., Mitilineos, D., Baloyannis, I. S., and Costa, V. G. (2018). *The Hypothalamus in Alzheimer's Disease*. London, UK: IntechOpen, 76–97. doi:10.5772/intechopen.81475

Bao, A. M., and Swaab, D. F. (2019). The Human Hypothalamus in Mood Disorders: The HPA axis in the center. *IBRO Rep.* 6, 45–53. doi:10.1016/j.ibror.2018.11.008

Belujon, P., and Grace, A. A. (2017). Dopamine System Dysregulation in Major Depressive Disorders. *Int. J. Neuropsychopharmacol.* 20, 1036–1046. doi:10.1093/ijnp/pyx056

Blardi, P., De Lalla, A., Leo, A., Auteri, A., Iapichino, S., Di Muro, A., et al. (2002). Serotonin and Fluoxetine Levels in Plasma and Platelets after Fluoxetine Treatment in Depressive Patients. *J. Clin. Psychopharmacol.* 22, 131–136. doi:10.1097/00004714-200204000-00005

Bobinski, F., Ferreira, T. A. A., Córdova, M. M., Dombrowski, P. A., Da Cunha, C., Santo, C. C. D. E., et al. (2015). Role of Brainstem Serotonin in Analgesia Produced by Low-Intensity Exercise on Neuropathic Pain after Sciatic Nerve Injury in Mice. *Pain* 156, 2595–2606. doi:10.1097/j.pain.0000000000000372

Bove, M., Mhillaj, E., Tucci, P., Giardino, I., Schiavone, S., Morgese, M. G., et al. (2018). Effects of N-3 PUFA Enriched and N-3 PUFA Deficient Diets in Naïve and Aβ-Treated Female Rats. *Biochem. Pharmacol.* 155, 326–335. doi:10.1016/j.bcp.2018.07.017

Bushnell, M. C., Ceko, M., and Low, L. A. (2013). Cognitive and Emotional Control of Pain and its Disruption in Chronic Pain. *Nat. Rev. Neurosci.* 14, 502–511. doi:10.1038/nrn3516

Chuo, L. J., Sheu, W. H., Pai, M. C., and Kuo, Y. M. (2007). Genotype and Plasma Concentration of Cystatin C in Patients with Late-Onset Alzheimer Disease. *Dement Geriatr. Cogn. Disord.* 23, 251–257. doi:10.1159/000100021

Colaianna, M., Tucci, P., Zotti, M., Morgese, M. G., Schiavone, S., Govoni, S., et al. (2010). Soluble Beta Amyloid(1-42): a Critical Player in Producing Behavioural and Biochemical Changes Evoking Depressive-Related State? *Br. J. Pharmacol.* 159, 1704–1715. doi:10.1111/j.1476-5381.2010.00669.x

Couch, Y., Martin, C. J., Howarth, C., Raley, J., Khrapitchev, A. A., Stratford, M., et al. (2013). Systemic Inflammation Alters central 5-HT Function as Determined by Pharmacological MRI. *Neuroimage* 75, 177–186. doi:10.1016/j.neuroimage.2013.02.046

Cox, V. C., and Valenstein, E. S. (1965). Attenuation of Aversive Properties of Peripheral Shock by Hypothalamic Stimulation. *Science* 149, 323–325. doi:10.1126/science.149.3681.323

Czyrak, A., Maćkowiak, M., Chocyk, A., Fijał, K., and Wedzony, K. (2003). Role of Glucocorticoids in the Regulation of Dopaminergic Neurotransmission. *Pol. J. Pharmacol.* 55, 667–674.

Defrin, R., Amanzio, M., De Tommaso, M., Dimova, V., Filipovic, S., Finn, D. P., et al. (2015). Experimental Pain Processing in Individuals with Cognitive Impairment: Current State of the Science. *Pain* 156, 1396–1408. doi:10.1097/j.pain.0000000000000195

Deuis, J. R., Dvorakova, L. S., and Vetter, I. (2017). Methods Used to Evaluate Pain Behaviors in Rodents. *Front. Mol. Neurosci.* 10, 284. doi:10.3389/fnmol.2017.00284

Di Cesare Mannelli, L., Marcoli, M., Micheli, L., Zanardelli, M., Maura, G., Ghelardini, C., et al. (2015). Oxaliplatin Evokes P2X7-dependent Glutamate Release in the Cerebral Cortex: A Pain Mechanism Mediated by Pannexin 1. *Neuropharmacology* 97, 133–141. doi:10.1016/j.neuropharm.2015.05.037

Dowben, J. S., Grant, J. S., and Keltner, N. L. (2013). Ketamine as an Alternative Treatment for Treatment-Resistant Depression. *Perspect. Psychiatr. Care* 49, 2–4. doi:10.1111/ppc.12006

Ernberg, M., Voog, U., Alstergren, P., Lundeberg, T., and Kopp, S. (2000). Plasma and Serum Serotonin Levels and Their Relationship to Orofacial Pain and Anxiety in Fibromyalgia. *J. Orofac Pain* 14, 37–46.

Farhanchi, A., Karkhanei, B., Amani, N., Aghajanloo, M., Khanlarzadeh, E., and Emami, Z. (2018). Association of Serum Serotonin and Pain in Patients with Chronic Low Back Pain before and after Spinal Surgery. *Pain Res. Treat.* 2018, 4901242. doi:10.1155/2018/4901242

Ferrari, C., and Sorbi, S. (2021). The Complexity of Alzheimer's Disease: an Evolving Puzzle. *Physiol. Rev.* 101, 1047–1081. doi:10.1152/physrev.00015.2020

Finckh, U., Von Der Kammer, H., Velden, J., Michel, T., Andresen, B., Deng, A., et al. (2000). Genetic Association of a Cystatin C Gene Polymorphism with Late-Onset Alzheimer Disease. *Arch. Neurol.* 57, 1579–1583. doi:10.1001/archneur.57.11.1579

Findley, C. A., Bartke, A., Hascup, K. N., and Hascup, E. R. (2019). Amyloid Beta-Related Alterations to Glutamate Signaling Dynamics during Alzheimer's Disease Progression. *ASN Neuro* 11, 1759091419855541. doi:10.1177/1759091419855541

Hayley, S., and Litteljohn, D. (2013). Neuroplasticity and the Next Wave of Antidepressant Strategies. *Front Cel Neurosci* 7, 218. doi:10.3389/fncel.2013.00218

He, H., Dong, W., and Huang, F. (2010). Anti-amyloidogenic and Anti-apoptotic Role of Melatonin in Alzheimer Disease. *Curr. Neuropharmacol* 8, 211–217. doi:10.2174/157015910792246137

Herman, J. P., Mueller, N. K., and Figueiredo, H. (2004). Role of GABA and Glutamate Circuitry in Hypothalamo-Pituitary-Adrenocortical Stress Integration. *Ann. N. Y Acad. Sci.* 1018, 35–45. doi:10.1196/annals.1296.004

Holck, A., Wolkowitz, O. M., Mellon, S. H., Reus, V. I., Nelson, J. C., Westrin, Å., et al. (2019). Plasma Serotonin Levels Are Associated with Antidepressant Response to SSRIs. *J. Affect Disord.* 250, 65–70. doi:10.1016/j.jad.2019.02.063

Hossain, M. F., Uddin, M. S., Uddin, G. M. S., Sumsuzzman, D. M., Islam, M. S., Barreto, G. E., et al. (2019). Melatonin in Alzheimer's Disease: A Latent Endogenous Regulator of Neurogenesis to Mitigate Alzheimer's Neuropathology. *Mol. Neurobiol.* 56, 8255–8276. doi:10.1007/s12035-019-01660-3

Huang, Y., Huang, W., Wei, J., Yin, Z., and Liu, H. (2021). Increased Serum Cystatin C Levels Were Associated with Depressive Symptoms in Patients with Type 2 Diabetes. *Diabetes Metab. Syndr. Obes.* 14, 857–863. doi:10.2147/DMSO.S295088

Ishii, M., and Iadecola, C. (2015). Metabolic and Non-cognitive Manifestations of Alzheimer's Disease: The Hypothalamus as Both Culprit and Target of Pathology. *Cell Metab* 22, 761–776. doi:10.1016/j.cmet.2015.08.016

Kim, J. Y., Tillu, D. V., Quinn, T. L., Mejia, G. L., Shy, A., Asiedu, M. N., et al. (2015). Spinal Dopaminergic Projections Control the Transition to Pathological Pain Plasticity via a D1/D5-Mediated Mechanism. *J. Neurosci.* 35, 6307–6317. doi:10.1523/JNEUROSCI.3481-14.2015

Kumar, A. M., Sevush, S., Kumar, M., Ruiz, J., and Eisdorfer, C. (1995). Peripheral Serotonin in Alzheimer's Disease. *Neuropsychobiology* 32, 9–12. doi:10.1159/000119205

Lau, W. W., Ng, J. K., Lee, M. M., Chan, A. S., and Wong, Y. H. (2012). Interleukin-6 Autocrine Signaling Mediates Melatonin MT(1/2) Receptor-Induced STAT3 Tyr(705) Phosphorylation. *J. Pineal Res.* 52, 477–489. doi:10.1111/j.1600-079X.2011.00965.x

Lautenbacher, S., and Krieg, J. C. (1994). Pain Perception in Psychiatric Disorders: a Review of the Literature. *J. Psychiatr. Res.* 28, 109–122. doi:10.1016/0022-3956(94)90023-x

Li, C., Liu, S., Lu, X., and Tao, F. (2019a). Role of Descending Dopaminergic Pathways in Pain Modulation. *Curr. Neuropharmacol* 17, 1176–1182. doi:10.2174/1570159X17666190430102531

Li, H., Wang, A., Qi, G., Guo, J., Li, X., Wang, W., et al. (2019b). Cystatin C and Risk of New-Onset Depressive Symptoms Among Individuals with a normal Creatinine-Based Estimated Glomerular Filtration Rate: A Prospective Cohort Study. *Psychiatry Res.* 273, 75–81. doi:10.1016/j.psychres.2019.01.009

Li, J. X. (2015). Pain and Depression Comorbidity: a Preclinical Perspective. *Behav. Brain Res.* 276, 92–98. doi:10.1016/j.bbr.2014.04.042

Lin, L., Huang, Q. X., Yang, S. S., Chu, J., Wang, J. Z., and Tian, Q. (2013). Melatonin in Alzheimer's Disease. *Int. J. Mol. Sci.* 14, 14575–14593. doi:10.3390/ijms140714575

Löfberg, H., and Grubb, A. O. (1979). Quantitation of Gamma-Trace in Human Biological Fluids: Indications for Production in the central Nervous System. *Scand. J. Clin. Lab. Invest.* 39, 619–626. doi:10.3109/00365517909108866

Luo, G. Q., Liu, L., Gao, Q. W., Wu, X. N., Xiang, W., and Deng, W. T. (2017). Mangiferin Prevents Corticosterone-Induced Behavioural Deficits via Alleviation of Oxido-Nitrosative Stress and Down-Regulation of Indoleamine 2,3-dioxygenase (Ido) Activity. *Neurol. Res.* 39, 709–718. doi:10.1080/01616412.2017.1310705

Lv, J., Chen, L., Zhu, N., Sun, Y., Pan, J., Gao, J., et al. (2020). Beta Amyloid-Induced Time-dependent Learning and Memory Impairment: Involvement of HPA axis Dysfunction. *Metab. Brain Dis.* 35, 1385–1394. doi:10.1007/s11011-020-00613-3

Ma, J., Gao, Y., Jiang, L., Chao, F. L., Huang, W., Zhou, C. N., et al. (2017). Fluoxetine Attenuates the Impairment of Spatial Learning Ability and Prevents Neuron Loss in Middle-Aged APPswe/PSEN1dE9 Double Transgenic Alzheimer's Disease Mice. *Oncotarget* 8, 27676–27692. doi:10.18632/oncotarget.15398

Malejko, K., Huss, A., Schönfeldt-Lecuona, C., Braun, M., and Graf, H. (2020). Emotional Components of Pain Perception in Borderline Personality Disorder and Major Depression-A Repetitive Peripheral Magnetic Stimulation (rPMS) Study. *Brain Sci.* 10, 905. doi:10.3390/brainsci10120905

Mannes, A. J., Martin, B. M., Yang, H. Y., Keller, J. M., Lewin, S., Gaiser, R. R., et al. (2003). Cystatin C as a Cerebrospinal Fluid Biomarker for Pain in Humans. *Pain* 102, 251–256. doi:10.1016/s0304-3959(02)00403-7

Mathiasen, J. R., and Dicamillo, A. (2010). Social Recognition Assay in the Rat. *Curr. Protoc. Neurosci.* 8, Unit 8 5I. doi:10.1002/0471142301.ns0805is53

Meller, S. T. (1994). Thermal and Mechanical Hyperalgesia. *APS J.* 3, 215–231. doi:10.1016/s1058-9139(05)80269-4

Mhillaj, E., Morgese, M. G., Tucci, P., Furiano, A., Luongo, L., Bove, M., et al. (2018). Celecoxib Prevents Cognitive Impairment and Neuroinflammation in Soluble Amyloid β-treated Rats. *Neuroscience* 372, 58–73. doi:10.1016/j.neuroscience.2017.12.046

Minev, E., Unruh, M., Shlipak, M. G., Simsonick, E., Yaffe, K., Leak, T. S., et al. (2010). Association of Cystatin C and Depression in Healthy Elders: the Health, Aging and Body Composition Study. *Nephron Clin. Pract.* 116, c241–6. doi:10.1159/000317205

Mitani, H., Shirayama, Y., Yamada, T., and Kawahara, R. (2006). Plasma Levels of Homovanillic Acid, 5-hydroxyindoleacetic Acid and Cortisol, and Serotonin Turnover in Depressed Patients. *Prog. Neuropsychopharmacol. Biol. Psychiatry* 30, 531–534. doi:10.1016/j.pnpbp.2005.11.021

Morgese, M. G., Bove, M., Francavilla, M., Schiavone, S., Dimonte, S., Colia, A. L., et al. (2021a). Sublingual AKBA Exerts Antidepressant Effects in the Aβ-Treated Mouse Model. *Biomolecules* 11, 686. doi:10.3390/biom11050686

Morgese, M. G., Colaianna, M., Mhillaj, E., Zotti, M., Schiavone, S., D'antonio, P., et al. (2015). Soluble Beta Amyloid Evokes Alteration in Brain Norepinephrine Levels: Role of Nitric Oxide and Interleukin-1. *Front. Neurosci.* 9, 428. doi:10.3389/fnins.2015.00428

Morgese, M. G., Schiavone, S., Bove, M., Colia, A. L., Dimonte, S., Tucci, P., et al. (2021b). N-3 PUFA Prevent Oxidative Stress in a Rat Model of Beta-Amyloid-Induced Toxicity. *Pharmaceuticals (Basel)* 14, 339. doi:10.3390/ph14040339

Morgese, M. G., Schiavone, S., Bove, M., Mhillaj, E., Tucci, P., and Trabace, L. (2018). Sub-chronic Celecoxib Prevents Soluble Beta Amyloid-Induced Depressive-like Behaviour in Rats. *J. Affect Disord.* 238, 118–121. doi:10.1016/j.jad.2018.05.030

Morgese, M. G., Schiavone, S., Maffione, A. B., Tucci, P., and Trabace, L. (2020). Depressive-like Phenotype Evoked by Lifelong Nutritional omega-3 Deficiency in Female Rats: Crosstalk Among Kynurenine, Toll-like Receptors and Amyloid Beta Oligomers. *Brain Behav. Immun.* 87, 444–454. doi:10.1016/j.bbi.2020.01.015

Morgese, M. G., Schiavone, S., and Trabace, L. (2017). Emerging Role of Amyloid Beta in Stress Response: Implication for Depression and Diabetes. *Eur. J. Pharmacol.* 817, 22–29. doi:10.1016/j.ejphar.2017.08.031

Morgese, M. G., and Trabace, L. (2019). Monoaminergic System Modulation in Depression and Alzheimer's Disease: A New Standpoint? *Front. Pharmacol.* 10, 483. doi:10.3389/fphar.2019.00483

Morgese, M. G., Tucci, P., Colaianna, M., Zotti, M., Cuomo, V., Schiavone, S., et al. (2014). Modulatory Activity of Soluble Beta Amyloid on HPA axis Function in Rats. *Curr. Pharm. Des.* 20, 2539–2546. doi:10.2174/13816128113199990500

Moriarty, O., Mcguire, B. E., and Finn, D. P. (2011). The Effect of Pain on Cognitive Function: a Review of Clinical and Preclinical Research. *Prog. Neurobiol.* 93, 385–404. doi:10.1016/j.pneurobio.2011.01.002

Mura, E., Lanni, C., Preda, S., Pistoia, F., Sarà, M., Racchi, M., et al. (2010). Beta-amyloid: a Disease Target or a Synaptic Regulator Affecting Age-Related Neurotransmitter Changes? *Curr. Pharm. Des.* 16, 672–683. doi:10.2174/138161210790883723

Nakagawa, T., Hasegawa, Y., Uekawa, K., and Kim-Mitsuyama, S. (2017). Chronic Kidney Disease Accelerates Cognitive Impairment in a Mouse Model of Alzheimer's Disease, through Angiotensin II. *Exp. Gerontol.* 87, 108–112. doi:10.1016/j.exger.2016.11.012

Nous, A., Engelborghs, S., and Smolders, I. (2021). Melatonin Levels in the Alzheimer's Disease Continuum: a Systematic Review. *Alzheimers Res. Ther.* 13, 52. doi:10.1186/s13195-021-00788-6

Onodera, Y., Teramura, T., Takehara, T., Shigi, K., and Fukuda, K. (2015). Reactive Oxygen Species Induce Cox-2 Expression via TAK1 Activation in Synovial Fibroblast Cells. *FEBS Open Bio* 5, 492–501. doi:10.1016/j.fob.2015.06.001

Pacini, A., Micheli, L., Maresca, M., Branca, J. J. V., Mcintosh, J. M., Ghelardini, C., et al. (2016). The α9α10 Nicotinic Receptor Antagonist α-conotoxin RgIA Prevents Neuropathic Pain Induced by Oxaliplatin Treatment. *Exp. Neurol.* 282, 37–48. doi:10.1016/j.expneurol.2016.04.022

Pan, X., Kaminga, A. C., Wen, S. W., Wu, X., Acheampong, K., and Liu, A. (2019). Dopamine and Dopamine Receptors in Alzheimer's Disease: A Systematic Review and Network Meta-Analysis. *Front. Aging Neurosci.* 11, 175. doi:10.3389/fnagi.2019.00175

Paredes, S., Cantillo, S., Candido, K. D., and Knezevic, N. N. (2019). An Association of Serotonin with Pain Disorders and its Modulation by Estrogens. *Int. J. Mol. Sci.* 20, 5729. doi:10.3390/ijms20225729

Paul-Savoie, E., Potvin, S., Daigle, K., Normand, E., Corbin, J. F., Gagnon, R., et al. (2011). A Deficit in Peripheral Serotonin Levels in Major Depressive Disorder but Not in Chronic Widespread Pain. *Clin. J. Pain* 27, 529–534. doi:10.1097/AJP.0b013e31820dfede

Paxinos, G. W. (1986). *The Rat Brain in Stereotaxic Coordinates*. Netherlands: Elsevier, Amsterdam.

Pereira, V., and Goudet, C. (2018). Emerging Trends in Pain Modulation by Metabotropic Glutamate Receptors. *Front. Mol. Neurosci.* 11, 464. doi:10.3389/fnmol.2018.00464

Petho, G., and Reeh, P. W. (2012). Sensory and Signaling Mechanisms of Bradykinin, Eicosanoids, Platelet-Activating Factor, and Nitric Oxide in Peripheral Nociceptors. *Physiol. Rev.* 92, 1699–1775. doi:10.1152/physrev.00048.2010

Pomara, N., and Sidtis, J. J. (2010). Brain Neurotoxic Amyloid-Beta Peptides: Their Potential Role in the Pathophysiology of Depression and as Molecular Therapeutic Targets. *Br. J. Pharmacol.* 161, 768–770. doi:10.1111/j.1476-5381.2010.00948.x

Preda, S., Govoni, S., Lanni, C., Racchi, M., Mura, E., Grilli, M., et al. (2008). Acute Beta-Amyloid Administration Disrupts the Cholinergic Control of Dopamine Release in the Nucleus Accumbens. *Neuropsychopharmacology* 33, 1062–1070. doi:10.1038/sj.npp.1301485

Puopolo, M. (2019). The Hypothalamic-Spinal Dopaminergic System: a Target for Pain Modulation. *Neural Regen. Res.* 14, 925–930. doi:10.4103/1673-5374.250567

Rea, K., Roche, M., and Finn, D. P. (2007). Supraspinal Modulation of Pain by Cannabinoids: the Role of GABA and Glutamate. *Br. J. Pharmacol.* 152, 633–648. doi:10.1038/sj.bjp.0707440

Rosales-Corral, S. A., Acuña-Castroviejo, D., Coto-Montes, A., Boga, J. A., Manchester, L. C., Fuentes-Broto, L., et al. (2012). Alzheimer's Disease: Pathological Mechanisms and the Beneficial Role of Melatonin. *J. Pineal Res.* 52, 167–202. doi:10.1111/j.1600-079X.2011.00937.x

Sastre, M., Calero, M., Pawlik, M., Mathews, P. M., Kumar, A., Danilov, V., et al. (2004). Binding of Cystatin C to Alzheimer's Amyloid Beta Inhibits *In Vitro* Amyloid Fibril Formation. *Neurobiol. Aging* 25, 1033–1043. doi:10.1016/j.neurobiolaging.2003.11.006

Savaskan, E., Ayoub, M. A., Ravid, R., Angeloni, D., Fraschini, F., Meier, F., et al. (2005). Reduced Hippocampal MT2 Melatonin Receptor Expression in Alzheimer's Disease. *J. Pineal Res.* 38, 10–16. doi:10.1111/j.1600-079X.2004.00169.x

Schiavone, S., Tucci, P., Mhillaj, E., Bove, M., Trabace, L., and Morgese, M. G. (2017). Antidepressant Drugs for Beta Amyloid-Induced Depression: A New Standpoint? *Prog. Neuropsychopharmacol. Biol. Psychiatry* 78, 114–122. doi:10.1016/j.pnpbp.2017.05.004

Schwarcz, R. (2016). Kynurenines and Glutamate: Multiple Links and Therapeutic Implications. *Adv. Pharmacol.* 76, 13–37. doi:10.1016/bs.apha.2016.01.005

Shen, Y., Zhang, G., Liu, L., and Xu, S. (2007). Suppressive Effects of Melatonin on Amyloid-Beta-Induced Glial Activation in Rat hippocampus. *Arch. Med. Res.* 38, 284–290. doi:10.1016/j.arcmed.2006.10.007

Sun, Y., Drevets, W., Turecki, G., and Li, Q. S. (2020). The Relationship between Plasma Serotonin and Kynurenine Pathway Metabolite Levels and the Treatment Response to Escitalopram and Desvenlafaxine. *Brain Behav. Immun.* 87, 404–412. doi:10.1016/j.bbi.2020.01.011

Sundelöf, J., Arnlöv, J., Ingelsson, E., Sundström, J., Basu, S., Zethelius, B., et al. (2008). Serum Cystatin C and the Risk of Alzheimer Disease in Elderly Men. *Neurology* 71, 1072–1079. doi:10.1212/01.wnl.0000326894.40353.93

Suzuki, R., Rygh, L. J., and Dickenson, A. H. (2004). Bad News from the Brain: Descending 5-HT Pathways that Control Spinal Pain Processing. *Trends Pharmacol. Sci.* 25, 613–617. doi:10.1016/j.tips.2004.10.002

Thompson, T., Correll, C. U., Gallop, K., Vancampfort, D., and Stubbs, B. (2016). Is Pain Perception Altered in People with Depression? A Systematic Review and Meta-Analysis of Experimental Pain Research. *J. Pain* 17, 1257–1272. doi:10.1016/j.jpain.2016.08.007

Torta, R. G., and Munari, J. (2010). Symptom Cluster: Depression and Pain. *Surg. Oncol.* 19, 155–159. doi:10.1016/j.suronc.2009.11.007

Trabace, L., Kendrick, K. M., Castrignanò, S., Colaianna, M., De Giorgi, A., Schiavone, S., et al. (2007). Soluble Amyloid Beta1-42 Reduces Dopamine Levels in Rat Prefrontal Cortex: Relationship to Nitric Oxide. *Neuroscience* 147, 652–663. doi:10.1016/j.neuroscience.2007.04.056

Tu, H., Rady, P. L., Juelich, T., Smith, E. M., Tyring, S. K., and Hughes, T. K. (2005). Cytokine Regulation of Tryptophan Metabolism in the Hypothalamic-Pituitary-Adrenal (HPA) axis: Implications for Protective and Toxic Consequences in Neuroendocrine Regulation. *Cell Mol Neurobiol* 25, 673–680. doi:10.1007/s10571-005-4007-1

Tucci, P., Mhillaj, E., Morgese, M. G., Colaianna, M., Zotti, M., Schiavone, S., et al. (2014). Memantine Prevents Memory Consolidation Failure Induced by Soluble Beta Amyloid in Rats. *Front. Behav. Neurosci.* 8, 332. doi:10.3389/fnbeh.2014.00332

Vercruysse, P., Vieau, D., Blum, D., Petersén, Å., and Dupuis, L. (2018). Hypothalamic Alterations in Neurodegenerative Diseases and Their Relation to Abnormal Energy Metabolism. *Front. Mol. Neurosci.* 11, 2. doi:10.3389/fnmol.2018.00002

Vezzani, A., and Viviani, B. (2015). Neuromodulatory Properties of Inflammatory Cytokines and Their Impact on Neuronal Excitability. *Neuropharmacology* 96, 70–82. doi:10.1016/j.neuropharm.2014.10.027

Wood, P. B. (2008). Role of central Dopamine in Pain and Analgesia. *Expert Rev. Neurother* 8, 781–797. doi:10.1586/14737175.8.5.781

Wu, J., Khan, G. M., and Nichols, R. A. (2007). Dopamine Release in Prefrontal Cortex in Response to Beta-Amyloid Activation of Alpha7 * Nicotinic Receptors. *Brain Res.* 1182, 82–89. doi:10.1016/j.brainres.2007.08.079

Wu, Y. H., Feenstra, M. G., Zhou, J. N., Liu, R. Y., Toranõ, J. S., Van Kan, H. J., et al. (2003). Molecular Changes Underlying Reduced Pineal Melatonin Levels in Alzheimer Disease: Alterations in Preclinical and Clinical Stages. *J. Clin. Endocrinol. Metab.* 88, 5898–5906. doi:10.1210/jc.2003-030833

Xie, Y., Liu, P. P., Lian, Y. J., Liu, H. B., and Kang, J. S. (2019). The Effect of Selective Serotonin Reuptake Inhibitors on Cognitive Function in Patients with Alzheimer's Disease and Vascular Dementia: Focusing on Fluoxetine with Long Follow-Up Periods. *Signal. Transduct Target. Ther.* 4, 30. doi:10.1038/s41392-019-0064-7

Yaffe, K., Lindquist, K., Shlipak, M. G., Simonsick, E., Fried, L., Rosano, C., et al. (2008). Cystatin C as a Marker of Cognitive Function in Elders: Findings from the Health ABC Study. *Ann. Neurol.* 63, 798–802. doi:10.1002/ana.21383

Yang, S., and Chang, M. C. (2019). Chronic Pain: Structural and Functional Changes in Brain Structures and Associated Negative Affective States. *Int. J. Mol. Sci.* 20, 3130. doi:10.3390/ijms20133130

Zeng, Q., Huang, Z., Wei, L., Fang, J., and Lin, K. (2019). Correlations of Serum Cystatin C Level and Gene Polymorphism with Vascular Cognitive Impairment after Acute Cerebral Infarction. *Neurol. Sci.* 40, 1049–1054. doi:10.1007/s10072-019-03777-8

Zhai, J. L., Ge, N., Zhen, Y., Zhao, Q., and Liu, C. (2016). Corticosteroids Significantly Increase Serum Cystatin C Concentration without Affecting Renal Function in Symptomatic Heart Failure. *Clin. Lab.* 62, 203–207. doi:10.7754/clin.lab.2015.150701

Zhang, C. Y., He, F. F., Su, H., Zhang, C., and Meng, X. F. (2020). Association between Chronic Kidney Disease and Alzheimer's Disease: an Update. *Metab. Brain Dis.* 35, 883–894. doi:10.1007/s11011-020-00561-y

Zieglgänsberger, W. (2019). Substance P and Pain Chronicity. *Cell Tissue Res* 375, 227–241. doi:10.1007/s00441-018-2922-y

Zotti, M., Colaianna, M., Morgese, M. G., Tucci, P., Schiavone, S., Avato, P., et al. (2013). Carvacrol: from Ancient Flavoring to Neuromodulatory Agent. *Molecules* 18, 6161–6172. doi:10.3390/molecules18066161

Conflict of Interest: The authors declare that the research was conducted in the absence of any commercial or financial relationships that could be construed as a potential conflict of interest.

Publisher's Note: All claims expressed in this article are solely those of the authors and do not necessarily represent those of their affiliated organizations, or those of the publisher, the editors and the reviewers. Any product that may be evaluated in this article, or claim that may be made by its manufacturer, is not guaranteed or endorsed by the publisher.

Copyright © 2022 Morgese, Bove, Di Cesare Mannelli, Schiavone, Colia, Dimonte, Mhillaj, Sikora, Tucci, Ghelardini and Trabace. This is an open-access article distributed under the terms of the Creative Commons Attribution License (CC BY). The use, distribution or reproduction in other forums is permitted, provided the original author(s) and the copyright owner(s) are credited and that the original publication in this journal is cited, in accordance with accepted academic practice. No use, distribution or reproduction is permitted which does not comply with these terms.

frontiers in Pharmacology

ORIGINAL RESEARCH
published: 02 February 2022
doi: 10.3389/fphar.2022.763678

Blimp-1 Upregulation by Multiple Ligands *via* EGFR Transactivation Inhibits Cell Migration in Keratinocytes and Squamous Cell Carcinoma

Hyemin Lee[1†], *Duen-Yi Huang*[1†], *Hua-Ching Chang*[1,2], *Chia-Yee Lin*[1], *Wan-Yu Ren*[1], *Yang-Shia Dai*[3] *and Wan-Wan Lin*[1,4,5*]

[1]Department of Pharmacology, College of Medicine, National Taiwan University, Taipei, Taiwan, [2]Department of Dermatology, Taipei Medical University Hospital, Taipei, Taiwan, [3]Department of Dermatology, National Taiwan University Hospital, Taipei, Taiwan, [4]Department and Graduate Institute of Pharmacology, National Defense Medical Center, Taipei, Taiwan, [5]Graduate Institute of Medical Sciences, Taipei Medical University, Taipei, Taiwan

OPEN ACCESS

Edited by:
Salvatore Salomone,
University of Catania, Italy

Reviewed by:
Sun Jung Kim,
Northwell Health, United States
Xiaobo Wang,
UMR5088 Laboratoire de Biologie Cellulaire et Moléculaire du Contrôle de la Prolifération (LBCMCP), France

***Correspondence:**
Wan-Wan Lin
wwllaura1119@ntu.edu.tw

[†]These authors have contributed equally to this work

Specialty section:
This article was submitted to Experimental Pharmacology and Drug Discovery, a section of the journal Frontiers in Pharmacology

Received: 24 August 2021
Accepted: 07 January 2022
Published: 02 February 2022

Citation:
Lee H, Huang D-Y, Chang H-C, Lin C-Y, Ren W-Y, Dai Y-S and Lin W-W (2022) Blimp-1 Upregulation by Multiple Ligands via EGFR Transactivation Inhibits Cell Migration in Keratinocytes and Squamous Cell Carcinoma. Front. Pharmacol. 13:763678. doi: 10.3389/fphar.2022.763678

B lymphocyte-induced maturation protein-1 (Blimp-1) is a transcriptional repressor and plays a crucial role in the regulation of development and functions of various immune cells. Currently, there is limited understanding about the regulation of Blimp-1 expression and cellular functions in keratinocytes and cancer cells. Previously we demonstrated that EGF can upregulate Blimp-1 gene expression in keratinocytes, playing a negative role in regulation of cell migration and inflammation. Because it remains unclear if Blimp-1 can be regulated by other stimuli beyond EGF, here we further investigated multiple stimuli for their regulation of Blimp-1 expression in keratinocytes and squamous cell carcinoma (SCC). We found that PMA, TNF-α, LPS, polyIC, H_2O_2 and UVB can upregulate the protein and/or mRNA levels of Blimp-1 in HaCaT and SCC cells. Concomitant EGFR activation was observed by these stimuli, and EGFR inhibitor gefitinib and Syk inhibitor can block Blimp-1 gene expression caused by PMA. Reporter assay of Blimp-1 promoter activity further indicated the involvement of AP-1 in PMA-, TNF-α-, LPS- and EGF-elicited Blimp-1 mRNA expression. Confocal microscopic data indicated the nuclear loclization of Blimp-1, and such localization was not changed by stimuli. Moreover, Blimp-1 silencing enhanced SCC cell migration. Taken together, Blimp-1 can be transcriptionally upregulated by several stimuli in keratinocytes and SCC via EGFR transactivation and AP-1 pathway. These include growth factor PMA, cytokine TNF-α, TLR ligands (LPS and polyIC), and ROS insults (H_2O_2 and UVB). The function of Blimp-1 as a negative regulator of cell migration in SCC can provide a new therapeutic target in SCC.

Keywords: EGFR transactivation, keratinocytes, squamous cell carcinoma, migration, Blimp-1

Abbreviations: Blimp-1, B lymphocyte-induced maturation protein-1; EGF, epidermal growth factor; EGFR, EGF receptor; PMA, phorbol 12-myristate 13-acetate; Q-PCR, quantitative polymerase chain reaction; RIPA, radioimmunoprecipitation assay; ROS, reactive oxygen species; SCC, squamous cell carcinoma; TNF-α, tumor necrotic factor-α.

INTRODUCTION

B lymphocyte-induced maturation protein-1 (Blimp-1) encoded by the *PRDM1* gene is a member of PRDM family. Blimp-1 is a transcriptional repressor that can regulate cell growth and differentiation. Blimp-1 lacks intrinsic histone methyltransferase activity and serves as a scaffold to epigenetically modulate DNA binding, gene silencing and chromatin reorganization (Bikoff et al., 2009; Minnich et al., 2016). Blimp-1 is a well-known master regulator required for the differentiation and function of hematopoietic lineages like B lymphocytes (Chang et al., 2000; Martins and Calame, 2008; Wang et al., 2019), T lymphocytes (Martins and Calame, 2008; Jain et al., 2016; Fu et al., 2017), dendritic cells (Chan et al., 2009), macrophages (Chang et al., 2000), and granulocytes (Chang et al., 2000). Accordingly Blimp-1 is critical in maintenance of immune homeostasis, and deficiency of Blimp-1 function may contribute to autoimmune disorders (Fu et al., 2017) and inflammation (Chiang et al., 2013).

Several studies have demonstrated the pathways to regulate Blimp-1 expression, in particular in lymphocytes. In this context, IL-21 and IL-23 which are crucial for lymphocytes differentiation and functions have been demonstrated to induce Blimp-1 expression (Ozaki et al., 2004; Jain et al., 2016). In lymphocytes, Blimp-1 expression is controlled by multiple transcriptional factors including AP-1, IRF4, STAT3, STAT5, NF-κB, FOXP3, and NFAT (Calame, 2008; Martins and Calame, 2008), and is also regulated by histone deacetylation (Tanaka et al., 2016). Study indicates that TGF-β acts as a suppressor of Blimp-1 expression during Th17 differentiation (Salehi et al., 2012). In contrast, in breast cancer cells TGF-β1 induces Blimp-1 expression via a c-Raf/ERK/AP-1 pathway and Blimp-1 mediates TGF-β-induced EMT *via* repression of BMP-5 (Romagnoli et al., 2012). On the other hands, TGF-β can induce Blimp-1 expression via Wnt/β-catenin signaling in fibroblasts (Magnusdottir et al., 2007). In addition, in macrophages and B lymphocytes Blimp-1 is a target of unfolded protein response and can be induced by PERK signaling pathway (Doody et al., 2006). Apart from transcription, Blimp-1 can be degraded by proteasome when it undergoes SUMOylation (Shimshon et al., 2011). Besides proteasomal degradation, Blimp-1 can undergo lysosomal degradation in keratinocytes (Chang et al., 2018).

Besides immune cells, Blimp-1 plays various roles in skin biology. Conditional Blimp-1 knockout in skin impedes terminal cornification (Magnusdottir et al., 2007), revealing crucial functions of Blimp-1 in skin homeostasis. Mice specifically lacking Blimp-1 in keratinocytes spontaneously develop neutrophils-predominant skin inflammation (Chiang et al., 2013). Furthermore, our study indicates that activation of EGFR can upregulate the Blimp-1 gene transcription *via* the PKC, p38, and ERK pathways in keratinocytes (Chang et al., 2018). Reciprocally the expression of Blimp-1 in keratinocytes exerts a negative role in EGF-induced inflammation and migration, and in turn controls keratinocyte differentiation via regulation of gene expression (Chang et al., 2018).

Given that Blimp-1 is involved in skin biology and can be induced by EGF and PMA in human keratinocytes (Chang et al., 2018), we were interested to further explore the regulation and function of Blimp-1 in keratinocytes and squamous cell carcinoma (SCC). Therefore, we examined several stimuli besides EGF and attempted to understand their regulation depending on EGFR activation or not. The tested stimuli included tumor promoter PMA, inflammatory response activators TNF-α and TLR ligands, and stressors H_2O_2 and UVB. The reasons we chose these agents are due to their functions in keratinocytes biology and skin disorders, in particular relating to EGFR activation which is the major growth factor to control keratinocyte biology (Nanba et al., 2013). PKC-dependent activation by phorbol ester PMA has been implicated in the regulation of keratinocyte differentiation and skin tumor formation, which in part depend on the EGFR activation (Snoek et al., 1987; Ando et al., 1993). TNF-α, a key cytokine in inflammatory skin disease, also has been shown to induce EGFR activation in keratinocytes (Segawa et al., 2018). TLRs, the major pattern recognition receptors for host defense, are expressed in keratinocytes (Lebre et al., 2007). On the other hands, UVB and reactive oxygen species (ROS) can lead to DNA damage-associated EGFR transactivation and inflammation in keratinocyte (Chiu et al., 2021). Moreover, the role of Blimp-1 in cell migration of keratinocytes and SCC was addressed.

MATERIALS AND METHODS

Reagents

DMEM (high glucose; Cat. No. 12100-046) and trypsin-EDTA were from Gibco (Carlsbad, CA, United States). FBS was from HyClone (Logan, UT, United States). Penicillin-streptomycin solution and penicillin-streptomycin-amphotericin B solution were from Biological Industries (Kibbutz Beit Haemek, Israel). Poly (I:C) was from InvivoGen (San Diego, CA, United States). TNF-α was from Biolegend (San Diego, CA, United States). PMA, PBS, mitomycin C, LPS, and H_2O_2 were from Sigma-Aldrich (St. Louis, MO, United States). Gefitinib was from Selleckchem (Houston, TX, United States). Recombinant human EGF was from PeproTech (Rocky Hill, NJ, United States). Blimp-1 (#9115), p-EGFR (Y1068, #2234) and Syk (#2712) antibodies were from Cell Signaling (Beverly, MA, United States). EGFR antibody (sc-03) was from Santa Cruz (Santa Cruz, CA, United States). p-Syk antibody (PK1010) was from Millipore (Burlington, Ma, United States).

Cell Culture

Human immortalized HaCaT keratinocytes, oral SCC Cal-27 and SAS cells were cultured in high glucose Dulbecco's modified Eagle's medium (DMEM) supplemented with 10% FBS and 1% penicillin-streptomycin-amphotericin B. NHEKs (normal human epidermal keratinocytes) were obtained from normal adult human foreskin and isolated as described previously (Chiu et al., 2021). The experiments were conducted according to the Declaration of Helsinki principles and approved by the Ethics Committee of Mackay Memorial Hospital (Institutional Review Board codes 19MMHIS173e). All cell lines were

incubated at 37°C under a humidified atmosphere of 5% CO_2 in air. HaCaT and SCC cell lines were seeded in 6-well or 12-well tissue culture plates at a density of 8×10^4 cells/well.

Generation of Knockdown Cells Using Lentiviral shRNAs

In construction of stable short hairpin RNA (shRNA) knockdown cell lines, lentiviral particles encoding shRNA targeting human *PRDM1* (Sigma-Aldrich, St. Louis, MO, United States) were used for transfection. Lentivirus-containing supernatants were harvested 24 h after transfection, filtered using a 0.45 μm filter, and diluted with fresh culture media to transduce target cells in the presence of 8 μg/ml PolyBrene (hexadimethrinebromide). Transduced cells were selected with puromycin (3 μg/ml) (Thermo Fisher Scientific, Waltham, MA, United States) for 2 weeks to select successful transfection.

Immunoblotting

Cells were lysed by adding radioimmunoprecipitation assay (RIPA) buffer. The extracts were sonicated for 10-15 sec to complete cell lysis and shear DNA, and then centrifuged at 16,200 g, 4°C for 30 min. The protein concentrations of the supernatants were determined using the Bio-Rad protein assay. Equal amounts of the protein were loaded and electrophoresed on 8–15% SDS-PAGE, and then electro-transferred to Immobilon-P (0.45 μm PVDF; Millipore). After transfer, the membrane was blocked with Tris-buffered saline with Tween 20 (TBST) containing 5% (w/v) nonfat dry milk for 1 h at room temperature. After incubation with the primary antibodies (at the appropriate dilution as recommended in the product data sheet) with gentle agitation overnight at 4°C, the membranes were washed with TBST for three times and incubated with horseradish-peroxidase-linked secondary antibodies with gentle agitation for 1 h at room temperature. After washing with TBST for three times, the protein bands were detected on X-ray film with ECL reagents.

Quantitative Polymerase Chain Reaction

After stimulation, cells were harvested with TriPure isolation reagent (Roche Diagnostics, Indianapolis, IN, United States) and RNA was extracted according to the manufacturer's procedure. Total RNA (1–2 μg) was converted into cDNA by reverse transcription system kit (Promega, Heidelberg, Germany). Q-PCR was performed using FastStart SYBR Green Master (Roche Diagnostics, Indianapolis, IN, United States) in 96-well plates, and determined using ABI Prism 7900 (Applied Biosystems, Oakland, CA, United States). The primers used for human *RPDM1* were 5′-CGAAATGCCCTTCTACCCT-3′ and 5′-GCGTTCAAGTAAGCGTAGGA-3′ and the primers used for human *β-actin* were 5′-AGGAAGGCTGGAAGAGTG C-3′ and 5′-CGGGGACCTGACTGACTACC-3'.

Wound Healing Assay

Cells were seeded (4×10^4 cm^2) into 12-well culture-insert purchased from ibidi (Martinsried, Germany). After attachment, the culture-insert was gently removed from each well, and the well was washed three times with PBS to remove the suspended cells. Before adding the drugs, the cells were incubated with anti-proliferative agent mitomycin C (5 μg/ml) for 30 min. Finally, cells were incubated in medium in the absence or presence of PMA (30 nM) or TNF-α (10 ng/ml) in HaCaT cells, and TNF-α (10 ng/ml) or EGF (50 ng/ml) in SCC. The process was recorded by photographs, and cell migration was quantified.

Luciferase Assay

Blimp-(wt) and Blimp-(AP1 mt) report constructs (human Blimp-1 promoter in pGL3-basic) were gifts from Alexander Dent (Addgene plasmid # 40340 and #40341). Following the commercial standard protocol, HaCaT cells were transfected with Blimp-1 reporter plasmid and β-galactosidase expression vector by using Lipofectamine 2000 reagent (Invitrogen) and then EGF (50 ng/ml) was treated for 24 h. After harvest, the luciferase activity was determined by luciferase assay system kit (Promega, Heidelberg, Germany), followed by microplate luminometer. Luciferase activity was normalized with activity of β-galactosidase, and expressed as fold of control without stimulus treatment.

Confocal Microscopy

HaCaT, Cal-27, and SAS cells in full serum DMEM medium were fixed with 4% paraformaldehyde and permeabilized with 0.2% Triton X-100 in PBS for 20 min. After this process, the samples were blocked with 4% BSA for 1 h and incubated with primary antibody for 2 h at room temperature or overnight at 4°C after aspiration of blocking solution. The primary antibody was then discarded and cells were washed three times with PBS. The samples were incubated with fluorochrome-conjugated secondary antibody for 1 h in the dark afterwards. Following immunostaining process, the coverslip was counterstained with 4′6-diamidino-2-phenylindole (DAPI), and mounted on microscope slides in dark. Samples were analyzed by LSM 880 confocal microscope (Zeiss).

Statistical Analysis

Values were expressed as the mean ± S.E.M. of at least three independent experiments. Student's t-test or one-way ANOVA was performed to analyze the statistical significance of the differences, and the P value <0.05 was considered statistically significant.

RESULTS

PMA, TNF-α, LPS, UVB, and H_2O_2 Upregulate Blimp-1 Expression and Activate EGFR in HaCaT Keratinocytes

To understand the regulation of Blimp-1 expression in keratinocytes, we tested several agents including tumor promoter PMA, TLR4 ligand lipopolysaccharide (LPS), cytokine TNF-α, ROS stressors H_2O_2 and UVB in human HaCaT keratinocytes. We found that LPS (1 μg/ml) (**Figure 1A**), PMA (30 nM), TNF-α (10 ng/ml) and H_2O_2 (200 μM) (**Figure 1B**) can increase Blimp-1 protein expression. Compared to other stimuli, the effect of H_2O_2 is much weaker. Nevertheless, polyIC (TLR3 ligand) (50 μg/ml) had

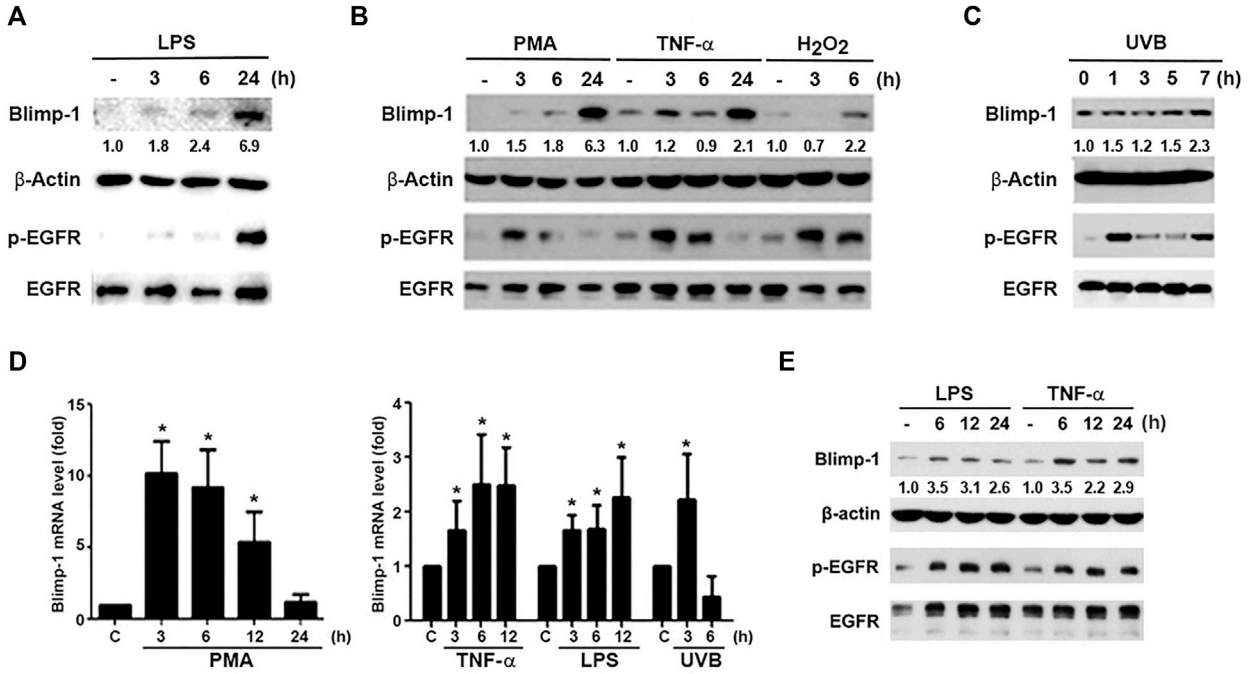

FIGURE 1 | LPS, PMA, TNF-α, UVB, and H_2O_2 upregulate Blimp-1 gene and protein expressions in HaCaT cells and NHEKs. HaCaT cells were stimulated with LPS (1 μg/ml) **(A)**, PMA (30 nM), TNF-α (10 ng/ml), H_2O_2 (200 μM) **(B)** or UVB (50 mJ/cm^2) **(C)** for indicated time periods. **(E)** NHEKs were stimulated with LPS (1 μg/ml) and TNF-α (10 ng/ml) for indicated times. After stimulation cell lysates were collected to determine Blimp-1 and β-actin expression by immunoblotting. **(D)** HaCaT cells were stimulated with PMA (30 nM), TNF-α (10 ng/ml), LPS (1 μg/ml), or UVB at 50 mJ/cm^2 for indicated time periods and then Q-PCR was performed to evaluate the mRNA level of Blimp-1. *$p < 0.05$ (mean ± S.E.M., $n = 5$) as compared to control group.

no significant effect Blimp-1 expression in HaCaT cells (data not shown). On the other hands, UVB (50 mJ/cm^2) could also induce Blimp-1 expression within 5–7 h (**Figure 1C**). Consistently the data from the Q-PCR study indicated that PMA, TNF-α, LPS and UVB can increase Blimp-1 mRNA level (**Figure 1D**).

Because previously EGF was shown to upregulate Blimp-1 expression in keratinocytes (Chang et al., 2018) and EGFR can be transactivated via extracellular and intracellular manners in various cell types including keratinocytes (Nanba et al., 2013; Wu et al., 2016), we interested to explore if Blimp-1 inducers mentioned above might exert actions related to EGFR. To this end, we determined the effects of these stimuli on EGFR expression and activation. We found that LPS (**Figure 1A**), PMA, TNF-α, H_2O_2 (**Figure 1B**) and UVB (**Figure 1C**) could activate EGFR in HaCaT cells. Strengthening these observations not only in HaCaT cells, we found that LPS and TNF-α also can induce Blimp-1 expression in NHEKs (**Figure 1E**). In our experimental conditions and time intervals, we ruled out the death effect of all tested agents including H_2O_2 and UVB in keratinocytes and SCC.

PMA, TNF-α, TLRs Ligands, UVB, and H_2O_2 Upregulate Blimp-1 Expression and Activate EGFR in Cal-27 and SAS Cells

Besides keratinocytes, we chose two SCC cell lines Cal-27 and SAS to understand the Blimp-1 regulation. In the same manners as seen in HaCaT cells, PMA, TNF-α, LPS, H_2O_2 and UVB could time-dependently increase Blimp-1 protein expression in Cal-27 cells (**Figures 2A,B**). Unlike HaCaT cells where polyIC failed to increase Blimp-1 protein, we found it can exert this action in Cal-27 cells (**Figure 2A**). In Q-PCR study, our data revealed the abilities of PMA, LPS, TNF-α, H_2O_2 and UVB to upregulate Blimp-1 gene expression (**Figure 2C**). Moreover, in SAS cells PMA, TNF-α, LPS, polyIC, H_2O_2 and UVB all increased Blimp-1 protein expression (**Figures 2D,E**), and UVB also increased Blimp-1 mRNA level (**Figure 2F**). All these data suggest that Blimp-1 can be induced by PMA, TNF-α, LPS, H_2O_2 and UVB in both keratinocytes and SCC. Similarly, we also determined EGFR activation in SCC cells. We found that PMA, TNF-α, LPS, polyIC, H_2O_2 and UVB all activated EGFR in Cal-27 cells (**Figures 2A,B**). In SAS cells, the EGFR was also activated by PMA, TNF-α, LPS, polyIC, H_2O_2 and UVB (**Figures 2D,E**). All these findings indicate that transactivation of EGFR is induced by all Blimp-1 regulators, suggesting the role of EGFR activation in Blimp-1 gene expression as we previously reported in the case of exogenous EGF (Chang et al., 2018).

EGFR Activation Mediates Blimp-1 Gene Expression *via* AP-1 Activation

Previous studies indicated that AP-1 is involved in BCR-mediated and TGF-β-induced Blimp-1 gene expression in B lymphocytes (Calame, 2008) and breast cancer cells (Romagnoli et al., 2012), respectively. We also found that PMA-induced Blimp-1 is

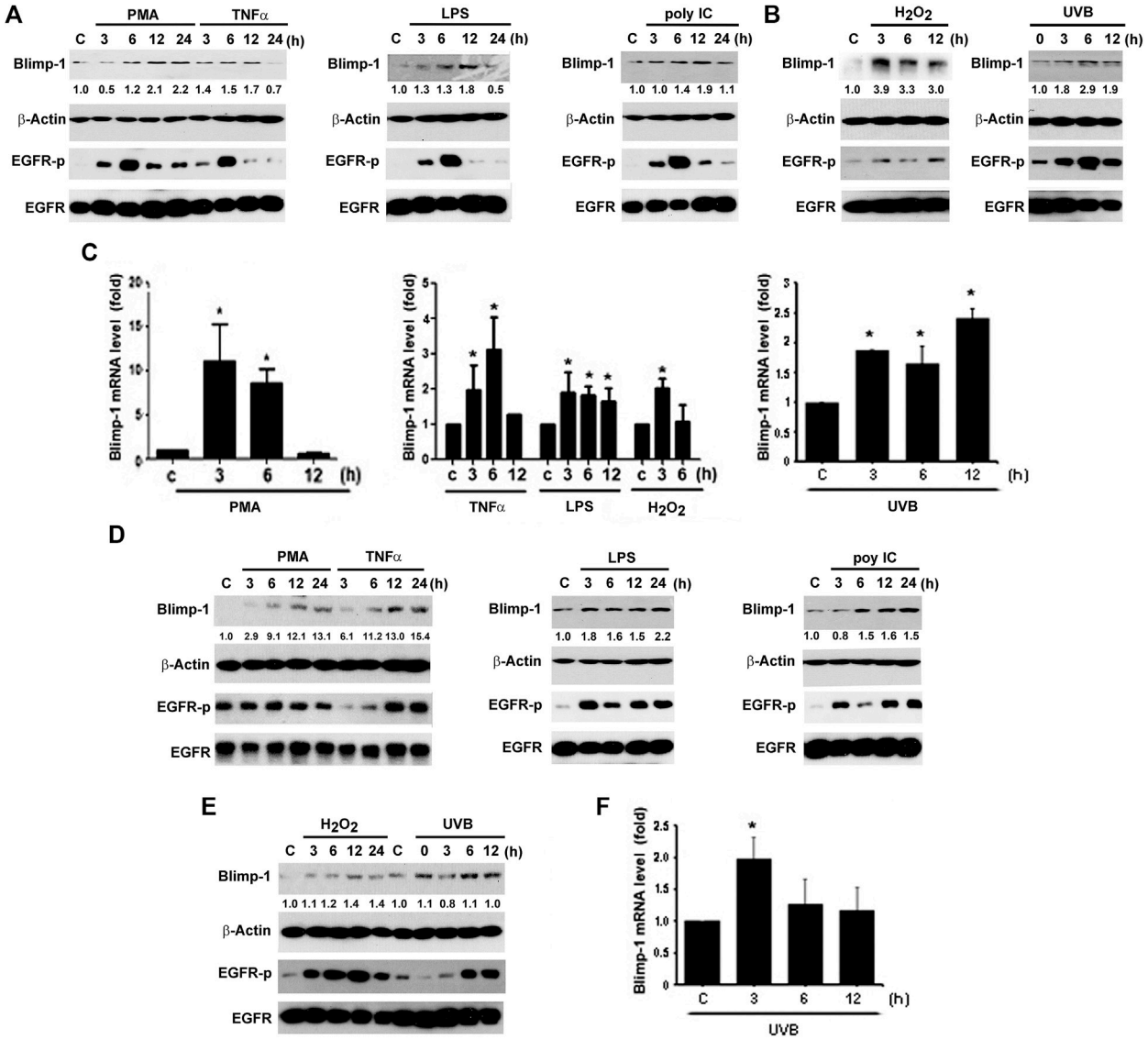

FIGURE 2 | Blimp-1 expression was induced by various stimuli in Cal-27 and SAS cells. Cal-27 cells **(A–C)** and SAS cells **(D–F)** were treated with PMA (30 nM), TNF-α (10 ng/ml), LPS (1 μg/ml), polyIC (50 μg/ml), H_2O_2 (200 μM) or UVB (50 mJ/cm^2) for indicated times. Protein expression of Blimp-1 and β-actin were analyzed by immunoblotting **(A,B,D,E)**. Q-PCR was performed to evaluate the mRNA level of Blimp-1 **(C,F)**. *$p < 0.05$ (mean ± S.E.M., $n = 3$) as compared to control group.

dependent on EGFR transactivation in keratinocytes, because EGFR inhibitor gefitinib can reduce this effect (Chang et al., 2018). Here we used reporter assay to check if AP-1 is required for Blimp-1 expression caused by various agents in keratinocytes. As shown in **Figure 3A**, PMA, LPS, TNF-α and EGF treatment could increase the luciferase activity of Blimp-1 in HaCaT cells with the highest effect of EGF, and AP-1 mutation abolished these effects of different agents (**Figure 3A**). In addition, we also observed the ability of gefitinib to reduce PMA-induced Blimp-1 gene expression in Cal-27 cells (**Figure 3B**). To clarify if gefitinib might have off-target effect on PMA signaling, we used PKCδ phosphorylation as the index of PKC activation. We found that gefitinib did not change PMA-induced PKCδ phosphorylation in Cal-27 cells (**Figure 3C**).

Moreover, previously we found that Syk is not only an upstream signaling molecule of EGFR in keratinocytes (Wu et al., 2016) but also can be activated by PKC in monocytes (Chang et al., 2012). Therefore, we wonder if Syk is involved in the action of PMA for Blimp-1 expression. First, as our previous study showing the effect of PMA on Syk activation in monocytes (Chang et al., 2012), we found that in HaCaT cells, PMA could also increase active phospho-Syk level (**Figure 3D**, left panel) and Syk inhibitor GS-9973 could block PMA-induced Blimp-1 upregulation (**Figure 3E**). Likewise, TNF-α also can activate Syk (**Figure 3D**, right panel). In Cal-27 cells, GS-9973 was also found to inhibit PMA-induced Blimp-1 gene expression (**Figure 3F**) as well as EGFR activation (**Figure 3C**). These findings suggest the

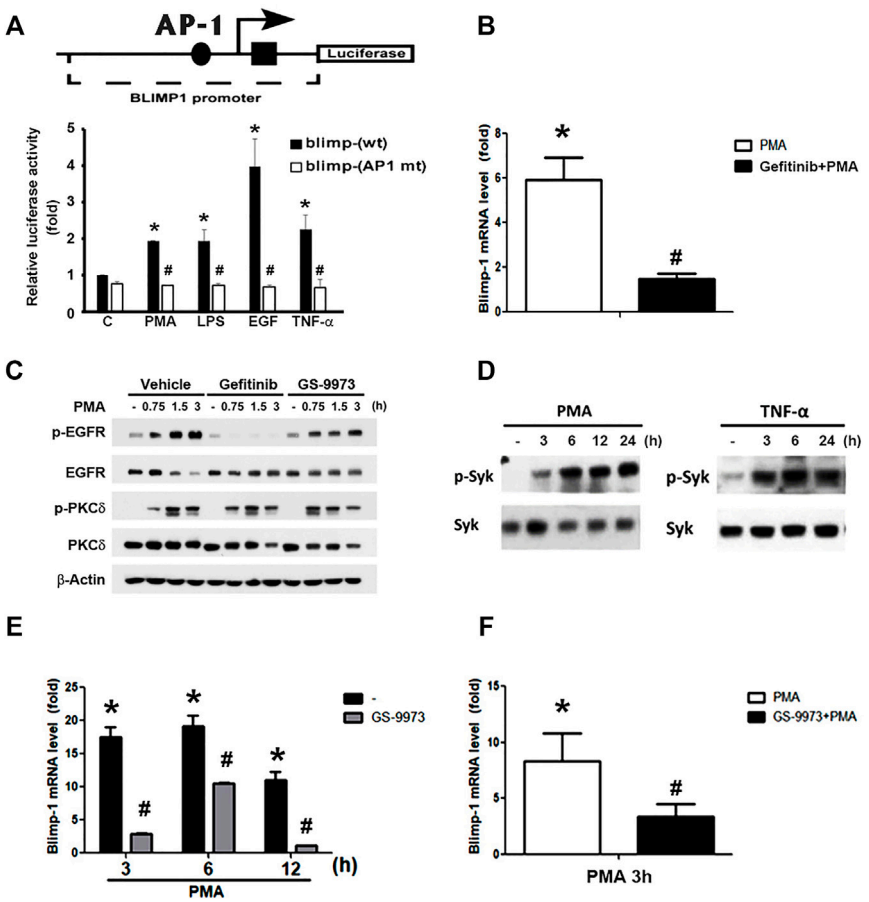

FIGURE 3 | Roles of EGFR and Syk activation in PMA- and TNF-α-induced Blimp-1 gene expression. **(A)** The indicated luciferase constructs in lentiviral vectors were transiently transfected in HaCaT cells and then PMA (30 nM), LPS (1 μg/ml), EGF (50 ng/ml), and TNF-α (10 ng/ml) was treated for 15 h. After harvesting, the luciferase luminescence was measured. Bars showed means ± S.E.M. ($n = 3$). *$p < 0.05$ as compared to control group. #$p < 0.05$, indicating the abolishment of agent-induced luciferase activity by AP-1 deletion. **(B)** After pretreatment with gefitinib (1 uM) for 30 min, Cal-27 cells were treated with PMA (30 nM) for 3 h, and then mRNA level of Blimp-1 was evaluated by Q-PCR. **(C)** HaCaT cells were pre-treated with gefitinib (1 uM) or GS-9973 (1 uM) for 30 min prior to the stimulation with PMA (30 nM). HaCaT cells **(D,E)** and Cal-27 cells **(F)** were stimulated with PMA (30 nM) or TNF-α (10 ng/ml) for indicated time periods, and in some experiments GS-9973 (1 μM) was pre-treated for 30 min **(E,F)**. EGFR, PKCδ and Syk were analyzed by immunoblotting **(C,D)**, and Q-PCR was performed to evaluate the mRNA levels of Blimp-1 **(E,F)**. *$p < 0.05$ (mean ± S.E.M., $n = 3$), as compared to control group. #$p < 0.05$, indicating the significant inhibitory effects of AP-1 mutation, gefitinib and GS-9973 on Blimp-1 gene transcription.

involvement of PKC-Syk axis in PMA-induced EGFR transactivation and subsequent Blimp-1 gene expression.

Nuclear Localization of Blimp-1 in Keratinocytes and SAS Cells

After observing the relationship between Blimp-1 expression and EGFR activity, we determined the subcellular localization of Blimp-1 and EGFR in keratinocytes and SCC. Data of immunoblotting analysis of subcellular fractions revealed that Blimp-1 is located in the nuclei and EGFR is present in both nuclei and plasma membrane in HaCaT cells (**Figure 4A**). Data of confocal microscopy revealed that Blimp-1 and EGFR are mainly present in the nuclei and plasma membrane, respectively (**Figure 4B**). Similar intracellular distributions of Blimp-1 and EGFR were also observed in NHEK. In addition, PMA and TNF-α treatment for 6 h cannot alter both proteins' localization in HaCaT cells (data not shown). Besides we checked the subcellular location of Blimp-1 and EGFR in Cal-27 and SAS cells before and after stimuli treatment. We found that Blimp-1 is localized in the nuclei of both cancer cell lines (**Figure 4B**) and is still kept in the nuclei after PMA, TNF-α or UVB stimulation (**Supplementary Figure S1**).

Blimp-1 Negatively Regulates Cell Migration in SCC Cells But Not HaCaT Cells

Next to know the role of Blimp-1 in cell migration, we knocked down Blimp-1 in HaCaT cells using shRNA. We found silencing of Blimp-1 increases wound closure percentages as compared to control group in SAS (**Figure 5B**) and Cal-27 cells (**Figure 5C**), but not in HaCaT cells (**Figure 5A**). PMA slightly inhibited the cell migration of HaCaT keratinocytes. The inhibitory effect of PMA is

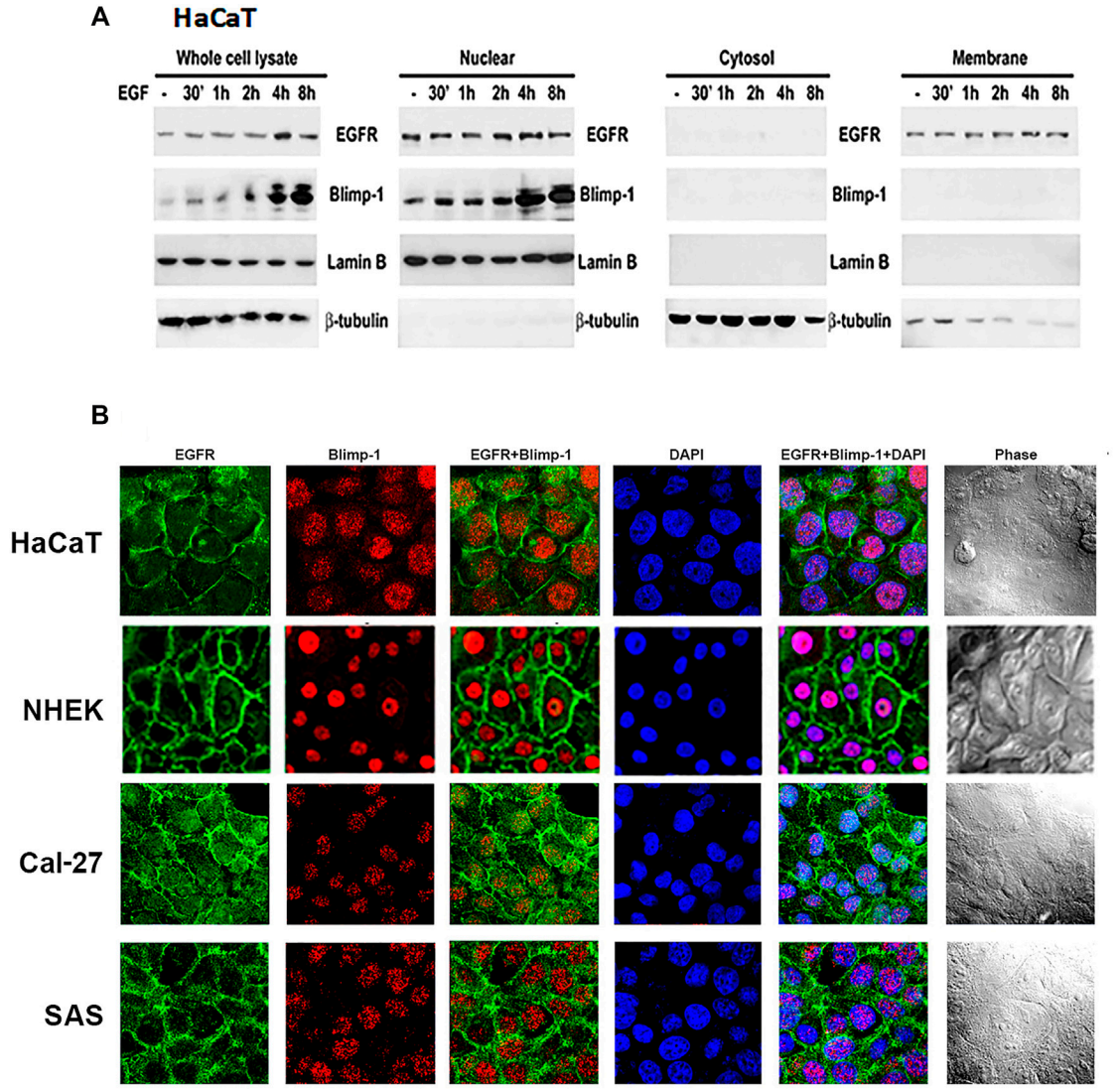

FIGURE 4 | Intracellular localization of Blimp-1 in keratinocytes and SCC. **(A)** Total cell lysates of EGF-stimulated HaCaT cells were separated into cytosol, membrane and nuclear fractions. Protein levels of Blimp-1, EGFR, lamin B and β-tubulin were determined. Lamin B and β-tubulin were the nuclear and cytosol markers, respectively. Data were representative from three independent experiments. **(B)** HaCaT cells, NHEKs, Cal-27, and SAS cells were seeded in 12-well plates. Immunofluorescence staining was performed to detect EGFR and Blimp-1 expression. Nuclei were counterstained with DAPI (blue color).

similar to previous finding and possibly is due to the keratinocyte differentiation action of PMA (Ando et al., 1993). In both SCC, EGF but not TNF-α can promote cell migration. shBlimp-1 induced a significant enhancement on cell migration in both types of SCC, and this effect was still observed upon TNF-α treatment and was non-additive to the stimulating response of EGF (**Figures 5B,C**). These effects indicate that Blimp-1 is a negative regulator of cell migration in SCC.

DISCUSSION

Blimp-1 was initially identified as a post viral induction repressor of transcription of IFNB1 (Keller and Maniatis, 1991). Later on accumulating evidence suggests Blimp-1 as an essential regulator of immune cells differentiation, particularly in B and T lymphocytes (Nutt et al., 2007). Although so far the roles of Blimp-1 in various cell types beyond immune cells remain largely unclear, some studies have demonstrated the pathways to regulate Blimp-1 gene expression. In this aspect, we previously demonstrated that EGF can increase Blimp1 gene transcription in keratinocytes through PKC-p38, ERK signaling pathway (Chang et al., 2018). Apart from EGF, Blimp-1 is also induced by TGF-β *via* Wnt/β-catenin signaling to regulate hair follicle growth (Telerman et al., 2017). Also in breast cancer cells TGF-β1 induces Blimp-1 expression via the c-Raf/Erk/AP-1 pathway (Romagnoli et al., 2012). Notably, analyses using microarray datasets in Oncomine reveal an elevated Blimp-1 mRNA expression in samples of tongue

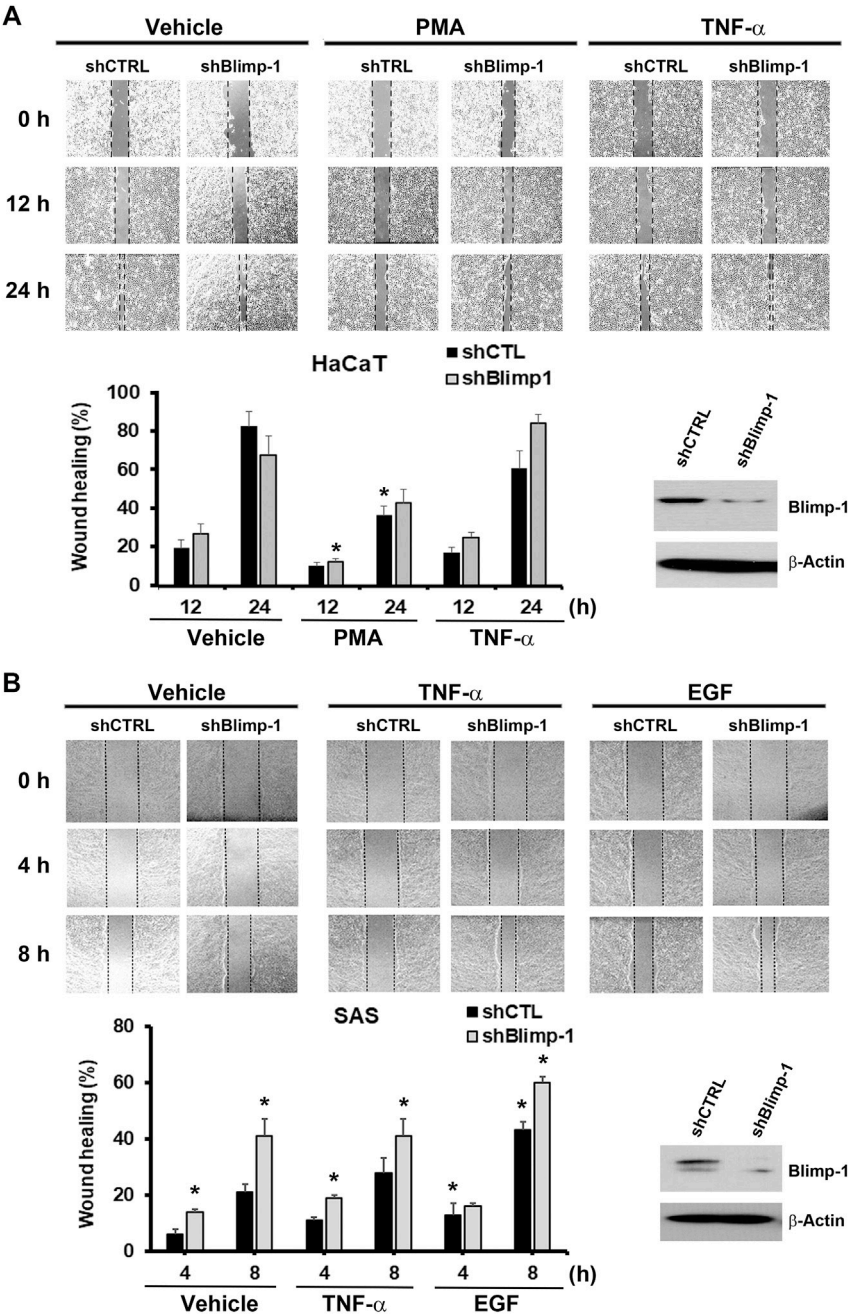

FIGURE 5 | Blimp-1 negatively regulates cell migration in SCC but not HaCaT cells. After transfection of silencing Blimp-1 and control shRNA, HaCaT **(A)**, SAS **(B)** and Cal-27 **(C)** cells were seeded in wound-healing assay kit and grown overnight for attachment. Then the kits were removed and fresh DMEM medium with mitomycin C (5 μg/ml) was treated. After 30 min, cells were stimulated with PMA (30 nM), TNF-α (10 ng/ml) or EGF (50 ng/ml). Photography (100x) was taken by microscopy. Dashed lines represent boundaries of the wounds. The percentage of wound closure from the denuded gap after incubation for different times was determined. *$p < 0.05$ (mean ± S.E.M., $n = 3$), indicating the significant enhancement effects of shBlimp-1 and EGF, and the inhibitory effect of PMA on cell migration as compared to control cells.

squamous cell carcinoma (Yu et al., 2012), correlating to the high frequencies of EGFR overexpression in squamous cell carcinomas (Molinolo et al., 2009). Moreover, interaction of Reishi-F3 with TLR4/TLR2 followed by signaling through p38 MAPK is involved in the induction of Blimp-1 mRNA level (Lin et al., 2006). Blimp-1 is promptly induced in plasmacytoid dendritic cells after exposure to TLR7 and TLR9 ligands *via* a unique Ras-related C3 botulinum toxin substrate (Rac)-mediated pathway (Ko et al., 2018). Blimp-1 is also greatly induced in bone marrow-derived dendritic cells cultured with LPS, TNF-α, CpG, and poly I:C (Chan et al., 2009).

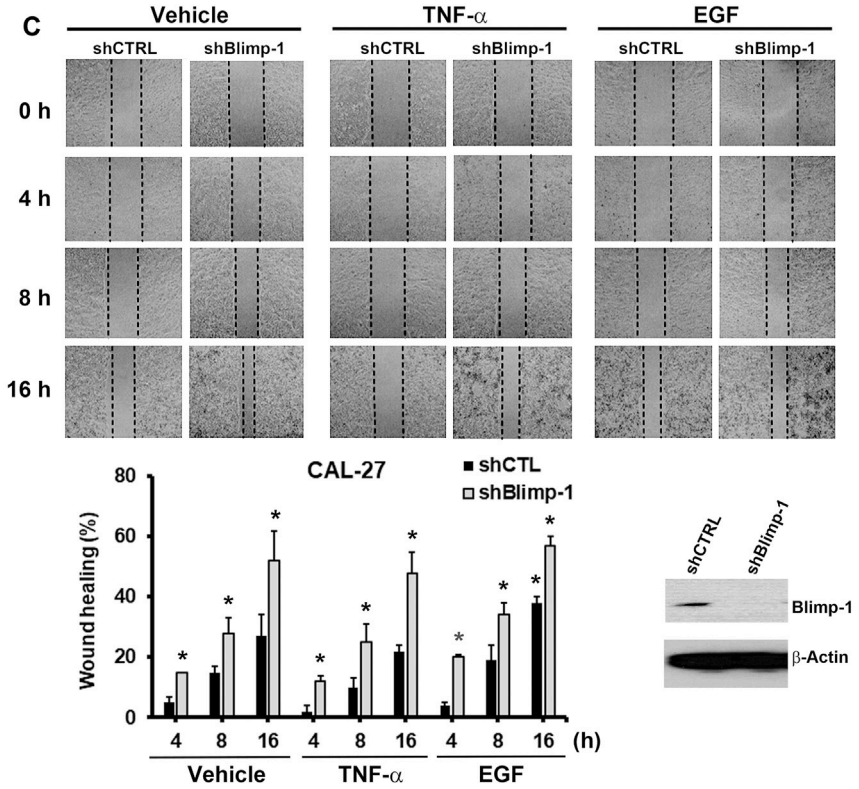

FIGURE 5 | (Continued)

All these findings suggest that Blimp-1 gene induction might be highly responsive to multiple stimuli and pathophysiological conditions.

To date studies on Blimp-1 are quite few in keratinocytes and cancer cells, and only EGFR activation is known to mediate Blimp-1 expression in keratinocytes (Chiang et al., 2013; Chang et al., 2018). The factors capable of inducing Blimp-1 and action mechanisms in relation with EGFR are still insufficiently investigated in keratinocytes and cancer cells. In this study, we examined several stimuli, and found that PKC activator PMA, cytokine TNF-α, TLRs ligands (LPS and polyIC), ROS stressors H_2O_2 and UVB can upregulate Blimp-1 protein expression in HaCaT and SCC (Cal-27, SAS) with different extents. Our current data indicate that Blimp-1 increase caused by these factors results from the gene transcription. Some transcriptional factors for Blimp-1 gene expression like AP-1, NF-κB, and IRF4 have been identified (Calame, 2008; Martins and Calame, 2008). Our data indicate that AP-1 is indispensable for EGF-, TNF-α-, PMA- and LPS-induced Blimp-1 gene expression in keratinocytes. Of note, we further demonstrated that EGFR activation contributes to Blimp-1 gene expression caused by these stimuli in these cell types. First of all we found that most stimulation conditions that we tested also can trigger EGFR activation. This is evidenced by the increasing EGFR phosphorylation upon treatment of LPS, PMA, TNF-α, H_2O_2, and UVB in HaCaT, Cal-27 and/or SAS cells. Second, these treatments do not affect the protein level of EGFR but increase EGFR phosphorylation of a late onset prior to Blimp-1 induction. Third, EGFR TKI gefitinib can block Blimp-1 induction caused by PMA. The no effect of gefitinib on PMA-induced PKC activation rules out the possibly non-specific action of gefitinib beyond EGFR. Therefore, we suggest that EGFR transactivation is occurred under these treatments and orchestrates an essential signal for Blimp-1 gene expression.

The EGFR and its ligands are recognized to centrally involve in the growth and repair process of epithelia and in carcinogenesis. Constitutive EGFR activation via ligand shedding as well as ligand-independent EGFR transactivation in keratinocytes and some EGFR-dependent cancer cell types including SCC has been reported. In keratinocytes, UVB can activate EGFR signaling by inducing shedding of EGFR ligand like HB-EGF (Pastore et al., 2008), which in turn regulates oxidative stress and inflammation (Seo and Juhnn, 2010; El-Abaseri et al., 2013; Chiu et al., 2021). Vice versa, ROS production in response to UVB or arsenite can reciprocally promote EGFR transactivation (Tseng et al., 2012; Chiu et al., 2021). Additionally, proinflammatory cytokines like TNF-α can transactivate EGFR via ERK signaling and EGFR ligand shedding in keratinocytes (Ziv et al., 2008; Potapovich et al., 2011; Wu et al., 2013; Segawa et al., 2018), and IL-1β also can induce EGFR-dependent MMP-1 expression in keratinocytes (Wan et al., 2001). On the other hand, EGFR transactivation in SCC is similarly demonstrated in response to H_2O_2 (Finch et al., 2006), PMA (Moon et al., 1984), LPS (Shuyi et al., 2011), UV

radiation (Rodust et al., 2009), and TNF-α (Donato et al., 1989). PMA was shown to induce secretion of EGFR ligand TGF-α in A431 cells (Thornley and Jones, 1992). In head and neck SCC biopsies TLR4 expression is correlated to EGFR, and the amplifying crosstalk between EGFR and TLR4 signaling pathways leads to anti-EGFR therapy resistance (Ju et al., 2020). Taken together, because of the well-known ERK-dependent EGFR activation and EGFR-ERK pathway for AP-1 activation, we suggest EGFR-ERK-AP-1 pathway contributes to Blimp-1 gene transcription in response to the stimuli tested in this study.

In this study, we also highlight the role of Syk in PMA-dependent Blimp-1 expression. We found that Syk activity is increased by PMA and TNF-α in HaCaT cells, and Syk inhibitor GS-9973 could suppress PMA-induced Blimp-1 increase in both HaCaT and Cal-27 cells. Because PMA can activate Syk in monocytes (Chang et al., 2012), and EGFR activation also transduces Syk signaling in keratinocytes (Wu et al., 2016) and SCC (Huang et al., 2020), we treated GS-9973 and took PMA as an example to understand the signaling cascade among PKC, Syk and EGFR. Our data that GS-9973 can reduce PMA-induced EGFR-p without affecting PKC activation suggest that PKC-Syk-EGFR-ERK-AP-1 signaling pathway is involved in Blimp-1 gene transcription.

According to published data, the role of Blimp-1 in cell migration remains controversial. Blimp-1 is a negative regulator of NHEKs migration (Chang et al., 2018), but promotes breast cancer cell motility and metastasis (Sciortino et al., 2017). In SAS and Cal-27 cells, we found Blimp-1 also acts as a negative regulator of cell migration, but does not affect HaCaT cell migration, and PMA as reported inhibits keratinocyte mobility possibly due to induction of keratinocyte differentiation (Ando et al., 1993). It remains unclear for the different role of Blimp-1 in keratinocyte migration between primary NHEKs and HaCaT cell line. EGF can enhance cell migration in SCC, and this action of EGF is non-additive to the effect of Blimp-1 silencing. Collectively, Blimp-1 functioning to regulate cell migration is cell type dependent. Currently it remains unclear how Blimp-1 negatively regulates cell migration, and future study on the molecular mechanisms underlying this event is required.

CONCLUSION

We demonstrate that the transcriptional regulator Blimp-1 can be transcriptionally upregulated by various stimuli including PKC activator, proinflammatory cytokine, TLR ligands, ROS and UVB in keratinocytes and SCC. The common mechanism of Blimp-1 gene induction is via the EGFR transactivation, which evokes ERK-AP-1 pathway for activation of Blimp-1 promoter. We further show that Blimp-1 can negatively regulate SCC cell migration. Combining our previous findings that Blimp-1 negatively regulates inflammation and keratinocyte differentiation, Blimp-1 is suggested to be a potential target to develop new intervention in therapy of skin diseases.

DATA AVAILABILITY STATEMENT

The raw data supporting the conclusion of this article will be made available by the authors, without undue reservation.

ETHICS STATEMENT

The studies involving human participants were reviewed and approved by The Ethics Committee of Mackay Memorial Hospital (Institutional Review Board codes 19MMHIS173e). The patients/participants provided their written informed consent to participate in this study.

AUTHOR CONTRIBUTIONS

W-WL designed the study. HL, D-YH, C-YL, H-CC, W-YR and Y-SD performed the experiments and analyzed the data. W-WL and HL wrote the paper. All authors read and approved the final manuscript.

FUNDING

The authors thank the research funding from the Ministry of Science and Technology (MOST 107-2320-B-002-036-MY3), National Taiwan University College of Medicine (NSCCMOH-145-61), and National Taiwan University Hospital (109-M4754).

SUPPLEMENTARY MATERIAL

The Supplementary Material for this article can be found online at: https://www.frontiersin.org/articles/10.3389/fphar.2022.763678/full#supplementary-material

Supplementary Figure S1 | PMA, UVB and TNF-a do not change intracellular Blimp-1 localization in SCC cells. Cal-27 **(A)** and SAS **(B)** cells were treated with PMA (30 nM), TNF-α (10 ng/ml) or UVB (50 mJ/cm^2) for 6 h, and immunofluorescence staining was performed to detect Blimp-1. Nuclei were counterstained with DAPI.

REFERENCES

Ando, Y., Lazarus, G. S., and Jensen, P. J. (1993). Activation of Protein Kinase C Inhibits Human Keratinocyte Migration. *J. Cel Physiol* 156, 487–496. doi:10.1002/jcp.1041560308

Bikoff, E. K., Morgan, M. A., and Robertson, E. J. (2009). An Expanding Job Description for Blimp-1/PRDM1. *Curr. Opin. Genet. Dev.* 19, 379–385. doi:10.1016/j.gde.2009.05.005

Calame, K. (2008). Activation-dependent Induction of Blimp-1. *Curr. Opin. Immunol.* 20, 259–264. doi:10.1016/j.coi.2008.04.010

Chan, Y. H., Chiang, M. F., Tsai, Y. C., Su, S. T., Chen, M. H., Hou, M. S., et al. (2009). Absence of the Transcriptional Repressor Blimp-1 in Hematopoietic

Lineages Reveals its Role in Dendritic Cell Homeostatic Development and Function. *J. Immunol.* 183, 7039–7046. doi:10.4049/jimmunol.0901543

Chang, D. H., Angelin-Duclos, C., and Calame, K. (2000). BLIMP-1: Trigger for Differentiation of Myeloid Lineage. *Nat. Immunol.* 1, 169–176. doi:10.1038/77861

Chang, H. C., Huang, D. Y., Wu, N. L., Kannagi, R., Wang, L. F., and Lin, W. W. (2018). BLIMP1 Transcriptionally Induced by EGFR Activation and post-translationally Regulated by Proteasome and Lysosome Is Involved in Keratinocyte Differentiation, Migration and Inflammation. *J. Dermatol. Sci.* 92, 151–161. doi:10.1016/j.jdermsci.2018.08.011

Chang, M. Y., Huang, D. Y., Ho, F. M., Huang, K. C., and Lin, W. W. (2012). PKC-dependent Human Monocyte Adhesion Requires AMPK and Syk Activation. *PLoS One* 7, e40999. doi:10.1371/journal.pone.0040999

Chiang, M. F., Yang, S. Y., Lin, I. Y., Hong, J. B., Lin, S. J., Ying, H. Y., et al. (2013). Inducible Deletion of the Blimp-1 Gene in Adult Epidermis Causes Granulocyte-Dominated Chronic Skin Inflammation in Mice. *Proc. Natl. Acad. Sci. U S A.* 110, 6476–6481. doi:10.1073/pnas.1219462110

Chiu, L. Y., Wu, N. L., Hung, C. F., Bai, P., Dai, Y. S., and Lin, W. W. (2021). PARP-1 Involves in UVB-Induced Inflammatory Response in Keratinocytes and Skin Injury via Regulation of ROS-dependent EGFR Transactivation and P38 Signaling. *Faseb J.* 35, e21393. doi:10.1096/fj.202002285RR

Donato, N. J., Gallick, G. E., Steck, P. A., and Rosenblum, M. G. (1989). Tumor Necrosis Factor Modulates Epidermal Growth Factor Receptor Phosphorylation and Kinase Activity in Human Tumor Cells. Correlation with Cytotoxicity. *J. Biol. Chem.* 264, 20474–20481. doi:10.1016/s0021-9258(19)47086-5

Doody, G. M., Stephenson, S., and Tooze, R. M. (2006). BLIMP-1 Is a Target of Cellular Stress and Downstream of the Unfolded Protein Response. *Eur. J. Immunol.* 36, 1572–1582. doi:10.1002/eji.200535646

El-Abaseri, T. B., Hammiller, B., Repertinger, S. K., and Hansen, L. A. (2013). The Epidermal Growth Factor Receptor Increases Cytokine Production and Cutaneous Inflammation in Response to Ultraviolet Irradiation. *ISRN Dermatol.* 2013, 848705. doi:10.1155/2013/848705

Finch, J. S., Tome, M. E., Kwei, K. A., and Bowden, G. T. (2006). Catalase Reverses Tumorigenicity in a Malignant Cell Line by an Epidermal Growth Factor Receptor Pathway. *Free Radic. Biol. Med.* 40, 863–875. doi:10.1016/j.freeradbiomed.2005.10.036

Fu, S. H., Yeh, L. T., Chu, C. C., Yen, B. L., and Sytwu, H. K. (2017). New Insights into Blimp-1 in T Lymphocytes: a Divergent Regulator of Cell Destiny and Effector Function. *J. Biomed. Sci.* 24, 49. doi:10.1186/s12929-017-0354-8

Huang, D. Y., Chen, W. Y., Chen, C. L., Wu, N. L., and Lin, W. W. (2020). Synergistic Anti-tumour Effect of Syk Inhibitor and Olaparib in Squamous Cell Carcinoma: Roles of Syk in EGFR Signalling and PARP1 Activation. *Cancers (Basel)* 12, 489. doi:10.3390/cancers12020489

Jain, R., Chen, Y., Kanno, Y., Joyce-Shaikh, B., Vahedi, G., Hirahara, K., et al. (2016). Interleukin-23-induced Transcription Factor Blimp-1 Promotes Pathogenicity of T Helper 17 Cells. *Immunity* 44, 131–142. doi:10.1016/j.immuni.2015.11.009

Ju, H., Hu, Z., Lu, Y., Wu, Y., Zhang, L., Wei, D., et al. (2020). TLR4 Activation Leads to Anti-EGFR Therapy Resistance in Head and Neck Squamous Cell Carcinoma. *Am. J. Cancer Res.* 10, 454–472.

Keller, A. D., and Maniatis, T. (1991). Identification and Characterization of a Novel Repressor of Beta-Interferon Gene Expression. *Genes Dev.* 5, 868–879. doi:10.1101/gad.5.5.868

Ko, Y. A., Chan, Y. H., Liu, C. H., Liang, J. J., Chuang, T. H., Hsueh, Y. P., et al. (2018). Blimp-1-mediated Pathway Promotes Type I IFN Production in Plasmacytoid Dendritic Cells by Targeting to Interleukin-1 Receptor-Associated Kinase M. *Front. Immunol.* 9, 1828. doi:10.3389/fimmu.2018.01828

Lebre, M. C., van der Aar, A. M., van Baarsen, L., van Capel, T. M., Schuitemaker, J. H., Kapsenberg, M. L., et al. (2007). Human Keratinocytes Express Functional Toll-like Receptor 3, 4, 5, and 9. *J. Invest. Dermatol.* 127, 331–341. doi:10.1038/sj.jid.5700530

Lin, K. I., Kao, Y. Y., Kuo, H. K., Yang, W. B., Chou, A., Lin, H. H., et al. (2006). Reishi Polysaccharides Induce Immunoglobulin Production through the TLR4/TLR2-Mediated Induction of Transcription Factor Blimp-1. *J. Biol. Chem.* 281, 24111–24123. doi:10.1074/jbc.M601106200

Magnúsdóttir, E., Kalachikov, S., Mizukoshi, K., Savitsky, D., Ishida-Yamamoto, A., Panteleyev, A. A., et al. (2007). Epidermal Terminal Differentiation Depends on B Lymphocyte-Induced Maturation Protein-1. *Proc. Natl. Acad. Sci. U S A.* 104, 14988–14993. doi:10.1073/pnas.0707323104

Martins, G., and Calame, K. (2008). Regulation and Functions of Blimp-1 in T and B Lymphocytes. *Annu. Rev. Immunol.* 26, 133–169. doi:10.1146/annurev.immunol.26.021607.090241

Minnich, M., Tagoh, H., Bönelt, P., Axelsson, E., Fischer, M., Cebolla, B., et al. (2016). Multifunctional Role of the Transcription Factor Blimp-1 in Coordinating Plasma Cell Differentiation. *Nat. Immunol.* 17, 331–343. doi:10.1038/ni.3349

Molinolo, A. A., Amornphimoltham, P., Squarize, C. H., Castilho, R. M., Patel, V., and Gutkind, J. S. (2009). Dysregulated Molecular Networks in Head and Neck Carcinogenesis. *Oral Oncol.* 45, 324–334. doi:10.1016/j.oraloncology.2008.07.011

Moon, S. O., Palfrey, H. C., and King, A. C. (1984). Phorbol Esters Potentiate Tyrosine Phosphorylation of Epidermal Growth Factor Receptors in A431 Membranes by a Calcium-independent Mechanism. *Proc. Natl. Acad. Sci. U S A.* 81, 2298–2302. doi:10.1073/pnas.81.8.2298

Nanba, D., Toki, F., Barrandon, Y., and Higashiyama, S. (2013). Recent Advances in the Epidermal Growth Factor Receptor/ligand System Biology on Skin Homeostasis and Keratinocyte Stem Cell Regulation. *J. Dermatol. Sci.* 72, 81–86. doi:10.1016/j.jdermsci.2013.05.009

Nutt, S. L., Fairfax, K. A., and Kallies, A. (2007). BLIMP1 Guides the Fate of Effector B and T Cells. *Nat. Rev. Immunol.* 7, 923–927. doi:10.1038/nri2204

Ozaki, K., Spolski, R., Ettinger, R., Kim, H. P., Wang, G., Qi, C. F., et al. (2004). Regulation of B Cell Differentiation and Plasma Cell Generation by IL-21, a Novel Inducer of Blimp-1 and Bcl-6. *J. Immunol.* 173, 5361–5371. doi:10.4049/jimmunol.173.9.5361

Pastore, S., Mascia, F., Mariani, V., and Girolomoni, G. (2008). The Epidermal Growth Factor Receptor System in Skin Repair and Inflammation. *J. Invest. Dermatol.* 128, 1365–1374. doi:10.1038/sj.jid.5701184

Potapovich, A. I., Lulli, D., Fidanza, P., Kostyuk, V. A., De Luca, C., Pastore, S., et al. (2011). Plant Polyphenols Differentially Modulate Inflammatory Responses of Human Keratinocytes by Interfering with Activation of Transcription Factors NFκB and AhR and EGFR-ERK Pathway. *Toxicol. Appl. Pharmacol.* 255, 138–149. doi:10.1016/j.taap.2011.06.007

Rodust, P. M., Stockfleth, E., Ulrich, C., Leverkus, M., and Eberle, J. (2009). UV-induced Squamous Cell Carcinoma-Aa Role for Antiapoptotic Signalling Pathways. *Br. J. Dermatol.* 161 (Suppl. 3), 107–115. doi:10.1111/j.1365-2133.2009.09458.x

Romagnoli, M., Belguise, K., Yu, Z., Wang, X., Landesman-Bollag, E., Seldin, D. C., et al. (2012). Epithelial-to-mesenchymal Transition Induced by TGF-B1 Is Mediated by Blimp-1-dependent Repression of BMP-5. *Cancer Res.* 72, 6268–6278. doi:10.1158/0008-5472.CAN-12-2270

Salehi, S., Bankoti, R., Benevides, L., Willen, J., Couse, M., Silva, J. S., et al. (2012). B Lymphocyte-Induced Maturation Protein-1 Contributes to Intestinal Mucosa Homeostasis by Limiting the Number of IL-17-producing CD4+ T Cells. *J. Immunol.* 189, 5682–5693. doi:10.4049/jimmunol.1201966

Sciortino, M., Camacho-Leal, M. D. P., Orso, F., Grassi, E., Costamagna, A., Provero, P., et al. (2017). Dysregulation of Blimp1 Transcriptional Repressor Unleashes p130Cas/ErbB2 Breast Cancer Invasion. *Sci. Rep.* 7, 1145. doi:10.1038/s41598-017-01332-z

Segawa, R., Shigeeda, K., Hatayama, T., Dong, J., Mizuno, N., Moriya, T., et al. (2018). EGFR Transactivation Is Involved in TNF-α-Induced Expression of Thymic Stromal Lymphopoietin in Human Keratinocyte Cell Line. *J. Dermatol. Sci.* 89, 290–298. doi:10.1016/j.jdermsci.2017.12.008

Seo, M., and Juhnn, Y. S. (2010). Gq Protein Mediates UVB-Induced Cyclooxygenase-2 Expression by Stimulating HB-EGF Secretion from HaCaT Human Keratinocytes. *Biochem. Biophys. Res. Commun.* 393, 190–195. doi:10.1016/j.bbrc.2010.01.085

Shimshon, L., Michaeli, A., Hadar, R., Nutt, S. L., David, Y., Navon, A., et al. (2011). SUMOylation of Blimp-1 Promotes its Proteasomal Degradation. *FEBS Lett.* 585, 2405–2409. doi:10.1016/j.febslet.2011.06.022

Shuyi, Y., Feng, W., Jing, T., Hongzhang, H., Haiyan, W., Pingping, M., et al. (2011). Human Beta-Defensin-3 (hBD-3) Upregulated by LPS via Epidermal Growth Factor Receptor (EGFR) Signaling Pathways to Enhance Lymphatic Invasion of Oral Squamous Cell Carcinoma. *Oral Surg. Oral Med. Oral Pathol. Oral Radiol. Endod.* 112, 616–625. doi:10.1016/j.tripleo.2011.02.053

Snoek, G. T., Boonstra, J., Ponec, M., and de Laat, S. W. (1987). Phorbol Ester Binding and Protein Kinase C Activity in normal and Transformed Human Keratinocytes. *Exp. Cel Res* 172, 146–157. doi:10.1016/0014-4827(87)90101-7

Tanaka, H., Muto, A., Shima, H., Katoh, Y., Sax, N., Tajima, S., et al. (2016). Epigenetic Regulation of the Blimp-1 Gene (Prdm1) in B Cells Involves Bach2 and Histone Deacetylase 3. *J. Biol. Chem.* 291, 6316–6330. doi:10.1074/jbc.M116.713842

Telerman, S. B., Rognoni, E., Sequeira, I., Pisco, A. O., Lichtenberger, B. M., Culley, O. J., et al. (2017). Dermal Blimp1 Acts Downstream of Epidermal TGFβ and Wnt/β-Catenin to Regulate Hair Follicle Formation and Growth. *J. Invest. Dermatol.* 137, 2270–2281. doi:10.1016/j.jid.2017.06.015

Thornley, A. L., and Jones, G. J. (1992). *In Vitro* secretion of Transforming Growth Factor Alpha (TGF-Alpha): a Comparison of the A431 Cell Line with Three Human Oesophageal Squamous Cell Carcinoma Lines. *Biosci. Rep.* 12, 293–302. doi:10.1007/BF01122801

Tseng, H. Y., Liu, Z. M., and Huang, H. S. (2012). NADPH Oxidase-Produced Superoxide Mediates EGFR Transactivation by C-Src in Arsenic Trioxide-Stimulated Human Keratinocytes. *Arch. Toxicol.* 86, 935–945. doi:10.1007/s00204-012-0856-9

Wan, Y., Belt, A., Wang, Z., Voorhees, J., and Fisher, G. (2001). Transmodulation of Epidermal Growth Factor Receptor Mediates IL-1 Beta-Induced MMP-1 Expression in Cultured Human Keratinocytes. *Int. J. Mol. Med.* 7, 329–334. doi:10.3892/ijmm.7.3.329

Wang, Y. H., Tsai, D. Y., Ko, Y. A., Yang, T. T., Lin, I. Y., Hung, K. H., et al. (2019). Blimp-1 Contributes to the Development and Function of Regulatory B Cells. *Front. Immunol.* 10, 1909. doi:10.3389/fimmu.2019.01909

Wu, N. L., Huang, D. Y., Hsieh, S. L., Hsiao, C. H., Lee, T. A., and Lin, W. W. (2013). EGFR-driven Up-Regulation of Decoy Receptor 3 in Keratinocytes Contributes to the Pathogenesis of Psoriasis. *Biochim. Biophys. Acta* 1832, 1538–1548. doi:10.1016/j.bbadis.2013.05.020

Wu, N. L., Huang, D. Y., Wang, L. F., Kannagi, R., Fan, Y. C., and Lin, W. W. (2016). Spleen Tyrosine Kinase Mediates EGFR Signaling to Regulate Keratinocyte Terminal Differentiation. *J. Invest. Dermatol.* 136, 192–201. doi:10.1038/JID.2015.381

Yu, Z., Sato, S., Trackman, P. C., Kirsch, K. H., and Sonenshein, G. E. (2012). Blimp1 Activation by AP-1 in Human Lung Cancer Cells Promotes a Migratory Phenotype and Is Inhibited by the Lysyl Oxidase Propeptide. *PLoS One* 7, e33287. doi:10.1371/journal.pone.0033287

Ziv, E., Rotem, C., Miodovnik, M., Ravid, A., and Koren, R. (2008). Two Modes of ERK Activation by TNF in Keratinocytes: Different Cellular Outcomes and Bi-directional Modulation by Vitamin D. *J. Cel Biochem* 104, 606–619. doi:10.1002/jcb.21650

Conflict of Interest: The authors declare that the research was conducted in the absence of any commercial or financial relationships that could be construed as a potential conflict of interest.

Publisher's Note: All claims expressed in this article are solely those of the authors and do not necessarily represent those of their affiliated organizations, or those of the publisher, the editors and the reviewers. Any product that may be evaluated in this article, or claim that may be made by its manufacturer, is not guaranteed or endorsed by the publisher.

Copyright © 2022 Lee, Huang, Chang, Lin, Ren, Dai and Lin. This is an open-access article distributed under the terms of the Creative Commons Attribution License (CC BY). The use, distribution or reproduction in other forums is permitted, provided the original author(s) and the copyright owner(s) are credited and that the original publication in this journal is cited, in accordance with accepted academic practice. No use, distribution or reproduction is permitted which does not comply with these terms.

frontiers in Pharmacology

ORIGINAL RESEARCH
published: 17 February 2022
doi: 10.3389/fphar.2022.806837

Levistilide A Promotes Expansion of Human Umbilical Cord Blood Hematopoietic Stem Cells by Enhancing Antioxidant Activity

Mei He[1†], Hui Xu[1†], Guangju Liu[2], Ming Yang[1], Wenshan Zhang[1], Yafang Li[1], Hexiao Zhang[1], Chaoqun Wang[1], Yiran Zhang[1], Xiaolei Liu[1], Shiqi Xu[1], Yahui Ding[3], Yinghui Li[1]*, Yingdai Gao[1]* and Quan Zhang[2]**

[1]State Key Laboratory of Experimental Hematology, PUMC Department of Stem Cell and Regenerative Medicine, CAMS Key Laboratory of Gene Therapy for Blood Diseases, National Clinical Research Center for Blood Diseases, Haihe Laboratory of Cell Ecosystem, Institute of Hematology and Blood Diseases Hospital, Chinese Academy of Medical Sciences and Peking Union Medical College, Tianjin, China, [2]State Key Laboratory of Medicinal Chemical Biology, College of Pharmacy and Tianjin Key Laboratory of Molecular Drug Research, Nankai University, Tianjin, China, [3]College of Chemistry, Nankai University, Tianjin, China

Several approaches to expand human hematopoietic stem cells (hHSCs) clinically along with retainable capability of multipotential differentiation have been reported, but only a few have advanced to evaluation in clinical trials, which limits the application of HSC-based therapy. Here we show a phthalide derivative, Levistilide A (LA), can serve as a promising molecule to expand functional human umbilical cord blood (UCB) HSCs *ex vivo*. An in-house screen identified LA out of nine natural products as an outstanding candidate for hHSCs expansion. Additionally, our data indicated that LA treatment not only increased the numbers of phenotype-defined HSCs, but also enhanced their colony formation ability. Xenotransplantation assays showed that LA treatment could maintain unaffected engraftment of hHSCs with multilineage differentiation capacity. Further experiments revealed that LA enhanced the antioxidant activity of hHSCs by reducing intracellular and mitochondrial reactive oxygen species (ROS) levels. The identification of LA provides a new strategy in solving the clinical issue of limited numbers of UCB HSCs.

Keywords: natural product, human hematopoietic stem cell, *ex vivo* expansion, phthalide derivatives, reactive oxygen species (ROS), Levistilide A

OPEN ACCESS

Edited by:
Salvatore Salomone, University of Catania, Italy

Reviewed by:
Valentina Salvestrini, University of Bologna, Italy
Christoph Schaniel, Icahn School of Medicine at Mount Sinai, United States
Eran Zimran, Hadassah Medical Center, Israel

****Correspondence:***
Quan Zhang
zhangquan612@163.com
Yingdai Gao
ydgao@ihcams.ac.cn
Yinghui Li
liyinghui@ihcams.ac.cn
Yahui Ding
017095@nankai.edu.cn

[†]These authors have contributed equally to this work and share first authorship

Specialty section:
This article was submitted to Experimental Pharmacology and Drug Discovery, a section of the journal Frontiers in Pharmacology

Received: *01 November 2021*
Accepted: *12 January 2022*
Published: *17 February 2022*

Citation:
He M, Xu H, Liu G, Yang M, Zhang W, Li Y, Zhang H, Wang C, Zhang Y, Liu X, Xu S, Ding Y, Li Y, Gao Y and Zhang Q (2022) Levistilide A Promotes Expansion of Human Umbilical Cord Blood Hematopoietic Stem Cells by Enhancing Antioxidant Activity. Front. Pharmacol. 13:806837. doi: 10.3389/fphar.2022.806837

INTRODUCTION

Development and maintenance of the hematopoietic system rely on a small heterogeneous pool of HSCs which are characterized by the capability of self-renewal and multipotent differentiation (Seita and Weissman, 2010). For individuals with defects in the hematopoietic system, such as hematological malignancies, hematopoietic stem cell transplantation (HSCT) has become the most practical form of stem cell therapy currently (Chivu-Economescu and Rubach, 2017). Hematopoietic stem and progenitor cells (HSPCs) in the graft will generate healthy cells to cure or replace the impaired cells. Superior to bone marrow (BM) and mobilized peripheral blood (mPB), UCB collections can be cryopreserved for over 20 years with efficient recovery of HSPCs after being thawed, and require lower human leukocyte antigen (HLA)-matching (Ballen et al., 2013). However, widespread use of UCB is still limited by two major obstacles: an insufficient dose of HSPCs in a single UCB collection, and subsequent delay of immune recovery post-transplantation (Ballen et al.,

2013; Huang et al., 2019). Thus, the top priority at present for UCB transplantation is to develop efficient methods to expand HSPCs *ex vivo* functionally and in turn improve the outcomes of transplantation.

To overcome the aforementioned obstacles, various strategies of expanding HSPCs *ex vivo* have been tested in the laboratory and even in the clinic, including genetic or epigenetic operations, modified culture systems with distinct combinations of cytokines such as stem cell factor (SCF), FMS-like tyrosine kinase-3 ligand (FLT3-L), and thrombopoietin (TPO), and also small molecules targeting certain signaling pathways (Zimran et al., 2021). However, small molecules show more advantages in aspects of safety, operational feasibility, expansion efficiency, and economy (Zhang et al., 2012). As exemplified by the surprising successes demonstrated for StemRegenin 1 (SR1) and UM171, the potential of small molecules to expand HSPCs has gradually been tapped. *Ex vivo* expansion by small molecules can either improve the homing of engrafted HSPCs (Christopherson et al., 2007; Goessling et al., 2011) or expand the absolute number of HSPCs in UCB collections (Fares et al., 2015; Zimran et al., 2021). SR1 (Boitano et al., 2010) and UM171 (Fares et al., 2014) are two potent small molecules that can preferentially expand hematopoietic progenitor cells (HPCs) and long-term HSCs, respectively, *ex vivo*. These approaches will ultimately contribute to improved engraftment of hHSCs.

The functionality of HSCs is affected by intrinsic regulations such as transcription factors and epigenetic modifiers, and extrinsic cues from the BM environment, including ionizing radiation (IR), chemotoxicity, and particularly the surrounding metabolic status (Boulais and Frenette, 2015; Testa et al., 2016). IR- or chemotherapy-induced BM injury leads to defects in HSCs and then senescence, which is caused by increased ROS and oxidative DNA damage (Wang et al., 2010; Wang et al., 2006). Similarly, metabolic status has a great influence on HSCs' functions by regulating the ROS level of the cell (Testa et al., 2016; Vlaski-Lafarge and Ivanovic, 2015). Different from the environment of downstream progenitors, HSCs are settled in a hypoxic BM environment, in which anaerobic metabolism is the main source of energy (Suda et al., 2011). An elevated intracellular ROS level increases DNA damage, which can promote the expression of cell-cycle inhibitors, causing senescence and loss of functions of HSCs (Yahata et al., 2011). HSCs are thus highly sensitive to oxidative stress (Suda et al., 2011), and their quiescence and functions must be maintained by low oxygen levels both intracellularly and mitochondrially. Therefore, many antioxidants such as ferulic acid, chlorophyllin, and Nicotinamide (NAM) have been developed to protect HSCs from excessive oxidative stress and ultimately to maintain self-renewal and the multipotent differentiation potential of HSCs (Hinge et al., 2010; Zeng-Chun MA, 2010; Baena-Gomez et al., 2015; Suryavanshi et al., 2015; Hwang and Song, 2017), which verifies an important link between ROS and HSCs.

Based on our previous research work (Gao et al., 2015; Xie et al., 2015; Ding et al., 2020; Li et al., 2020; Li et al., 2021), both the platform for chemical compound screening and the following efficacy evaluation of the *ex vivo* expansion of HSCs have been maturely established and put into service to find novel promising candidate compounds. In this study, we screened an in-house collection of natural products to find potential candidates able to expand functional long-term HSCs *ex vivo*. Among these compounds, LA, a dimer of a phthalide derivative, exhibited superior activity in expanding phenotype defined HSPCs and long-term HSCs proportionally and quantitatively. Moreover, LA maintained the engraftment capacity with uncompromised multipotency of hHSCs in NOG mice, suggesting the potential of LA for the *ex vivo* expansion of human UCB stem cells with functionally validated long-term repopulating capability.

MATERIALS AND METHODS

Compounds

All compounds (**1**–**9**) are >95% pure by HPLC analysis.

Compound **1** (neocnidilide): Purity: 98.3% by HPLC. ^{1}H NMR (400 MHz, $CDCl_3$) δ 6.75 (s, 1H), 4.08-3.88 (m, 1H), 2.48 (s, 1H), 2.40-2.10 (m, 2H), 1.97 (m, 2H), 1.74 (d, J = 5.8 Hz, 2H), 1.58-1.44 (m, 2H), 1.39 (m, 3H), 1.25 – 1.07 (m, 1H), 0.96 – 0.84 (m, 3H). ^{13}C NMR (100 MHz, $CDCl_3$) δ 170.4, 135.3, 131.3, 85.5, 43.2, 34.5, 27.7, 25.5, 25.1, 22.7, 20.9, 14.0. HRMS(ESI) calculated for $C_{12}H_{18}NaO_2^+$ $[M + Na]^+$: 217.1199, found 217.1205.

Compound **2** (levistilide A, LA): Purity: 98.8% by HPLC. ^{1}H NMR (400 MHz, $CDCl_3$) δ 7.34 (d, J = 6.6 Hz, 1H), 5.06 (t, J = 7.9 Hz, 1H), 4.99 (t, J = 7.5 Hz, 1H), 3.24 (d, J = 8.9 Hz, 1H), 2.98 (dd, J = 6.5, 2.1 Hz, 1H), 2.54 (t, J = 7.7 Hz, 1H), 2.28 (q, J = 7.6 Hz, 2H), 2.24 – 2.14 (m, 3H), 2.13 – 1.98 (m, 2H), 1.97 – 1.82 (m, 2H), 1.63 – 1.40 (m, 6H), 1.30 (ddd, J = 12.2, 4.7, 2.6 Hz, 1H), 0.98 – 0.87 (m, 6H). ^{13}C NMR (100 MHz, $CDCl_3$) δ 168.6, 165.0, 155.1, 150.6, 148.1, 142.2, 134.3, 126.7, 112.3, 108.7, 47.7, 41.7, 41.6, 38.4, 31.2, 29.1, 28.1, 27.6, 25.9, 22.4, 22.4, 19.9, 14.1, 13.9. HRMS (ESI) calculated for $C_{24}H_{29}O_4^+$ $[M^+H]^+$: 381.2060, found 381.2062.

Compound **3**: ^{1}H NMR (400 MHz, CDCl3) δ 5.32 – 5.22 (m, 1H), 4.48 (dt, J = 6.2, 1.7 Hz, 1H), 3.95 (ddd, J = 9.4, 6.0, 3.1 Hz, 1H), 3.43 (s, 2H), 2.64 – 2.44 (m, 2H), 2.34 (q, J = 7.6 Hz, 2H), 2.09 (dtd, J = 13.7, 5.3, 3.1 Hz, 1H), 1.88 (dddd, J = 13.7, 9.6, 8.3, 6.1 Hz, 1H), 1.49 (h, J = 7.4 Hz, 2H), 0.94 (t, J = 7.4 Hz, 3H); ^{13}C NMR (100 MHz, $CDCl_3$) δ 169.12, 152.86, 148.10, 125.98, 114.53, 71.92, 68.09, 28.21, 26.77, 22.39, 19.32, 13.91.

Compound **4**: ^{1}H NMR (400 MHz, CDCl3) δ 6.39 – 6.09 (m, 1H), 5.91 (dq, J = 9.5, 3.2 Hz, 1H), 4.92 (dd, J = 7.7, 3.9 Hz, 1H), 2.63 – 2.41 (m, 4H), 1.88 (dtt, J = 14.3, 6.9, 3.0 Hz, 1H), 1.59-1.48 (m, 1H), 1.39 (tdd, J = 17.7, 8.5, 4.6 Hz, 4H), 0.91 (td, J = 7.1, 2.6 Hz, 3H); ^{13}C NMR (100 MHz, $CDCl_3$) δ 171.39, 161.53, 128.45, 124.66, 117.04, 82.64, 32.05, 26.87, 22.58, 22.43, 20.94, 14.00.

Compound **5**: ^{1}H NMR (400 MHz, CDCl3) δ 7.85 (dq, J = 7.7, 1.0 Hz, 1H), 7.68 – 7.60 (m, 2H), 7.48 (ddt, J = 7.5, 6.4, 1.1 Hz, 1H), 5.62 (t, J = 7.8 Hz, 1H), 2.47-2.38 (m, 2H), 1.53 (h, J = 7.4 Hz, 2H), 0.96 (td, J = 7.4, 0.8 Hz, 3H); ^{13}C NMR (100 MHz, $CDCl_3$) δ 167.29, 145.80, 139.63, 134.31, 129.40, 125.25, 124.47, 119.72, 109.55, 27.85, 22.58, 13.87.

Compound **6**: ^{1}H NMR (400 MHz, CDCl3) δ 5.30 (t, J = 7.9 Hz, 1H), 4.61 (dd, J = 4.2, 2.3 Hz, 1H), 4.05 (ddt, J = 8.0, 4.0, 2.1 Hz, 1H), 3.40 (d, J = 2.8 Hz, 1H), 2.83 (d, J = 4.1 Hz, 1H), 2.65

(dddd, J = 18.4, 7.3, 5.6, 1.7 Hz, 1H), 2.45 – 2.28 (m, 3H), 2.13 (ddt, J = 13.7, 7.9, 5.8 Hz, 1H), 1.82 (tdd, J = 9.9, 6.4, 2.4 Hz, 1H), 1.49 (h, J = 7.3 Hz, 2H), 0.94 (t, J = 7.4 Hz, 3H); ^{13}C NMR (100 MHz, $CDCl_3$) δ 169.43, 153.38, 148.32, 125.47, 114.59, 67.41, 63.56, 28.21, 25.76, 22.39, 18.48, 13.91.

Compound **7**: ^{1}H NMR (400 MHz, CDCl3) δ 7.85 (d, J = 7.6 Hz, 1H), 7.64 (td, J = 7.5, 1.1 Hz, 1H), 7.49 (t, J = 7.5 Hz, 1H), 7.42 (dd, J = 7.6, 0.9 Hz, 1H), 5.45 (dd, J = 7.9, 4.1 Hz, 1H), 2.02 (dddd, J = 14.2, 10.0, 5.8, 4.1 Hz, 1H), 1.73 (dddd, J = 14.5, 10.0, 7.9, 4.7 Hz, 1H), 1.52-1.25 (m, 4H), 0.87 (t, J = 7.1 Hz, 3H); ^{13}C NMR (100 MHz, $CDCl_3$) δ 170.71, 150.15, 133.99, 129.03, 126.12, 125.63, 121.80, 81.47, 34.44, 26.89, 22.44, 13.87.

Compound **8**: ^{1}H NMR (400 MHz, CDCl3) δ 6.24 (dt, J = 9.6, 2.1 Hz, 1H), 5.97 (dt, J = 9.7, 4.2 Hz, 1H), 5.20 (t, J = 8.0 Hz, 1H), 2.57 (td, J = 9.5, 1.7 Hz, 2H), 2.49 – 2.39 (m, 2H), 2.34 (q, J = 7.6 Hz, 2H), 1.47 (h, J = 7.3 Hz, 2H), 0.92 (t, J = 7.4 Hz, 3H); ^{13}C NMR (100 MHz, $CDCl_3$) δ 167.70, 148.62, 147.19, 130.01, 124.02, 117.12, 113.02, 28.19, 22.47, 18.58, 13.85.

Compound **9**: ^{1}H NMR (400 MHz, CDCl3) δ 7.51 (d, J = 6.7 Hz, 1H), 6.16 (dt, J = 9.6, 2.0 Hz, 1H), 5.92 (dt, J = 9.6, 4.2 Hz, 1H), 4.62 (dd, J = 8.7, 6.8 Hz, 1H), 3.10 (dt, J = 7.0, 2.4 Hz, 2H), 2.52-2.45 (m, 1H), 2.33 – 2.24 (m, 2H), 2.23-1.91 (m, 6H), 1.70 – 1.63 (m, 1H), 1.51-1.41 (m, 1H), 1.39 – 1.20 (m, 4H), 1.17 – 1.07 (m, 1H), 0.88 (t, J = 7.1 Hz, 3H), 0.81 (t, J = 7.4 Hz, 3H); ^{13}C NMR (100 MHz, $CDCl_3$) δ 170.57, 164.37, 161.88, 148.58, 145.02, 133.09, 129.48, 125.65, 116.70, 107.64, 89.76, 50.18, 42.85, 36.75, 28.46, 28.26, 27.13, 22.73, 21.29, 21.19, 17.06, 14.27, 13.67.

Animals

Female NOD/Shi-scid/IL2Rγnull (NOG) mice (6-7 weeks) were purchased from Charles River and were housed in specific-pathogen-free (SPF) conditions, with free access to food and water. All animal protocols were approved by the Animal Care and Use Committee of State Key Laboratory of Experimental Hematology, Institute of Hematology and Blood Diseases Hospital.

Human UCB CD34$^+$ Cells Collection and Processing

Samples were collected from consenting donors by Shandong Qilu Stem Cell Engineering Co., Ltd. in accordance with the declaration of Helsinki and approved by the Ethics Review Board of the Institute of Hematology and Blood Diseases Hospital, Chinese Academy of Medical Sciences. Fresh collected human umbilical cord blood CD34$^+$ cells were isolated using LS Column and QuadroMACS Separator (Miltenyi Biotec), according to the manufacturer's protocol after collecting CD34 MicroBead-labeled cells by magnetic activated cells sorting (MACS) CD34 MicroBeads (Miltenyi Biotec).

Ex vivo HSC Expansion

For compound screening assays and mechanism research, fresh human UCB CD34$^+$ cells were cultured in HSC expansion medium consisting of Iscove's Modified Dulbecco's Medium (IMDM, Gibco) supplemented with 10% fetal bovine serum (FBS, Gibco), 100 ng/ml human stem cell factor (hSCF, PeproTech), 100 ng/ml human Fms-related tyrosine kinase three ligand (hFlt3-L, PeproTech), 100 ng/ml human thrombopoietin (hTPO, PeproTech), and 1% penicillin-streptomycin (P/S, Sigma-Aldrich). Isolated human CD34$^+$ UCB cells were resuspended in HSC expansion medium (5.3×10^4 cells/mL) before being seeded into 96 well plates (Corning). Small molecule compounds were dissolved in dimethyl sulfoxide (DMSO, Sigma-Aldrich) and stored as stock solutions. Stock solutions were diluted to working solutions at the desired concentration by HSC expansion media, and then added into cell suspension in 96 well plates. Each well contained 190 μL cell suspension (1×10^4 cells) and 10 μL small molecule compound working solution, which were fully blended. The final concentration of DMSO did not exceed 0.1% (v/v). Cells were incubated at 37°C with 5% CO_2 for 7 days. For further phenotype and function assays, fresh human UCB CD34$^+$ cells were cultured in HSC expansion medium consisting of StemSpan Serum-free Expansion Medium (SFEM, StemCell Technologies), 100 ng/ml hSCF, 100 ng/ml hFlt3-L, 100 ng/ml hTPO, 1% P/S, and supplemented with vehicle control (0.05% DMSO, v/v) or SR1 (Selleck) [1 μM] or LA [10 μM] or a combination of LA [10 μM] + SR1 [1 μM]. Isolated human CD34$^+$ UCB cells were resuspended in HSC expansion medium (2×10^6 cells/mL) before being seeded into 24 well plates (Corning). Each well contained 100 μL cell suspension (2×10^5 cells), 100 μL small molecule compound working solution, and 1800 μL expansion medium, which were fully blended. For transplantation experiments, human CD34$^+$CD38$^-$CD45RA$^-$CD90$^+$ cells were sorted into 96 well plates at 300 cells per well in 250 μL culture system. HSC expansion media composed of SFEM, 100 ng/ml hSCF, 100 ng/ml hFlt3-L, 100 ng/ml hTPO, 1% P/S, and supplemented with vehicle control (0.05% DMSO, v/v) or SR1 [1 μM] or LA [10 μM] or a combination of LA [10 μM] + SR1 [1 μM]. Cells were incubated at 37°C with 5% CO_2 for 4 days.

Flow Cytometry Analysis

UCB CD34$^+$ cells were seeded at 1×10^4 cells per well in the presence of chemical compounds. Total expanded cells were collected, and the live cells were counted using trypan blue and an automated cell counter (Bio-Rad, TC20) after 4–7 days of culture. Cell phenotypes in expanded cells were stained at 4°C for 30–60 min in PBS supplemented with a combination of the following antibodies and fluorophores: APC-labeled anti-human CD34 (BD; 555824), PE-Cy7-labeled anti-human CD38 (BD; 560,677), APC-H7-labeled anti-human CD45RA (BD; 560,674), PerCP-Cy5.5-labeled anti-human CD90 (BD; 561557), and PE-labeled anti-human CD49f (BD; 555736). Following a wash step, stained cells were analyzed using an LSRII (BD) or FACS CantoII (BD) flow cytometer. The absolute numbers of input cells were calculated based on FACS data of freshly isolated CD34$^+$ cells and the initial seeding number in the culture. The absolute numbers of output cells were obtained by multiplying the viable cell counts of expanded progeny by FACS proportion data.

Colony Forming Cell Assay (CFC)

The concentration of cultured human UCB CD34$^+$ cells was adjusted to 50 μL/1000 initial cells in Iscove's Modified Dulbecco's Medium (IMDM). Frequencies of colony-forming

cells were estimated by plating 10 μL cell suspension (equivalent to 200 initial cells) in 1 ml MethoCult™ GF H4434 (StemCell Technologies) in 6 well plates (Corning). After 14 days in culture, plates were visually scored for CFU-GM (colony-forming unit-granulocyte/macrophage), CFU-E (colony-forming unit-erythrocyte), BFU-E (burst-forming unit-erythroid), and CFU-GEMM (colony-forming unit granulocyte/erythrocyte/macrophage/megakaryocyte).

Cobblestone Area Forming Cell Assay (CAFC)

The frequency of Week 5 CAFC was determined using a limiting dilution assay. Cultured UCB $CD34^+$ cells were seeded on cryopreserved irradiated (8000 cGy) M2-10B4 bone marrow stromal cells (ATCC) in flat-bottomed collagen-coated 96 well plates at five different concentrations (63, 125, 250, 500, and 1000 cells) with 12 replicates per dilution. For assessment of CAFC after 5 weeks of culture, all wells were scored microscopically. Wells were scored as being positive for the presence of at least one cobblestone area (CA, tightly knit group of phase-dark, angular cells in the stroma). The CA-forming cell frequencies were calculated by ELDA software (http://bioinf.wehi.edu.au/software/elda/).

Transplantation and Monitoring of Human HSCs in NOG Mice

At 7–8 weeks of age, mice were irradiated at a dose of 250 cGy 4 h prior to transplantation. Experiments were conducted in sodium pentobarbital-anesthetized mice. For the uncultured group, freshly sorted UCB $DAPI^-CD34^+CD38^-CD45RA^-CD90^+$ cells were counted and resuspended in 300 cells/25 μL PBS per mouse and injected into mouse tibiae. For the compound-treated groups, 3000 sorted $DAPI^-CD34^+CD38^-CD45RA^-CD90^+$ cells were cultured for 4 days in the presence of chemical compounds as previously described. The expanded bulk-cell cultures were washed by PBS and adjusted to 300 equivalent initial cells/25 μL PBS per mouse and injected into mouse tibiae. Human cell chimerism was calculated at 4-, 8-, and 12-weeks post transplantation in the peripheral blood and 16-weeks post transplantation in bone marrow, using FITC-labeled anti-human CD45 (BD; 555482). At least 2% donor chimerism in PB or 15% in BM was determined as the threshold for positive engraftment. Multilineage reconstitution in BM was analyzed 16 weeks post-transplantation, using APC-labeled anti-human CD33 (BD; 551378), PE-Cy7-labeled anti-human CD3 (BD; 557851), PerCP-Cy5.5-labeled anti-human CD56 (BD; 560842), APC-labeled anti-human CD235a (BD; 561,775), and PE-labeled anti-human CD41a (BD; 557297).

ROS Assay

The cultured UCB $CD34^+$ cells treated with LA, SR1, DMSO, or LA plus SR1 were resuspended at a density of 5×10^5 to 1×10^6 cells/mL. Prior to adding working solution to cell suspensions prepared according to the manufacturer's instructions (Fluorometric Intracellular ROS Kit, Siga-Aldrich, cat: MAK144; MitoSOX™ Red mitochondrial superoxide indicator, Invitrogen, cat: M36008), the extracellular fluorescein labeled antibodies were first labeled for 30 min at 4°C. The fluorescence intensity of ROS was measured within 2 h by FACSArialll (BD) flow cytometer. The median level of MFI (mean fluorescence intensity) of ROS was obtained after Downsample in software FlowJo 10 (BD) of each sample to the same measuring cell number (for intracellular ROS: downsample $CD34^+$ subpopulation to 424,800 cells and $CD34^+CD38^-$ subpopulation to 47,808 cells; for MitoSox: downsample $CD34^+$ subpopulation to 111,430 cells and $CD34^+CD38^-$ subpopulation to 11,780 cells).

RNA Extraction

Cultured human UCB $CD34^+$ cells were lysed, and RNA was extracted using Trizol. RNA degradation and contamination were monitored on 1% agarose gels. RNA purity was checked using the NanoPhotometer spectrophotometer (IMPLEN, CAUnited State). RNA concentration was measured using Qubit RNA Assay Kit with Qubit 2.0 Flurometer (Life Technologies, CA, United States). RNA integrity was assessed using the RNA Nano 6000 Assay Kit of the Bioanalyzer 2100 system (Agilent Technologies, CA, United States).

RNA-Sequencing

A total amount of 3 μg RNA per sample was used as input material for the RNA sample preparations. Sequencing libraries were generated using NEBNext UltraTM RNA Library Prep Kit for Illumina (NEB, United States) following manufacturer's recommendations, and index codes were added to attribute sequences to each sample. The PCR products were purified with AMPure XP system (Beckman Coulter, Beverly, MA, United States) and library quality was assessed on the Agilent Bioanalyzer 2100 system. The clustering of the index-coded samples was performed on a cBot Cluster Generation System using TruSeq PE Cluster Kit v3-cBot-HS (Illumina) according to the manufacturer's instructions. After cluster generation, the library preparations were sequenced on an Illumina Hiseq platform and 125 bp/150 bp paired-end reads were generated. After mapping to the reference genome and quantification, DESeq2 (R package, 1.10.1) was used to analyze the differentially expressed genes. $|Log2(FoldChange)| > 0.0$ and the adjusted p-value (qadj) < 0.05 were used as a standard of cutting off for significance. The significantly changed genes were used in GO. GO terms results of molecules function (MF) were summarized and clustered based on semantic similarity measures using the online tool REVIGO (Supek et al., 2011). Total gene list was used in GSEA analysis, and gene sets used were searched from the GSEA gene set database (http://www.gsea-msigdb.org/gsea/msigdb/index.jsp).

Quantitative Real-Time PCR (qRT-PCR)

Reverse transcription of extracted RNA was performed using M-MLV Reverse transcriptase (Invitrogen, 28025-013) to obtain cDNA, following the manufacturer's instructions. qRT-PCR was then performed in a 384 well plate PCR reaction system using TB Green Premix Ex Taq (Tli RNaseH lusP) (Takara Bio, RR420A), according to the manufacturer's instructions. The PCR was run in QuantStudio six Flex (Thermo Fisher Scientific) selecting standard procedure for two-step PCR amplification: pre-denaturation (one cycle of 95°C for 30 s) and PCR reaction (40 cycles of 95°C for 5 s

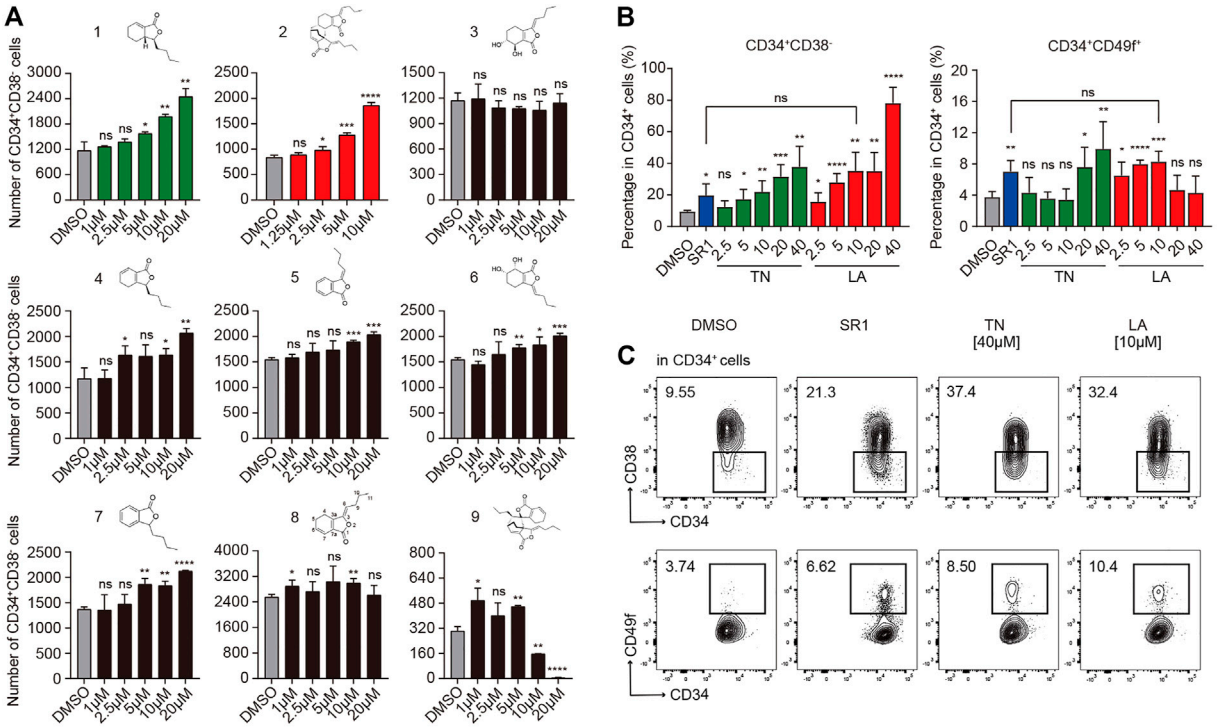

FIGURE 1 | Identification of proliferative activities of phthalide derivatives 1 to 9 and the optimal working concentration of candidate compounds for *in vitro* expansion of human UCB CD34$^+$ cells. **(A)** The structures of phthalide derivatives 1 to 9 and the corresponding absolute number of CD34$^+$CD38$^-$ cells after a serum-based 7-d culture in gradient concentrations as specified ($n = 6$). **(B)** The percentages of CD34$^+$CD38$^-$ and CD34$^+$CD49f$^+$ subpopulations in CD34$^+$ cells after a serum-based 7-d culture supplemented with DMSO (0.05%, v/v), SR1 (1 μM), Levistilide A (LA, 2.5 –40 μM), or Tetrahydrophthalide Neocnidilide (TN, 2.5 –40 μM) ($n = 5$). **(C)** Representative FACS profiles of CD34$^+$CD38$^-$ and CD34$^+$CD49f$^+$ subpopulations in cultured CD34$^+$ cells as described in **(B)**. All data represent the means ± SD. Compared with fresh unless specified. $^*p < 0.05$, $^{**}p < 0.01$, $^{***}p < 0.001$, $^{****}p < 0.0001$ and ns = not significant by two-tailed unpaired Students' *t*-test.

and then 60°C for 30 s). The expression of target transcripts was normalized to that of internal control GAPDH, and their relative expressions were processed based on their $2^{-\Delta\Delta Ct}$. The primers for target genes are listed in Supporting Information 1.

Statistical Analysis

All data are presented as the mean ± standard deviation (SD) and all statistical analyses were done using the software Graphpad Prism version 8.4.0 (GraphPad Software). Two tailed Student's t-test was used to generate *p* values for most of the data sets and *p*-values < .05 were considered statistically significant. Additionally, $^*p < .05$, $^{**}p < .01$, $^{***}p < .001$, $^{****}p < .0001$, ns = no significance. Chi-square test was used and performed by ELDA software in CAFC assay.

RESULTS

Screening of Nine Phthalide Derivatives That Can Expand HSPCs From UCB CD34$^+$Cells

To confirm the activity of expanding HSPCs among candidate compounds, primary human CD34$^+$ cells isolated from UCB using MACS were seeded into 96 well plates (1×10^4 cells per well) in medium (IMDM +10%FBS +100 ng/ml hSCF +100 ng/ml hTPO +100 ng/ml hFLT3-L + 1%P/S) supplemented with each compound (1–20 μM) or DMSO (0.05%, v/v, used in subsequent experiments unless otherwise noted), respectively. After 7 days incubation, the mixture of expanded cells was processed and the absolute number of HSPCs (**Figure 1A**) were analyzed by flow cytometry based on immunophenotype: CD34$^+$CD38$^-$. As is shown in **Figure 1A**, compound **2** (Levistilide A, LA) exhibited the most potent activity to expand HSPCs, followed by compound **1** (Tetrahydrophthalide Neocnidilide, TN), and next followed by other compounds **4**–**7**. LA is the dimer of compound **8** ((Z)-ligustilide, a common phthalide), but the monomer **8** demonstrated nearly no expansion activity. It appears that the dimer is more efficient than the monomer on expanding HSPCs and monomer **4** to **7** might be potential small molecular fragments to form effective compounds, similarly to monomer **8**. Significantly, the dimer **9** nearly lost potency to expand HSPCs. It is noteworthy that dimer **2** illustrates that the 6,7-alkene unit undergoes 4 + 2 cycloaddition as the dienophile with the monomer **8** 1,3-diene system, while dimer **9** is derived from 4 + 2 cycloaddition of the cross-conjugated 3,8-alkene. Therefore, for dimers, the pattern of 4 + 2 cycloaddition could be important for their HSPC expansion activity. Based on the results above, TN and

LA were identified as candidate compounds for HSPC expansion deserving further functional investigation.

Identification of Optimal HSPC Expansion Concentration of LA

To investigate the optimal expansion concentration of candidate TN and LA, UCB $CD34^+$ cells were incubated for 7 days in medium (IMDM +10%FBS +100 ng/ml hSCF +100 ng/ml hTPO +100 ng/ml hFLT3-L + 1%P/S) with TN or LA (2.5, 5, 10, 20, or 40 μM, respectively). SR1 (1 μM, used in subsequent experiments unless otherwise noted) was used as a positive control and equivalent DMSO as a negative control. Flow cytometry analysis was performed to analyze the percentage of subpopulations in live cells based on the expression of cell surface markers: CD34, CD38, and CD49f (Notta et al., 2011), which were always used to define a more primitive subpopulation of HSCs. Both LA and TN led to a dose-dependent increase in the percentage of $CD34^+CD38^-$ HSPCs (**Figure 1B**, left panel). As for $CD34^+CD49f^+$ HSCs, LA expanded cells in the concentration range of 2.5–10 μM, while TN worked at a concentration of at least 20 μM (**Figure 1B**, right panel). This indicated that LA was more potent expanding more primitive cell subsets than TN. SR1 treatment led to a twofold increase compared to DMSO in the percentage of both $CD34^+CD38^-$ HSPCs and $CD34^+CD49f^+$ HSCs (20 vs. 10% and 8 vs. 4%, respectively), which was similar to the expansion effects of LA at 10 μM (**Figures 1B,C**). Thus, our group identified LA as the most potent out of nine phthalide derivatives, and 10 μM (used in subsequent experiments) as the optimal concentration to expand HSPCs initiated with UCB-$CD34^+$ cells.

LA Enhanced Expansion of Phenotype-Defined Long-Term HSCs *in vitro*

It is known that CD34, CD38, CD90, CD45RA, and CD49f are common cell surface markers used for identifying human HSPCs *in vitro* and *in vivo*, and the detection of different combinations of these markers is a close estimate of HSCs (Tajer et al., 2019). Thus, we compared the difference of percentage in live cells and absolute number between the fresh UCB $CD34^+$ cells and cultured cells (treated with DMSO, SR1, LA or LA + SR1, respectively) by flow cytometry analysis to determine the expansion activity of LA alone and LA + SR1 at 10 μM on certain subpopulations of HSCs. When in a serum-free culture system (SFEM+100 ng/ml hSCF+100 ng/ml hTPO+100 ng/ml hFLT3-L+1%P/S) for 4 days, LA treatment significantly increased the number of $CD34^+$ cells and $CD34^+CD38^-$ cells rather than in percentage compared with fresh or DMSO, while it increased primitive $CD34^+CD38^-CD45RA^-CD90^+$ HSCs and $CD34^+CD38^-CD45RA^-CD90^+CD49f^+$ long-term HSCs obviously in both percentage and cell number, especially the latter subset (**Figure 2A**). LA incubation increased $CD34^+CD38^-CD45RA^-CD90^+CD49f^+$ cells up to sixfold compared with the fresh or DMSO, which is significantly more effective than SR1 treatment (**Figure 2A**). Notably, combining LA with SR1 could significantly improve the problem of insufficient SR1 expansion in counts of $CD34^+CD38^-CD45RA^-CD90^+CD49f^+$ cells (**Figure 2A**). When the culture time was prolonged to 7 days in this system, LA treatment could significantly expand both the percentage and cell number of these 4 cell populations, the fold change of which was nearly similar with that of 4-day culture. Additionally, 7-day LA treatment led to a 10-fold increase in the cell number of $CD34^+$ cells, $CD34^+CD38^-$ cells, or $CD34^+CD38^-CD45RA^-CD90^+$ cells compared with 4-day culture, while up to 25-fold in cell number for $CD34^+CD38^-CD45RA^-CD90^+CD49f^+$ cells and up to twofold in percentage (**Figure 2A**, **Supplementary Figure S1A**). Additionally, the expansion effect of SR1 on $CD34^+CD38^-CD45RA^-CD90^+CD49f^+$ cells was also manifested by prolonging the culture time (**Figure 2A**, **Supplementary Figure S1A**). When it comes to a 7-d serum-based culture, we found that treatment with DMSO, SR1, LA, LA + SR1 is inferior to that of serum-free culture neither in percentage nor in cell number (**Figure 2A**, **Supplementary Figure S2A**). However, regardless of the culture system with or without serum, the expansion of $CD34^+CD38^-CD45RA^-CD90^+CD49f^+$ long-term HSCs by LA was significantly superior to fresh or DMSO in both the percentage and cell number (**Figure 2A**, **Supplementary Figure S2A**). Representative FACS profiles of phenotypically defined subpopulations can be seen in **Figure 2B**, **Supplementary Figure S1B**, and **Supplementary Figure S2B**. These results indicated that incubation with LA can significantly expand phenotype defined HSPCs, in particular long-term HSCs.

LA Enhanced Colony Formation Capacity of HSCs

After identifying the *ex-vivo* expansion effect of LA on phenotype-defined HSPCs, we next evaluated the short-term differentiation potential of LA-treated cells in colony-forming cell (CFC) assays. First, we examined the clonogenic capacity of hUCB $CD34^+$ cells cultured *in vitro* in serum-free system added with DMSO, SR1, LA, or LA + SR1 for 4 d. It shows that LA-treated cells generated twofold, onefold, and onefold more total colonies than fresh, DMSO, and SR1, respectively. A combination of LA and SR1 can generate more total colonies than LA alone (**Figure 3A**). The number of erythrocyte colonies by the treatment of both LA and LA + SR1 were significantly higher than that of fresh and SR1. For BFU-E, both LA and LA + SR1 treatment generated significantly increased colonies as compared with fresh and SR1 and there was no significance between LA and LA + SR1. LA could also significantly increase the numbers of total colonies and CFU-E compared with DMSO in the 7-day serum-based culture system (**Supplementary Figure S3A**). Representative morphological images of different types of colonies are shown in **Figure 3B** and **Supplementary Figure S3B**. Then, cobblestone area-forming cell (CAFC) assays were carried out to assess the long-term hematopoietic activity of LA-treated cells initiated with UCB-$CD34^+$ cells. Limiting dilution analysis (LDA) showed that 0.88% (1 out of 113) of LA-treated $CD34^+$ cells had long-term repopulating activity, which was 1.7 times that of the DMSO group (0.52%, 1 out of 192) (**Supplementary Figure S3C**), suggesting that LA

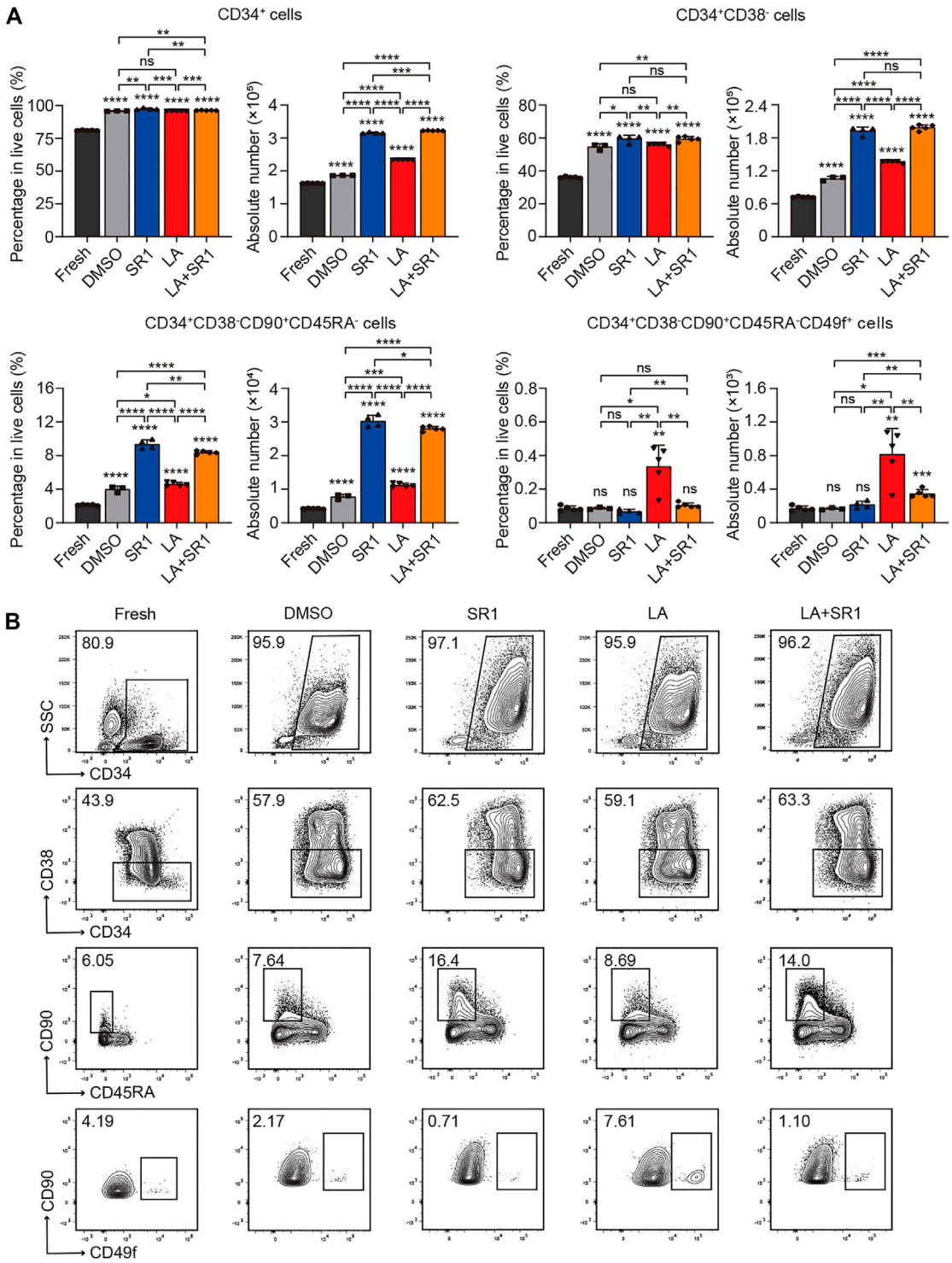

FIGURE 2 | LA promoted expansion of UCB HSCs *in vitro*. **(A)** The percentages in live cells and absolute number of $CD34^+$, $CD34^+CD38^-$, $CD34^+CD38^-CD45RA^-CD90^+$ and $CD34^+CD38^-CD45RA^-CD90^+CD49f^+$ subpopulations before (fresh, $n = 5$) and after a serum-free 4 days culture with DMSO (0.05%, v/v) ($n = 3$), SR1 (1 μM) ($n = 4$), LA (10 μM) ($n = 5$), or LA + SR1 ($n = 5$). All data represent the means ± SD. Compared with fresh unless specified. $^*p < 0.05$, $^{**}p < 0.01$, $^{***}p < 0.001$, $^{****}p < 0.0001$ and ns = not significant by two-tailed unpaired Students' *t*-test. **(B)** Representative FACS profiles of phenotypically defined subpopulations in cultured $CD34^+$ cells as described in **(A)**.

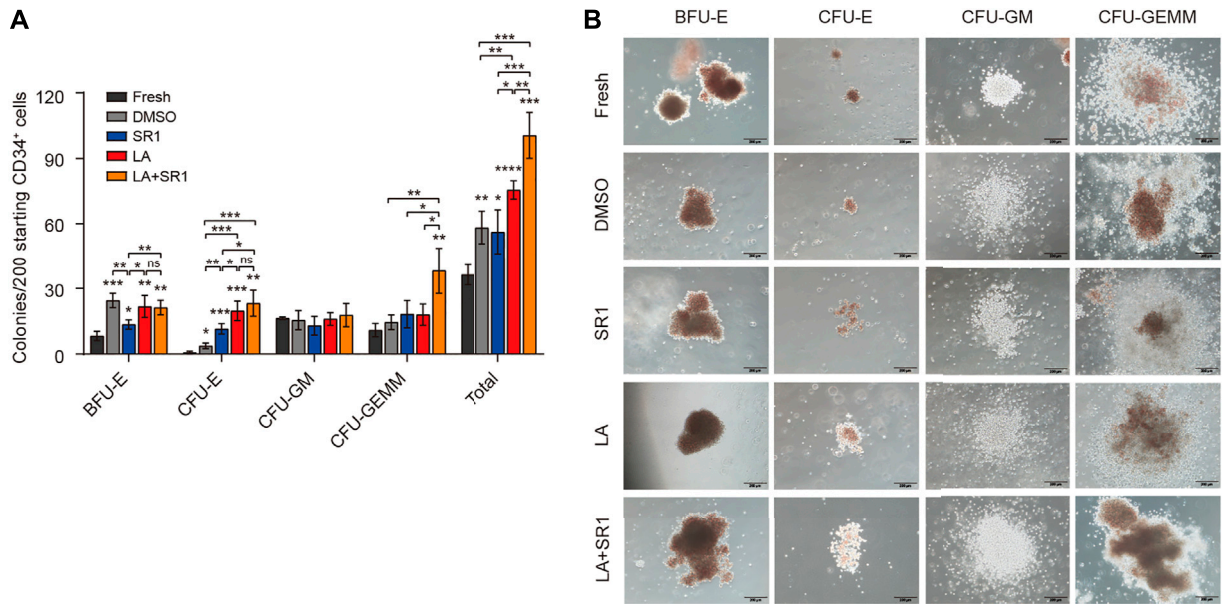

FIGURE 3 | LA enhanced the short-term clonogenic capacity of HSPCs *in vitro*. **(A)** Colonies derived from LA-treated (10 μM) cells in serum-free 4-d system following an additional 14-d culture in H4434 methylcellulose ($n = 3$). All data represent the means ± SD. Compared with fresh unless specified. *$p < 0.05$, **$p < 0.01$, ***$p < 0.001$, ****$p < 0.0001$ and ns = not significant by two-tailed unpaired Students' *t*-test. **(B)** Representative morphological images of CFU colonies (BFU-E, CFU-E, CFU-GM, CFU-GEMM). Scale bar, 200 μm.

maintained the long-term viability of HSPCs. Taken together, these results indicated that LA sustains the multipotentiality and long-term repopulating activity of HSPCs and promotes erythroid differentiation during *in vitro* culture.

LA Maintained Human HSCs Engraftment in a Xenograft Model

Although CFU and CAFC assays are usually used for assessing activities of HSCs and progenitors *in vitro*, xenotransplantation into immunodeficient mice is reported to be a gold standard assay to assess whether cultured cells *in vitro* can maintain the ability of HSCs to indefinitely repopulate all blood cell lineages (Goyama et al., 2015). We thus sorted $CD34^+CD38^-CD45RA^-CD90^+$ cells from the fresh and cultured groups (treated with DMSO, SR1, LA, or SR1 plus LA, respectively) initiated with UCB $CD34^+$ cells, which were injected respectively into sub-lethally irradiated severe combined immunodeficient NOD/Shi-scid/IL2Rγnull (NOG) mice *via* tail vein.

Flow cytometry was performed to measure human cell engraftment in peripheral blood (PB) at 4, 8, and 12 weeks and in BM at 16-weeks post-transplantation. We regarded the level of $CD45^+$ human cells not less than 2% in PB and not less than 15% in BM of mice recipients as a baseline of successful engraftment. Although human cells engraftment in PB of recipient NOG showed no significant difference among all groups at both 4- and 8-weeks post-transplantation, some mice in the SR1 group and SR1 plus LA group generated a slightly higher level of engraftment at week 8 (**Figure 4B**). At 12 weeks, we observed a significant increase of engraftment in the LA group compared to the fresh group. In addition, the SR1 plus LA group also increased the engraftment levels notably when compared with the fresh group, indicating that LA treatment may maintain engraftment of human cells (**Figure 4B**). These results indicated that LA treatment could maintain normal engraftment of human cells in recipient PB. Consistent with the results analyzed in PB at 12 weeks, when LA was administered, either the LA group or the SR1 plus LA group exhibited a generally higher level of human $CD45^+$ cells in BM at 16-weeks post-transplantation (**Figure 4C**, upper panel), which suggested that LA treatment retained the long-term engraftment of human cells. Except for the LA group and the SR1 plus LA group, there were recipients that did not achieve positive engraftment (the percentage of human $CD45^+$ cells less than 15%) in the fresh group (3 out of 6), the DMSO group (2 out of 6), or the SR1 group (1 out of 6) (**Figure 4C**, lower panel), which implied an unaffected engraftment of human cells after culturing with LA *ex vivo*.

Assessment of hematopoietic reconstitution in BM at 16-weeks post-transplantation was subsequently conducted, including total leukocytes ($CD45^+$), myeloid cells ($CD45^+CD33^+$), B lymphoid cells ($CD45^+CD19^+$), T lymphoid cells ($CD45^+CD3^+$), natural killer cells (NK cells, $CD45^+CD56^+$), megakaryocytes ($CD45^-CD41a^+$), and erythroid cells ($CD45^-CD235a^+$). As shown in **Figures 4D,E**, multiple lineages could be observed in both the LA group and the SR1 plus LA group, suggesting that LA treatment did not affect the multilineage differentiation potential of HSPCs. Differentiation into megakaryocytes and erythroid cells was significantly improved by LA treatment (**Figure 4D**), which was consistent with the results of functional verification *in vitro* by CFC assays. Notably, the combination of SR1 and LA resulted in a reconstruction level of

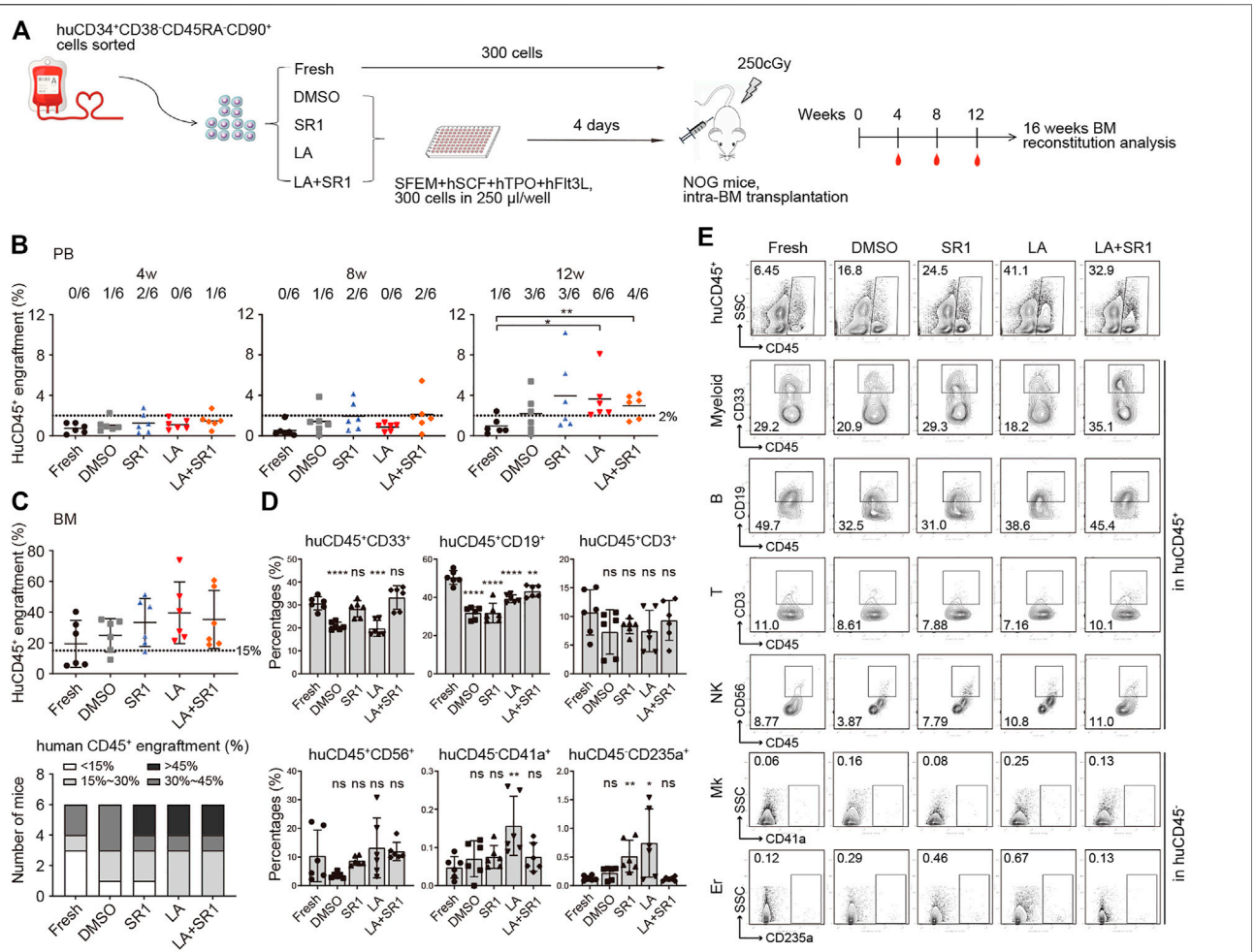

FIGURE 4 | Engraftment and reconstruction of human UCB CD34$^+$CD38$^-$CD45RA$^-$CD90$^+$ cells before (fresh) and after a 4-d culture with DMSO, SR1, LA alone, or in combination with SR1 (LA + SR1) in sublethal irradiated NOG mice. **(A)** Schematic representation of xenograft experiment. NOG mice were transplanted with 300 fresh or cultured cells (n = 6 mice per group). **(B)** Human engraftment in peripheral blood (PB) of NOG mice was detected at 4-, 8-, and 12-weeks post-transplantation and mice were sacrificed at 16-weeks post-transplantation for bone marrow (BM) analysis. **(B)** The percentage of human CD45$^+$ cells in PB of NOG mice. Numbers of mice with ≥2% engraftment percentage are specified. **(C)** The percentage of human CD45$^+$ cells in BM of NOG mice (upper panel) and the number of mice at different engraftment levels (<15%; 15%–30%; 30%–45%; >45%) (lower panel) in each group at 16-weeks post-transplantation. **(D)** Levels of myeloid (CD45$^+$CD33$^+$), B lymphocytes (CD45$^+$CD19$^+$), T lymphocytes (CD45$^+$CD3$^+$), natural killer cells (CD45$^+$CD56$^+$), megakaryocytes (CD45$^-$CD41a$^+$), and erythroid (CD45$^-$CD235a$^+$) reconstitution in BM of NOG mice at 16-weeks post-transplantation. **(E)** Representative FACS profiles showing engraftment of human CD45$^+$ cells and multilineage reconstruction described in **(C,D)**.

each lineage similar to that of fresh (**Figures 4D,E**). Taken together, our data revealed that LA treatment led to unaffected engraftment of human cells both in PB and BM of immunodeficient mice and did not alter the capacity of the engrafted cells to retain long-term hematopoietic repopulation. Importantly, the combination of reagents such as SR1 and LA could optimize outcomes of engraftment.

LA Enhanced the Antioxidant Activity of HSCs by Reducing ROS Levels Intracellularly and Mitochondrially

To elucidate the molecular mechanism by which LA expands HSCs, RNA-sequencing (RNA-seq) of the *in vitro* human UCB-CD34$^+$ cells was performed to obtain gene expression profiling in both the DMSO- and LA-treated groups, which showed that LA treatment resulted in significantly differential expression of 3384 upregulated and 3613 downregulated genes (**Figure 5A**). Based on these differentially expressed genes, we visualized the interactions among major gene ontology molecular function (GO:MF) terms by REVIGO, which showed that numerous genes have significantly increased oxidoreductase activity and antioxidant activity in the LA-treated group (**Figure 5B**), indicating that oxidation-reduction reactions might be one key focal point to explore how LA regulates HSCs' functions. Consistent with the results of REVIGO analysis, subsequent gene set enrichment analysis (GSEA) data revealed that two sets of genes in antioxidant- and glutathione-related pathways (see in Methods) were upregulated in LA-treated UCB-CD34$^+$ cells (**Figure 5C**). Furthermore, qRT-PCR analysis showed that the genes phosphatidylinositol 3-kinase (PI3KCA), protein kinase B

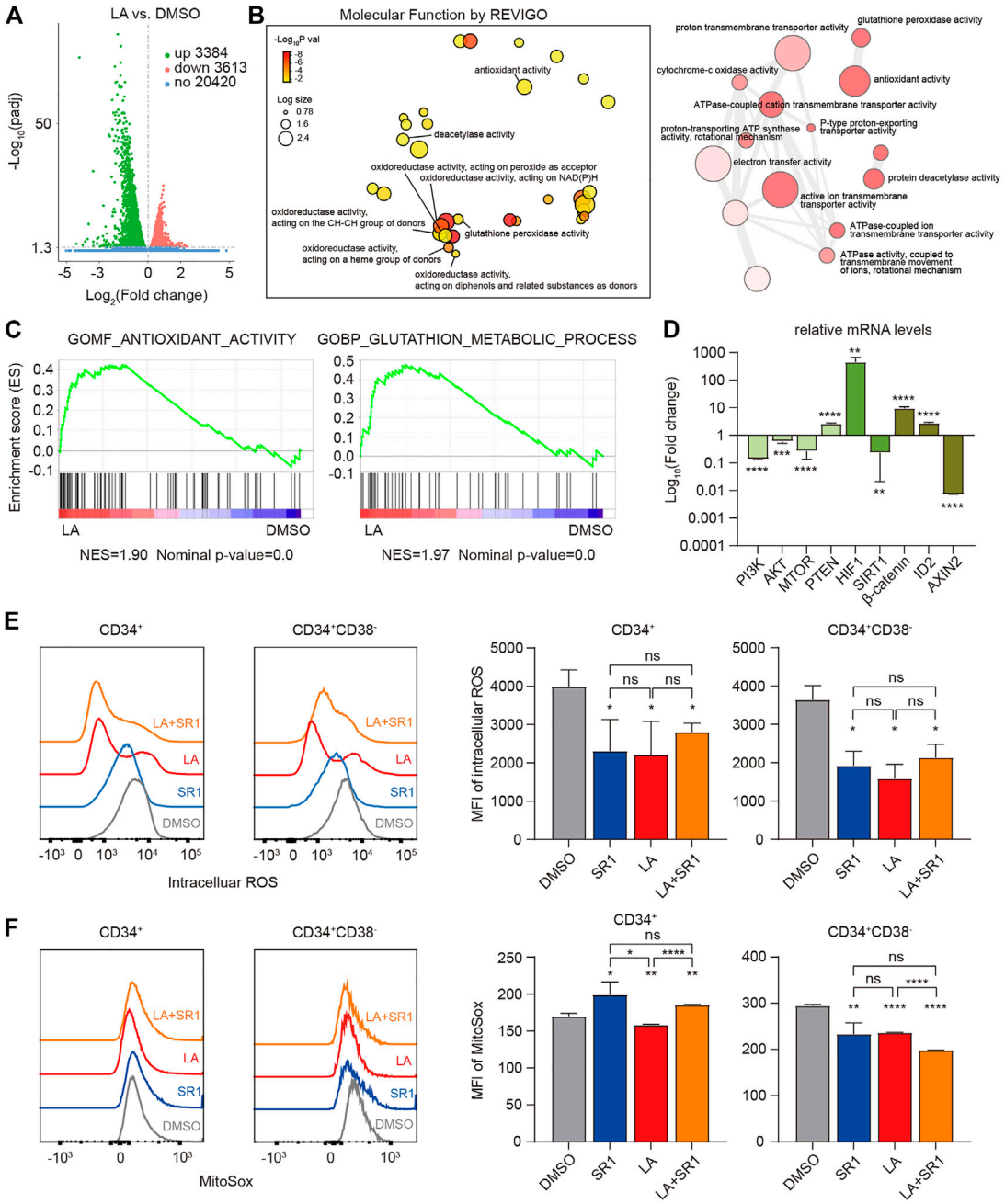

FIGURE 5 | LA-induced HSCs maintenance works by enhanced antioxidant capacity. **(A,B)**, RNA-seq profiling of LA cultured UCB CD34$^+$ cells. **(A)** Volcano plot of differentially expressed genes (DEGs) between LA- and DMSO-cultured UCB CD34$^+$ cells (3384 up-regulated and 3613 downregulated, |log2 fold change | > 0.0, and padj <0.05). **(B)** Interactive graph of major gene ontology molecular function (GO:MF) terms analysis by REVIGO (left). Bubble color indicates -Log10 *p* value; bubble size indicates the frequency of the GO term. Highly similar GO terms are linked by edges in the graph, where the line width indicates the degree of similarity (right). **(C)** GSEA enrichment plots of the gene sets enriched in LA vs. DMSO. Normalized enrichment score (NES) is shown. **(D)** Relative expression of metabolism-related and stemness-related genes using real-time PCR. Log_{10} of the fold change of mRNA levels of LA/DMSO is shown (n = 3). GAPDH served as a loading control. **(E,F)** Intracellular ROS levels **(E)** and mitochondrial ROS levels **(F)** of CD34$^+$ and CD34$^+$CD38$^-$ subpopulations in UCB CD34$^+$ cells after a serum-based 7-d culture with DMSO, SR1, LA ,or LA + SR1 (n = 3). All data represent the means ± SD. Compared with DMSO unless specified. *p < 0.05, **p < 0.01, ***p < 0.001, ****p < 0.0001 and ns = not significant by two-tailed unpaired Students' t-test.

(AKT3), mammalian target of rapamycin (mTOR), hypoxia-inducible factor-1 A (HIF-1A), catenin beta 1, β-catenin (CTNNB1), and inhibitor of DNA binding (ID2) were upregulated while the genes phosphate and tensin homolog (PTEN), sirtuins 1 (SIRT1), and axin two which degrades β-catenin (CTNNB1) were downregulated (**Figure 5D**), which

suggested that the PI3K/Akt/mTOR (Mansell et al., 2021; Testa et al., 2016), SIRT1/HIF-1A (Ballen et al., 2013; Suda et al., 2011; Testa et al., 2016), and Wnt/β-catenin signaling pathways (Huang et al., 2012) might participate in the regulation of HSCs by LA.

Several studies have demonstrated that HSCs tend to reside in a hypoxic BM microenvironment and generate energy merely through anaerobic glycolysis by limiting the production of ROS to maintain their stemness and quiescence, which varies from their progenitor cells (Suda et al., 2011; Testa et al., 2016, Vlaski-Lafarge and Ivanovic, 2015). Therefore, we measured the ROS levels in both the cytoplasm and mitochondria of $CD34^+$ and $CD34^+CD38^-$ cells from human UCB-$CD34^+$ cells cultured *in vitro* with DMSO, LA, SR1, or SR1 plus LA by flow cytometry. Mean fluorescence intensity (MFI) of intracellular ROS measurement showed that SR1 treatment or LA treatment significantly decreased the ROS levels in $CD34^+$ and $CD34^+CD38^-$ cells compared with that of the DMSO-treated group, while combining SR1 and LA did not decrease the ROS level further (**Figure 5E**). We also found that LA-treated cells had significantly lower mitochondrial ROS levels in $CD34^+$ and $CD34^+CD38^-$ cells when compared with the DMSO- or SR1-treated groups (**Figure 5F**). In addition, mitochondrial ROS was reduced by SR1 treatment only in the $CD34^+CD38^-$ subpopulation rather than in the $CD34^+$ subpopulation and combining SR1 with LA could reduce mitochondrial ROS further (**Figure 5F**). In summary, our experiments measuring ROS after treatment indicated that LA treatment led to significantly reduced intracellular and mitochondrial ROS levels in both $CD34^+$ and $CD34^+CD38^-$ cells, and the combination treatment of SR1 with LA selectively reduced mitochondrial ROS level in $CD34^+$ and $CD34^+CD38^-$ cells.

DISCUSSION

In this study, we identified LA, a dimeric phthalide derivative that could be a promising candidate to expand HSPCs *ex vivo*. Our data confirmed that LA treatment could not only expand phenotype-defined HSPCs *in vitro*, in particular in long-term HSCs which can be significantly expanded by LA in culture system with or without serum, but also retain their capacities of short-term and long-term colony formation and multilineage reconstitution in immunodeficient mice at the optimal dose of 10 μM. Phthalides are mainly extracted from the volatile oil of the plant Chuanxiong and with the rapid development of analytical techniques, hundreds of new phthalides have been identified and isolated in recent years (Chen et al., 2018). The superior activity of LA in proliferating HSCs suggests that nature is a rich library for storing diverse lead compounds which can be structurally modified or reorganized to achieve different bioactivities. Strikingly, we observed that monomer **8** itself exhibits no expansion effect on HSPCs, yet its dimer **2** (LA) exhibits potent activity, which suggests that the size and structure of the compound have a great influence on the potential target of LA. Moreover, although they are both dimers of compound **8**, the activity of LA (compound **2**) is totally different from that of compound **9** due to a different pattern of 4 + 2 cycloaddition. Perhaps the polymerization pattern subsequently impacts the spatial structure of the molecule, which determines its preferred binding targets and, in turn, distinct physiological reactions. If extending screening, more candidates belonging to phthalide derivatives may be identified. Additionally, it is notable that the expansion activity on HSPCs of phthalides is novel and varies from that of previously reported pharmacological properties such as anti-inflammation, analgesia, anti-thrombosis, anti-tumor, etc. (Chen et al., 2018), reminding us of the "new use of old medicine".

Drug combination is likely to represent a key strategy for the future treatment of various diseases. Our experiments of xenotransplantation in immunodeficient mice demonstrated that UCB-$CD34^+$ cells cultured with SR1 plus LA prior to transplantation exhibited slightly improved engraftment in PB and BM and a similar reconstitution level as that of the fresh UCB group. The aim of a drug combination is to achieve complementary advantages and reduce adverse effects. SR1 is reported to be mostly active on primitive normal hematopoietic progenitors and leukemia stem cells (LSCs) (Fares et al., 2015), while our data showed that LA had superior activity on long-term HSCs. Thus, combining SR1 and LA could make up for the deficiency of LA in expanding HPCs to fulfill complete proliferation of UCB-derived cells, even if the combination of LA and SR1 did not achieve expected combined effect on some type of colony and engraftment capacity, which is consistent with previous studies that show synergistic effect of the combination of SR1 and UM171 merely restricted to progenitor cell subpopulation (Zimran et al., 2021). This phenomenon reminds us that a combination of various agents with stem cell activity may lead to senescence or simply prove redundant. Essentially, drug combinations in this context refers to simultaneous activation of several signaling pathways related to hematopoiesis to gain ideal expansion outcomes. Previous studies have provided distinct mechanisms whereby small molecules expand *ex vivo* UCB-$CD34^+$ cells, taking SR1 as an example, which serves as an aryl hydrocarbon receptor (AhR) antagonist (Boitano et al., 2010); this has extended our understanding of hematopoiesis and the mechanisms involved. Additionally, increasing the number of investigations in the biology of HSCs will provide strong theoretical foundations for this work. Notably, this area of elucidation is not limited only to a combination between small molecules, but also extends to a combination among small molecules, cytokines, and three-dimensional microcarriers exemplified by zwitterionic hydrogel (ZTG) (Bai et al., 2019), which has been regarded as a novel efficient culture system for HSCs' expansion and merits further consideration.

Through our research into the mechanisms underlying our observations, we primarily revealed that LA treatment led to inhibition of the PI3K/Akt/mTOR signaling pathway, which plays a crucial role in regulating metabolism through complex mechanisms. For example, activation of mTORC1 by Akt and upregulation of HIF1 promote glycolysis by converting pyruvate to ATP molecules and lactate (Nepstad et al., 2020). Transferring to glycolysis means less NAD^+, a deacetylated substrate of SIRT1, will be generated. A lower NAD^+ level cannot make SIRT1 better for deacetylation (Hwang and Song, 2017). On the contrary, upregulated HIF1A combines with downregulated SIRT1 which in turn acetylates and activates HIF1A. Different substrates that

SIRT1 binds to determine different biological functions it exerts. Activation by downregulated SIRT1 is critical for HIF1A to function because upregulated SIRT1 leads to the deacetylation and inactivation of HIF1A even in hypoxia (Lim et al., 2010). This is the reason why some studies found that loss of SIRT1 leads to elevated ROS and DNA damage in mice (Bigarella et al., 2014). In contrast to HIF2A and HIF3A, HIF1A remains stable and promotes transcription of genes in the nucleus under hypoxic conditions to attenuate high ROS levels and severe DNA damage in cells (Bigarella et al., 2014; Lim et al., 2010; Testa et al., 2016). A number of studies have indicated that HIF activation can induce HSCs both *in vitro* and *in vivo* and potentiate their self-renewal potential (Forristal et al., 2013; Nombela-Arrieta et al., 2013), which may be because HIF1A drives cellular metabolism toward anaerobic glycolysis instead of mitochondrial respiration (Papa et al., 2019). However, the specific molecular mechanism whereby LA regulates the biology of HSCs through HIF1A deserves further study, including the reason why HIF1A was upregulated and SIR1 was downregulated after LA treatment. Additionally, the Wnt/β-catenin signaling pathway was activated, which could partially account for maintenance of HSCs (Huang et al., 2012).

In conclusion, we identified a phthalide derivative dimer, LA, which can expand HSPCs *in vitro* and maintain unaffected homing or engraftment of human HSCs cultured with LA *in vivo* with functional long-term hematopoietic reconstitution capability. Based on the relationship between hematopoiesis and redox status, we found that LA maintained quiescence and stemness of HSCs via terminal SIRT1/HIF1 collaboration to reduce intracellular and mitochondrial ROS level.

DATA AVAILABILITY STATEMENT

The datasets presented in this study can be found in online repositories. The names of the repository/repositories and accession number(s) can be found in the article/**Supplementary Material**.

ETHICS STATEMENT

The studies involving human participants were reviewed and approved by the Ethics Review Board of the Institute of Hematology and Blood Diseases Hospital, Chinese Academy of Medical Sciences. The patients/participants provided their written informed consent to participate in this study. The animal study was reviewed and approved by the Animal Care and Use Committee of State Key Laboratory of Experimental Hematology, Institute of Hematology and Blood Diseases Hospital.

AUTHOR CONTRIBUTIONS

MH and HX co-first authors performed the experiments, made the figures, and wrote the paper. MY, WZ, YFL, HZ, CW, YZ, XL, SX, YD and YL helped performed the experiments. GL provided the mass spectrometry and NMR information of compounds **3**–**9**. YL was responsible for critical reading of the manuscript and important intelligent content. QZ and YD completed chemical experiments. YG, LY, QZ contributed to the conception and design of the study. All authors have given approval to the final version of the manuscript.

FUNDING

This work was supported by grants from the Ministry of Science and Technology of China (No. 2017YFA0104900 and 2016YFA0100600), the National Science Foundation of China (NSFC 92068204, 81870083, 81970105, 81872764 and 81903456), Tianjin Science and Technology Planning Project (No. 18ZXXYSY00010), CAMS Innovation Fund for Medical Science No. 2021-I2M-1-019, Natural Science Foundation of Tianjin (No. 20JCQNJC02080) and a SKLEH-Pilot Research Grant.

ACKNOWLEDGMENTS

We would like to thank the staff of our animal housing facility who provided excellent care for our mice, and other workers who kindly provided professional assistance in performing flow cytometry analysis and RNA-seq, especially Wei Ch. Fu.

SUPPLEMENTARY MATERIAL

The Supplementary Material for this article can be found online at: https://www.frontiersin.org/articles/10.3389/fphar.2022.806837/full#supplementary-material

REFERENCES

Baena-Gómez, M. A., Aguilar, M. J., Mesa, M. D., Navero, J. L., and Gil-Campos, M. (2015). Changes in Antioxidant Defense System Using Different Lipid Emulsions in Parenteral Nutrition in Children after Hematopoietic Stem Cell Transplantation. *Nutrients* 7 (9), 7242–7255. doi:10.3390/nu7095335

Bai, T., Li, J., Sinclair, A., Imren, S., Merriam, F., Sun, F., et al. (2019). Expansion of Primitive Human Hematopoietic Stem Cells by Culture in a Zwitterionic Hydrogel. *Nat. Med.* 25 (10), 1566–1575. doi:10.1038/s41591-019-0601-5

Ballen, K. K., Gluckman, E., and Broxmeyer, H. E. (2013). Umbilical Cord Blood Transplantation: the First 25 Years and beyond. *Blood* 122 (4), 491–498. doi:10.1182/blood-2013-02-453175

Bigarella, C. L., Liang, R., and Ghaffari, S. (2014). Stem Cells and the Impact of ROS Signaling. *Development* 141 (22), 4206–4218. doi:10.1242/dev.107086

Boitano, A. E., Wang, J., Romeo, R., Bouchez, L. C., Parker, A. E., Sutton, S. E., et al. (2010). Aryl Hydrocarbon Receptor Antagonists Promote the Expansion of Human Hematopoietic Stem Cells. *Science* 329 (5997), 1345–1348. doi:10.1126/science.1191536

Boulais, P. E., and Frenette, P. S. (2015). Making Sense of Hematopoietic Stem Cell Niches. *Blood* 125 (17), 2621–2629. doi:10.1182/blood-2014-09-570192

Chen, Z., Zhang, C., Gao, F., Fu, Q., Fu, C., He, Y., et al. (2018). A Systematic Review on the Rhizome of Ligusticum Chuanxiong Hort. (Chuanxiong). *Food Chem. Toxicol.* 119, 309–325. doi:10.1016/j.fct.2018.02.050

Chivu-Economescu, M., and Rubach, M. (2017). Hematopoietic Stem Cells Therapies. *Curr. Stem Cel Res Ther* 12 (2), 124–133. doi:10.2174/1574888x10666151026114241

Christopherson, K. W., 2nd, Paganessi, L. A., Napier, S., and Porecha, N. K. (2007). CD26 Inhibition on CD34+ or Lineage- Human Umbilical Cord Blood Donor Hematopoietic Stem Cells/hematopoietic Progenitor Cells Improves Long-Term Engraftment into NOD/SCID/Beta2null Immunodeficient Mice. *Stem Cell Dev* 16 (3), 355–360. doi:10.1089/scd.2007.9996

Ding, Y., Gao, S., Shen, J., Bai, T., Yang, M., Xu, S., et al. (2020). TNFSF15 Facilitates Human Umbilical Cord Blood Haematopoietic Stem Cell Expansion by Activating Notch Signal Pathway. *J. Cel Mol Med* 24 (19), 11146–11157. doi:10.1111/jcmm.15626

Fares, I., Chagraoui, J., Gareau, Y., Gingras, S., Ruel, R., Mayotte, N., et al. (2014). Cord Blood Expansion. Pyrimidoindole Derivatives Are Agonists of Human Hematopoietic Stem Cell Self-Renewal. *Science* 345 (6203), 1509–1512. doi:10.1126/science.1256337

Fares, I., Rivest-Khan, L., Cohen, S., and Sauvageau, G. (2015). Small Molecule Regulation of normal and Leukemic Stem Cells. *Curr. Opin. Hematol.* 22 (4), 309–316. doi:10.1097/MOH.0000000000000151

Forristal, C. E., Winkler, I. G., Nowlan, B., Barbier, V., Walkinshaw, G., and Levesque, J. P. (2013). Pharmacologic Stabilization of HIF-1α Increases Hematopoietic Stem Cell Quiescence *In Vivo* and Accelerates Blood Recovery after Severe Irradiation. *Blood* 121 (5), 759–769. doi:10.1182/blood-2012-02-408419

Gao, Y., Yang, P., Shen, H., Yu, H., Song, X., Zhang, L., et al. (2015). Small-molecule Inhibitors Targeting INK4 Protein p18(INK4C) Enhance *Ex Vivo* Expansion of Haematopoietic Stem Cells. *Nat. Commun.* 6, 6328. doi:10.1038/ncomms7328

Goessling, W., Allen, R. S., Guan, X., Jin, P., Uchida, N., Dovey, M., et al. (2011). Prostaglandin E2 Enhances Human Cord Blood Stem Cell Xenotransplants and Shows Long-Term Safety in Preclinical Nonhuman Primate Transplant Models. *Cell Stem Cell* 8 (4), 445–458. doi:10.1016/j.stem.2011.02.003

Goyama, S., Wunderlich, M., and Mulloy, J. C. (2015). Xenograft Models for normal and Malignant Stem Cells. *Blood* 125 (17), 2630–2640. doi:10.1182/blood-2014-11-570218

Hinge, A. S., Limaye, L. S., Surolia, A., and Kale, V. P. (2010). *In Vitro* protection of Umbilical Cord Blood-Derived Primitive Hematopoietic Stem Progenitor Cell Pool by Mannose-specific Lectins via Antioxidant Mechanisms. *Transfusion* 50 (8), 1815–1826. doi:10.1111/j.1537-2995.2010.02647.x

Huang, J., Nguyen-McCarty, M., Hexner, E. O., Danet-Desnoyers, G., and Klein, P. S. (2012). Maintenance of Hematopoietic Stem Cells through Regulation of Wnt and mTOR Pathways. *Nat. Med.* 18 (12), 1778–1785. doi:10.1038/nm.2984

Huang, X., Guo, B., Capitano, M., and Broxmeyer, H. E. (2019). Past, Present, and Future Efforts to Enhance the Efficacy of Cord Blood Hematopoietic Cell Transplantation. *F1000Res* 8, 1833. doi:10.12688/f1000research.20002.1

Hwang, E. S., and Song, S. B. (2017). Nicotinamide Is an Inhibitor of SIRT1 *In Vitro*, but Can Be a Stimulator in Cells. *Cell Mol Life Sci* 74 (18), 3347–3362. doi:10.1007/s00018-017-2527-8

Li, Y., He, M., Zhang, W., Yang, M., Ding, Y., Xu, S., et al. (2020). Antioxidant Small Molecule Compound Chrysin Promotes the Self-Renewal of Hematopoietic Stem Cells. *Front. Pharmacol.* 11, 399. doi:10.3389/fphar.2020.00399

Li, Y., Zhang, W., Zhang, Y., Ding, Y., Yang, M., He, M., et al. (2021). Enhanced Self-Renewal of Human Long-Term Hematopoietic Stem Cells by a Sulfamoyl Benzoate Derivative Targeting p18INK4C. *Blood Adv.* 5 (17), 3362–3372. doi:10.1182/bloodadvances.2020004054

Lim, J. H., Lee, Y. M., Chun, Y. S., Chen, J., Kim, J. E., and Park, J. W. (2010). Sirtuin 1 Modulates Cellular Responses to Hypoxia by Deacetylating Hypoxia-Inducible Factor 1alpha. *Mol. Cel* 38 (6), 864–878. doi:10.1016/j.molcel.2010.05.023

Mansell, E., Sigurdsson, V., Deltcheva, E., Brown, J., James, C., Miharada, K., et al. (2021). Mitochondrial Potentiation Ameliorates Age-Related Heterogeneity in Hematopoietic Stem Cell Function. *Cell Stem Cell* 28 (2), 241–e6. doi:10.1016/j.stem.2020.09.018

Nepstad, I., Hatfield, K. J., Grønningsæter, I. S., and Reikvam, H. (2020). The PI3K-Akt-mTOR Signaling Pathway in Human Acute Myeloid Leukemia (AML) Cells. *Int. J. Mol. Sci.* 21 (8). doi:10.3390/ijms21082907

Nombela-Arrieta, C., Pivarnik, G., Winkel, B., Canty, K. J., Harley, B., Mahoney, J. E., et al. (2013). Quantitative Imaging of Haematopoietic Stem and Progenitor Cell Localization and Hypoxic Status in the Bone Marrow Microenvironment. *Nat. Cel Biol* 15 (5), 533–543. doi:10.1038/ncb2730

Notta, F., Doulatov, S., Laurenti, E., Poeppl, A., Jurisica, I., and Dick, J. E. (2011). Isolation of Single Human Hematopoietic Stem Cells Capable of Long-Term Multilineage Engraftment. *Science* 333 (6039), 218–221. doi:10.1126/science.1201219

Papa, L., Djedaini, M., and Hoffman, R. (2019). Mitochondrial Role in Stemness and Differentiation of Hematopoietic Stem Cells. *Stem Cell Int* 2019, 4067162. doi:10.1155/2019/4067162

Seita, J., and Weissman, I. L. (2010). Hematopoietic Stem Cell: Self-Renewal versus Differentiation. *Wiley Interdiscip. Rev. Syst. Biol. Med.* 2 (6), 640–653. doi:10.1002/wsbm.86

Suda, T., Takubo, K., and Semenza, G. L. (2011). Metabolic Regulation of Hematopoietic Stem Cells in the Hypoxic Niche. *Cell Stem Cell* 9 (4), 298–310. doi:10.1016/j.stem.2011.09.010

Supek, F., Bošnjak, M., Škunca, N., and Šmuc, T. (2011). REVIGO Summarizes and Visualizes Long Lists of Gene Ontology Terms. *PLoS One* 6 (7), e21800. doi:10.1371/journal.pone.0021800

Suryavanshi, S., Sharma, D., Checker, R., Thoh, M., Gota, V., Sandur, S. K., et al. (2015). Amelioration of Radiation-Induced Hematopoietic Syndrome by an Antioxidant Chlorophyllin through Increased Stem Cell Activity and Modulation of Hematopoiesis. *Free Radic. Biol. Med.* 85, 56–70. doi:10.1016/j.freeradbiomed.2015.04.007

Tajer, P., Pike-Overzet, K., Arias, S., Havenga, M., and Staal, F. J. T. (2019). *Ex Vivo* Expansion of Hematopoietic Stem Cells for Therapeutic Purposes: Lessons from Development and the Niche. *Cells* 8 (2). doi:10.3390/cells8020169

Testa, U., Labbaye, C., Castelli, G., and Pelosi, E. (2016). Oxidative Stress and Hypoxia in normal and Leukemic Stem Cells. *Exp. Hematol.* 44 (7), 540–560. doi:10.1016/j.exphem.2016.04.012

Vlaski-Lafarge, M., and Ivanovic, Z. (2015). Reliability of ROS and RNS Detection in Hematopoietic Stem Cells-Ppotential Issues with Probes and Target Cell Population. *J. Cel Sci* 128 (21), 3849–3860. doi:10.1242/jcs.171496

Wang, Y., Liu, L., Pazhanisamy, S. K., Li, H., Meng, A., and Zhou, D. (2010). Total Body Irradiation Causes Residual Bone Marrow Injury by Induction of Persistent Oxidative Stress in Murine Hematopoietic Stem Cells. *Free Radic. Biol. Med.* 48 (2), 348–356. doi:10.1016/j.freeradbiomed.2009.11.005

Wang, Y., Schulte, B. A., LaRue, A. C., Ogawa, M., and Zhou, D. (2006). Total Body Irradiation Selectively Induces Murine Hematopoietic Stem Cell Senescence. *Blood* 107 (1), 358–366. doi:10.1182/blood-2005-04-1418

Xie, X. Q., Yang, P., Zhang, Y., Zhang, P., Wang, L., Ding, Y., et al. (2015). Discovery of Novel INK4C Small-Molecule Inhibitors to Promote Human and Murine Hematopoietic Stem Cell *Ex Vivo* Expansion. *Sci. Rep.* 5, 18115. doi:10.1038/srep18115

Yahata, T., Takanashi, T., Muguruma, Y., Ibrahim, A. A., Matsuzawa, H., Uno, T., et al. (2011). Accumulation of Oxidative DNA Damage Restricts the Self-Renewal Capacity of Human Hematopoietic Stem Cells. *Blood* 118 (11), 2941–2950. doi:10.1182/blood-2011-01-330050

Zhang, Y., Li, W., Laurent, T., and Ding, S. (2012). Small Molecules, Big Roles -- the Chemical Manipulation of Stem Cell Fate and Somatic Cell Reprogramming. *J. Cel Sci* 125 (Pt 23), 5609–5620. doi:10.1242/jcs.096032

Zhang, Y., Li, W., Tan, Hong-Ling., Laurent, X. I. A. O., Ding, S., and Yue Gao, A. (2010). Small Molecules, Big Roles - the Chemical Manipulation of Stem Cell Fate and Somatic Cell Reprogramming. *Biol. Pharm. Bull.* 33, 29–34.

Zimran, E., Papa, L., and Hoffman, R. (2021). *Ex Vivo* expansion of Hematopoietic Stem Cells: Finally Transitioning from the Lab to the Clinic. *Blood Rev.* 50, 100853. doi:10.1016/j.blre.2021.100853

Conflict of Interest: The authors declare that the research was conducted in the absence of any commercial or financial relationships that could be construed as a potential conflict of interest.

Publisher's Note: All claims expressed in this article are solely those of the authors and do not necessarily represent those of their affiliated organizations, or those of the publisher, the editors, and the reviewers. Any product that may be evaluated in this article, or claim that may be made by its manufacturer, is not guaranteed or endorsed by the publisher.

Copyright © 2022 He, Xu, Liu, Yang, Zhang, Li, Zhang, Wang, Zhang, Liu, Xu, Ding, Li, Gao and Zhang. This is an open-access article distributed under the terms of the Creative Commons Attribution License (CC BY). The use, distribution or reproduction in other forums is permitted, provided the original author(s) and the copyright owner(s) are credited and that the original publication in this journal is cited, in accordance with accepted academic practice. No use, distribution or reproduction is permitted which does not comply with these terms.

frontiers in Pharmacology

ORIGINAL RESEARCH
published: 21 February 2022
doi: 10.3389/fphar.2022.818116

Apigenin, a Single Active Component of Herbal Extract, Alleviates Xerostomia *via* ERα-Mediated Upregulation of AQP5 Activation

Wei Wei[1], *Tingting Cao*[2], *Janak L. Pathak*[2], *Xintong Liu*[3,4], *Tianjiao Mao*[2,5], *Nobumoto Watanabe*[3,4], *Xiaomeng Li*[1]*, *Manli Zhang*[2] *and Jiang Li*[2]*

[1]The Key Laboratory of Molecular Epigenetic, Institute of Genetics and Cytology, Northeast Normal University, Changchun, China, [2]Guangdong Engineering Research Center of Oral Restoration and Reconstruction, Affiliated Stomatology Hospital of Guangzhou Medical University, Guangzhou, China, [3]Chemical Biology Research Group, RIKEN Center for Sustainable Resource Science, Saitama, Japan, [4]Bio-Active Compounds Discovery Unit, RIKEN Center for Sustainable Resource Science, Saitama, Japan, [5]Hospital of Stomatology, Jilin University, Changchun, China

OPEN ACCESS

Edited by:
Andres Trostchansky,
Universidad de la República, Uruguay

Reviewed by:
Lyanne Rodriguez,
University of Talca, Chile
Anna Zalewska,
Medical University of Bialystok, Poland
Olga Juliana Baker,
University of Missouri, United States

***Correspondence:**
Xiaomeng Li
lixm441@nenu.edu.cn
Jiang Li
ljiang@gzhmu.edu.cn

Specialty section:
This article was submitted to Experimental Pharmacology and Drug Discovery, a section of the journal Frontiers in Pharmacology

Received: 19 November 2021
Accepted: 26 January 2022
Published: 21 February 2022

Citation:
Wei W, Cao T, Pathak JL, Liu X, Mao T, Watanabe N, Li X, Zhang M and Li J (2022) Apigenin, a Single Active Component of Herbal Extract, Alleviates Xerostomia via ERα-Mediated Upregulation of AQP5 Activation. Front. Pharmacol. 13:818116. doi: 10.3389/fphar.2022.818116

Xerostomia is a common symptom in menopausal women, suggesting the role of sex steroids in disease development. Shreds of literature had reported the potential use of herbal extracts to relieve xerostomia. However, a cocktail of multiple components in herbal extract makes it difficult to understand the exact mechanism of action. Aquaporin5 (AQP5), the specific aquaporin expressed in salivary glands, plays an important role in salivary secretion as a downstream of estrogen signaling. In this study, we aimed to unravel a single active herbal component as a therapeutic for xerostomia and investigate its mechanism of action. The effects of apigenin (flavonoid), dauricine (alkaloids), protopine (alkaloids), and lentinan (polysaccharides) on AQP5 transcription were screened *in vitro*. Only apigenin robustly induced AQP5 transcription and expression, and this effect was even robust compared to the effect of estradiol (E2, a positive control). Overexpression of estrogen receptor α (ERα) in the human salivary gland cell line (HSG) upregulated the AQP5 transcription and expression and the knockdown ERα reversed this effect, suggesting the role of ERα signaling on AQP5 activation in HSG cells. Docking results showed apigenin-specific binding sites in ERα. We further analyzed the therapeutic effect of apigenin on ovariectomized mice as a xerostomia model. The saliva secretion in the xerostomia group was reduced to one-third of the sham group, whereas the apigenin or E2 treatment for 12 weeks reversed this effect. Meanwhile, the water consumption in the xerostomia group was augmented obviously compared to the sham group, whereas the water consumption in the apigenin and E2 group was declined to the level of the sham group. Immunohistochemistry of submandibular glands revealed the downregulation of AQP5 expression in xerostomia mice compared to control. Apigenin, or E2 treatment, upregulated AQP5 expression in xerostomia mice. In conclusion, apigenin, a single active component of herbal extract, upregulated AQP5 expression in HSG cells via activation of ERα signaling and restored saliva flow rates in OVX mice. These results revealed apigenin as a single active component of herbal extract with the potential to treat xerostomia.

Keywords: apigenin, xerostomia, aquaporin5 (AQP5), estrogen receptor α (ERα), ovariectomized (OVX) mice

INTRODUCTION

Xerostomia is the subjective feeling of oral dryness (Delli et al., 2014). The main symptoms of xerostomia are thick saliva, chapped lips, and abnormal taste; it destroys oral functions such as chewing, swallowing, and speaking (Liu et al., 2018). Xerostomia has a significant negative effect on patients' quality of life (Millsop et al., 2017). Xerostomia affects millions of patients throughout the world, and the prevalence is between 12 and 30% (Tanasiewicz et al., 2016). Reports from the literature suggest that xerostomia affects mostly menopausal women and individuals older than 65 years (Minicucci et al., 2013; D R et al., 2014). Clinical studies have demonstrated that estrogen therapy could effectively alleviate oral dryness by augmenting salivary secretion in menopausal women (Eliasson et al., 2003; Lago et al., 2015). However, long-term estrogen therapy possesses a risk for endometrial and breast cancer (Liang and Shang, 2013; Marjoribanks et al., 2017). Therefore, alternative therapeutic approaches to treat xerostomia are still in high demand.

Shreds of evidence from the literature had shown the therapeutic potential of several herbal extracts to treat xerostomia (Murakami et al., 2009; Chang et al., 2015). However, the cocktail of multiple components in the herbal extract is a key hurdle to unraveling the molecular mechanism and mode of action of the therapy. To overcome this issue, researchers are currently focused on isolating a single active therapeutic component from the herbal extract. Flavonoids, alkaloids, and polysaccharides are commonly isolated active therapeutic components from plant extracts (Almadi and Almohaimede, 2018; Ibrahim et al., 2018). The therapeutic potential and mechanisms of action of these active components, from plant extract, in treating xerostomia are not fully understood.

Aquaporins (AQPs), as transmembrane channel proteins, mediate transcellular water permeability (Delporte et al., 2016). Aquaporin5 (AQP5) is specifically expressed in salivary glands and plays an important role in salivary secretion (Hosoi, 2016). The decreased expression or abnormal distribution of AQP5 diminishes saliva secretion (Krane et al., 2001; Matsuzaki et al., 2012). AQP5 null mice show a 30% reduction in salivary secretion compared to wild type mice (WT) (Ma et al., 1999). Similarly, irradiated rats show decreased saliva secretion and AQP5 protein expression (Li et al., 2006). Since xerostomia is common in postmenopausal women, estrogen deficiency could play a role in the development of this disease. Salivary epithelium expresses a functional estrogen receptor (ER) α and ERβ (Tsinti et al., 2009; Wei et al., 2019). The estrogen response element (ERE) is located in the promoter region of the AQP5 gene (Kobayashi et al., 2006; Jiang et al., 2015). This suggests AQP5 as a downstream signaling protein of estrogen signaling. Therefore, the single active component from plant extract that can modulate estrogen AQP5 signaling in the salivary gland could be a possible drug to rescue xerostomia.

In this study, we aimed to identify a single active herbal component as a therapeutic for xerostomia. First, the effect of apigenin (flavonoid), dauricine (alkaloids), protopine (alkaloids), or lentinan (polysaccharides) on AQP5 transcription was screened *in vitro*. We further investigated the mechanism of apigenin-induced AQP5 transcription in human submandibular gland (HSG) cells. The effect of overexpression and knockdown of ERα in HSG cells on AQP5 expression was analyzed. Since only the apigenin upregulated AQP5, docking analysis was performed to unravel the apigenin-specific binding sites in ERα. The effect of apigenin treatment on xerostomia was further investigated in ovariectomized (OVX) mice as a xerostomia model. Our results revealed apigenin as a single active component of herbal extract with the potential to treat xerostomia *via* modulating ERα-AQP5 signaling.

MATERIAL AND METHODS

Chemicals and Reagents

HSG cell line was provided by Prof. Hongchen Sun from the Stomatological Hospital of Jilin University. Apigenin and estradiol (E2) (Baoji Herbest Bio-Tech Co., Ltd. Shanxi, China), fetal bovine serum (FBS, Sijiqing Biological Engineering Materials Co. Ltd., Hangzhou, China), Dulbecco's modified Eagle's medium (DMEM, Thermo Fisher Scientific, Shanghai, China), EndoFectin Max Transfection Reagent (GeneCopoeia, Rockville, MD, United States), luciferase reported detection reagents (Promega, Madison, WI, United States), total RNA extraction kit (Shanghai, Yeasen, China), anti-mouse monoclonal AQP5 antibodies (Santa Cruz Biotechnology, Dallas, TX, United States), anti-mouse monoclonal ERα antibodies (Santa Cruz Biotechnology, Dallas, TX, United States), anti-rabbit ERα antibodies (Bioss Biosynthesis Biotechnology, Beijing, China), anti-mouse and anti-rabbit secondary antibodies (Bioss Biosynthesis Biotechnology, Beijing, China), and Chromatin Immunoprecipitation (ChIP) Assay Kit (Beyotime, China) were used in this study.

Cell Culture and Plasmid Transient Transfection

The HSG cells were seeded and cultured in a 10 cm culture dish with DMEM containing 10% FBS, then incubated at 37°C in a humidified incubator supplied with 5% CO2. The AQP5 promoter–luciferase (AQP5p-luc) plasmid was constructed by amplifying the AQP5 promoter sequence, from -2,000 bp to + 200 bp (Homo sapiens), then linking to pGL3 basic vector *via* KpnI and XhoI sites to create an artificial pGL3/AQP5 promoter–reporter system. The ERα plasmid and ERαshRNA plasmid were purchased from Genepharma, Inc.

The HSG cells were seeded into 48-well plates containing 1% FBS, transfected with 100 ng appropriate AQP5p-luc plasmid together with 25 ng pREP7 plasmid, or/and 10 ng ERα/ERαshRNA plasmid using transfection reagent following the manufacturer's protocol. HSG cells were seeded into 6-well plates containing 1% FBS and transfected with 1 μg ERα/ERαshRNA plasmid using transfection reagent following the manufacturer's protocol.

Dual-Luciferase Reporter Assay

HSG cells were seeded in a 48-well plate with a DMEM containing 1% FBS. Cells of each well were transfected with 100 mg appropriate AQP5p-luc plasmid together with 25 ng pREP7 plasmid for 48 h. Then the cells were stimulated by dauricine (1 μM), protopine (1 μM), lentinan (1 μM), apigenin (1 μM), or E2 (0.1 μM) for 24 h. The apigenin was divided into 0.01, 0.1, and 1 μM. The cells were lysed in 65 μL passive lysis buffer rocking on ice for 30 min. The lysate was transferred into a new tube and centrifuged at a speed of 13,500 rpm for 10 min. For firefly luciferase activity detection, 30 μL of the supernatant was measured by using the dual-luciferase reporter assay system. The ratio of firefly luciferase activity to Renilla luciferase activity was calculated as relative luciferase activity.

Real-Time Quantitative PCR

HSG cells (Jaiboonma et al., 2020) were seeded in 6-well plates with a DMEM containing 1% FBS. The cells were stimulated with apigenin (0.01, 0.1, and 1 μM) and E2 (0.1 μM) for 48 h. The total RNA from differently treated cells was extracted using a total RNA extraction reagent. RNA was then reverse-transcribed by first strand cDNA synthesis supermix for qPCR and amplified using SYBR Green Master Mix by the real-time PCR detection system. Primers used for qPCR were as follows: human AQP5 (forward primer: 5′-TGCCATCCTTTACTTCTACCTG-3′, reverse primer: 5′-CTCATACGTGCCTTTGATGATG-3′) and human β-actin (forward primer: 5′-GGCACCACACCTTCT ACAATGAGC-3′, reverse primer: 5′-GATAGCACAGCCTGG ATAGCAACG-3′). The thermal cycling condition for PCR amplification was 95°C for 5 min, 40 cycles of 95°C for 10 s, 60°C for 30 s, followed by 40°C for 20 min. The relative expression ratio was calculated from real-time PCR efficiencies and the crossing point deviation of a given gene vs. β-actin house-keeping gene. In each independent experiment, the mean gene expression ratios obtained with regularly submerged cultures were given a value of 1 (fold).

Western Blot Assay

HSG cells were seeded in a 6-well plate with a DMEM containing 1% FBS. Cells of each well were stimulated with apigenin (0.01, 0.1, and 1 μM) and E2 (0.1 μM) for 48 h. To verify whether apigenin upregulated AQP5 transcription through the ERα pathway HSG cells were seeded in 6-well plates containing 1% FBS, transfected with 1 μg ERα/ERαshRNA plasmid using transfection reagent for 48 h, and induced with 1 μM apigenin for 24 h. The cells were lysed on ice with RIPA for 30 min. The submandibular glands tissues of mice were lysed on ice with RIPA. The protein samples were resolved on 12% SDS-PAGE and transferred to the PVDF membrane. The membranes were incubated with 5% (w/v) skimmed milk in TBST, followed by incubation with primary antibodies (AQP5 1:200, β-actin 1: 1,000) at 4°C overnight. The membranes were further incubated with HRP conjugated respective goat anti-mouse (1: 500) secondary antibody IgG at room temperature for 1 h. Signals were detected using ECL plus chemiluminescence kit on X-ray film. The protein expression in the Western blots was quantified using Image J software.

Immunofluorescence Study

HSG cells were seeded in DMEM complemented with 1% FBS. The cells were stimulated with 1 μM apigenin and 0.1 μM E2 for 48 h. The cells were fixed with 4% paraformaldehyde for 10 min, permeabilized in 0.2% Triton X-100 for 10 min, and blocked with 1% bovine serum albumin (BSA) for 1 h. Then the cells were incubated with anti-mouse AQP5 antibodies in 1:100 dilution at 4°C overnight, followed by incubation with fluorophore-conjugated secondary antibodies 1:500 for 1 h at room temperature. DAPI staining for 5 min was carried out after secondary antibody incubation.

To verify whether apigenin upregulated AQP5 transcription through the ERα pathway, HSG cells were transfected with ERα/ ERαshRNA plasmid using transfection reagent for 48 h and induced with 1 μM apigenin for 24 h. The cells were fixed with 4% paraformaldehyde for 10 min, permeabilized in 0.2% Triton X-100 for 10 min, and blocked with 1% bovine serum albumin (BSA) for 1 h. Then the cells were incubated with anti-mouse AQP5 antibodies in 1:100 dilution at 4°C overnight and anti-rabbit ERα antibodies in 1:100 dilution for 2 h at room temperature. The cells were incubated with fluorophore-conjugated goat anti-mouse (red) secondary antibodies 1:500 for 1 h at room temperature, followed by fluorophore-conjugated goat anti-rabbit (green) secondary antibodies 1: 1,000 for 1 h at room temperature. DAPI staining for 5 min was carried out after secondary antibody incubation. Staining was detected using fluorescent microscopy (model IX71; Olympus, Tokyo, Japan).

ChIP Assay

HSG cells were treated with 1 μM apigenin for 48 h. The chromatin immunoprecipitation (ChIP) assays were performed according to the manufacturer's protocol (Beyotime Co.). Chromatin solutions were sonicated and incubated with anti-ERα and rotated overnight at 4°C. DNA–protein cross-links were reversed and chromatin DNA was purified and subjected to PCR analysis. The primers ERE1 (forward primer: 5′-GGAACTGGA AGAAAGTGTCA-3′, reverse primer: 5′-TGCCTTTTGCTG TCTTAGTC-3′), ERE2 (forward primer: 5′- TTGGGAGGT CAGTGGTGC-3′, reverse primer: 5′-TGGAAGGCTGGCGTT TT-3′), ERE3 (forward primer: 5′-CAAAACGCCAGCCTTCCA A-3′, reverse primer: 5′-TCCTCCTTTTCCTCCTGCGAC -3′), ERE4 (forward primer: 5′-AGCTAGACGCCCCGAGGTCG-3′, reverse primer: 5′-TCTCCGTCGTCCAGCGCAAC-3′), which were designed to amplify the AQP5 promoter region that contains ERα binding sites by Jaspar database, were used. After amplification, PCR products were resolved on a 1.5% agarose gel.

Autodock Analyses

For docking purposes, the structure of apigenin (PubChem CID: 5280443), E2 (PubChem CID: 5756), and lentinan (PubChem CID: 37723) were retrieved from the PubChem Compound repository of small molecules in NCBI. The macromolecular structures of the human ERα ligand binding region were retrieved from the PDB protein data bank. Docking was carried out by AutoDock software to analyze the binding

energy and amino acid residues of apigenin and ERα in the docking model.

Animal Study

Twenty-four female ICR mice (aged 6 weeks, weighing 30 ± 2 g) were purchased from the Hua Fukang Biotechnology Co., Ltd. (Beijing, China). All mice were free to obtain soy-based food and water under the light/dark cycle for 12/12 h at a constant temperature of 25 ± 1°C. The mice were divided randomly into four groups (sham operation, OVX/control, OVX/apigenin, and OVX/E2) with six mice in each group. For ovariectomy and sham surgery, the mice were anesthetized with intraperitoneal administration of 10 mg/kg 0.7% sodium pentobarbital. An incision was made in the middle of the abdomen and then the bilateral ovaries were removed. In the sham group, the ovaries were exposed and a small piece of adipose tissue was removed. The incision was layered and sutured. Then the mice received daily drug treatment by oral gavage. The OVX/apigenin group mice were gavaged with apigenin (dissolved in 0.5% carboxymethyl cellulose sodium) 50 mg/kg/day (Yang et al., 2018). The OVX/E2 group mice were gavaged with E2 (dissolved in 0.5% carboxymethyl cellulose sodium) 1 mg/kg/day (Liu et al., 2018). The sham operation group and OVX/control group mice were administrated by 0.5% carboxymethyl cellulose sodium in the same way. The saliva secretion and water consumption were recorded before ovariectomy and after 4, 8, and 12 weeks of drug administration as described previously (Lai et al., 2016; Liu et al., 2018). After 12 weeks of drug administration, mice were anesthetized and submandibular glands were used for immunohistochemistry and Western blot assay.

Saliva Secretion and Water Consumption Assessment

The saliva secretion was measured by a previously described method before ovariectomy and after 4, 8, and 12 weeks of drug administration (Nakamura et al., 2004; Tajiri et al., 2019). Before the saliva was collected, the mice were fasted for the night. The mice were routinely anesthetized with intraperitoneal administration of 10 mg/kg 0.7% sodium pentobarbital. Then pilocarpine (1.0 mg/kg) was injected subcutaneously. We collected saliva from the oral cavity using pre-weighed pieces of cotton every 5 min for a total of 30 min, then weighed the pieces of cotton again. The saliva secretion index was calculated by the amount of increase in weight (mg)/body weight (g).

The water consumption for 7 days was recorded before ovariectomy and after, 4, 8, and 12 weeks of drug administration. The average water consumption index of each group was calculated by the water consumption (ml)/body weight (g), and then the changes among each group were observed.

Histology and Immunostaining

After 12 weeks of drug administration, mice were anesthetized and submandibular glands were removed by routine surgery and fixed in 4% polyformaldehyde. Then the specimen was dehydrated with alcohol gradient, transparent to xylene, embedded in paraffin, and cut into 5-μm-thick tissue sections. For immunohistochemistry, tissue sections were incubated with primary antibodies, AQP5 (1:100) at 4°C overnight. Then the tissue sections were incubated with biotinylated goat anti-rabbit/mouse IgG antibody at room temperature for 60 min and followed by DAB color rendering hematoxylin counterstaining for 3 min. Then the same tissue sections were counterstained with hematoxylin and eosin (H&E) staining. Staining was visualized in the same structural area and quantified using a model IX71 light microscope (Olympus, Tokyo, Japan). Plaque number and staining area were calculated by Image J software.

Statistical Analysis

All data are presented as mean ± standard deviation (SD). Statistical significance was evaluated using a one-way analysis of variance. Each experiment was repeated at least three times. Statistical analysis was performed using SPSS 22.0 statistics software. Image J software was used for data analysis in Western blot and immunohistochemical staining. Differences were considered to be statistically significant at $p < 0.05$.

RESULTS

Apigenin, a Natural Flavone, Screened to Activate AQP5 Transcription

To screen the natural products activating AQP5 transcription, we performed a dual-luciferase reporter assay. In this study, three categories of effective components from plant extract, that is, flavonoids (apigenin), alkaloids (dauricine and protopine), and polysaccharides (lentinan) were selected to screen their effect on AQP5 expression. Apigenin, a natural flavone, can be extracted from parsley, celery, chamomile, and so on (**Figure 1A**). Estradiol (E2), a positive transcriptional regulator of AQP5, was used as a positive control. We transfected the luciferase reporter pGL3/AQP5p (-2,000-+200 bp, *Homo sapiens*) plasmid (**Figure 1B**) into HSG cells, induced by PBS, 1 μM dauricine, protopine, lentinan, apigenin, and 0.1 μM E2, and then tested AQP5 transcription. The data showed that dauricine, protopine, and lentinan did not affect the AQP5 transcription, whereas E2 treatment enhanced AQP5 transcription by approximately 2.0-fold. Interestingly, apigenin (1 μM) robustly induced AQP5 transcription by 3.0-fold (**Figure 1C**). Furthermore, to investigate the dose-dependent effect of apigenin on the AQP5 transcription, we performed a dual-luciferase reporter assay in HSG cells in the presence of different concentrations of apigenin. Apigenin upregulated AQP5 transcription in a dose-dependent manner (**Figure 1D**). The data indicate that apigenin, a natural flavone, activates AQP5 transcription.

Apigenin Upregulates AQP5 Transcription and Expression

To monitor the changes of the endogenous AQP5 transcription level, we performed the real-time quantitative PCR in HSG cells induced by different concentrations of apigenin. Apigenin

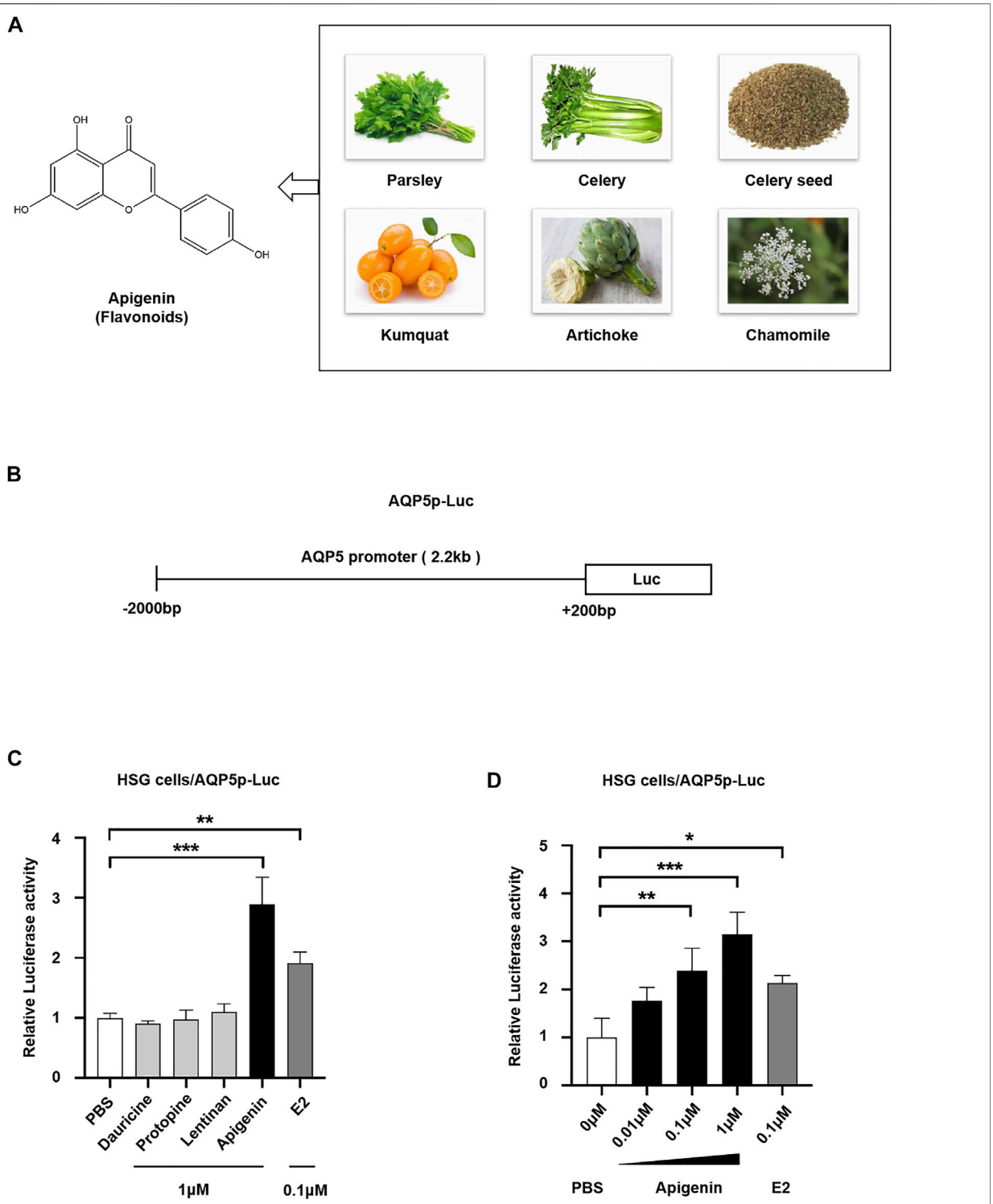

FIGURE 1 | Natural product apigenin upregulates AQP5 transcription. **(A)** Structure of apigenin. **(B)** Luciferase reporter pGL3/AQP5 promoter (AQP5p) plasmid. **(C)** Relative luciferase activity showing the AQP5p activation induced by apigenin in HSG cells. **(D)** Apigenin activated the AQP5p in dose dependence. Data are presented as the mean ± SD, $n = 3$. Significant effect of the treatment, $^{*}p < 0.05$, $^{**}p < 0.01$.

upregulated AQP5 transcription in a dose-dependent manner, and the AQP5 mRNA relative expression level was increased by 4.0-fold compared to the control group (**Figure 2A**). The effect of apigenin (1 μM) on AQP5 transcription was more prominent than that of E2 (0.1 μM). These data suggest the AQP5 transcription potential of apigenin.

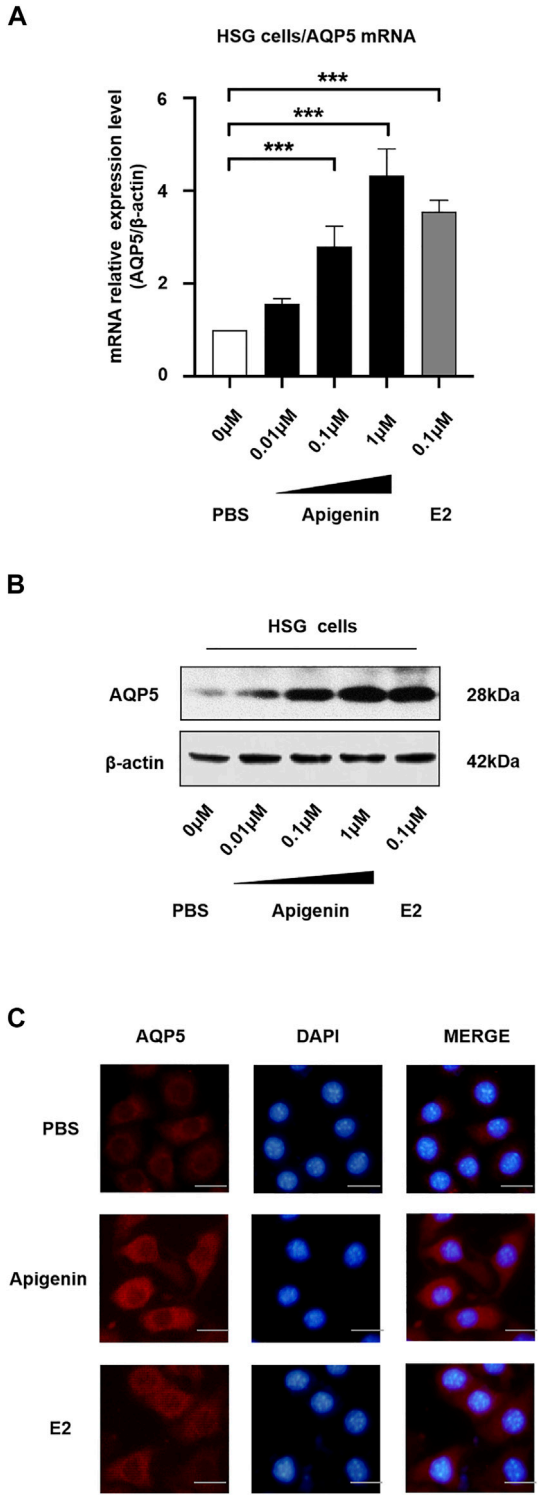

FIGURE 2 | Apigenin upregulates AQP5 transcription and expression. **(A)** mRNA relative expression level (AQP5/β-actin) showing the AQP5 transcription in HSG cells by qPCR. **(B)** Apigenin upregulates AQP5 expression. Representative Western blot image showing endogenous AQP5 protein expression in HSG cells. **(C)** Immunofluorescence staining showing the AQP5 protein level and localization in HSG cells. Bar scale, 50 μm. Data are presented as the mean ± SD, $n = 3$. Significant effect of the treatment, $^{*}p < 0.05$, $^{**}p < 0.01$.

To verify the endogenous AQP5 protein level and localization in HSG cells, we performed Western blot and immunofluorescence staining. We observed there was a dose-dependent increase in AQP5 protein level in the HSG cells treated with apigenin (**Figure 2B**). The results of Western blot analysis were in accordance with the results of qPCR. As shown in **Figure 2C**, AQP5 protein expression was upregulated in the apigenin-treated group. The AQP5 protein was mainly localized in the cell membrane and cytoplasm. Taken together, these data indicate that apigenin upregulates AQP5 transcription and expression in HSG cells.

Apigenin Upregulates Transcription and Translation of AQP5 Through the ERα Pathway

We demonstrated that apigenin upregulates AQP5 transcription. Apigenin is a flavone with estrogen activity; therefore, we analyzed potential ERα binding sites in the AQP5 promoter and explored whether the ERα pathway involved in the AQP5 transcriptional activation.

First, to evaluate the existence of ERα binding sites in the AQP5 promoter sequence, we searched the AQP5 promoter in NCBI databases and predicted transcription factor binding sites in the JASPAR database. As shown in **Figure 3A**, four ERα binding sites are located in the AQP5 promoter sequence. The ERE sequence is at −1,430 to −1,416, −690 to −676, −478 to −464, and −223 to −209 bp in AQP5 promote. These data suggest that ERα binding sites exist in the AQP5 promoter sequence.

To ascertain the direct recruitment of the ERα complex on the AQP5 promoter, ChIP assays were performed with ERα antibodies in HSG cells. In order to further verify ERE binding sites in apigenin and AQP5 promoter sequences, we designed 4 pairs of ChIP primers, whose products were −1,444 to −1,211, −883 to −643, −660 to −442, and −374 to −143 bp, respectively, included ERE binding sites predicted by JASPER database. ChIP results showed that ERα occupancy was apparently increased at ERE3 in the presence of apigenin (**Figure 3B**). These data suggest the direct increased recruitment of ERα on the AQP5 promoter is the response to apigenin.

Then, we aimed to verify whether apigenin upregulated AQP5 transcription through the ERα pathway. We performed a dual-luciferase reporter assay and Western blot by gene overexpression and interference of ERα. As shown in **Figure 3C**, the overexpression of ERα induced AQP5 activation in HSG cells by 2.0-fold. Intriguingly, while interference of ERα, the AQP5 activation was downregulated. Meanwhile, an approximately 4.0-fold induction of AQP5 activation was observed in apigenin-treated ERα overexpressed HSG cells. This effect was nullified in ERα-knocked down HSG cells. A similar effect of apigenin in AQP5 expression was observed in ERα-overexpressed and -knocked down in Western blot in HSG cells (**Figure 3D**). Taken together, the aforementioned results indicate that apigenin activates AQP5 transcription and upregulates the AQP5 protein expression through the ERα pathway.

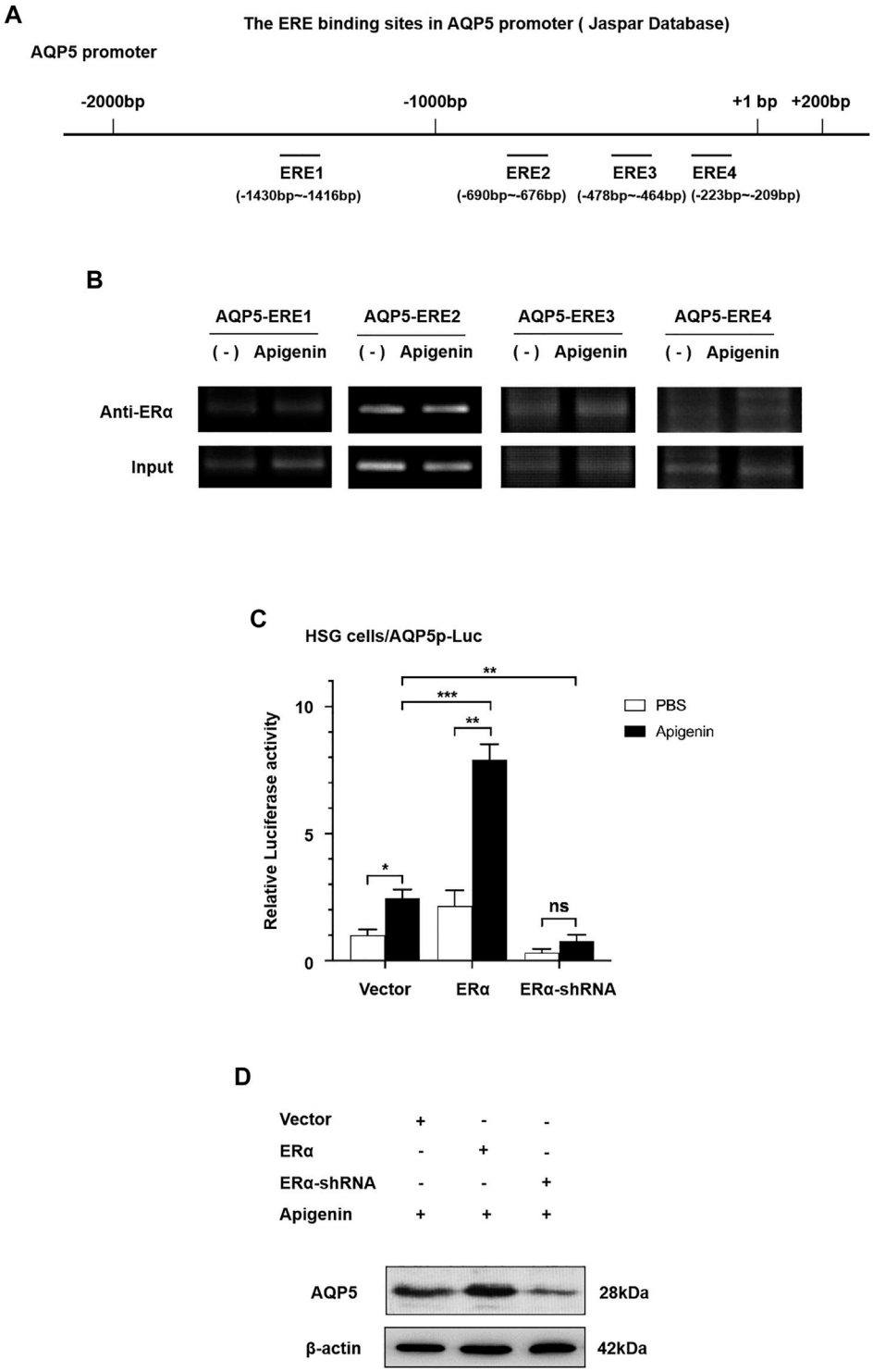

FIGURE 3 | Apigenin upregulates the transcription and translation of AQP5 through the ERα pathway. **(A)** Scheme showing AQP5 promoter sequence with ERα binding sites. **(B)** ChIP results showed that ERα occupancy was apparently increased at ERE3 in the presence of apigenin. **(C)** Relative luciferase activity (the indication of AQP5 expression) in ERα-overexpressed and -knocked down with or without 1 μM apigenin in HSG cells. **(D)** Western blot analysis showing the effect of apigenin treatment on AQP5 protein expression in ERα-overexpressed and -knocked down HSG cells. Data are presented as the mean ± SD, $n = 3$. Significant effect of the treatment, $^{*}p < 0.05$, $^{**}p < 0.01$.

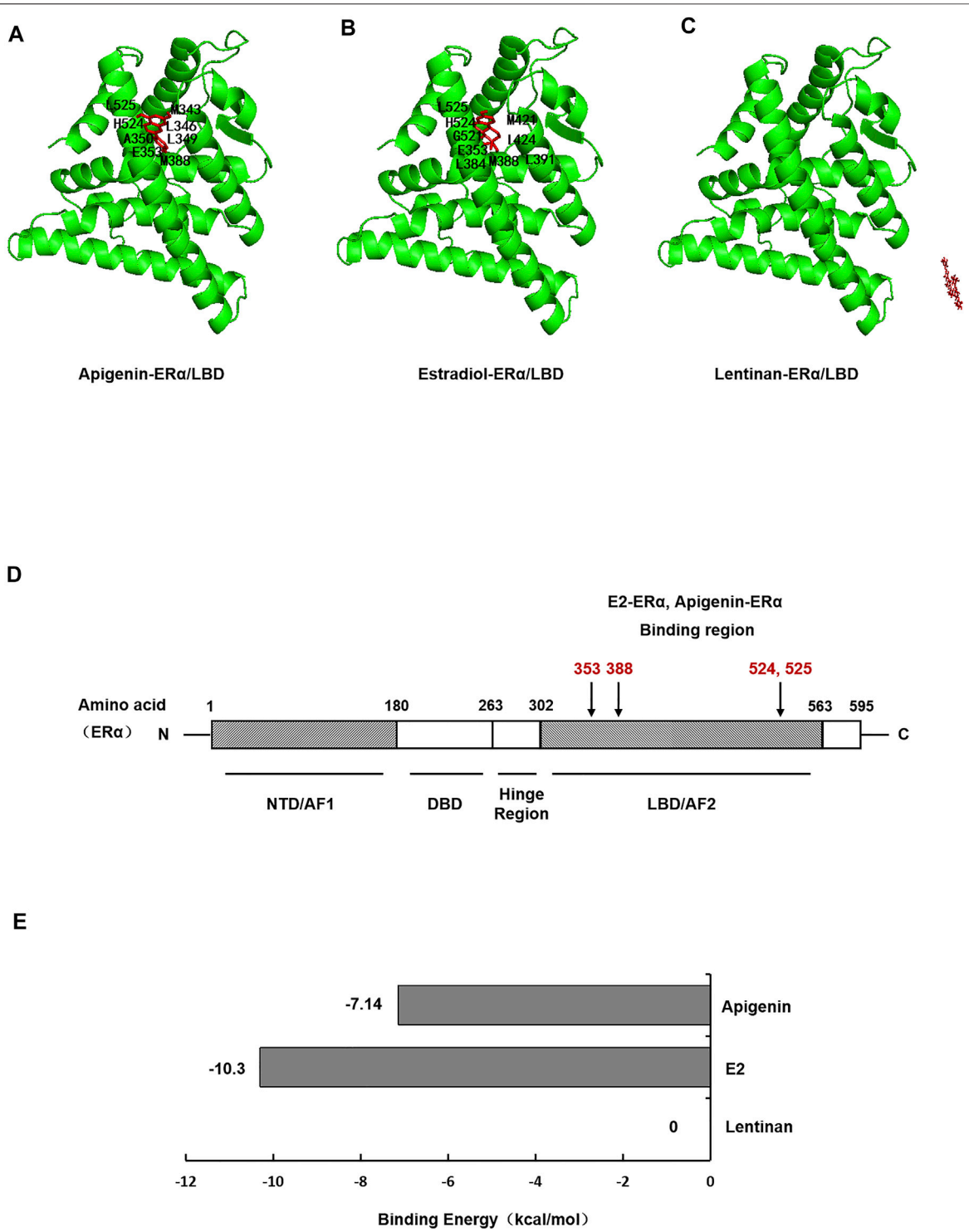

FIGURE 4 | Molecular docking shows specific binding of apigenin to ERα within the E2-ligand binding domain. Images showing the binding site of apigenin **(A)**, E2 **(B)**, and lentinan **(C)** in ERα. **(D)** Interaction of amino acid residues located in the ligand binding domain (LBD) of ERα. **(E)** Binding energy of apigenin, E2, and lentinan with ERα.

TABLE 1 | Amino acid residues in the apigenin, E2, and lentinan binding sites of ERα.

Ligand	Macromolecule	Amino acid residues
Apigenin	ERα	MET343, LEU346, LEU349, LAA350, GLU353, MET388, HIS524, LEU525
E2	ERα	GLU353, LEU384, MET388, LEU391, ARG394, MET421, ILE424, GLY521, HIS524, LEU525
Lentinan	ERα	—

Apigenin Specifically Binds to ERα Within Its Ligand Binding Domain by Molecular Docking of Apigenin to ERα

To investigate whether apigenin functioned as a ligand of ERα protein, then formed complexes with ERα protein, autodock software was performed to dock the molecule of apigenin to ERα protein. E2, the natural ligand of ERα, was set as a positive control, while lentinan was a negative control. First, the docking results showed that apigenin is located within the ligand binding (LBD) site of ERα (**Figure 4A**), at the same position in ERα as its natural ligand E2 (**Figure 4B**). The negative control lentinan could not enter the LBD region of ERα (**Figure 4C**).

ERα protein contains 595 amino acids, which is composed of three functional domains: the NH2-terminal domain (NTD/AF1, 1–180 amino acids), the DNA binding domain (DBD, 180–263 amino acids), and the COOH-terminal ligand binding domain (LBD/AF2, 302–563 amino acids) (Jia et al., 2015). In our docking study, apigenin was found to interact with the LBD of ERα with the amino acid residues MET343, LEU346, LEU349, LAA350, GLU353, MET388, HIS524, and LEU52. The positive control E2 was found to interact with LBD of ERα with the amino acid residues GLU353, LEU384, MET388, LEU391, ARG394, MET421, ILE424, GLY521, HIS524, and LEU525 (**Table 1**). Interestingly, the amino acid residues of apigenin binding to ERα were similar to E2 with the same amino acid residues including GLU353, MET388, HIS524, and LEU525 (**Figure 4D**), whereas the negative control lentinan was free outside of the LBD of ERα. The results suggest that apigenin is a natural product that plays an estrogen-like role.

Finally, the binding energy (**Figure 4E**) between apigenin and ERα was −7.14 kcal/mol, which approached the binding energy between E2 and ERα. However, the binding energy between lentinan and ERα was 0 kcal/mol. These data indicate that apigenin has strong binding abilities to ERα. Taken together, the aforementioned results suggest that apigenin specifically bound to ERα within its ligand binding domain and then activated the AQP5 transcription.

Apigenin Ameliorates the Impairment of Saliva Secretion and Reduced the Water Consumption Rate in OVX Mice

To verify the effect of apigenin *in vivo*, we constructed the OVX mice model. The mice were divided randomly into four groups, including sham operation, OVX/control, OVX/apigenin (drug group), and OVX/E2 (positive group) with six mice in each group. The animal study was performed as illustrated in **Figure 5**.

The saliva secretion was measured before ovariectomy and after 4, 8, and 12 weeks of treatment in **Figure 6A**. Saliva secretion was similar in the four groups before ovariectomy. The saliva secretion in the sham operation group did not change significantly at various stages, and the salivary secretion index was 20–25 mg/g. The saliva secretion in the OVX/control group decreased sharply at 4 weeks after administration, which was reduced to half of that in the sham operation group. The saliva secretion decreased gradually at 8–12 weeks after administration and was maintained at a low-level stage. At 12 weeks, the saliva secretion of the OVX/control group was reduced to 1/3 of that of the sham operation group. The saliva secretion in the OVX/apigenin group and OVX/E2 group was significantly lower at 4 weeks than that of the sham operation group. However, after 4 weeks of administration, the saliva secretion index began to increase, and the saliva secretion index increased gradually and approached the level of the sham operation group at 4–12 weeks of administration. At 12 weeks of administration, the saliva secretion index of the OVX/apigenin group and OVX/E2 group almost reached the level of the sham operation group. These results indicate that apigenin can significantly ameliorate saliva secretion in OVX mice, which is effective from 4 to 12 weeks.

To further illustrate the results, we analyzed the saliva secretion index in each group after 12 weeks of administration. As shown in **Figure 6B**, the saliva secretion index in the OVX/control group was 1/3 of that in the sham operation group. However, the saliva secretion index of the OVX/apigenin group and OVX/E2 group was completely different from that of the OVX/control group, while close to that of the sham operation group. These results indicate that apigenin rescues the impairment of saliva secretion in OVX mice.

To demonstrate the effects of apigenin on the thirsty symptom, we measured the water consumption rate before ovariectomy and after 4, 8, and 12 weeks of treatment in **Figure 6C**. The water consumption in the sham operation group showed no significant change at each stage, and the water consumption index was 0.75–1.0 ml/g. The water consumption in the OVX/control group increased to nearly 1.5 times of the sham operation group at 4 weeks of administration. During 8–12 weeks of administration, water consumption increased slowly and remained at a high level. At 12 weeks, the water consumption in OVX/control group increased nearly 1.7 times to that of the sham operation group. These results indicate that water consumption in ovariectomized mice increased significantly, suggesting the symptoms of xerostomia. Water consumption in the OVX/apigenin group and OVX/E2 group was higher at 4 weeks than that in the sham operation group. However, after 4 weeks of

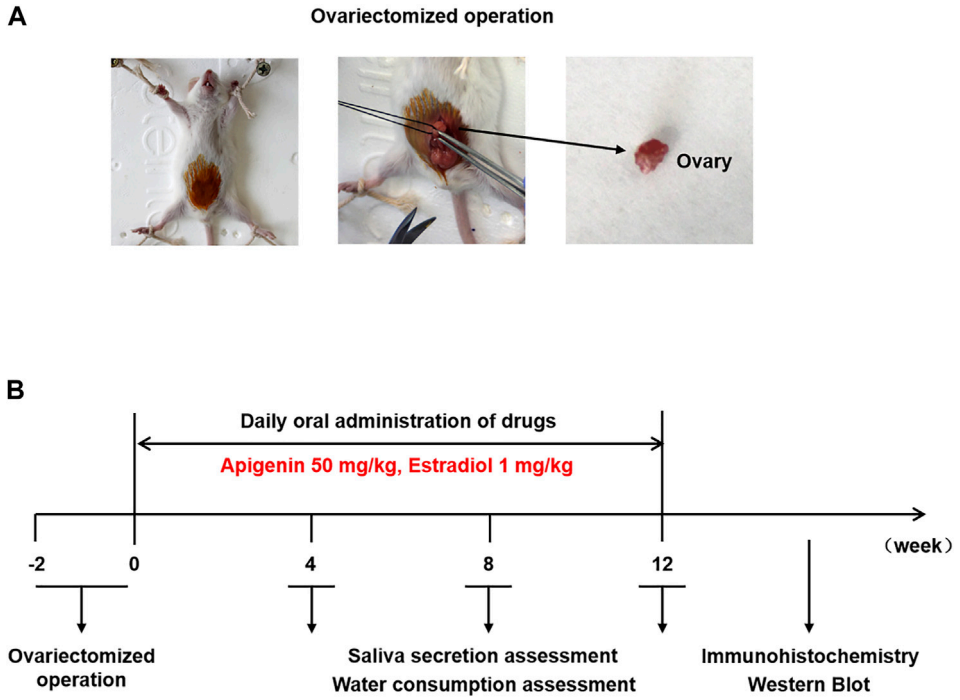

FIGURE 5 | (A) Ovariectomized operation. **(B)** Scheme of animal experiment and treatment.

administration, water consumption began to decline, decreased gradually, and was close to the level of the sham operation group. At 12 weeks of administration, the water consumption of the OVX/apigenin group and OVX/E2 group almost reached the level of the sham operation group. These results indicate that apigenin significantly reduces water consumption in ovariectomized mice, which is effective at 4–12 weeks.

We further analyzed water consumption in each group after 12 weeks of administration. As shown in **Figure 6D**, the water consumption in the OVX/control group was about 1.7 times that in the sham operation group. The water consumption in the OVX/apigenin group and OVX/E2 group was close to that in the sham operation group. The results suggest that apigenin relieves the thirsty symptom in OVX mice.

Apigenin Upregulates the Expression of AQP5 in the Submandibular Glands of OVX Mice

Based on the fact that apigenin ameliorates the impairment of saliva secretion in the OVX mice, we next investigated the expression of the key protein AQP5 that is involved in saliva secretion in the submandibular glands. As indicated by H&E staining, there was no significant change in the histology of submandibular gland tissue among the groups (**Figure 7A**).

As described previously (D'Agostino et al., 2020), both the apical and basolateral membranes of acinar cells display positive AQP5 labeling in mice (Delporte, 2014; Hosoi et al., 2020). In addition, intercalated ducts express AQP5 (Larsen et al., 2011). As shown in **Figure 7A**, in the sham operation group, AQP5 immunostaining was distributed at the membrane of acinar cells. In the OVX/control group, AQP5 immunostaining at the membrane of acinar cells, especially at the apical membrane, was severely declined. While AQP5 immunostaining at the membrane of acinar cells was augmented approaching the level of the sham operation group in the OVX/apigenin and OVX/E2 group. In quantitative analysis (**Figure 7B**), the AQP5 immunostaining in acinar cells in the OVX/control group declined severely compared to the sham operation group. As indicated, the AQP5 immunostaining in the OVX/apigenin and OVX/E2 groups was augmented approaching the level of the sham operation group. Furthermore, to detect the AQP5 protein expression level in the mice's submandibular glands, we performed a Western blot analysis. In the OVX/control group, the AQP5 protein level was declined severely compared to the sham operation group. As indicated, the AQP5 protein level in the OVX/apigenin and OVX/E2 groups was augmented approaching the level of the sham operation group (**Figure 7C**). These data indicate that apigenin upregulates the expression of AQP5 in the submandibular glands in OVX mice.

DISCUSSION

Xerostomia has high incidence with age, which was demonstrated by the reports from the literature that one in ten for younger and one in four for elder Australians (55 years old as cutoff) experienced dry mouth, with a prevalence of 9.3% among 15- to 34-year-olds, 11% among 35- to 54-year-olds, 17.6% among

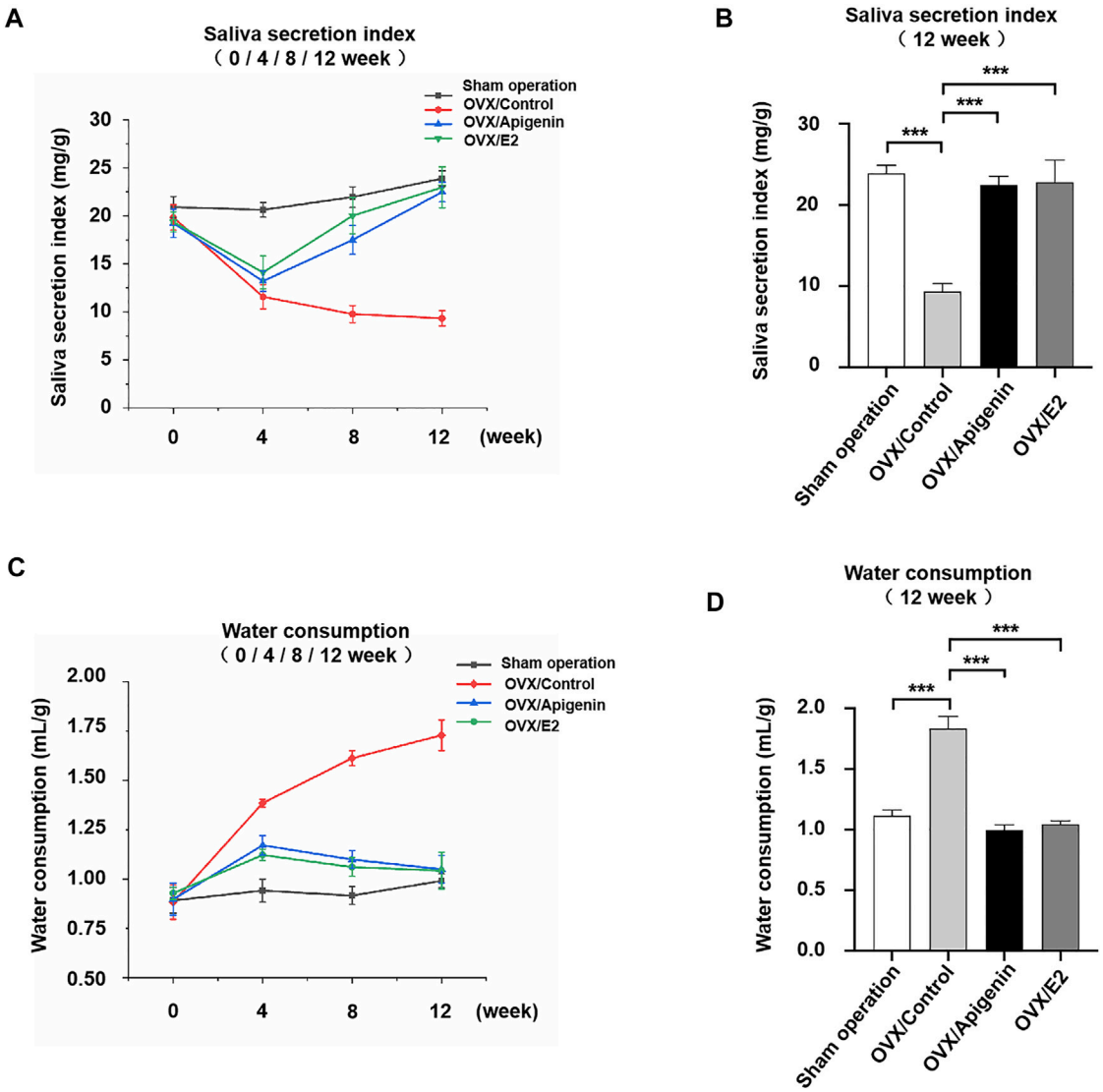

FIGURE 6 | Apigenin ameliorates the impairment of saliva secretion and reduced the water consumption rate in OVX mice. **(A)** Salivary secretion index before ovariectomy and after 4, 8, and 12 weeks of treatments. **(B)** Salivary secretion index after 12 weeks of treatment. **(C)** Water consumption rate before ovariectomy and after 4, 8, and 12 weeks of treatments. **(D)** Water consumption rate after 12 weeks of treatment. Data are presented as the mean ± SD, $n = 6$. Significant effect of the treatment, $^{*}p < 0.05$, $^{**}p < 0.01$.

55- to 74-year-olds, and 26.5% among those older than 75 years old (Jamieson and Thomson, 2020). Another study also reported xerostomia was one in five (19.1%) by 293 elderly people older than 60 years in Vanini, Brazil (Fornari et al., 2021). Moreover, xerostomia affects more than one-third of postmenopausal women (Nederfors, 2000). Salivary glands are sensitive to changes in female sex steroid blood levels (Agha-Hosseini et al., 2009). The decrease in estrogen levels during menopause is thought to affect salivary secretion (Forabosco et al., 1992). AQP5 is a key protein involved in salivary secretion and its expression downregulates in xerostomia. Effective therapy for xerostomia is still lacking. In this study, we unraveled that apigenin, an active flavone, directly binds with ERα and enhances AQP5 expression and activity in HSG cells via ERα signaling. Furthermore, apigenin treatment alleviated xerostomia and upregulated AQP5 expression in the submandibular gland in OVX mice. The results of this study unravel the therapeutic potential of apigenin for xerostomia and the underlying mechanism.

Apigenin, a natural flavone, is present in a significant amount as a glycosylated form in vegetables (parsley, celery, and onions), fruits (oranges), herbs (chamomile, thyme, oregano, and basil), and plant-based beverages (tea, beer, and wine) (Hostetler et al., 2017; Salehi et al., 2019). Apigenin has antidiabetic and anticancer potential (Yan et al., 2017; Ginwala et al., 2019). Moreover, apigenin treatment had shown a beneficial role in

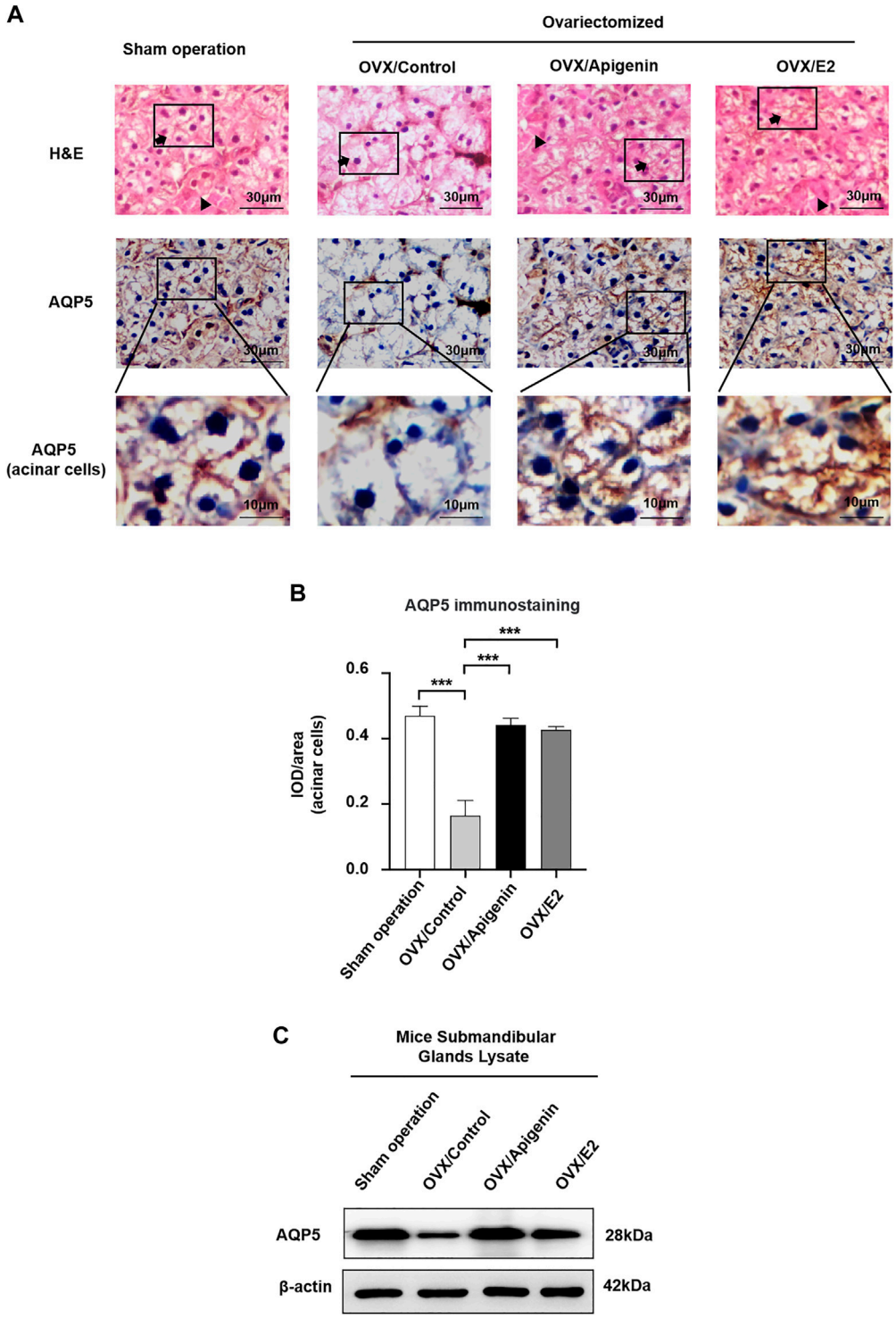

FIGURE 7 | Apigenin treatment upregulates AQP5 expression in the submandibular gland of OVX mice. **(A)** Histological images (H&E stained) and immunohistochemistry images of AQP5 of mice submandibular gland tissues. Arrows, acinar cells. Triangles, ducts cells. **(B)** Quantitative analysis of immunohistochemistry images. **(C)** AQP5 protein expression in the submandibular gland lysate. Data are presented as the mean ± SD, $n = 6$ mice per group. Significant effect of the treatment, $^{*}p < 0.05$, $^{**}p < 0.01$.

amnesia, Alzheimer's disease, depression, and insomnia (Venigalla et al., 2015; Salehi et al., 2019). Shreds of literature had reported anti-inflammatory and antimicrobial properties of apigenin, suggesting its application in various diseases. Apigenin is considered safe even in high doses and can be extracted easily from its natural sources. Considering these facts, we tested the effect of apigenin treatment on xerostomia and signaling molecules involved in xerostomia. AQP5 are key proteins involved in the pathophysiology of xerostomia. We found upregulation of ERα/AQP5 protein expression in apigenin-treated HSG cells and the submandibular gland of OVX mice. These findings indicate that apigenin has the potential to activate ERα/AQP5 signaling on salivary glands.

Postmenopausal estrogen deficiency is linked to various diseases, including xerostomia, osteoporosis, diabetes, and other inflammatory diseases (Caputo and Costa, 2014; Baer and Walitt, 2018). Hormone replacement therapy (HRT) had been reported to increase salivary secretion in postmenopausal women (Yalçin et al., 2005; Lago et al., 2015). However, HRT possesses a risk of adverse side effects, including the development of endometrial and breast cancer (Pietrzak et al., 2015). Phytoestrogens are plant-derived dietary compounds with structural similarity to E2 (Rietjens et al., 2017). This structural similarity to E2 enables phytoestrogens to cause estrogenic effects by binding to the estrogen receptors. The docking study revealed the similar binding sites of apigenin and E2 on ERα, indicating apigenin as a decoy of E2. Goto et al. reported that apigenin treatment prevents estrogen deficiency-induced bone loss in OVX mice (Goto et al., 2015). Therefore, apigenin could have the potential to alleviate estrogen deficiency-related diseases including xerostomia.

Reports from the literature and our previous studies revealed the role of AQP5 on the pathophysiology of xerostomia (Matsuzaki et al., 2012). In this study, treatment of apigenin robustly upregulated ERα and AQP5 expression in HSG cells *in vitro* and the submandibular gland of OVX mice. AQP5 expression and activity were increased in apigenin-treated HSG cells with the overexpression of ERα. Interestingly, apigenin failed to increase the AQP5 expression and activity in ERα-knocked down HSG cells indicating the ERα-mediated effect of apigenin on AQP5 expression and activity. Reports from the literature also reported the stimulatory effect of E2 on AQP5 expression (Jiang et al., 2015; Wei et al., 2019). Moreover, the apigenin and E2 treatment increased the salivary secretion index and decreased water consumption in OVX mice in a similar extent. This is the first study to report the anabolic role of apigenin on AQP5 expression and activity via binding with ERα. These results unravel the therapeutic potential of apigenin for xerostomia via ERα/AQP5 signaling. Our results indicate promising potential of apigenin to treat xerostomia.

CONCLUSION

Xerostomia is defined as decreased salivary flow or hypofunction of the salivary glands. Among the 4 plant extracts tested in this study, only apigenin showed robust potential to activate the expression. Since AQP5 is a key protein involved in salivary secretion *via* ERα signaling, we further investigated the role of apigenin on ERα/AQP5 pathway-mediated salivary secretion. Apigenin, an active flavone component of herbal extract, upregulated AQP5 expression *via* activation of ERα signaling and restored saliva flow rates in OVX mice. Our results revealed the possible therapeutic potential of apigenin to alleviate the clinical symptoms of xerostomia.

DATA AVAILABILITY STATEMENT

The original contributions presented in the study are included in the article/**Supplementary Material**, further inquiries can be directed to the corresponding authors.

ETHICS STATEMENT

The animal study was reviewed and approved by the Ethics Committee of Northeast Normal University.

AUTHOR CONTRIBUTIONS

JL, XML, and NW: study design. WW: *in vitro* and *in vivo* experimental conduct. TC and JP: manuscript writing and editing. XTL, TM, TC, and MZ: data analysis and interpretation. All authors approved the final version of the manuscript.

FUNDING

This study was supported by grants from the Ministry of Science and Technology (Nos. 2021YFE0108000 and 2016YFE0128500), Jilin Provincial Science and Technology Department (No. 20200201025JC), National Natural Science Foundation of China (Nos. 31870758 and 82150410451), and Jilin Provincial Department of Finance (No. jsz2018170-3).

SUPPLEMENTARY MATERIAL

The Supplementary Material for this article can be found online at: https://www.frontiersin.org/articles/10.3389/fphar.2022.818116/full#supplementary-material

REFERENCES

Agha-Hosseini, F., Mirzaii-Dizgah, I., Mansourian, A., and Khayamzadeh, M. (2009). Relationship of Stimulated Saliva 17beta-Estradiol and Oral Dryness Feeling in Menopause. *Maturitas* 62, 197–199. doi:10.1016/j.maturitas.2008.10.016

Almadi, E. M., and Almohaimede, A. A. (2018). Natural Products in Endodontics. *Saudi Med. J.* 39, 124–130. doi:10.15537/smj.2018.2.21038

Baer, A. N., and Walitt, B. (2018). Update on Sjögren Syndrome and Other Causes of Sicca in Older Adults. *Rheum. Dis. Clin. North. Am.* 44, 419–436. doi:10.1016/j.rdc.2018.03.002

Caputo, E. L., and Costa, M. Z. (2014). Influence of Physical Activity on Quality of Life in Postmenopausal Women with Osteoporosis. *Rev. Bras Reumatol* 54, 467–473. doi:10.1016/j.rbr.2014.02.008

Chang, C. M., Chu, H. T., Wei, Y. H., Chen, F. P., Wang, S., Wu, P. C., et al. (2015). The Core Pattern Analysis on Chinese Herbal Medicine for Sjögren's Syndrome: A Nationwide Population-Based Study. *Sci. Rep.* 5, 9541. doi:10.1038/srep09541

D R, M., G, K., G, J., D, D., T V, S., and Dinesh, P. (2014). Evaluation of Salivary Flow Rate, pH and Buffer in Pre, Post & Post Menopausal Women on HRT. *J. Clin. Diagn. Res.* 8, 233–236. doi:10.7860/JCDR/2014/8158.4067

D'agostino, C., Elkashty, O. A., Chivasso, C., Perret, J., Tran, S. D., and Delporte, C. (2020). Insight into Salivary Gland Aquaporins. *Cells* 9.

Delli, K., Spijkervet, F. K., Kroese, F. G., Bootsma, H., and Vissink, A. (2014). Xerostomia. *Monogr. Oral Sci.* 24, 109–125. doi:10.1159/000358792

Delporte, C. (2014). Aquaporins in Salivary Glands and Pancreas. *Biochim. Biophys. Acta* 1840, 1524–1532. doi:10.1016/j.bbagen.2013.08.007

Delporte, C., Bryla, A., and Perret, J. (2016). Aquaporins in Salivary Glands: From Basic Research to Clinical Applications. *Int. J. Mol. Sci.* 17, 166. doi:10.3390/ijms17020166

Eliasson, L., Carlén, A., Laine, M., and Birkhed, D. (2003). Minor Gland and Whole Saliva in Postmenopausal Women Using a Low Potency Oestrogen (Oestriol). *Arch. Oral Biol.* 48, 511–517. doi:10.1016/s0003-9969(03)00094-3

Forabosco, A., Criscuolo, M., Coukos, G., Uccelli, E., Weinstein, R., Spinato, S., et al. (1992). Efficacy of Hormone Replacement Therapy in Postmenopausal Women with Oral Discomfort. *Oral Surg. Oral Med. Oral Pathol.* 73, 570–574. doi:10.1016/0030-4220(92)90100-5

Fornari, C. B., Bergonci, D., Stein, C. B., Agostini, B. A., and Rigo, L. (2021). Prevalence of Xerostomia and its Association with Systemic Diseases and Medications in the Elderly: a Cross-Sectional Study. *Sao Paulo Med. J.* 139 (4), 380–387. doi:10.1590/1516-3180.2020.0616.R3.1902021

Ginwala, R., Bhavsar, R., Chigbu, D. I., Jain, P., and Khan, Z. K. (2019). Potential Role of Flavonoids in Treating Chronic Inflammatory Diseases with a Special Focus on the Anti-inflammatory Activity of Apigenin. *Antioxidants (Basel)* 8. doi:10.3390/antiox8020035

Goto, T., Hagiwara, K., Shirai, N., Yoshida, K., and Hagiwara, H. (2015). Apigenin Inhibits Osteoblastogenesis and Osteoclastogenesis and Prevents Bone Loss in Ovariectomized Mice. *Cytotechnology* 67, 357–365. doi:10.1007/s10616-014-9694-3

Hosoi, K. (2016). Physiological Role of Aquaporin 5 in Salivary Glands. *Pflugers Arch.* 468, 519–539. doi:10.1007/s00424-015-1749-6

Hosoi, K., Yao, C., Hasegawa, T., Yoshimura, H., and Akamatsu, T. (2020). Dynamics of Salivary Gland AQP5 under Normal and Pathologic Conditions. *Int. J. Mol. Sci.* 21. doi:10.3390/ijms21041182

Hostetler, G. L., Ralston, R. A., and Schwartz, S. J. (2017). Flavones: Food Sources, Bioavailability, Metabolism, and Bioactivity. *Adv. Nutr.* 8, 423–435. doi:10.3945/an.116.012948

Ibrahim, N, Wong, S. K., Mohamed, I. N., Mohamed, N., Chin, K. Y., Ima-Nirwana, S., et al. (2018). Wound Healing Properties of Selected Natural Products. *Int. J. Environ. Res. Public Health* 15. doi:10.3390/ijerph15112360

Jaiboonma, A., Kaokaen, P., Chaicharoenaudomrung, N., Kunhorm, P., Janebodin, K., Noisa, P., et al. (2020). Cordycepin Attenuates Salivary Hypofunction through the Prevention of Oxidative Stress in Human Submandibular Gland Cells. *Int. J. Med. Sci.* 17, 1733–1743. doi:10.7150/ijms.46707

Jamieson, L. M., and Thomson, W. M. (2020). Xerostomia: its Prevalence and Associations in the Adult Australian Population. *Aust. Dent J.* 65 (Suppl. 1), S67–S70. doi:10.1111/adj.12767

Jia, M., Dahlman-Wright, K., and Gustafsson, J. (2015). Estrogen Receptor Alpha and Beta in Health and Disease. *Best Pract. Res. Clin. Endocrinol. Metab.* 29, 557–568. doi:10.1016/j.beem.2015.04.008

Jiang, X. X., Fei, X. W., Zhao, L., Ye, X. L., Xin, L. B., Qu, Y., et al. (2015). Aquaporin 5 Plays a Role in Estrogen-Induced Ectopic Implantation of Endometrial Stromal Cells in Endometriosis. *PLoS One* 10, e0145290. doi:10.1371/journal.pone.0145290

Kobayashi, M., Takahashi, E., Miyagawa, S., Watanabe, H., and Iguchi, T. (2006). Chromatin Immunoprecipitation-Mediated Target Identification Proved Aquaporin 5 Is Regulated Directly by Estrogen in the Uterus. *Genes Cells* 11, 1133–1143. doi:10.1111/j.1365-2443.2006.01009.x

Krane, C. M., Melvin, J. E., Nguyen, H. V., Richardson, L., Towne, J. E., Doetschman, T., et al. (2001). Salivary Acinar Cells from Aquaporin 5-deficient Mice Have Decreased Membrane Water Permeability and Altered Cell Volume Regulation. *J. Biol. Chem.* 276, 23413–23420. doi:10.1074/jbc.M008760200

Lago, M. L., De Oliveira, A. E., Lopes, F. F., Ferreira, E. B., Rodrigues, V. P., and Brito, L. M. (2015). The Influence of Hormone Replacement Therapy on the Salivary Flow of post-menopausal Women. *Gynecol. Endocrinol.* 31, 109–112. doi:10.3109/09513590.2014.959918

Lai, Z., Yin, H., Cabrera-Pérez, J., Guimaro, M. C., Afione, S., Michael, D. G., et al. (2016). Aquaporin Gene Therapy Corrects Sjögren's Syndrome Phenotype in Mice. *Proc. Natl. Acad. Sci. U S A.* 113, 5694–5699. doi:10.1073/pnas.1601992113

Larsen, H. S., Aure, M. H., Peters, S. B., Larsen, M., Messelt, E. B., and Kanli Galtung, H. (2011). Localization of AQP5 during Development of the Mouse Submandibular Salivary Gland. *J. Mol. Histol.* 42, 71–81. doi:10.1007/s10735-010-9308-0

Li, Z., Zhao, D., Gong, B., Xu, Y., Sun, H., Yang, B., et al. (2006). Decreased Saliva Secretion and Down-Regulation of AQP5 in Submandibular Gland in Irradiated Rats. *Radiat. Res.* 165, 678–687. doi:10.1667/RR3569.1

Liang, J., and Shang, Y. (2013). Estrogen and Cancer. *Annu. Rev. Physiol.* 75, 225–240. doi:10.1146/annurev-physiol-030212-183708

Liu, S., Niu, K., Da, Y., Liu, Y., Zhang, J., Wang, W., et al. (2018). Effects of Standardized Isopropanolic Black Cohosh and Estrogen on Salivary Function in Ovariectomized Rats. *Biomed. Pharmacother.* 97, 1438–1444. doi:10.1016/j.biopha.2017.11.038

Ma, T., Song, Y., Gillespie, A., Carlson, E. J., Epstein, C. J., and Verkman, A. S. (1999). Defective Secretion of Saliva in Transgenic Mice Lacking Aquaporin-5 Water Channels. *J. Biol. Chem.* 274, 20071–20074. doi:10.1074/jbc.274.29.20071

Marjoribanks, J., Farquhar, C., Roberts, H., Lethaby, A., and Lee, J. (2017). Long-term Hormone Therapy for Perimenopausal and Postmenopausal Women. *Cochrane Database Syst. Rev.* 1, Cd004143. doi:10.1002/14651858.CD004143.pub5

Matsuzaki, T., Susa, T., Shimizu, K., Sawai, N., Suzuki, T., Aoki, T., et al. (2012). Function of the Membrane Water Channel Aquaporin-5 in the Salivary Gland. *Acta Histochem. Cytochem.* 45, 251–259. doi:10.1267/ahc.12018

Millsop, J. W., Wang, E. A., and Fazel, N. (2017). Etiology, Evaluation, and Management of Xerostomia. *Clin. Dermatol.* 35, 468–476. doi:10.1016/j.clindermatol.2017.06.010

Minicucci, E. M., Pires, R. B., Vieira, R. A., Miot, H. A., and Sposto, M. R. (2013). Assessing the Impact of Menopause on Salivary Flow and Xerostomia. *Aust. Dent J.* 58, 230–234. doi:10.1111/adj.12057

Murakami, M., Wei, M. X., Ding, W., and Zhang, Q. D. (2009). Effects of Chinese Herbs on Salivary Fluid Secretion by Isolated and Perfused Rat Submandibular Glands. *World J. Gastroenterol.* 15, 3908–3915. doi:10.3748/wjg.15.3908

Nakamura, T., Matsui, M., Uchida, K., Futatsugi, A., Kusakawa, S., Matsumoto, N., et al. (2004). M(3) Muscarinic Acetylcholine Receptor Plays a Critical Role in Parasympathetic Control of Salivation in Mice. *J. Physiol.* 558, 561–575. doi:10.1113/jphysiol.2004.064626

Nederfors, T. (2000). Xerostomia and Hyposalivation. *Adv. Dent Res.* 14, 48–56. doi:10.1177/08959374000140010701

Pietrzak, B., Wlaźlak, E., and Zwierzyńska, E. (2015). Long-term Use of Estrogens: Benefit or Risk. *Postepy Hig Med. Dosw (Online)* 69, 285–293. doi:10.5604/17322693.1142582

Rietjens, I. M. C. M., Louisse, J., and Beekmann, K. (2017). The Potential Health Effects of Dietary Phytoestrogens. *Br. J. Pharmacol.* 174, 1263–1280. doi:10.1111/bph.13622

Salehi, B., Venditti, A., Sharifi-Rad, M., Kręgiel, D., Sharifi-Rad, J., Durazzo, A., et al. (2019). The Therapeutic Potential of Apigenin. *Int. J. Mol. Sci.* 20, 1305. doi:10.3390/ijms20061305

Tajiri, A., Higuchi, H., and Miyawaki, T. (2019). Hyperoxia Reduces Salivary Secretion by Inducing Oxidative Stress in Mice. *Arch. Oral Biol.* 98, 38–46. doi:10.1016/j.archoralbio.2018.11.001

Tanasiewicz, M., Hildebrandt, T., and Obersztyn, I. (2016). Xerostomia of Various Etiologies: A Review of the Literature. *Adv. Clin. Exp. Med.* 25, 199–206. doi:10.17219/acem/29375

Tsinti, M., Kassi, E., Korkolopoulou, P., Kapsogeorgou, E., Moutsatsou, P., Patsouris, E., et al. (2009). Functional Estrogen Receptors Alpha and Beta Are Expressed in normal Human Salivary Gland Epithelium and Apparently Mediate Immunomodulatory Effects. *Eur. J. Oral Sci.* 117, 498–505. doi:10.1111/j.1600-0722.2009.00659.x

Venigalla, M., Gyengesi, E., and Münch, G. (2015). Curcumin and Apigenin - Novel and Promising Therapeutics against Chronic Neuroinflammation in Alzheimer's Disease. *Neural Regen. Res.* 10, 1181–1185. doi:10.4103/1673-5374.162686

Wei, W., He, X., Liu, X., Lan, C., and Li, J. (2019). Estradiol Induced Estrogen Receptor-Mediated Transcription and Expression of Aquaporin5. *Chem. Res. Chin. Univ.* 35, 239–244. doi:10.1007/s40242-019-9016-6

Yalçin, F., Gurgan, S., and Gurgan, T. (2005). The Effect of Menopause, Hormone Replacement Therapy (HRT), Alendronate (ALN), and Calcium Supplements on Saliva. *J. Contemp. Dent Pract.* 6, 10–17.

Yan, X., Qi, M., Li, P., Zhan, Y., and Shao, H. (2017). Apigenin in Cancer Therapy: Anti-cancer Effects and Mechanisms of Action. *Cell Biosci* 7, 50. doi:10.1186/s13578-017-0179-x

Yang, M., Jiang, Z. H., Li, C. G., Zhu, Y. J., Li, Z., Tang, Y. Z., et al. (2018). Apigenin Prevents Metabolic Syndrome in High-Fructose Diet-Fed Mice by Keap1-Nrf2 Pathway. *Biomed. Pharmacother.* 105, 1283–1290. doi:10.1016/j.biopha.2018.06.108

Conflict of Interest: The authors declare that the research was conducted in the absence of any commercial or financial relationships that could be construed as a potential conflict of interest.

Publisher's Note: All claims expressed in this article are solely those of the authors and do not necessarily represent those of their affiliated organizations, or those of the publisher, the editors, and the reviewers. Any product that may be evaluated in this article, or claim that may be made by its manufacturer, is not guaranteed or endorsed by the publisher.

Copyright © 2022 Wei, Cao, Pathak, Liu, Mao, Watanabe, Li, Zhang and Li. This is an open-access article distributed under the terms of the Creative Commons Attribution License (CC BY). The use, distribution or reproduction in other forums is permitted, provided the original author(s) and the copyright owner(s) are credited and that the original publication in this journal is cited, in accordance with accepted academic practice. No use, distribution or reproduction is permitted which does not comply with these terms.

frontiers in Pharmacology

ORIGINAL RESEARCH
published: 28 February 2022
doi: 10.3389/fphar.2021.816477

β-Sitosterol Inhibits Rheumatoid Synovial Angiogenesis Through Suppressing VEGF Signaling Pathway

Kai Qian[1,2], Xue-Xia Zheng[1], Chen Wang[1], Wen-Guang Huang[1], Xiao-Bao Liu[1,3], Shu-Di Xu[1,3], Dan-Kai Liu[1], Min-Ying Liu[1,3] and Chang-Song Lin[1,3]**

[1]Guangzhou University of Chinese Medicine, Guangzhou, China, [2]Postdoctoral Research Station, Guangzhou University of Traditional Chinese Medicine, Guangzhou, China, [3]Department of Rheumatology, First Affiliated Hospital of Guangzhou University of Chinese Medicine, Guangzhou, China

Background: Rheumatoid arthritis (RA) is a chronic disabling inflammatory disease that causes synovial angiogenesis in an invasive manner and leads to joint destruction. Currently available pharmacotherapy for RA has unwanted side effects and limitations. Although anti-angiogenic therapy is regarded as a new potential treatment for RA, only a few anti-angiogenic drugs are available. An increasing number of studies have shown that *β*-sitosterol (BSS) may exert inhibitory effects against angiogenesis. However, the mechanisms involved are still unclear.

Methods: Based on the results of the gene set enrichment analysis (GSEA) of the transcriptome data of endothelial cells from RA patients, we evaluated the pharmacological effects of BSS on the tube formation, cell proliferation, and migration of human umbilical vein endothelial cells (HUVECs). Furthermore, the effects of BSS treatment on vascular endothelial growth factor receptor 2 (VEGFR2) were determined using molecular docking and Western blotting. Additionally, in the presence or absence of BSS, synovial angiogenesis and joint destruction of the ankle were investigated in collagen-induced arthritis (CIA) mice. The effect of BSS treatment on VEGFR2/p-VEGFR2 expression was verified through immunohistochemical staining.

Results: The immunohistochemistry results revealed that BSS treatment inhibited angiogenesis both *in vitro* and *in vivo.* In addition, the results of 5-ethynyl-2′-deoxyuridine and cell cycle analysis showed that BSS treatment suppressed the proliferation of HUVECs, while the Transwell migration and stress fiber assays demonstrated that BSS treatment inhibited the migration of HUVECs. Notably, the inhibitory effect of BSS treatment on VEGFR2/p-VEGFR2 was similar to that of axitinib. In CIA mice, BSS also exerted therapeutic effects on the ankles by reducing the degree of swelling, ameliorating bone and cartilage damage, preventing synovial angiogenesis, and inhibiting VEGFR2 and *p*-VEGFR2 expression.

OPEN ACCESS

Edited by:
Andres Trostchansky, Universidad de la República, Uruguay

Reviewed by:
Ana Paula Silva De Azevedo Santos, Federal University of Maranhão, Brazil
Chien-Chung Huang, China Medical University, Taiwan

***Correspondence:**
Chang-Song Lin
linchs@gzucm.edu.cn
Min-Ying Liu
liuminying5343@163.com

Specialty section:
This article was submitted to Experimental Pharmacology and Drug Discovery, a section of the journal Frontiers in Pharmacology

Received: 16 November 2021
Accepted: 30 December 2021
Published: 28 February 2022

Citation:
Qian K, Zheng X-X, Wang C, Huang W-G, Liu X-B, Xu S-D, Liu D-K, Liu M-Y and Lin C-S (2022) β-Sitosterol Inhibits Rheumatoid Synovial Angiogenesis Through Suppressing VEGF Signaling Pathway. Front. Pharmacol. 12:816477. doi: 10.3389/fphar.2021.816477

Abbreviations: BSS, β-sitosterol; CIA, collagen-induced arthritis; ECM, endothelial cell medium; ECL, enhanced chemical luminescent; ECs, endothelial cells; GSEA, gene set enrichment analysis; HUVECs, human umbilical vein endothelial cells; RA, rheumatoid arthritis; VEGF, vascular endothelial growth factor.

Conclusion: Therefore, our findings demonstrate that BSS exerts an inhibitory effect on synovial angiogenesis by suppressing the proliferation and migration of endothelial cells, thereby alleviating joint swelling and bone destruction in CIA mice. Furthermore, the underlying therapeutic mechanisms may involve the inhibition of VEGF signaling pathway activation.

Keywords: rheumatoid arthritis, β-sitosterol, VEGFR2, angiogenesis, endothelial cells, collagen-induced arthritis

INTRODUCTION

Rheumatoid arthritis (RA) is a common inflammatory disease with a prevalence of about 1% of people worldwide (O'neil et al., 2020), leading to joint deformity and disability constituting a burden both on individuals and society. RA is characterized by persistent synovitis and developing synovial angiogenesis, which leads to subsequent hyperplasia of the synovium and the erosion of cartilage and bone (Mcinnes and Schett, 2011; Bottini and Firestein, 2013). In the course of RA, active tissue neovascularization is necessary for the expansion, hyperplasia, and invasiveness of synovium (Fearon et al., 2016). Accordingly, RA was as well regarded as one of the "angiogenic family of diseases" because of the notably increased number and density of new synovial blood vessels in synovium. What is more, increasing evidence support that angiogenesis appears to be a central part involved in the development and maintenance of RA (Leblond et al., 2017).

In the progress of angiogenesis, endothelial cells (ECs) are an indispensable source of new synovial blood vessels (Leblond et al., 2017). Vascular endothelial growth factor (VEGF) is a main "on" switch controlling nearly all steps of angiogenesis (Apte et al., 2019), and vascular endothelial growth factor receptor 2 (VEGFR2) is the principal endothelial VEGF signaling receptor (Simons et al., 2016). VEGF binds to homologous VEGFR2 and induces phosphorylation of Y1173 and Y949 sites in VEGFR2. Phosphorylated Y1173 binds and activates phosphorylated phospholipase C γ (PLCγ), while PLCγ mediates the activation of the ERK1/2 pathway, leading to gene transcription changes that affect biological processes such as cell migration, proliferation, and homeostasis (Sakurai et al., 2005). The phosphorylation of Y949 leads to the activation of sarcoma gene (c-SRC) at the cell-to-cell junction, which determines the downstream signaling events of cell shape, survival, and vascular permeability (Li et al., 2016). Nowadays, anti-VEGF/VEGFR2 therapies seem to be beneficial for animal models of RA and also have a great therapeutic promise for RA (Le and Kwon, 2021), such as Avastin (Bevacizumab, a VEGF humanized monoclonal antibody) (Wang et al., 2013) and Sorafenib (a proangiogenic receptor tyrosine kinase inhibitor, which mainly suppresses the expression of VEGFR2) (Wang et al., 2018).

With a long history of nutritional complement and pharmaceutical products, BSS is a common bioactive phytosterol that can be derived from many kinds of plants. It has antioxidant, cholesterol-lowering, anti-inflammatory effects, and is widely used in pharmaceutical raw materials and functional foods (Babu and Jayaraman, 2020). Phytosterols were reported to be involved in various mechanisms, such as inhibiting cancer cell growth, angiogenesis, and promoting cancer cells apoptosis (Woyengo et al., 2009). In addition, the expression of VEGF was decreased by BSS in renal tissue, and angiogenesis was inhibited by BSS in renal cell carcinoma (Sharmila and Sindhu, 2017). As we know, the characteristics of synovial angiogenesis were similar to tumor angiogenesis (Fearon et al., 2016). Therefore, we hypothesized that BSS may inhibit synovial angiogenesis in RA by affecting ECs, thereby reducing joint swelling and joint destruction. In our study, we implemented the gene set enrichment analysis (GSEA) method to analyze the transcriptome of synovial ECs in RA, and results showed that ECs were significantly enriched in proliferation and migration. Furthermore, we found that VEGF, PI3K-AKT-mTOR, and TGF-β signaling pathways, related to angiogenesis, were activated in ECs. Therefore, we used human umbilical vein endothelial cells (HUVECs) and collagen-induced arthritis (CIA) mice to explore the effect of BSS on synovial angiogenesis and its possible mechanism.

MATERIALS AND METHODS

Reagents and Antibodies

BSS (drug purity ≥95%, batch number S1270) was derived from Sigma-Aldrich (St. Louis, MO, United States). For *in vivo* experiments, BSS was dissolved in anhydrous ethanol to 200 mM and stored at −20°C, and then diluted with EC medium (ECM). For *in vitro* experiments, BSS was dissolved in corn oil using anhydrous ethanol as cosolvent (final concentration of ethanol was 5%). Axitinib (drug purity was 99.76%, lot number S1005) was derived from Selleck (Houston, TX, United States). Recombinant human TNF-α (lot number 300-01A) and Recombinant human $VEGF_{165}$ (lot number 100–20) were purchased from Peprotech (Cranbury, NJ, United States). ECM (lot number 1001) was purchased from ScienCell (Carlsbad, CA, United States). In addition, anti-VEGFR2 (lot number AF6281), anti-phospho-VEGFR2 (lot number AF3279) antibodies were obtained from Affinity Biosciences LTD. (Changzhou, Jiangsu, China). Anti-phospho-AKT (lot number 9271S) and anti-phospho-smad2 (lot number 3108S) antibodies were obtained from CST (Danvers, MA, United States).

Animal Experimental Design

Twenty-four male DBA/1 mice (7–8 weeks), weighing 18 ± 2 g, were purchased from Beijing Weitong Lihua Laboratory Animal Technology, license number SCXK (Beijing) 2016-0011, animal

certificate number 1100112011028365. The animals (animal ethics number 2020006) were maintained in the Experimental Animal Centre of the First Affiliated Hospital of Guangzhou University of Traditional Chinese Medicine, and experimental unit license number: SYXK [Guangdong] 2018-0092. This study was reviewed and approved by the Ethics Committee of the First Affiliated Hospital of Guangzhou University of Traditional Chinese Medicine, and conducted therapeutic intervention on laboratory animals in accordance with the NIH Laboratory Animal Care and Use Guidelines.

CIA mice were guided by a previous study (Pan et al., 2018), and the mice were randomly divided into four experimental groups ($n = 6$ each): normal control + vehicle (NC group), CIA + vehicle (CIA group), CIA + methotrexate (MTX group), and CIA + BSS (BSS group). The mice were treated *via* gastric irrigation of either vehicle, MTX (1 mg/kg every 3 days) or BSS (100 mg/kg daily) for 28 days, beginning on the day after the second immunization. Arthritis index score: scoring was initiated on day 21 and subsequently performed every 3 days (Li et al., 2017).

Cell Culture

The HUVECs purchased from ScienCell (lot number 28433) were identified by CD31 fluorescent staining. The HUVECs were cultured in ECM, at 37°C and 5% CO_2. Operations such as medium exchange, subculture, cryopreservation, resuscitation, or seeding were performed according to the state and density of the cells. In this study, 4–6 generations of cell cultures were tested.

Cell Counting Kit-8 Assay

The HUVECs were inoculated (6×10^3 cells/well) in 96-well plates and then treated with different dosage groups of BSS for 24 h, each group included five duplicate wells, and the experiment was repeated thrice. After discarding the culture medium, the plates were washed with PBS, and 100 μl of fresh complete medium and 10 μl CCK-8 assay reagent (Dojindo, Kunamoto, Japan) were added to each well, and the cells were cultured for another 1 h. Absorbance (A value) was measured at 450 nm using a microplate reader, and cell viability was subsequently assessed.

Tube Formation Assay

The Normal control + vehicle (NC group), VEGF + vehicle (VEGF group), and VEGF + BSS groups were first established. A 100-μl cell suspension (4×10^5 cells/ml) was placed into each well of a 96-well plate, coated with 35 μl/well matrix adhesive (BD Biosciences, CA, United States). The HUVECs were treated with vehicle or BSS (10 and 20 μM) and stimulated with or without VEGF (50 ng/ml) for 6 h. The tube formation of HUVECs was observed and photographed using an inverted phase contrast microscope (Olympus, Tokyo, Japan). The Angiogenesis Analyser plug-in in ImageJ software (NIH, Bethesda, MD, United States; http://rsb.info.nih.gov/nih-image/) was used to analyze the number of tube-cavity nodes and connection intersections (Carpentier et al., 2020).

Microarray Data Analysis

Following the experimental design, the gene expression profile data of ECs from 18 RA patients and 11 healthy controls in the GSE121894 dataset under basic conditions were selected (Leblond et al., 2020). GSEA was performed through the "clusterProfiler" R package, with "c5.all.v7.4.symbols.gmt" and "c2.cp.kegg.v7.4.symbols.gmt" as the reference gene set.

Proliferation Assays

The HUVECs (6×10^3 cells/well) were treated with vehicle or BSS (10 and 20 μM) and stimulated with or without VEGF (50 ng/ml) for 24 h. Cell proliferation was assessed using Apollo 488 Cell Proliferation Kit (Ruibo Biotechnology Co., Ltd., Guangzhou, China). Image was obtained using an inverted fluorescence microscope (Olympus) and ImageJ software (NIH) was used to count the 5-ethynyl-2′-deoxyuridine positive (EdU) cells and $Hoechst^+$ cells in the photomicrographs. The positive rate of EdU staining was calculated using the formula: (positive rate = EdU^+ cell number/$Hoechst^+$ cell number).

Cell Cycle Assays

The HUVECs (3×10^5 cells/well) were treated with vehicle or BSS (10 and 20 μM) and stimulated with or without VEGF (50 ng/ml) for 24 h. The samples were centrifuged at 1,000 × *g* for 5 min to collect cells, and the supernatant was discarded. The cells were washed twice with cold PBS, and the precipitate was fixed with pre-cooled 75% ethanol overnight at 4°C. The fixed cells were collected by centrifugation at 1,000 × *g* and the supernatant was discarded. Then, 1 ml of PBS was added, and the cells were incubated for 15 min at 20–25°C. The cells were collected again by centrifugation and the supernatant was discarded. A 500-μl propidium iodide staining solution (Beyotime Biotechnology, Shanghai, China) was added to each tube, and the cells were incubated for 30 min. Accuri™ C6 flow cytometer (BD Biosciences) and FlowJo software (BD Biosciences) were used for cell cycle detection and analysis, respectively.

Transwell Migration Assays

A 100-μl cell suspension (4×10^5 cells/ml) was added to the upper chamber (total volume: 200 μl, with serum-free medium as solvent) of the Transwell apparatus (Costar, NY, United States), while medium (600 μl) containing 5% FBS was added to the lower chamber. The HUVECs were treated with vehicle or BSS (10 and 20 μM) and stimulated with or without VEGF (50 ng/ml) for 24 h. The migrated cells were stained with 0.1% crystal violet (Beyotime Biotechnology). Cells that migrated to the lower chamber were photographed under an inverted phase contrast microscope (Olympus). ImageJ software (NIH) was used to count the cells, and the average number of cells were determined.

Stress Fiber Fluorescent Staining

The HUVECs (2×10^4 cells/well) were seeded in 24-well plates, treated with vehicle or BSS (10 and 20 μM), and stimulated with or without tumor necrosis factor-alpha (TNF-α, 20 ng/ml) for 24 h. Then, the HUVECs were fixed on a glass slide with 4% paraformaldehyde for 20 min and infiltrated with 0.1% Triton X-100 in PBS for 5 min at 37°C. The cells were blocked with 1% BSA for 20 min, and incubated with Invitrogen Alexa Fluo™ r-546 phalloidin (Thermo Fisher Scientific, Waltham, MA,

United States) for 20 min at 37°C to stain the F-actin. Subsequently, the glass cover was fixed on the glass slide using DAPI anti-fading mounting medium (Beyotime Biotechnology). Images were obtained using a laser confocal microscope (×630 oil objective). ImageJ software (NIH) was used for fluorescence quantification (Jensen, 2013), to obtain the arbitrary unit (AU). The mean was computed, and the experiment was repeated thrice.

Molecular Docking

For molecular docking, we used CB-Dock (http://cao.labshare.cn/cb-dock/), which employs a new curvature-based cavity detection method to predict the binding sites of specific proteins, calculate their centers and sizes, and integrate them with AutoDock Vina, with an optimization success rate that reaches 70% (Liu et al., 2020). The VEGFR2 protein PDB format (PDB ID: 6GQQ) file was obtained from the Protein Database (http://www.rcsb.org). The ligand files in SDF format for BSS and axitinib compounds were obtained from PubChem (https://pubchem.ncbi.nlm.nih.gov/).

Western Blot Analysis

The HUVECs were homogenized in a lysis buffer, and centrifugated at 12,000 × *g* for 15 min at 4°C. The protein concentration in the supernatant was determined using the BCA protein assay kit (Beyotime Biotechnology). Equal amounts of protein were separated using 7.5% or 10% PAGE Gel Rapid Preparation Kit (Yazyme Biotechnology, Shanghai, China) under denaturing and non-reducing conditions and then transferred to a PVDF membrane. The membrane was blocked with Protein Free Rapid Blocking buffer (Yazyme) for 1 h and incubated with the primary antibody overnight at 4°C. After washing thrice with TBST, the blots were incubated with the horseradish-coupled secondary antibody. The signals were visualized using enhanced chemiluminescence reagent (Pierce Biotechnology, Rockford, IL, United States) and recorded using ChemiScope 3500 mini chemiluminescence imaging system (Clinx, Shanghai, China).

Histological Evaluation

The ankles were fixed after the mice were sacrificed. Decalcification and paraffin embedding were subsequently performed. Sections of the ankle samples (4 μm thick) were stained with hematoxylin and eosin (H and E) and safranin O-fast green (Sigma-Aldrich). A digital pathological scanner (3DHISTECH Ltd., Budapest, Hungary) was used for slide scanning.

Micro-CT Scan

The ankle was fixed with paraformaldehyde, and the skeletal structure was scanned by micro-CT system (SKYSCAN 1172, BRUKER, Belgium). Scanning parameter: resolution 4 μm, voltage 80 kV, current 88 μA. Three-dimensional reconstruction was performed using CT-Vox software after scanning. The bone destruction score was analyzed by Micro-CT (the erosion degree of knee and ankle was divided into 0–4 points according to the median, medial, and lateral planes, and the total score was 12 points) (Najm et al., 2020), and the results were expressed as mean ± standard deviation.

Immunohistochemistry Staining

Sections of the ankle samples (4 μm thick) were stained. After dewaxing, sections were submitted to antigen retrieval and further blocked with blocking fluid. The slices were rinsed in PBS for 5 min, 3 times, and then incubated with primary antibody (1:100 dilution) at 4°C overnight. After washing with PBS, the slices were incubated with secondary antibody for 1 h. Digital pathological scanner (3DHISTECH) was used for slide scanning, and three visual fields were selected at the joint site. ImageJ software was used to calculate the integral absorbance (IOD)/mm^2 (Van Kuijk et al., 2010), and the mean was taken for statistical analysis.

Statistical Analysis

The data were analyzed using SPSS software version 22.0 (IBM SPSS, Armonk, NY, United States) and GraphPad Prism version 5.0 (GraphPad, San Diego, CA, United States). Data were expressed as means ± standard deviations. The *t*-test, one-way analysis of variance (ANOVA), and Kruskal–Wallis non-parametric test were performed to evaluate the differences between experimental groups. The statistical significance was set at $p < 0.05$.

RESULTS

BSS Treatment Inhibits the VEGF-Induced Tube Formation of HUVECs

The chemical formula of BSS is shown in **Figure 1A**. The HUVECs were successfully identified using CD31 fluorescent staining **(Figure 1B)**. The CCK-8 assay was used to evaluate the effects of BSS on HUVECs viability **(Figure 1C)**, Specifically, a cell viability of >80% was observed in cells treated with 10 and 20 μM BSS. Hence, these were identified as the non-toxic dosages and used for subsequent experiments.

To investigate the anti-angiogenic effect of BSS, we performed a tube formation test. We determined that BSS significantly inhibited VEGF-induced tube formation in HUVECs **(Figure 1D)**. Our data also showed that the two dosage groups of BSS significantly reduced the number of junction points **(Figure 1E)** and cross-junction points **(Figure 1F)** in the tube formation of HUVECs ($p < 0.001$).

BSS Treatment Suppresses VEGF-Induced Proliferation of HUVECs

Angiogenesis is closely related to EC proliferation, and GSEA analysis of the GSE121894 dataset showed that "endothelial cell proliferation" and "positive regulation of endothelial cell proliferation" were significantly enriched in patients with RA, so we investigated the effect of BSS on endothelial cell proliferation **(Figure 2A)**. The EC transcriptome profile data were standardized and displayed (**Supplementary Figure S1A**), and the differential gene expression was displayed as a volcano graph (**Supplementary Figure S1B**).

To evaluate the inhibitory effect of BSS on the proliferation of HUVECs, we conducted EDU proliferation and cell cycle

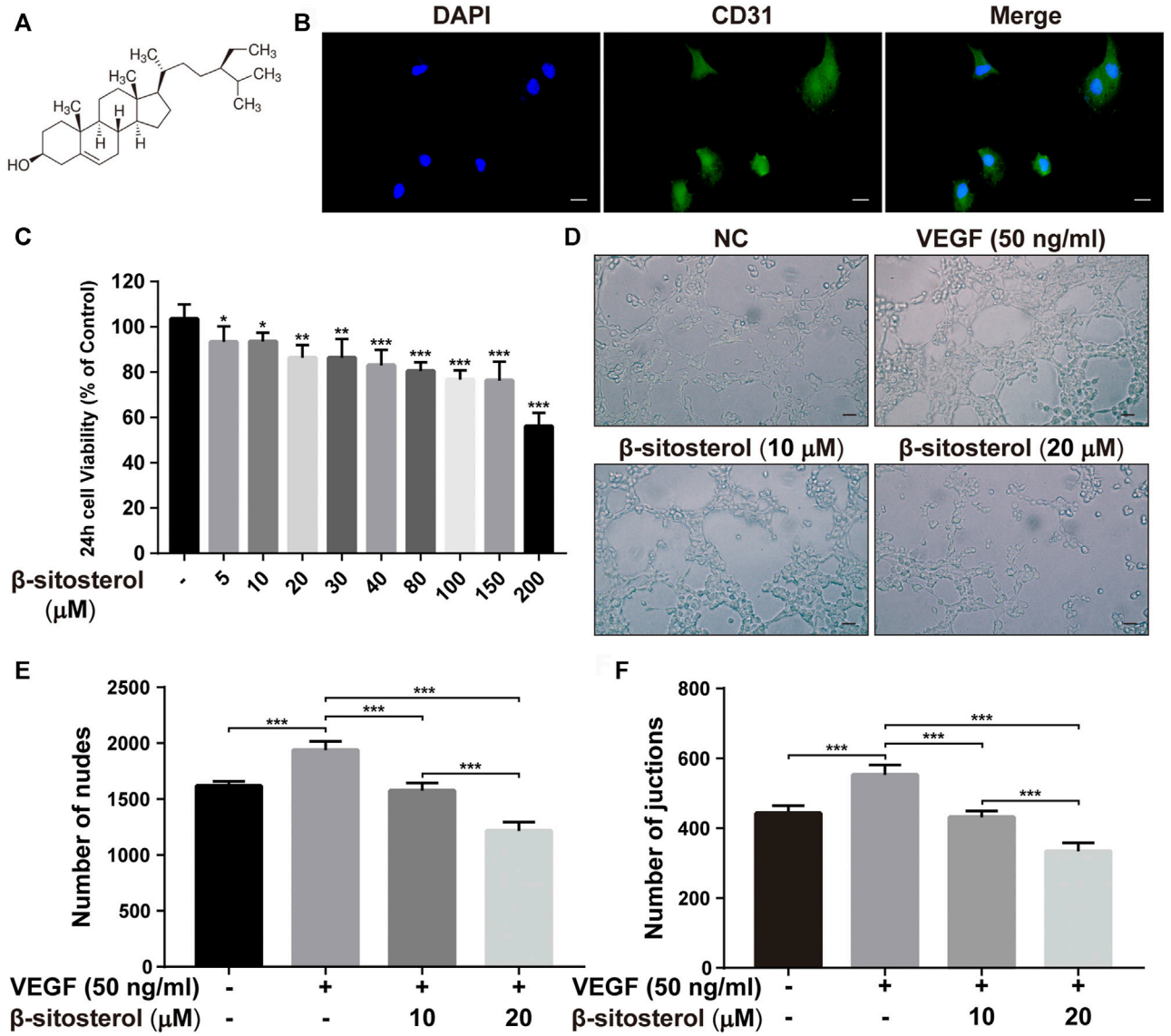

FIGURE 1 | BSS inhibits angiogenesis in HUVECs. **(A)** BSS chemical formula (quoted from sigma official website). **(B)** CD31 fluorescent staining identification (×630, scale bar = 20 μm). **(C)** Effects of different concentrations of BSS on CCK-8 in HUVECs after 24 h ($n = 3$). **(D)** Representative images of tube formation at 6 h in HUVECs (×200, scale bar = 50 μm), *Y*-axis shows the nodes **(E)** and junction numbers **(F)** ($n = 3$). All data are shown as the mean ± SEM. $^{*}p < 0.05$, $^{**}p < 0.01$, $^{***}p < 0.001$.

experiments. We determined that BSS significantly inhibited the VEGF-induced proliferation of HUVECs **(Figures 2B,C)**. Furthermore, cell cycle **(Figure 2D)** analysis showed that BSS induced S phase arrest in VEGF-stimulated HUVECs **(Figure 2E)**. These data suggest the inhibitory effect of BSS on cell proliferation of HUVECs.

BSS Treatment Prevents VEGF and TNF-α Induced Migration of HUVECs

It is well known that endothelial angiogenesis is closely related to endothelial cell migration, and GSEA analysis of GSE121894 dataset showed that "endothelial cell migration" and "regulation of endothelial cell migration" were significantly enriched in patients with RA. Therefore, we evaluated the effect of BSS on endothelial cell migration, measured using transwell assays **(Figure 3A)**. We determined that BSS treatment reduced VEGF-induced HUVECs migration **(Figures 3B,C)**. Since stress fibers provide the mechanical basis for cell migration (Fischer et al., 2021), we evaluated the effect of BSS on intensity of F-actin stress fibers. As shown in **Figures 3D,E**, BSS reduced the TNF-α-induced formation of stress fibers, further confirming the role of BSS in regulating EC migration. Collectively, our data indicate that

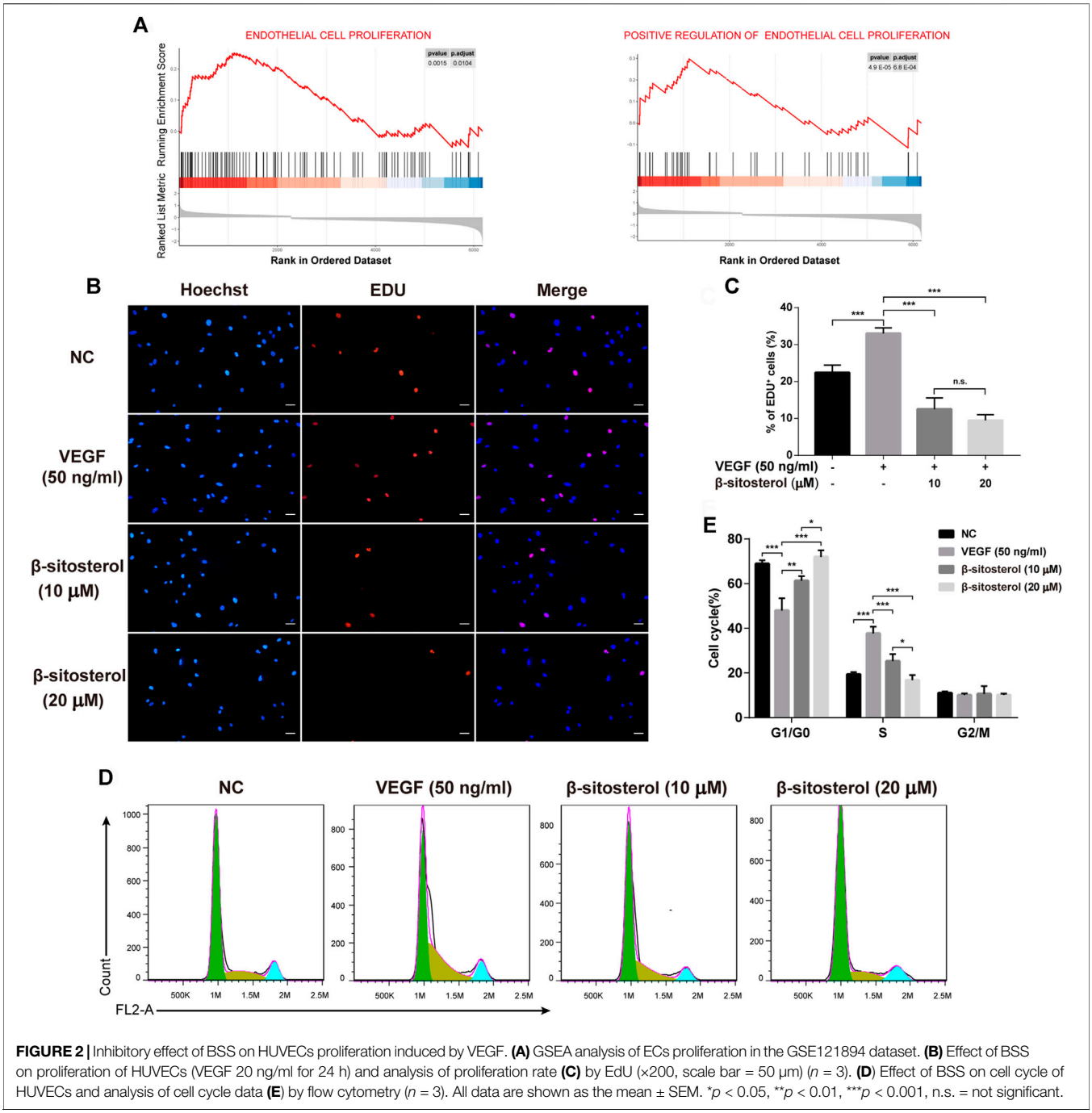

FIGURE 2 | Inhibitory effect of BSS on HUVECs proliferation induced by VEGF. **(A)** GSEA analysis of ECs proliferation in the GSE121894 dataset. **(B)** Effect of BSS on proliferation of HUVECs (VEGF 20 ng/ml for 24 h) and analysis of proliferation rate **(C)** by EdU (×200, scale bar = 50 μm) (n = 3). **(D)** Effect of BSS on cell cycle of HUVECs and analysis of cell cycle data **(E)** by flow cytometry (n = 3). All data are shown as the mean ± SEM. $^{*}p < 0.05$, $^{**}p < 0.01$, $^{***}p < 0.001$, n.s. = not significant.

BSS suppressed angiogenesis through, at least in part, regulating ECs migration.

BSS Treatment Inhibits the TNF-α-Induced Expression of VEGFR2 and *p*-VEGFR2 in HUVECs

GSEA was used to analyze the enrichment of ECs and angiogenesis-related signaling pathways in patients with RA. The results showed that VEGF signaling, PI3K-AKT-mTOR signaling pathway, and TGF-β signaling pathway were significantly activated in ECs of patients with RA (**Figure 4A**). In addition, previous studies have shown that BSS inhibits activation of PI3K-AKT and TGF-β signaling pathways (Xu et al., 2018; Park et al., 2019); the AKT and Smad2 as the major proteins in these pathways were suppressed by BSS in phosphorylated protein level in our data (**Supplementary Figure S2**). However, the effect of BSS on VEGF signaling pathway is unknown.

To evaluate the binding ability of BSS with VEGFR2 by molecular docking technology, we selected axitinib as a

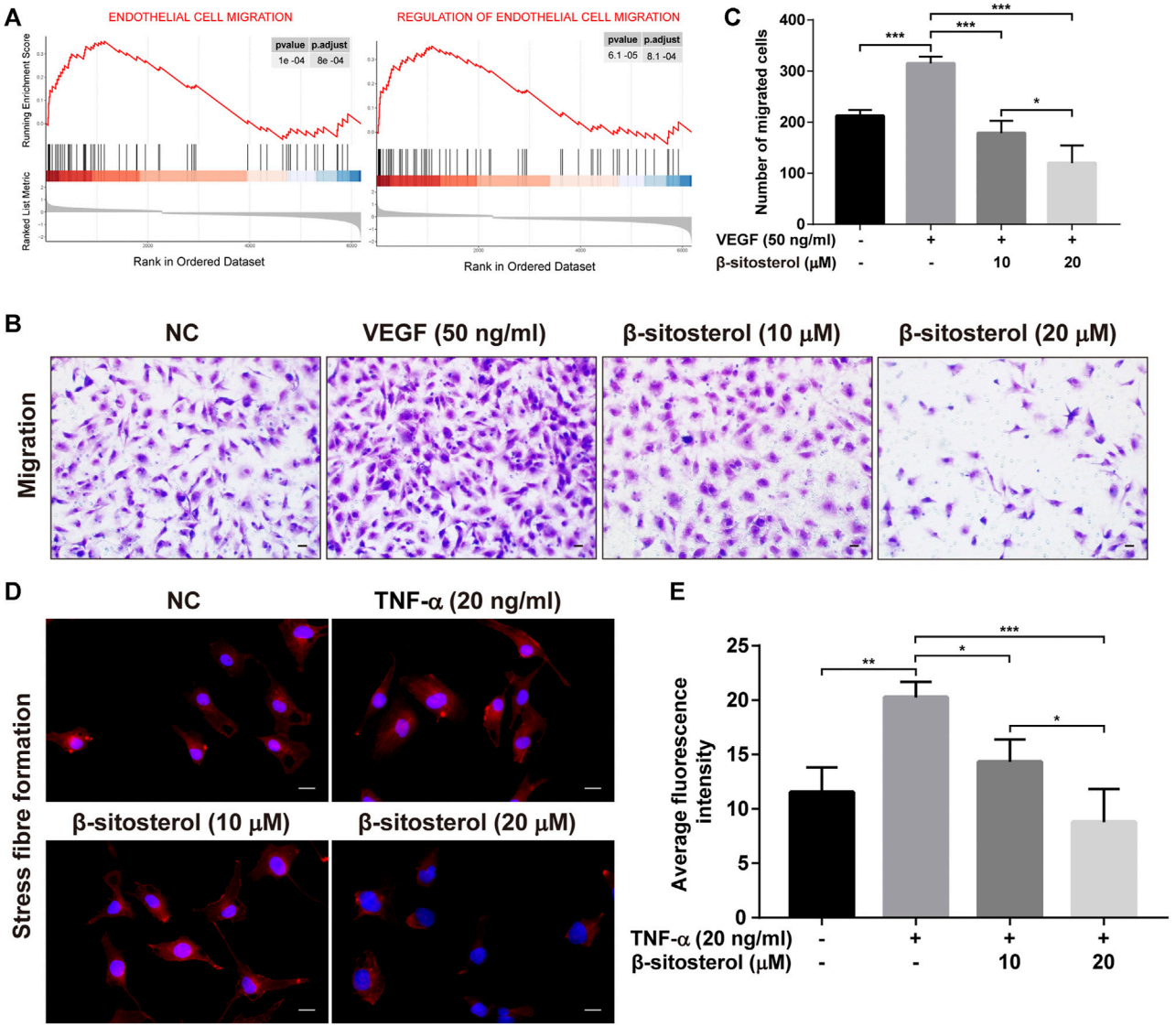

FIGURE 3 | Inhibitory effect of BSS on HUVECs migration induced by VEGF or TNF-α. **(A)** GSEA analysis of ECs migration in GSE121894 dataset. **(B)** Representative images of cell migration in a modified Boyden chamber following HUVECs induced by VEGF stimulation (×200, scale bar = 50 μm). **(C)** *Y*-axis shows the number of migrated cells ($n = 3$). **(D)** Representative images of stress fiber formation on TNF-α stimulation (20 ng/ml for 24 h) (×630, scale bar = 20 μm), Nuclei are stained with DAPI (blue). **(E)** *Y*-axis shows fluorescence intensity quantified by ImageJ ($n = 3$). All data are shown as the mean ± SEM. $^{*}p < 0.05$, $^{**}p < 0.01$, $^{***}p < 0.001$.

positive control drug for comparison. The more negative the Vina score (kcal/mol) and the larger the binding cavity, the more stable the binding of the receptor to the ligand (Liu et al., 2020). The results showed that the Vina scores of BSS **(Figure 4B)** and axitinib **(Figure 4C)** with VEGFR2 were close (−9.0 vs. −8.9, respectively), and the binding cavities of BSS and axitinib to VEGFR2 were 1,633 **(Table 1)**. With further verification by Western blot, the results showed that BSS (10 and 20 μM) significantly inhibited the expression of VEGFR2 and *p*-VEGFR2 **(Figures 4D,E)**. We also demonstrated that the inhibitory effect was more obvious under the combined treatment with axitinib and BSS **(Figures 4F,G)**.

BSS Treatment Attenuates the Severity of RA in CIA Mice

The *in vivo* effect of BSS on joint inflammation was evaluated in mice with CIA. As shown in **Figure 5A**, BSS alleviated the arthritis index score of CIA mice and reduced the degree of ankle swelling **(Figures 5B,C)**. Furthermore, compared with the CIA group, HE staining and safranin O green staining revealed that BSS administration reduced the joint inflammation and cartilage erosion **(Figure 5D)**. Moreover, micro-CT showed that, compared with the CIA group, BSS (100 mg/kg) ameliorated the bone destruction of ankle in mice **(Figures 5E,F)**.

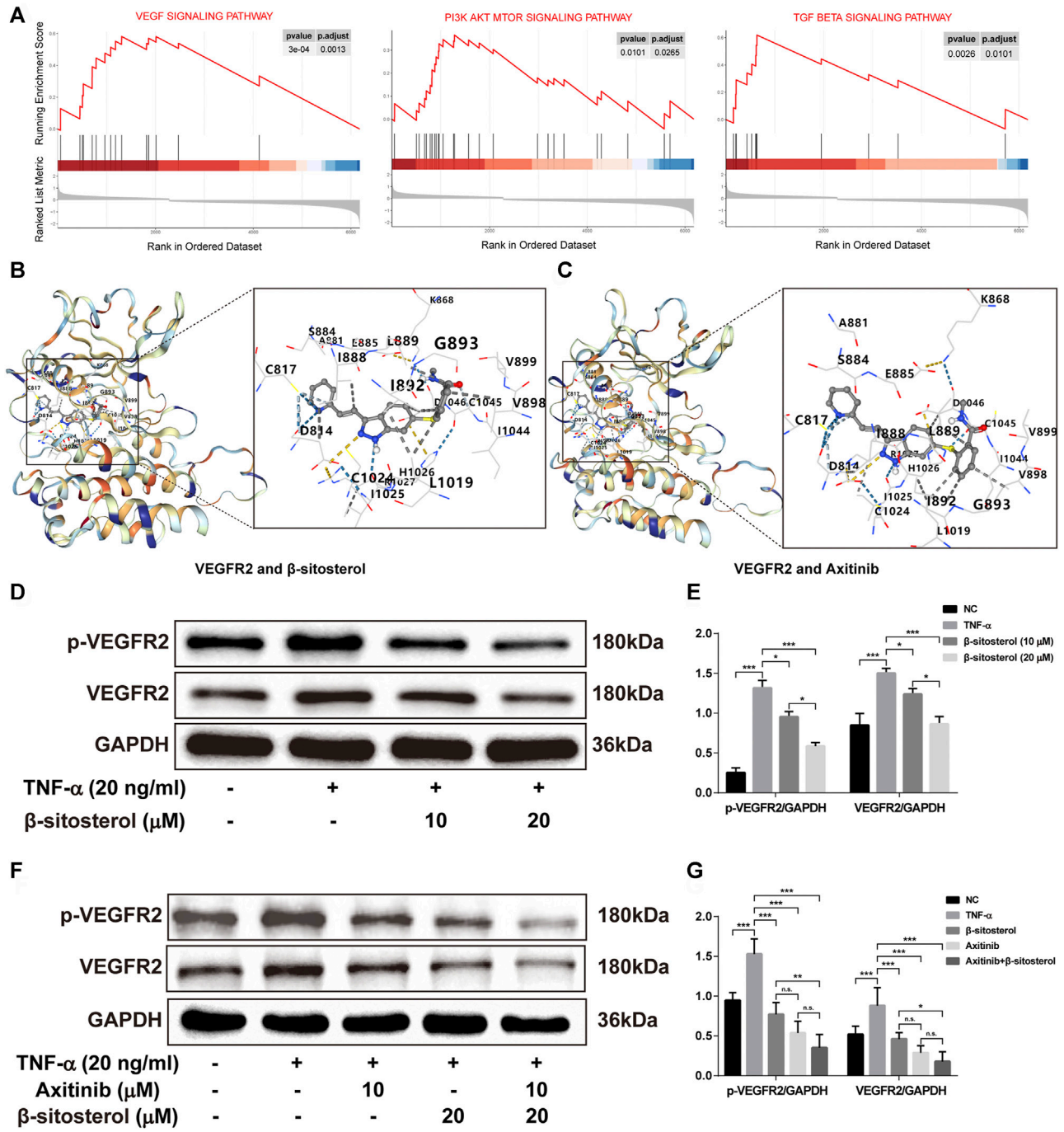

FIGURE 4 | The effect of VEGF signaling pathway in TNF-α-induced HUVECs regulated by BSS. **(A)** GSEA analysis of KEGG signaling pathway in the GSE121894 dataset. The structural interactions between VEGFR2 and BSS **(B)** and between VEGFR2 and axitinib **(C)** were described by molecular simulation, and binding affinity of VEGFR2 with BSS and axitinib is shown in **Table 1**. **(D)** *p*-VEGFR2 and VEGFR2 protein levels in HUVECs (on TNF-α 20 ng/ml for 1 h) intervened with BSS dosage groups were detected by immunoblotting and the relative expression levels **(E)** of proteins were corrected by GAPDH ($n = 3$). **(F)** *p*-VEGFR2 and VEGFR2 protein levels in HUVECs intervened with BSS and axitinib were detected by immunoblotting, and the relative expression levels **(G)** of proteins were corrected by GAPDH ($n = 3$). All data are shown as the mean ± SEM. $^{*}p < 0.05$, $^{**}p < 0.01$, $^{***}p < 0.001$, n.s. = not significant.

TABLE 1 | Binding affinity between VEGFR2 and BSS.

Compound name	Molecular formula	PubChem Cid	Molecular weight (g/mol)	Cavity size	Affinity (kcal/mol)
BSS	$C_{29}H_{50}O$	521199	414.7	1633	−9.0
Axitinib	$C_{22}H_{18}N_4OS$	6450551	386.5	1633	−8.9

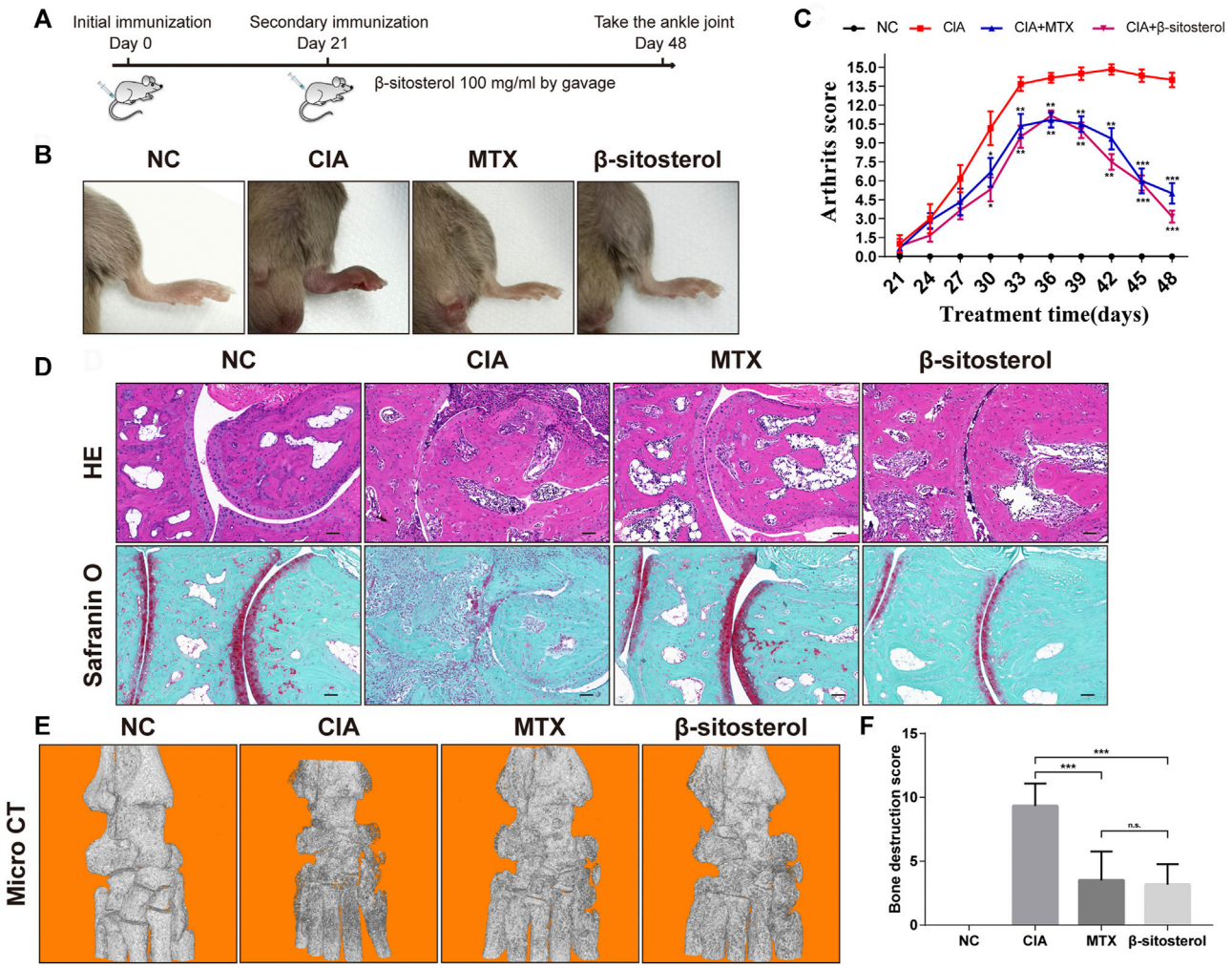

FIGURE 5 | Effects of BSS on experimental arthritis. **(A)** Animal experiment process, **(B)** the mice foot swelling photos, **(C)** Arthritis scores were shown. **(D)** Ankle HE and safranin O-fast green staining in the mice from each group ($n = 6$). **(E)** Micro-CT detection of bone destruction in the ankle joint of each group of mice, and analysis of **(F)** bone destruction scores in each group ($n = 6$). $^{*}p < 0.05$, $^{**}p < 0.01$, $^{***}p < 0.001$, n.s. = not significant.

BSS Treatment Inhibits Synovial Angiogenesis and the VEGFR2 and *p*-VEGFR2 Expression in CIA Mice

We further determined the effects of BSS treatment on CD31, VEGFR2, and *p*-VEGFR2 in ankle of CIA *via* the immunohistochemical examination of synovial angiogenesis. The results showed that BSS (100 mg/kg) significantly inhibited the CD31 expression in the synovial tissues (**Figures 6A,B**). Furthermore, consistent with our *in vitro* results, BSS treatment (100 mg/kg) significantly reduced the expression of VEGFR2 and *p*-VEGFR2 (**Figures 6C–F**) positive cells in the synovial tissues of CIA mice.

DISCUSSION

Synovial angiogenesis is an invasive tumor-like tissue that plays a vital role in the pathological process of RA synovitis and can lead to joint damage and cartilage destruction (Bottini and Firestein,

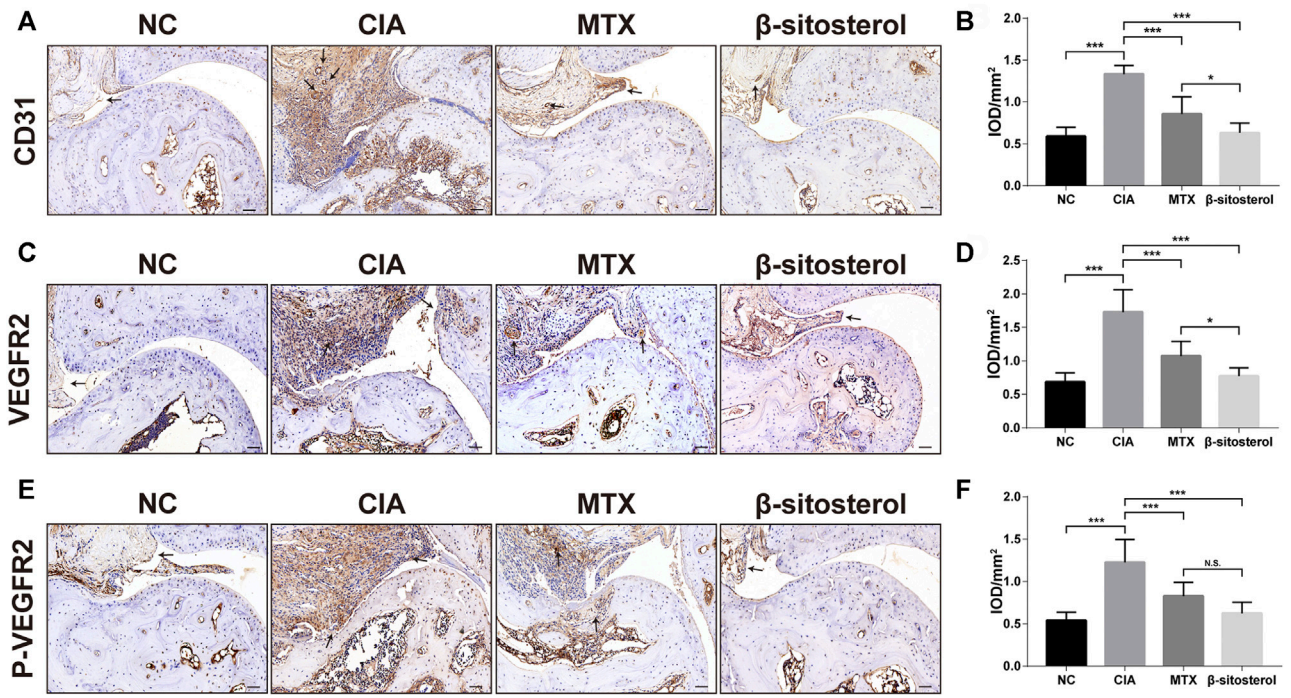

FIGURE 6 | Effect of BSS on immunohistochemistry of CD31, VEGFR2, and P-VEGFR2 on experimental arthritis. **(A)** CD31 immunohistochemical staining of the ankle joints in each group, and the optical density value **(B)** analysis using ImageJ ($n = 6$) (×200, scale bar = 50 μm). **(C)** VEGFR2 immunohistochemical staining of the ankle joints in each group, and the optical density value **(D)** analysis using ImageJ ($n = 6$) (×200, scale bar = 50 μm). **(E)** *p*-VEGFR2 immunohistochemical staining of the ankle joints in each group, and **(F)** the optical density value analysis using ImageJ ($n = 6$) (×200, scale bar = 50 μm). All data are shown as the mean ± SEM. $^{*}p < 0.05$, $^{**}p < 0.01$, $^{***}p < 0.001$, n.s. = not significant.

2013). During the development of synovium angiogenesis, the most important process is the formation of new blood vessels, which is necessary for the expansion, proliferation, and invasion of RA synovium (Fearon et al., 2016). Activation of ECs, including proliferation, migration, adhesion, and tube formation, play a central role in promoting the formation of new blood vessels. This study confirmed that BSS could significantly suppressed the tube formation, proliferation, and migration of HUVECs. At the same time, BSS could also obviously inhibit the formation of ankle and alleviated the degree of joint damage in the CIA mice. Its mechanism was related to the inhibition of VEGF signaling pathway activation.

The different aspects of angiogenesis can be observed in HUVECs capable of simulating the proliferation, migration, adhesion, and lumen formation of ECs. TNF-α and VEGF play a key role in RA and angiogenesis. TNF-α directly affects the migration and proliferation of ECs and the formation of new blood vessels (Leibovich et al., 1987). Meanwhile, studies have shown that TNF-α can affect the level of VEGF in serum of RA patients (Elshabrawy et al., 2015). Therefore, based on the previous studies (Leblond et al., 2020), HUVECs were intervened by TNF-α and VEGF to simulate the *in vivo* environment. We found that BSS significantly inhibited the tube formation of HUVECs and cell proliferation stimulated by VEGF, and prevent the entry of the cell into the S phase. In addition, BSS also restrained migration of HUVECs from the upper chamber to the lower chamber under VEGF stimulation and reduced the formation of stress fibers under TNF-α stimulation. Therefore, BSS may affect the synovial angiogenesis by affecting the proliferation, migration, and tube formation of ECs.

To further evaluate the effect of BSS on synovial angiogenesis and joint destruction *in vivo*, we selected CIA mice to study. CIA is an effective animal model in the study of RA. The pathological changes of CIA mice are highly similar to RA patients, which can simulate the main pathological features of RA (Miyoshi and Liu, 2018). For example, the CIA mice also have pathological changes such as joint involvement, synovial hyperplasia, synovial angiogenesis, bone, and cartilage destruction. The incidence of CIA was 90%–100% at 42–56 days after initial immunization and reached the peak at 40–50 days after initial immunization (Brand et al., 2007). In this study, the joint swelling of mice in the CIA group was obvious, and the success rate of modeling was 100%. The incidence peak reached 51 days after the initial immunization, which was consistent with the description of previous CIA mice studies, and BSS markedly decreased ankle swelling in CIA mice. In addition, HE staining showed the integrity of the articular surface structure of the ankle in the BSS group, but a small amount of inflammatory cell infiltration was observed. Safranin O-fast green staining and micro-CT results showed that compared with the CIA group, the ankle cartilage of mice in the BSS group was more complete, and there

was no obvious bone destruction. Overall, CIA mice results confirmed that BSS could significantly improve the joint swelling, protect the integrity of joint structure, and reduce the damage of joint bone and cartilage.

CD31 is a six-domain molecule that mediates the adhesion and the migration of ECs. It is a member of the immunoglobulin superfamily that constitutes the main protein for the connection between ECs. CD31 can be used to show the presence of ECs and help to evaluate the degree of angiogenesis, which expresses on platelets, most white blood cells, and ECs (Liu and Shi, 2012). In the present study, CD31 immunohistochemistry was used to evaluate the synovial angiogenesis in the ankle synovial tissue of CIA mice. The results showed that there was obvious angiogenesis labeled by CD31 in the ankle synovial tissue of CIA mice, and BSS could significantly inhibit the synovial angiogenesis of CIA mice.

Angiogenesis is mediated mainly by VEGF/VEGFR2 signaling, which is considered to be an important target of anti-angiogenic therapies (Karaman et al., 2018). The combination of VEGF with VEGFR2 leads to the phosphorylation of VEGFR2 on multiple tyrosine residues that trigger signaling cascades promoting ECs proliferation, migration, survival, and permeability (Simons et al., 2016). Thus, VEGFR2 activation is a key step in angiogenesis-related course, and blockage of VEGF/VEGFR2 signaling by VEGFR2 inhibitors can suppress angiogenic responses (Roskoski, 2017). In this study, the affinity of BSS and VEGFR2 was predicted by molecular docking. Molecular docking is also able to assess the binding affinity between drugs and targets (Saikia and Bordoloi, 2019), and binding affinity determines bioactivity of drug against the target quantified by the docking score (kcal/mol) (Quiroga and Villarreal, 2016). It was somewhat surprising in our molecular docking results that BSS had a similar binding affinity to VEGFR2 compared with axitinib, a potent inhibitor of VEGFR2 mainly suppressing the phosphorylation of VEGFR2 (Hu-Lowe et al., 2008). According to this finding, it could conceivably be hypothesized that BSS played an analogous role for VEGFR2 block as axitinib. Therefrom, we detected the expression levels of VEGFR2 and *p*-VEGFR2 proteins by Western blot assays, and we indeed found a declining trend of both in HUVECs. On the other hand, we measured their expression in synovial tissues of CIA mice joint using IHC staining that validated our hypothesis. In a word, we confirmed that BSS had an inhibitory effect on the expression and activation of VEGFR2. In addition, previous studies had demonstrated that BSS exerted anti-angiogenesis functions through inhibition of VEGF or inflammatory cytokine expression (Yang et al., 2019). These results added to a growing body of evidence that suggests that BSS probably acted on the VEGF pathway to treat RA.

BSS is considered a safe and potential drug, structurally similar to cholesterol, that inhibits the absorption of cholesterol in the intestines and elevates the levels of enzymatic and non-enzymatic antioxidants, effectively exerting anti-diabetic and lipid-lowering effects (Babu and Jayaraman, 2020). Studies have also shown that BSS has immunomodulatory effects (Fraile et al., 2012), and analgesic and anti-inflammatory effects (Nirmal et al., 2012), which are beneficial for the treatment of RA. In recent years, the effects of BSS in other aspects of RA have also been investigated. In particular, BSS was discovered to reduce the swelling of the ankle and to decrease the levels of collagen-specific antibodies and serum cytokines in CIA mice, by triggering polarization of macrophage to an anti-inflammatory phenotype (Liu et al., 2019). In addition, treatments using the combination of BSS and imperatorin (Guo et al., 2020) and BSS-loaded solid lipid nanoparticles (Zhang et al., 2020) have been reported to ameliorate RA.

In our study, we proved that BSS improved the joint symptoms of CIA mice by affecting synovial angiogenesis. BSS may have a more obvious improvement effect on patients with multiple comorbidities, such as RA with diabetes or RA with hyperlipidemia. In addition, it needs to be pointed out that this study also has shortcomings, and other cell models have not been used for further verification. The effect of BSS on the hypoxia model of HUVECs induced by cobalt oxide and the co-culture model of fibroblast-like synovial cells and HUVECs will be used for in-depth study.

Therefore, we have proved that BSS has a strong restrained effect on synovial angiogenesis *in vivo* and *in vitro*, and alleviated joint swelling and bone destruction in CIA mice. Its mechanism may be related to the suppression of VEGF signaling pathway activation. In a word, BSS might be a potential candidate drug for treating RA.

DATA AVAILABILITY STATEMENT

The datasets presented in this study can be found in online repositories. The names of the repository/repositories and accession number(s) can be found in the article/ **Supplementary Material**.

ETHICS STATEMENT

The animal study was reviewed and approved by Ethics Committee of the First Affiliated Hospital of Guangzhou University of Traditional Chinese Medicine.

AUTHOR CONTRIBUTIONS

C-SL and KQ designed this study. KQ, X-XZ, CW, W-GH, X-BL, S-DX, and D-KL performed the experiments. C-SL, KQ, and X-XZ analyzed the data. KQ wrote the manuscript. C-SL and M-YL revised the manuscript. All authors critically participated in the discussion and commented on the manuscript.

FUNDING

This work is supported by grants from the National Natural Science Foundation of China (Grant Nos. 81774262 and 82174301), and the Natural Science Foundation of Guangdong Province (Grant No. 2017A030311009).

ACKNOWLEDGMENTS

We would like to thank the Lingnan Medical Center of Guangzhou University of Chinese Medicine for the technical assistance provided.

SUPPLEMENTARY MATERIAL

The Supplementary Material for this article can be found online at: https://www.frontiersin.org/articles/10.3389/fphar.2021.816477/full#supplementary-material

REFERENCES

Apte, R. S., Chen, D. S., and Ferrara, N. (2019). VEGF in Signaling and Disease: Beyond Discovery and Development. *Cell* 176, 1248–1264. doi:10.1016/j.cell.2019.01.021

Babu, S., and Jayaraman, S. (2020). An Update on β-sitosterol: A Potential Herbal Nutraceutical for Diabetic Management. *Biomed. Pharmacother.* 131, 110702. doi:10.1016/j.biopha.2020.110702

Bottini, N., and Firestein, G. S. (2013). Duality of Fibroblast-like Synoviocytes in RA: Passive Responders and Imprinted Aggressors. *Nat. Rev. Rheumatol.* 9, 24–33. doi:10.1038/nrrheum.2012.190

Brand, D. D., Latham, K. A., and Rosloniec, E. F. (2007). Collagen-induced Arthritis. *Nat. Protoc.* 2, 1269–1275. doi:10.1038/nprot.2007.173

Carpentier, G., Berndt, S., Ferratge, S., Rasband, W., Cuendet, M., Uzan, G., et al. (2020). Angiogenesis Analyzer for ImageJ - A Comparative Morphometric Analysis of "Endothelial Tube Formation Assay" and "Fibrin Bead Assay". *Sci. Rep.* 10, 11568. doi:10.1038/s41598-020-67289-8

Elshabrawy, H. A., Chen, Z., Volin, M. V., Ravella, S., Virupannavar, S., and Shahrara, S. (2015). The Pathogenic Role of Angiogenesis in Rheumatoid Arthritis. *Angiogenesis* 18, 433–448. doi:10.1007/s10456-015-9477-2

Fearon, U., Canavan, M., Biniecka, M., and Veale, D. J. (2016). Hypoxia, Mitochondrial Dysfunction and Synovial Invasiveness in Rheumatoid Arthritis. *Nat. Rev. Rheumatol.* 12, 385–397. doi:10.1038/nrrheum.2016.69

Fischer, R. S., Sun, X., Baird, M. A., Hourwitz, M. J., Seo, B. R., Pasapera, A. M., et al. (2021). Contractility, Focal Adhesion Orientation, and Stress Fiber Orientation Drive Cancer Cell Polarity and Migration along Wavy ECM Substrates. *Proc. Natl. Acad. Sci. U S A.* 118, e2021135118. doi:10.1073/pnas.2021135118

Fraile, L., Crisci, E., Córdoba, L., Navarro, M. A., Osada, J., and Montoya, M. (2012). Immunomodulatory Properties of Beta-Sitosterol in Pig Immune Responses. *Int. Immunopharmacol* 13, 316–321. doi:10.1016/j.intimp.2012.04.017

Guo, Q., Li, L., Zheng, K., Zheng, G., Shu, H., Shi, Y., et al. (2020). Imperatorin and β-sitosterol Have Synergistic Activities in Alleviating Collagen-Induced Arthritis. *J. Leukoc. Biol.* 108, 509–517. doi:10.1002/JLB.3MA0320-440RR

Hu-Lowe, D. D., Zou, H. Y., Grazzini, M. L., Hallin, M. E., Wickman, G. R., Amundson, K., et al. (2008). Nonclinical Antiangiogenesis and Antitumor Activities of Axitinib (AG-013736), an Oral, Potent, and Selective Inhibitor of Vascular Endothelial Growth Factor Receptor Tyrosine Kinases 1, 2, 3. *Clin. Cancer Res.* 14, 7272–7283. doi:10.1158/1078-0432.CCR-08-0652

Jensen, E. C. (2013). Quantitative Analysis of Histological Staining and Fluorescence Using ImageJ. *Anat. Rec. (Hoboken)* 296, 378–381. doi:10.1002/ar.22641

Karaman, S., Leppänen, V. M., and Alitalo, K. (2018). Vascular Endothelial Growth Factor Signaling in Development and Disease. *Development* 145, dev151019. doi:10.1242/dev.151019

Le, T. H. V., and Kwon, S. M. (2021). Vascular Endothelial Growth Factor Biology and its Potential as a Therapeutic Target in Rheumatic Diseases. *Int. J. Mol. Sci.* 22, 5387. doi:10.3390/ijms22105387

Leblond, A., Allanore, Y., and Avouac, J. (2017). Targeting Synovial Neoangiogenesis in Rheumatoid Arthritis. *Autoimmun. Rev.* 16, 594–601. doi:10.1016/j.autrev.2017.04.005

Leblond, A., Pezet, S., Cauvet, A., Casas, C., Pires Da Silva, J., Hervé, R., et al. (2020). Implication of the Deacetylase Sirtuin-1 on Synovial Angiogenesis and Persistence of Experimental Arthritis. *Ann. Rheum. Dis.* 79, 891–900. doi:10.1136/annrheumdis-2020-217377

Leibovich, S. J., Polverini, P. J., Shepard, H. M., Wiseman, D. M., Shively, V., and Nuseir, N. (1987). Macrophage-induced Angiogenesis Is Mediated by Tumour Necrosis Factor-Alpha. *Nature* 329, 630–632. doi:10.1038/329630a0

Li, N., Xu, Q., Liu, Q., Pan, D., Jiang, Y., Liu, M., et al. (2017). Leonurine Attenuates Fibroblast-like Synoviocyte-Mediated Synovial Inflammation and Joint Destruction in Rheumatoid Arthritis. *Rheumatology (Oxford)* 56, 1417–1427. doi:10.1093/rheumatology/kex142

Li, X., Padhan, N., Sjöström, E. O., Roche, F. P., Testini, C., Honkura, N., et al. (2016). VEGFR2 pY949 Signalling Regulates Adherens junction Integrity and Metastatic Spread. *Nat. Commun.* 7, 11017. doi:10.1038/ncomms11017

Liu, L., and Shi, G. P. (2012). CD31: beyond a Marker for Endothelial Cells. *Cardiovasc. Res.* 94, 3–5. doi:10.1093/cvr/cvs108

Liu, R., Hao, D., Xu, W., Li, J., Li, X., Shen, D., et al. (2019). β-Sitosterol Modulates Macrophage Polarization and Attenuates Rheumatoid Inflammation in Mice. *Pharm. Biol.* 57, 161–168. doi:10.1080/13880209.2019.1577461

Liu, Y., Grimm, M., Dai, W. T., Hou, M. C., Xiao, Z. X., and Cao, Y. (2020). CB-dock: a Web Server for Cavity Detection-Guided Protein-Ligand Blind Docking. *Acta Pharmacol. Sin* 41, 138–144. doi:10.1038/s41401-019-0228-6

Mcinnes, I. B., and Schett, G. (2011). The Pathogenesis of Rheumatoid Arthritis. *N. Engl. J. Med.* 365, 2205–2219. doi:10.1056/NEJMra1004965

Miyoshi, M., and Liu, S. (2018). Collagen-Induced Arthritis Models. *Methods Mol. Biol.* 1868, 3–7. doi:10.1007/978-1-4939-8802-0_1

Najm, A., Masson, F. M., Preuss, P., Georges, S., Ory, B., Quillard, T., et al. (2020). MicroRNA-17-5p Reduces Inflammation and Bone Erosions in Mice with Collagen-Induced Arthritis and Directly Targets the JAK/STAT Pathway in Rheumatoid Arthritis Fibroblast-like Synoviocytes. *Arthritis Rheumatol.* 72, 2030–2039. doi:10.1002/art.41441

Nirmal, S. A., Pal, S. C., Mandal, S. C., and Patil, A. N. (2012). Analgesic and Anti-inflammatory Activity of β-sitosterol Isolated from Nyctanthes Arbortristis Leaves. *Inflammopharmacology* 20, 219–224. doi:10.1007/s10787-011-0110-8

O'neil, L. J., Barrera-Vargas, A., Sandoval-Heglund, D., Merayo-Chalico, J., Aguirre-Aguilar, E., Aponte, A. M., et al. (2020). Neutrophil-mediated Carbamylation Promotes Articular Damage in Rheumatoid Arthritis. *Sci. Adv.* 6, eabd2688. doi:10.1126/sciadv.abd2688

Pan, D., Li, N., Liu, Y., Xu, Q., Liu, Q., You, Y., et al. (2018). Kaempferol Inhibits the Migration and Invasion of Rheumatoid Arthritis Fibroblast-like Synoviocytes by Blocking Activation of the MAPK Pathway. *Int. Immunopharmacol* 55, 174–182. doi:10.1016/j.intimp.2017.12.011

Park, Y. J., Bang, I. J., Jeong, M. H., Kim, H. R., Lee, D. E., Kwak, J. H., et al. (2019). Effects of β-Sitosterol from Corn Silk on TGF-B1-Induced Epithelial-Mesenchymal Transition in Lung Alveolar Epithelial Cells. *J. Agric. Food Chem.* 67, 9789–9795. doi:10.1021/acs.jafc.9b02730

Quiroga, R., and Villarreal, M. A. (2016). Vinardo: A Scoring Function Based on Autodock Vina Improves Scoring, Docking, and Virtual Screening. *PLoS One* 11, e0155183. doi:10.1371/journal.pone.0155183

Roskoski, R., Jr. (2017). Vascular Endothelial Growth Factor (VEGF) and VEGF Receptor Inhibitors in the Treatment of Renal Cell Carcinomas. *Pharmacol. Res.* 120, 116–132. doi:10.1016/j.phrs.2017.03.010

Saikia, S., and Bordoloi, M. (2019). Molecular Docking: Challenges, Advances and its Use in Drug Discovery Perspective. *Curr. Drug Targets* 20, 501–521. doi:10.2174/1389450119666181022153016

Sakurai, Y., Ohgimoto, K., Kataoka, Y., Yoshida, N., and Shibuya, M. (2005). Essential Role of Flk-1 (VEGF Receptor 2) Tyrosine Residue 1173 in Vasculogenesis in Mice. *Proc. Natl. Acad. Sci. U S A.* 102, 1076–1081. doi:10.1073/pnas.0404984102

Sharmila, R., and Sindhu, G. (2017). Modulation of Angiogenesis, Proliferative Response and Apoptosis by β-Sitosterol in Rat Model of Renal Carcinogenesis. *Indian J. Clin. Biochem.* 32, 142–152. doi:10.1007/s12291-016-0583-8

Simons, M., Gordon, E., and Claesson-Welsh, L. (2016). Mechanisms and Regulation of Endothelial VEGF Receptor Signalling. *Nat. Rev. Mol. Cel Biol* 17, 611–625. doi:10.1038/nrm.2016.87

Van Kuijk, A. W., Wijbrandts, C. A., Vinkenoog, M., Zheng, T. S., Reedquist, K. A., and Tak, P. P. (2010). TWEAK and its Receptor Fn14 in the Synovium of

Patients with Rheumatoid Arthritis Compared to Psoriatic Arthritis and its Response to Tumour Necrosis Factor Blockade. *Ann. Rheum. Dis.* 69, 301–304. doi:10.1136/ard.2008.090548

Wang, Y., Da, G., Li, H., and Zheng, Y. (2013). Avastin Exhibits Therapeutic Effects on Collagen-Induced Arthritis in Rat Model. *Inflammation* 36, 1460–1467. doi:10.1007/s10753-013-9687-y

Wang, Z. Z., Liu, F., Gong, Y. F., Huang, T. Y., Zhang, X. M., and Huang, X. Y. (2018). Antiarthritic Effects of Sorafenib in Rats with Adjuvant-Induced Arthritis. *Anat. Rec. (Hoboken)* 301, 1519–1526. doi:10.1002/ar.23856

Woyengo, T. A., Ramprasath, V. R., and Jones, P. J. (2009). Anticancer Effects of Phytosterols. *Eur. J. Clin. Nutr.* 63, 813–820. doi:10.1038/ejcn.2009.29

Xu, H., Li, Y., Han, B., Li, Z., Wang, B., Jiang, P., et al. (2018). Anti-breast-Cancer Activity Exerted by β-Sitosterol-d-glucoside from Sweet Potato via Upregulation of MicroRNA-10a and via the PI3K-Akt Signaling Pathway. *J. Agric. Food Chem.* 66, 9704–9718. doi:10.1021/acs.jafc.8b03305

Yang, Q., Yu, D., and Zhang, Y. (2019). β-Sitosterol Attenuates the Intracranial Aneurysm Growth by Suppressing TNF-α-Mediated Mechanism. *Pharmacology* 104, 303–311. doi:10.1159/000502221

Zhang, F., Liu, Z., He, X., Li, Z., Shi, B., and Cai, F. (2020). β-Sitosterol-loaded Solid Lipid Nanoparticles Ameliorate Complete Freund's Adjuvant-Induced Arthritis in Rats: Involvement of NF-Kb and HO-1/Nrf-2 Pathway. *Drug Deliv.* 27, 1329–1341. doi:10.1080/10717544.2020.1818883

Conflict of Interest: The authors declare that the research was conducted in the absence of any commercial or financial relationships that could be construed as a potential conflict of interest.

Publisher's Note: All claims expressed in this article are solely those of the authors and do not necessarily represent those of their affiliated organizations, or those of the publisher, the editors, and the reviewers. Any product that may be evaluated in this article, or claim that may be made by its manufacturer, is not guaranteed or endorsed by the publisher.

Copyright © 2022 Qian, Zheng, Wang, Huang, Liu, Xu, Liu, Liu and Lin. This is an open-access article distributed under the terms of the Creative Commons Attribution License (CC BY). The use, distribution or reproduction in other forums is permitted, provided the original author(s) and the copyright owner(s) are credited and that the original publication in this journal is cited, in accordance with accepted academic practice. No use, distribution or reproduction is permitted which does not comply with these terms.

Advantages of publishing in Frontiers

OPEN ACCESS
Articles are free to read for greatest visibility and readership

FAST PUBLICATION
Around 90 days from submission to decision

HIGH QUALITY PEER-REVIEW
Rigorous, collaborative, and constructive peer-review

TRANSPARENT PEER-REVIEW
Editors and reviewers acknowledged by name on published articles

Frontiers
Avenue du Tribunal-Fédéral 34
1005 Lausanne | Switzerland

Visit us: www.frontiersin.org
Contact us: frontiersin.org/about/contact

REPRODUCIBILITY OF RESEARCH
Support open data and methods to enhance research reproducibility

DIGITAL PUBLISHING
Articles designed for optimal readership across devices

FOLLOW US
@frontiersin

IMPACT METRICS
Advanced article metrics track visibility across digital media

EXTENSIVE PROMOTION
Marketing and promotion of impactful research

LOOP RESEARCH NETWORK
Our network increases your article's readership